Awareness and Localization of Explosives-Related Threats

A Department of Homeland Security Center of Excellence

Phase 2, Year 7 Annual Report
September 2020

ALERT
AWARENESS AND LOCALIZATION OF EXPLOSIVES-RELATED THREATS

This page intentionally left blank.

Table of Contents

This page intentionally left blank.

Section 1: ALERT Phase 2 Overview and Year 7 Highlights

1.1 ALERT OVERVIEW

ALERT (Awareness and Localization of Explosives-Related Threats) is a Department of Homeland Security (DHS) funded Center of Excellence (COE). This report reflects the work performed during the seventh year (July 1, 2019–June 30, 2020) and final year of funding under the Phase 2 award made by DHS in September 2013. Due to the impact of the COVID-19 pandemic beginning in March 2020 and continuing to present, ALERT leadership requested a no-cost extension which was granted by DHS. The pandemic and related shutdowns and social distancing requirements resulted in necessitated delays in the research, education and outreach elements of the ALERT COE. As a result, a no-cost extension was granted through May 31, 2021. This will enable the Center to achieve its final goals and deliverables.

Vision

A world protected from the catastrophic consequences of explosives-related threats.

Mission

ALERT seeks to conduct transformational research, technology development, and educational initiatives for effective characterization, detection, mitigation, and response to the explosives-related threats facing the country and the world.

The report that follows contains information on ALERT research, transition, and education programs. The major elements of the ALERT COE are as follows:

Partners

The ALERT academic partnership is led by Northeastern University. Currently, the partnership consists of three core partners: Boston University, Purdue University, and the University of Rhode Island. In addition, there are six research partners: Duke University, Marquette University, Rensselaer Polytechnic Institute, Tufts University, University of Notre Dame, and the University of Puerto Rico at Mayagüez.

Research Program

The ALERT research program was and continues to be driven by inspiring challenges such as ultrareliable screening, explosives detection at a distance, and actionable trace sampling. These challenges have defined the four core fundamental science research thrusts: Characterization and Elimination of Illicit Explosives (R1), Trace and Vapor Sensors (R2), Bulk Sensors and Sensor Systems (R3), and Video Analytics and Signature Analysis (R4). Examples of cutting-edge projects within these thrusts include characterization of signatures and properties of potential threat materials, cost-effective sensors and sampling methods, standoff infrared spectroscopy, advanced multi-modality concealed threat imaging, and model-based iterative reconstruction for single- and dual-energy X-ray computed tomography (CT). With the collaboration of its industrial and national laboratory partners, ALERT has worked to transition research to systems in the field, such as a video-analytics-based anomaly detection system for use in airports and other venues. Researchers from the partnership brought strengths in advanced sensor design, standoff weak-target detection, signal processing, sensor integration, explosives characterization, chemistry, and material science. The ALERT team was able to meet the challenges of its daunting mission by combining the expertise

of its core researchers with national lab affiliates and other strategic academic, industrial, and government partners. The research program is discussed in more detail in Section 2.

Education Program

A key ALERT objective has been to build an outstanding educational program that includes pre-college, undergraduate, graduate, and career professional components. Examples include distance-learning courses in homeland security–related technologies, an Engineering Leadership Program available to DHS personnel, and the Science and Engineering Workforce Development Program (SEWDP) for undergraduate and graduate students aimed at building the homeland security workforce. Workshops and short courses have been developed to review new threat detection and mitigation technologies for first responders such as the Secret Service, Transportation Safety Administration, police, firefighters, and emergency medical technicians. The education program is discussed in more detail in Section 3.

Transition Efforts

The COE's transition efforts transferred the science and technologies developed by the ALERT Research Program Thrusts to DHS stakeholders and the homeland security enterprise, HSE. Transition required focused engagement of the ALERT researchers and the HSE end users to identify research results and users' needs, which then led to collaborative research, implementation, and ultimately, transition of the developed technology to the user. Transition of the ALERT science and technology solutions into relevance for the HSE is the first of a two-step process. The second step is a focused DHS task order that will lead to a deployment of the technology in the field. Current and future transition efforts are described in detail in Section 4.

Strategic Studies

Part of ALERT's mandate from DHS is to develop a research strategy to identify the fundamental science key objectives, such as Improvised Explosive Device (IED) Detect and Defeat capabilities. To support this effort, ALERT continues to lead its strategic study workshop series, known as the Advanced Development for Security Applications (ADSA). The outcomes of each workshop are documented in a report that articulates a roadmap recommending prioritized areas of long-range fundamental research. One ADSA workshop was held in Year 7, supplementing the twenty held previously. Due to the COVID-19 pandemic, the workshop scheduled for May 2020 needed to be rescheduled and will now be held virtually in the fall of 2020. We anticipate that two or three workshops will be held on a variety of topics relating to the ALERT mission through the remainder of the no-cost extension period through May 2021. The strategic studies activities are discussed in more detail in Section 5.

Safety Program

While striving for the goal of effective characterization, detection, and response to the explosives-related threats facing the country and the world, safety has been of paramount importance. Handling of energetic materials requires constant vigilance. The ALERT Safety Program components include a Safety Review Board, a Safety Awareness Education Program, a set of Safety Protocols and Standard Operating Procedures, and a Safety Compliance Assurance Program. It has been our intent that by taking the time to create and review these safe-operating procedures, faculty and students have had a heightened awareness of the hazards and taken appropriate care. The safety program is discussed in more detail in Section 6.

Information Protection Plan

The ALERT Phase 1 Cooperative Agreement was modified to include an Information Protection Program, and similar language was built into the ALERT Phase 2 Cooperative Agreement. There are four components of the ALERT Information Protection Program: Sensitive Information Protection Policy, Sensitive Information Review Process, Data Procurement and Dissemination Process, and Information Protection Education and Training Procedure. The Information Protection Plan is discussed in more detail in Section 7. That section also describes the Information Protection Program Board, which oversees the successful implementation of the program components and reviews them on an annual basis.

Industrial Liaison Initiatives and Partnerships

ALERT Phase 2 benefited from the prior collaborative links forged by ALERT Phase 1 and by Northeastern's National Science Foundation (NSF)-funded Engineering Research Center, Gordon-CenSSIS, with industry, practitioners (e.g., hospitals), and government organizations. These partners have provided ALERT with financial support and opportunities for researchers and students to work at their facilities, as well as access to research and development (R&D) leaders, real system-level applications, state-of-the-art hardware and software, willing partners for technology transfer, and team members for proposals for additional funding and sustainability. Conversely, ALERT has provided its collaborators with access to talented professors, postdocs, graduate students, undergraduate students, and innovative research. Together, the industrial/practitioner, government, and academic collaboration has been a powerful vehicle for advanced development. The COE's industrial/practitioner and government partnerships are discussed in more detail in Section 8.

Infrastructure

The ALERT management team has been comprised of faculty and staff from the core partners, and it has been augmented by our partnership with strategic affiliates, companies, and government agencies. Effectively managing this complex enterprise has presented a challenge equal to the basic research challenges. To meet this challenge, ALERT has been managed by experienced personnel with proven records of accomplishment. In doing so, we understood and embraced the concept that each entity within the center must maintain its own unique charter and work environment while also striving for coherence. The ALERT Center infrastructure is discussed in more detail in Section 9.

Summary

This report provides a broad overview of the strategic plan, goals, and deliverables for the ALERT Center of Excellence. With these elements in place, the ALERT leadership has had a firm base from which to quickly adapt to new research and education priorities related to the daunting mission of DHS to protect our nation from terrorist threats. Before turning to the detailed description of the ALERT program, we first present a brief description of several Year 7 highlights.

1.2 ALERT PHASE 2 YEAR 7 HIGHLIGHTS

A. ALERT Faculty and Student Honors, Awards, and Accomplishments

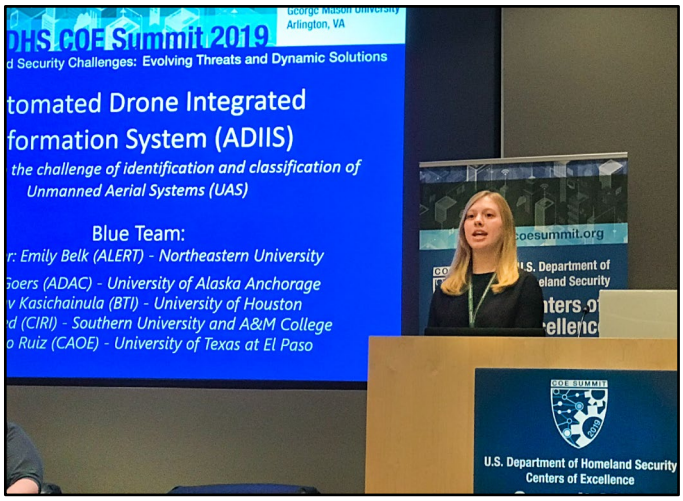

Figure 1-1: Northeastern University student Emily Belk presents her team's work during the 2019 Department of Homeland Security Centers of Excellence Summit Grand Challenge Student Competition.

Northeastern University Computer Engineering and Computer Science BS student Emily Belk was part of the winning team at the 2019 Department of Homeland Security Centers of Excellence Summit Grand Challenge Student Competition held on July 31 at George Mason University in Arlington, Virginia. The DHS COE Summit is an annual event held to showcase the innovative research being conducted by the COE community as they work with industry partners, government collaborators, and end users to develop R&D tools and solutions to respond to the evolving threats and challenges facing the nation. Emily works as an undergraduate researcher on the ALERT project known as Multi-Transmitter/Multi-Receiver Blade Beam Torus Reflector for Efficient Advanced Imaging Technology, led by ALERT deputy director, Professor Carey Rappaport. In addition, ALERT graduate student Annette Colón Mercado of the University of Puerto Rico at Mayagüez was a participant in the second place team through which she was able to integrate some of her research work with Dr. Samuel Hernandez on ALERT Project R3-C: Standoff Detection of Explosives: Infrared Spectroscopy Chemical Sensing.

Notre Dame graduate student, David Benirschke accepted the prized Intelligence Community (IC) Postdoctoral Research Fellowship. The Oak Ridge Institute for Science and Education oversees this fellowship, funded primarily by the Office of the Director of National Intelligence, to support Postdoctoral Fellows to conduct unclassified basic research in areas of interest to the IC, such as David's research in infrared-based explosive detection conducted while pursuing his PhD in electrical engineering at Notre Dame. David has been a key contributor on the ALERT Project R2-C.2: Multiplexed Mid-Infrared Imaging of Trace Explosives, led by ALERT researcher Dr. Scott Howard, an associate professor at Notre Dame. Through his participation, David worked with the project team to build upon prior ALERT research to create lower cost MIR technology for field use. With the aspiration of identifying explosive residue on objects in mind, David engineered many experimental prototypes, utilizing his deep theoretical knowledge in the area, eventually creating a spotlight on mid-infrared as well.

ALERT Department of Chemical Engineering graduate student Cara Coultas-Mckenney, of Purdue University, won first place at Purdue's Chemical Engineering 28th Annual Research Symposium poster competition, in the material science category, for her poster, "Characterizing Powder Behavior via the Enhanced Centrifuge Method" on August 15, 2019. Cara works as a student researcher on ALERT Project R2-A.3: A Novel Method for Evaluating the Adhesion of Explosive Residues under the direction of ALERT Research Thrust 2 leader, Dr. Stephen P. Beaudoin of Purdue University.

As Northeastern University associate professor of electrical and computer engineering and principal investigator for Project R2-B.3, Matteo Rinaldi is part of a research team that was awarded a $437K grant in

August of 2019 from the NSF for "fully integrated parametric filters for extensive phase-noise reduction in low-power RF front-ends and resonant sensing platforms."

In May 2020, Professor Matteo Rinaldi and research assistant Professor Zhenyun Qian of Northeastern University received two significant awards related to their research. They received a $550K NSF grant for their proposal, "Zero Power Wireless Flame Detector for Ubiquitous Fire Monitoring." This award was made through NSF's technology translation program, Partnerships for Innovation. The goal of the award is to develop a novel micromechanical flame detector which will consume near-zero power while in standby mode until triggered by the specific infrared signature emitted by a flame. Professors Rinaldi and Qian were also awarded a patent for a "zero power plasmonic microelectromechanical device." Drs. Rinaldi and Qian's research with ALERT focuses on understanding and exploiting the fundamental properties of micro/nanomechanical structures and advanced nanomaterials to engineer new classes of micro and nanoelectromechanical systems with unique and enabling features applied to the areas of chemical, physical, and biological sensing and low-power reconfigurable radio communication systems.

ALERT researcher and URI professor Dr. Jimmie Oxley was featured on CBS News discussing TSA projects aimed at improving the security screening process for travelers. The story detailed new technology being developed as part of ALERT research at URI, such as the desensitizing agent known as SCHMOO (Safe Control of Hazard Materials or Others Onsite) recently developed by Dr. Oxley's team. SCHMOO is a unique gel that can be applied to hazardous materials to neutralize them and allow for safe removal and transportation for later analysis.

Figure 1-2: ALERT researcher and URI professor, Dr. Jimmie Oxley.

Featured on ABC News, ALERT researcher and URI professor Otto Gregory was invited to speak about the "digital dog nose" being developed. Dr. Gregory described one benefit of the digital dog nose as being available around the clock, thereby not requiring breaks and reinforcement, which is otherwise necessary for the dogs. Dr. Gregory's related journal article titled, "Orthogonal Sensors for the Trace Detection of Explosives" appeared in *IEEE Sensors* in October 2019 and was the subject of a lead story in *IEEE Spectrum*.

B. ALERT Hosts 2019 Industrial Advisory Board Meeting and ADSA21

ALERT's annual IAB Meeting was held on November 4 at the Northeastern Innovation Campus in Burlington, Massachusetts. As the most attended IAB yet, the agenda included a keynote address from Len Polizzotto, partner at the Practice of Innovation, on maximizing the innovation process utilizing some interesting techniques to keep companies moving in the right direction. The presentation by ALERT researcher Professor Matteo Rinaldi on near-zero power sensors was extremely well received with DHS S&T requesting further information to initiate the next steps for potentially providing additional funding for the project.

IAB attendees also took an in-depth tour of the Northeastern Drone Test Facility and the ALERT Video Analytics Lab. The day concluded with a student poster session and networking reception. Thirteen students, both undergraduate and graduate, presented their current research projects while networking with industrial members. A video highlighting the students and their contributions can be found at http://www.northeastern.edu/alert/news-article/meet-the-alert-students/.

The topic of practicing and supporting innovation continued throughout the week on November 5–6 at ADSA21, which addressed the theme "Effective Integrated Systems for Aviation Security." During the two days of workshops, subject matter experts and leaders discussed defining and developing effective integrated systems including human operators, detection versus deterrence versus displacement, and the role of interconnectivity with open architectures, among others. In particular, attendees highlighted the Day One Q&A session, overall TSA presence and the introduction of machine learning to projects as their favorite moments during the two days of workshops.

C. ALERT Hosts Second Advanced Developments Encompassing Processes and Technologies for Customs and Border Protection (CBP-ADEPT-02) Workshop

The second workshop, Advanced Developments Encompassing Processes and Technologies for Customs and Border Protection (CBP-ADEPT-02), was held on July 17–18, 2019 at Northeastern University in Boston. This workshop brought together 130 attendees from government, industry, and academia to discuss topics related to current technology in improving port and cargo security. Presentations were given in the following areas of expertise: an adaptive adversary, integration of equipment and data, collection and use of metadata, deterrence/hardening, insider threats, con-ops, adaptation of TSA technologies, simulation tools, and war gaming applications.

D. ALERT Collaborates with CBP on Technology Demonstration at LA / Long Beach Seaport

On Thursday, November 21, 2019, the US Customs and Border Protection (CBP) Office of Field Operations at the Los Angeles / Long Beach Seaport headed by Chief Victor Todorov, hosted an all-day technology demonstration organized and led by ALERT industrial liaison officer Emel Bulat. The meeting was well-attended with six ALERT researchers and staff, seven industry representatives, six senior DHS personnel, and twenty-five CBP officers participating.

Figure 1-3: ALERT Industrial Liaison Officer, Ms. Emel Bulat, welcoming attendees at Long Beach Seaport in Los Angeles.

To kick off the meeting, Major General Robert Newman (retired), executive director for the Office of Mission and Capability Support at DHS S&T, gave welcoming remarks, along with Dr. Laura Parker, program manager at DHS S&T; Mr. David Taylor, portfolio manager at DHS S&T; and Mr. Edward Morones, assistant port director at CBP. In preparation for the event, four of ALERT's industry partners—including Pendar Technologies, Rapiscan Systems, Rigaku Analytical Equipment, and Smiths Detection—prepared live demonstrations of six instruments, including handheld Raman spectroscopy units as well as benchtop and handheld ion mobility spectrometry systems.

One week prior to the event, vendors were given a list of approximately forty compounds, mostly from a Drug Enforcement Agency list of precursors, to add to their instruments' lookup libraries for sample identification. Ten samples consisting of one to four compounds from the list were prepared for analysis and scanned. At the end of the meeting, six "live" shipments were scanned on the warehouse floor. The

enthusiasm with which the CBP officers and vendors prepared for and participated in the technology demonstration made this event a great success.

E. ALERT at the Second Annual DHS COE Summit

The 2019 Department of Homeland Security Centers of Excellence Summit was held on Wednesday, July 31 and Thursday, August 1 at George Mason University in Arlington, Virginia. The summit focused on the topic of homeland security challenges, "Evolving Threats and Dynamic Solutions." The ALERT management team collaborated with other COE leadership to coordinate the second year of this unique event. The 2019 summit involved stimulating panel discussions on homeland security topics, intriguing demonstrations of COE technologies, and focused engagement opportunities for students, industry, and DHS end users. The attendees included a broad range of participants including COE researchers and collaborators, members of industry, and several divisions of the US government. During the summit, interaction amongst these attendees helped create new connections, inspire ideas, and advance collaboration toward solving homeland security issues.

Director Michael Silevitch moderated a panel focused on physical soft targets and crowded places on the second day of the summit. The panelists included Larry Balding of Advanced Law Enforcement Rapid Response Training, Kevin Clement of University of Houston College of Technology, Carl Crawford of Csuptwo, Benji Hutchinson of NEC Corporation of America, and Neil Sandhoff of Evolv Technology.

Figure 1-4: ALERT Director Michael Silevitch moderating a panel during the DHS COE Summit in Arlington, Virginia.

Outside the Innovation Showcase area, ALERT students Mohammad Nemati of Northeastern University and Annette Colón Mercado of the University of Puerto Rico at Mayagüez (UPRM) were on hand to represent ALERT's research in Thrust R3 related to bulk sensors and sensor systems as part of the summit's COE Student Poster Display and Competition.

DHS COEs take pride in their students' contributions and efforts. To foster student innovation, student participants were encouraged to take part in the summit's Grand Challenge competition. Leading up to and culminating at the summit, talented undergraduate and graduate students from each of the COEs collaborated on solutions to address emerging homeland security concerns. ALERT students Emily Belk of Northeastern University and Annette Colón Mercado of UPRM both participated in this challenge, and both were recognized for their efforts.

This page intentionally left blank.

Section 2: Research and Transition Program: A Strategic Overview

The ALERT research and transition program is derived from a top-down understanding of the technical and societal issues related to characterizing, detecting, and mitigating explosives-related threats to our homeland. These issues have been crystallized by considering a set of "Grand Challenges," which in turn, inform and drive the ALERT programs through an organizing three-level strategy, as shown in Figure 2-1. In the following sections, we will describe how the research and transition program was defined and provide an overview of the specific programs. Detailed project reports are provided in Appendix A.

2.1 RATIONALE

The ALERT strategy is focused on advancing cutting-edge basic and applied research, buttressed by experienced management, enhanced by education and workforce development programs, and linked to stakeholders and stakeholder needs within the homeland security rnterprise (HSE). This detailed and flexible strategy allows ALERT to nimbly adapt to new Department of Homeland Security (DHS) priorities and needs. The Grand Challenges for the overarching ALERT research and transition programs are based on the goals described in the Aviation Security Technology Research and Development Strategy, issued by DHS in 2011:

- Transportation Security Administration (TSA) G1: Improve understanding of homemade explosives (HME) threats and address HME threat vulnerabilities.
- TSA G2: Reduce passenger privacy concerns in aviation security through increased integration and automation of security screening processes.
- TSA G3: Develop enhanced technologies and capabilities to enable risk-based screening processes.
- TSA G4: Increase capability to respond to emerging threats through flexible security solutions.
- TSA G5: Apply science and technology breakthroughs to advance security solutions.

Additionally, there are ten capability gaps which were first described in the December 2017 TSA Strategic Technology Investment Plan (TSA CG1–CG10). These capability gaps are listed below. With the exceptions of CG 4 and 9, all capability gaps are incorporated into the ALERT program.

- TSA CG1: Enhance the ability to resolve alarms.
- TSA CG2: Enhance operators' ability to screen passenger carry-ons and checked baggage.
- TSA CG3: Support risk-based screening throughput goals.
- TSA CG4: Enhance the ability to verify a passenger's identification and determine vetting status.
- TSA CG5: Minimize physical contact with passengers.
- TSA CG6: Reduce divestiture screening requirements.
- TSA CG7: Enhance the ability to identify and screen a passenger and his/her baggage based on an assigned risk level.
- TSA CG8: Enhance the ability to integrate systems to support risk-based screening to support more efficient security screening.
- TSA CG9: Support remote access and data collection from Transportation Security Equipment (TSE) by strengthening the TSE cybersecurity infrastructure.

- TSA CG10: Enhance the ability to adjust security posture based on risk.

2.2 THE THREE-LEVEL ALERT STRATEGY: GRAND CHALLENGES

The ALERT research and transition program is described by the three-level strategy, shown in Figure 2-1, that ties real-world Grand Challenges to fundamental research and technology transition, keeping them synchronized but able to adapt as societal and DHS needs change. The three-level structure is not static; spiral development occurs as the plan evolves.

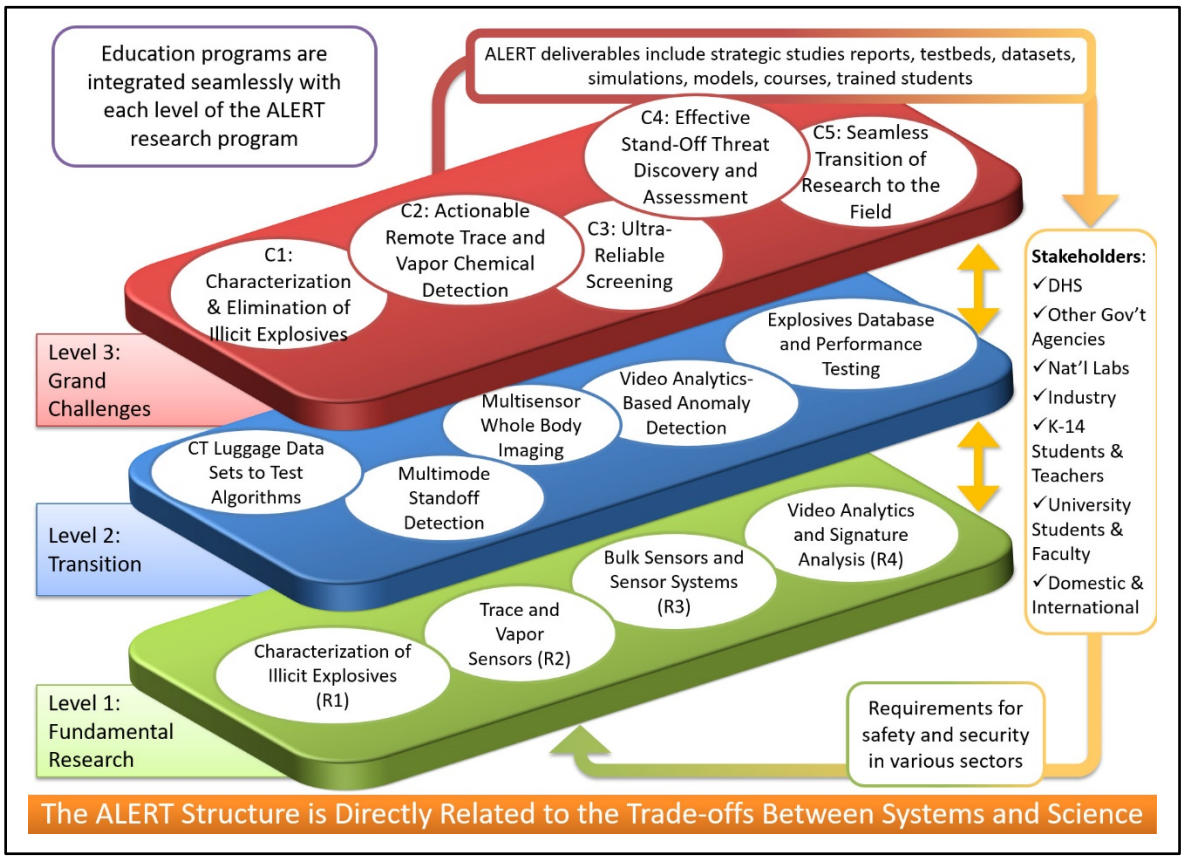

Figure 2-1: The ALERT three-level strategy focuses resources on achieving protection from explosive threats.

The Grand Challenges level (the top level, in red) contains the challenges C1–C5 that must be addressed in order to achieve a high level of protection from explosives-related threats. The Grand Challenges inform and drive the ALERT research and transition/E2E program, as shown in Figure 2-1. Each Grand Challenge has specific goals, which are correlated with the TSA recommendations and capability gaps described earlier. The Challenges and associated goals are as follows.

C1: Characterization & Elimination of Illicit Explosives (TSA G1, 3 and TSA CG1, 5–6)

- Identify future explosives threats and develop small-scale "early warning" tests.
- Prevent commonly available chemicals from being used to make explosives.
- Characterize explosive formulas to facilitate detection, destruction, and protection.

- Safely and gently render an explosive inactive or less sensitive.

C2: Actionable Remote Trace and Vapor Chemical Detection (TSA G3–5 and TSA CG2–3, 8)

- Create versatile, specific sensors to detect emerging homemade explosives.
- Create fieldable sampling processes to enable detection.
- Detect threats in large crowds (e.g., sports events, subways, and nightclubs).
- Noninvasively identify trace explosives on or within cargo containers in transit.
- Develop miniaturized detection sensors suitable for fusion into larger systems.

C3: Ultrareliable Screening (TSA G2–3, 5 and TSA CG1–3, 5–8, 10)

- Integrate multi-mode sensors to enhance threat identification.
- Improve the speed and performance of computed-tomography–based luggage screening.
- Improve the speed, accuracy, and threat coverage of whole body imaging (i.e., advanced imaging technology) systems for passenger screening.
- Integrate new screening concepts and algorithms into vendor systems.

C4: Effective Standoff Threat Discovery and Assessment (TSA G2–3, 5 and TSA CG1, 5, 8, 10)

- Reliably pinpoint trace explosives on packages or vehicles left behind.
- Recognize potential suicide bombers through anomaly detection.
- Identify and track anomalous behavior in mass transit environments.
- Develop video analytics tools to be integrated into TSA airport camera systems.

C5: Seamless Transition of Research to the Field (TSA G5 and TSA CG7–8, 10)

- Actively identify DHS stakeholder emerging needs to ensure research relevance.
- Define transition plans for mature research results and prototypes.
- Transfer and support emerging technologies and tools to DHS stakeholders.

2.3 THE THREE-LEVEL ALERT STRATEGY: FUNDAMENTAL RESEARCH

The program at the Fundamental Research level in Figure 2-1 (the bottom level, in green) is the result of an analysis to determine the barriers that must be overcome in order to address the Grand Challenges C1–C4. This program is divided into four interrelated research thrusts (R1–R4): Characterization & Elimination of Illicit Explosives (R1), Trace and Vapor Sensors (R2), Bulk Sensors and Sensor Systems (R3), and Video Analytics and Signature Analysis (R4). A brief overview of each follows, and details are provided in Appendix A.

R1: Characterization & Elimination of Illicit Explosives

- Thrust Lead: Jimmie Oxley, University of Rhode Island (URI)
- Key Personnel: Jim Smith (URI), Steve Son (Purdue University), Joel Greenberg (Duke University)

Detection of explosives requires knowledge of the signature characteristics of various threat materials and seeks to answer the following questions: What makes a chemical capable of being explosive or detonating? Can we prevent terrorist acquisition and/or use of precursor chemicals to make explosives? Are there characteristics of terrorist-used explosives that exhibit observable signatures by current or envisioned sensor systems? Can we concentrate sample collection to enhance our ability to detect these signatures? What properties of terrorist-used explosives pertain to safe handling and creation of realistic simulants? Activities in this thrust include (1) characterization of signatures and properties of a variety of potential threat materials; (2) design of protocols for safe handling and disposal of these threats, including ways to prevent common chemicals from being used to make illicit explosives while still allowing their intended uses; and (3) determination of surface-explosive particle interaction in order to best locate and collect explosive residue.

R2: Trace and Vapor Sensors

- Thrust Lead: Steve Beaudoin (Purdue University)
- Key Personnel: Otto Gregory (URI), Scott Howard, Anthony Hoffman (Notre Dame), Matteo Rinaldi (Northeastern University)

This thrust concentrates on understanding the fundamental problems of trace and vapor detection of explosives. The goal of this effort is to enable development of sensing and sampling systems capable of detecting ultralow amounts of explosives, systems that are both selective (i.e., able to reduce the number of false positives and false negatives) and adaptable (i.e., can accommodate new explosives as they become threats). This effort requires fundamental material research for next-generation sensors, such as development of hybrid quantum dot/polymer array structures. The sensor concepts developed here can be integrated into multi-sensor systems, as discussed in Thrusts R3 and R4.

R3: Bulk Sensors and Sensor Systems

- Thrust Lead: Carey Rappaport (Northeastern University)
- Key Personnel: Jose Martinez-Lorenzo (Northeastern University), Samuel Hernandez (University of Puerto Rico at Mayagüez)

This thrust is focused on designing and implementing novel bulk sensors and multi-sensor detection systems, including the optimization of mm-wave–based sensing of anomalies under clothing to detect explosives on and within the human body. Both portal and standoff systems were considered and used as the basis for the development and evaluation of multi-modal sensors and algorithms for advanced imaging technologies (AIT), enabling experimentation, model-based reconstruction, and automatic threat detection of explosives. Improved algorithms for existing bulk sensor systems and multi-modal fusion systems will be investigated in Thrust R4.

R4: Video Analytics and Signature Analysis

- Thrust Lead: David Castañón (Boston University)
- Key Personnel: Octavia Camps, Mario Sznaier (Northeastern University), Clem Karl (Boston University), Charles Bouman (Purdue University), Rich Radke (Rensselaer Polytechnic Institute), Eric Miller (Tufts University), Henry Medeiros (Marquette University)

This thrust focuses on multi-camera video anomaly detection in scenarios relevant to passengers, divested object tracking, and area monitoring in public spaces; signature analysis work based on developing fundamental processing algorithms for trace; and bulk and multi-sensor systems extracting maximal information from available sensed signals to increase the probability of detection and classification of

explosives while reducing the number of false alarms. The research also includes improved model-based iterative reconstruction for single- and dual-energy X-ray computed tomography (CT), exploitation of new signatures such as multi-spectral CT and X-ray diffraction, threat detection in our novel trace sensors in Thrust R2, and algorithms for sensor fusion in AIT and standoff threat detection.

2.4 THE THREE LEVEL ALERT STRATEGY: TECHNOLOGY TRANSITION

The Transition level, shown in Figure 2-1 (the middle level, in blue), is needed to address Grand Challenge C5. This contains the testbeds, tools, and facilities needed to validate fundamental research results and enable these research breakthroughs to actively address Grand Challenges C1–C4 through technology transition projects that benefit DHS and HSE stakeholders. Implementation of this level depends on close collaboration between academic researchers, national laboratories, industry, and DHS, with the goal to accelerate transition from bench to field. Five testbeds are currently identified to test basic research results.

- Testbed T1: Computed Tomography Luggage Datasets to Test Algorithms
- Testbed T2: Multimode Standoff Detection
- Testbed T3: Advanced Imaging Technologies (Whole Body Imaging)
- Testbed T4: Video Analytics–Based Anomaly Detection
- Testbed T5: Explosives Database and Performance Testing

Initial versions of these testbeds were developed during the first five years of ALERT (Phase 1) and are continuing to evolve during the current phase of ALERT (Phase 2). A brief overview of these testbeds follows.

Testbed T1: CT Luggage Datasets to Test Algorithms

T1 leverages the ongoing effort of ALERT to develop advanced luggage screening algorithms via calibrated X-ray CT datasets. Through task-order funding, ALERT leveraged the advances made within medical CT and contracted with a vendor to obtain representative datasets of packed luggage and reference objects. Approximately 900 objects were used to form 62 luggage datasets, which spanned the spectrum of packing, density, arrangement, orientation, and size. The data was intended to provide security-like images to academic researchers, to be used in evaluating, improving, and refining state-of-the-art techniques while fostering deeper communication within the segmentation reconstruction and recognition algorithm community. More details on this effort are given in Section 2.5.

Figure 2-2: (left) Segmented image of (center) doll extracted from (right) CT image dataset of luggage.

Testbed T2: Multimode Standoff Detection

There are two indicators for most suicide bombers: the metal for shrapnel and the explosive itself. Using signatures of these indicators, the Multimode Standoff Detection testbed is envisioned as leading to a product in which multiple detection technologies are integrated into surveillance platforms for suicide bomber detection. Possible "bombers" will be identified and continuously tracked at distances up to 50 meters, as shown in Figure 2-3. More details are given in the reports in the R3-B section of Appendix A.

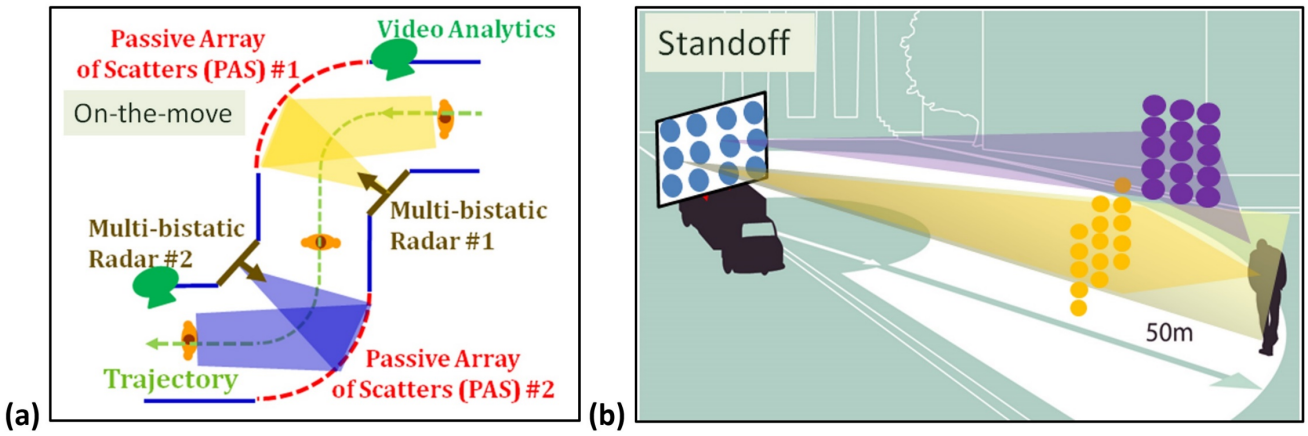

Figure 2-3: General sketch of the inexpensive system being developed for the use of detecting security threats: at (a) mid-ranges using an on-the-move configuration; and (b) standoff-ranges using a van-based configuration.

Testbed T3: Advanced Imaging Technologies (Whole Body Imaging)

The objective of the AIT testbed is the creation of an unbiased, academic-oriented facility for development and evaluation of millimeter-wave (mm-wave) sensors and algorithms for whole body imaging. Specific objectives include (1) enabling experimentation with new sensing modalities, via sensor configuration and scanning mode optimization; (2) exploring new algorithm concepts, such as model-based versus Fourier inversion, high-resolution fused imaging, and automated anomaly detection; (3) providing experimental validation of multistatic radar imaging; and (4) characterizing the dielectric constant of concealed body-worn foreign objects to rule out those that are benign. The facility development is led by R3 Thrust lead, Carey Rappaport. It is being advanced with equipment provided by Rapiscan, Smiths Detection, and Analog Devices. Rapiscan provided equipment as part of a John Adams Innovation Institute grant to use mm-wave sensing to reconstruct an object placed between the transmitters' and receivers' wave path. Analog devices supplied RF communications modules that have been adapted for radar use in our experimental scanners. It has been shown both theoretically and experimentally that by choosing the right positions for transmitters and receivers in a multistatic system, it is possible to reconstruct 2D and 3D images that cover all 360 degrees of the target with minimal dihedral artifacts that plague currently deployed scanning systems. The algorithms and datasets generated

Figure 2-4: Professor Carey Rappaport and ALERT student researchers answer the questions of TSA Administrator David Pekoske during his visit to the Advanced Imaging Technology Laboratory at Northeastern University in May 2018.

are anticipated to be of great value to TSA in the analysis of enhancements to the state-of-the-art. More details are given in the reports in the R3-A and R3-B sections of Appendix A.

Testbed T4: Video Analytics–Based Anomaly Detection

ALERT's video analytics effort addresses the needs of the TSA to increase the speed of screening, improve the passenger experience, and monitor and mitigate threats by individuals in an effort to improve airport security. Testbed T4 began as an installation in the Cleveland Hopkins International Airport (CLE), and in Year 4 it transitioned to a 1,225 square-foot Video Analytics Laboratory at Northeastern University's George J. Kostas Research Institute for Homeland Security (KRI) in Burlington, MA.

T4's first installation at CLE was a result of ALERT and the TSA Ohio senior federal security director working together to assemble a team of researchers from three universities (Northeastern University, Boston University, and Rensselaer Polytechnic Institute), Siemens Corporate Research, and TSA practitioners to develop and transition video analytics–based solutions to address two security issues: first, to identify when an airport exit lane is breached ("in-the-exit"), and second, to identify and track individuals moving through a camera system. The in-the-exit solution, identified as the "Video Analytic Surveillance Transition Project" (VAST), resulted in a proof of principle system installed in the TSA command center. The system leveraged live video from a portion of the existing CLE video network without interfering with airport operations and obtained 99.9% probability of detection and <10 false alarms per week.

As a result of ALERT's successes at CLE as well as other video analytics–based work, the center has partnered with the DHS "Screening at Speed" program manager. This partnership allowed ALERT not only to acquire the funding to construct the latest T4 facility at KRI but also to establish a significant research program titled, "Research and Development of Systems for Tracking Passengers and Divested Items at the Checkpoint", also referred to as CLASP (Correlating Luggage and Specific Passengers). The objective of CLASP is to track people and their associated items within a TSA airport security checkpoint, with a focus on improving screening speed, the passenger experience, and security at the checkpoint.

The current T4 lab installation, as seen in Figure 2.5, includes a full-scale mock airport security checkpoint using TSA-approved equipment and design guidelines, screening equipment donated by ALERT industrial members Smiths and Rapiscan, and a camera grid of twenty networked 1080p CCTV cameras. To date, the testbed has been leveraged to hold seven data collection events involving students, actors, TSO trainers, and a service dog to produce twenty-one video datasets. These datasets contain scripted scenarios of actions relevant to the TSA and serve to allow the research team to better hone algorithms developed for the CLASP program.

Figure 2-5: ALERT's Video Analytics Laboratory provides a space to collect non-SSI data for the Center's CLASP project, which supports the DHS S&T "Screening at Speed" initiative tasked with improving throughput, security, and passenger experience at airport checkpoints.

Strong progress made in the first phase of CLASP resulted in additional funds being allocated to the program in the form of a Basic Ordering Agreement Task Order (this funding vehicle is further described in Section 2.5) to enhance the effort. With a team from Boston University, Northeastern University, Rensselaer Polytechnic Institute, and Marquette University, the CLASP Task Order's objectives are to (1) refine the algorithms developed in phase one to manage more complex scenarios, such as person-to-person transfer, a higher density of people, and variations in lighting and occlusion; (2) investigate the

requirements for a real-time implementation; (3) acquire and process video data from actual airport security checkpoints; and (4) demonstrate an integrated, real-time system at KRI. The program is currently in partnership with Dulles International Airport (IAD), Logan International Airport (BOS), Portsmouth International Airport at Pease (PSM), Seattle-Tacoma International Airport (SEATAC), and T. F. Green Airport (PVD), thanks to the support of former Logan federal security director and MassPort CIO, Rear Admiral George N. Naccara (retired).

Testbed T5: Explosives Database and Performance Testing

In 2011, URI set aside several hundred acres for an explosive testing range and a standoff detection range. Each range has storage for one hundred pounds of explosives and is licensed to manufacture and store explosives. While funding of this project has not come through the Center of Excellence (COE) but rather the US Army, these facilities are outstanding assets to the Center. Vendors come to test their explosives detection instrumentation, and bomb squads from both Massachusetts and Rhode Island have used the testing range to prepare training aids (Figure 2-6). This is a premier site for first-responder training, both "hands-on" and in the classroom.

Figure 2-6: Standoff detection test at URI field range.

URI has also maintained a database of explosive properties for the last eleven years. This extensive database contains physical properties (e.g., infrared, Raman, mass, and NMR spectra) and was intended to serve forensic labs; however, the URI database has been a much more extensively utilized resource. Over a thousand registered members are a testament to its usefulness to diversify HSE stakeholders from the United States and twenty-six other countries.

2.5 BASIC ORDERING AGREEMENT TASK ORDERS

In 2009, ALERT was awarded a Basic Ordering Agreement (BOA), HSQDC-10-D-00030, that allowed the DHS components to establish specific task orders for homeland-security–related research, analysis, and services aligned with the unique expertise, facilities, experience, and thrust area of focus of the respective university-based COE. The BOA and the associated task orders became a means for ALERT to enhance its research and transitions programs by:

1. Creating groups of third party researchers in X-ray CT explosives detection, similar to the community of researchers in medical CT.
2. Improving the performance of future explosives detection systems, which includes increased probability of detection and decreased probability of false alarm for a larger set of objects and reduced minimum masses.
3. Creating a technical interchange near the end of each task order so researchers could present their results to the security industry vendors, DHS, and other third parties to transfer the science and technology they created during the task order into the security enterprise.

To date, the following thirteen major task orders have been awarded under the BOA.

A. Segmentation of Objects from Volumetric CT Data [COMPLETED]

This was a program to stimulate the development of advanced segmentation algorithms from volumetric CT data. The results from this and the next task order enabled the development of Testbed T1. This program ended during ALERT Phase 1.

B. Research and Development of Reconstruction Advances in CT-Based Object Detection Systems [COMPLETED]

This was a program to improve the image quality of CT-based object detection equipment using advanced reconstruction algorithms to reduce artifacts. As indicated above, Testbed T1 was a byproduct of this and the previous task order. This program ended during ALERT Phase 1.

C. Advances in Automatic Target Recognition for CT-Based Object Detection Systems [COMPLETED]

This program was initiated in ALERT Phase 1 and continued in Phase 2. It addressed improving automatic target recognition (ATR) capabilities and made use of the improvements in segmentation and reconstruction algorithms that were developed in the core research program and via the results obtained in A and B above. In that vein, the program was designed to improve the performance of the complete algorithmic system (e.g., reconstruction, segmentation, and object recognition). The validation of the ATR algorithms was aided by the datasets in Testbed T1.

D. Development and Transition of a Video Analytics System for Tracking Tagged Suspects in Airports (VAST) [COMPLETED]

This program focused on video analytics and was initiated in ALERT Phase 1 and continued in Phase 2. This research effort was an integral part of the transition and E2E strategy for ALERT. It enabled the development of the first iteration of Testbed T4 (described in Section 2.4).

E. Improved Millimeter-Wave Radar AIT Characterization of Concealed Low-Contrast Body-Bourne Threats [COMPLETED]

This program focused on enhancing mm-wave personnel screening systems using a single frequency, rapidly scanned flying focal spot to enable materials discrimination. The results were incorporated into Testbed T3.

F. Research and Development of Adaptive ATR for CT-Based Object Detection Systems [COMPLETED]

This program focused on the development of adaptive ATR (AATR) algorithms that can be configured in the field to add new targets after deployment without having to retrain and retest the ATR. In addition, an AATR algorithm has the ability in the field to add or subtract targets, vary minimum target mass, vary minimum sheet thickness, and trade off probability of detection (PD) for probability of false alarm (PFA) or PFA for PD. As a result of this project, the researchers within this group developed AATR algorithms and presented these algorithms to experts in the field at a recent program review for the AATR project (May 17, 2018). The applicability of the AATR algorithms to certified explosives detection equipment and the steps needed for continuing research in this area were also discussed. Presentations and summaries from the most recent program review are available at http://www.northeastern.edu/alert/task-order-07/.

G. Standardization of Procedures and Methodology to Measure Trace Explosives Sampling Efficiency and Baseline Performance [COMPLETED]

This development and transition effort addressed the need for a set of reference materials for dry sampling of explosives and an associated procedure for each step of the sampling process.

H. Maturation and Validation of Dielectric Characterization Algorithms

Built upon advanced mm-wave research, this program is tasked to develop and deploy AIT material characterization algorithms to minimize false alarms and the need for physical pat-downs at the airport

security checkpoint. The team has been investigating new approaches to processing data generated by AIT systems data to determine the dielectric constant and thickness of foreign objects attached to persons. Current AIT systems provide sufficient information about the scattering to generate the overall shape of a foreign dielectric object, but with appropriate processing they could also calculate its thickness and dielectric constant. This allows ruling out benign objects, such as paper cash or medical items, but alerts when the dielectric constant is consistent with a threat material, thereby requiring additional investigation by security personnel.

ALERT's algorithms have shown sufficient progress in the initial phase of the project that DHS Science and Technology Directorate (DHS S&T) has allocated an additional $600,000 to supplement the original $600,000 award allowing the group to further refine the algorithms and develop a software-based tool to be incorporated with existing fielded AIT systems.

I. Correlation of Luggage and Specific Passengers (CLASP) Algorithm Maturation and Deployment

This program is tasked with developing automated tracking algorithms (ATAs) to track passengers and divested objects at the checkpoint. The ATAs are being designed to detect exceptions such as divested items left behind at the checkpoint and the theft of items. The CLASP project's Testbed T4 facility at KRI supports this effort by providing video datasets to be used in this task.

Initial funding was allocated as a supplement to the core grant, not via the BOA. Follow-on funding for Phase 2 of this program is utilizing both the cooperative agreement and the BOA mechanism. This program is described in more detail in section 2.4.

J. Research and Development of Tools for the Simulation of Palletized Air Cargo Skids

The purpose of this task order is to develop a capability to provide the mathematical description of simulated air cargo. The air cargo shall be packed on skids. The mathematical descriptions, when used in conjunction with extant x-ray simulation tools, lead to simulated projections of air cargo contents. The deliverable for this project is a software tool that can be used by DHS S&T and TSL to augment the detection capabilities of current inspection systems to detect anomalies. A demonstration at TSL is planned for the Fall of 2020.

K. Comprehensive Database of Contact Explosives Sampling Efficiency and Baseline Performance

This task order is an extension of work performed under the earlier task order that resulted in the creation of a standardized method and common language to measure sampling efficiency related to explosives trace detection devices (ETDs) resulting in a set of reference materials, procedures to use the reference materials, and a limited database of contact sampling. This current task order seeks to establish a more thorough database of contact sampling by extending the number and type of sample traps and type of explosives. Emphases are placed on commercial off-the-shelf traps and reagent-enhanced traps.

L. Novel Features and Emerging Technologies for Opioid Detection

This task order was initiated in 2019 and is an effort to support the opioid detection prize competition launched by the DHS S&T. The main task is identifying new signatures and predicting optimum detection performance for opioids entering the country through international mail. The outcome of this work will provide DHS with the capability to decide which new technologies to develop into prototypes to demonstrate effective detection capability.

M. Enhanced Trace Explosives Detection, an Ambient Desorption Ionization Retrofitted ETD Solution and a Continuous Automatic Non-Contact Sampler Based on Remote Heating

This task order was initiated in August 2020. Its focus is threefold: (1) a contactless sampler based on remote heating and integrated with a mass spectrometer for explosive detection and confirmation; (2) an ambient desorption ionization (ADI) module retrofitted into a currently deployed Smiths Detection IONSCAN 600 (ADI-IS600) for inorganic and homemade explosives trace detection; and (3) a scenario-based feasibility study on explosive vapor detection.

In conclusion, it is anticipated that several of these task orders will advance into future phases, resulting in deployment in fieldable systems. Specific examples are Task Orders G, H and J.

2.6 ENSURING PROGRAMMATIC RELEVANCE

The ALERT leadership is acutely aware of the need to demonstrate the relevance of its programs to the HSE stakeholders. Mechanisms that have been actively used for ensuring relevance include:

- Alignment with DHS S&T programs (Office of University Programs and Homeland Security Advanced Research Projects Agency Explosives Division).
- Collaborations with researchers at National Labs (Lawrence Livermore National Laboratory, Los Alamos National Laboratory, Sandia National Laboratory, Pacific Northwest National Laboratory).
- Collaborations with critical DHS components (TSA, Transportation Science and Logistics, Customs and Border Protection).
- Collaborations with DHS vendors (AS&E, Analogic, L3, Morpho, Smiths, Siemens).
- Linkage with a broad national and international R&D community to identify strategic research issues (Advanced Development for Security Applications workshops, Trace Explosives Sampling for Security Applications workshops).
- Connection with other DHS COEs (ADAC, CINA, CREATE, VACCINE).
- Internal review of projects emphasizing relevance and potential transition (video analytics tag and track systems, enhancements for CT baggage and cargo systems, next-generation whole body passenger screening system development, cell phone networked instruments for trace explosives detection, and signatures for opioid detection in international mail).

2.7 CONCLUSION

As indicated by its strategic three-level structure, ALERT has maintained a balance of high-risk, high-payoff research combined with transition projects meeting immediate DHS and customer needs. As of May 2021, ALERT ends its funding under the OUP Cooperative Agreement and moves toward BOA Task Order support. This will result in the pragmatic transition of ALERT developed technologies that DHS will be able to incorporate into requirements for future systems to help safeguard our nation.

This page intentionally left blank.

Section 3: Education Program

It is widely recognized that our country still needs to put more emphasis on providing a workforce pipeline into the science, technology, engineering, and mathematics (STEM) disciplines. The development of the ALERT Education Program was guided by the need to provide a meaningful impact on the communities of university students, K–14 students and their teachers, first responders, and career professionals who are important contributors to the Department of Homeland Security (DHS) and to the success of its critical mission. In addition to developing the next generation of fundamental research advances, the ALERT team of educational institutions addresses the strong and continuing need for personnel trained in homeland-security–related technologies. This section describes the elements of the ALERT Education Program and the results of the Year 7 initiatives.

As shown in Figure 3-1, the ALERT Education Program initiatives have focused on the following areas:

- University graduate and undergraduate programs;
- Professional development programs and short courses for DHS professionals and first responders; and
- Community college, pre-college, and minority-serving institution outreach and involvement.

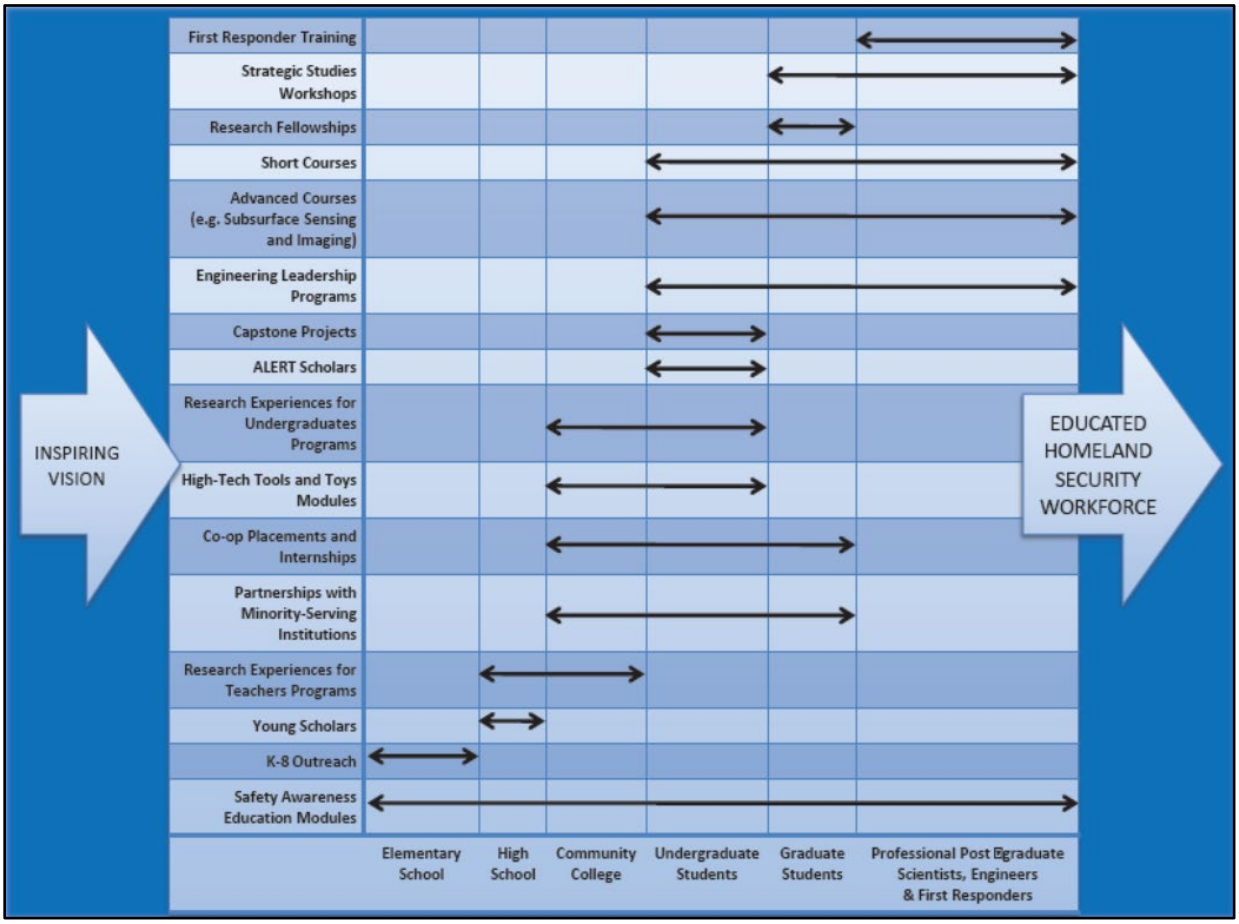

Figure 3-1: The ALERT education program supports students at every stage.

The ALERT Education Program has been co-led by Professor Charles DiMarzio of Northeastern University (NU) and Professor James Smith of the University of Rhode Island (URI) with support from Kristin Hicks, director of operations at NU. The main goals of the ALERT Education Program have included introducing new students to ALERT research at an early stage in their career through outreach to K–12 schools, community colleges, and freshmen undergraduates; enhancing the professional development opportunities of our undergraduate and graduate students; and providing courses and workshops to the DHS workforce to build on their foundational training and expertise. By engaging K–12, community college, undergraduate, graduate, and professional students in our research, we were able to build a broad awareness of the ALERT and DHS mission and prepare a new workforce for careers within the homeland security enterprise.

While the following sections of this report (Sections 3.1 through 3.5) provide a description of the major components of the ALERT Education Program, this section summarizes some of the special accomplishments realized by our talented student pool.

NU Computer Engineering and Computer Science BS student Emily Belk was part of the winning team at the 2019 Department of Homeland Security Centers of Excellence (COE) Summit Grand Challenge Student Competition held on July 31 at George Mason University in Arlington, Virginia. The DHS COE Summit is an annual event held to showcase the innovative research being conducted by the COE community as they work with industry partners, government collaborators, and end users to develop R&D tools and solutions to respond to the evolving threats and challenges facing the nation. Emily worked as an undergraduate researcher on the ALERT project Multi-Transmitter/Multi-Receiver Blade Beam Torus Reflector for Efficient Advanced Imaging Technology, led by ALERT deputy director Professor Carey Rappaport. In addition, ALERT graduate student Annette Colón Mercado of the University of Puerto Rico at Mayagüez (UPRM) was a participant in the second-place team through which she was able to integrate some of her research work with Dr. Samuel Hernandez on ALERT Project R3-C, Standoff Detection of Explosives: Infrared Spectroscopy Chemical Sensing.

Notre Dame graduate student David Benirschke accepted the prized Intelligence Community (IC) Postdoctoral Research Fellowship. The Oak Ridge Institute for Science and Education oversees this fellowship, funded primarily by the Office of the Director of National Intelligence, to support Postdoctoral Fellows to conduct unclassified basic research in areas of interest to the IC, such as David's research in infrared-based explosive detection conducted while pursuing his PhD in electrical engineering at Notre Dame. David has been a key contributor on the ALERT Project R2-C.2: Multiplexed Mid-Infrared Imaging of Trace Explosives, led by ALERT researcher Dr. Scott Howard, an associate professor at Notre Dame. Through his participation, David worked with the project team to build on prior ALERT research to create lower cost MIR technology for field use. With the aspiration of identifying explosive residue on objects in mind, David engineered many experimental prototypes, utilizing his deep theoretical knowledge in the area, eventually creating a spotlight on mid-infrared as well.

Figure 3-2: ALERT Notre Dame PhD graduate David Benirschke received the prestigious Intelligence Community Postdoctoral Research Fellowship in the summer of 2019.

ALERT Department of Chemical Engineering graduate student Cara Stevenson, of Purdue University, won first place at Purdue's Chemical Engineering 28th Annual Research Symposium poster competition, in the material science category, for her poster, "Characterizing Powder Behavior via the Enhanced Centrifuge Method" on August 15, 2019. Cara worked as a student researcher on ALERT Project R2-A.3: A Novel Method for Evaluating the Adhesion of Explosive Residues, under the direction of ALERT Research Thrust 2 leader, Dr. Stephen P. Beaudoin of Purdue University.

Over the years, many of our ALERT graduate students have gone on to work in the homeland security enterprise and other prestigious locations for both internships and full-time positions including:

- Owen Dominguez, a 2020 Notre Dame PhD graduate, is now working with the Detonation Science and Technology group at Los Alamos National Laboratory.
- Bianca López-Pagán, a 2019 UPRM BS graduate, is now working at the Naval Surface Warfare Center, Indian Head Explosives Ordnance Disposal Technology Division.
- Gabriela Padilla Rivera, a 2020 UPRM MS graduate, is working at the US Army Construction Engineering Research Laboratory.
- Can Uner, a 2020 NU MS graduate, is working at Tytovision, Inc.
- Meng Zheng, a 2020 Rensselaer Polytechnic Institute (RPI) PhD graduate, is now working with other ALERT RPI alumni, Srikrishna Karanam and Ziyan Wu, at United Imaging Healthcare Co., Ltd.

3.1 GRADUATE PROGRAMS

Graduate Programs Overview

Each of the universities involved in ALERT have doctoral-level and master's-level graduate programs that train the students who will be the professors and research leaders of tomorrow. Within the ALERT program, these students completed theses on topics related to homeland security problems. Research areas require background coursework and seminars, as well as mentoring from faculty, researchers, and industry personnel. In Year 7, ALERT universities supported forty-four PhD and fourteen MS students with thesis topics such as:

- "Realization of a Commercially Available, Low-Cost, Spectroscopic, Mid-Infrared Imaging Platform for Enabling Applications and Thermal Time-Harmonic Imaging "
- "Mathematical Models for Dielectrics on the Human Body Using Millimeter-Wave Security Scanners"
- "Automatic Characterization of Low-Loss Low-Permittivity Body-Born Threats Using Wideband Millimeter-Wave Radar"

ALERT graduate students are encouraged to become involved in many Center-related events to build on their research work and enhance their knowledge of homeland security topics. For example, ALERT graduate students are invited to attend the ADSA workshops, and ADSA21 was held in November 2019 for Year 7. The ADSA planned for May 2020, as well as the ADEPT-03 (Customs and Border Protection) workshop planned for July 2020 were both postponed due to COVID-19. The ADSA21 workshop allowed students to participate in the cross-disciplinary discussion of homeland security topics with representatives from academia, government, and industry. ALERT has also coordinated a professional development event, ASPIRE (Annual Student Pipeline Industry Roundtable Event), specifically aimed at connecting students with ALERT partner industries. ASPIRE gives students the opportunity to meet with industry and government members looking to recruit for internships and full-time positions. ASPIRE's unique format covers a broad range of topics, and provides students and industry members with meaningful and effective networking opportunities. Unfortunately, due to COVID-19 shutdowns, ASPIRE was not held in 2020.

ALERT students are key participants in the ALERT Industrial Advisory Board Meetings, and thirteen students attended the Year 7 event held on November 4, 2019 at the Northeastern Innovation Campus in Burlington, Massachusetts. In addition to attending the presentations from industry and academia, the students presented their research at a networking poster session, which concluded the event on a high note.

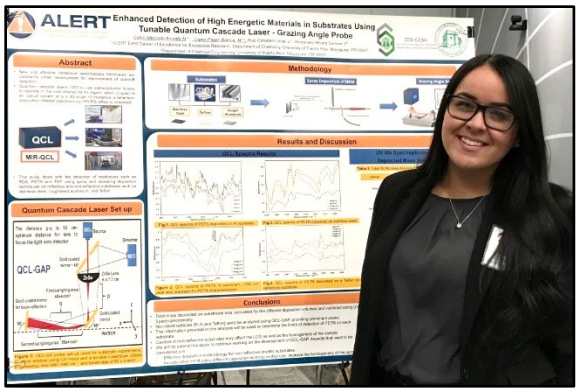

Figure 3-3: ALERT graduate student Annette Colón Mercado from UPRM presents at the 2019 Industrial Advisory Board Meeting.

Engineering Leadership in DHS Technologies

Since the fall of 2007, NU has offered a graduate program in engineering leadership that allows academically talented graduate students to pursue a graduate certificate in engineering leadership, as well as an MS degree in the engineering discipline of their choice. The Gordon Institute of Engineering Leadership (GIEL) Program was established as a result of a generous gift from the Bernard M. Gordon Foundation. The program began its thirteenth year in September 2019 with a class of Gordon Fellows, mainly from industry and government, who are educated and mentored by faculty and senior industry leaders. A key element of this program is the year-long Challenge Project that each Gordon Fellow undertakes with the goal of developing and deploying a system or commercializing an innovative product. Under the tutelage of Gordon Program mentors, the Fellows learn how to achieve technological impact firsthand.

The GIEL Program provides a valuable resource, helping sponsors working on DHS technologies to develop their engineers into more effective leaders who are experts in homeland security technologies and adept at transitioning research; and the development of concepts into deployable systems. In the program's fourteen years of existence, Gordon Fellows have been sponsored by more than seventy industrial firms and government organizations and four ALERT-related government organizations: Army Night Vision Electronics and Sensors Directorate, Hanscom Air Force Base, US Air Force, and US Coast Guard. The Challenge Projects of these participants have focused on areas that are of strategic importance to the sponsoring organization, such as the demonstration of the effectiveness of infrared standoff explosives detection. The thirteenth-year class included a candidate sponsored by ALERT member Raytheon.

ALERT DHS Science and Engineering Workforce Development Program (previously known as the Career Development Grant)

In September 2011, ALERT deputy director Professor Carey Rappaport received a DHS HS-STEM Career Development Grant (CDG), which provided funding for four fellowships to full-time graduate students pursuing MS or PhD degrees in electrical and computer engineering. Under the terms of this program, selected students received full tuition and a stipend of $2,300 per month for up to three years. Multi-year continuation was granted based on satisfactory progress. Award recipients engaged in research work, class work, and career development activities that provided them with a skill set that was further strengthened by the completion of a ten-week summer research experience at a DHS laboratory, industrial venue engaged in relevant DHS-related R&D, or other DHS-related federal, state, or local facility engaged in R&D.

In January 2012, the first ALERT DHS HS-STEM CDG Fellow, Richard (Alex) Showalter-Bucher, was selected to participate in the program, engaging in research on security threat detection. Alex's work specifically focused on radar technologies for tunnel detection. It was performed at NU and at a summer internship at Lawrence Livermore National Laboratory (LLNL). After Alex completed the program requirements and

received his MS degree in electrical and computer engineering, as well as a graduate certificate in engineering leadership through the Gordon Engineering Leadership Program, he accepted a position at the MIT Lincoln Laboratory Federally Funded Research and Development Center in Lexington, MA, and he completed his one year of service in April 2015.

In September 2012, ALERT selected three additional ALERT DHS HS-STEM CDG Fellows to begin their MS studies. Ted Bednarcik began working with Professor Carey Rappaport on a continuation of the work that Alex Showalter-Bucher began during his ten-week summer research experience at LLNL, and he spent his ten-week summer research experience there as well. Ted also completed the GIEL Program in the summer of 2013 and completed his MS degree in electrical and computer engineering leadership in January 2015. Ted began his one year of service at the Portsmouth Naval Shipyard on June 1, 2015 and completed it as of May 31, 2016. Michael Collins began working with Professor Rappaport on investigating nuclear quadrupole resonance sensing for noninvasive detection of concealed explosives. He spent the summer of 2013 at Los Alamos National Laboratory for his ten-week summer research experience and completed his MS degree in electrical and computer engineering in Summer 2014. Michael completed his one year of service as a visiting researcher with the NATO Science and Technology Organization's Centre for Maritime Research and Experimentation in October of 2015. Finally, ALERT CDG Fellow, Thomas Hebble, continued to work with Professor Octavia Camps on video-analytics–based detection and tracking of suspicious behavior in airports. Tom intended to move from the MS degree to the PhD degree but did not end up continuing with the program.

In Fall 2014, Joseph Robinson began the program working with Professor Yun (Raymond) Fu at NU. Joe is nearing the end of his studies for the PhD in computer engineering, and as of July 30, 2017, he completed the second of two ten-week internships to fulfill that requirement of the program. Joe worked at Systems & Technology Research (STR) in Woburn, MA on defense related projects, many of which are in line with ALERT's mission.

In Summer 2015, with support from the DHS Office of University Programs, ALERT updated and expanded the ALERT CDG Program—changing the name of the program for all future participants to the ALERT Science and Engineering Workforce Development Program (SEWDP). A major change to the program was that undergraduates and students from other ALERT partner universities could now apply. Our first undergraduate participant, Matthew Tivnan, an NU student pursuing the BS in electrical engineering and physics, began participation in Fall 2015, working with Professor Carey Rappaport. As an undergraduate, Matt was allowed to complete one six-month co-op experience in place of the two ten-week internships. In January 2016, Matt worked at Photo Diagnostic Systems, Inc. in Boxboro, MA and was exposed to the design, development, manufacture, installation, and service of positron emission tomography (PET) and hybrid PET/CT imaging systems and accessories. In May 2017, Matt completed his degree and participation in the ALERT SEWDP and began working full time at Photo Diagnostic Systems. He continued in that position through May 2018, thereby satisfying his final program requirement of one year of service in the DHS enterprise.

In Fall 2016, Christian Sorensen began pursuing a PhD in mechanical engineering at Purdue University as an ALERT SEWDP participant under the direction of ALERT Thrust R1 researcher, Professor Steven Son. Christian completed his second year with the program in spring 2018 and did the first of his two ten-week internships in summer 2018, working on macroscale explosives phenomena at Lawrence Livermore National Labs. Christian completed his work with the program through the spring of 2019.

In Fall 2017, Katherine Graham (Figure 3-5), an undergraduate at NU pursuing the BS in mechanical engineering, began participation in the ALERT SEWDP working with Professor Jose Martinez on hardware

design for stand-off and on-the-move detection of security threats. Katherine completed her six-month co-op experience at MIT Lincoln Laboratories and continued her participation in the ALERT SEWDP through the Summer of 2019. Katherine completed her BS degree in May of 2020.

Finally, ALERT was authorized to use SEWDP funds to support ALERT students who were being supported via ALERT core funding through their participation on research projects that were cut as a result of the ALERT DHS 2015/2016 Biennial Review. A student from Notre Dame and a student from Texas Tech received funding in Year 5.

Figure 3-4: Katherine Graham is an NU BS graduate and a former ALERT SEWDP participant.

3.2 UNDERGRADUATE PROGRAMS

Research Experiences for Undergraduates Program

ALERT held its last Research Experiences for Undergraduates (REU) program in the summer of 2018 during Year 6 and provided seven opportunities for undergraduate students to engage in exciting ALERT projects related to identifying, sensing, and managing explosives-related threats (Figure 3-5). These opportunities took place at NU and UPRM.

ALERT and Gordon-CenSSIS Scholars NU

Many of the undergraduate students involved in ALERT were introduced to research through their participation in the ALERT Scholars Program, which was aimed at freshmen. Students applied to the program in the first semester of their freshman year and accepted students attended lectures and seminars, including Research Ethics, Engineering Leadership, and Research Presentation Skills, as well as presentations on ALERT and other research opportunities. Scholars participated in ALERT research, volunteered for Boston-area K–12 outreach programs related to ALERT and other STEM research initiatives, and gave a final research presentation at the end of the program. In recognition of participation, the ALERT Scholars who completed the program received a $1,000 book voucher.

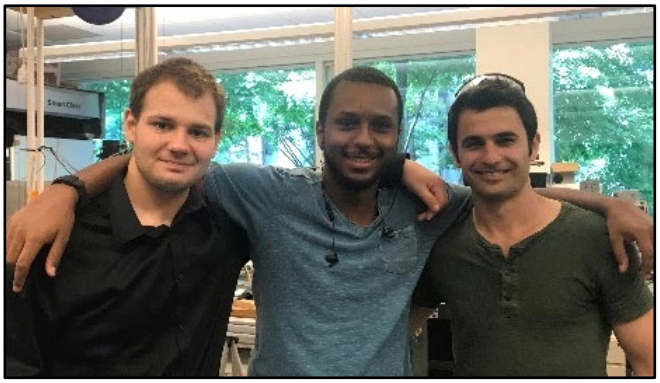

Figure 3-5: Year 6 ALERT REUs in Professor Rappaport's AIT Lab at NU.

In addition to the ALERT REU Program and the ALERT Scholars Program, all the ALERT university partners involve undergraduate students in research efforts and outreach. In Year 7, thirty-nine undergraduate students were involved in ALERT, working on projects including radar suicide bomber detection, creation of explosive simulants, segmentation of luggage images, whole body imaging and characterization, synthesis, detection, and identification of energetic materials.

3.3 PROFESSIONAL DEVELOPMENT PROGRAMS AND SHORT COURSES FOR DHS PROFESSIONALS AND FIRST RESPONDERS

There is an increasing need for advanced study on special topics related to homeland security technologies for graduate students, DHS personnel, and other professionals. To address this need, we have developed a series

of strategic study workshops and short courses, including the biannual ADSA (Advanced Development for Security Applications) workshops and a second, newer workshop series, ADEPT (Advanced Development for Security Applications for Customs and Border Protection). The purpose of these workshops is to present cutting-edge research with a focus on identifying current "gaps" and providing tutorials on explosives-related areas such as CT screening, whole body imaging, video analytics, and stand-off detection. The strategic study workshops are discussed in greater detail in Section 5.

First responder and professional training courses continue to be offered through URI (Figure 3-6) to representatives from various agencies, such as the Army, Air Force, and Navy facilities, as well as for the Transportation Security Administration (TSA) and the TSA Systems Integration Facility. In Year 7, ten specialty classes, such as the recurring Explosives Analysis course, served over 225 professionals.

Figure 3-6: Participants at one of URI's ongoing training courses.

3.4 COMMUNITY COLLEGE OUTREACH

An important ALERT goal is to increase the number of community college students retained in STEM majors and to enhance their desire to matriculate into a four-year program. Strong partnerships have been developed by the COE to reach that goal.

Since the summer of 2012, Michael Pelletier, a faculty member at Northern Essex Community College (NECC), began working with Professor McKnight through the Research Experiences for Teachers (RET) program at NU, partially funded by ALERT. His summer work involved developing a new High Tech Tools & Toys Lab (HTT&TL) experiment to detect hidden objects with 40 kHz ultrasound in air and producing written material on the HTT&TL experiments that would be useful to classroom instructors at NECC and other community colleges. Since that summer, Mr. Pelletier continued to teach two sections (Essentials in Design) in both the fall and spring semesters.

Chitra Javdekar, a faculty member at MassBay Community College, attended a summer program at NU in 2011 where she experienced the HTT&TL teaching style. On her return to MassBay, she introduced the HTT&TL experiments with the stepper motor and video-cam color identification and separation of painted Ping-Pong balls in an Engineering Computation class in the spring of 2012. Dr. Javdekar has subsequently been appointed as dean of the Science, Technology, Engineering and Mathematics (STEM) Division at MassBay, and the HTT&TL modules are continuing to be used in the Engineering Computation course.

3.5 PRE-COLLEGE PROGRAMS

ALERT continues to foster the education pipeline through pre-college programs provided at NU, URI, Purdue University, and the University of Notre Dame. Examples of relevant pre-college programs and activities that ALERT has participated in over the years include:

- RET summer program, which immerses high school teachers and community college faculty in research laboratories at NU and URI;
- Clay Middle School outreach event through Notre Dame;

- Summer program at Notre Dame, in which high school students and teachers participated;
- Summer research internships for high school students at Duke University;
- Hosting the Young Scholars (YS) program at NU for gifted high school students;
- Offering a STEM Field Trip series at NU for urban students throughout the academic year;
- Participating in Building Bridges Programs at NU; and
- Hosting middle school students for two weeks each summer to build and support their STEM interests.

Over the years, ALERT continued its ongoing collaboration with Claire Duggan, director for programs and operations for the Center for STEM Education at NU, to host participants of the Young Scholars program for Boston-area high school students.

3.6 CONCLUSION

In summary, ALERT has provided a pipeline of educational support for students from middle school through the university level and beyond. Through residential programs, summer research experiences, courses, and workshops, we have introduced hundreds of students and career professionals to DHS-related material. Through our professional development opportunities, we will continue to introduce many students in STEM to the work of ALERT, and ultimately to the workforce of DHS and its stakeholders.

Section 4: Technology Transition and Engagement

4.1 INTRODUCTION

As the ALERT Center of Excellence (COE) is concluding its final year, the Transition Team, shown in Figure 4-1 (Emel Bulat, Kristy Provinzano, and Deanna Beirne), has focused on the goal of transitioning the research and development (R&D) from the last twelve years over to the commercial sector. Transitions represent a shift to industry, government lab, or government agency. Our longstanding collaboration with our industrial partners has been the key to ensuring this goal and has allowed ALERT to be adaptive and responsive to the needs of our partners in the ever-evolving homeland security landscape.

Figure 4-1: The ALERT Transition Team. Of note, in November of 2019, Kristy Provinzano resigned, and in March of 2020, Gustavo Bottan was hired to support the Transition and Industrial Liaison Teams.

To facilitate this drive to transition, the team developed new ways of evaluating and promoting Center work. As an outcome of the second ALERT Biennial Review, we culled the number of research projects from a total of thirty-two projects to nineteen projects, most of which continue to work closely with our industrial partners throughout Year 7 to ensure a smooth transition. The Transition Team worked with all research faculty to establish milestones that closely parallel those used by industry. These milestones were focused on driving technology maturation and transition rather than basic and applied research (with some exceptions). The team established quarterly reviews focused on these transition milestones, which provided the Transition Team an opportunity to not only develop stronger ties to the project teams but also offer transition support where it would be beneficial to achieving milestones. In preparation for ALERT's final year, the Transition Team conducted an extensive review of all the remaining projects, assigned technology readiness levels (TRLs), and prioritized them so that we can optimize the remaining funds to maximize the number of successful transition outcomes.

There are six pathways to successfully transition technologies developed at the ALERT COE into the marketplace:

- Licensing and/or spin-off companies;
- Directed research with funds from an industrial partner;
- Joint proposals;

- Task orders through ALERT's Basic Ordering Agreement;
- The transfer of ALERT students to the homeland security enterprise (HSE) on graduation; and
- Databases and Datasets for the HSE community.

Of the nineteen remaining projects, eight have already transitioned algorithms or other intellectual property (IP)—such as equipment configuration concepts—to our industrial partners, with nine more projects on the verge of doing so.

In the transition area of databases and datasets, ALERT's Explosives Database developed by URI and supplemented by Duke University has amassed over one thousand subscribers, and ten vendors of explosives detection instrumentation have leveraged this resource. ALERT Airport Re-Identification Dataset, developed by teams at Northeastern University and Rensselaer Polytechnic Institute, currently has over 280 users, including thirteen different industrial organizations.

In addition to transitioning various types of IP and data resources to the HSE, we have leveraged core research findings to pursue and acquire task orders and directed research projects. These efforts are focused on providing specific deliverables for homeland security end users and industrial partners within a one to two year time period, our current efforts are outlined later in this section. These task orders and projects help move research out of the lab and into the field and are a key component to ALERT's continued viability beyond core funding.

To expand our reach to other Department of Homeland Security (DHS) components, we have started working closely with Customs and Border Protection (CBP). In addition to the CBP-Advanced Developments Encompassing Processes and Technologies (ADEPT) Workshop started in 2018, we orchestrated and attended a day-long visit at the Los Angeles / Long Beach Seaport on April 2, 2019. The visit yielded valuable insight into the daily operations and the technology gaps faced by CBP, and it led to organizing a second day-long Technology Demonstration event involving five of ALERT's industrial partners, as discussed in detail below.

Finally, instead of our Annual Technology Showcase, which was postponed due to the COVID-19 pandemic, this year ALERT instituted an online biweekly seminar series, beginning in late June and running through September 2020, focused on eight projects that are all working closely with industry to transfer the R&D from the lab into the commercial sector. We intend to host a virtual Technology Showcase in late spring of 2021 to coincide with the successful completion of ALERT's core activity at the end of the current no-cost extension in May 2021.

4.2 TRANSITION IMPLEMENTATIONS

The Transition Process Requires Resources Beyond Core Funding

Our experience thus far has shown that successful transition requires resources beyond core funding (e.g., task orders or directed research from a vendor). Finding a funding partner can be difficult because the outcome of the research is uncertain and the market is unproven. However, the successes listed in the following section demonstrate that if resources can be found, researchers will help adapt their research to fit an uncertain market, and industrial partners can envision the impact of new research in their relevant market.

For example, ALERT's core funding resulted in X-ray computed tomography (CT) segmentation algorithms, reconstruction algorithms, automatic target recognition algorithms, and associated datasets, which have all

been transitioned to the X-ray CT industry. This work paved the way for our partnership with Astrophysics, Inc., which provides supplemental funding to the core grant. This work focuses on developing and optimizing unique single- and dual-energy reconstruction algorithms for Astrophysics's Multi-View CT (MVCT™) cargo scanning system. This system is now deployed at John F. Kennedy International Airport. Astrophysics is a shining example of how core funding plus directed research funding can yield a great result.

Beyond this work, we have initiated transition programs for adaptive automatic target recognition (AATR) for the X-ray industry, developed algorithms to evaluate and utilize the dielectric constant of materials to reduce false alarm rates of millimeter-wave (mm-wave) advanced imaging technology (AIT) scanning systems, and leveraged video analytics to track passengers and their associated items in a checkpoint.

There Is More Than One Way to Transition

As highlighted in the introduction, there are many ways to transition technology into the HSE; one pathway does not fit all. The Transition Team must be imaginative and willing to adapt to changing circumstances to achieve the goal. To illustrate this point, here are a few examples of the different pathways used for different technologies:

1. Task Orders
    a. **CLASP (Correlation of Luggage and Specific Passengers):** Funded by the DHS Science and Technology (DHS S&T) Screening at Speed program, this is the second phase of development for an automated video-analytics–based system to associate air passengers with their belongings. The directive of this project is to identify items left behind and potential theft events; optimize security checkpoint throughput; and pave the way for risk-based screening in the airport security checkpoint. The project involves direct partnerships with multiple airports and the TSA.
    b. **Maturation and Validation of Dielectric Characterization Algorithms:** Also funded by the DHS S&T Screening at Speed program, ALERT researchers are leveraging data generated by Pacific Northwest National Laboratory for the DHS Passenger Screening Algorithm Challenge to derive the dielectric constant of objects located on a person and use that information to determine if it is a potential threat or not. This project strives to produce a tool to be integrated into the next generation of AIT systems that will reduce the false alarm rate of these scanners, thereby minimizing the need for pat-downs, which in turn improves throughput rates and the passenger experience.
    c. **Simulated Air Cargo Skids:** This task order is working on developing methods to create simulated descriptions of palletized air cargo for use in assessing scanning systems such as 3D CT. The software tools developed under this contract, when used in conjunction with extant X-ray simulation tools, will provide the following benefits to the HSE: (1) an increase in the number of people developing anomaly detection algorithms by providing publicly available data sets for unrestricted use by third parties such as academia and industry vendors; (2) an ability to utilize training and testing data generated from the simulation engine for the development of artificial intelligence and deep learning methods to automatically detect anomalies; and (3) a faster assessment of emerging scanning modalities by obviating the cost and time of developing prototypes.
    d. **Comprehensive Database of Contact Explosives Sampling Efficiency and Baseline Performance (TESSA2) Materials:** Sampling is a critical step in enhancing the sensitivity of explosives trace detectors (ETDs), and the more sample delivered to an ETD's sampling inlet the more sensitive the ETD is. This is an extension of work performed under an earlier task order that resulted in the creation of a standardized method and common language to measure sampling efficiency related to ETDs, resulting in a set of reference materials, procedures to use the reference

materials, and a limited database of contact sampling. This current task order seeks to establish a more thorough database of contact sampling by extending the number and type of sample traps and type of explosives. Emphases are placed on commercial off-the-shelf (COTS) traps and reagent-enhanced traps.

e. **Novel Features and Emerging Technologies for Opioid Detection:** This program seeks to develop technologies to support US Customs and Border Protection in their mission to detect and interdict illicit drugs in packages entering the United States through international mail facilities and express consignment facilities at speeds that do not disrupt legitimate commerce.

2. Directed Research

   a. **MVCT Cargo Screening:** The industrial partner Astrophysics asked ALERT to provide science and technology for their commercial instrument. They are providing the resources for the transfer and have the ownership of the IP. ALERT provided significantly faster 3D CT reconstruction algorithms to Astrophysics for use in the MVCT that is currently deployed at John F. Kennedy International Airport in New York.

3. Licensing/Spin-Off Companies

   a. **Model-Based Iterative Reconstruction (MBIR):** ALERT researchers started their own company and obtained a Small Business Innovation Research (SBIR) fund to provide resources to transition a security product.

   b. **MatrixSpace:** A new spin-off company started by R3-B.1 principal investigator, Dr. Jose Martinez of Northeastern University, and Gregory Waters (former CEO of Integrated Device Technology) that is currently developing lower cost mm-wave chips that can be used to increase resolution and performance of the prototype "on-the-move" scanning radar system being developed in that project.

   c. **Zepsor Technologies:** Zepsor Technologies is in the process of incorporating their new start-up by the end of the year and will license near-zero power sensor patents developed under the ALERT funding no later than Q2 2021.

4. Knowledge Product

   a. Dissemination of the datasets related to the task orders for CT Segmentation, Reconstruction, Automated Threat Recognition, and Airport Re-Identification to academic institutions as well as government laboratories and industry.

The ALERT Transition Team will continue to work with researchers, government, and industrial partners throughout the no-cost extension period to steer the projects toward successfully transitioning ALERT's R&D into the homeland security marketplace.

4.3 TRANSITION DRIVEN THROUGH FREQUENT FACE-TO-FACE INTERACTION

ALERT pursues DHS security needs by communicating with the DHS components, national laboratories, and industrial partners. There is an ongoing dialogue between our academic, government, and industrial partners at events such as the Advanced Development for Security Applications (ADSA) and CBP-ADEPT Workshops, COE directors' meetings, and Annual and Biennial Reviews with members of the Federal Coordinating Committee. In Year 6, we held ALERT's first Technology Showcase to highlight how the COE has addressed the HSE needs (by categorizing them as Grand, Medium, or Small Challenges). In Year 7 (our final year), the Transition Team did a deep-dive on all of the current projects, traveling to most of the university partners to discuss their project status, their TRLs, and whether or not an industry partner was

working with them to transition their research. As discussed in Section 4.1, we established a series of quarterly reviews to help guide researchers in the ultimate goal of transitioning their technology to industry and the HSE, which has proven extremely helpful in aiding our objectives. In summary, ALERT will continue to monitor their progress through the no-cost extension period (May 31, 2021) so that we can steer the projects toward the goals of these Challenges to maximize successful transition as we sunset our center.

ADSA Helps ALERT Understand the Needs of the Security Enterprise

Every spring and fall, ADSA workshops are held at ALERT's Northeastern University campus, bringing the DHS security community together to discuss relevant topics. During the semiannual two-day workshop, more than thirty presentations and panel discussions are used to initiate discussions among approximately 150–175 participants from the security and aviation industry, DHS components, DHS S&T, national laboratories, and academics. Information pertaining to the most recent ADSA workshops are available at http://www.northeastern.edu/alert/transitioning-technology/adsa/.

Due to the COVID-19 pandemic, ADSA22 has been postponed to fall of 2020 and will be held as a virtual workshop series.

CBP-ADEPT Focuses on the Needs of Customs and Border Protection

Modeled after the ADSA Workshop Series, CBP-ADEPT focuses on addressing the technology requirements facing CBP officers on a daily basis. This two-day event is held once a year in the summer and features approximately twenty-five to thirty presentations and panels. Topics include illegal immigration, contraband interdiction, radiation detection to prevent dirty bombs, and trace explosives detection. As with ADSA, due to the COVID-19 pandemic, CBP-ADEPT has been postponed to fall of 2020 and will be held as a virtual workshop series.

Information pertaining to the most recent CBP-ADEPT workshops are available at http://www.northeastern.edu/alert/transitioning-technology/cbpadept .

Los Angeles / Long Beach Seaport Technology Demonstration

On April 2, 2019, a team of ten people from the ALERT community—including academics, government, and industry representatives—traveled to the Los Angeles / Long Beach Seaport for a day-long visit focused on the daily operations of the seaport. We learned about the routine challenges facing the CBP officers, discussed their needs for various forms of state-of-the-art sensors and sensor systems, and formulated some next steps on how to establish closer collaboration. With that end goal in mind, we were pleased when two of the CBP officers from Los Angeles / Long Beach attended our Technology Showcase and ADSA20 in May of 2019, as well as participated in the CBP-ADEPT in July of 2019. These interactions resulted in ALERT working hand-in-hand with LA/LB CBP Chief Victor Todorov and his team to organize a day-long Technology Demonstration aimed at detecting opioids, their precursors, and other contraband. This Technology Demonstration was held on November 21, 2019, and it was highly successful and well-attended. Present at the event were six members of the ALERT researcher team and staff, seven industry representatives from five industrial partners (Astrophysics, Pendar, Rapiscan, Rigaku, and Smiths Detection), six senior DHS personnel, and twenty-five CBP officers. Details are summarized in the newsletter article found at http://www.northeastern.edu/alert/news-article/alert-collaborates-with-cbp-on-technology-demonstration-at-los-angeleslong-beach-seaport/.

As a direct result, two of our industrial partners, Pendar and Rigaku, were invited back for a three-week in-depth technology analysis of their instruments. Both vendors were gracious enough to loan their Raman

systems that were used in conducting the day-to-day operations at the Seaport's A-TCET Warehouse in Carson, CA.

CBP has generously offered their warehouse facilities to ALERT as testbeds for our technologies. This year ALERT industrial partners, Pendar and Rigaku, have taken advantage of this opportunity. We anticipate that in the coming year, ALERT researchers will leverage this resource for some of our continuing task orders (as much as the COVID-19 pandemic permits).

Technology Showcase

Last year we held the first Technology Showcase on May 14, 2019 highlighting ALERT's successes. The showcase consisted of nineteen technical project posters, many of which were jointly manned with an industrial partner supporting the development of that project. In addition, we presented seven demonstrations highlighting the research projects that are at TRL 4 or greater. ALERT's intent is to show that our COE's R&D will transition into the HSE and affect positive change. The event was extremely well received with many of the attendees asking us to conduct another showcase in 2020. However, due to the COVID-19 pandemic, we had to postpone this year's Technology Showcase. In lieu of the Technology Showcase, the ALERT COE is hosting a biweekly webinar series, which started on June 24, 2020, discussing updates on Technology Transition Projects, many of which were initially presented at last year's showcase.

Final decisions and dates on rescheduling all the events above will depend on the COVID-19 pandemic status.

4.4 SUMMARY

As the core funding for the ALERT Phase 2 COE draws to a close, our focus continues to be the transition of technologies developed over the twelve years of ALERT Phases 1 and 2. Transitions, as counted here, represent a shift to industry, government lab, or government agency. To date, across the nineteen active projects, there have been nine transitions and eight transitions "on the verge," where some projects have yielded multiple transitions. The Center has seen many successes supporting the HSE, including commercialized products, spin-off companies, the development of groundbreaking technologies, advancements in security scanning capabilities, the transfer of knowledge products, and workforce development. The Transition Team will pursue new opportunities for partnerships while also continuing to leverage our cohort of industrial members, DHS funded task orders, and HSE collaborators to move ALERT technologies to market.

Section 5: Strategic Studies Program

Part of ALERT's mandate from the Department of Homeland Security (DHS) has been to develop a strategy to identify gaps in the knowledge for effective improvised explosive device (IED) Detect and Defeat capabilities. The prime vehicle for this has been a series of strategic studies workshops on relevant DHS topical areas. Since 2008, ALERT has held two to three workshops per year, as part of the originally titled Algorithm Development for Security Applications (ADSA) series. In 2014, due to the evolving nature of these workshops (expanding from an original focus on algorithms), the series was renamed as Advanced Development for Security Applications. ALERT Director Michael Silevitch convenes these workshops in concert with Carl Crawford, an expert in security imaging and consultant to ALERT. The audience for the ADSA workshops is comprised of government, academic, industry (aviation and security), and national lab participants in the Homeland Security Enterprise. Since 2018, a new series of workshops have emerged in addition to ADSA. These workshops are known as ADEPT, which stands for Advanced Developments Encompassing Processes and Technologies. The ADEPT workshops are focused on the priorities of DHS Customs and Border Protection (CPB). This new focus enables ALERT to be much more relevant and responsive to the overall needs of DHS.

Comprehensive lists of ALERT Phase 1 and Phase 2 workshops follow.

ALERT Phase 1

In the first five years of ALERT (i.e., ALERT Phase 1), these strategic studies resulted in nine workshops, each with a full report:

- **Terahertz Imaging and Sensing:** October 30, 2008.
- **ADSA01:** April 23–24, 2009. Focused on development of new algorithms for detecting explosives at an integrated checkpoint.
- **ADSA02:** October 7–8, 2009. Dealt with segmenting objects of interest from volumetric computed tomography (CT) scans of baggage.
- **ADSA03:** April 27–28, 2010. Focused on Advanced Imaging Technology (AIT) for whole body screening.
- **ADSA04:** October 5–6, 2010. The purpose of this workshop was to discuss how third parties could participate in the development of reconstruction algorithms for explosive detection equipment based on CT scanning.
- **ADSA05:** May 3–4, 2011. Focused on sensor fusion techniques.
- **ADSA06:** November 8–9, 2011. Addressed specific topics related to developing and deploying multi-sensor systems.
- **ADSA07:** May 15–16, 2012. Focused on advanced reconstruction algorithms for CT-based luggage scanning systems.
- **ADSA08:** October 24–25, 2012. Focused on Automatic Target Recognition (ATR) algorithms for explosives detection systems.

ALERT Phase 2

Over the past seven years of ALERT Phase 2, our strategic studies efforts have resulted in eighteen workshops. Fifteen of these workshops were held over the first six years of ALERT Phase 2. These are listed next. The three Year 7 workshops are discussed in more detail following this list.

- **ADSA09:** October 22–23, 2013. Focused on new methods for explosive detection and addressed new hardware for aviation security.
- **ADSA10:** May 6–7, 2014. Focused on explosives detection in air cargo. Going forward, the title of this series of workshops was changed from "Algorithm Development for Security Applications" to "Advanced Development for Security Applications." The change reflects the broad scope of the workshops, which evolved to include hardware, such as sensors.
- **TESSA01:** August 13–14, 2014. This workshop was the second in a series dealing with the development of a research plan for organizing the community's understanding of contact sampling during trace explosives detection.
- **ADSA11:** November 4–5, 2014. Focused on explosives detection in air cargo to support the Department of Homeland Security's objective of improving the performance of existing technologies.
- **ADSA12:** May 12–13, 2015. Focused on screening of personnel and divested items at the checkpoint to support the Department of Homeland Security's objective of improving the performance of existing technologies and improving the passenger experience at checkpoints.
- **TESSA02:** August 5–6, 2015. This workshop was the second in a series dealing with the development of a research plan for organizing the community's understanding of contact sampling during trace explosives detection, and it focused on three enabling components of trace explosives detection.
- **ADSA13:** October 28–29, 2015. Focused on screening of personnel and divested items at airport security checkpoints to support the DHS objective of improving the performance of existing technologies.
- **ADSA14:** May 10–11, 2016. Focused on the development and deployment of fusible technologies at airport security checkpoint to support the DHS objective of improving the performance of existing technologies.
- **ADSA15:** November 15–16, 2016. Focused on next generation screening technologies and processes for airport security checkpoints to support the DHS objective of improving the performance of existing technologies. This workshop was a continuation of ADSA12, ADSA13, and ADSA14.
- **ADSA16:** May 2–3, 2017. Focused on addressing the requirement for different stakeholders in transportation security to support the DHS objective of improving the performance of existing technologies.
- **ADSA17:** October 17–18, 2017. Focused on systems engineering of aviation security systems.
- **ADSA18:** May 15–16, 2018. Focused on the collection and use of metadata for improving aviation security systems.
- **CBP-ADEPT-01:** June 20–21, 2018. Focused on advanced development for security applications for the Customs and Border Protection branch of DHS.
- **ADSA19:** October 16–17, 2018. Focused on rapid response to an adapting adversary.
- **ADSA20:** May 15–16, 2019. Focused on design, development, testing, deployment and operation of effective systems.

5.1 WORKSHOPS DURING YEAR 7

The **ADSA21** workshop entitled, "Effective Integrated Systems for Aviation Security" convened at Northeastern University (NU) in Boston on November 5–6, 2019. The ADSA21 Workshop featured more than thirty presentations from subject matter experts and leaders from industry and government over the course of two days. Over 170 participants from academia, industry, and government gathered to discuss topics such as exposing third parties to problems that need to be solved in the aviation security field, understanding what third parties need to participate in with the aviation field, including access to funding and problem statements, developing databases that can be used by third parties, dealing with classified information and export control restrictions, protecting intellectual property, protecting the business interests of incumbent vendors, and publishing the results.

The **ADSA22** workshop entitled "Reducing Cognitive Load in Aviation Security Equipment" was scheduled to convene at NU in Boston on May 6–7, 2020 but was postponed due to COVID-19 restrictions. This workshop is now planned to take place virtually as a series of two-hour webinars occurring on Tuesdays between November 17 and December 8. Presentation and discussion will focus on topics such as automating operator functions to reduce the vigilance decrement of operators and TIP, target shifting and insider threats, adaptability of machine learning algorithms and open architectures and third-party involvement.

The **CBP-ADEPT-02** workshop entitled "Advanced Developments Encompassing Processes and Technologies for Customs and Border Protection" convened at NU in Boston on July 17–18, 2019. This workshop brought together 130 attendees from government, industry, and academia to discuss topics related to current technology in improving port and cargo security. Presentations were given in the following areas of expertise: an adaptive adversary, integration of equipment and data, collection and use of metadata, deterrence/hardening, insider threats, con-ops, adaptation of TSA technologies, simulation tools, and war gaming applications. A third workshop in the ADEPT series was scheduled to be held in July 2020 but was postponed due to COVID-19 restrictions. It will be rescheduled in 2021.

Full reports and presentations from Phase 1 and Phase 2 workshops are available at http://www.northeastern.edu/alert/transitioning-technology/adsa/final-reports-and-presentations/.

5.2 SUMMARY

In summary, the ADSA and CBP-ADEPT strategic studies workshops have been and will continue to be valuable in creating collaborative opportunities by engaging participants from industry, national labs, vendors, government, and academia in an integrated setting where the Center acts as a "neutral broker." This is vital in the further development of a dynamic network that can foster the innovative basic research, education, and technology needed to help DHS in its mission to safeguard our nation.

This page intentionally left blank.

Section 6: Safety Program

6.1 INTRODUCTION

On January 7, 2010, an accident occurred in the chemistry department at Texas Tech University (TTU) in the laboratory of Associate Professor Louisa Hope-Weeks, a past ALERT researcher. A senior graduate student, Preston Brown, injured himself while synthesizing nickel hydrazine perchlorate. Northeastern University (NU) was notified about the accident on January 8, by e-mail and by phone. In light of this incident, ALERT undertook a comprehensive reassessment of the "safety culture" within the ALERT COE and instituted a center-wide safety program as outlined below in Figure 6-1.

The following year, the ALERT Cooperative Agreement (and those of the other Department of Homeland Security COEs) was modified to require the establishment of a center-wide safety program. For the past eight years, we have been operating with the ALERT Safety Program and have maintained a culture of safety. During the last six years, ALERT has broadened the Safety Awareness Education Program (SAEP) to include general laboratory safety. The Safety Protocol & Standard Operating Procedures and Safety Compliance Assurance parts of the program have remained and will remain focused on explosives safety.

In terms of the safety program, the ALERT team recognized that handling energetic materials, screening instruments, etc., requires constant vigilance; any lapses in safety can have severe consequences. The issue with any safety program is that it can become stale and lose the attention of its audience. As shown in Figure 6-1, the ALERT Safety Program components are (1) a Safety Review Board, (2) a Safety Awareness Education Program, (3) Safety Protocols and Standard Operating Procedures, and (4) a Safety Compliance Assurance Program. It is the ALERT Center's intent that by taking the time to create and review safety elements, practitioners will have a heightened awareness of the hazards and take appropriate care. To keep the program vital, ALERT worked to change the focus and implementation of the safety program's educational and compliance components. The rest of this section describes, in detail, the components shown in Figure 6-1.

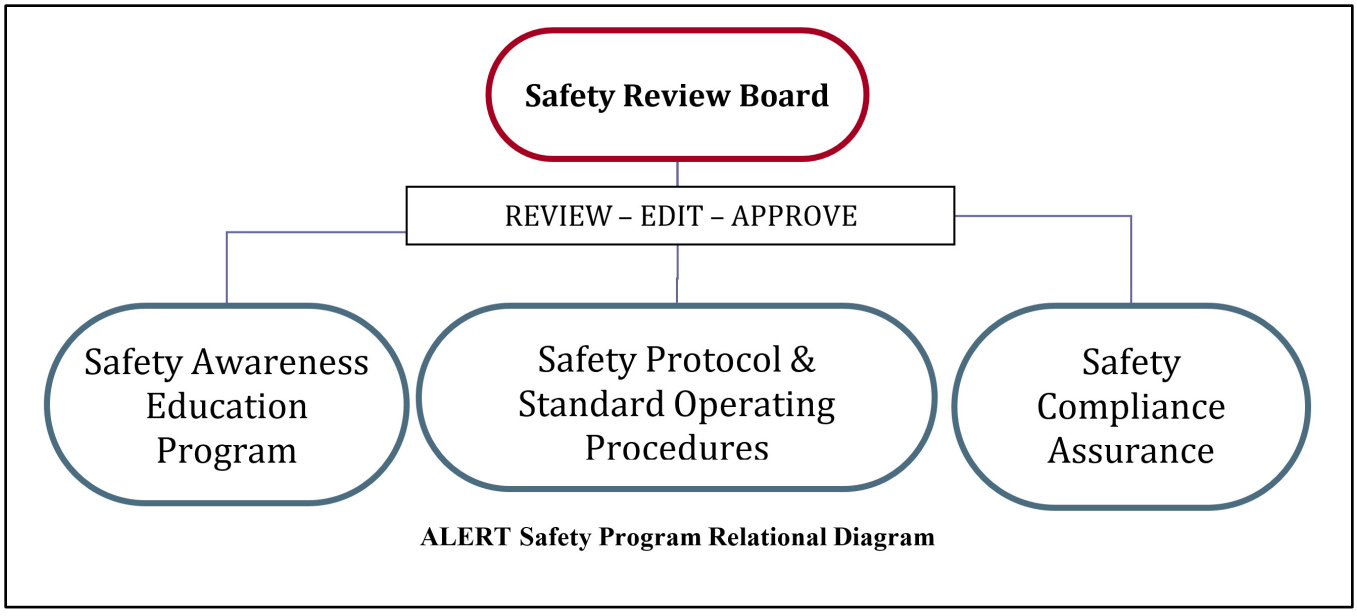

Figure 6-1: Safety Review Program components.

6.2 SAFETY REVIEW BOARD

A team of outside experts assembled to aid in creating, adding, and updating appropriate overarching safety protocols. The members of this Safety Review Board (SRB) have a wide variety of explosive research, explosive handling, radiation safety, and chemical process safety backgrounds (see Table 6-1). The SRB and safety protocols are not intended to supersede the existing safety protocols at each ALERT institution; rather, these protocols and the SRB are put in place to offer basic guidance. ALERT is responsible for making the SRB available for ongoing consultation and periodic oversight of each academic partner's safety awareness and compliance processes. Each institution and each individual is responsible for safety, and each must create and maintain safety protocols and standard operating procedures (SOP), which meet the minimum level established by the "ALERT Safety Protocols and Standard Operating Procedures."

The functions of the Safety Review Board are to review and provide input for:

1. The baseline ALERT Safety Protocol and Standard Operating Procedures;
2. The Safety Awareness Education Program;
3. The Safety Compliance Assurance Program (SCAP);
4. Any corrective actions resulting from the SCAP audits; and
5. Other issues as needed.

Name	Title	Organization	Phone Number	Email
Jimmie Oxley (Chair)	Professor of Chemistry	University of Rhode Island	401-874-2103	joxley@chm.uri.edu
John (Jack) Price	Director Environmental Health and Safety	Northeastern University	617-373-2769	j.price@neu.edu
Bill Koppes	Synthetic Chemist	Navy, Indian Head (retired)	301-659-3701	bilsukopp@verizon.net
Mike Coburn	Synthetic Chemist	Los Alamos National Lab (retired)	505-709-9158	mdcoburn@cybermesa.com

Table 6-1: Composition of the 2019–2020 Safety Review Board.

6.3 SAFETY AWARENESS EDUCATION PROGRAM

The most important features needed to create a "culture of safety" are safety education in the laboratory and best practices for use in the laboratory and the field. Most of the ALERT institutions already provide these features; however, researchers should be periodically re-indoctrinated about lab safety practices, protocols, and hazards. The center has developed a program on laboratory safety with a focus specifically on explosives safety. To keep the education program vital, while remaining focused on safety, the topics will shift to different explosives, practices, protocols, and hazards.

Drawing on the resources of ALERT researchers and those of the Department of Defense (DoD) and National Laboratories, a Safety Awareness Education Program has been created to supplement the safety education at participating institutions.

The SRB has input into the Safety Awareness Education Program. It was intended for the "Explosive Safety Protocols and Procedures" course to be offered once every year, online and in person, with instructors visiting each institution, if able, so that researchers will have the opportunity to meet the instructors face to face. Principal Investigators at each institution will have an opportunity to supplement the instruction as appropriate for their institution. Each individual who participates in the ALERT program must attend the course within one year of joining the program and at least once every other year thereafter.

The Safety Awareness Education Program was designed to promote a culture of safety in ALERT laboratories working with energetic materials and ancillary equipment. Over the life of the center, ALERT has broadened the SAEP to include general laboratory safety. The majority of ALERT laboratories do not handle explosives and general laboratory safety in those laboratories is important. While there has been a shift in the SAEP, the primary focus of working with energetic materials and ancillary equipment remains. The ALERT Safety Review Board is responsible for creating, implementing, and maintaining the ALERT leadership, and the chairperson of the SAEP will select the instructor who will lead the training sessions associated with the SAEP. The SRB has reviewed the SAEP on an annual basis and as necessary for emergent issues.

The SAEP is intended to meet the highest standards of safety achievable for explosives-based research work and has become the reference protocol for the ALERT partnership. Additional Safety Awareness Education efforts by the partners are encouraged. The content of the training sessions has been created by the selected instructors, then edited and approved by the SRB. Any changes or additions to the training sessions are to be edited and approved by the SRB. The training sessions associated with the SAEP will be offered on an annual basis through real-time webinars that will also be recorded for future viewing online. Each individual who uses energetic materials in their research must attend the training session.

6.4 SAFETY COMPLIANCE ASSURANCE PROGRAM

How can safety be ensured? Education is the first step, but education must be coupled with the knowledge that unsafe practices will not be tolerated. As with written protocols, compliance must start with the practitioners. Coworkers must be vigilant when it concerns the safety of their colleagues.

The Safety Compliance Assurance Program will require the SRB to periodically review each of the components of the Safety Program:

- The ALERT Safety Protocols and Standard Operating Procedures;
- The ALERT Safety Awareness Education Program; and
- The on-site safety practices of each ALERT partner institution using energetic materials.

Annually, the SRB reviewed and edited, as necessary, the overarching Safety Protocols and Standard Operating Procedures. Recommendations were made to the ALERT administration at NU when appropriate.

Periodically, the SRB would visit each NU-led ALERT partner institution using energetic materials to audit each institution's safety program as practiced, which includes safety protocols and standard operating procedures, additional safety awareness education efforts, and on-site safety practices. The SRB decided how best to audit these safety programs. For example, the SRB may make use of reviews performed by an institution's Safety and Risk Management department. If the safety program is found to be deficient, recommendations and a plan for remediation will be provided by the SRB, and a schedule for compliance will be created and followed. NU will monitor compliance. Failure to comply in a timely fashion will result in a stop work order.

6.5 SAFETY PROTOCOLS AND STANDARD OPERATING PROCEDURES

To create a common culture of safety, a Safety Protocol and Standard Operating Procedure (SOP) document has been created and reviewed by the participants, researchers, and the Safety Review Board. ALERT researchers are responsible for creating, implementing, and maintaining this overarching document. It may be necessary to periodically augment or alter this document; such changes or additions will require a fresh review. Each institution and researcher is responsible for creating and maintaining safety protocols and SOPs appropriate for the research area. The overarching Safety Protocols and Standard Operating Procedures serve as a guideline, a minimum standard. The next level of action is written protocols for operations, written by the researcher, reviewed and modified by colleagues and supervisors, and signed by an institutional safety committee and the researcher. Signing the protocol is the researcher's agreement to operate in a safe manner. It is up to each institution to demonstrate that they have created a culture of safety.

Safety Philosophy

In working with chemicals, certain "best practices" are overarching. These practices are outlined in a number of texts, most notably the National Research Council's *Prudent Practices in the Laboratory: Handling and Disposal of Chemicals* (1995, ISBN-10: 0-309-05229-7). The book provides general guidance on good housekeeping, personnel protective equipment, preplanning and documentation of operations, storage, and disposal. Common sense demands that SDS (safety data sheets) be available and reviewed for all materials handled and that personnel in the laboratory wear appropriate protective gear (e.g., safety glasses, face shields, or full-face masks). Established laboratory safety protocols should be followed or adapted as necessary with review. However, safety ultimately rests on the individual's attitude and knowledge. As new protocols become necessary, they should be added. Every researcher must be part of this process; it is essential for their safety and for the safety of everyone around them.

The safety document is not intended to replace or supersede protocols already in place; all the normal safety precautions applicable to chemicals apply. The additional hazard is uncontrolled release of energy. In handling a known energetic material (e.g., TNT) sufficient literature exists that the researcher should know the specific hazards faced. For unknown species or mixtures, some general guidelines can be followed until more specific information is obtained. A useful source for general hazard warnings is *Bretherick's Handbook of Reactive Chemical Hazards*, 7th edition, P. Urben, 2006.

In general, the concern in the laboratory is synthesis and handling of bulk energetic materials. The issues are sensitivity and stability. Sensitivity is the ease with which a material can be caused to react by relatively mild insult (something a human might inadvertently impart—impact, friction, electrostatic discharge) as opposed to the input of a shock wave (e.g., from a detonator). Sensitivity is generally determined experimentally at a small scale. It is essential to get this information as soon as possible. Furthermore, although a scaled-up formulation is more hazardous, it is usually not more sensitive. (A possible exception is a change to more sensitive impurities with increase in batch size.) Stability refers to the capacity of an energetic material to maintain its chemical composition for long periods at ambient temperature (such as during storage). A material that lacks stability may undergo catastrophic reaction on its own with no apparent additional input of energy. The temperature at which an energetic material maintains stability is a function of its chemistry, its quantity, and its degree of contamination. Generally, contaminated materials degrade more readily than pure ones; their degradation may be quiescent or violent. Large quantities of material undergo self-heating more readily than small quantities because their decomposition generates heat that raises the temperature that accelerates decomposition.

Therefore, during scale-up of a synthetic process, stability tests are run at various stages. In handling energetic material, the rule is to:

- Minimize quantity of material;
- Minimize time of exposure;
- Minimize number of people exposed; and
- Maximize distance, or introduce an adequate barrier commensurate with the amount of material.

6.6 SAFETY ACTIVITIES

Since the initial implementation of the Safety Program, ALERT has gone through multiple iterations of each component.

ALERT Phase 2 Activities

In Year 1, ALERT SRB members, Ronald J. Willey, William Koppes, Michael Coburn, and Jack Price visited the University of Rhode Island (URI) in May 2014. The report is available upon request.

In Year 2, telephone interviews occurred in early August 2014 with University of Puerto Rico at Mayagüez (UPRM), TTU, and Washington State University (WSU). The SRB also visited the newest ALERT member, Purdue University, in late August 2014.

In Year 3, ALERT SRB members, Ronald J. Willey, William Koppes, Michael Coburn, and Jack Price visited TTU in October 2015. A report of their visit and their findings is available upon request.

In Year 4, ALERT SRB members, Ronald J. Willey, William Koppes, Michael Colburn, and Jack Price visited UPRM in February 2017. A report of their visit and their findings are available upon request.

In Year 5, ALERT SRB members, Ronald J. Willey, Jack Price, Mike Coburn, and Jimmie Oxley visited WSU on April 30, 2018. A report of their visit and their findings is available upon request.

In Year 6, the ALERT Safety Program Webinar covered lab safety as it relates to the use of chemicals, millimeter-wave imaging and lasers. Presenters included ALERT R1 Thrust leader Professor Jimmie Oxley of URI; ALERT R3 Thrust leader Professor Carey Rappaport of NU and ALERT education program leader Professor Charles DiMarzio of NU. The webinar was held on February 14, 2019, and there was time for questions and answers following each presenter.

Safety Review Courses

The ALERT SRB has led ten Safety Review courses beginning with the first on April 23, 2010, followed by courses on October 25, 2010, April 7, 2011, November 2011 and July 31, 2012, and included presentations by William Koppes, Ronald J. Willey, and Dr. Geneva Peterson, a postdoctoral research associate working with Professor Hope-Weeks and Professor Weeks at TTU. The sixth Safety Review course and the first course of ALERT Phase 2 was held on September 19, 2014 so that all new professors, graduate, and undergraduate students joining the various groups were included. The seventh Safety Review course taught by Ronald J. Willey and Jimmie Oxley was held on April 1, 2016. The eighth Safety Review course taught by Ronald J. Willey was held on April 21, 2017. The ninth Safety Review course and Training for the Thrust 1 and Thrust 2 researchers was held on April 11, 2018. As indicated above, the tenth Safety Review course was held on February 14, 2019 and included material relevant to all four thrusts of the COE. All of the safety courses were recorded. These mandatory short courses were broadcast to the lead professors and students working with energetic materials at each ALERT partner institution working with such materials. Our short course agendas contain materials common throughout the center and institution-specific items based on the work being

conducted at the location. These short courses have typically been offered annually, adhering to the time frame laid out earlier in this section. Short course topics have included:

- Basic laboratory best practices;
- DoD contractor safety manuals and storage regulations;
- Required testing and the meaning of test results;
- Handling requirements specific to each explosive; and
- Historic explosive accidents for "lessons learned."

Section 7: Information Protection Program

7.1 INTRODUCTION

As a part of conducting explosives detection, mitigation, and response research for DHS, ALERT has gathered relevant X-ray computed tomography (CT) data, video data, and advanced imaging technology (AIT) data, and has developed a method to disseminate the data to researchers. In the ALERT Phase 2 Cooperative Agreement, the Information Protection Program was created to formalize the ALERT Information Protection Plan. This section of the Year 7 Annual Report provides a description of the four components of the ALERT Information Protection Program (IPP): Sensitive Information Protection Policy, Sensitive Information Review Process, Data Procurement and Dissemination Process, and Information Protection Education and Training Procedure. It also describes the Information Protection Program Board, which oversees the implementation of the four program components and reviews them on an annual basis.

The ALERT IPP has been in operation for eleven years and has procured, maintained, protected, and disseminated data for security research. During that time, the ALERT IPP has been responsible for reviewing ALERT public disclosures of information to ensure DHS that no sensitive, secure information (SSI) has been generated or disseminated. Each year, ALERT holds an Information Protection webinar for all of the faculty and students affiliated with the COE. These webinars are recorded and are made available to the ALERT community. We are planning to hold the Year 7 webinar in the fall of 2020 due to pending changes in the submission process.

IPP Mission

The Information Protection Program was established to create and enforce policies and procedures that will ensure that ALERT research does not involve, use, or generate sensitive or classified information, intentionally or accidentally. The IPP also provides guidance on the proper handling, maintenance, and dissemination of research information and data. Figure 7-1 shows the organization of the IPP.

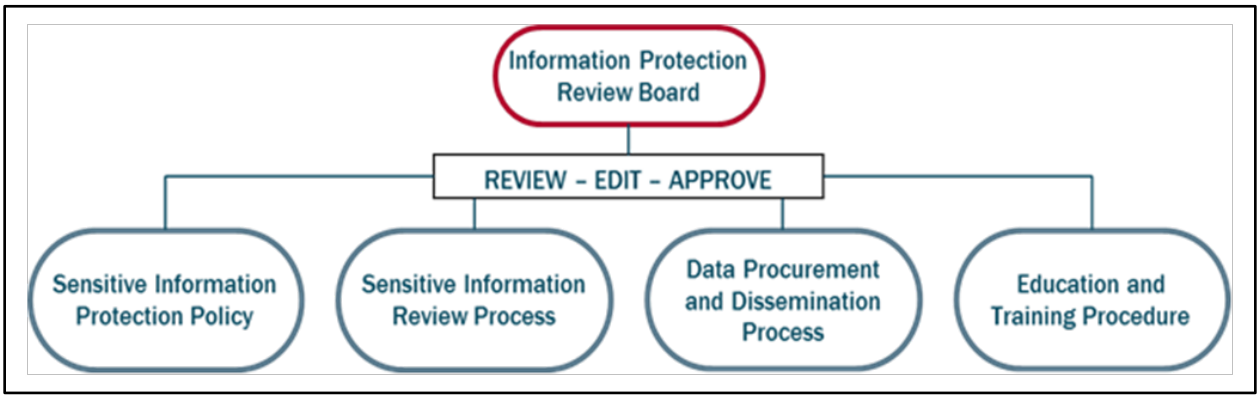

Figure 7-1: Information Protection Program organization.

7.2 INFORMATION PROTECTION PROGRAM REVIEW BOARD

The Information Protection Program Review Board is an operational board, composed of an IT expert for the development and maintenance of the secure data repositories and web-based components; a data handling expert, charged with tracking and distributing requested datasets; an SSI expert for reviewing ALERT

produced materials; and the co-chairs, the ALERT director of technology programs, and the ALERT director of operations (see Table 7-1).

All members of the board are familiar with the ALERT Center of Excellence management and research activities and have knowledge of the history of the Information Protection Program policies and procedures created and implemented under the Phase 1 ALERT award. The board reports directly to the ALERT director and meets on an annual basis to review and update the Information Protection Program policies and procedures. If necessary, the board will convene additional meetings to address emergent issues or situations that require resolution prior to the next annual meeting review date. The co-chairs are responsible for the management of the Information Protection Program and report directly to the ALERT director for this purpose.

The board is currently composed of the members listed in Table 7-1.

Last Name	First Name	Role	Institution	Title	Phone Number	Email
Beirne	Deanna	Co-Chair/ IT Expert	Northeastern University	Director of Technology Programs, ALERT	617-373-3473	d.beirne@neu.edu
Hicks	Kristin	Co-Chair	Northeastern University	Director of Operations, ALERT	617-373-5384	k.hicks@neu.edu
Potter	David	Data Expert	Northeastern University	Research Project Coordinator	617-373-5110	d.potter@neu.edu
Wittmann	Horst	SSI Expert	Retired	Former Senior Research Development Officer, NU	—	h.wittmann@neu.edu

Table 7-1: Composition of the 2019–2020 Information Protection Program Review Board.

7.3 INFORMATION PROTECTION PLAN EDUCATION PROGRAM

An Education and Training Procedure was developed to inform the ALERT community of its obligation not to generate SSI data or information and to clarify how to handle and protect SSI in the event that it is generated or obtained, intentionally or accidentally. The Education and Training Procedure also describes the Sensitive Information Protection Policy, the Sensitive Information Review Process, and the Data Procurement and Dissemination Process.

The ALERT Leadership and the Information Protection Program Review Board have developed an SSI training webinar that is provided to the ALERT principal investigators on an annual basis. These webinars include a presentation that is derived from the TSA SSI Training Module, which can be found at https://www.tsa.gov/for-industry/sensitive-security-information. ALERT chooses to use the TSA guidance and training module because SSI is a TSA-defined designation. TSA is the authority upon which ALERT has built the IPP. These webinars review the specific Sensitive Information Review Process and Data Procurement and Dissemination Process that must be followed by all ALERT principal investigators and their teams. These webinars are recorded and posted on the ALERT website so that they can be referred to regularly, and they are also reviewed by those who are unable to attend the annual presentation.

7.4 SENSITIVE INFORMATION REVIEW PROCESS

As defined in ALERT's Sensitive Information Protection Policy, all material containing information on work funded by ALERT must be reviewed for SSI content in advance of any public disclosure or submission for publication. This review process was established to ensure that sensitive information is not distributed, either intentionally or accidentally.

ALERT has established a Sensitive Information Research Evaluation and Assessment Process (REAP) for the purpose of reviewing ALERT-generated material for potential SSI content. Members of a REAP panel are approved by the ALERT center director as being capable of identifying potential SSI and classified information. Materials are reviewed by panel members on a rolling basis. Typically, materials are reviewed once per week.

ALERT project investigators (PIs) are asked to submit any materials containing ALERT funded work for REAP review at least two weeks prior to any publication submission, distribution, or presentation. Exceptions may be accommodated on a case-by-case basis by the Review Panel if the material needs to be distributed externally prior to the next scheduled review date. Due to the possibility of materials containing SSI, PIs are told not to submit files via email. PIs are asked to upload files for review via ALERT's secure online repository, formerly MyFiles and currently OneDrive.

The REAP panel members review submitted materials for potential SSI. If the REAP review finds that the material contains no potential SSI, communication is sent to the PI that the material has been approved and cleared for distribution. If the REAP review finds that the material contains content that has been identified as possible SSI, depending on the content, the reviewer either (1) provides suggested edits to the author and the author implements the change(s) or (2) finds another way of removing the SSI. In either case, the revision must be submitted for REAP review again. This process is illustrated in Figure 7-2.

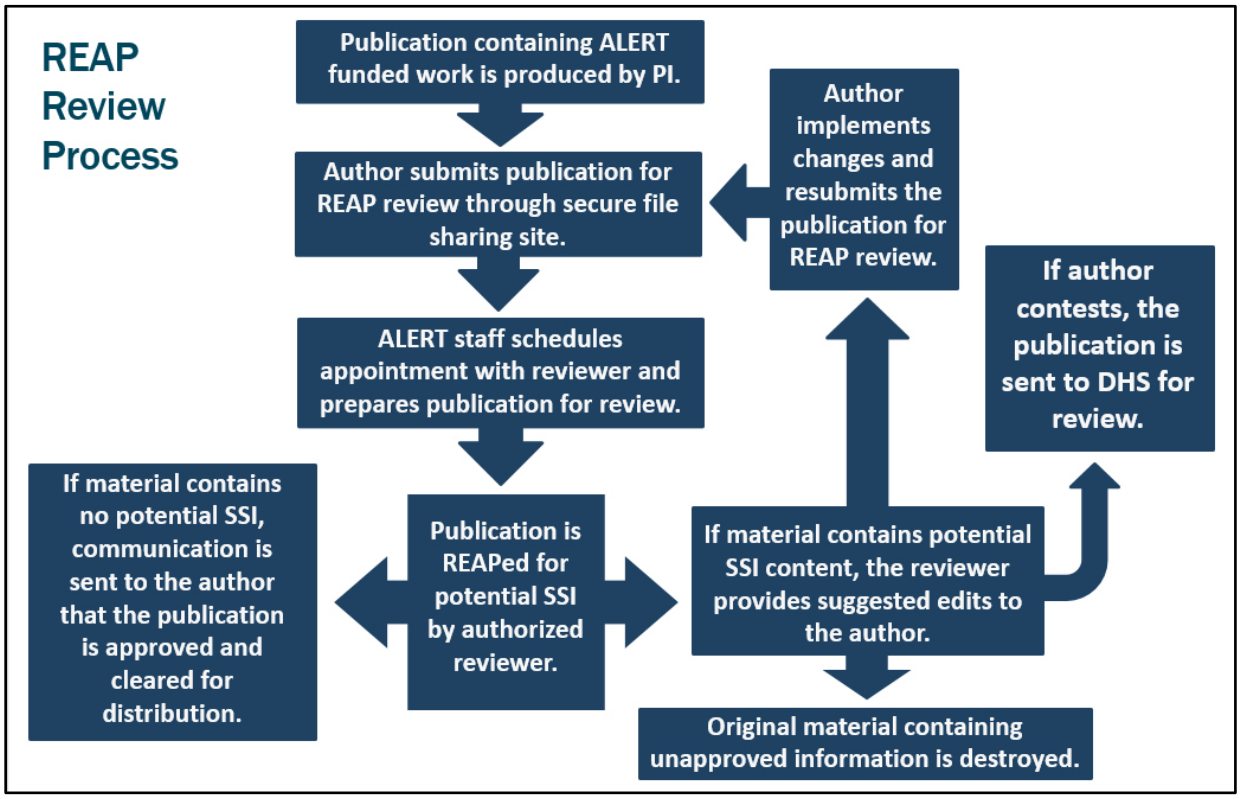

Figure 7-2: The REAP review flowchart.

If the REAP reviewer identifies content that could be possible SSI and provides recommendations or appropriate changes to the author and the author then implements the change(s), the document must be resubmitted and the modified document must be reviewed. If the material is approved as written, communication is sent and the material is then approved for distribution. The process continues until the materials submitted for REAP review do not contain SSI.

The original material containing SSI and a brief description of the process is archived, as institutional memory. The SSI materials is maintained in accord with the TSA approved methods.

7.5 DATA PROCUREMENT AND DISSEMINATION PROCESS

ALERT acquires data to support its DHS research efforts. The possibility exists that the data may be SSI. In all cases, ALERT data is treated as if it were SSI. The data acquired is documented, stored, and maintained to be ready for distribution in accordance with the TSA SSI approved process.

The Data Procurement and Dissemination Process, as illustrated in Figure 7-3, is designed to define the key steps that should be taken when ALERT Thrust leaders, principal investigators, or staff receive or distribute data that has the potential to be SSI. Data recipients must always be vigilant to:

1. Obtain, maintain, protect, and distribute data sets consistent with the required SSI REAP Process.
2. Maintain the integrity of data sets by prohibiting distribution to third parties unless properly authorized and documented; and
3. Require that any public disclosure of ALERT-managed data or its derivatives must be submitted in accordance with the ALERT REAP Process.

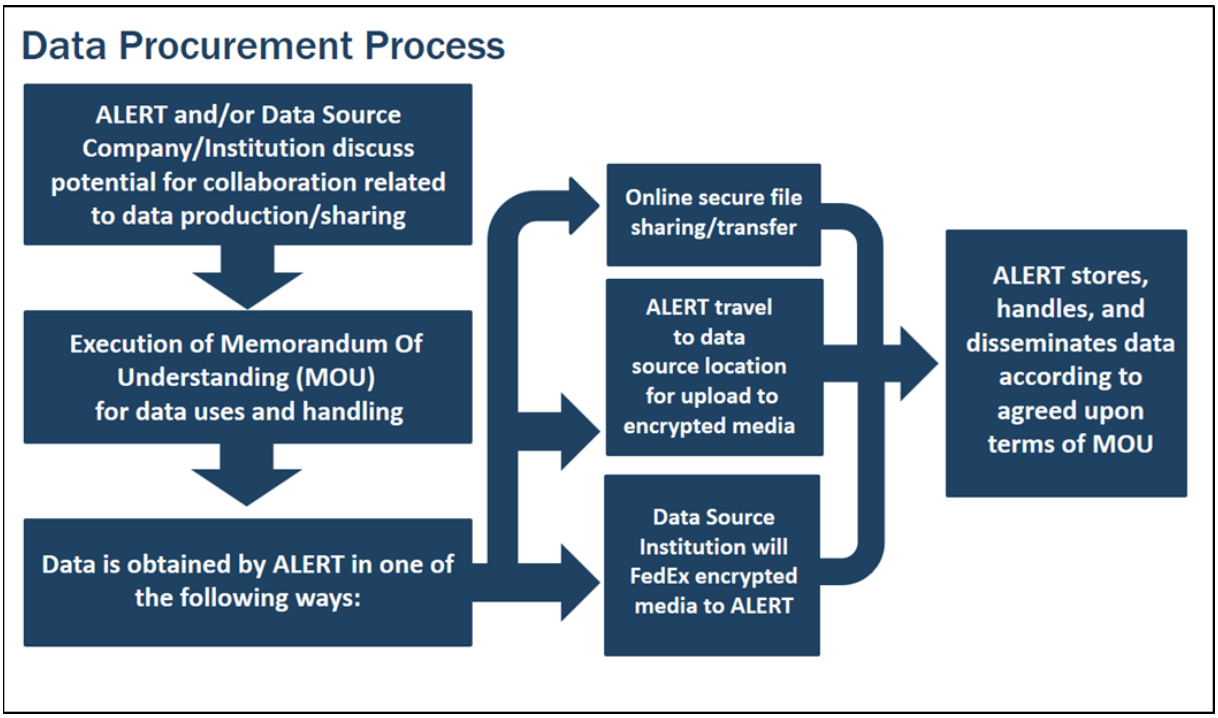

Figure 7-3: Steps involved in the data procurement and dissemination process.

Any researcher can request available non-SSI ALERT datasets using the online dataset request form. When a request is received, the requestor will be contacted via email and asked to review and sign the DHS Non-Disclosure Agreement (NDA).

When a signed NDA is received, ALERT personnel will provide access to the data requested. If the data is online, the requestor will receive instructions to access the online data repository. If it is not online, the individual will receive an encrypted external hard drive containing the data via Federal Express for tracking purposes and an email with instructions on how to decrypt the files.

ALERT treats non-SSI data with the same precautions as if it were potential SSI, so the data should be downloaded, kept, and transferred only to encrypted devices or systems with password protection.

7.6 INFORMATION PROTECTION PROGRAM ACTIVITIES

The Information Protection Program developed from an expanding need to protect data being dispersed to the research community. ALERT has developed and refined a process to procure, store, protect, and disseminate data. In summary, this is a vitally important element of the COE's mission.

ALERT received data from the security research community, including AIT whole body imaging data (X-ray and millimeter wave), and video data. These data sets were recognized as being valuable to other parties, and, as a result, ALERT created a process to release the data, under NDA, for research purposes. This data is available by request on the ALERT website. Many other data sets were the result of task orders received by ALERT from DHS. Examples include:

- CT Segmentation of Luggage Data
- Video Data from Cleveland Airport
- Imatron CT Image Volumes and Associated Information for Reconstruction
- Automatic Target Recognition Dataset
- Airport Re-Identification Dataset
- Video Data from the Kostas Homeland Security Research Institute

This page intentionally left blank.

Section 8: Industrial Liaison Initiatives and Partnerships

8.1 INTRODUCTION

The ALERT Center of Excellence (COE) has a long history of collaborating with key Department of Homeland Security (DHS) stakeholders within the security community. ALERT's desire to work with our industrial base to develop and transition research that addresses the capability gaps outlined in the strategic objectives of DHS components has been highly successful in fostering long-term university-industry partnerships. This strategy is one of the hallmarks that ensures ALERT's relevance to the DHS community.

The ALERT industrial partners provide support for the COE through membership funds, joint proposals, and career opportunities for students at partner facilities. The partners also provide access to research and development (R&D) leaders, real system-level applications, state-of-the-art hardware and software, and real applications data. Each year, for the last eleven years, ALERT demonstrates that our industry members are willing partners in technology transfer efforts, as team members on proposals for mutual funding, and as potential employers for students. Emel Bulat, the ALERT corporate and government liaison, works to find opportunities and provide resources that enable collaboration between ALERT academics, industry, and government sponsors. With this mindset, the ALERT COE brings value to its industrial partners by assisting in developing solutions for the DHS security enterprise.

This year, Kristy Provinzano left the ALERT COE and Gustavo Bottan was hired as a new addition to the team. Mr. Bottan comes to ALERT with a broad background in the security field, including both national and international experience as well as a B.S. in industrial engineering (University of Buenos Aires), specialization in chemical engineering (KTH Royal Institute of Technology), and an M.S. in management from MIT Sloan. Previously, he was vice president of business development at Passport Systems, an ALERT industrial partner from 2014–2016. As such, Mr. Bottan is familiar with DHS Science and Technology (S&T) and many of the program managers our Center is currently working with. He is a welcome addition to our Industrial Liaison Team and will assume the lead corporate and government liaison role by the end of the year. Ms. Bulat will transition to supporting the ALERT COE on task orders and special projects as needed.

Figure 8-1: ALERT Center of Excellence Industrial Liaison Team.

A. ALERT Industrial Membership

The ALERT Center's strategy of a multi-tier industrial membership continues to serve our COE, our government sponsors, and our broader security community well. This year, we added one new industrial member:

- Astrophysics Inc., founded in 2002 by imaging scientist François Zayek, has since emerged as the industry innovator. With over thirty years in imaging technology, Mr. Zayek is experienced in both the medical and security industry. Mr. Zayek is joined by a team of field-leading scientists and software developers that transform theory into cutting-edge products. With a specific focus on security X-ray

imaging and detection, Astrophysics delivers the best in technology. Astrophysics does not just manufacture X-ray systems, they develop the security technology of tomorrow.

Astrophysics has been a long-time collaborator of the ALERT COE through funding a sponsored research project focused on improving detection algorithms for their compact X-ray inspection systems. We are happy to say that they have also decided to join us as an Industrial Advisory Board member in addition to continuing the sponsored research project.

During the no-cost extension through May 2021, we will continue to look for networking opportunities and will follow up on leads to further grow our industry membership. Over its life, the Center has advanced its research in the areas of target signature detection and identification, novel sensors, image processing, advanced algorithms, and enhancements through the use of Artificial Intelligence, which has expanded the possibility for new fields of application for our technologies, databases, and expertise. One such field, for example, pertains to the protection of large venues and infrastructure. One company that has entered this market with success is Evolv Technology, based in Waltham, Massachusetts. We've initiated contact with Evolv's CEO, Peter George to explore collaborative opportunities leading to a potential membership. Based on what we have learned about their objectives, we expect to present our capabilities to them in the coming months.

We are pleased to report that all of our current members are continuing their membership.

B. Partners and Government Collaborators

ALERT's Year 7 strategic industrial and government partners include:

- **908 Devices** develops products ranging from rugged, handheld chemical detection tools to compact footprint analyzers and fast separation devices. These purpose-built and user-centric devices serve a range of industries including safety and security, oil and gas, life sciences, and other applied markets.
- **American Science & Engineering (AS&E)**, recently acquired by OSI Systems, Inc., specializes in detection technologies that can uncover dangerous and elusive threats. AS&E's X-ray inspection systems are used by governments and corporations around the world.
- **Astrophysics Inc.,** founded in 2002 by imaging scientist François Zayek, has since emerged as the industry innovator. With over thirty years in imaging technology, Mr. Zayek is experienced in both the medical and security industry. Mr. Zayek is joined by a team of field-leading scientists and software developers that transform theory into cutting-edge products. With a specific focus on security X-ray imaging and detection, Astrophysics delivers the best in technology.
- **Guardian Centers, LLC** is a disaster preparedness and tactical training center. Guardian Centers provides custom services including complete exercise design and planning, training and certification, and full service logistics support at its state-of-the-art flagship training campus in Perry, Georgia, or at any client location throughout the world. Guardian Centers demonstrates exceptional performance and results delivering specialized training courses and practical exercises for special skills certification and professional services training. They are a total solutions company dedicated to testing, evaluating, and validating skills through training and exercise in dynamic and immersive urban terrain replicating the most realistic natural and manmade disasters.
- **HXI, LLC**, a subsidiary of Renaissance Electronics & Communications, LLC, is a leading supplier of millimeter-wave products, including LNAs, power amplifiers, mixers, detectors, oscillators, switches, transmitters, receivers, and transceivers for radars, communications systems, and sensors.

- **The John Adams Innovation Institute** is the economic development division of the Massachusetts Technology Collaborative. The Innovation Institute serves as the convergence point in creating productive, collaborative partnerships between Massachusetts companies and academic research institutions to compete for business, talent, and opportunities in the global marketplace.
- **Kiernan Group Holdings** (KGH) utilizes competitive intelligence, market analysis, tailored case studies, and vast executive experience in diverse fields to provide expert insight into emerging challenges. Kiernan Group Holdings provides comprehensive access to insular markets with an insightful understanding of existing wants and needs for federal, defense, intelligence, and law enforcement communities.
- **Lawrence Livermore National Laboratory** (LLNL) is a premier research and development institution for science and technology applied to national security. They are responsible for ensuring that the nation's nuclear weapons remain safe, secure, and reliable. LLNL also applies its expertise to prevent the spread and use of weapons of mass destruction and strengthen homeland security.
- **Pacific Northwest National Laboratory** (PNNL) is one of the US Department of Energy's (DOE's) ten national laboratories, managed by DOE's Office of Science. PNNL also performs research for other DOE offices as well as government agencies, universities, and industry to deliver breakthrough science and technology to meet today's key national needs.
- **Pendar Technologies** is a privately held product development company focused on bringing to market breakthrough portable analysis and monitoring systems that include proprietary data science driven analysis modules. With experts in innovative spectroscopy and data science, the company has a pipeline of products in development. The company was formed by a merger of Pendar Medical and Eos Photonics in 2015.
- **Rapiscan Systems**, an OSI Systems Division, provides state-of-the-art security screening products, solutions, and services that meet the most demanding threat detection needs of customers worldwide, while improving operational efficiency. The technical staff at Rapiscan Laboratories, the R&D arm of Rapiscan Systems, is focused on leading edge physics, algorithm, and software-based research and development work in the detection of explosives, nuclear materials, and other contraband.
- **Raytheon Company** is a technology and innovation leader specializing in defense, security, and civil markets throughout the world. With a history of innovation spanning 91 years, Raytheon provides state-of-the-art electronics, mission systems integration, and other capabilities in the areas of sensing, effects, and command, control, communications and intelligence systems, as well as a broad range of mission support services.
- **Rigaku Analytical Devices** is a leading pioneer and innovator of handheld and portable spectroscopic analyzers for use in the protection of public health and safety, aid in the advancement of scientific and academic study, enable the recycle and reuse of metal alloys, and ensure quality of key metal alloy components in mission-critical industries. Their advanced and rugged products deliver unparalleled accuracy and extensive application support, empowering their customers to achieve rapid lab-like results any time, any place.
- **Smiths Detection** is a global leader in threat detection and screening technologies for aviation, ports and borders, urban security and military. Deploying a broad range of solutions based around X-ray imaging, computed tomography (CT), ion mobility spectrometry (IMS) and a range of other sensing technologies, we accurately detect and identify hidden weapons, explosives, narcotics, contraband and toxic industrial

chemicals. Our goal is simple- to provide the security, peace of mind, and freedom of movement upon which the world depends.

8.2 INDUSTRIAL ADVISORY BOARD AND MEMBERSHIP STRUCTURE

In 2015, as part of the membership benefits for companies, the ALERT COE formalized and restructured its Industrial Advisory Board (IAB). The IAB is a body comprised of companies that have contributed membership fees to support ALERT. Industrial members are invited to an annual IAB meeting in the fall, plus the Annual Student Pipeline Industry Roundtable Event (ASPIRE) in the spring. As discussed in the Members-only Event section below, these meetings continuously evolve to meet the expectations of our paying members. We also have a password-protected portal on our website that allows members more in-depth access to students and current activities that are not yet in the public domain.

To our knowledge, the ALERT COE is the only DHS Center that has a paying industrial membership strategy with an active IAB that interfaces regularly with its faculty, students, and government sponsors. Through ASPIRE and the IAB meetings, ALERT has created close collaboration amongst a broad industrial base, while finding the "right" match for our students and partner institutions. We seek these collaborations to allow for agile responses to future market opportunities, as well as government BAAs and RFPs, thereby fostering effective technology transfer.

To become a member and join the Industrial Advisory Board (IAB), a company has to make a membership commitment. The four levels of membership are:

1. Strategic Partner: $100K+
2. Corporate Partner: $50K
3. Associate Industrial Partner: $25K
4. Small Business Partner: $10K (reserved for companies whose yearly sales are less than $25M).

The current ALERT IAB members include:

- Corporate Partners ($50K): AS&E/Rapiscan, Raytheon
- Associate Industrial Partner ($25K): Smiths Detection
- Small Business Partner ($10K): Pendar Technologies
- Small Business Partners (in-kind): Kiernan Group Holdings; HXI, LLC; Guardian Centers, LLC; 908 Devices; Rigaku Analytical Devices

Based on the level of engagement, the industrial members have a say in how their membership fees are spent. $10K goes toward supporting the ALERT research and development infrastructure (funding the front office). For small business industrial members, this is reduced to $5K. After that, members can allocate the remainder of their membership fee as follows.

A. Member Allocations

- Targeted (nonproprietary) research ($15K or $20K increments).
- In tuition credit for an employee to participate in the Gordon Institute of Engineering Leadership (GIEL) Program and an associated master's degree at Northeastern University ($40K).

- Tuition credit for an employee to participate in the GIEL Program and an associated graduate certificate in engineering leadership at Northeastern University ($20K).
- Stipend support for one K–14 (including community college) teacher to participate in a summer Research Experiences for Teachers Program hosted by Gordon-CenSSIS and its affiliates ($10K).
- Stipend and housing support for one undergraduate (including community college) student to participate in a summer Research Experiences for Undergraduates Program hosted by Gordon-CenSSIS and its affiliates, and stipend support for one undergraduate student to participate in one semester of part-time research while in school ($10K).
- Stipend support for one high school student to participate in a summer Research for Young Scholars Program hosted by Gordon-CenSSIS and its affiliates ($5K).
- One-day, targeted seminar tailored to the industrial member's request ($5K).
- Leasing space and/or the use of the Kostas Research Institute's secure conference room facilities with encrypted video and audio feeds, subject to availability, review by the Kostas facility security officer, and validation of security clearances ($5K).
- Membership dollars to be allocated at the discretion of the ALERT director for research, education, and/or infrastructure development ($5K).

Our experience shows that having "skin in the game" incentivizes our members to work more closely with ALERT. In addition to the benefits discussed above, our industrial members have formed close ties with our faculty, resulting in joint proposal/publications and teaming opportunities.

8.3 ALERT INDUSTRIAL MEMBERSHIP BENEFITS

Becoming an ALERT industrial member comes with several important advantages. It gives companies priority access to ALERT faculty and students for hiring, joint proposal activity, and proprietary research projects. Events such as ASPIRE, the Industrial Advisory Board, and Candidate Central are available only to members and are intended to create a close, collaborative university-industry-government network. This year, due to COVID-19, all the members-only events will be virtual. As such, ALERT has decided to waive all 2020 membership fees for existing IAB members. New members are not exempt.

All industrial members enjoy the following benefits:

- Facilitation of joint proposal opportunities.
- Facilitation of the development of sponsored (proprietary) research contracts.
- Preferential access to students associated with ALERT, including undergraduate and graduate co-op assignments, internships, and fellowships (Candidate Central on website).
- Invitations to multiple members-only meetings (ASPIRE and IAB) to facilitate R&D collaborations.
- Invitations to special events (Technology Demonstration for Customs and Border Protection, Los Angeles / Long Beach Seaport)
- Free admission to ALERT Workshops: Advanced Development for Security Applications (ADSA), Customs and Border Protection Advanced Developments Encompassing Processes and Technologies (CBP-ADEPT)

A. Members-Only Events

Throughout ALERT Phase 2, the ALERT COE was praised by DHS S&T for having the strongest industrial membership base with a long history of close collaboration with industrial partners. An example of this strong collaboration with our members is the annual IAB meeting, which features a guest lecturer, in-depth faculty presentation segments, and a presentation by an industrial partner to the gathered members. We have also invited government sponsors and labs from DHS components to be part of the roundtables at our signature Annual Student Pipeline to Industry Roundtable Event (ASPIRE).

A.1. Industrial Advisory Board Meeting

ALERT held its annual IAB meeting at the Northeastern Innovation Campus's new "Building V" meeting space in Burlington, Massachusetts on November 4, 2019. In attendance were many of ALERT's industrial members, representatives from ALERT's DHS Office of University Program (OUP) customers and other DHS components, such as DHS S&T and Customs and Border Protection (CBP). For the second year in a row, it was ALERT'S highest attended IAB meeting to date, and many new relationships were established, laying the groundwork for potential future collaboration.

The agenda included welcoming remarks from Director Michael Silevitch and Ms. Emel Bulat, from ALERT, and Dr. Laura Parker and Director Matt Coats, from the Office of University Programs at DHS S&T. The day continued with the presentations as detailed below. This year, in lieu of the Industry Presentation, and in addition to a tour of the ALERT Video Analytics Laboratory, we toured Northeastern's unique indoor/outdoor Drone Facility, which was extremely well received by our industry partners. A lengthy networking reception with student posters concluded the event. Presenters included:

Figure 8-2: Dr. Len Polizzotto presented on creating value through transitioning break-through technology into the marketplace to the engaged 2019 IAB audience consisting of DHS representatives, IAB members, and faculty.

- **New-Member Introducer**: Bree Allen, president, Rigaku Analytical Devices, and François Zayek, CEO, Astrophysics, Inc.
- **Guest Presenter**: "Innovation for Impact," Leonard Polizzotto, partner, Practice of Innovation
- **Faculty Presenter**: "Zero Power Sensors," Matteo Rinaldi, Associate Professor, Department of Electrical and Computer Engineering, Northeastern University.
- **Guest Presenter**: "Intersection of Research, Innovation, Education and Training," Craig Gruber, research associate professor, Northeastern University

Due to the COVID-19 pandemic, the next IAB meeting has not been scheduled.

A.2. Annual Student Pipeline Industry Roundtable Event (ASPIRE)

Due to the COVID-19 pandemic, the ASPIRE meeting was cancelled for 2020. ALERT plans to resume the event in the Spring of 2021.

To complement ASPIRE on an ongoing basis, the Candidate Central Portal is an integral portion of the ALERT website. This supports the DHS technologies workforce pipeline by providing our partners with biographies and resumes of exceptional ALERT students and recent graduates who are interested in homeland-security jobs or internships. Candidate Central, in conjunction with ASPIRE, and the restructured IAB meeting have allowed our partners to find highly trained students to fill several internships and full-time positions.

Figure 8-3: Stefan Lukow, Director of R&D at Rapiscan Systems, hosts students for a networking roundtable at ASPIRE 2019.

A.3. Special Event: Technology Demonstration at the CBP Port of Los Angeles / Long Beach

On Thursday, November 21, 2019, the CBP Office of Field Operations at the Los Angeles / Long Beach (LA/LB) Seaport, headed by Chief Victor Todorov, hosted an all-day Technology Demonstration organized and led by ALERT industrial liaison officer, Ms. Emel Bulat. The meeting was well-attended with six members of the ALERT researchers and staff, seven industry representatives, six senior DHS personnel, and twenty-five CBP officers participating.

To kick off the meeting, Major General Robert Newman (retired), executive director for the Office of Mission and Capability Support at DHS S&T, gave welcoming remarks along with Dr. Laura Parker, program manager for DHS S&T; Mr. David Taylor, portfolio manager for DHS S&T; and Mr. Edward Morones, assistant port director at CBP. In preparation for the event, four of ALERT's industry partners, including Pendar Technologies, Rapiscan Systems, Rigaku Analytical Equipment, and Smiths Detection, prepared live demonstrations of six instruments, including handheld Raman spectroscopy units and benchtop or handheld IMS systems.

Figure 8-4: Major General Robert Newman (retired), executive director for the Office of Mission and Capability Support at DHS S&T, participated in various opioids testing experiments during the 2019 ALERT Tech Demo at the CBP LA/LB Seaport.

One week prior to the event, vendors were given a list of approximately forty compounds, mostly from a Drug Enforcement Agency list of precursors, to add to their instruments' lookup libraries for sample identification. Ten samples consisting of one to four compounds from the aforementioned list were prepared for analysis and scanned. At the end of the meeting, six "live" shipments were scanned on the warehouse floor. A team of CBP/DHS S&T/ALERT evaluators reviewed the results. The Raman spectroscopy systems performed best for the day-to-day operations of detecting large quantities of contraband and their

precursors. Pendar and Rigaku were invited back for a three-week in-depth demonstration. This event is a fantastic example of academia/industry/government working together to achieve a great outcome for all parties. As a result, CBP at the LA/LB Seaport has offered their facility as a testbed for ALERT/industry R&D. We are very pleased that our partnership with the LA/LB Seaport continues to grow stronger.

8.4 CONCLUSION

In summary, Year 7 was another productive year where the ALERT team continued to grow its membership and foster collaboration between ALERT researchers, industry/practitioners, and government partners. These partnerships are essential to achieve early engagement and effective transition of innovative science and technology into the security enterprise. ALERT's industrial liaison strategy is to listen to our members, researchers, and government sponsors; to identify opportunities to develop and mature technology through partnership; and to facilitate the building of teams that will ultimately result in successful technology transition. With this strategy, ALERT has built and maintains strong relationships with security industry stakeholders to sustain ALERT's relevance to DHS.

Section 9: Infrastructure and Evaluation

The technical challenges outlined in the ALERT program are significant. Overcoming the underlying research barriers required fundamentally new approaches. Effectively managing and evaluating the outcomes of this complex enterprise presents a challenge equal to the basic research challenges themselves. To support this effort, the ALERT management team is comprised of faculty and staff from the core partners and augmented by our partnership with national labs, companies, and government agencies. We understand that each entity within the Center must maintain its own unique charter and work environment while also striving for coherence. In this section, we first discuss the ALERT organizational structure, followed by the processes for evaluating the ALERT research, transition projects, and outcomes. Both are needed to ensure continued relevance of the Center of Excellence (COE) to the DHS mission.

9.1 MANAGEMENT APPROACH

ALERT is led by Northeastern University (NU) and is managed by experienced personnel with proven records of accomplishment. Dr. Michael Silevitch is the director of the COE. As director, he has full management responsibility, including budgeting funds, resource allocation, risk identification and mitigation, and management of progress tracking and reporting. He holds the Robert D. Black Chair in the College of Engineering at Northeastern and brings over thirty years of experience leading and managing large, multi-institution, multitask, high-stakes initiatives. He has an outstanding track record for creating effective university-industry teams oriented to address important DHS problems. In addition to his role at ALERT, Professor Silevitch is the director of the Bernard M. Gordon Center for Subsurface Sensing and Imaging Systems (Gordon-CenSSIS), a graduated National Science Foundation Engineering Research Center. The Gordon-CenSSIS focus on detecting, locating, and identifying objects hidden beneath surfaces, such as under the ground or inside the human body, is clearly linked to the mission of ALERT. Dr. Silevitch's dual leadership positions at ALERT and Gordon-CenSSIS enable the two centers to maximize their synergy and sharing of infrastructure.

Professor Carey Rappaport, Northeastern Distinguished Professor of Electrical and Computer Engineering, serves as the ALERT deputy director (as well as the R3 Thrust leader). Professor Rappaport is internationally recognized for his research contributions in the areas of electromagnetics and antenna theory, which are key disciplines of ALERT. Previously, Professor Rappaport led multiple grants, including a $5 million army demining Multidisciplinary University Research Initiatives (MURI).

The ALERT Organization Chart in Figure 9-1 shows that in addition to NU, ALERT has three key academic partners: Boston University (BU), Purdue University, and the University of Rhode Island (URI). Each of these four institutions is represented within the ALERT management structure by a faculty member who directs one of the fundamental science research thrusts: Professor Jimmie Oxley (URI), R1 Thrust lead; Professor Stephen Beaudoin (Purdue), R2 Thrust lead; Professor Carey Rappaport (NU), R3 Thrust lead; and Professor David Castañón (BU), R4 Thrust lead. All of the thrust leaders have the necessary credentials to oversee the progress of their individual programmatic responsibilities. Professors Charles DiMarzio (NU) and James Smith (URI) are the Education Program co-leads. In the area of technology transition, Emel Bulat, Kristy Provinzano, and Deanna Beirne together bring over forty years of experience in technology development. This team is responsible for the transition of ALERT R&D programs to DHS. In the domain of industry and government liaison, Emel Bulat and Kristy Provinzano focus on identifying strategic ALERT technologies for corporate development. They are responsible for fostering industrial linkages with both large and small companies.

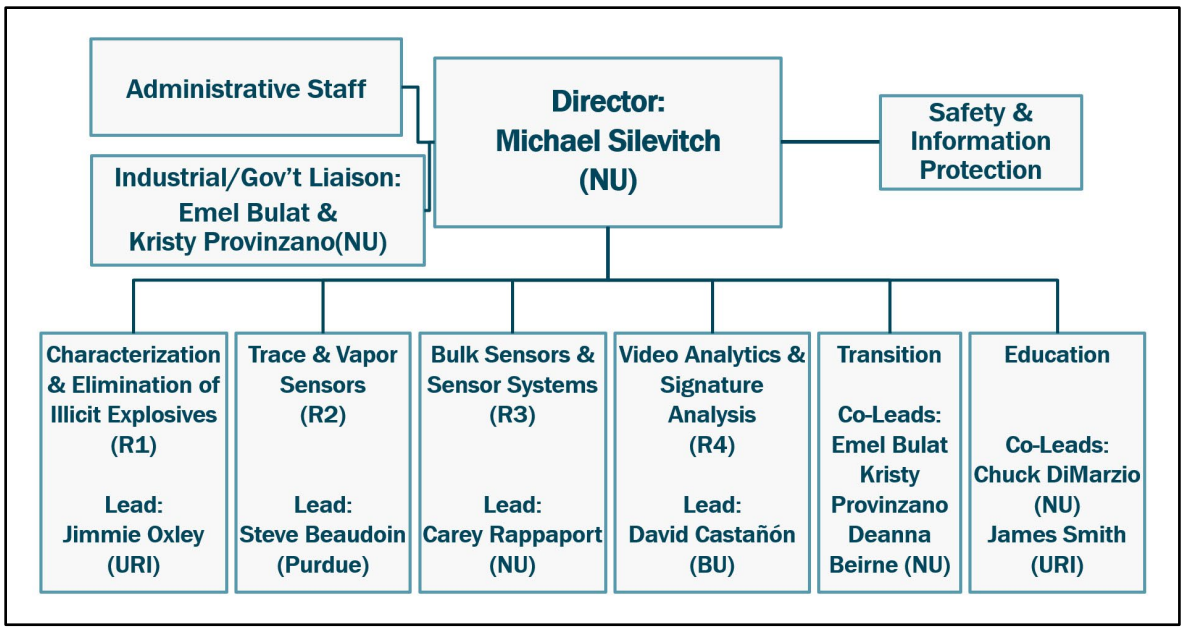

Figure 9-1: The ALERT Organization Chart enables integration of its research, transition, and education elements.

The administrative team is comprised of Kristin Hicks, director of operations; Anne Magrath, director of finance and research contracts; Diane Hubbard, senior grants administrator; Deanna Beirne, director of research computing and technology transfer; Pooja Ravichandran, software applications developer; and Tiffany Lam, events and communications specialist. This team enables ALERT to seamlessly organize and implement the multitude of events and deliverables that are inherent in the portfolio of the complex ALERT Center.

As part of the industrial/government liaison efforts, ALERT has created an Industrial Advisory Board (IAB). This body is comprised of all companies supporting the COE with membership funds that augment the funding from DHS. The IAB provides strategic guidance to the COE in areas such as new sensor developments, educational needs, and system applications. The IAB and industry membership is described in greater detail in Section 8. In addition, the ALERT Safety Review Board (SRB) is a team of outside experts employed to aid in creating appropriate overarching safety protocols. The SRB is drawn from a variety of backgrounds: academia, industry, Department of Defense, Department of Homeland Security, and Department of Energy. The ALERT SRB is described in detail in Section 6. Finally, the Information Protection Review Board is a team of NU personnel who are tasked with reviewing and administering the Information Protection Program as described in detail in Section 7.

9.2 RESEARCH EVALUATION PROCESS

The ALERT management team is actively engaged in the ongoing assessment of research relevance for both existing and potential new partnerships. Existing research efforts are evaluated as part of a cyclical review process. Input is solicited for this review from both DHS and thrust leaders, while ultimate responsibility for funding decisions lies with the Director. Figure 9-2 illustrates the project evaluation process.

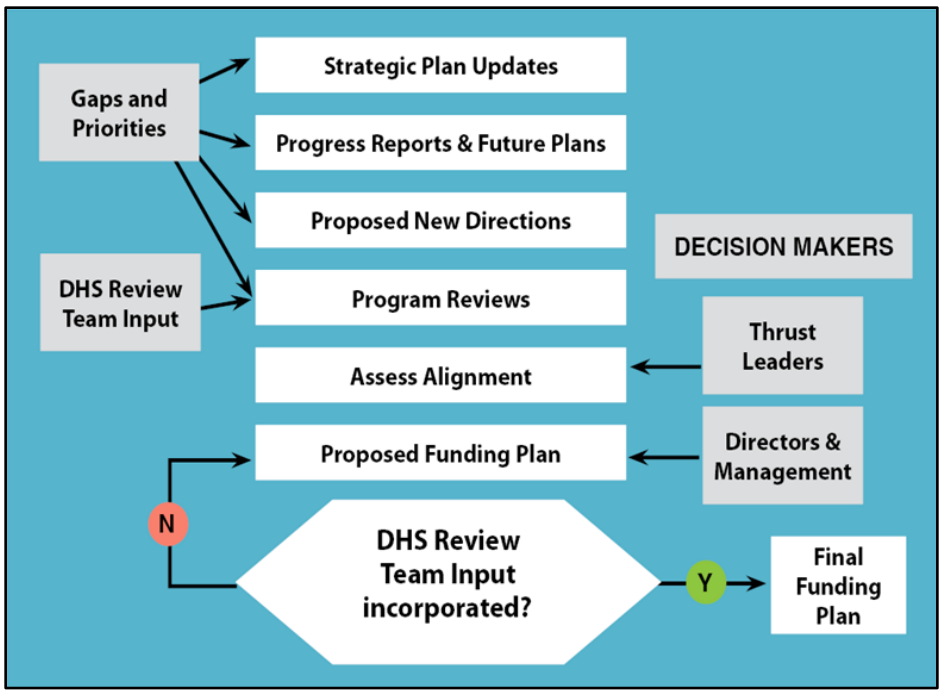

Figure 9-2: The ALERT Project Evaluation Process is aligned with COE goals and mission.

9.3 METRICS OF SUCCESS

A successful program is one that achieves its strategic goals and produces meaningful deliverables. We must keep the Grand Challenges detailed earlier as the ultimate measure of success, while we also note our related steps to success along the way. To that end, we attempt to track not just frequently cited measures such as publications or numbers of students but other measures as well. Just a few of the examples of metrics that paint a broader picture of the COE success follow:

- External accomplishments:
  1. What funding has been received as a consequence of ALERT?
  2. Which faculty and students have received awards recognizing their efforts?
- Knowledge transfer (in addition to publications):
  1. Which groups from the homeland security enterprise (HSE) are we interacting with?
  2. How are we interacting with them and positively affecting their environment?
  3. Is our work being reported in the broader media for public consumption?
- Technology transfer:
  1. How many invention disclosures and patents do we have?
  2. Has our work been incorporated into commercial prototypes or products?
- Impact on DHS:
  1. What recommendations have been made to DHS? Has DHS acted as a result?

2. How has ALERT's near-term knowledge and technology transfer influenced long-term DHS investments?

- Student impact (in addition to the number of K–12, undergraduate, and graduate students):
  1. Where do students go after graduation?
  2. Are they serving the HSE?
- Diversity:
  1. Is the center representative of the overall US population in regards to participation by women and underrepresented minorities?
  2. Are we engaging minority-serving institutions and their faculty/students?

9.4 EVALUATION OF RESEARCH AND TRANSITION/E2E OUTCOMES

The thrust leaders from the Research and Results Transition/E2E domains have the primary interaction with the individual project leaders and staff. As such, they will provide the first level of evaluation. Research thrust leaders in particular have crafted research programs after carefully reviewing research pertinent to the HSE. The thrust leader has immediate oversight of his/her research program; requests for reports coming from management or requests for publication coming from PIs will go through the thrust leader. This allows the thrust leader to continually monitor the technical quality of the projects while maintaining active communication between the project investigators. There are various opportunities to showcase the Center throughout the year, so it is expected that the thrust leaders will present their programs in a cohesive fashion. In doing so, thrust leaders can evaluate the success or failure of each project, link successful programs, and disseminate research data to the interested government or industry partners. Not only does this ensure integration of projects, but it also pinpoints areas of weakness or lack of relevance.

DHS schedules annual programs and biennial reviews, and requires annual reports and many intermittent calls for data or outcomes over a given year. Meeting these reporting deadlines gives the thrust leaders and the Director insight into weak or lagging program areas. It is difficult to use a single metric to evaluate all programs. Some research efforts involve short-term projects or fielding of off-the-shelf technology. Their success is easy to see and appreciate. Others focus on fundamental research that lays the groundwork for the next generation of sensor systems or other protection. It is our intention to maintain a healthy mix of projects ready to go to the field (see Section 4 for more on ALERT's transition efforts) and projects supporting the long-term goals of DHS. These long-term projects are also essential; otherwise, a decade from now there will be no new technologies in the pipeline nor new scientists and engineers.

More important than the success or failure of individual projects is the health of the entire program. The evaluation of each project is tied not only to its success in meeting its stated goals, but the relative importance of those goals to DHS. For example, about five years ago, a great deal of emphasis and funding was placed on terahertz spectroscopy. Research in that area has been excellent, but the technology itself has proven limited, which dictated that Center funding should be directed elsewhere. Those decisions are informed by DHS strategic analyses. However, the addition of new projects will be made with caution and consultation, since one appealing idea should not distort the entire research program. Sometimes a midcourse correction is necessary and projects need to be pruned, either for nonperformance or low relevance. That decision will be made by the director in consultation with the thrust leaders and DHS program managers, along with the benefit of outside expertise. For example, during Year 3 of the ALERT program, DHS conducted an extensive Biennial Review of the COE. A second Biennial Review was held in March 2018.

As a result of the ongoing Biennial Review process, projects were pruned and new projects were launched. Those were determined as a result of a wide dissemination of a request for white papers. The white papers were subjected to a two-stage review process to determine the most relevant new projects. The most recent Biennial review was focused on the viability of the Year 6 transition plans for each project. As a result, seven projects were pruned. The resources freed up by this action were used to intensify the transition efforts of the remaining nineteen projects in Year 7.

In summary, the ALERT Center of Excellence has developed a strong strategic base, fundamentally supported by both a meaningful vision and a mission that integrates research and education. As described in this section, this base is complemented by a strong organizational infrastructure coupled with a quantitative evaluation process. As a result, the ALERT programs will continue to evolve in response to the future technological advances needed by DHS to thwart terrorism. Going forward, using the task order mechanism and other funding opportunities, we will strive to identify potential customers and align research to their needs at an earlier stage. This will keep research relevant to DHS requirements and provide partners, collaborators, and mentors for ALERT.

This page intentionally left blank.

Section 10: Conclusion

The ALERT Center of Excellence has established a strong strategic base, supported by both a meaningful vision and a mission that integrates research and education. Over the past seven years the ALERT Phase 2 program has evolved to incorporate the needs of DHS into its three-level strategy. This approach has proven successful, as evidenced by the research and education deliverables and outcomes achieved to date. The research programs and testbeds have led to a continued emphasis and development on ways to transition basic research results to end users. ALERT educational modules are engaging students at all levels; ALERT has been able to leverage successful educational programs at Northeastern University and affiliated universities and adapt them for instruction in homeland security-related technologies.

Associated programs have also been established and broadened as a result of the Center's efforts. ALERT has continued the implementation of its Safety Program, led by a Safety Review Board (a team comprised of outside experts), to aid in creating appropriate overarching safety protocols. ALERT has also continued its Strategic Study Workshop series, creating collaborative opportunities by engaging participants from industry, national labs, vendors, government, and academia in an integrated setting where the Center acts as a "neutral broker." This is vital in the further development of a dynamic network that can foster the innovative basic research, education, and technology transition needed to help DHS in its mission to safeguard our nation.

In summary, the ALERT leadership has developed and reinforced a firm base from which it can quickly adapt to encompass new research and education priorities to address DHS needs. Beyond Year 7 and using the Basic Ordering Agreement vehicle, ALERT will move forward with its dynamically evolving three-level strategy to advance the state-of-the-art in homeland security technologies. The ALERT team is proud to be able to help DHS meet the demands of its daunting mission.

This page intentionally left blank.

APPENDIX A: Project Reports

Detailed fundamental science progress reports on each fundamental science project follow. These projects are part of "Awareness and Localization of Explosives-Related Threats," a Center of Excellence for Explosives Detection, Mitigation, and Response, and are supported by the US Department of Homeland Security under Award Number 2013-ST-061-ED0001.

This page intentionally left blank.

THRUST R1

CHARACTERIZATION & ELIMINATION OF ILLICIT EXPLOSIVES

Project Number	Project Title	Lead Investigator(s)	Other Faculty Investigator(s)
R1-A.1	Characterization of Explosives & Precursors	Jimmie Oxley Jim Smith	Gerald Kagan
R1-B.1	Metrics for Explosivity, Inerting, & Compatibility	Jimmie Oxley Jim Smith	
R1-B.2	Small-Scale Characterization of Homemade Explosives	Steven F. Son	Vasant Vuppuluri
R1-C.2	Compatibilities & Simulants: Explosive Polymer Interactions	Jimmie Oxley Jim Smith	Gerald Kagan
R1-C.3	Characterizing, Modeling, and Mitigating Texturing in X-Ray Diffraction Tomography	Joel Greenberg Anuj Kapadia	Dean Hazineh

This page intentionally left blank.

R1-A.1: Characterization of Explosives & Precursors

I. PARTICIPANTS INVOLVED FROM JULY 1, 2019 TO JUNE 30, 2020

Faculty/Staff			
Name	**Title**	**Institution**	**Email**
Jimmie Oxley	Co-PI	URI	joxley@chm.uri.edu
Jim Smith	Co-PI	URI	jsmith@chm.uri.edu
Gerald Kagan	Post-Doc	URI	gkagan@chm.uri.edu
Graduate, Undergraduate and REU Students			
Name	**Degree Pursued**	**Institution**	**Month/Year of Graduation**
Taylor Busby	PhD	URI	5/2021
Lindsay McLennan	PhD	URI	5/2020
Robert Ichiyama	PhD	URI	5/2023

II. PROJECT DESCRIPTION

A. Project Overview

This project sought to determine the physical properties, synthesis, and destruction mechanisms of improvised explosives, often called homemade explosives (HMEs). In Year 7, we performed further characterization on erythritol tetranitrate (ETN) and on the nitro-sugars mannitol and sorbitol hexanitrate and HMTD. For ETN, we examined its synthesis and sought stable isotope signatures that might allow attribution to particular groups. For the sugars we are attempting to establish basic properties and observing different polymorphs. The existence of polymorphs was also found with HMTD.

B. State of the Art and Technical Approach

Stable isotope analysis is a technique capable of determining the subtle differences between the stable isotope ratios of hydrogen ($^{2}H/^{1}H$), carbon ($^{13}C/^{12}C$), nitrogen ($^{15}N/^{14}N$), oxygen ($^{18}O/^{16}O$), and, with special modifications, sulfur ($^{34}S/^{32}S$). Stable isotope analyses are important for provenance studies, where minute differences in isotope ratios can determine production location. Stable isotope ratio mass spectrometry (IRMS) has been considered as a forensic science technique for attribution that has been applied to illicit drugs, chemical weapon agents, and recently to explosives. Now we have used IRMS to examine the signatures indicative of the method by which the homemade explosive erythritol tetranitrate (ETN) is synthesized. In an exhaustive study conducted by our lab at URI and the Netherlands Forensic Institute, we found only IRMS provided the unique signatures necessary for attribution to a particular synthetic route.[1,2] (Paper accepted in *International Journal of Forensic Science*)

The hexanitrates of the sugars mannitol and sorbitol were studied to resolve issues regarding their relative stability. During the course of preparing and characterizing these materials, a new polymorph of each was

discovered. Mannitol hexanitrate (MHN) that had been exposed to elevated temperatures exhibited a different crystal structure seen by X-ray diffraction and Raman spectroscopy, but no differences in the thermal behavior were observed. Sorbitol hexanitrate (SHN) has two distinct structures that are visibly different and that differ in structural spectra and thermal behavior. The thermal stability of these nitrate esters was also examined; despite being isomers, SHN and MHN differ in their long-term thermal stability. (Manuscript in preparation)

While exploring the synthesis pathway of HMTD, an unexpected new route for preparing HMTD was found through the reaction of formaldehyde, hydrogen peroxide, and ammonium hydroxide. The recovered HMTD was characterized by Raman spectroscopy and powder X-ray diffraction and found to be a different crystal structure. This HMTD is believed to be the result of a different confirmation of the HMTD, only previously predicted by computational methods and through the use of specialized NMR reagents. (Paper submitted, see R1-A.1 Appendix)

C. Major Contributions

- Extensive TATP characterization—safe-scent aids, gentle destruction (Years 1–4)
- The limitations of certain oxidizers in terms of terrorist use (Years 1–6)
- Baseline information about HMTD chemical properties and reactivity (Years 1–7)
- Identifying the hazards of humidity to HMTD (Years 2–3)
- Formation mechanism of HMTD initiated (Years 2–3)
- Gentle destruction methods for HMTD (Years 3–4)
- Safe-scent aids for HMTD (Years 3–4)
- Revealing modes by which peroxide explosive signature can be masked by solvent (Years 3–4)
- Canine training aids for TATP and HMTD (Years 3–4)
- Determining best practices in analyzing peroxide explosives (Years 5–6)
- An extremely reliable standard for HMTD quantification work has been developed (Year 5)
- Examination of ETN, tracking synthesis routes, and attribution (Years 6–7)
- Creating new method of “neutralizing” any small-scale (1-lb. scale) hazard SCHMOO & SCHMOO 2 (Years 6–7)
- Examination of toxicity issues for canines (Year 5) and humans (Years 6–7)
- Development of a new method for “injecting” nonvolatile explosives (e.g., chlorate) into IMS (Year 7)

D. Milestones

A major milestone was the examination of the six-carbon sugars. This study is close to complete. We expect to submit a paper by the end of the summer.

HMTD transformations required laboratory study, and that student has not been able to come into the lab due to COVID-19.

The book chapter(s) are still in progress. Cover and foreword have been submitted.

E. Final Results at Project Completion (Year 7)

Thirty-five papers on HME (TATP, HMTD, ETN, AN, UN), one full patent (safe-scent training aids), two full patents in process (SCHMOO and ADI), and one provisional patent (sheet pyrotechnics) in process.

Nine PhD, three MS, and numerous BS students have graduated, and many have entered the homeland security enterprise.

Safe-scent explosive training aids are on the market and have recently been suggested for authentication aids for TSA.

SCHMOO (Safe Control of Hazardous Materials or Others Onsite) has received a great deal of free publicity, and we expect to find a vendor for it shortly.

Ambient desorption ionization (ADI) with an additional task order from DHS S&T is being integrated into the Smiths 6000 ETD.

Explosive database has over a thousand subscribers.

It is difficult to separate these projects by project number. The basic chemical characteristic had to be established in R1-A.1 before any work could progress on other projects.

III. RELEVANCE AND TRANSITION

A. Relevance of Research to the DHS Enterprise

Characterization of HMEs is an ongoing research effort within DHS, involving vendors and associated researchers. It impacts the entire HSE. In many cases, our methods of analysis have led the way for other members of the HSE. Our studies on the extreme sensitivity of HMTD to moisture and acidity may have prevented mishandling in a number of laboratories. Many vendors of explosives detection instrumentation have requested access to the explosives database, or have asked for help in working with various materials characterized in this project. The characterization of these materials is published on our database (URI Explosives Database), which is subscribed to by over a thousand people, about a quarter of which are from US government agencies. Furthermore, our work is cited in the DHS HME Safety Protocols Handbook, and we were invited to participate in the DHS Chemical Security Analysis Center & Explosives Division 1st Inter-agency Explosives Terrorism Risk Assessment Working Group. We have worked directly with ten vendors of explosive detection instrumentation.

B. Status of Transition at Project End

Safe-scent aids have been licensed to Detectachem. ADI is moving forward with Smiths Detection. Many papers on HME are available in the open literature.

C. Transition Pathway and Future Opportunities

The ADI-Smiths project is ongoing with a task order through Northeastern.

D. Customer Connections

The connections to DHS (central), TSL, and TSA are strong. To date the FBI is the major agency outside of DHS that is aware of the details of this project.

IV. PROJECT ACCOMPLISHMENTS AND DOCUMENTATION

A. *Education and Workforce Development Activities*

1. Course, Seminar, and/or Workshop Development
   a. Since June 2019, we have held seven classes with 105 attendees. The new class was CTH.
   b. Dr. Oxley gave an invited lecture at the International Pyrotechnic Symposium in Tours, FR, summer 2019.
2. Student Internship, Job, and/or Research Opportunities
   a. Five graduate students who were supported by ALERT and graduated are now at Signature Science supporting TSL (two students), the Navy Research Lab (two students), and Los Alamos National Laboratory (one student).
3. Interactions and Outreach to K–12, Community College, and/or Minority-Serving Institution Students or Faculty
   a. We ran two two-week workshops introducing high school students to chemical analysis. This program will end with the end of ALERT.
4. Training to Professionals or Others
   a. Since June 2019 we have held seven classes with 105 attendees. The new class was CTH.

B. *Peer Reviewed Journal Articles*

1. Bezemer, K., McLennan, L., van Duin, L., Kuijpers, C.-J., Koeberg, M., van den Elshout, J., van der Heijden, A., Busby, T., Yevdokimov, A., Schoenmakers, P., Smith, J., Oxley, J., & van Asten, A. "Chemical Attribution of the Home-Made Explosive ETN—Part I: Liquid Chromatography–Mass Spectrometry Analysis of Partially Nitrated Erythritol Impurities." *Forensic Science International*, *307*(110102), December 2019. https://doi.org/10.1016/j.forsciint.2019.110102.
2. Rettinger, R.C., Porter, M., Canaria, J., Smith, J.L., & Oxley, J.C. "Fuel-Oxidizer Mixtures: A Lab and Field Study." *Journal of Energetic Materials*, *38*(2), 23 October 2019, pp. 170–190. https://doi.org/10.1080/07370652.2019.1679282.

Pending –

1. Bezemer, K., McLennan, L., van Duin, L., Kuijpers, C.-J., Koeberg, M., van den Elshout, J., van der Heijden, A., Busby, T., Yevdokimov, A., Schoenmakers, P., Smith, J., Oxley, J., & van Asten, A. "Chemical Attribution of the Home-made Explosive ETN—Part II: Use of Isotopic Ratio." *Forensic Science International*, in preparation.
2. Gonsalves, M.D., Colizza, K., Smith, J., & Oxley, J.C. "In Vitro Metabolism and Enzyme Phenotyping of Triacetone Triperoxide (TATP) in Humans." *Forensic Toxicology*, submitted June 2020.
3. McLennan, L., Smith, J., & Oxley, J. "A New Polymorph of HMTD." Manuscript in preparation.

C. *Peer Reviewed Conference Proceedings*

1. Oxley, J.C., Smith, J.L., Colizza, K., & Gonsalves, M. "In Vitro Metabolism of TATP." *NTREM*, April 2020, meeting proceedings, meeting canceled.

D. Seminars

1. Oxley, J. "Evaluation of Explosive Characteristics via Energy-Resolved MS." *ISADE*, April 2020 canceled.
2. Yevdokimov, A. "A Novel Approach to IMS Sampling and Analysis." Student Award Winner, *ISADE*, April 2020 canceled.

E. Poster Sessions

1. Gonsalves, M. "Metabolism of TATP." *ISADE*, April 2020 canceled.

F. Interviews and/or News Articles

1. CBS News. "'Innovative Checkpoint' and 'digital dog nose': TSA tests new security technology." *CBS News*, 25 November 2019. https://www.cbsnews.com/news/tsa-testing-advanced-airport-security-technology-digital-dog-nose-innovation-checkpoint/.
2. Interview by Scripps the NOW November 2019.

G. Other

1. Consulted with American Chemical Society on July 2019 script for Gunpowder & Moon Smell; January 2020 advice on Explosive Vapor Detection.

H. New and Existing Courses Developed and Student Enrollment

New or Existing	Type	Title	Description	Enrollment
Existing	Short course	Explosive Stability	Analysis & safety of explosives	3
Existing	Short course	Propellants	Propellants	12
Existing	Short course	Fundamentals of Explosives	Fundamentals of explosives	26
Existing	Short course	Explosive Components	Device design	17
Existing	Short course	Explosive Components	Device design	17
Existing	Short course	Dynamic Diagnostics	Instrumentation & analysis	17
New	Short course	CTH for China Lake	Sandia computer code	13

I. Technology Transfer/Patents

1. Patent Applications Filed (Including Provisional Patents)
   a. Oxley, J.C., Smith, J.L., Yevdokimav, A.V., & Colizza, K. "Apparatus and Methods for Explosive Trace Detection Sample Preparation and Introduction into an Ionizing Detection System." Provisional Patent 62/816,253, 11 March, 2019.
   b. Oxley, J.C., Smith, J.L, Ichiyama, R., & Kagan, G. "Safe Control of Hazardous Materials or Others Onsite." US 62/837,520, April 2019
   c. Oxley, J.C., Smith, J.L., Kominia, A., Busby, T., & Stubbs, V. "Plasticized Flexible Pyrotechnic Material and Methods of Using the Same." Provisional Patent 62/993,992, 24 April 2020.

J. Requests for Assistance/Advice

1. From DHS
    a. Oxley is part of the DHS-formed Inter-Agency Explosive Terrorism Risk Assessment Working Group (IExTRAWG).
    b. On call for a variety of TSA TSS-E personnel.
2. From Federal/State/Local Government
    a. The URI bomb dog and his trainer rely on our lab for advice and explosives.

R1-A.1. APPENDIX

This page intentionally left blank.

A New Polymorph of HMTD

Lindsay McLennan, James L. Smith, and Jimmie C. Oxley*

Chemistry Department
University of Rhode Island
Kingston, RI 02881
Phone: 401-874-2103
Email: joxley@chm.uri.edu

ABSTRACT

While exploring the synthesis pathway of HMTD, an unexpected new polymorph of HMTD was found. Both Raman spectroscopy and powder x-ray diffraction support a different crystal structure. This HMTD is believed to be the result of a different confirmation of the HMTD, only previously predicted by computational methods and through the use of specialized NMR reagents.

1 INTRODUCTION

Hexamethylene triperoxide diamine (HMTD) is a peroxide-based explosive that was first synthesized in 1885 by the German chemist Legler. Its structure was proposed in 1900, but not confirmed by X-ray analysis until 1985 [1-3]. HMTD is an amine peroxide compound with bridgehead nitrogens that lie nearly planar. Combined with ring strain, planar nitrogens may contribute to the overall sensitivity of HMTD. Yet, even though it is considered one of the more sensitive peroxide molecules, it still is used by terrorists; most recently in the 2016 NY/NY pipe bomb incident [4]. Its simple synthesis from hexamine, hydrogen peroxide, and a weak acid such as citric acid, has made HMTD the focus of several research groups [5-8].

Like HMTD, triacetone triperoxide (TATP) is a cyclic organic that contains three peroxide functionalities. Both have been studied due to their use as a homemade explosive (Figure 1). In TATP the peroxide bonds in the cage compound can adopt two conformations, the "twist-boat-chair" confirmation (D_3) and "twist-chair-chair" confirmation (C_2) [9,10]. The barrier for the conversion from C_2 to the stable D_3 conformer is reported at 24 kcal/mol, supporting that the two conformers coexist in solution and are separable by chromatography methods [9-11]. Additionally, TATP is found to exhibit polymorphism beyond the crystal structures of the D_3 and C_2 conformers through the use of different acid catalysts or recrystallization solvents [12,13]. HMTD has been isolated as only the D_3 conformer [14]. The first crystal structure of HMTD was proposed by Schaefer et al. in 1985, where they found that the bridgehead nitrogens adopted a relatively planar geometry [1]. Shortly after, the infrared, Raman, and NMR spectra of HMTD were published [15]. Assignments of IR and Raman peaks were in good agreement with HMTD having D_3 symmetry. The ^1H NMR of HMTD in the same work showed that HMTD retains D_3 molecular symmetry in solution, and no other conformers were observed. Wierbizcki et al. sought to explain the interesting geometry of HMTD through density functional theory studies and additional X-ray techniques [16,17]. Initially, they performed their calculations without symmetry constraints but imposed the D_3 symmetry after additional X-ray analysis. In 2006, Guo et al. examined the helical chirality in HMTD via the use chiral shift agents [14]. The authors were able to observe the C_2 conformer via ^1H and ^{13}C NMR.

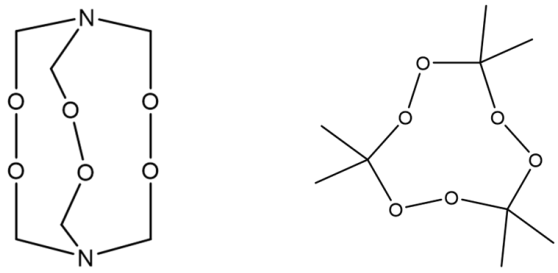

Figure 1. Hexamethylene triperoxide diamine (HMTD, left) and triacetone triperoxide (TATP, right)

2 EXPERIMENTAL SECTION

Warning: HMTD is a sensitive peroxide explosive and should only be synthesized and handled by trained personnel.

2.1 Synthesis of Hexamethylene triperoxide diamine (HMTD, Form I)

In a 50 mL round bottom flask, hexamine (2.43 g, 17.3 mmol) was slowly added to stirring chilled 50wt% hydrogen peroxide (9.87 g, 145 mmol). Once hexamine dissolved, 3.61 g (18.8 mmol) of anhydrous citric acid was added portion-wise. The reaction flask was covered with Parafilm and left in the ice bath to warm overnight. After 14 to 18 hours, the white precipitate was collected by filtration and rinsed with 600 mL of deionized water, followed by 200 mL of room temperature methanol [1]. Clumps were gently broken on the filter paper to prevent caking and allowed to dry under vacuum for at least 30 minutes (2.3 grams, 64% yield). The final powder was stored at -20°C until use.

2.2 Synthesis of HMTD polymorph (Form II)

In a 25 mL round bottom flask, 37% formaldehyde (5 mL, 67.1 mmol) was mixed with 50wt% hydrogen peroxide (2.48 g, 36.5 mmol) for 1 hr. The reaction mixture was then cooled via ice bath and concentrated ammonium hydroxide was added dropwise to slow the temperature increase (0.5 mL, 7.4 mmol) [2,3]. The reaction was left to warm overnight. The white precipitate was collected by vacuum filtration, rinsed with 300 mL deionized water and 100 mL room temperature methanol. The white solid was dried under vacuum for a minimum of 30 minutes and stored at -20°C until use (0.15 g, 20% yield).

2.3 Instrumentation

Raman spectra were obtained with an Ondax 785 nm laser and an Andor Shamrock 500i-D2-R spectrometer using a 1200 lines/mm grating. Unless noted, spectra were obtained five 5-second accumulations over the full range. Infrared (IR) spectra were collected on a Nicolet 6700 FT-IR at 4 cm^{-1} resolution and an average of 32 scans. Powder X-ray diffraction (XRD) spectra were collected on a Rigaku MiniFlex600 benchtop powder x-ray diffractometer. Differential scanning calorimetry (DSC) was done on a TA Q100 DSC (New Castle, DE, USA). Samples (150-250 µg) were sealed in aluminum hermetic pans and run in duplicate at 10 °C/min. NMR spectra were collected on a Bruker Ascend 400 MHz spectrometer.

3 Results and Discussion

TATP has two common conformers (C_2 and D_3); D_3 is the most stable conformer, but depending on reaction conditions (acid strength, recrystallization solvent, etc.) the ratio of the two conformers may vary in a given sample [12]. While studying the synthesis pathway of HMTD, an unexpected precipitate from a reaction mixture containing formaldehyde, hydrogen peroxide, and ammonium hydroxide was observed. ^1H NMR analysis of a d6-DSMO solution of this material confirmed that it was HMTD (Figure 2) [14]. DSC analysis

revealed that the two forms behave similarly; a single sharp peak for the exothermic decomposition of HMTD at 162°C and the absence of a melting point (Figure 3).

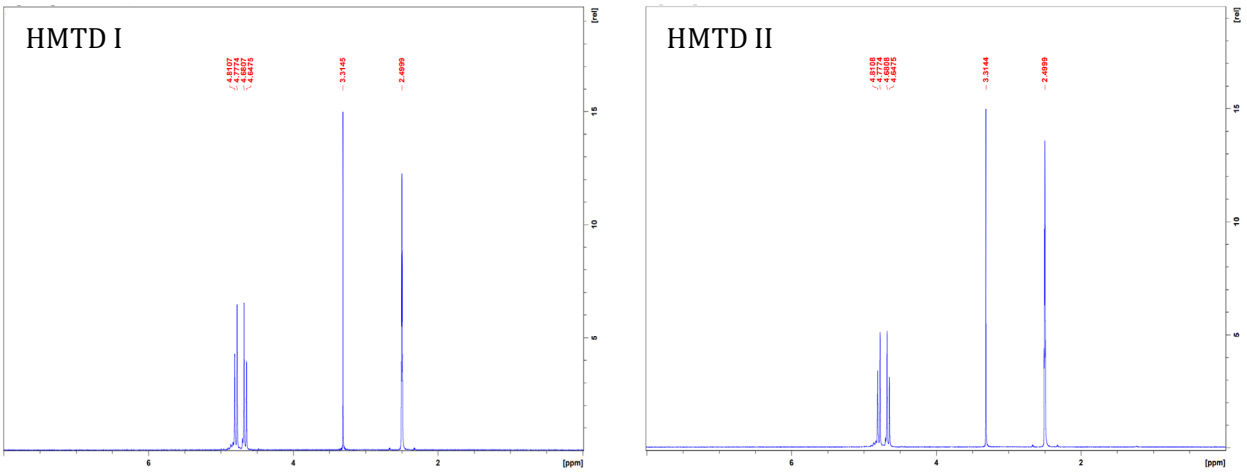

Figure 2. ^{1}H NMR of standard HMTD I (left) and HMTD II (right)

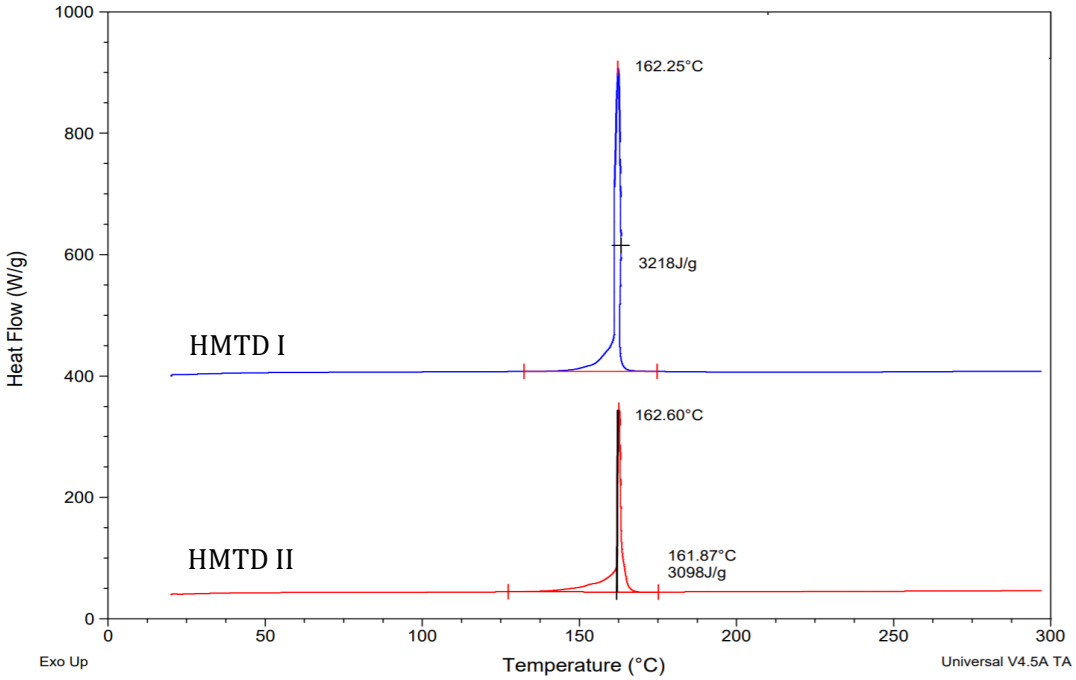

Figure 3. DSC of HMTD I (top) and HMTD II (bottom)

Structural analysis of the solid HMTDs suggested that there was a difference between the two solids. Powder XRD analysis (Figure 4) showed differences in the structure between the two solids. A major difference between the two patterns is the more complex spectra in the 10-20 degree 2-θ. Over multiple samples of suspected HMTD II, the peak locations matched, suggesting that the differences were not a factor of preferred orientation.

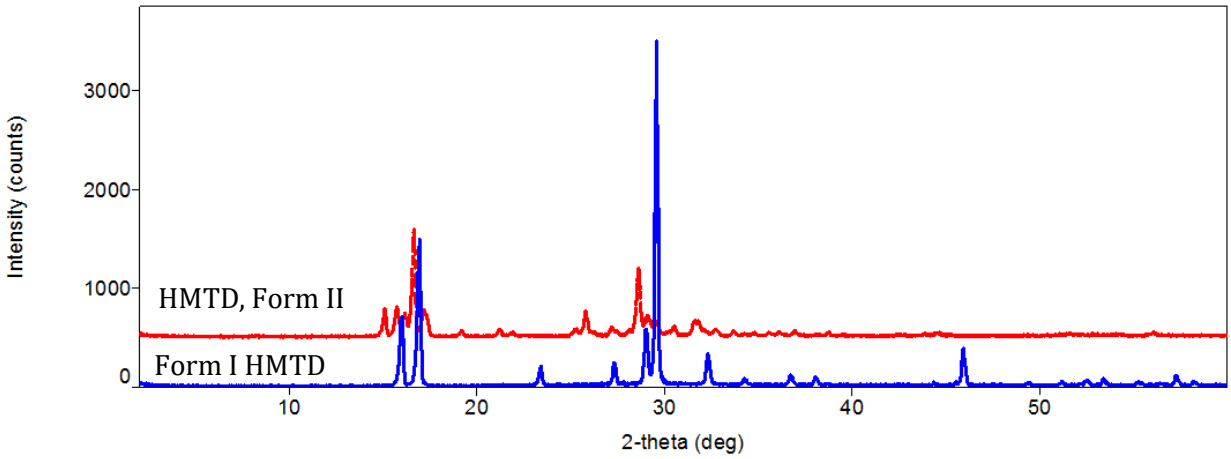

Figure 4. Powder XRD of HMTD I (solid line, bottom) and HMTD II (dashed line, top)

The Raman spectra of both forms of HMTD are relatively similar but differ in some key regions. The low wavenumber region of the Raman spectrum (often referred to as the THz Raman region) often contains vibrations that correspond to the movement of the entire molecular structure. Differences in Raman spectra in this region may be used to discriminate between different polymorphs of materials [18] and Figure 4 indicates several distinguishable differences. The THz region of Form II HMTD contains additional peaks, as well as some apparent shifting of peaks from those in HMTD I. Additional peaks in this region may indicate that there are different crystal structure interactions occurring in HMTD II.

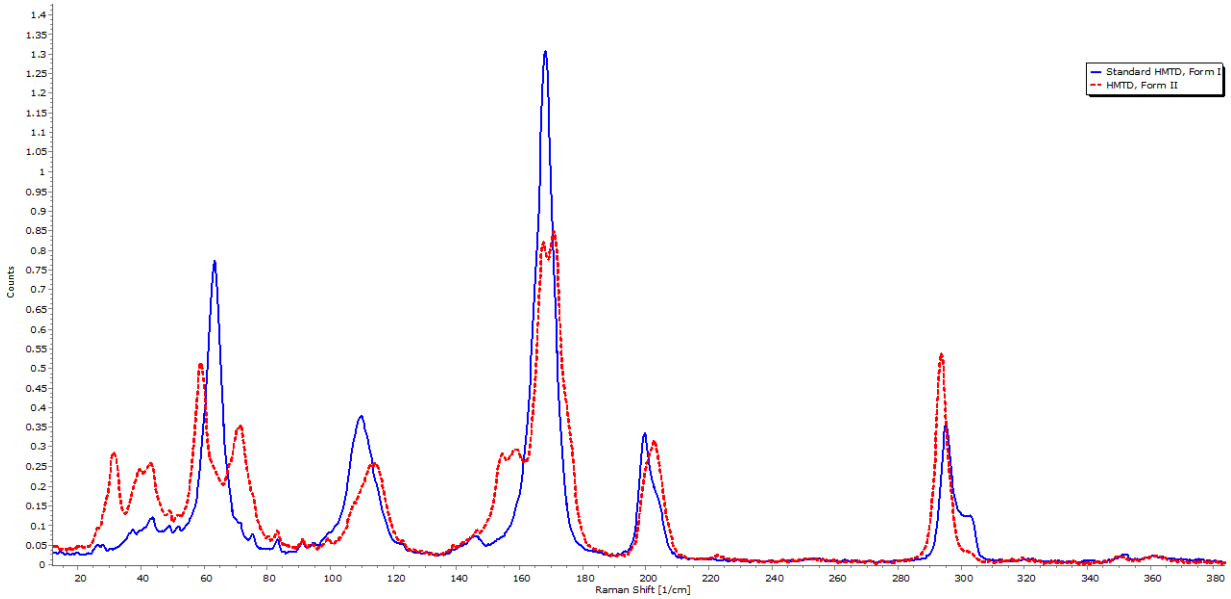

Figure 5. Low-wavenumber region of HMTD I (solid line) and HMTD II (dashed line)

In the fingerprint region of the HMTD spectra, assignments to vibrational modes have previously been made [15,19,20]. Only slight differences are seen here between the two forms of HMTD (Figure 6). In the middle of the spectral window, around 770 cm^{-1}, is the characteristic O-O stretch. The splitting of this peak may be attributed one of the three peroxide bonds having a different orientation, as is suggested by calculations for the C_2 conformer [14]. In the 1300-1500 cm^{-1} region, where CH_2 motions, e.g. CH_2 twist, wag, and scissor are observed, there are changes which support the theory that at least one of the peroxide arms in the HMTD molecule is in a different orientation.

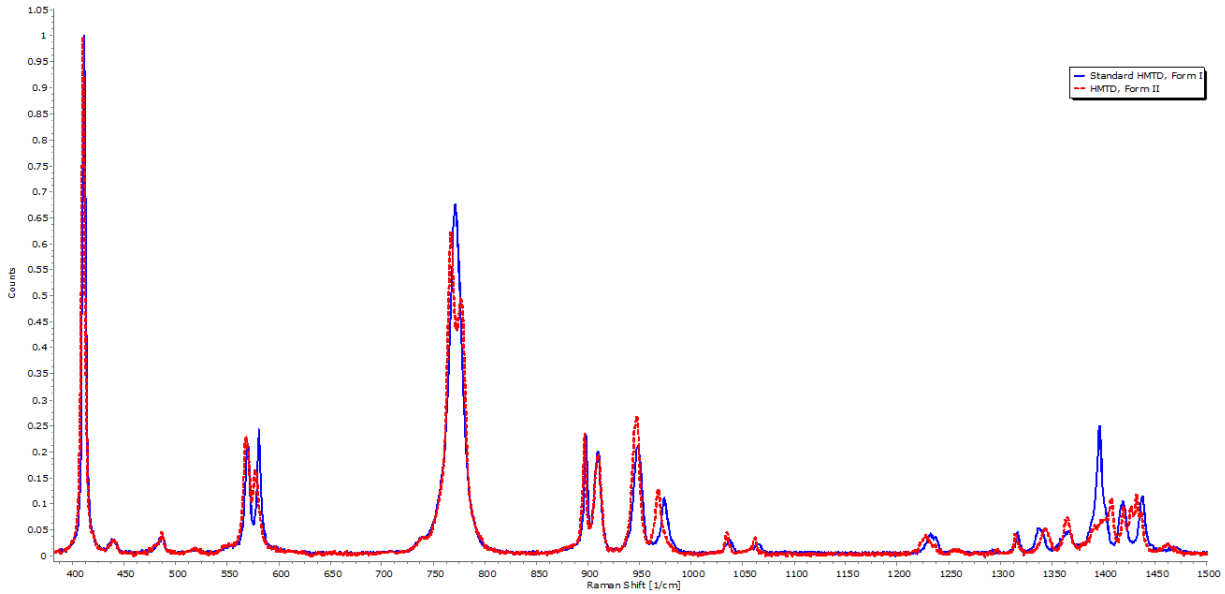

Figure 6. Mid-wavenumber region of HMTD I (solid line) and HMTD II (dashed line)

There are also differences in the high-wavenumber region of the HMTD spectra. Normal HMTD has symmetric (2917 and 2930 cm^{-1}) and asymmetric (2963 and 2976 cm^{-1}) C – H stretches. Though hardly resolved under these conditions, it is still clear that there are changes to both the symmetric and asymmetric C – H stretches in the new HMTD polymorph (Figure 7).

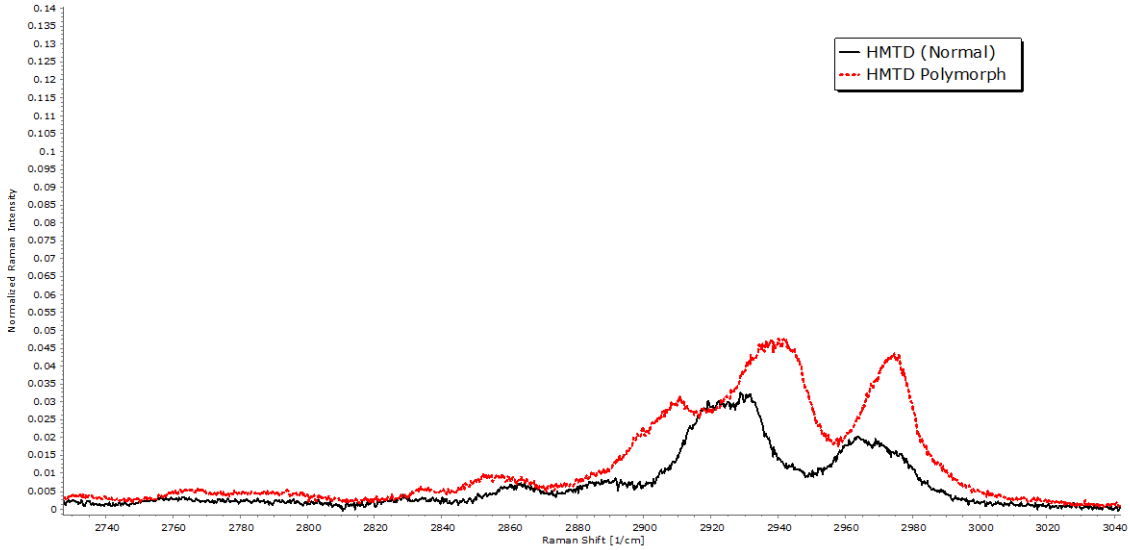

Figure 7. High-wavenumber region of HMTD I (solid line) and HMTD II (dashed line)

The infrared spectra of HMTD I and HMTD II also supports structural differences (Figure 8). There are shifts in the fingerprint region of HMTD II to higher frequencies, specifically in the transitions that correspond to C-O stretching modes [19,21,22]. The slight blue shift of these modes suggests that there are different, if not new, interactions in HMTD II.

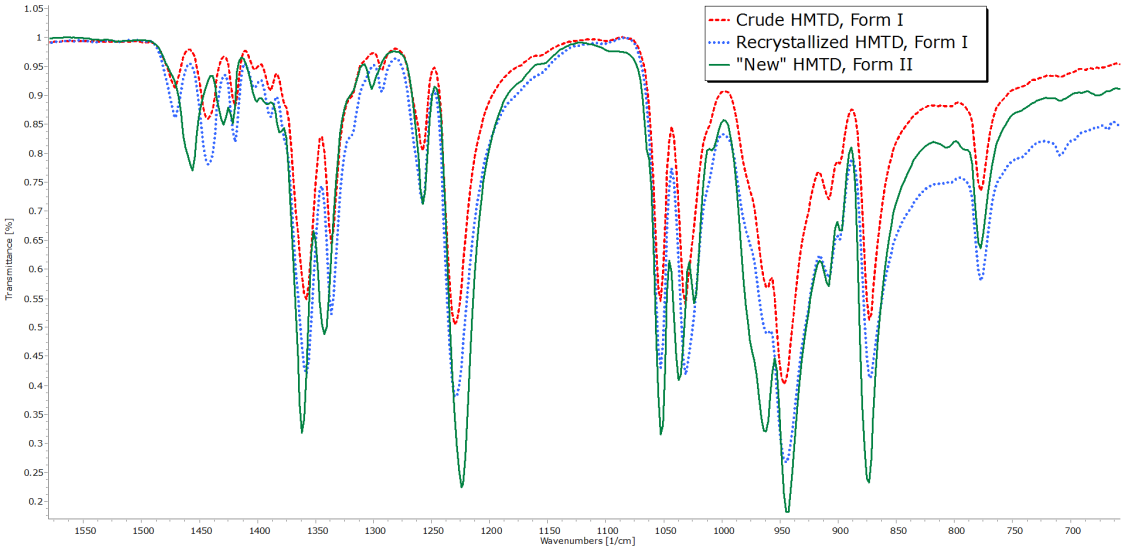

Figure 8. IR spectra of HMTD I (dotted, dashed lines) and HMTD II (solid)

HMTD synthesis requires an acid catalyst (often citric acid) for the reaction to optimally proceed, however, HMTD will form in the absence of acid after 5-7 days [8]. Ammonium hydroxide was used as the source of the nitrogen in the reaction. Several sources of ammonium were tested with hydrogen peroxide and formaldehyde to determine if any HMTD formed. The results are summarized in Table 1 below. Under the reaction conditions, even hexamine was able to form HMTD in appreciable amounts without the addition of acid. The greater than 100% yield is a factor of assuming a 1:1 ratio of hexamine to HMTD; the addition of formaldehyde provides extra carbon into the system to generate more product. When the ammonium salt anion is a weak acid/weak base, no HMTD formation was observed. The reaction mixtures were tested with pH paper prior to disposal; in cases where HMTD was not formed, the reaction mixture was very acidic. This is likely due to the formation of formic acid from the decomposition reaction of hydrogen peroxide and formaldehyde [23]. When the ammonium counterion was more basic, HMTD formation was seen, and as with the ammonium hydroxide, the recovered HMTD was HMTD II.

That these basic ammonium salts can form HMTD at all is surprising. The reaction has an increased danger during synthesis due to the incompatibility of bases and peroxides. The temperature of the reaction must be monitored; the decomposition reaction can generate enough heat to rapidly boil the reactants. Espinosa-Fuentes et al. found that the use of strong acids to prepare TATP led to the C_2 conformer and postulated that the energy release associated with strong acids in the system may give way to products of higher energy [24]. A similar phenomenon may occur with preparing HMTD under basic conditions.

Table 1. Summary of HMTD synthesis from hydrogen peroxide and formaldehyde using alternative nitrogen sources

Ammonium Salt/Nitrogen Source		% Yield*	Comments/Observations
Hexamine	$C_6H_{12}N_4$	105**	HMTD I formed
Ammonium acetate	$NH_4C_2H_3O_2$	34.6	HMTD I formed
Ammonium sulfate	$(NH_4)_2SO_4$	0	No HMTD formed, pH ~3
Ammonium chloride	NH_4Cl	0	No HMTD formed, pH ~1-2
Ammonium nitrate	NH_4NO_3	0	No HMTD formed, pH ~1-2
Ammonium hydroxide (28%)	NH_4OH	44.0	HMTD II formed
Ammonium carbonate	$(NH_4)_2CO_3$	28.4	HMTD II formed
Ammonium bicarbonate	NH_4HCO_3	43.2	HMTD II formed
Monoammonium phosphate	$(NH_4)H_2PO_4$	0	No HMTD formed
Diammonium phosphate	$(NH_4)_2HPO_4$	10.3	HMTD I formed

*% yield based off 500 mg theoretical yield (assuming 2 N to 1 HMTD)
**Assumed a 1:1 hexamine to HMTD ratio

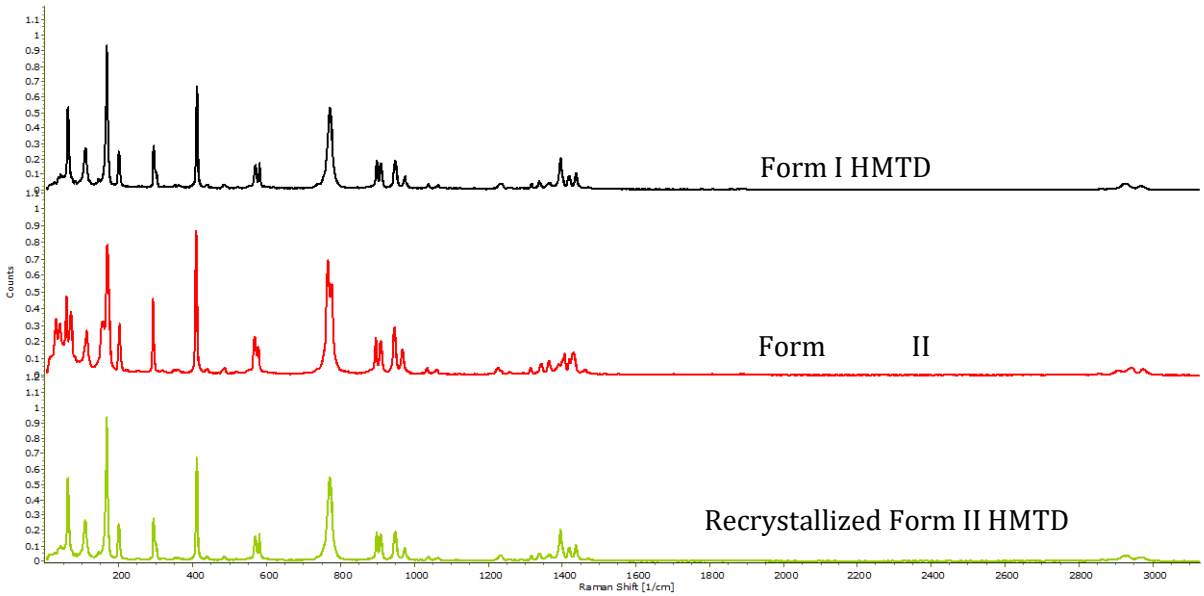

Figure 9. Comparison of Form I HMTD, Form II HMTD, and recrystallized Form II HMTD

Obtaining a crystal suitable in size for single crystal x-ray analysis was difficult. Altering the synthetic procedure to promote larger particle size only resulted in the normal HMTD structure. Different recrystallization solvents were also tried, to no success. In Figure 9, the Raman spectrum of a recrystallization of HMTD with acetonitrile is shown. After dissolving and reprecipitating out, the HMTD recovered was the standard Form I HMTD. Apparently, in solution, HMTD reverts to the stable D_3 conformer. Despite being stored at -20°C, the HTMD polymorph will convert to normal HMTD on extended storage.

4 CONCLUSION

Though only predicted and observed through the use of chiral shift reagents in ^{1}H and ^{13}C NMR, it was thought that HMTD had a C_2 conformer in addition to the easily prepared D_3 conformer. While studying a reaction mixture of formaldehyde, hydrogen peroxide, and ammonium hydroxide, a precipitate was

collected. The precipitate was determined to be HMTD, and subsequent structural analysis through XRD and Raman techniques suggested a new crystal structure of HMTD. Without single crystal XRD it can only be hypothesized that the new crystal structure is the result of HMTD adopting a higher energy confirmation in the C_2 form.

5 ACKNOWLEDGMENTS

This material is based upon work supported by U.S. Department of Homeland Security (DHS), Science & Technology Directorate, Office of University Programs, under Grant 2013-ST-061-ED0001. Views and conclusions are those of the authors and should not be interpreted as necessarily representing the official policies, either expressed or implied, of DHS.

REFERENCES

[1] Schaefer, W. P.; Fourkas, J. T.; Tiemann, B. G., Structure of hexamethylene triperoxide diamine. *J. Am. Chem. Soc.* **1985,** *107* (8), 2461-2463.
[2] Legler, L., Ueber Producte der langsamen Verbrennung des Aethyläthers. *Ber. Dtsch. Chem. Ges.* **1885,** *18* (2), 3343-3351.
[3] Baeyer, A.; Villiger, V., Ueber die Nomenclatur der Superoxyde und die Superoxyde der Aldehyde. *Ber. Dtsch. Chem. Ges.* **1900,** *33* (2), 2479-2487.
[4] Santora, M.; Rashbaum, W. K.; Goldman, A. Ahmad Khan Rahami Is Arrested in Manhattan and New Jersey Bombings. (accessed 14 February 2018).
[5] Simon, A. G.; DeGreeff, L. E., Variation in the headspace of bulk hexamethylene triperoxide diamine (HMTD): Part II. Analysis of non-detonable canine training aids. *Forensic Chem.* **2019,** *13*, 100155.
[6] DeGreeff, L. E.; Cerreta, M. M.; Katilie, C. J., Variation in the headspace of bulk hexamethylene triperoxide diamine (HMTD) with time, environment, and formulation. *Forensic Chem.* **2017,** *4*, 41-50.
[7] Steinkamp, F. L.; DeGreeff, L. E.; Collins, G. E.; Rose-Pehrsson, S. L., Factors affecting the intramolecular decomposition of hexamethylene triperoxide diamine and implications for detection. *J. Chromatogr. A* **2016,** *1451*, 83-90.
[8] Oxley, J. C.; Smith, J. L.; Porter, M.; McLennan, L.; Colizza, K.; Zeiri, Y.; Kosloff, R.; Dubnikova, F., Synthesis and Degradation of Hexamethylene Triperoxide Diamine (HMTD). *Propellants Explos. Pyrotech.* **2016,** *41* (2), 334-350.
[9] Denekamp, C.; Gottlieb, L.; Tamiri, T.; Tsoglin, A.; Shilav, R.; Kapon, M., Two Separable Conformers of TATP and Analogues Exist at Room Temperature. *Org. Lett.* **2005,** *7* (12), 2461-2464.
[10] Widmer, L.; Watson, S.; Schlatter, K.; Crowson, A., Development of an LC/MS method for the trace analysis of triacetone triperoxide (TATP). *Analyst* **2002,** *127* (12), 1627-1632.
[11] Haroune, N.; Crowson, A.; Campbell, B., Characterisation of triacetone triperoxide (TATP) conformers using LC-NMR. *Sci. Justice.* **2011,** *51* (2), 50-56.
[12] Reany, O.; Kapon, M.; Botoshansky, M.; Keinan, E., Rich Polymorphism in Triacetone-Triperoxide. *Cryst. Growth Des.* **2009,** *9* (8), 3661-3670.
[13] Peterson, G. R.; Bassett, W. P.; Weeks, B. L.; Hope-Weeks, L. J., Phase Pure Triacetone Triperoxide: The Influence of Ionic Strength, Oxidant Source, and Acid Catalyst. *Cryst. Growth Des.* **2013,** *13* (6), 2307-2311.
[14] Guo, C.; Persons, J.; Harbison, G. S., Helical chirality in hexamethylene triperoxide diamine. *Magn. Reson. Chem.* **2006,** *44* (9), 832-837.
[15] Sülzle, D.; Klaeboe, P.; S. B. Grace, D.; Hopf, H.; Lehrich, F.; J. Nielsen, C.; L. Powell, D.; Trætteberg, M., The Infrared, Raman and NMR Spectra of Hexamethylene Triperoxide Diamine. *Acta Chem. Scand.* **1988,** *42a*, 165-170.
[16] Wierzbicki, A.; Cioffi, E., Density Functional Theory Studies of Hexamethylene Triperoxide Diamine. *J. Phys. Chem. A* **1999,** *103* (44), 8890-8894.
[17] Wierzbicki, A.; Salter, E. A.; Cioffi, E. A.; Stevens, E. D., Density Functional Theory and X-ray Investigations of P- and M-Hexamethylene Triperoxide Diamine and Its Dialdehyde Derivative. *J. Phys. Chem. A* **2001,** *105* (38), 8763-8768.
[18] Roy, S.; Chamberlin, B.; Matzger, A. J., Polymorph Discrimination Using Low Wavenumber Raman Spectroscopy. *Org. Process Res. Dev.* **2013,** *17* (7), 976-980.

[19] Oxley, J.; Smith, J.; Brady, J.; Dubnikova, F.; Kosloff, R.; Zeiri, L.; Zeiri, Y., Raman and infrared fingerprint spectroscopy of peroxide-based explosives. *Appl. Spectrosc.* **2008,** *62* (8), 906-915.
[20] Leigh, B. S.; Monson, K. L.; Kim, J. E., Visible and UV resonance Raman spectroscopy of the peroxide-based explosive HMTD and its photoproducts. *Forensic Chem.* **2016,** *2*, 22-28.
[21] Schulte-Ladbeck, R.; Edelmann, A.; Quintás, G.; Lendl, B.; Karst, U., Determination of Peroxide-Based Explosives Using Liquid Chromatography with On-Line Infrared Detection. *Anal. Chem.* **2006,** *78* (23), 8150-8155.
[22] Pena-Quevedo, A. J.; Figueroa, J.; Rodriguez, N.; Nieves, D.; Hernandez, N.; Rivera, R.; Mina, N.; Hernandez-Rivera, S. P., Effect of water and common salts on the vibrational spectra of high energy cyclic organic peroxides. *Proc. SPIE-Int. Soc. Opt. Eng.* **2006,** *6201* (Sensors, and Command, Control, Communications, and Intelligence (C31) Technologies for Homeland Security and Homeland Defense V), 62012D/1-62012D/11.
[23] Satterfield, C. N.; Wilson, R. E.; LeClair, R. M.; Reid, R. C., Analysis of Aqueous Mixtures of Hydrogen Peroxide and Aldehydes. *Anal. Chem.* **1954,** *26* (11), 1792-1797.
[24] Espinosa-Fuentes, E.; Colpas-Castillo, F.; Meza-Fuentes, E.; Ropero, J., An Easy Method to Prepare D3 and C2-TATP Crystals. *Propellants Explos. Pyrotech.* **2016,** *41* (4), 713-718.

This page intentionally left blank.

R1-B.1: Metrics for Explosivity, Inerting, & Compatibility

I. PARTICIPANTS INVOLVED FROM JULY 1, 2019 TO JUNE 30, 2020

Faculty/Staff			
Name	**Title**	**Institution**	**Email**
Jimmie Oxley	Co-PI	URI	joxley@chm.uri.edu
Jim Smith	Co-PI	URI	jsmith@chm.uri.edu
Graduate, Undergraduate and REU Students			
Name	**Degree Pursued**	**Institution**	**Month/Year of Graduation**
Ryan Rettinger	PhD	URI	5/2019
Taylor Busby	PhD	URI	5/2021
Alex Yevdokimov	PhD	URI	12/2020
Rachael Lenher	BS	URI	5/2021

II. PROJECT DESCRIPTION

A. *Project Overview*

To reveal detonability/initiability with small-scale tests was our ultimate goal. There has been no precedent for this type of test, but the goal is of such value to the homeland security enterprise (HSE) that it was worth the effort. To double our chances of achieving this goal, two very different approaches were pursued: (1) detonation studies, which require a special facility where explosives can be tested, and (2) using a research-grade mass spectrometer found in many chemical laboratories. A mass spectrometric technique, termed "survival yield," has been adapted to our purpose. We employed energy-resolved mass spectrometry (ERMS), a similar technique to monitor and collect the energy required to "break down" a species using a linear ion trap mass spectrometer.

In working with mass spectrometry and delving into issues of ionization, we examined a technique termed paper spray ionization. Because of the known difficulty with nonvolatile species entering the IMS, we decided to attempt a similar transfer technique. The technique involved using the swab as the platform for ionization and adduct formation, if necessary. Presently, it is performed on commercial swabs, which are shaped after swabbing and treated with solvent, and exposed to high voltage. This approach both ionizes the sample and drives it from the swab, making both thermal desorption and subsequent ionization sources unnecessary. It has been demonstrated to allow detection of high melting inorganic species as well as the current IMS library of threat materials. Voltage requirements are no higher than currently available internal to IMS instruments, and solvent requirements are minimal (a few microliters).

B. State of the Art and Technical Approach

B.1. Approach 1: Detonation Studies

Studies developing new small-scale detonability tests are underway and will be continued through the no-cost extension period provided to ALERT through May 2021. Characterizing detonation behavior for

subcritical diameters of non-ideal energetics is extremely challenging. A material may fail to detonate because it is below its critical diameter or because it has no explosive character at all. We are attempting to probe the explosivity of materials labeled "nonexplosive" but possessing fragmentation energies similar to explosive materials. We have developed a small-scale test using photon Doppler velocimetry where less than a pound of the material of interest is impacted by a shock wave from a booster and the profile of shock wave structure through that material is captured at early times before edge effects become important. Evaluation of such profiles will reveal whether a material is detonable but failed to detonate due to its small charge size or whether the material's chemical contribution is too slow and low energy ever to grow to detonation. We have demonstrated visualization of the detonation wave, but now we find that the curvature of the input shock is too great to allow use of a flat flyer plate required for these small-scale detonation tests with hydrogen peroxide. Creating a flat input wave could be accomplished with a gas gun, which we and many HSE facilities do not have. Therefore, our approach is to develop an inexpensive, simple plane wave. This development was of interest to the US Army; thus, the project has transitioned to their funding.

B.2. Approach 2: MS and IMS Studies

In pursuing methods of evaluating potential detonability, we examined the detailed workings of our liquid chromagraph-mass spectrometer (LC-MS). We have previously reported development of the ERMS technique by which we hope to understand detonability or at least stability. The LC-MS ionizes the analyte-solvent mix by a number of methods; one common one is ESI (electron spray ionization). By this route the laboratory-grade LC-MS can analyze chlorate salts. This is something the fielded IMS cannot do. We took on this challenge.

Unlike the MS, the IMS requires no high vacuum or special gases. Its versatility, speed, and portability has made the IMS a common tool for explosive detection, and it is widely used in airports, border security, and controlled check-points screenings. Because of these characteristics, there are many commercially available IMS devices. The Transportation Security Administration groups these devices as explosives trace detection (ETD). Standalone IMS systems are widely used at a variety of security checkpoints; however, they suffer from a number of limitations (e.g., high rate of false positive detection, missing true alarms, and inability to detect nonvolatile compounds). To improve the operation of the IMS (i.e., lower false alarm rate and increase the number of detectable species), we have developed ambient desorption ionization (ADI). ADI offers a new way to introduce the analyte into the IMS. Instead of relying on heat to drive the analyte into the instrument to be ionized, ADI performs the ionization first; this facilitates the introduction of the analyte into the IMS. In ADI the swab containing the analyte is treated with both high voltage and solvent to create an environment somewhat analogous to that created in electrospray ionization (ESI) used in many mass spectrometers. In other words, ionization, volatilization, and possibly adduct formation are all performed as part of the process of introducing the sample into the IMS. This novel approach allows normally nonvolatility species to be moved into the instrument. This improved detection of nonvolatile species might be compared to the improved detection offered by the liquid chromatography-MS compared to the gas chromatography-MS. Use of ADI with an IMS adds detection capability not attainable with commercial desorbers; perchlorate, chlorate and nitrate salts—all major parts of threat explosive compositions—can be added to the libraries of IMS instruments. ADI effectively eliminates the use of radioactive or any other type of ionization source that is required under current instrumentation configurations. Additionally, the high voltage required is no more than IMS instruments already have included in the components, and solvent requirements are a few microliters. The solvent eliminates the need for added dopants (presently part of the IMS consumable list), while providing potential adducting species. We believe use of ADI can mitigate many of the IMS shortcomings, but we need to be able to directly compare IMS ionization to that of an MS. If we can combine IMS and an MS, we will be able to characterize the manner in which ADI ionizes fragments species.

ADI can be used on a variety of benchtop MSs. In fact, a high resolution MS was used to prove that the proposed technique results in proper compound ionization. IMS on its own lacks the specificity, precision, and accuracy

of molecular identification, solely relying on time-space separations. The benchtop MS, on the other hand, possesses these important attributes and adds confidence to the results. Unfortunately, an MS with these capabilities lack the IMS mobility and field deployability. (We believe ADI can add detection capabilities to the present handheld MS.) We have a provision patent on ADI and are applying for a full patent. We have teamed with Smiths Detection and have been promised DHS funding to create a prototype.

B.3. Advantages of ADI Versus Existing Sources

- ADI allows volatilization and ionization of low volatility materials (e.g., chlorates, perchlorates, sulfides, phosphides, and cyanides) without the need of heat or chemical reaction.
- Power needed to operate the ADI source utilizes high voltage supply already incorporated in the ETD.
- The ADI source obviates the need for any other ionization approach.
- The ADI requires a small amount of aqueous buffer, which may also act as a dopant to aid ionization.

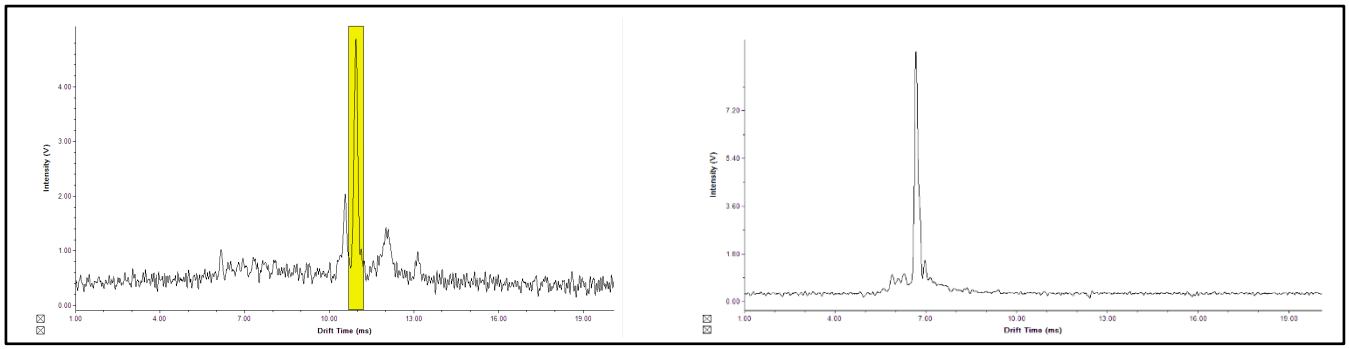

Figure 1: ADI used to detect PETN (acetonitrile solvent; left) and potassium perchlorate (methanol/water solvent; right). Floating voltage is 3 kV.

C. Major Contributions

- Extensive triacetone triperoxide (TATP) characterization—safe-scent aids, gentle destruction (Years 1–4)
- The limitations of certain oxidizers in terms of terrorist use (Years 1–6)
- Baseline information about hexamethylene triperoxide diamine (HMTD) chemical properties and reactivity (Years 1–7)
- Identifying the hazards of humidity to HMTD (Years 2–3)
- Formation mechanism of HMTD initiated (Years 2–3)
- Gentle destruction methods for HMTD (Years 3–4)
- Safe-scent aids for HMTD (Years 3–4)
- Revealing modes by which peroxide explosive signature can be masked by solvent (Years 3–4)
- Canine training aids for TATP and HMTD (Years 3–4)
- Determining best practices in analyzing peroxide explosives (Years 5–6)
- An extremely reliable standard for HMTD quantification work has been developed (Year 5)
- Examination of ETN, tracking synthesis routes, and attribution (Years 6–7)

- Creating new methods of "neutralizing" any small-scale (1-lb. scale) hazard SCHMOO (Safe Control of Hazardous Materials or Others Onsite) & SCHMOO II (Years 6–7)
- Examination of toxicity issues for canines (Years 5 and 7) and humans (Years 6 and 7)
- Development of a new method for "injecting" nonvolatile explosives (e.g., chlorate) into an IMS (Year 7)

D. Milestones

A major milestone was the examination of the six-carbon sugars. This study is close to complete. We expect to submit a paper by the end of the summer.

HMTD transformations required laboratory study, and that student has not been able to come into the lab due to COVID-19.

The book chapter(s) are still in progress. Cover and foreword have been submitted.

E. Final Results at Project Completion (Year 7)

- Thirty-five papers on HME (TATP, HMTD, ETN, AN, UN), one full patent (safe-scent training aids), two full patents in process (SCHMOO and ADI), and one provisional patent (sheet pyrotechnics) in process.
- Nine PhD, three master's degree students, and numerous BS students have graduated, and many have entered the homeland security enterprise.
- Safe-scent explosive training aids are on the market and have recently been suggested for authentication aids for TSA.
- SCHMOO has received a great deal of free publicity, and we expect to find a vendor for it shortly.
- Ambient desorption ionization (ADI), with an additional task order from DHS S&T, is being integrated into the Smiths 6000 ETD.
- Explosive database has over a thousand subscribers.

It is difficult to separate these projects by project number. The basic chemical characteristic had to be established in R1-A.1 before any work could progress on other projects.

III. RELEVANCE AND TRANSITION

A. Relevance of Research to the DHS Enterprise

Characterization of HMEs is an ongoing research effort within DHS, involving vendors and associated researchers. It impacts the entire HSE. In many cases, our methods of analysis led the way for other members of the HSE. Our studies on the extreme sensitivity of HMTD to moisture and acidity may have prevented mishandling in a number of laboratories. Many vendors of explosives detection instrumentation have requested access to the explosives database, or asked for help in working with various materials characterized in this project. The characterization of these materials is published on our database (URI Explosives Database), which is subscribed to by over a thousand people, about a quarter of which are from US government agencies. Furthermore, our work is cited in the DHS HME Safety Protocols Handbook, and we were invited to participate in the DHS Chemical Security Analysis Center & Explosives Division 1st Inter-agency Explosives Terrorism Risk Assessment Working Group. We have worked directly with ten vendors of explosive detection instrumentation.

B. Status of Transition at Project End

Safe-scent aids have been licensed to Detectachem. ADI is moving forward with Smiths Detection. Many papers on HME are available in the open literature.

C. Transition Pathway and Future Opportunities

The ADI-Smiths project is ongoing with a task order through Northeastern.

D. Customer Connections

The connections to DHS (central), TSL, and TSA are strong. To date the FBI is the major agency outside of DHS that is aware of the details of this project.

IV. PROJECT ACCOMPLISHMENTS AND DOCUMENTATION

A. Education and Workforce Development Activities

1. Course, Seminar, and/or Workshop Development
    a. Since June 2019 we have held seven classes with 105 attendees. The new class was CTH.
    b. Dr. Oxley gave an invited lecture at the International Pyrotechnic Symposium in Tours, France, summer 2019.
2. Student Internship, Job, and/or Research Opportunities
    a. Five graduate students who were supported by ALERT and graduated are now at Signature Science supporting TSL (two students), the Navy Research Lab (two students), and Los Alamos National Laboratory (one student).
3. Interactions and Outreach to K–12, Community College, and/or Minority Serving Institution Students or Faculty
    a. We ran two 2-week workshops introducing high school students to chemical analysis. This program will end with the end of ALERT.
4. Training to Professionals or Others
    a. Since June 2019 we have held seven classes with 105 attendees. The new class was CTH.

B. Peer Reviewed Journal Articles

1. Bezemer, K., McLennan, L., van Duin, L., Kuijpers, C.J., Koeberg, M., van den Elshout, J., van der Heijden, A., Busby, T., Yevdokimov, A.V., Schoenmakers, P., Smith, J., Oxley, J., & van Asten, A. "Chemical Attribution of the Home-Made Explosive ETN—Part I: Liquid Chromatography–Mass Spectrometry Analysis of Partially Nitrated Erythritol Impurities." *Forensic Science International*, 307(110102), December 2019. https://doi.org/10.1016/j.forsciint.2019.110102.
2. Rettinger, R.C., Porter, M., Canaria, J., Smith, J.L., & Oxley, J.C. "Fuel-Oxidizer Mixtures: A Lab and Field Study." *Journal of Energetic Materials*, *38*(2), 23 October 2019, pp. 170–190. https://doi.org/10.1080/07370652.2019.1679282.

Pending –

1. Bezemer, K., McLennan, L., van Duin, L., Kuijpers, C.J., Koeberg, M., van den Elshout, J., van der Heijden, A., Busby, T. Yevdokimov, A.V., Schoenmakers, P., Smith, J.L., Oxley, J.C., & van Asten, A. "Chemical Attribution of the Home-Made Explosive ETN—Part II: Use of Isotopic Ratio." *Forensic Science International*, in preparation.
2. Gonsalves, M.D., Colizza, K., Smith, J., & Oxley, J.C. "In Vitro Metabolism and Enzyme Phenotyping of Triacetone Triperoxide (TATP) in Humans." *Forensic Toxicology*, submitted.

C. Peer Reviewed Conference Proceedings

b. Oxley, J.C., Smith, J.L., Colizza, K., & Gonsalves, M. "In Vitro Metabolism of TATP." *NTREM*, April 2020, meeting proceedings, meeting canceled.

D. Seminars

1. Oxley, J.C. "Evaluation of Explosive Characteristics via Energy-Resolved MS." *ISADE*, April 2020 canceled.
2. Yevdokimov, A.V. "A Novel Approach to IMS Sampling and Analysis." Student Award Winner, *ISADE*, April 2020 canceled.

E. Poster Sessions

1. Gonsalves, M. "Metabolism of TATP." *ISADE*, April 2020 canceled.

F. Interviews and/or News Articles

1. CBS News. "'Innovative Checkpoint' and 'digital dog nose': TSA tests new security technology." *CBS News*, 25 November 2019. https://www.cbsnews.com/news/tsa-testing-advanced-airport-security-technology-digital-dog-nose-innovation-checkpoint/.

G. Other

1. Jimmie Oxley is an on-call American Chemical Society (ACS) expert. Consulted on July 2019 script for Gunpowder & Moon Smell and January 2020 on Explosive Vapor Detection.

H. New and Existing Courses Developed and Student Enrollment

New or Existing	Type	Title	Description	Enrollment
Existing	Short course	Explosive Stability	Analysis and safety of explosives	3
Existing	Short course	Propellants	Propellants	12
Existing	Short course	Fundamentals of Explosives	Fundamentals of explosives	26
Existing	Short course	Explosive Components	Device design	17
Existing	Short course	Explosive Components	Device design	17
Existing	Short course	Dynamic Diagnostics	Instrumentation and analysis	17
New	Short course	CTH for China Lake	Sandia computer code	13

I. Patent Applications Filed (Including Provisional Patents)

1. Oxley, J.C., Smith, J.L., Yevdokimav, A.V., & Colizza, K. "Apparatus and Methods for Explosive Trace Detection Sample Preparation and Introduction into an Ionizing Detection System." Provisional Patent 62/816,253, 11 March, 2019.
2. Oxley, J.C., Smith, J.L, Ichiyama, R., & Kagan, G. "Safe Control of Hazardous Materials or Others Onsite." US 62/837,520, April 2019.
3. Oxley, J.C., Smith, J.L., Kominia, A., Busby, T., & Stubbs, V. "Plasticized Flexible Pyrotechnic Material and Methods of Using the Same." Provisional Patent 62/993,992, 24 April, 2020.

J. Requests for Assistance/Advice

1. From DHS
    a. Oxley is part of the DHS-formed Inter-Agency Explosive Terrorism Risk Assessment Working Group (IExTRAWG). In addition to group meetings, a representative was sent to URI for two days in August 2018, so that we could finalize the metric for selecting threat materials.
    b. On call for a variety of TSA TSS-E personnel.
2. From Federal/State/Local Government
    a. The URI bomb dog and his trainer rely on our lab for advice and explosives.

This page intentionally left blank.

R1-B.2: Small-Scale Characterization of Homemade Explosives

I. PARTICIPANTS INVOLVED FROM JULY 1, 2019 TO JUNE 30, 2020

Faculty/Staff			
Name	**Title**	**Institution**	**Email**
Steven F. Son	PI	Purdue University	sson@purdue.edu
Vasant S. Vuppuluri	Research Scientist	Purdue University	vvuppulu@purdue.edu
Graduate, Undergraduate and REU Students			
Name	**Degree Pursued**	**Institution**	**Month/Year of Graduation**
Dakota Scott	MS	Purdue University	7/2019

II. PROJECT DESCRIPTION

A. Project Overview

- **Small-scale detonability testing:** We developed the capability to perform small-scale detonation performance testing, using as little as 10 g of material. Normally, detonation performance tests require several kilograms of material, making it very resource-intensive to obtain data with the necessary breadth to parametrize models. We started with a microwave interferometer that could provide a near-continuous shock front position history. We have also performed testing with systems not amenable to microwave using high-speed imaging.
- **Model development and calibration:** Reliable models are required for the Department of Homeland Security (DHS) to be able to perform accurate threat assessments. We have demonstrated the ability to use data from small-scale detonation failure experiments to calibrate computational models. Through this work, we have determined the small-scale experimental configuration that would be most amenable to computational modeling.
- **Collaboration with national research laboratories:** We have collaborated with multiple national laboratories, including Lawrence Livermore National Laboratory and Los Alamos National Laboratory. Multiple students have completed internships at these locations.

B. State of the Art and Technical Approach

Typical homemade explosive (HME) formulations consist of a combination of ammonium nitrate (AN), an oxidizer, and an appropriate fuel. A mixture of 94% AN and 6% fuel oil (ANFO) is a common HME formulation. In some HME formulations, AN is mixed with nitromethane (ANNM) instead of fuel oil. AN, NM, and fuel oil have widely accepted civilian uses, making it relatively easy to acquire them for malicious use. ANFO and other HMEs behave as nonideal explosives that are characterized by a long reaction zone length (on order of mm). Their detonation behavior is highly dependent on a variety of parameters, including the particle size and morphology of the AN, confinement, etc. This makes the modeling of their behavior for threat assessment challenging. The dearth of data on these formulations exacerbates the challenge. Typical detonation performance tests to calibrate models are dependent on having a fully developed detonation. Being nonideal

explosives, HMEs have large critical diameters (25 mm or greater). This requires several kilograms of material, making it expensive and time-consuming to perform multiple experiments necessary to parametrize models.

To measure detonation velocity, microwave interferometry is a well-established diagnostic. In a detonating explosive, the reaction front acts as a conductor, which reflects microwaves [1,2]. The incident and reflected microwave signals are mixed, resulting in a beat frequency measured by a detector that can be seen on a digitizer. From this, the position and velocity history of the shock front can be inferred. In addition to measuring fully developed detonations, microwave interferometry can also be used to measure failing detonations. It has been shown that under appropriate conditions, shock front history in a failing detonation can be used to calibrate models [3]. Most explosives are partially transparent to microwaves. For explosives that absorb microwaves, high-speed imaging may be substituted. A 10 MHz camera can be used to obtain the shock front position. An appropriate numerical differentiation scheme may be used to obtain velocity history, from which failure rate may be calculated.

C. Major Contributions

Year 7

- Dakota Scott graduated with an MS in mechanical engineering and has accepted a position at Army Research Laboratory.

Year 6

- Performed detonation failure experiments on the AN/NM system using high-speed imaging. The AN/NM system is not amenable to being studied with microwave interferometry due to nitromethane-absorbing microwaves.

Year 5

- Developed an experiment to measure shock front position using high-speed imaging and calculate velocity history and failure rate. We have compared these data to microwave interferometry data and found them to be comparable.
- Published paper on shock sensitivity of AN and aluminum additives.

Year 4

- Developed an experiment to quantify and rank shock sensitivity using small-scale subcritical diameter experiments. We applied this approach to characterize the effect of aluminum additives of various particle sizes as well as other inert additives.
- Published results of ANFO modeling.

Year 3

- David Kittell graduated with a PhD and joined Sandia National Laboratories.
- Characterized effects of density and confinement on ANFO detonation failure behavior.
- Successfully simulated detonation failure using reaction flow modeling in CTH.

Year 2

- Peter Renslow graduated with an MS in mechanical engineering and joined Sandia National Laboratories.
- Obtained initial results on AN and aluminum (ammonal) and ANFO compositions.

- Published results of time-frequency analysis of microwave interferometry.

Year 1

- Developed a small-scale detonation experiment using microwave interferometry.

D. Milestones

- **Characterize effect of desensitizing agents:** We tested various diluents reported in the literature, including diammonium phosphate (DAP) and calcium carbonate ($CaCO_3$). These additives were reported as having inhibited the detonation of ANFO. We also considered ascorbic acid, an antioxidant. Our results show that all these materials appear to behave as diluents and do not appear to desensitize ANFO.
- **Develop small-scale disc-acceleration experiment (DAX):** We obtained initial results with our photonic doppler velocimetry (PDV) system. However, we were not able to make further progress due to the COVID-19 pandemic impacting shipment of additional PDV probes and shutdown of university operations.
- **Heated experiments to quantify shock sensitivity:** We were unable to meet this milestone due to COVID-19 pandemic impeding implementation of this technique.

E. Final Results at Project Completion (Year 7)

In Year 7, we focused primarily on studying the effect of desensitizing agents on ANFO. Given the wide availability of AN and fuel oil, identification of an additive that mitigates the potential for malicious use of AN is useful. Many additives such as DAP and $CaCO_3$ have been claimed to inhibit detonation of ANFO. However, there is significant variability in the methods of evaluating the efficacy of these additives. In addition, it is not known whether these materials suppress reaction or behave primarily as diluents.

In our approach, we prepared various formulations of ANFO plus additive and compared their effect on detonation failure. We prepare compositions of ANFO plus 2.5% additive by mass and also ANFO plus 20% additive by mass. We compared DAP, $CaCO_3$, aluminum oxide (AlO), glass beads, and ascorbic acid. A picture of a test sample is shown in Figure 1. The sample is initiated with an RP-80 detonator. A booster charge of LX-14 is used to initiate the sample material.

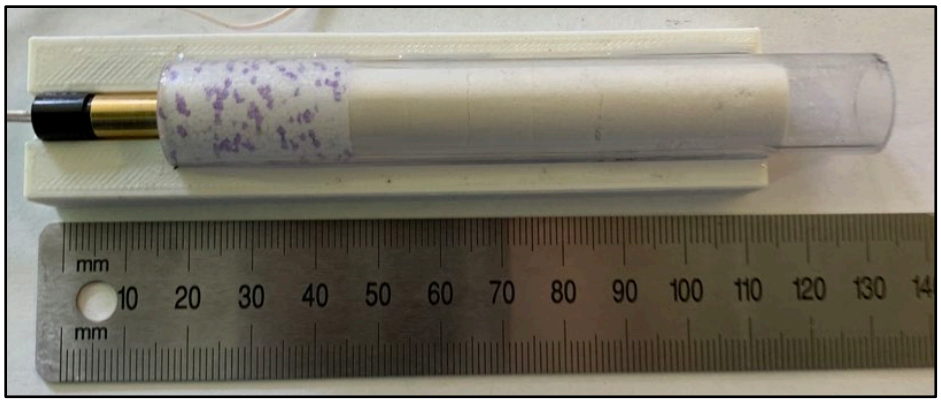

Figure 1: Image of test samples for characterizing desensitizing agents.

Using a Shimadzu HPV-X2 camera, we imaged the detonation of these materials at a 10 MHz frame rate and 50 ns exposure time. Using manual tracking, we obtained the position history of the shock front. A series of 256 images were acquired for each shot. Representative images are shown in Figure 2.

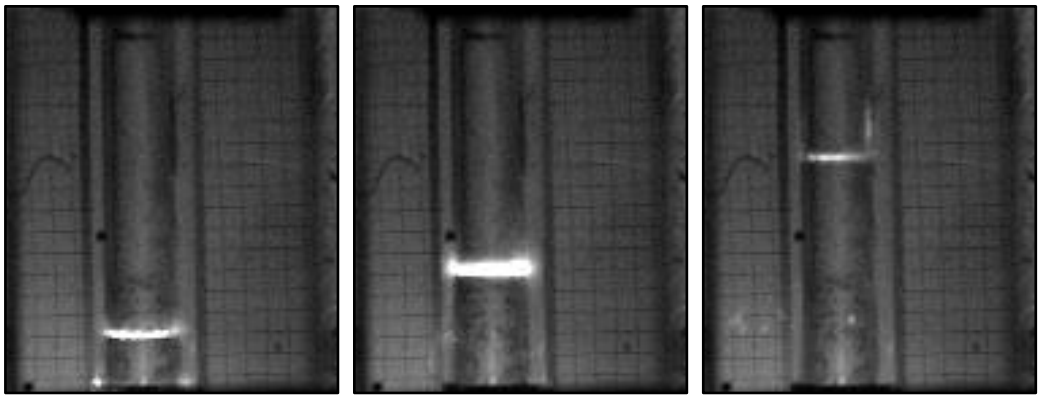

(a) (b) (c)

Figure 2: Representative images from detonation of test samples. In (a), the reaction front is propagating through the LX-14 booster. In (b), the reaction front has reached the booster/sample interface. In (c), the detonation is failing but at a relatively slow rate.

Position histories are shown for both the 2.5% and 20% additive cases (both by mass). The shock velocity is relatively steady initially for about 2.5 μs, which is the time taken for the shock to travel through the booster charge. After about 2.5 μs, the shock reaches the sample material, at which point failure begins.

It can be seen from Figure 3 that the position histories are nearly indistinguishable from one another. The shock front positions appear to diverge at later times. The type of additive does not appear to make a significant difference in the detonation failure behavior. In Figure 4, the position histories shortly after the booster/sample interface are relatively similar. Again, the nature of the material added appears to have little effect on the detonation failure behavior.

From this, it appears that all these materials function primarily as diluents and do not suppress reaction.

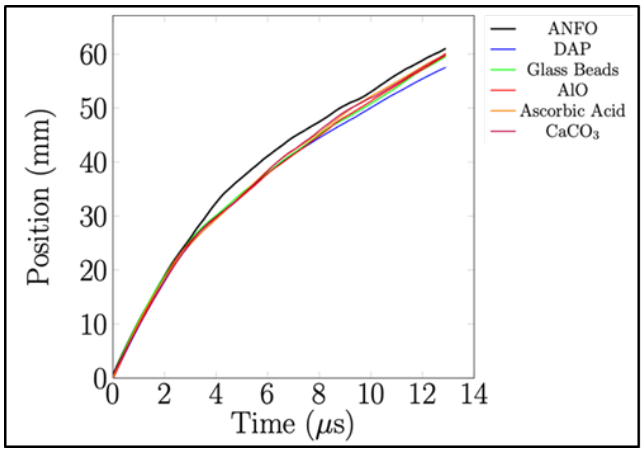

Figure 3: Results from 2.5% additive by mass. ANFO, diammonium phosphate (DAP), aluminum oxide (AlO), ascorbic acid, and calcium carbonate ($CaCO_3$) are shown.

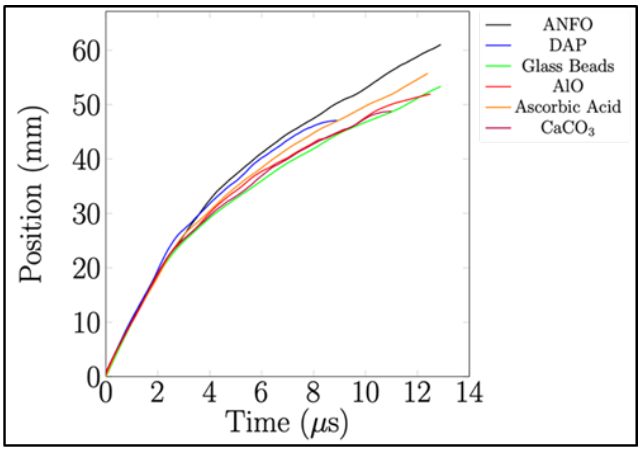

Figure 4: Results from 20% additive by mass. ANFO, diammonium phosphate (DAP), aluminum oxide (AlO), ascorbic acid, and calcium carbonate ($CaCO_3$) are shown.

Over the life of this project, we developed an experimental framework for performing small-scale detonation testing of nonideal explosive formulations. Our results demonstrated that one can obtain an understanding of shock sensitivity from small-scale experiments. In addition, our modeling results showed that overdriving highly confined HME samples will yield results that are amenable to modeling. As a result of this work, we have graduated three MS students and one PhD student, all of whom are currently working in the national security enterprise.

III. RELEVANCE AND TRANSITION

A. Relevance of Research to the DHS Enterprise

1. Explosive behavior of AN-based HME formulations is highly dependent on a variety of factors, including size and morphology of the AN, presence of sensitizing agents, and type of fuel. Performing standard detonation performance tests with HMEs would normally require kilograms of material. This makes it challenging and costly to obtain enough data to parametrize models. We focused on methods to study AN-based explosives at small scale. With use of as little as 10 g of material, we were able to obtain data that could be used to calibrate computational models, representing a ten-times reduction in material requirement.
2. Our work has resulted in multiple journal articles and conference proceedings. As a result, we have made our results available to a variety of customers. In addition, all of the students who have been involved in this project are currently working in the national security enterprise.
3. We also studied the efficacy of desensitization agents. We focused on determining whether an additive could function as a true reaction suppressant. The key metric was effect on rate of detonation failure.

B. Status of Transition at Project End

We recently submitted a proposal to the Defense Advanced Research Projects Agency on small-scale detonation performance evaluation that was heavily based on the expertise we developed as a result of this project.

C. Transition Pathway and Future Opportunities

From this project, we have graduated three MS students and one PhD student. Also, our work on this project has produced over three journal publications.

D. Customer Connections

- David Kittell, Sandia National Laboratories—former ALERT student
- Scott Jackson, Los Alamos National Laboratory—mentored Nicholas Cummock in summer 2015
- Brian Bockmon, founder of Rocky Mountain Scientific Laboratory
- Mike Lindsay, Air Force Research Laboratory
- Rob Reeves, Lawrence Livermore National Laboratory—mentored Christian Sorensen, former ALERT student

IV. PROJECT ACCOMPLISHMENTS AND DOCUMENTATION

A. Education and Workforce Development Activities

1. This project provided partial support to Vasant Vuppuluri, research scientist.

V. REFERENCES

[1] Cawsey, G. F., Farrands, J. L., & Thomas, S. (1958). Observations of detonation in solid explosives by microwave interferometry. Proceedings of the Royal Society of London. Series A. *Mathematical and Physical Sciences*, *248*(1255), 499-521.

[2] Kittell, D. E., Mares Jr, J. O., & Son, S. F. (2015). Using time-frequency analysis to determine time-resolved detonation velocity with microwave interferometry. *Review of Scientific Instruments*, *86*(4), 044705.

[3] Kittell, D. E., Cummock, N. R., & Son, S. F. (2016). Reactive flow modeling of small scale detonation failure experiments for a baseline non-ideal explosive. *Journal of Applied Physics*. *120*(6), 064901.

R1-C.2: Compatibilities & Simulants: Explosive Polymer Interactions

I. PARTICIPANTS INVOLVED FROM JULY 1, 2019 TO JUNE 30, 2020

Faculty/Staff			
Name	**Title**	**Institution**	**Email**
Jimmie Oxley	Co-PI	URI	joxley@chm.uri.edu
Jim Smith	Co-PI	URI	jsmith@chm.uri.edu
Gerald Kagan	Post-Doc	URI	gkagan@chm.uri.edu
Graduate, Undergraduate and REU Students			
Name	**Degree Pursued**	**Institution**	**Month/Year of Graduation**
Michelle Gonsalves	PhD	URI	12/2020
Robert Ichiyama	PhD	URI	5/2023
Jeff Canaria	PhD	URI	5/2021
Victoria Stubbs	MS	URI	8/2020

II. PROJECT DESCRIPTION

A. Project Overview

This project has examined the interaction of explosives with polymers with the aim at revealing new swabs. In the process we have catalyzed research in other groups that remain ongoing. We hope for the same success with our exploration of the biological effects of the peroxide explosives. We have succeeded in identifying a biomarker indicating triacetone triperoxide (TATP) exposure. It may take some time before forensic labs become aware of this useful evidence of illicit explosive handling.

SCHMOO was developed to sequester hazardous materials and preserves the evidentiary value. This it does very well. However, first responders appear more concerned with destroying the hazardous material than preserving evidence.

B. State of the Art and Technical Approach

TATP is a volatile but powerful explosive that appeals to terrorists due to its ease of synthesis from household items. For this reason, bomb squads, canine (K9) units, and scientists must work with this material to mitigate this threat. However, no information on the metabolism of TATP is available.

In vitro experiments using human liver microsomes and recombinant enzymes were performed on TATP and TATP-OH (hydroxy-TATP) for metabolite identification and enzyme phenotyping. Enzyme kinetics for TATP hydroxylation were also investigated. Urine from laboratory personnel collected before and after working with TATP was analyzed for TATP and its metabolites.

While experiments with flavin-containing monooxygenases (FMOs) were inconclusive, those with recombinant cytochrome P450s (CYPs) strongly suggested that CYP2B6 was the principle enzyme responsible for TATP hydroxylation. TATP-O-glucuronide was also identified, and incubations with

recombinant uridine diphosphoglucuronosyl transferases (UGTs) indicated that UGT2B7 catalyzes this reaction. Michaelis-Menten kinetics were determined for TATP hydroxylation, with $K_{M\,=}$ 1.4 μM and $v_{max\,=}$ 8.7 nmol/min/nmol CYP2B6. TATP-O-glucuronide was present in the urine of all three volunteers after being exposed to TATP vapors showing good in vivo correlation to in vitro data. TATP and TATP-OH were not observed.

Since scientists working to characterize and detect TATP to prevent terrorist attacks are constantly exposed to this volatile compound, attention should be paid to its metabolism. This paper is the first to elucidate any metabolism and excretion of TATP in humans. Also, TATP-O-glucuronide can be exploited as a marker of exposure to TATP in urine. (See R1-C.2 Appendix)

C. Major Contributions

- Extensive TATP characterization—safe-scent aids, gentle destruction patented and licensed (Years 1–4)
- The limitations of certain oxidizers in terms of terrorist use (Years 1–6)
- Baseline information about HMTD chemical properties and reactivity (Years 1–7)
- Identifying the hazards of humidity to HMTD (Years 2–3)
- Formation mechanism of HMTD initiated (Years 2–3)
- Gentle destruction methods for HMTD (Years 3–4)
- Safe-scent aids for HMTD (Years 3–4)
- Revealing modes by which peroxide explosive signature can be masked by solvent (Years 3–4)
- Canine training aids for TATP and HMTD (Years 3–4)
- Determining best practices in analyzing peroxide explosives (Years 5–6)
- An extremely reliable standard for HMTD quantification work has been developed (Year 5)
- Examination of ETN, tracking synthesis routes, and attribution (Years 6–7)
- Creating new method of "neutralizing" any small-scale (1-lb. scale) hazard SCHMOO & SCHMMO 2 (Years 6–7)
- Examination of toxicity issues for canines (Year 5) and humans (Year 6), with publication (Years 6–7)
- Development of a new method for "injecting" nonvolatile explosives (e.g., chlorate) into IMS (Year 7)

D. Milestones

A major milestone was the examination of the six-carbon sugars. This study is close to complete. We expect to submit a paper by the end of the summer.

HMTD transformations is just now complete, slowed by COVID-19.

The book chapter(s) are still in progress. Cover and foreword have been submitted.

E. Final Results at Project Completion (Year 7)

- Thirty-five papers on HME (homemade explosives, including TATP, HMTD, ETN, AN, and UN), one full patent (safe-scent training aids), two full patents in process (SCHMOO and ADI), and one provisional patent (sheet pyrotechnics) in process.
- Nine PhD, three master's degree students, and numerous BS students have graduated, and many have entered the homeland security enterprise.
- Safe-scent explosive training aids are on the market and have recently been suggested for authentication aids for TSA.
- SCHMOO has received a great deal of free publicity, and we expect to find a vendor for it shortly.
- Ambient desorption ionization (ADI) with an additional task order from DHS S&T is being integrated into the Smiths 6000 ETD.
- Explosive database has over a thousand subscribers.

It is difficult to separate these projects by project number. The basic chemical characteristic had to be established in R1-A.1 before any work could progress on other projects.

III. RELEVANCE AND TRANSITION

A. Relevance of Research to the DHS Enterprise

Characterization of HMEs is an ongoing research effort within DHS, involving vendors and associated researchers. It impacts the entire HSE. In many cases, our methods of analysis lead the way for other members of the HSE. Our studies on the extreme sensitivity of HMTD to moisture and acidity may have prevented mishandling in a number of laboratories. Many vendors of explosives detection instrumentation have requested access to the explosives database, or asked for help in working with various materials characterized in this project. The characterization of these materials is published on our database (URI Explosives Database), which is subscribed to by over a thousand people, about a quarter of which are from US government agencies. Furthermore, our work is cited in the DHS HME Safety Protocols Handbook, and we were invited to participate in the DHS Chemical Security Analysis Center & Explosives Division 1st Inter-agency Explosives Terrorism Risk Assessment Working Group. We have worked directly with ten vendors of explosive detection instrumentation.

B. Status of Transition at Project End

Safe-scent aids have been licensed to Detectachem. ADI is moving forward with Smiths Detection. Many papers on HME are available in the open literature.

C. Transition Pathway and Future Opportunities

The ADI-Smiths project is ongoing with a task order through Northeastern.

D. Customer Connections

The connections to DHS (central), TSL, and TSA are strong. To date the FBI is the major agency outside of DHS which is aware of the details of this project.

IV. PROJECT ACCOMPLISHMENTS AND DOCUMENTATION

A. Education and Workforce Development Activities

1. Course, Seminar, and/or Workshop Development
   a. Since June 2019 we have held seven classes with 105 attendees. The new class was CTH.
   b. Dr. Oxley gave an invited lecture at the International Pyrotechnic Symposium in Tours, France, summer 2019.
2. Student Internship, Job, and/or Research Opportunities
   a. Five graduate students who were supported by ALERT and graduated are now at Signature Science supporting TSL (two students), the Navy Research Lab (two students), and Los Alamos National Laboratory (one student).
3. Interactions and Outreach to K–12, Community College, and/or Minority Serving Institution Students or Faculty
   a. We ran two two-week workshops introducing high school students to chemical analysis. This program will end with the end of ALERT.
4. Training to Professionals or Others
   a. Since June 2019 we have held seven classes with 105 attendees. The new class was CTH.

B. Peer Reviewed Journal Articles

1. Bezemer, K., McLennan, L., van Duin, L., Kuijpers, C.J., Koeberg, M., van den Elshout, J., van der Heijden, A., Busby, T., Yevdokimov, A.V., Schoenmakers, P., Smith, J.L., Oxley, J.C., & van Asten, A. "Chemical Attribution of the Home-Made Explosive ETN—Part I: Liquid Chromatography–Mass Spectrometry Analysis of Partially Nitrated Erythritol Impurities." *Forensic Science International*, 307(110102), December 2019. https://doi.org/10.1016/j.forsciint.2019.110102.
2. Rettinger, R.C, Porter, M., Canaria, J., Smith, J.L., & Oxley, J.C. "Fuel-Oxidizer Mixtures: A Lab and Field Study." *Journal of Energetic Materials*, *38*(2), 23 October 2019, pp. 170–190. https://doi.org/10.1080/07370652.2019.1679282.

Pending:

1. Bezemer, K., McLennan, L., van Duin, L., Kuijpers, C.J., Koeberg, M., van den Elshout, J., van der Heijden, A., Busby, T., Yevdokimov, A.V., Schoenmakers, P., Smith, J.L., Oxley, J.C., & van Asten, A. "Chemical Attribution of the Home-Made Explosive ETN—Part II: Use of Isotopic Ratio." *Forensic Science International*, in preparation.
2. Gonsalves, M.D., Colizza, K., Smith, J., & Oxley, J.C. "In Vitro Metabolism and Enzyme Phenotyping of Triacetone Triperoxide (TATP) in Humans." *Forensic Toxicology*, submitted.

C. Peer Reviewed Conference Proceedings

1. Oxley, J.C., Smith, J.L., Colizza, K., & Gonsalves, M. "In Vitro Metabolism of TATP." *NTREM*, April 2020, meeting proceedings, meeting canceled.

D. Seminars

1. Oxley, J.C. "Evaluation of Explosive Characteristics via Energy-Resolved MS." *ISADE*, April 2020 canceled.
2. Yevdokimov, A.V. "A Novel Approach to IMS Sampling and Analysis." Student Award Winner, *ISADE*, April 2020 canceled.

E. Poster Sessions

1. Gonsalves, M. "Metabolism of TATP." *ISADE*, April 2020 canceled.

F. Interviews and/or News Articles

1. CBS News. "'Innovative Checkpoint' and 'digital dog nose': TSA tests new security technology." *CBS News*, 25 November 2019. https://www.cbsnews.com/news/tsa-testing-advanced-airport-security-technology-digital-dog-nose-innovation-checkpoint/.

G. Other

1. Jimmie Oxley is an on-call American Chemical Society (ACS) expert. Consulted on July 2019 script for Gunpowder & Moon Smell and January 2020 on Explosive Vapor Detection.

H. New and Existing Courses Developed and Student Enrollment

New or Existing	Type	Title	Description	Enrollment
Existing	Short course	Explosive Stability	Analysis and safety of explosives	3
Existing	Short course	Propellants	Propellants	12
Existing	Short course	Fundamentals of Explosives	Fundamentals of explosives	26
Existing	Short course	Explosive Components	Device design	17
Existing	Short course	Explosive Components	Device design	17
Existing	Short course	Dynamic Diagnostics	Instrumentation & analysis	17
New	Short course	CTH for China Lake	Sandia computer code	13

I. Technology Transfer/Patents

1. Patent Applications Filed (Including Provisional Patents)
   a. Oxley, J.C., Smith, J.L., Yevdokimav, A.V., & Colizza, K. "Apparatus and Methods for Explosive Trace Detection Sample Preparation and Introduction into an Ionizing Detection System." Provisional patent 62/816,253, 11 March, 2019.
   b. Oxley, J.C., Smith, J.L, Ichiyama, R., & Kagan, G. "Safe Control of Hazardous Materials or Others Onsite." US 62/837,520, April 2019.
   c. Oxley, J.C., Smith, J.L., Kominia, A., Busby, T., & Stubbs, V. "Plasticized Flexible Pyrotechnic Material and Methods of Using the Same." Provisional Patent 62/993,992, 24 April 2020.

J. Requests for Assistance/Advice

1. From DHS
    a. Oxley is part of the DHS-formed Inter-Agency Explosive Terrorism Risk Assessment Working Group (IExTRAWG). In addition to group meetings, a representative was sent to URI for two days in August 2018, so that we could finalize the metric for selecting threat materials.
    b. On call for a variety of TSA TSS-E personnel.
2. From Federal/State/Local Government
    a. The URI bomb dog and his trainer rely on our lab for advice and explosives.

R1-C.2. APPENDIX

This page intentionally left blank.

In Vitro and *In Vivo* Studies of Triacetone Triperoxide (TATP) Metabolism in Humans

Michelle D. Gonsalves[1]; Kevin Colizza[1]; James L. Smith[1]; Jimmie C. Oxley[1,2]

[1] Chemistry Department, University of Rhode Island, 140 Flagg Rd, Kingston, RI 02881, USA.
[2] Corresponding author:
Address: 140 Flagg Rd, Kingston, RI 02881, USA.
Phone number: 401- 874-2103
Email: joxley@chm.uri.edu

ABSTRACT

Purpose Triacetone triperoxide (TATP) is a volatile but powerful explosive that appeals to terrorists due to its ease of synthesis from household items. For this reason, bomb squad, canine (K9) units, and scientists must work with this material to mitigate this threat. However, no information on the metabolism of TATP is available.

Methods *In vitro* experiments using human liver microsomes (HLM) and recombinant enzymes were performed on TATP and TATP-OH for metabolite identification and enzyme phenotyping. Enzyme kinetics for TATP hydroxylation were also investigated. Urine from laboratory personnel collected before and after working with TATP was analyzed for TATP and its metabolites.

Results While experiments with flavin-containing monooxygenases (FMOs) were inconclusive, those with recombinant cytochrome P450s (CYPs) strongly suggested that CYP2B6 was the principle enzyme responsible for TATP hydroxylation. TATP-O-glucuronide was also identified and incubations with recombinant uridine diphosphoglucuronosyl transferases (UGTs) indicated that UGT2B7 catalyzes this reaction. Michaelis-Menten kinetics were determined for TATP hydroxylation, with K_M = 1.4 μM and v_{max} = 8.7 nmol/min/nmol CYP2B6. TATP-O-glucuronide was present in the urine of all three volunteers after being exposed to TATP vapors showing good *in vivo* correlation to *in vitro* data. TATP and TATP-OH were not observed.

Conclusions Since scientists working to characterize and detect TATP to prevent terrorist attacks are constantly exposed to this volatile compound, attention should be paid to its metabolism. This paper is the first to elucidate any metabolism and excretion of TATP in humans. Also, TATP-O-glucuronide can be exploited as a marker of exposure to TATP in urine.

KEYWORDS energetic material, endoperoxide, human metabolism, TATP exposure, CYP2B6 hydroxylation, UGT2B7 glucuronidation.

INTRODUCTION

Triacetone triperoxide (3,3,6,6,9,9-hexamethyl-1,2,4,5,7,8-hexoxonane, TATP) is a homemade (HME) explosive, easily synthesized from household items.(1) For this reason, TATP has often been used by terrorists,(2) necessitating its research by bomb squad, canine (K9) units, and scientists.(3) In addition to being extremely hazardous, this peroxide explosive is highly volatile, with partial pressure of 4–7 Pa at 20°C.(4,5) Personnel exposed to TATP will most likely absorb it through inhalation and/or dermal absorption. However, no information on the human absorption, distribution, metabolism, excretion and toxicity (ADMET) of TATP is available. Therefore, this paper will investigate the *in vitro* metabolism of TATP and the *in vivo* excretion through urine analysis.

The toxicity of most military explosives has been well characterized.(6) The biotransformation of trinitrotoluene (TNT), for example, has been thoroughly investigated. It is metabolized by cytochrome P450 reductase, forming nitroso intermediates, and yielding 4-hydroxylamino-2,6-dinitrotoluene, 4-amino-2,6-dinitrotoluene and 2-amino-4,6-dinitrotoluene. These primary metabolites are further reduced by cytochrome P450 to 2,4-diamino-6-nitrotoluene and 2,6-diamino-4-nitrotoluene.(7,8) *In vivo* studies of Chinese ammunition factory workers found metabolites such as 4-amino-2,6-dinitrotoluene and 2-amino-4,6-dinitrotoluene in urine and bound to the hemoglobin in blood.(8,9) TATP has been studied for almost two decades, but its metabolism and toxicity are still unknown. TATP characterization is problematic since it is an extremely sensitive explosive, difficult to analyze and, due to its high volatility, difficult to concentrate in biological samples.(4)

Most xenobiotics are metabolized by cytochrome P450 (CYP) which is a family of heme-containing enzymes found in all tissues, particularly the liver endoplasmic reticulum (microsomes). CYPs catalyze phase I oxidative reactions (among others) in the presence of oxygen and a reducing agent (usually reduced nicotinamide adenine dinucleotide phosphate, NADPH). NADPH provides electrons to the CYP heme via cytochrome P450 reductase. This oxidation generally produces more polar metabolites that are either excreted in the urine or undergo phase II biotransformation, further increasing their hydrophilicity.(10) One of the most common phase II reactions is glucuronidation, which is catalyzed by uridine diphosphoglucuronosyl transferase (UGT) in the presence of the cofactor uridine diphosphate-glucuronic acid (UDPGA). In this reaction, glucuronic acid is conjugated onto an electron-rich nucleophilic heteroatom, frequently added to the substrate by phase I metabolism. Glucuronide metabolites increase the topical polar surface area (TPSA) and are ionized at physiological pH, thus, increasing the aqueous solubility of the compound for excretion.(10)

TATP is a cyclic peroxide, a motif shared with the anti-malarial drug, artemisinin. The endoperoxide functionality of artemisinin is thought to be crucial for its anti-malarial activity.(11) In the presence of ferrous ions, artemisinin undergoes homolytic peroxide cleavage to yield an oxygen radical that may be lethal to malaria parasite, *Plasmodium falciparum*. Biotransformation studies indicate that artemisinin is primarily metabolized by CYP2B6 to deoxy-artemisinin, deoxy-dihydroartemisinin, dihydroartemisinin and 'crystal-7'.(12,13) Similarly, we have previously shown that TATP is metabolized *in vitro* by canine CYP2B11, another CYP2B subfamily enzyme.(14) Artemisinin is further metabolized by glucuronidation, particularly by UGT1A9 and UGT2B7, to dihydroartemisinin-glucuronide, the principal metabolite found in urine, suggesting endoperoxides, like TATP, may be glucuronidated and excreted in urine. (15)

Laboratory personnel who work on synthesizing, characterizing and detecting TATP are inevitably exposed to this volatile compound. Even the small-size samples they work with can result in buildup of TATP in a confined space. Furthermore, bomb-sniffing dogs and their handlers are purposely exposed to these vapors for the sake of training. Our previous study revealed TATP metabolism in dog liver microsomes (DLM).(14) Now we evaluate its biotransformation in HLM and recombinant enzymes, identifying phase I and phase II metabolites, estimating enzyme kinetics and detecting urinary metabolites excreted from scientists exposed to TATP in their work environment.

MATERIAL AND METHODS

Chemicals

Optima HPLC grade methanol (MeOH), Optima HPLC grade water (H_2O), Optima HPLC grade acetonitrile (ACN), ACS grade acetone, ACS grade methanol, ACS grade pentane, hydrochloric acid (HCl), ammonium acetate (NH_4OAc), dipotassium phosphate (K_2HPO_4), monopotassium phosphate (KH_2PO_4), magnesium chloride ($MgCl_2$) and reduced glutathione (GSH) were purchased from Fisher Chemical (Fair Lawn, NJ, USA). Reduced nicotinamide adenine dinucleotide phosphate (NADPH), 1-aminobenzotriazole (1-ABT), methimazole (MMI), 1-naphthol and hydroxyacetone were purchased from Acros Organics (Morris Plain, NJ, USA). Uridine-5'-diphosphoglucuronic acid (UDPGA), saccharolactone and 2,4-dichloro-phenoxyacetic acid were purchased from Sigma-Aldrich (St. Louis, MO, USA). Bupropion (BUP), benzydamide (BZD) and alamethicin were purchased from Alfa Aesar (Ward Hill, MA, USA). Oxcarbazepine (OXC) was purchased from European

Pharmacopoeia Reference Standard (Strasbourg, France). Ticlopidine (TIC) was purchased from TCI (Tokyo, Japan). Hydroxybupropion (BUP-OH) was purchased from Cerilliant Corporation (Round Rock, Texas, USA). Deuterated acetone (d_6-acetone) was purchased from Cambridge Isotope Labs (Cambridge, MA, USA). Hydrogen peroxide (50 %) was purchased from Univar (Redmond, WA, USA). Human liver microsomes (HLM), rat liver microsomes (RLM), dog liver microsomes (DLM) and human lung microsomes (HLungM) were purchased from Sekisui XenoTech (Kansas City, KS, USA). Human CYP bactosomes (rCYP) expressed in *Escherichia coli* (*E. coli*) were purchased from Cypex (Dundee, Scotland). Human FMO supersomes (rFMO) and human UGT supersomes (rUGT) expressed in insect cells were purchased from Corning (Woburn, MA, USA).

TATP, Deuterated TATP (d_{18}-TATP) and Hydroxy-TATP (TATP-OH) Synthesis

TATP was synthesized following the literature methods using hydrochloric acid as the catalyst.(1) TATP was purified by recrystallization, first with 80/20 (w/w) methanol/water (MeOH/H_2O) and then with pentane. Deuterated TATP was synthesized as above using d_6-acetone. Hydroxy-TATP was synthesized as above using 2:1:1 hydrogen peroxide (50 wt%): acetone: hydroxyacetone.(14) TATP-OH was purified using a Teledyne Isco CombiFlash RF+ system with attached PurIon S MS system, followed by two cycles of drying and reconstituting in solvent to sublime away the TATP. Separation was performed using a C-18 cartridge combined with a liquid chromatograph (LC) flow of 18 mL/min with 10% MeOH (A) and 90% aqueous 10 mM ammonium acetate (NH4OAc) (B) for 1 minute, before ramping to 35% A/65% B over 1 minute, followed by another ramp to 95% A/5% B over the next 1 minute, holding for 2 minutes, before a 30 second transition to initial conditions, with a hold of 2 minutes.(14)

Instrumentation

Metabolite identification was performed by high performance liquid chromatography coupled to Thermo Scientific Exactive or LTQ Orbitrap XL high resolution mass spectrometer (HPLC-HRMS). A CTC Analytics PAL autosampler was used for LC injections, solvent delivery was performed using a Thermo Scientific Accela 1200 quaternary pump, and data collection/analysis was done using Xcalibur software (ver. 2.2 and 2.1, respectively).

Metabolite quantification was performed by high performance liquid chromatography coupled to AB Sciex Q-Trap 5500 triple quadrupole mass spectrometer (HPLC-MS/MS). A CTC Analytics PAL autosampler was used for LC injections, solvent delivery was performed using a Thermo Scientific Accela 1200 quaternary pump and data collection/analysis was done with Analyst software (ver. 1.6.2).

The HPLC method for all TATP derivatives was as follow: sample of 40 µL (Exactive and LTQ Orbitrap XL) or 20µL (Q-Trap 5500) in 50/50 acetonitrile/water (ACN/H_2O) were injected into LC flow of 250 µL/min of 10%A/90% B for introduction onto a Thermo Syncronis C18 column (50 X 2.1 mm, 5 µm). Initial conditions were held for 1 minute before ramping to 35% A/65% B over 1 minute, followed by another ramp to 95% A/5% B over the next 1 minute. This ratio was held for 2 minutes before reverting to initial conditions over 30 seconds, which was held for additional 2 minutes. The Exactive MS tune conditions for atmospheric pressure chemical ionization (APCI) positive mode were as follows: N_2 sheath gas flow rate, 30 arbitrary units (AU); N_2 auxiliary gas flow rate, 30 AU; discharge current, 6 µA; capillary temperature, 220 °C; capillary voltage, 25 V; tube lens voltage, 40 V; skimmer voltage, 14 V; and vaporizer temperature, 220 °C. The Exactive MS tune conditions for electrospray ionization (ESI) negative mode were as follows: N_2 sheath gas flow rate, 30 AU; N_2 auxiliary gas flow rate, 15 AU; spray voltage, -3.4 kV; capillary temperature, 275 °C; capillary voltage, -35 V; tube lens voltage, -150 V; and skimmer voltage, -22 V. The LTQ Orbitrap XL MS tune conditions for ESI-, used for TATP-O-gluc verification, were as follows: N_2 sheath gas flow rate, 30 AU; N_2 auxiliary gas flow rate, 15 AU; spray voltage, -4 kV; capillary temperature, 275 °C; capillary voltage, -15 V; and tube lens voltage, -84 V. The single reaction monitoring settings were as follows: m/z 413.13 with isolation width m/z 1.7, activated by higher-energy collision dissociation at 35 eV. The Q-trap 5500 MS tune and multiple reaction monitoring (MRM) conditions are shown in Table 1. TATP and TATP-OH quantification was done as the area ratio to d_{18}-TATP (internal standard, IS) using a standard curve

ranging 10-20,000ng/mL and 10-500 ng/mL (Fig. S-1) or 500-8,000 ng/mL, respectively. TATP-O-gluc relative quantification was done as the area ratio to 2,4-dichloro-phenoxyacetic acid (IS).

The HPLC method for bupropion (BUP), hydroxybupropion (BUP-OH), benzydamine (BZD), benzydamine N-oxide (BZD-NO), and oxcarbazepine (OXC, IS), was as follow: sample of 10 µL in 50/50 ACN/H_2O were injected into LC flow of 250 µL/min with 30% A/70% B for introduction onto a Thermo Scientific Acclaim Polar Advantage II C18 column (2.1 × 50 mm, 3 µm). Initial conditions were held for 1 minute before instant increase to 95% A/5% B and held for 2.5 minutes, then reversed to initial conditions over 30 seconds, with a hold of 1 minute for BUP, BUP-OH and OXC method or 3 minutes for BZD, BZD-NO and OXC method.

Metabolite Identification

All incubations were performed in triplicates in a Thermo Scientific Digital Heating Shaking Drybath set to body temperature 37 °C and 800 rpm. An incubation mixture containing phosphate buffer (pH 7.4), $MgCl_2$,(16) and NADPH (CYP cofactor(10)) was prepared so that at a final volume of 1 mL, their concentrations were 10 mM, 2 mM, 1 mM, respectively. When the incubation times were relatively long (greater than 15 minutes), it was thought necessary to use closed vessels to avoid loss of the volatile TATP or TATP-OH; as a result, prior to incubation, oxygen gas was bubbled through the buffer to ensure ample oxygen availability.(14) To this mixture, microsomes or recombinant enzymes were added and equilibrated for 3 minutes before the reaction was initiated by adding the substrate. Substrates included TATP in ACN, TATP-OH in MeOH, and BUP and BZD in H_2O. Organic solvents can disrupt metabolism, but the catalytic activity of most CYP enzymes is unaffected by less than 1 % ACN or MeOH.(17) At the end point, an aliquot was transferred to a vial containing equal volume of ice cold ACN and immediately vortex-mixed to quench the reaction. The sample was centrifuged for 5 minutes at 14000 rpm, and the supernatant analyzed by LC-MS.

Metabolite identification studies used microsomes (HLM, RLM, DLM) at protein concentrations of 1 mg/mL as part of the incubation mixture. The substrate, TATP, TATP-OH, or d_{18}-TATP (10 µg/mL) was allowed to incubate for several minutes before MS analysis. Negative controls consisted of the incubation mixture excluding either microsomes or NADPH. Positive control used 100 µM BUP, a probe substrate for CYP2B6.(18–20)

Phase II TATP metabolism was examined by two studies. Metabolism by glutathione S-transferase (GST) was probed by equilibrating 5 mM reduced glutathione (GSH, GST cofactor(10)) for 5 minutes in the incubation mixture including HLM before the substrate (TATP) was added. Ticlopidine (TIC, 10 µM) was the substrate for the GST the positive control (Fig. S-7).(21) To examine metabolism by UGT, HLM, buffer, and alamethicin (50 µg/mL in H_2O/MeOH) were equilibrate cold for 15 minutes before saccharolactone (1mg/mL, β-glucuronidase inhibitor(22)), $MgCl_2$, and NADPH were added and the mixture warmed to 37 °C and shaken at 800 rpm. After 3 minutes equilibration, the substrate (TATP or TATP-OH) was added, and in 2 minutes the reaction was started by the addition of 5.5mM UDPGA (UGT cofactor(10)).(23,24) Positive control used 100 µM 1-naphthol, an UGT1A6 substrate (Fig. S-8).(25,26) Alamethicin was employed to replace membrane transporters, in allowing UGT (located in the endoplasmic reticulum lumen) easy access to the UDPGA cofactor.(10)

Enzyme Identification

TATP was incubated as described in the previous section with various enzyme inhibitors in HLM (1 mg/mL). TATP-OH formation was monitored and benchmarked against incubations without inhibitors. Chemical inhibitors, such as 1-aminobenzotriazole (1mM, 1-ABT),(27,28) methimazole (500µM, MMI),(29,30) or TIC (100 µM),(31,32) were pre-equilibrated in the incubation mixture for 30 minutes prior to the addition of the substrate (100µM, TATP or controls). TATP was also tested as a possible CYP2B6 inhibitor; TATP or BUP was pre-equilibration in the incubation mixture before starting the reaction with a known CYP2B6 substrate (BUP) or TATP, respectively. Flavin-containing monooxygenase (FMO) inhibition by heat was also tested.(10,33) In that experiment, HLM was mixed with buffer and pre-heated at 37 °C or 45°C for 5 minutes. After an hour cooling on

ice, the incubation procedure was resumed. BUP, a CYP2B6 substrate,(18–20) and BZD, a FMO substrate,(33) were used as positive and negative control substrates to assess CYP, FMO and CYP2B6 inhibition. Samples not pre-incubated with chemical inhibitors nor heated to 45 °C were used as 100% TATP-OH formation. Inhibition studies were quenched after 15 minutes incubation.

Recombinant CYP and FMO enzymes were employed to identify the isoform responsible for the NADPH dependent metabolism. Human bactosomes expressed in *E. coli* were used for CYP isoform identification; CYP1A2, CYP2B6, CYP2C9, CYP2C19, CYP2D6, CYP2E1 and CYP3A4 (100 pmol CYP/mL) were tested. Human supersomes expressed in insect cells were used for FMO isoform identification; FMO1, FMO3 and FMO5 (100 µg protein/mL) were examined. Both TATP and TATP-OH were tested as the substrate (10 µg/mL) in the incubation mixture with the recombinant enzymes. Negative control incubations were done in *E. coli* control or insect cell control. Positive control incubations were done in HLM (200 pmol CYP/mL), which contains all CYP and FMO enzymes. Recombinant enzymes studies were quenched after 10 minutes incubation.

Recombinant UGT enzymes were used to identify the isoform responsible for phase II metabolism. Human supersomes expressed in insect cells were used for UGT isoform identification; UGT1A1, UGT1A3, UGT1A4, UGT1A6, UGT1A9 and UGT2B7 were examined. The incubation mixture was similar to the glucuronidation incubation previously described, except saccharolactone was not added;(34) 500 µg protein/mL was used; and the substrate was 10 µg/mL TATP-OH. Negative control incubations were done in insect cell control. Positive control incubations were done in HLM (1 mg/mL), which contains all UGT enzymes. Glucuronidation with recombinant enzymes were quenched after 2 hours incubation.

Enzyme Kinetics

Kinetics experiments were done to determine the affinity of the enzyme CYP2B6 to the substrate TATP. The human CYP2B6 bactosomes used contained human CYP2B6 and human cytochrome P450 reductase co-expressed in *E. coli*, supplemented with purified human cytochrome b_5. Cytochrome P450 reductase is responsible for the transfer of electrons from NADPH to CYP, a task sometimes extended to cytochrome b_5.(10) The incubation mixture (1 mL) contained 10 mM phosphate buffer (pH 7.4), 2 mM $MgCl_2$, 50 pmol/mL rCYP2B6, 1 mM NADPH, and various concentrations of 0.1 to 20 µM TATP. The reaction was initiated by adding TATP after a 3-minute pre-equilibration and stopped at different end points (up to 5 minutes) to determine rate of TATP hydroxylation. The rate of TATP hydroxylation in lungs was also investigated by incubating TATP (100 µM) in the incubation mixture containing 1 mg/mL HLM or HLungM, instead of rCYP2B6, for up to 10 minutes.

TATP-OH metabolism by CYP2B6 was evaluated by incubating 10 µg/mL TATP-OH in CYP2B6 bactosomes according to the above procedure, with or without NADPH, except the buffer was pre-oxygenated so that the incubation could be performed in a closed vessel. Aliquots were removed and quenched at different time points, up to 30 minutes. TATP-OH depletion by HLM was determined using the same procedure, except 1µM TATP-OH and up to 60 minutes reaction times were used.

Urine Analysis

Laboratory personnel testing TATP are constantly exposed to this volatile compound. Explosive sensitivity experiments, such as drop weight impact tests, are done in a small brick-walled room for explosivity precautions, unlike synthesis reactions which are performed inside a fume hood for coverage protection. Also, testing portable explosive trace detection (ETD) devices that are meant to be used in the field are tested as such, which also contribute to exposure. Urine from laboratory workers was tested for TATP and its metabolites after TATP exposure in the laboratory environment. Urine was collected at the beginning of the work week and 2 hours after performing activities that could lead to high TATP exposure. To determine the longevity of TATP in the body, urine from the day following TATP exposure was also tested. The fresh urine was cleaned and concentrated for analysis using solid-phase extraction (SPE). Restek RDX column was conditioned with 6 mL of MeOH, followed by 6 mL of H_2O, and sample introduction (20–250 mL urine). The sample was washed with two cycles of 3mL 50:50 (v/v)

MeOH:H_2O. Extraction was achieved with two cycles of 1mL ACN. Both the MeOH:H_2O wash and the ACN extraction were tested by LC-MS.

RESULTS

Metabolite Identification

When TATP was incubated in HLM, TATP was depleted and one observable product, hydroxyl-TATP, was formed over time (Fig. 1). Metabolism of TATP in HLM consists of hydroxylation at one methyl group with the peroxide bonds and nine-membered ring structure preserved (Fig. 2).(14) Solaja have reported various monohydroxylated and dihydroxylated products during microsomal incubations with cyclohexylidene and steroidal mixed tetraoxanes where the peroxide bond was also preserved.(11) A TATP-OH standard (Fig. S-2) was chemically synthesized to confirm the metabolite by retention time and mass-to-charge ratio (m/z). TATP-OH, identified as $[TATP\text{-}OH + NH_4]^+$ (m/z 256.1391) by accurate mass spectrometry, increased in incubation samples as time progressed. The hydroxylated metabolite could not be verified with deuterated TATP due to the persistence of a contaminant with the same mass. As previously observed, TATP incubations in different species (dogs and rats) yielded the same metabolite, TATP-OH (Fig. S-3).(14) Other suspected metabolites, including the dihydroxy-species and additional oxidation of the TATP-OH to the aldehyde and carboxylic acid were not observed. Small polar molecules, such as acetone and hydrogen peroxide, the synthetic reagents of TATP, could not be chromatographically separated or are below the lower mass filter limit.

TATP was investigated for phase II metabolism routes of glutathione and glucuronide conjugation. Incubation in HLM with GSH produced no detectable glutathione metabolite conjugates, indicating that TATP is most likely not a substrate for microsomal GSTs (Fig. S-4). When TATP was incubated with UDPGA, the TATP-OH glucuronic acid metabolite (TATP-O-gluc) was observed (Fig. 2). The m/z 432.1712 for $[TATP\text{-}O\text{-}gluc + NH_4]^+$ was observed at very low levels after 2 and 3 hours of incubation. When the sample was dried and reconstituted in low volume, the intensity of $[TATP\text{-}O\text{-}gluc + NH_4]^+$ increased, but TATP and TATP-OH were evaporated along with the solvent. TATP and TATP-OH are volatile, limiting their use in quantification experiments since sample concentration is not feasible.(4) However, TATP-O-gluc is a non-volatile TATP derivative that is amenable to sample preparation. Formation of TATP-O-gluc over time was monitored as an intensity increase of m/z 432.1712 (Fig. S-5). Even though TATP and TATP-OH generally form ammonia adducts under positive ion APCI, the glucuronide favors negative ion mode ESI. The m/z 413.1301 for $[TATP\text{-}O\text{-}gluc - H]^-$ was easily seen at 1 to 3 hours without sample concentration. The common fragments of glucuronic acid, m/z 175, 113, and 85, were observed in the fragmentation pattern of m/z 413.1301, confirming the presence of a glucuronic acid conjugate (Fig. 3).(35) TATP-O-glucuronide was not observed in negative controls without UDPGA or NADPH, indicating that TATP-OH must be formed and then be further metabolized into TATP-O-gluc. Glucuronide conjugates are highly polar compounds that are easily eliminated by the kidney, suggesting that TATP-O-gluc would likely progress via urinary excretion.(10)

Enzyme Identification

TATP was only metabolized into TATP-OH in HLM in the presence of NADPH, indicating that the metabolism is NADPH-dependent. The predominant microsomal enzymes that require NADPH for activity are CYP and FMO.(10)

The usual roles of CYP are hydroxylation of an aliphatic or aromatic carbons, epoxidation of double bonds, heteroatom oxygenation or dealkylation, oxidative group transfer, cleavage of esters and dehydrogenation reactions.(10) 1-ABT is considered a general mechanism-based inhibitor of CYPs, initiated by metabolism into benzyne, which irreversibly reacts with the CYP heme.(27,28) When CYP activity was inhibited by 1-ABT, TATP-OH formation was also inhibited, with only 3.6% formed, (Table 2), suggesting that CYP is involved in the

hydroxylation of TATP. To support this evidence and to narrow down the CYP isoform catalyzing TATP hydroxylation, TATP was incubated with rCYPs (Fig. 4). The CYPs selected for testing are responsible for the metabolism of 89% of common xenobiotics.(36) TATP-OH was not observed when TATP was incubated with CYP1A2, CYP2C9, CYP2C19, CYP2D6, CYP2E1 and CYP3A4. TATP hydroxylation was performed exclusively by CYP2B6, with 5.6 ± 0.3 μM TATP-OH produced in 10 minutes. CYP2B6 has been found to metabolize endoperoxides by hydroxylation, as observed for TATP.(12,13) HLM, which contains CYP2B6, also exhibited TATP hydroxylation (1.5 ± 0.1 μM).

Since dog liver microsomes studies indicated that TATP is metabolized by CYP2B11, it was not surprising that another CYP2B subfamily enzyme, CYP2B6, metabolizes TATP in humans.(14) CYP2B6 metabolism of TATP was further investigated by incubating TATP with TIC, a mechanism-based inhibitor of CYP2B6.(31,32) When CYP2B6 activity was inhibited by TIC, TATP-OH formation was also inhibited by 95% (Table 2), further supporting the primary involvement of CYP2B6 in the metabolism of TATP. BUP hydroxylation is catalyzed by CYP2B6; therefore, it was chosen as a positive control for CYP and CYP2B6 inhibition tests. BUP-OH formation was inhibited by 77 % and 90% when incubated with 1-ABT and TIC, respectively.(37)

FMO catalyzes oxygenation of nucleophilic heteroatoms, such as nitrogen, sulfur, phosphorous and selenium.(33,38) Although FMO involvement in the hydroxylation of the TATP methyl group is unlikely, it seemed prudent to examine this enzyme class. Addition of MMI, an FMO competitive inhibitor,(29,30) caused a decrease in TATP-OH formation by 66% (Table 2), but this is not necessarily direct inhibition of TATP metabolism by FMO since MMI has been reported to reduce CYP2B6 activity by up to 80%.(33,39) While this result was inconclusive about the FMO contributions to TATP metabolism, it could be considered further support for the role of CYP2B6. TATP was incubated with available rFMOs: FMO1, FMO3 and FMO5 (Fig. 4). FMO1 is expressed in adults in the kidneys, and it should not contribute to the liver metabolism of TATP;(33) indeed, none appeared to be involved as no TATP-OH was produced. Since FMO is inactivated by heat,(10,33) TATP was incubated in HLM preheated to 45 °C for 5 minute. Table 2 compares the formation of TATP-OH at 37°C to that at 45°C and to the N-oxidation of the positive control, BZD. Although, there was a decrease in TATP hydroxylation, the inhibitory effect was not as significant compared to the decrease in BZD N-oxidation, which is catalyzed by FMO.

TATP-OH also appears to be metabolized by HLM in an NADPH-dependent manner: therefore, TATP-OH was incubated for 10 minutes with recombinant enzymes (CYP and FMO), to determine which isoform is responsible for this secondary phase I metabolism (Table 3). Although in all incubations some TATP-OH was lost due to sublimation at 37 °C, the only notable loss was with CYP2B6. In that incubation TATP-OH was depleted by 40%, suggesting CYP2B6 metabolizes TATP-OH. TATP-OH depletion in CYP2B6 was faster in the presence of NADPH than its absence, supporting metabolism by CYP2B6 (Fig. S-6). Unfortunately, no subsequent metabolite was identified.

To identify which isoform is responsible for TATP glucuronidation, TATP-OH was incubated with the most clinically relevant rUGTs (Fig. 5).(40) Glucuronidation was not observed with UGT1A1, UGT1A3, UGT1A4, UGT1A6 and UGT1A9. TATP-O-glucuronide was formed only in UGT2B7 incubations with 0.05 ± 0.03 area count relative to IS produced after 2 hours of incubation. HLM, which contains UGT2B7, also displayed TATP-O-gluc (0.26 ± 0.02 area count relative to IS). Relative quantification of TATP-O-gluc was done by area ratio to the IS because a TATP-O-gluc standard is not available. Endoperoxide glucuronidation by UGT2B7 has been reported, in which urine analysis of patients treated with artesunate, an artemisinin derivative, found dihydroartemisinin-glucuronide to be the principal metabolite excreted.(15)

Enzyme Kinetics

Rate of TATP hydroxylation by CYP2B6 was evaluated by plotting concentration of TATP-OH formed over time. The initial rate of TATP hydroxylation at various TATP concentrations was used to estimate enzyme kinetics using the Michaelis-Menten model: $v = v_{max} * [S] / (K_M + [S])$. Here, [S] is the substrate (TATP) concentration, v_{max} is the maximum formation rate, K_M is the substrate concentration at half of v_{max}, and k_{cat} is the

turnover rate of an enzyme-substrate complex to product and enzyme.(41) The kinetic constants were obtained using nonlinear regression analysis on GraphPad Prism software (ver. 8.2.1). The Michaelis-Menten (Fig. 6) evaluation for TATP hydroxylation by CYP2B6 yielded K_M of 1.4 μM; v_{max} of 8.7 nmol/min/nmol CYP2B6; and k_{cat} of 174 min^{-1}. Other linearized models are in good agreement:

Lineweaver-Burk: $1/v = (K_M/v_{max} * 1/[S]) + 1/v_{max}$; K_M 3.1 μM; v_{max} 11.7 nmol/min/nmol CYP2B6

Eadie-Hofstee: $v = (-K_M * v /[S]) + v_{max}$; K_M 0.54 μM; v_{max} 4.9 nmol/min/nmol CYP2B6

Hanes-Woolf: $[S]/v = [S]/v_{max} + K_M/v_{max}$; K_M 1.2 μM; v_{max} 8.0 nmol/min/nmol CYP2B6

The low K_M indicates TATP has a high affinity for CYP2B6.(42) Table 2 shows that TATP inhibits BUP hydroxylation by CYP2B6, with only 62% BUP-OH formation in 15 minutes. However, in the presence of BUP, TATP-OH formation was enhanced, with 125% formed compared to the reaction uninhibited by BUP (Table 2). CYP2B6 preference for TATP affects the metabolism of BUP, but further testing is needed to establish the specific type of inhibition.

Using the Michaelis-Menten parameters, *in vitro* intrinsic clearance ($Cl_{int} = v_{max}/K_M$) was calculated to be 6.13 mL/min/nmol CYP2B6.(10,43,44) Scale-up of the Cl_{int} to yield intrinsic clearance on a per kilogram body weight was done using values of 0.088 nmol CYP2B6/mg microsomal protein, 45 mg microsomal protein/g liver wet weight and 20 g liver wet weight/kg human body weight.(43) Taking that into account, the scale-up Cl_{int} was calculated to be 485 mL/min/kg.

In vivo intrinsic clearance (Cl) is the ability of the liver to metabolize and remove a xenobiotic, assuming normal hepatic blood flow (Q = 21 mL/min/kg(43,45)) and no protein binding.(43) Cl can be extrapolated using the well-stirred model excluding all protein binding as $Cl = Q * Cl_{int} / Q + Cl_{int}$.(43) The *in vivo* intrinsic clearance of TATP was estimated as 20 mL/min/kg. Compared to common drugs, TATP has a moderate clearance.(46)

TATP-OH kinetics was also investigated by substrate depletion. Substrate depletion was plotted as the natural log of substrate percent remaining over time (Fig. 7). Half-life ($t_{1/2}$) was calculated to be 16 minutes, as the natural log 2 divided by the negative slope of the substrate depletion plot. *In vitro* intrinsic clearance (Cl_{int}) can also be estimated using half-life as $Cl_{int} = (0.693/t_{1/2})$ * (incubation volume/mg microsomal protein).(47,48) The *in vitro* intrinsic clearance of TATP-OH was estimated as 0.042 mL/min/mg. Even though we identified two metabolic pathways for TATP-OH, it appears to be cleared slower than TATP.

Lung metabolism

Inhalation is the most probable pathway for systemic exposure since TATP is both volatile and lipophilic. With passive diffusion into the bloodstream being very possible, TATP metabolism in the lung was also investigated. TATP was incubated in lung and liver microsomes for comparison of metabolic rate. The results, shown in Table 4, indicate that TATP hydroxylation in the lungs is negligible. Though CYP2B6 gene and protein are expressed in the lungs, enzyme activity in lungs is minimal compared to the liver, limiting TATP metabolism.(49,50) This suggests that TATP will most likely be distributed through the blood to the liver for metabolism. News reported that traces of TATP was found in the blood samples extracted from the Brussels suicide bombers.(51) This indicates the possibility of using blood tests as forensic evidence for TATP exposure.

Urine Analysis

Laboratory workers, who normally work with TATP on a daily basis, performing tasks like explosive sensitivity testing, were screened for TATP exposure. These laboratory workers volunteered to collect their urine

before and after exposure to TATP vapor. Since the health effects of TATP exposure are unknown, to minimize any additional risks to these workers, this pilot study was performed in duplicates using only three volunteers to establish some reproducibility. TATP and TATP-OH were not observed in the urine of any of the workers. However, TATP-O-gluc was present in all urine samples after TATP exposure (Fig. 8). TATP-O-glucuronide was identified in human urine samples as both $[TATP\text{-}O\text{-}gluc - H]^-$ and $[TATP\text{-}O\text{-}gluc + NH_4]^+$. The presence of TATP-O-gluc in the urine of all three volunteers is summarized in Table 5.

CONCLUSIONS

Because TATP has high volatility it is likely to be absorbed into the body by inhalation; however, no appreciable metabolism in lung was observed in either dog(14) or human microsomes. Therefore, systemic exposure and subsequent liver metabolic clearance was presumed. Across three species, dog, rat, and human, TATP was metabolized in liver microsomes by CYP to TATP-OH. Using recombinant enzymes, we have previously established that CYP2B11 is responsible for this metabolism in dogs.(14) Interestingly, human CYP2B6 appears to be the major phase I enzyme responsible for the same metabolism. Though heat inactivation and specific FMO inhibition appeared to affect TATP hydroxylation, incubations with recombinant FMO suggest FMO was not forming TATP-OH. MMI, an FMO inhibitor, inhibited TATP-OH formation; but, inhibition of BUP under these conditions suggests MMI also inhibits CYP2B6 activity.(39)

When incubated together, TATP and BUP, appear to compete for CYP2B6 metabolism, with BUP hydroxylation being inhibited by 38% in the presence of TATP. Considering CYP2B6 expression in the liver is low and exhibits broad genetic polymorphisms, CYP2B6 activity can be widely affected if TATP affects the metabolism of other compounds, like BUP.(52,53) TATP may be a serious perpetrator for drug-drug interactions (DDI) for compounds cleared by CYP2B6.(54,55)

In vitro clearance of TATP was calculated as 0.54 mL/min/mg protein with *in vivo* extrapolation to 20 mL/min/kg. *In vitro* clearance of TATP-OH was roughly estimated as 0.038 mL/min/mg protein. We also established the clearance of TATP in dogs as 0.36 mL/min/mg protein in our previous study in canine microsomes, which is significantly relevant to K9 units, where the dog and human handler are both exposed to the explosive.(14)

No glutathione adducts of any TATP metabolism products were observed in the microsomal incubations with GSH. However, glucuronidation converted TATP-OH to TATP-O-gluc in HLM with UGT2B7 specifically catalyzing this reaction. Considering glucuronides are often observed as urinary metabolites, the presence of TATP-O-gluc in urine can be exploited as an absolute marker of TATP exposure.

Urine from scientists working to prevent terrorist attacks by synthesizing, characterizing and detecting TATP, who are inevitably exposed to this volatile compound were negatively tested for TATP and TATP-OH, but TATP-O-gluc was present at high levels in their fresh urine. Even though working with TATP falls under the protection of several standard operating procedures (SOPs) to handling explosives, considering the breathing exposure these laboratory workers revealed, implementation of precautionary measures to absorption by inhalation, such as the use of respirators, should be considered. This paper is the first to examine some aspects of TATP ADMET, elucidating the metabolism and excretion of TATP in humans.

ACKNOWLEDGMENT

The authors would like to thank Alexander Yevdokimov for mass spectrometry support and Lindsay McLennan for synthesis of TATP-OH standard.

FUNDING INFORMATION

This material is based upon work supported by U.S. Department of Homeland Security (DHS), Science & Technology Directorate, Office of University Programs, under Grant 2013-ST-061-ED0001.

Views and conclusions are those of the authors and should not be interpreted as necessarily representing the official policies, either expressed or implied, of DHS.

COMPLIANCE WITH ETHICAL STANDARDS

Conflict of interest The authors declare that they have no conflict of interest.

Ethics approval This study was approved by the University of Rhode Island Institutional Review Board (IRB) for Human Subjects Research (approval number 1920-206).

REFERENCES

1. Oxley JC, Smith JL, Bowden PR, Rettinger RC. Factors Influencing Triacetone Triperoxide (TATP) and Diacetone Diperoxide (DADP) Formation: Part 1. Propellants, Explos Pyrotech. 2013 Dec 11;38:244–54.
2. Jacoby M. Explosive used in Brussels isn't hard to detect [Internet]. Chemical & Engineering News. 2016 [cited 2019 Sep 3]. Available from: https://cen.acs.org/articles/94/web/2016/03/Explosive-used-Brussels-isnt-hard.html
3. Oxley JC, Smith JL, Canino JN. Journal of Energetic Materials Insensitive TATP Training Aid by Microencapsulation. 2016; Available from: http://www.tandfonline.com/action/journalInformation?journalCode=uegm20
4. Colizza K, Yevdokimov A, Mclennan L, Smith JL, Oxley JC. Reactions of Organic Peroxides with Alcohols in Atmospheric Pressure Chemical Ionization — the Pitfalls. J Am Soc Mass Spectrom. 2018;29:393–404.
5. Oxley JC, Smith JL, Shinde K, Moran J. Determination of the vapor density of Triacetone Triperoxide (TATP) using a gas chromatography headspace technique. Propellants, Explos Pyrotech. 2005;30(2):127–30.
6. Yinon J. Toxicity and Metabolism of Explosives. Boca Raton, FL: CRC Press, Inc.; 1990.
7. Leung KH, Yao M, Stearns R, Chiu S-HL. Mechanism of bioactivation and covalent binding of 2,4 ,6-trinitrotoluene. Chem Interact. 1995;97:37–51.
8. Bell SC, Gayton-Ely M, Nida CM. Bioassays for bomb-makers: Proof of concept. Anal Bioanal Chem. 2009;395(2):401–9.
9. Sabbioni G, Liu Y, Yan H, Sepai O. Hemoglobin adducts , urinary metabolites and health effects in 2 , 4 , 6-trinitrotoluene exposed workers. Carcinogenesis. 2005;26(7):1272–9.
10. Parkinson A. Biotransformation of Xenobiotics. In: Klaassen CD, editor. Casarett & Doull's Toxicology: The Basic Science of Poisons. 5th ed. McGraw-Hill, Inc.; 1996. p. 113–86.
11. Opsenica DM, Šolaja BA. Antimalarial peroxides. J Serbian Chem Soc. 2009;74(11):1155–93.
12. Svensson USH, Ashton M. Identification of the human cytochrome P450 enzymes involved in the in vitro metabolism of artemisinin. Br J Clin Pharmacol. 1999;48:528–35.
13. Lee I-S, Hufford CD. Metabolism of Antimalarial Sesquiterpene Lactones. Pharmacol Ther. 1990;48:345–55.
14. Colizza K, Gonsalves M, Mclennan L, Smith JL, Oxley JC. Metabolism of triacetone triperoxide (TATP) by canine cytochrome P450 2B11. Forensic Toxicol [Internet]. 2019;37:174–85. Available from: https://doi.org/10.1007/s11419-018-0450-9
15. Ilett KF, Ethell BT, Maggs JL, Davis TME, Batty KT, Burchell B, et al. Glucuronidation of dihydroartemisinin in vivo and by human liver microsomes and expressed UDP-glucuronosyltransferases. Drug Metab Dispos. 2002;30(9):1005–12.

16. Yamazaki H, Ueng Y-F, Shimada T, Guengerich FP. Roles of Divalent Metal Ions in Oxidations Catalyzed by Recombinant Cytochrome P450 3A4 and Replacement of NADPH-Cytochrome P450 Reductase with Other Flavoproteins, Ferredoxin, and Oxygen Surrogates. Biochemistry. 1995;34:8380–9.

17. Chauret N, Gauthier A, Nicoll-Griffith DA. Effect of Common Organic Solvents on In Vitro Cytochrome P450- Mediated Metabolic Activities in Human Liver Microsomes. Drug Metab Dispos. 1998;26(1).

18. Hesse LM, Venkatakrishnan K, Court MH, Moltke LL Von, Duan SX, Shader RI, et al. CYP2B6 Mediates the in vitro Hydroxylation of Bupropion: Potential Drug Interactions with Other Antidepressants. Drug Metab Dispos. 2000;28(10):1176–83.

19. Faucette SR, Hawke RL, Lecluyse EL, Shord SS, Yan B, Laethem RM, et al. Validation of Bupropion Hydroxylation as a Selective Marker of Human Cytochrome P450 2B6 Catalytic Activity. Drug Metab Dispos. 2000;28(10):1222–30.

20. Chen Y, Liu H, Liu L, Nguyen K, Jones EB, Fretland AJ. The in vitro metabolism of bupropion revisited : concentration dependent involvement of cytochrome P450 2C19. Xenobiotica. 2010;40(8):536–46.

21. Ruan Q, Zhu M. Investigation of Bioactivation of Ticlopidine Using Linear Ion Trap/Orbitrap Mass Spectrometry and an Improved Mass Defect Filtering Technique. Chem Res Toxicol. 2010;23:909–17.

22. Oleson L, Court MH. Effect of the b-glucuronidase inhibitor saccharolactone on glucuronidation by human tissue microsomes and recombinant UDP-glucuronosyltransferases (UGTs). J Pharm Pharmacol. 2008;60(9):1175–82.

23. Schebb NH, Franze B, Maul R, Ranganathan A, Hammock BD. In Vitro Glucuronidation of the Antibacterial Triclocarban and Its Oxidative Metabolites. Drug Metab Dispos. 2012;40(1):25–31.

24. Sim J, Choi E, Jeong G, Lee S. Characterization of in vitro metabolites of cudratricusxanthone A in human liver microsomes. Biopharm Drug Dispos. 2015;35:325–36.

25. Fujiwara R, Nakajima M, Yamanaka H, Katoh M, Yokoi T. Product Inhibition of UDP-Glucuronosyltransferase (UGT) Enzymes by UDP Obfuscates the Inhibitory Effects of UGT Substrates. Drug Metab Dispos. 2008;36(2):361–7.

26. Kazmi F, Yerino P, Barbara JE, Parkinson A. Further Characterization of the Metabolism of Desloratadine and Its Cytochrome P450 and UDP-glucuronosyltransferase Inhibition Potential : Identification of Desloratadine as a Relatively Selective UGT2B10 Inhibitor. Drug Metab Dispos. 2015;43:1294–302.

27. Linder CD, Renaud NA, Hutzler JM. Is 1-Aminobenzotriazole an Appropriate in Vitro Tool as a Nonspecific Cytochrome P450 Inactivator? Drug Metab Dispos. 2009;37(1):10–3.

28. Montellano PRO de. 1-Aminobenzotriazole: A Mechanism-Based Cytochrome P450 Inhibitor and Probe of Cytochrome P450 Biology. Med Chem. 2018;8(3):38–65.

29. Nace CG, Genter MB, Sayre LM, Crofton KM. Effect of Methimazole, an FMO Substrate and Competitive Inhibitor, on the Neurotoxicity of 3,3′-Iminodipropionitrile in Male Rats. Fundam Appl Toxicol. 1997;37:131–40.

30. Foti RS, Dalvie DK. Cytochrome P450 and non-cytochrome P450 oxidative metabolism: Contributions to the pharmacokinetics, safety, and efficacy of xenobiotics. Drug Metab Dispos. 2016;44:1229–45.

31. Richter T, Murdter TE, Heinkele G, Pleiss J, Tatzel S, Schwab M, et al. Potent Mechanism-Based Inhibition of Human CYP2B6 by Clopidogrel and Ticlopidine. J Pharmacol Exp Ther. 2004;308(1):189–97.

32. Talakad JC, Shah MB, Walker GS, Xiang C, Halpert JR, Dalvie D. Comparison of In Vitro Metabolism of Ticlopidine by Human Cytochrome P450 2B6 and Rabbit Cytochrome P450 2B4. Drug Metab Dispos. 2011;39(3):539–50.

33. Jones BC, Srivastava A, Colclough N, Wilson J, Reddy VP, Amberntsson S, et al. An investigation into the

prediction of in vivo clearance for a range of flavin-containing monooxygenase substrates. Drug Metab Dispos. 2017;45(1):1060–7.

34. Walsky RL, Bauman JN, Bourcier K, Giddens G, Lapham K, Negahban A, et al. Optimized Assays for Human UDP-Glucuronosyltransferase (UGT) Activities : Altered Alamethicin Concentration and Utility to Screen for UGT Inhibitors. Drug Metab Dispos. 2012;40(3):1051–65.

35. Levsen K, Schiebel H, Behnke B, Reinhard D, Dreher W, Elend M, et al. Structure elucidation of phase II metabolites by tandem mass spectrometry : an overview. J Chromatogr A. 2005;1067:55–72.

36. Zanger UM, Schwab M. Cytochrome P450 enzymes in drug metabolism: Regulation of gene expression, enzyme activities, and impact of genetic variation. Pharmacol Ther [Internet]. 2013;138(1):103–41. Available from: http://dx.doi.org/10.1016/j.pharmthera.2012.12.007

37. Linder CD, Renaud NA, Hutzler JM. Is 1-Aminobenzotriazole an appropriate in vitro tool as a nonspecific cytochrome P450 inactivator? Drug Metab Dispos. 2009;37(1):10–3.

38. Jakoby WB, Ziegler DM. The Enzymes of Detoxication. J Biol Chem. 1990;265(34):20715–8.

39. Guo Z, Raeissi S, White RB, Stevens JC. Orphenadrine and Methimazole Inhibit Multiple Cytochrome P450 Enzymes in Human Liver Microsomes. Drug Metab Dispos. 1997;25(3):390–3.

40. Rowland A, Miners JO, Mackenzie PI. The UDP-glucuronosyltransferases : Their role in drug metabolism and detoxification. Int J Biochem Cell Biol [Internet]. 2013;45:1121–32. Available from: http://dx.doi.org/10.1016/j.biocel.2013.02.019

41. Rawn JD. Biochemistry. Row H&, editor. New York; 1983.

42. Cox PM, Bumpus NN. Single Heteroatom Substitutions in the Efavirenz Oxazinone Ring Impact Metabolism by CYP2B6. ChemMedChem. 2016;11:2630–7.

43. Obach RS. Nonspecific Binding to Microsomes: Impact on Scale-up of In Vitro Intrinsic Clearance to Hepatic Clearance as Assessed Through Examination of Warfarin, Imipramine, and Propranolol. Drug Metab Dispos. 1997;25(12).

44. Stringer RA, Strain-Damerell C, Nicklin P, Houston JB. Evaluation of Recombinant Cytochrome P450 Enzymes as an in Vitro System for Metabolic Clearance Predictions. Drug Metab Dispos. 2009;37(5):1025–34.

45. Davies B, Morris T. Physiological Parameters in Laboratory Animals and Humans. Pharm Res. 1993;10(7).

46. Di L, Obach RS. Addressing the Challenges of Low Clearance in Drug Research. AAPS J. 2015;17(2):352–7.

47. Słoczyńska K, Gunia-Krzyzak A, Koczurkiewicz P, Wójcik-Pszczoła K, Zelaszczyk D, Popiół J, et al. Metabolic stability and its role in the discovery of new chemical entities. Acta Pharm. 2019;69:345–61.

48. Schneider D, Oskamp A, Holschbach M, Neumaier B, Bauer A, Bier D. Relevance of in vitro metabolism models to PET radiotracer development: Prediction of in vivo clearance in rats from microsomal stability data. Pharmaceuticals. 2019;12(57):1–12.

49. Macé K, Bowman ED, Vautravers P, Shields PG, Harris CC, Pfeifer AMA. Characterisation of xenobiotic-metabolising enzyme expression in human bronchial mucosa and peripheral lung tissues. Eur J Cancer. 1998;34(6):914–20.

50. Hukkanen J. Xenobiotic-Metabolizing Cytochrome P450 Enzymes in Human Lung. Lung. University of Oulu; 2000.

51. Goulard H. Belgian breakthrough to help ID terror suspects: report [Internet]. Politico. 2016 [cited 2019 Jan 3]. Available from: https://www.politico.eu/article/belgian-breakthrough-to-help-id-terror-suspects-report/

52. Shimada T, Yamazaki H, Mimura M, Inui Y, Guengerich FP. Interindividual Variations in Human Liver Cytochrome P-450 Enzymes Involved in the Oxidation of Drugs, Carcinogens and Toxic Chemicals: Studies with Liver Microsomes of 30 Japanese and 30 Caucasians. J Pharmacol Exp Ther. 1994;270(1):414–23.

53. Zanger UM, Klein K. Pharmacogenetics of cytochrome P450 2B6 (CYP2B6): advances on polymorphisms, mechanisms, and clinical relevance. Front Genet. 2013;4(March):1–12.

54. Xing J, Kirby BJ, Whittington D, Wan Y, Goodlett DR. Evaluation of P450 inhibition and induction by artemisinin antimalarials in human liver microsomes and primary human hepatocytes. Drug Metab Dispos. 2012;40(9):1757–64.

55. Fahmi OA, Shebley M, Palamanda J, Sinz MW, Ramsden D, Einolf HJ, et al. Evaluation of CYP2B6 induction and prediction of clinical drug-drug interactions: Considerations from the IQ consortium induction working group - An industry perspective. Drug Metab Dispos. 2016;44:1720–30.

TABLES

Table 1: Triple quadrupole mass spectrometer (Q-trap 5500) operating parameters

Parameters	Method 1		Method 2	Method 3			
Source type	APCI+		ESI-	ESI+			
Source temperature °(C)	300		300	260			
Ion spray voltage (V)	N/A		-4500	4500			
Nebulizer current (μA)	0.8		N/A	N/A			
Ion source gas 1 (psi)	50		50	20			
Ion source gas 2 (psi)	2		2	2			
Curtain gas (psi)	28		28	30			
Collision gas (psi)	6		6	5			
Declustering potential (V)	26		-26	30			
Entrance potential (V)	10		-10	10			
Internal standard MRM transitions (m/z)	258 → 80, 46		219 → 161, 125	253 → 208, 180			
Collision energy (V)	11, 27		-13, -27	27, 39			
Collision cell exit potential (V)	14, 20		-36, -20	22, 14			
Analyte	TATP	TATP-OH	TATP-O-gluc	BUP	BUP-OH	BZD	BZD-NO
Analyte MRM transition (m/z)	240 → 74, 43	256 → 75	413 → 113, 87	240 → 184, 166	256 → 238, 139	310 → 86	326 → 102
Collision energy (V)	11, 28	13	-22, -34	17, 23	15, 33	21	19
Collision cell exit potential (V)	10, 11	36	-13, -9	20, 10	12, 16	10	12

Table 2: Average % metabolite formed (triplicates) in 15min incubations with chemical inhibitors or heat

Metabolite Formation in 15min	30 min pre-incubation in HLM					HLM pre-heated for 5min	
	No inhibitor	1-ABT CYP inhibitor	MMI FMO inhibitor	TIC CYP2B6 inhibitor	TATP or BUP	37°C	45°C
TATP-OH (%)	100 ± 5	3.6 ± 0.7	34 ± 2	4.8 ± 0.7	12µ± 21	100 ± 10	69 ± 4
BUP-OH (%)	100 ± 3	23 ± 1	62 ± 2	9.6 ± 0.4	62 ± 2	100 ± 6	99 ± 2
BZD-NO (%)	100 ± 2	97 ± 1	48 ± 1	98 ± 3	N/A	100 ± 2	44 ± 2

Table 3: Average % TATP-OH remaining (triplicates) after 10 min incubation in recombinant enzymes

Incubation matrix	% TATP-OH Remaining
HLM	69 ± 5
rCYP control	76 ± 4
rCYP1A2	77 ± 2
rCYP2B6	60 ± 3
rCYP2C9	71 ± 8
rCYP2C19	76 ± 5
rCYP2D6	76 ± 5
rCYP2E1	73 ± 5
rCYP3A4	78 ± 6
rFMO control	69 ± 3
rFMO1	78 ± 12
rFMO3	78 ± 6
rFMO5	72 ± 7

Table 4: Rate of TATP hydroxylation (triplicates) in HLM versus HLungM

Human Microsomes	Rate of TATP-OH Formation (nmol/min/mg)
Liver	0.425 ± 0.06
Lung lot1710142	< LOQ
Lung lot1410246	< LOQ

Table 5: Summary of TATP-O-glucuronide presence in human urine (triplicates). TATP glucuronide is observed as $[TATP\text{-}O\text{-}gluc - H]^-$ (m/z 413.1301) and $[TATP\text{-}O\text{-}gluc + NH_4]^+$ (m/z 432.1712, less sensitive)

Human	m/z 413.1301			m/z 432.1712		
	#1	#2	#3	#1	#2	#3
Before TATP exposure	-	-	-	-	-	-
2 hours after TATP exposure	+	+	+	+	+	+
1 day after TATP exposure[a]	+	+	-	+	-	-

[a] Only one trial performed on next day samples.

LEGENDS TO FIGURES

Fig. 1: TATP biotransformation into TATP-OH monitored over time in HLM. Performed in triplicates

Fig. 2: TATP metabolic pathways in HLM

Fig. 3: Mass spectrum of $[TATP\text{-}O\text{-}gluc - H]^-$ (m/z 413.1301), fragmented with 35 eV using ESI-. Proposed structure are shown(35)

Fig. 4: TATP-OH formation from TATP incubations with recombinant CYP and FMO. Experiments with rCYP or rFMO consisted of 10 µg/mL TATP incubated with phosphate buffer (pH 7.4), 2 mM $MgCl_2$ and 1 mM NADPH. Incubations done in triplicates and quenched at 10 minutes

Fig. 5: TATP-O-glucuronide formation from TATP-OH incubations with recombinant UGT. Experiments with rUGT consisted of 10 µg/mL TATP-OH incubated with phosphate buffer (pH 7.4), 2 mM $MgCl_2$, 50 µg/mL alamethicin, 1 mM NADPH, and 5.5µM UDPGA. Glucuronidation done in triplicates and quenched at 2 hours. Quantification was done using area ratio TATP-O-gluc/IS

Fig. 6: Rate of TATP hydroxylation by CYP2B6 versus TATP concentration. Incubations of various TATP concentrations consisted of 50 pmol CYP2B6/mL human bactosomes with phosphate buffer (pH 7.4), 2mM $MgCl_2$ and 1mM NADPH. Incubations done in triplicates and quenched every minute up to 5 minutes.

Fig. 7: Natural log of TATP-OH % remaining in HLM versus time. TATP-OH (1µM) incubated in 1 mg/mL HLM with pre-oxygenated phosphate buffer (pH 7.4), 2 mM $MgCl_2$ and 1 mM NADPH. Incubations done in closed vials, in triplicates and quenched every 10 minutes up to 1 hour.

Fig. 8: Extracted ion chromatogram of $[TATP\text{-}O\text{-}gluc - H]^-$ (m/z 413.1301) in HLM 2 hours after incubation with TATP, and in human urine, before TATP exposure and 2 hours after TATP exposure.

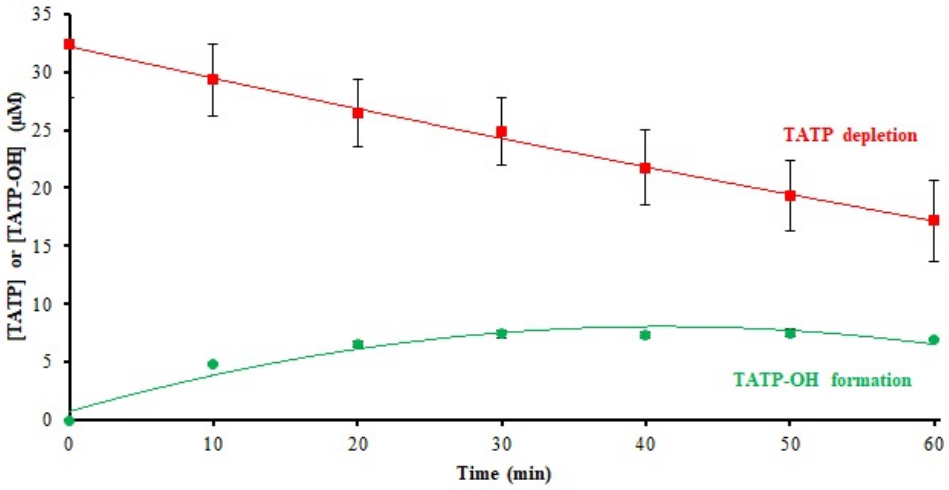

Figure 1

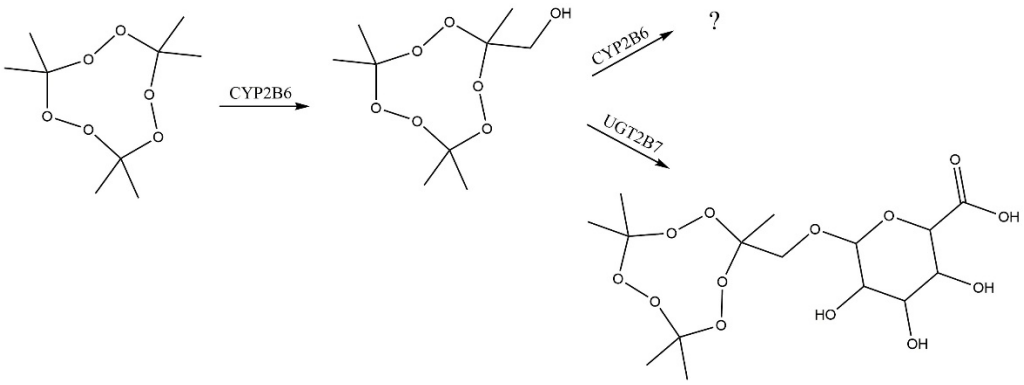

Figure 2

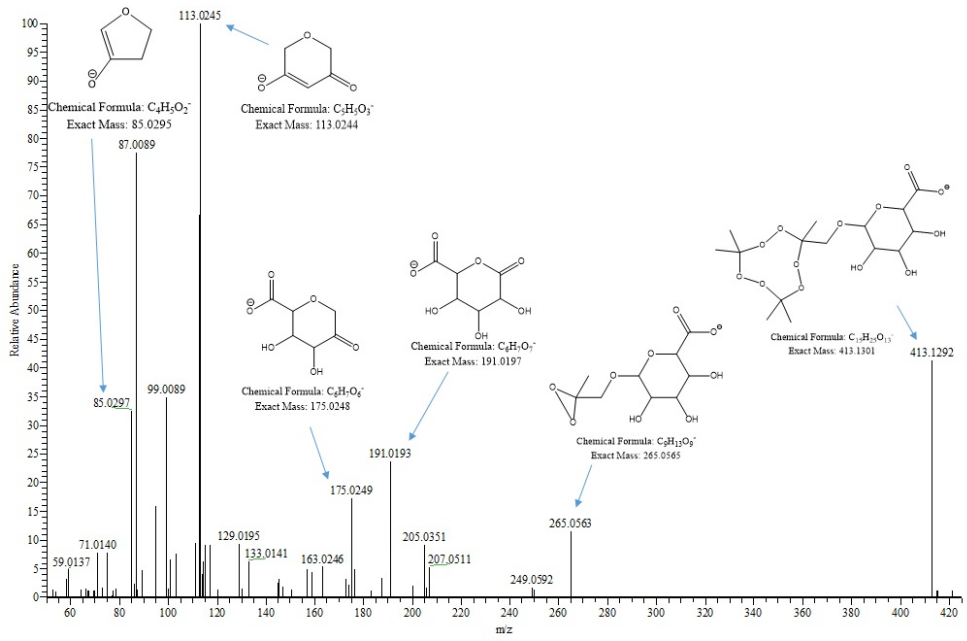

Figure 3

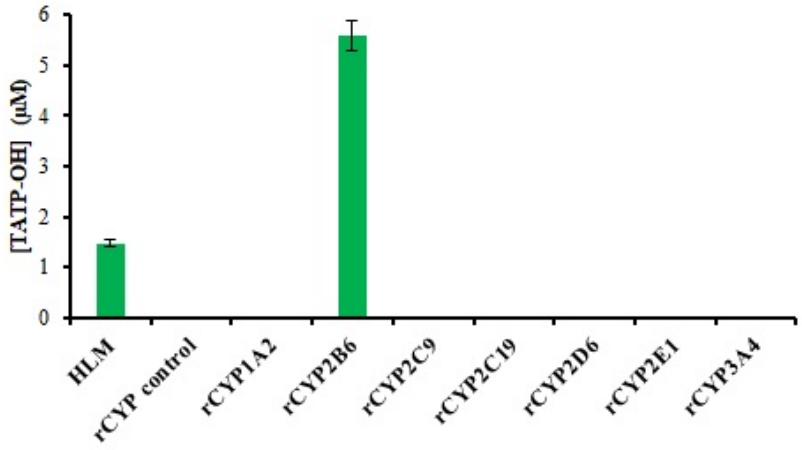

Figure 4

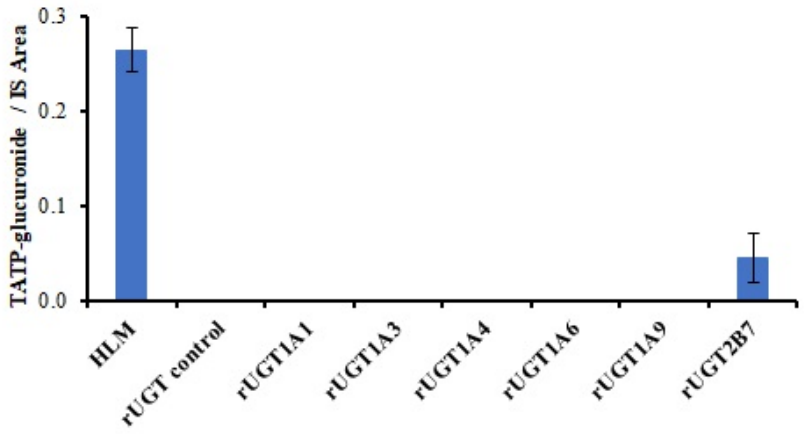

Figure 5

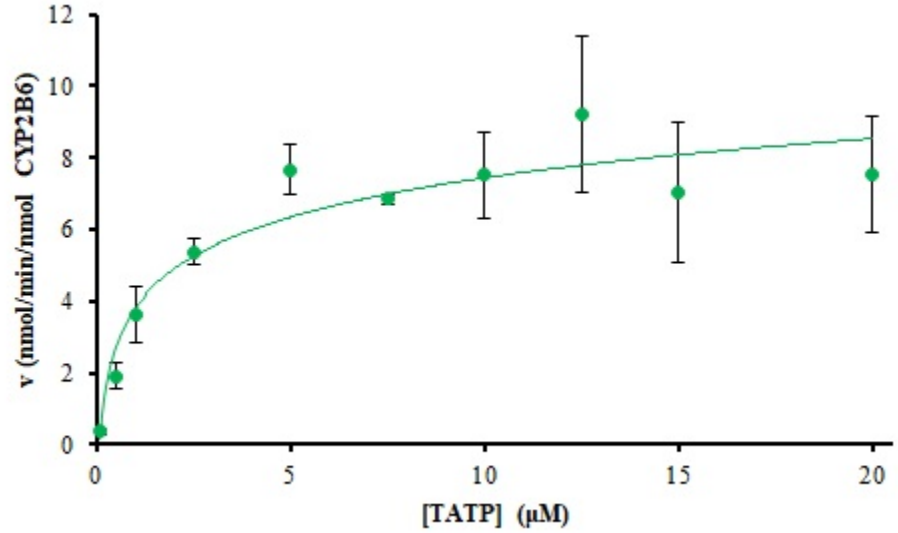

Figure 6

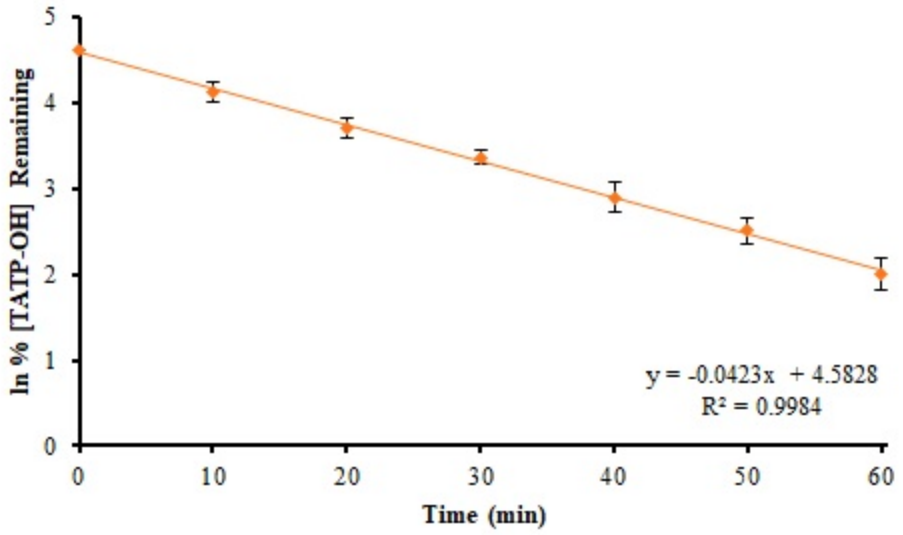

Figure 7

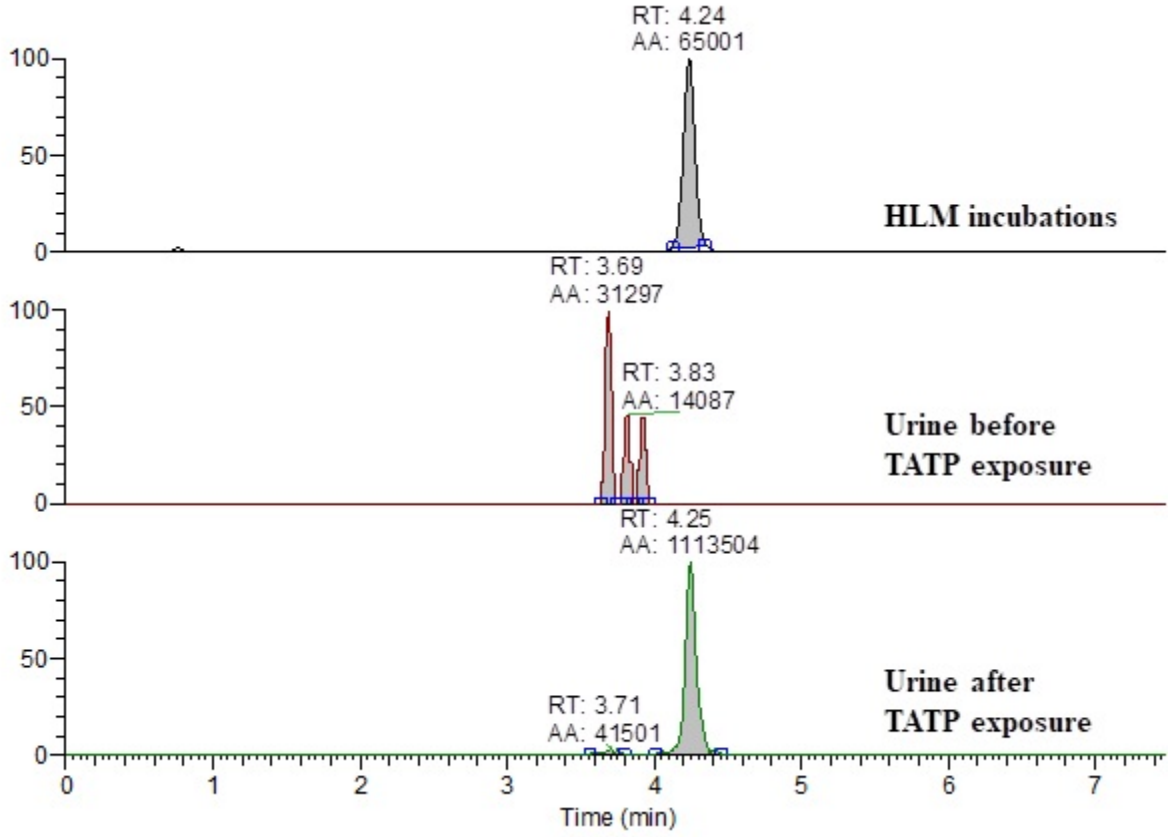

Figure 8

This page intentionally left blank.

R1-C.3: Characterizing, Modeling, and Mitigating Texturing in X-Ray Diffraction Tomography

I. PARTICIPANTS INVOLVED FROM JULY 1, 2019 TO JUNE 30, 2020

Faculty/Staff			
Name	**Title**	**Institution**	**Email**
Joel Greenberg	PI	Duke University	joel.greenberg@duke.edu
Anuj Kapadia	Co-PI	Duke University	anuj.kapadia@duke.edu
Dean Hazineh	Research Associate	Duke University	dean.hazineh@duke.edu
Graduate, Undergraduate and REU Students			
Name	**Degree Pursued**	**Institution**	**Month/Year of Graduation**
Stefan Stryker	PhD (Med Phys)	Duke University	5/2022
Oluwadamilola Fasina	MS (Med Phys)	Duke University	5/2021
Jordan Houri	MS (Med Phys)	Duke University	5/2021
Jeffrey Xiao	MS (Med Phys)	Duke University	5/2020

II. PROJECT DESCRIPTION

A. Project Overview

The detection of contraband and explosives concealed within a large volume of confounding items is a challenging task. X-ray based imaging has been central to this effort for nearly the last two decades, but conventional transmission-based methods lack the material specificity required to accurately detect the target items. X-ray diffraction tomography (XRDT) has the potential to dramatically improve the sensitivity and specificity of X-ray–based explosives detection systems because of its ability to identify concealed materials based on their microscopic atomic and/or molecular structures. As such, it has begun appearing on DHS roadmaps as a future solution for reducing false alarm rates while increasing the threat list. While this sensitivity to molecular composition is necessary for accurately assessing a host of benign and threat materials, it may at times be too sensitive: the details of the measured X-ray diffraction scatter signatures can depend on a variety of factors relating to environmental history and conditions. This can lead to a variation in the X-ray diffraction (XRD) "signatures" that complicate classification and reduce the efficacy of the XRD system. A well-known example of this effect is the dependence on the degree that crystallinity, orientation of crystalline grains, size of the grains, and other related factors result in seemingly random modulations of the powder XRD patterns, called texture. In this project, we took a multipronged approach to investigating the role of texture as it relates to aviation security in order to understand its impact as well as provide methods for mitigating its effects. In particular, we addressed the following topics, with the goal of improving the performance of current and future XRD systems:

- **Empirical testbed:** Built a novel experimental system to explore the prevalence of texture in both stream of commerce and explosive materials.

- **Database creation:** Acquired scatter data for multiple instantiations (e.g., different orientations, grain sizes, and processing history) of a broad range of materials of interest and incorporated the measurements into a shareable database (hosted by the University of Rhode Island [URI]).
- **Simulation tools:** Developed an empirically informed approach to modeling texture in arbitrary XRD systems and implemented it in both a deterministic and GPU-enhanced Monte Carlo (MCGPU) simulation approach. The MCGPU tool is available for sharing with interested parties.
- **Detection algorithms:** Explored machine learning and nonlinear dimension reduction techniques for robust detection performance in the presence of texture. We showed that support vector machine, random forest, convolutional neural net algorithms trained on simulated data lead to improved probability of error when applied to experimental data, as compared to the conventional matched-filter or correlation-based classifier approaches. These approaches generalize nicely to the case of mixtures (e.g., homemade explosives) and to situations when the library is incomplete.
- **System design:** Performed system-level studies that demonstrate measurement approaches that minimize the impact of texturing on detection and imaging performance.

The tools and findings of this project have already been adopted by other members of the aviation security industry and will be further applied and refined via separate DHS-funded efforts (e.g., the current BAA 14-02 T/Si program led by Duke in collaboration with Smiths, University of Arizona, and Quadridox) aimed at developing and deploying XRD systems at the checkpoint and in checked baggage.

B. State of the Art and Technical Approach

The topics of texturing, numerical simulation methods, and XRDT architectures have all been studied previously; however, none of these previous investigations have been unified. As a result, there exist critical gaps in quantifying and overcoming the effects of texturing that make accurate evaluation of XRDT impossible. We address these gaps and evaluate the utility of XRDT in aviation security applications.

B.1. X-Ray Diffraction Tomography

X-ray diffraction has been shown to greatly increase the material specificity of X-ray-based inspection; as a result, it can lead to significantly reduced false alarm rates [1]. XRDT involves determining the XRD signature associated with each voxel throughout an object. Unfortunately, the physics of XRD conflates the location and material composition of an object. While several methods for performing the XRDT task have been studied previously, the two methods most applicable to aviation security are direct tomography (DT) [2] and coded aperture XRDT (CA-XRDT) [3-6]. In DT, one uses collimators on the source and detector side of the object, such that each detector pixel images only a single voxel within the object. With the signal localized in this way, the XRD signature is recorded through the use of energy-sensitive detection at each pixel. This technique forms the basis of the Smiths HDX 10065 and Smiths XDi machines [7]. While DT has a well-defined spatial resolution and low computational overhead, the heavy collimation results in extreme photon starvation in the imaging system, making the scanning system slow and/or requiring expensive, complicated components [8]. In addition, the requirement of viewing an object voxel from only a single angle may result in the system measuring incorrectly or missing altogether the scatter in the case of a highly textured material.

B.2. Characterization of Texturing

For more than one hundred years, the fundamental science behind XRD has been developed and applied to understanding the structure and properties of materials. It is well known that the XRD signal depends on the molecular structure of the material at the microscopic scale. Because of this, XRD yields a signature for

distinguishing materials from one another (i.e., performing material identification); however, details in the microscopic structure of the material can impact the XRD signature. A particular example of this is known as texturing, in which the type, degree, and relative orientation of the crystal structure of a sample impacts the details of the XRD scatter signal (see Figure 1). While these details are useful for investigating the properties of a known material, they pose challenges (and therefore are usually ignored) in the case of performing material identification and/or threat detection of an unknown material.

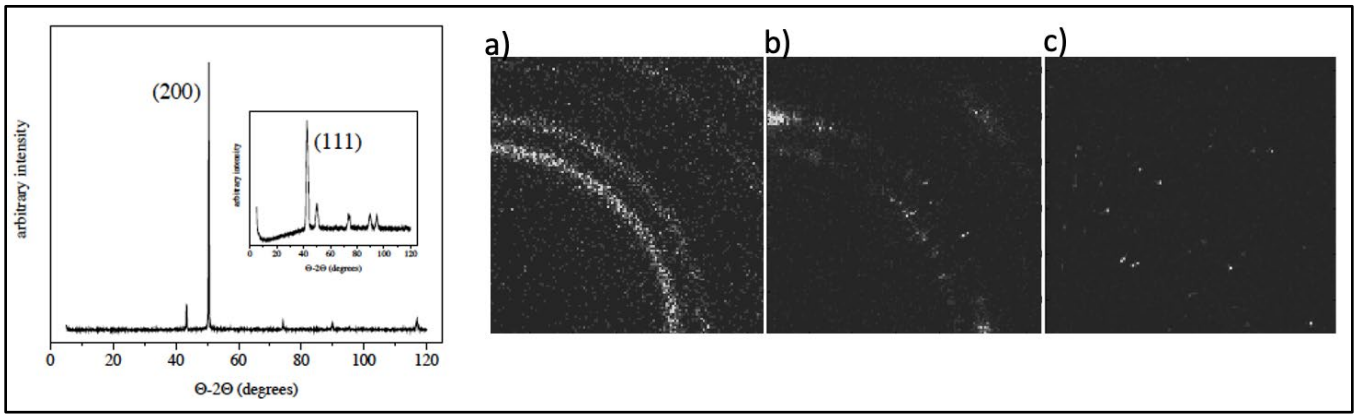

Figure 1: Degree of texturing; (left image) XRD form factor for the same copper sheet with two different orientations relative to the x-ray beam; (right three images, in order of increasing texturing from left to right) XRD scatter at 60 keV using a pencil-beam CAXSI system and 2D energy-sensitive detector spanning π/2 for (a) Al powder, (b) Al sheet, and (c) ammonium nitrate powder. Texture modulates the scatter intensity in both angle and energy in an unpredictable way.

A variety of XRD databases exist; however, they are of limited value to aviation security for several reasons. First, they typically involve measurements made with carefully prepared powder samples (as opposed to solid or highly crystalline samples), which guarantees that texturing is absent. Furthermore, they typically only cover specific classes of materials (e.g., biomolecules or metal alloys) which do not adequately represent many common objects found in luggage (such as toothpaste, cheese, paper, and water). Finally, existing databases usually include only a few instantiations for each unique material and do not included various orientations of textured materials. Without an adequate understanding of the inherent variability of the XRD signatures, one cannot evaluate the performance of any real-world XRDT system.

In addition, the conventional XRD measurements are made using a standard X-ray diffractometer operated in reflection mode at a single, low (e.g., 8 keV) X-ray energy to record the scatter form factors; however, for aviation security applications, measurements are made in transmission mode and require high energies (20–180 keV) in order to penetrate bags. Because the scatter cross-section changes as a function of energy and angle, it is important to record the complete energy- and angle-dependent scatter cross-sections. While a synchrotron system has recently been built to measure the angle- and energy-dependent XRD signal over a limited range of energies [9], this method is hardly practical for use in real labs and too expensive to use to generate large databases worth of data.

Without the aforementioned databases (which include stream of commerce materials measured at appropriate energies and including material variations), it is extremely difficult to design XRDT systems or develop appropriate detection algorithms, as material signatures and their associated variability are central to these tasks. We are therefore building a comprehensive database relevant to threat detection and developing a statistical description of texturing in order to improve the performance of existing systems and properly evaluate the performance of future scanners.

B.3. XRD Simulation Tools

Numerical tools that enable simulation of X-ray physics as well as dependencies on component behavior (e.g., source, detector, and collimator) and geometry are critical for understanding and evaluating the benefits of XRDT systems. The two dominant simulation methods are (1) deterministic numerical models for calculating mean quantities (which typically consider only first order scatter phenomena) and (2) Monte Carlo (MC) techniques (which are exhaustive but time-consuming). The advantage of a deterministic numerical model is that it is fast to run and can therefore be used to perform design studies over a broad trade space. A robust model of this sort is also necessary for performing model-based reconstruction for an XRDT system (e.g., recovering the threat status of an object based on the raw measurements). On the other hand, MC is the most physically accurate simulation technique and naturally accommodates stochastic processes (such as multiple scatter and noise). Although time-consuming, Monte Carlo enables realistic and accurate determination of system performance with all relevant sources of noise.

Models of both types have been developed previously by several groups [10-12]. We have previously developed state-of-the-art simulation models of both types: a deterministic numerical model of Compton scatter and XRD [8], as well as an MC model based on GEANT4 [13] that includes empirically measured XRD signatures in place of the conventional Hubble form factors. We have previously validated our models against experimental measurements and used them to study various XRDT configurations (see Figure 2) [3, 13]. In addition, the FDA has developed a GPU-accelerated MC approach (MCGPU) that is intended for simulating a limited range of materials at X-ray energies [14]. While useful, none of the models developed to date include the energy and angular dependencies exhibited by textured materials and are therefore constrained to describing a limited set of materials. We are therefore extending the current models to include a more complete description of texturing in order to faithfully represent real-world materials present in luggage.

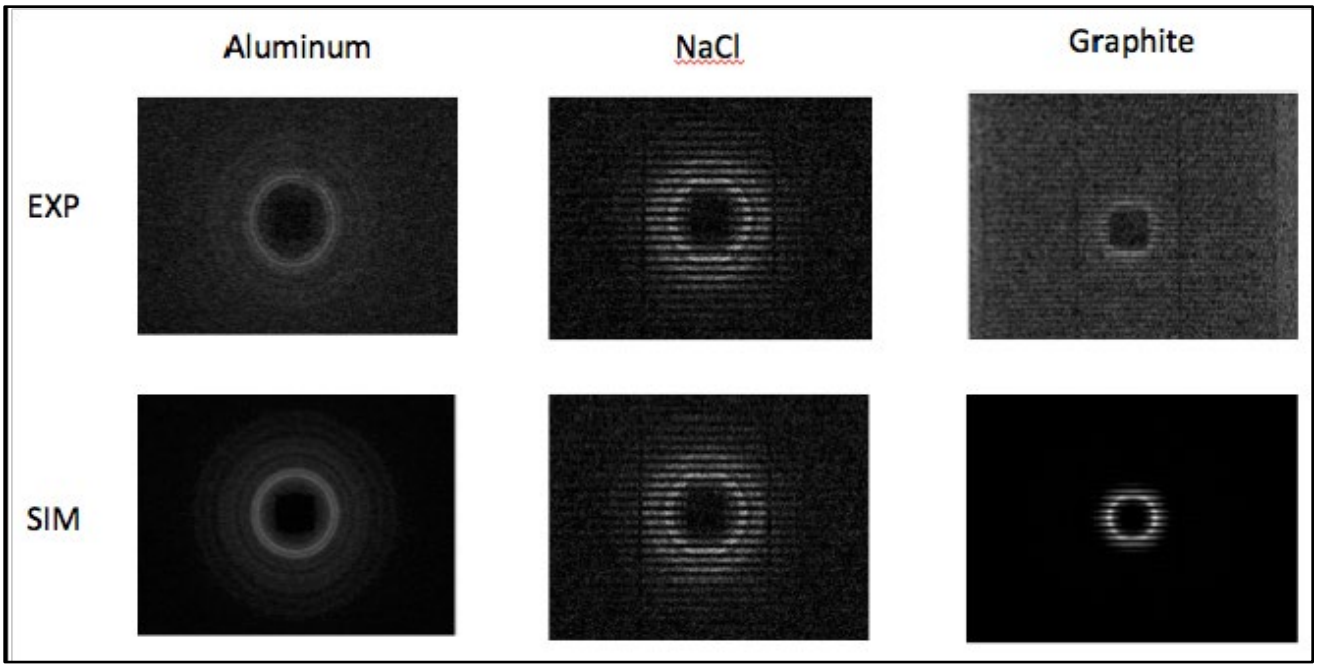

Figure 2: Comparison of raw experiment (top) and MC simulation (bottom) XRD data for Al, NaCl, and graphite powders (left to right).

B.4. Data-centric Analysis of XRD Signatures

Traditional XRD threat classification methods usually involve two separate steps in order to assign a class to a particular measured form factor. In the first step, one performs material identification, which is a multi-class classification problem, by comparing the unknown form factor to a premeasured library of form factors and determining the best match. Since X-ray diffraction is most often performed with crystalline materials (either naturally occurring or artificially crystallized) whose form factors consist of a multitude of narrow peaks, it is common to simply compare the locations (although not the amplitudes) of the prominent peaks against the locations of peaks of the form factors in the library. If enough of the peaks coincide within some predetermined accuracy, then a match is made. This approach, however, does not work for amorphous and liquid materials, in which scatter occurs at a broad range of momentum transfer values and the relative peak intensities are important in distinguishing materials. In this case, one can instead calculate a similarity metric, such as the correlation (which we use in this work), between the unknown form factor and all elements of the library. Whichever material is most similar to the unknown material is then matched with the unknown material. After the material identification process is complete, the second step is then to assign the class of the matched material to the previously unknown material. While this process can work in some situations, there are several challenges associated with it. For example, the entire process fails if the unknown material is not already in the library, which is a significant issue given the breadth and evolution of explosive-related threats. Furthermore, it can be difficult to accurately associate a given form factor with the correct library element in the presence of noise, measurement uncertainty, and material variability.

The problem of the traditional identify-then-classify approach stems from the fact that it does not make use of similarities between members of a given class (or, more specifically, does not take into account class differences). If one considers correlation-based classifiers, for example, it is clear that each feature (e.g., momentum transfer value or principal component) receives a uniform weight when performing the intermediate material identification step. In this case, a missing peak (as in the case of texturing) or a noise spike at a location that happens to coincide with that of a different material could produce an incorrect identification and, correspondingly, a classification error.

In order to improve the detection performance relative to traditional approaches, in this program, we turn to machine learning as a method to automatically generate a set of feature weights that are optimized for performing the specific task of interest. Note that this approach does not necessarily aid in the intermediate problem of identifying the unknown material or in obtaining any auxiliary data about the material (e.g., whether it is a solid or a crystalline material). Instead, it eliminates the need for the intermediate identification step entirely: the traditional process collapses to a single step that simply uses a previously-trained classier to identify directly whether a material is an explosive or not. With sufficient training data, the use of machine learning therefore provides the potential for increased robustness to noise and better performance in the face of "new" form factors (i.e., those on which the classier has not been trained). Some previous studies have investigated support vector machines (SVMs), principal component analysis, or hybrid discriminant analysis to identify classes of interest; however, these studies have always been limited to narrow categories such as the evaluation of only liquid materials, only considered linear dimension reduction methods, or did not account for XRD signature variability arising from intrinsic effects (such as texture).

C. Major Contributions

C.1. Construction of an Energy-Dispersive Laue Diffraction System (Year 4)

We built an experimental testbed X-ray system capable of collecting the XRD signal over a large range of energies and angles relevant to aviation security [15]. This allows us to collect the 3D scatter data (in terms

of 2D scatter angle and energy) that will be included in the XRD database. All components are commercial off-the-shelf (Figure 3), and a high SNR scan of a sample can take between 5 and 45 minutes, depending on the material.

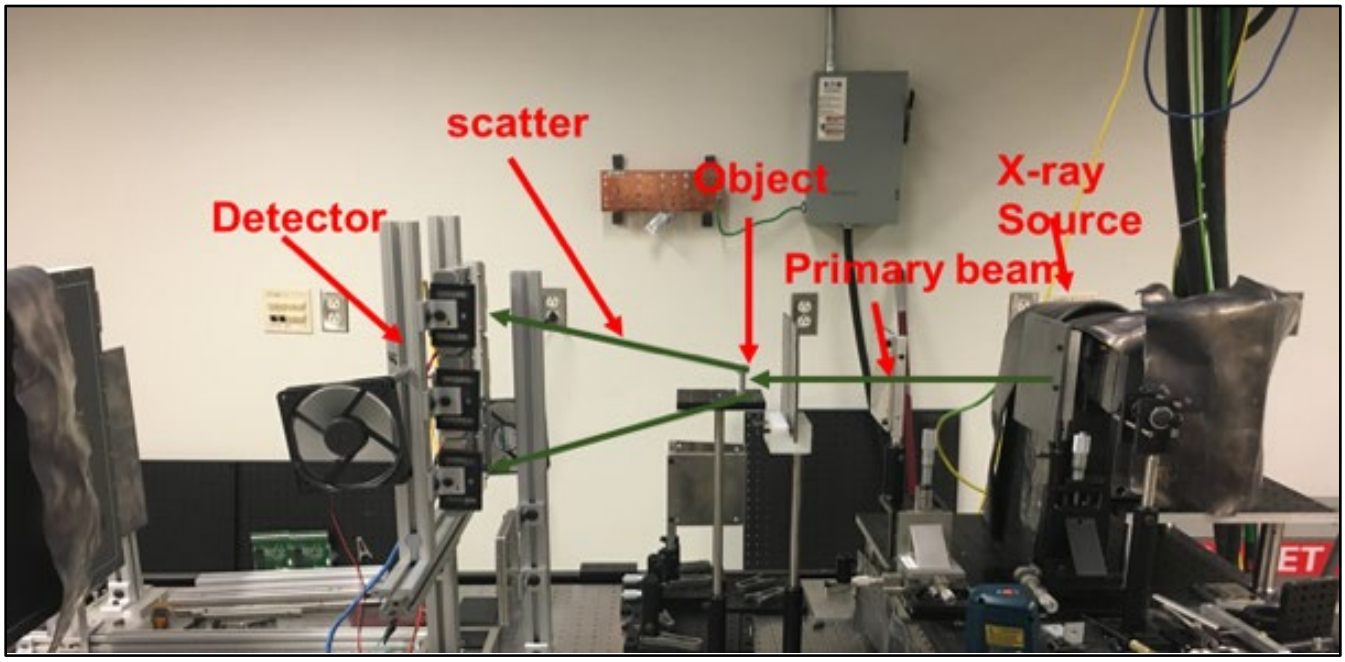

Figure 3: Experimental setup of our energy-dispersive Laue diffractometer. From right to left, we show the X-ray source, series of pinhole collimators, object, and energy-resolving, pixelated detectors. Both the detectors and object are placed on rotation and translation stages to enable flexible illumination and detection.

C.2. Commercial XRD Database Creation (Years 4–7)

Using a conventional, commercial diffractometer system (Bruker D2 Phaser, operated in reflection mode at the copper k-Alpha line), we acquire high-resolution scans of the XRD form factors. To record a wide range of materials in different orientations, we have modified the system to enable title and azimuthal rotation of the sample, to vibrate the sample to promote randomness, and to heat or cool the same to vary the sample temperature. Using this setup, we measured over four hundred different substances, including both benign and energetic materials. For explosives, we visited Professor Jimmie Oxley's (Projects R1-A.1, R1-B.1, and R1-C.2) lab at URI and scanned a variety of recipes of explosives (in powder and slurry form) at a range of different orientations on both her Rigaku XRD system and our Bruker system. Examples of the recipe dependence and orientation dependence of the XRD signatures are shown in Figure 4. Since it is extremely difficult to accurately predict the XRD signature from first principles for complicated materials, this empirical approach is necessary for understanding and simulating XRD scatter. In Year 6, we added more liquids to the database, provided additional material metadata (such as whether a material is solid/liquid, crystalline/amorphous), and included the energy-dependent attenuation coefficient for the materials in addition to their XRD signatures). In Year 7, we included additional stream of commerce materials of particular relevance to discrimination of organic materials with some degree of texturing.

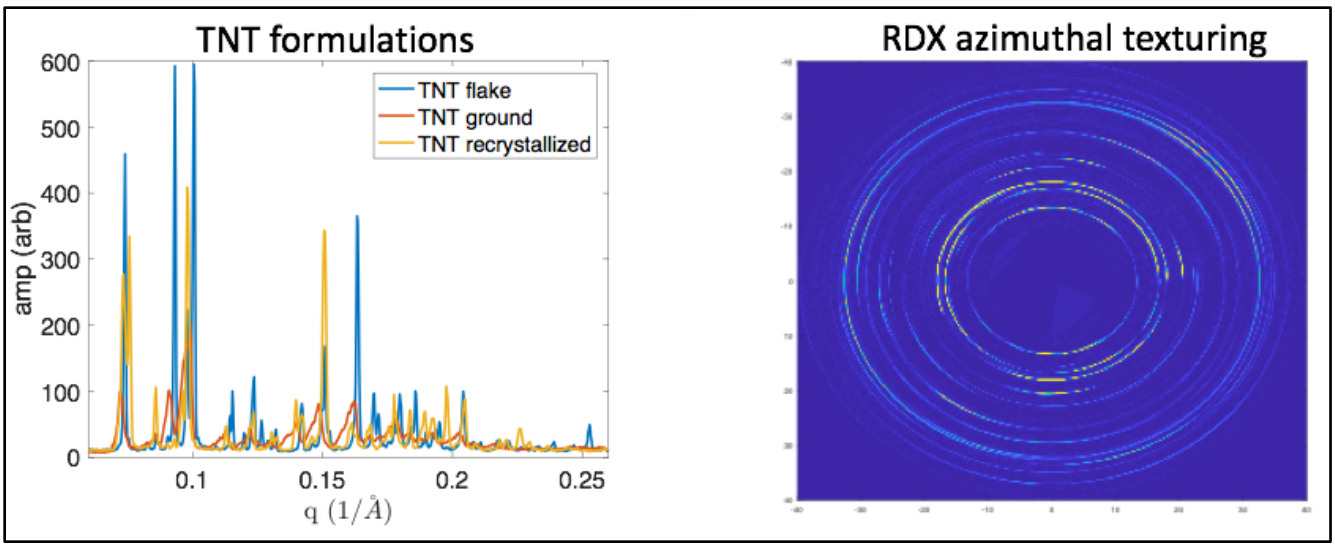

Figure 4: (Left) X-ray diffraction form factors for TNT in flake, ground powder, and recrystallized crystalline forms. The peaks occur at nearly identical locations, but the relative amplitudes vary significantly (despite the identical molecular composition of the samples). (Right) An image of the scatter pattern for a sample of RDX as it is rotated over 360 degrees in the sample holder. For all measurements, we use a Bruker D2 phaser system.

In Year 7, we formalized and organized the data and formatted it for inclusion in Jimmie Oxley's Explosives Database. An example of such a file is shown in Figure 5—each material has an associated PDF file showing a plot of the spectra and a list of the locations of the dominant peaks. The full data for scatter intensity versus diffraction angle is included explicitly in table form on the succeeding pages. The files were shared with Jimmie and her team.

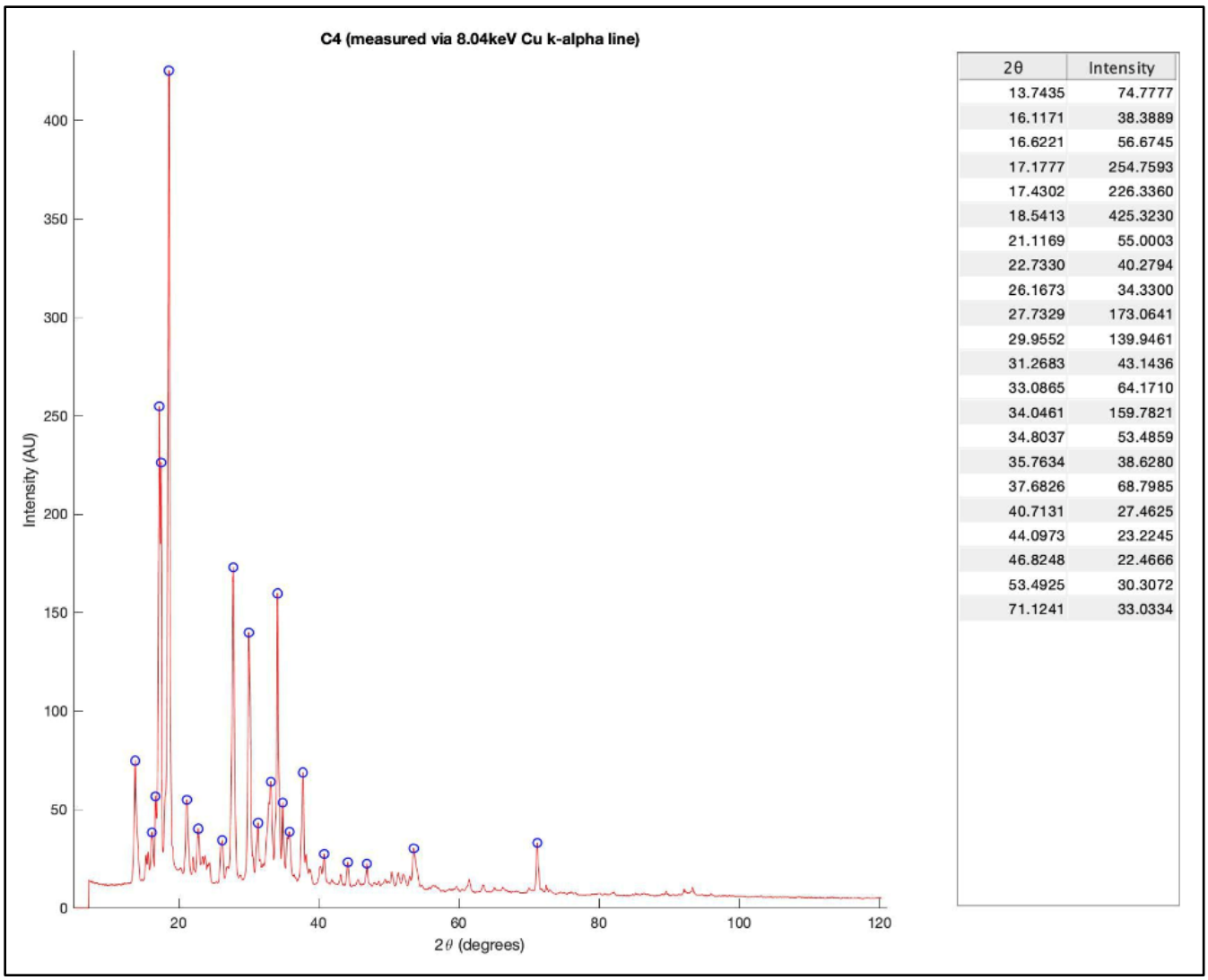

2θ	Intensity
13.7435	74.7777
16.1171	38.3889
16.6221	56.6745
17.1777	254.7593
17.4302	226.3360
18.5413	425.3230
21.1169	55.0003
22.7330	40.2794
26.1673	34.3300
27.7329	173.0641
29.9552	139.9461
31.2683	43.1436
33.0865	64.1710
34.0461	159.7821
34.8037	53.4859
35.7634	38.6280
37.6826	68.7985
40.7131	27.4625
44.0973	23.2245
46.8248	22.4666
53.4925	30.3072
71.1241	33.0334

Figure 5: Example cover page image for C4 as part of the URI Explosives Database.

C.3. Fundamental Study of the Relationship between Grain Size and Texturing (Year 5)

Powder material attributes of crystallinity, crystal faceting, and powder packing collectively influence texture and the corresponding diffraction spectra are shown in Figure 6. We have analyzed how the X-ray aperture size and crystal grain size influence the XRD signatures. Smaller powder size relative to the X-ray aperture (1 mm × 16 mm) showed diffraction features characteristic of randomly configured powder since many particles and their configuration were analyzed in the sampling volume. Figure 6 shows more spectral variability, or texturing, exists for larger powder grain size relative to the fixed aperture size due to the fact that fewer grains were included in the illuminated volume. A new finding was that the manner in which the powder is packed into the holder impacts texturing, as shown in Figure 6.

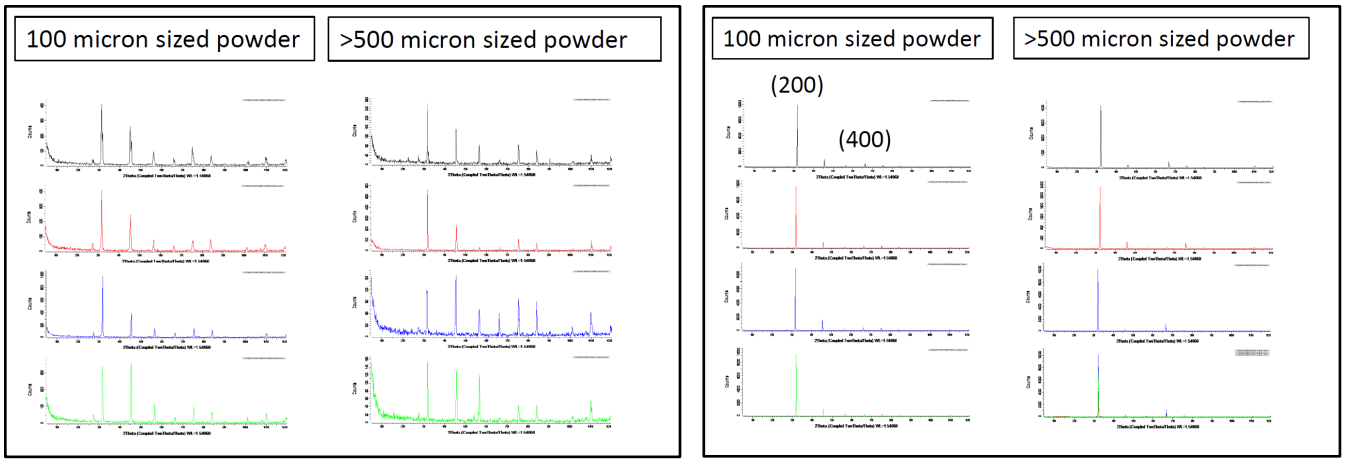

Figure 6: X-ray diffraction spectra for 100 mm and >500 mm NaCl powder for material loosely placed (left) and pressed into the sample holders (right).

C.4. Energy-Dispersive Laue Database Creation (Years 4–7)

Using the energy-dispersive (ED) Laue system, we scanned over one hundred materials and recorded the scatter signal from 20–170 keV and for a deflection angle between 1 and 30 degrees. As shown in Figure 7, each material was placed in the system with multiple orientations, and many in multiple forms (e.g., sheet, powder, different vendors, and different processing histories). We find that fine powders, such as Al, give symmetric rings with no texturing at all energies and orientations. Aluminum sheet, however, has textured rings that vary around the ring (azimuthally) and depend on the orientation of the sample relative to the beam, but have no variation or structure in energy. For polycrystalline powders with large grain sizes, such as salt in a shaker, scatter only arises at particular angles and energies, and depends sensitively on the configuration of the individual polycrystalline grains. This indicates the challenges associated with XRDT on highly textured materials, as both collecting and interpreting the signal can be very challenging (compared to an untextured material). In Year 6, we added fifty materials (in multiple orientations) to the database, focusing on materials with some degree of crystallinity that existed already in the XRD database (including some single crystals) [15].

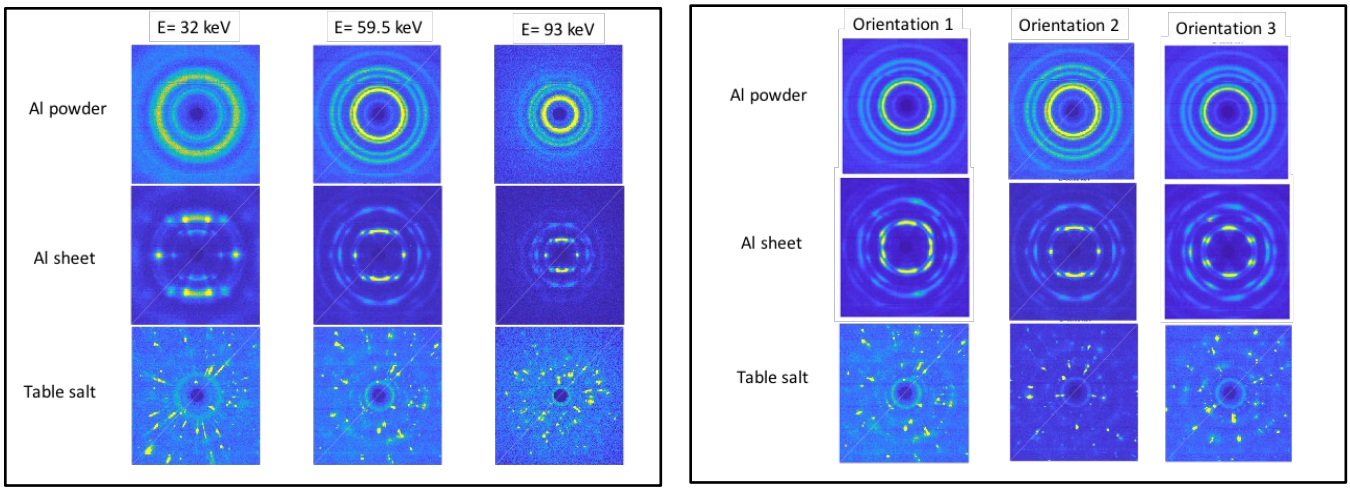

Figure 7: Scatter signals measured across different energies using the ED Laue system (left). The top, middle, and bottom rows show the scatter for aluminum powder, aluminum sheet, and large grain sodium chloride, respectively. From left to right, we show the scatter at 32, 59.5 and 93 keV. Together, this data shows examples of different ways in which the XRD signal may deviate from the Debye cones described by Bragg's law. Scatter signals measured for different orientations of the same samples in the ED Laue system (right). The top, middle, and bottom rows show the scatter for aluminum powder, aluminum sheet, and large grain sodium chloride, respectively. From left to right, we show the scatter for three different orientations of the sample in the system (with the rest of the parameters held fixed). This data shows examples of the orientation dependence for materials with different degrees of texturing.

In Year 7, we have continued scanning more materials to add to the database. These materials were chosen to both broaden the stream of commerce breadth of the database (e.g., including liquids and foods) and to include additional materials with "interesting" texture patterns (e.g., single crystals and formed metal objects). Due to COVID-19-related lab closures, this work is still ongoing.

C.5. Texturing Taxonomy (Year 5–6)

Using the ED Laue database results, we quantified the type and degree of texturing by developing a custom metric that characterizes the variation of the scatter signal around the ring (azimuthal texturing coefficient) and across different energies (energy texturing coefficient). By plotting each material in this space, we can visualize the distribution of materials (see Figure 8). A new result in Year 6 is that our metric places materials with similar structures and processing histories near each other and emphasizes these attributes over molecular structure. For example, copper sheet and aluminum sheet appear nearer to one another and farther away from copper powder and aluminum powder, despite having the exact same chemical and molecular composition. This shows that, rather than a nuisance, texture can be used to determine the processing history of a material. In addition, we find that only part of the texture space is filled—materials with a high degree of energy texturing generally also have a high degree of angular texturing. Finally, we can define a single parameter, referred to as the degree of texturing (DOT), which quantifies how textured the material is. For the materials in our library (which represent common, stream of commerce materials), we find that over half have at least some degree of texturing. These findings are important for simulating ensembles of objects with appropriate degrees of texturing, as well as giving insight into the texturing "categories" into which materials fall, so that we can get a representative understanding of the range of possible scenarios while studying only a limited number of cases [15].

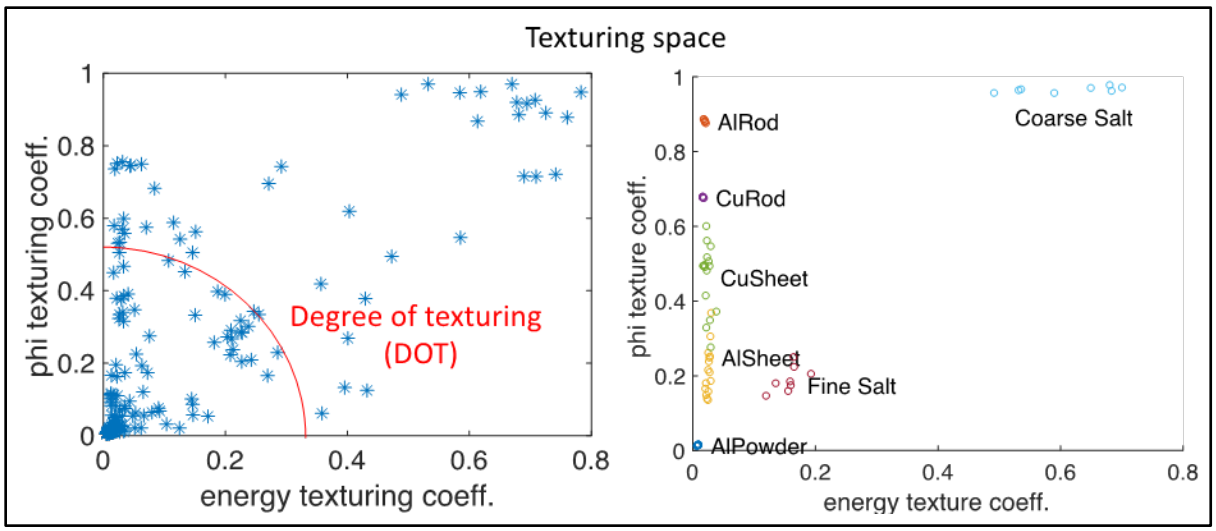

Figure 8: Texturing taxonomy showing the distribution of materials in the ED Laue database in terms of the degree of texturing of each material and in terms of energy and azimuthal scatter angle (left). The materials are clustered in the upper left hand corner of the plot. The degree of texturing is defined as the distance from the origin. Highlighting materials whose processing history can be distinguished based on texture alone (right).

C.6. Using Texture as a Feature for Material Identification (Year 7)

Based on the characterization of materials in texture space from the previous year, we investigated whether texture could be used as a useful feature (rather than a problem) in the XRDT detection paradigm. We focused on the case of aluminum, for which we had access to a single crystal, sheet, rod, and fine powder. Figure 9 shows that using texture features related to the intensity variation around a Debye ring (c_phi) and as a function of energy (c_E) allows one to separate powders from solid sheets and rods much more accurately than by using the conventional XRD form factor (fq) alone.

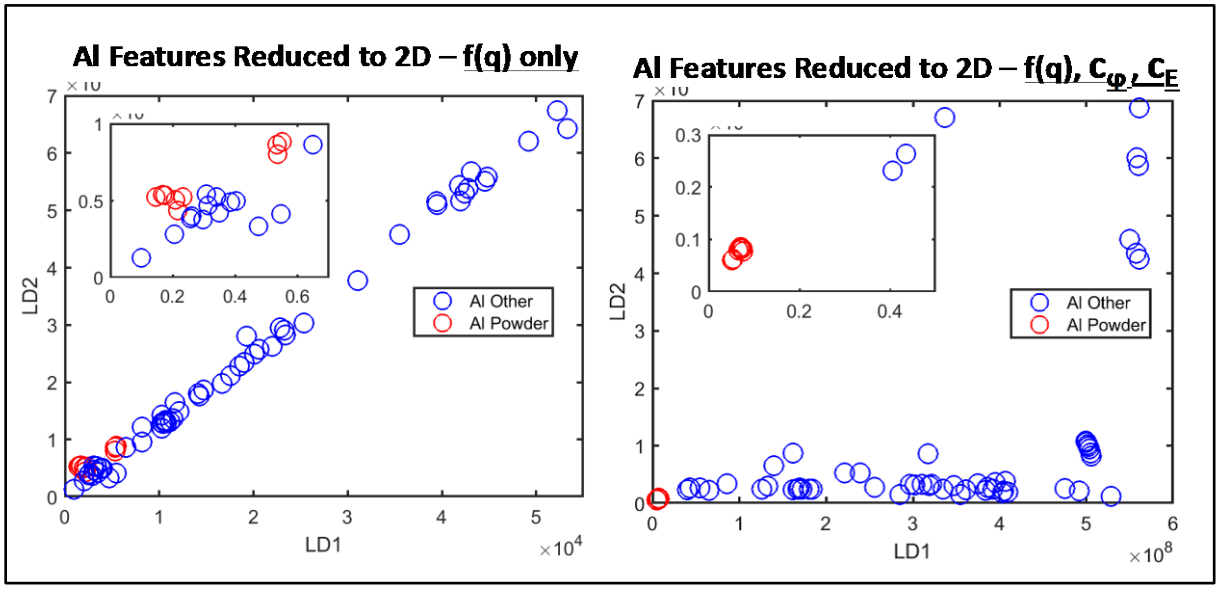

Figure 9: Plot showing Al powder (blue) and other forms of Al (red) in linear discriminant analysis space. When only f(q) is used, there is substantial overlap between the powder and other forms of Al, whereas when the texture features are used, the different forms of the same substance are easily separable.

C.7. Comparing Transmission Versus Diffraction for Material Identification (Years 4 and 7)

A natural question to ask is how well explosives and nonexplosives can be distinguished from one another based on their X-ray properties. We considered the class separation (average distance between explosives and nonexplosives) using three different feature sets: density and effective atomic number, the XRD signature, and a combination of the two. We find that the XRD features provide significantly better class separation, J, for reasonably high-quality XRD measurements (indicated in Figure 10 as Δq) as compared to the transmission-related features (density and the effective atomic number). Also, combining these features gives rise to better separation than either feature set alone. This shows that classifiers that combine transmission and XRD data should outperform those that use only one measurement approach, and that XRD fundamentally has the potential to outperform transmission measurements.

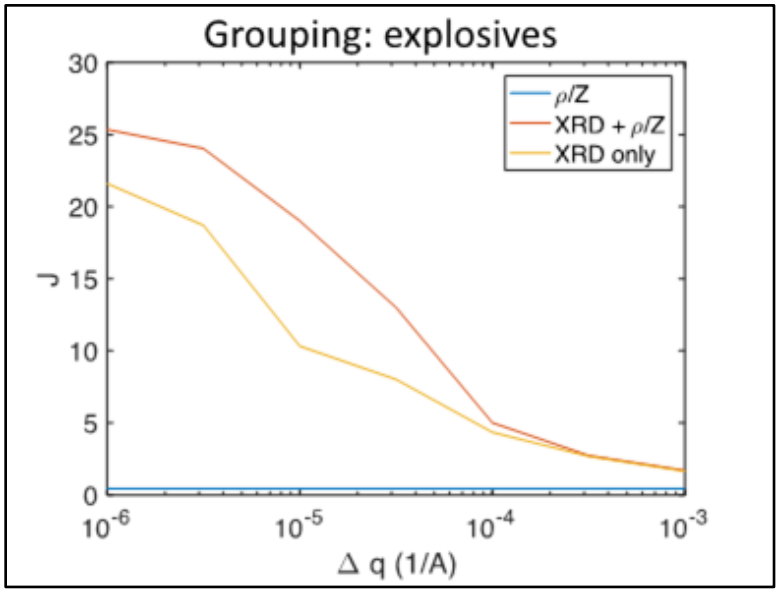

Figure 10: Class separation, J, as a function of XRD momentum transfer resolution (i.e., quality of the XRD measurement) when transmission (density and effective atomic number), XRD, or transmission + XRD features are used to discriminate between explosives and nonexplosives.

C.8. GPU-Based Monte Carlo: Fast and Accurate Simulation (Year 6–7)

We have built and implemented a Monte-Carlo simulation for X-ray diffraction using the software MCGPU. MCGPU is a freely available software developed and maintained by the US Food and Drug Administration. It is designed to model X-ray interactions at energies of relevance to our diffraction-based modeling and detection approach. The software utilizes GPU frameworks and can be fully parallelized across multiple GPU processors, either within a single computer or across multiple computers. Based on our early experiments to measure GPU-computing efficiency, we have found speed-ups of up to 50X compared to CPU-based computing, such as in GEANT4. We have created our own MATLAB wrapper for simple end-user interaction with the software and modified the default coherent scattering models in MCGPU to incorporate XRD signatures derived from our diffractometer database. Using this modified code, we have demonstrated preliminary validation against data generated via experiment and GEANT4 (see Figure 11).

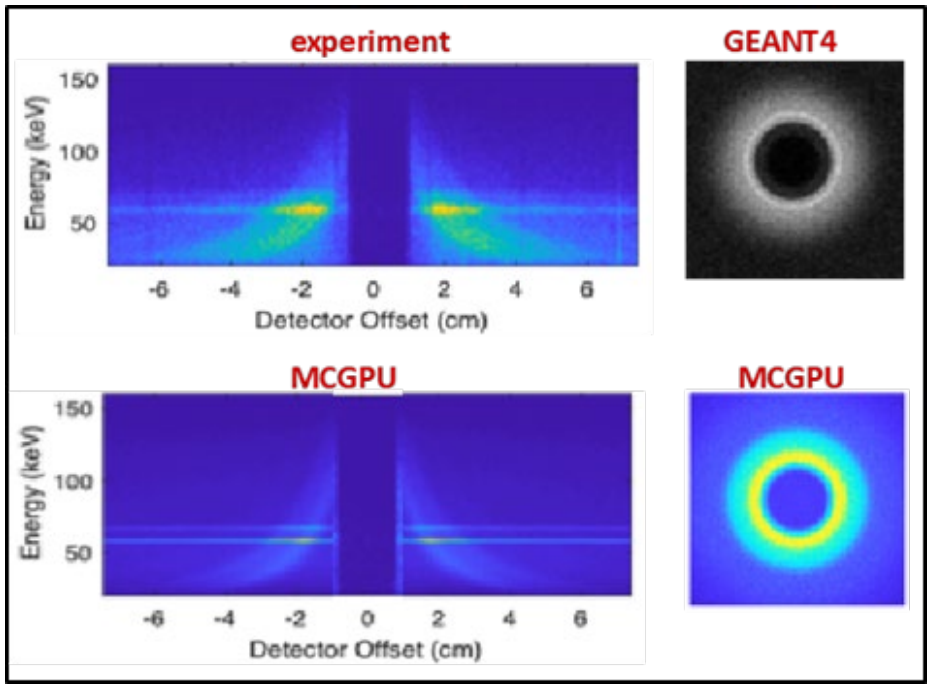

Figure 11: Validation of MCGPU against experiment (left) and GEANT4-based Monte Carlo (right).

In Year 7, the MCGPU model has been tested and validated against experimental data acquired using the ED Laue testbed system. Shown in Figure 12 are simulated versus experimental spectra from water, graphite, and aluminum. The total scatter signal was accurate to within 5% of the values obtained from literature. Furthermore, the peak locations and spectral shape are consistent with the experimental measurements. Additional validation of the accuracy and speed benchmarking against GEANT4 (the Monte Carlo "gold standard") show that MCGPU is over 100 times faster than GEANT4 while producing nearly identical results.

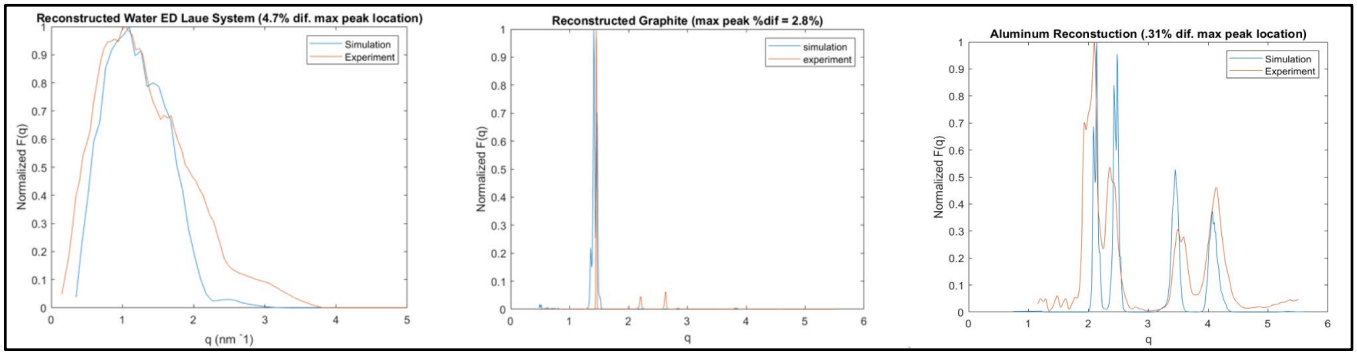

Figure 12: Simulated (blue) and experimental (orange) XRD signals for water, graphite, and aluminum powder (left to right, respectively).

C.9. Implementing Texturing in Simulation: Deterministic Model (Years 4–6)

We previously developed a fast, deterministic, first-order scatter model of XRD and Compton scatter for untextured materials. Because the details of the texture pattern are impossible to predict ab initio but the details of their structure are critical to system performance, we implemented an empirical approach to XRD texture modeling in which we use the ED Laue scatter measurements as a texture "mask" in the simulation system. By modulating the scatter at specific energies and angles in the simulation, we can create realistic

scatter distributions for materials whose texturing ranges from negligible to highly textured. We have validated our scatter simulation against experimental data. The simulation enables us to simulate arbitrary system architectures by changing component parameters (e.g., detector type), geometry, and optics (including coded apertures and collimators) for objects with spatial and material descriptions limited only by the extent of our material databases. The general description of this method is shown in Figure 13. In Year 6, we quantified this performance and showed that we can use the model to perform accurate recovery of the XRD form factor from experimental data despite the presence of texturing.

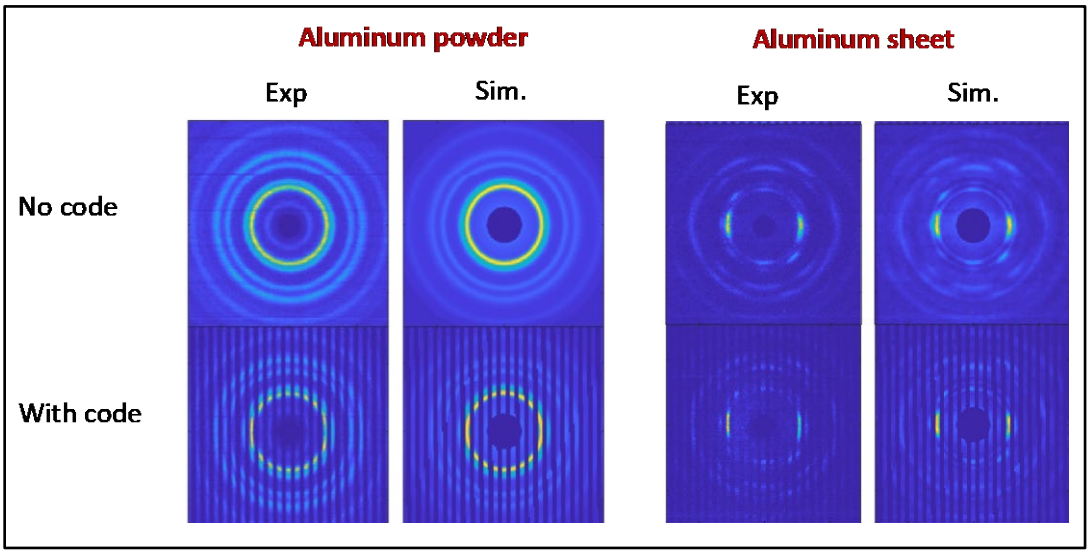

Figure 13: Example of experimental and simulated scatter from aluminum power and a textured sheet of aluminum at 60 keV (without and with a coded aperture).

C.10. Implementing Texturing in Simulation: Monte Carlo (Years 4–5)

We previously developed an accurate Monte Carlo tool (based on GEANT4) for simulating arbitrary scatter orders for untextured materials. As in the deterministic approach previously described, we have extended this MC tool to include texturing by modifying the scatter probabilities across different energies and angles according to empirical measurements made in the ED Laue system. The model has been validated against experiment.

C.11. Simulation-Based XRDT System Analysis (Year 6–7)

A number of methods have been proposed for performing XRDT at the airport. Among them, direct tomography (DT) has been implemented and deployed by Smiths and Morpho, and coded aperture XRDT (CA-XRDT) was invented at Duke and is currently under development by Rapiscan and Smiths. While these systems have been studied separately, they have never been compared head-to-head in a controlled analysis. We developed a method for analyzing these systems in a common framework and evaluated the performance as a function of the number of incident (or detected) photons as well as the size of the target object under analysis (in the absence of texturing). We found that, while the DT system has more information per detected photon, the CA-XRDT system can outperform the DT system overall by virtue of being able to measure orders of magnitude more photons (see Figure 14). Coded aperture XRDT is therefore a promising approach for aviation security [16].

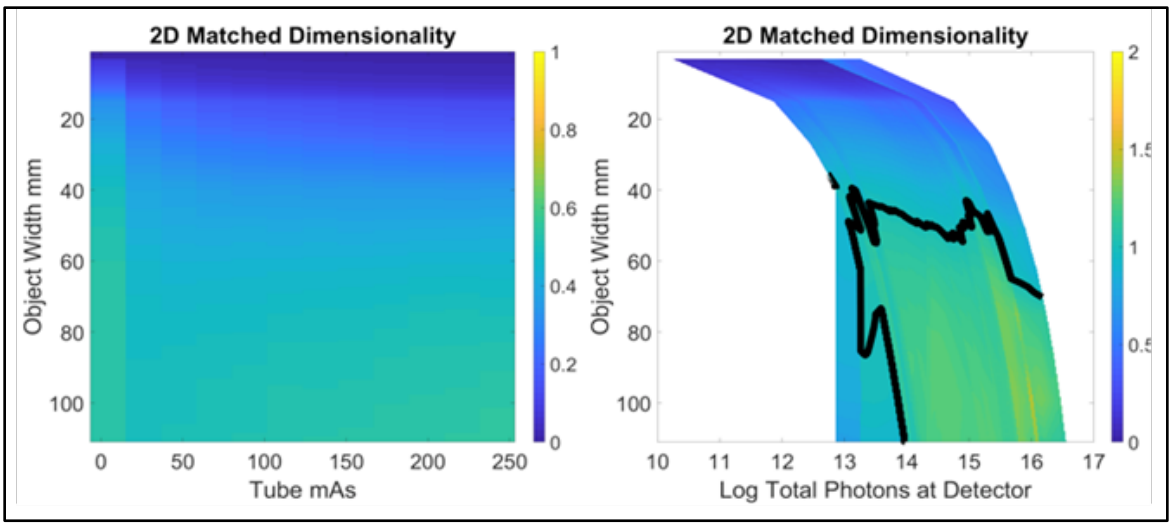

Figure 14: ratio of the error for the CA-XRDT system relative to the DT system as a function of object extend and (left) incident and (right) detected flux. The black line shows the transition between DT and CA-XRDT performing better.

In Year 7, we extended this analysis to include joint DT + CA-XRDT systems. This analysis showed that, while pure coding or pure collimation have individual strengths and weaknesses as the incident photon flux goes down or the object complexity goes up, the coding + collimation system (shown in green in Figure 15 for different degrees of collimation) is able to maintain the strengths of both symptoms and therefore outperform both alternatives.

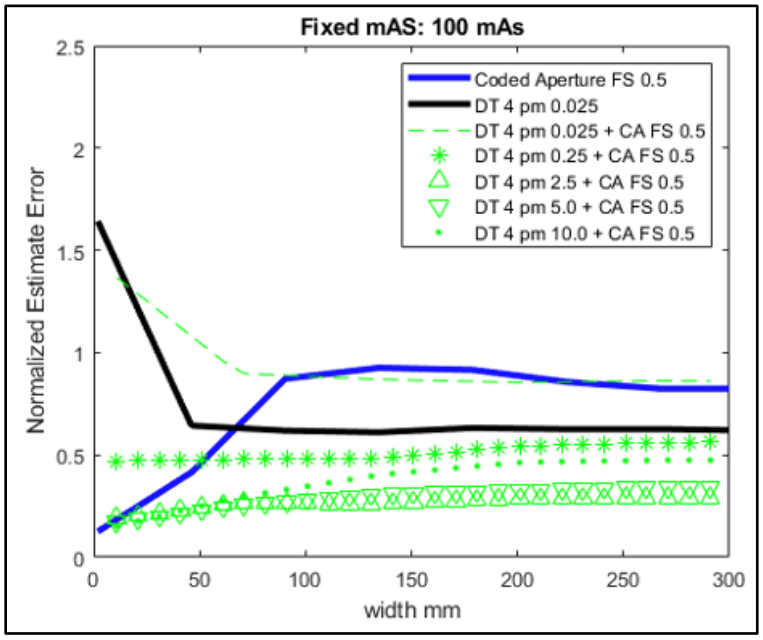

Figure 15: Reconstructed image error as a function of object extent for a coded aperture system (blue), DT system (black), and a CA+DT system (green) with varying degrees of collimation.

C.12. XRDT Performance Analysis with Texturing (Year 5)

We have performed an initial study comparing the impact of texturing on DT and CA-XRDT systems. We found that, while the imaging performance of both systems degrades with increased texturing, DT is somewhat more robust. For both systems, the effect of texturing can be greatly mitigated by using a higher dimensional detector that records both a range of scatter angles and energies [15].

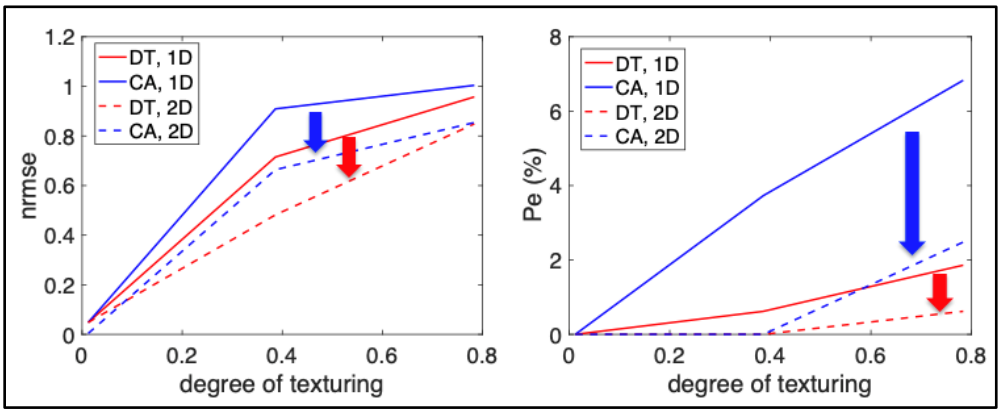

Figure 16: Comparison of reconstructed image error and probability of error in threat/nonthreat classification for a DT and CA system using a 1D and 2D detector as a function of the degree of texturing in the scatter signal.

C.13. Nonlinear Dimension Reduction of XRD Data (Year 6)

Our XRD databases are rich with information; however, considering that each material has multiple texture instantiations (each of which are high-dimensional in their own rights), this data volume can be difficult to interpret. To reduce the data dimension in a manner that preserves the features of interest, we have begun to investigate nonlinear dimension reduction approaches. In particular, we have identified UMAP (Figure 17) as a particularly promising approach—by projecting the high-dimensional XRD signal into a 2D space, for example, we find that individual materials appear as "islands," and clusters with meaningful properties naturally emerge. This is a promising approach both for data-centric analysis of material properties as well for feature engineering in classifier development (as discussed in the next section) [17].

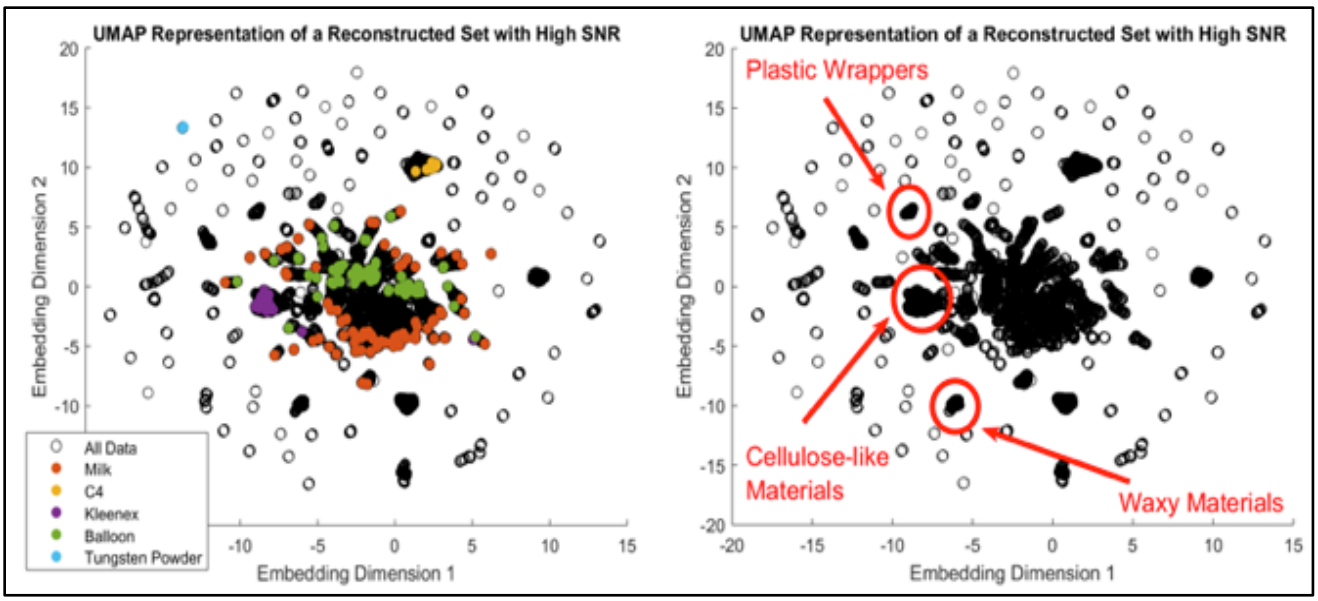

Figure 17: UMAP representation of the reconstructed XRDT data set color-coded to show certain materials (left) and groups (right). The islands represent well-separated materials and the clusters show harder-to-separate materials.

C.14. Machine Learning Analysis of XRD Signals (Year 5–7)

Over the last two years, we have tackled the challenge of building a classifier capable of distinguishing between threats and nonthreats in XRD space. This is a difficult problem because XRD signatures can be highly material-specific, often to the point that having a complete library against which to compare an unknown measurement is impossible: material variability and the large dimensionality of the signature create an infinite number of signatures. We have pioneered the use of machine learning techniques in the XRD space for performing "classification without identification": determining the threat status of an unknown sample without first having to identify what specific material it might be. In Year 6, we found that ML-based approaches, like a support vector machine (SVM) or convolutional neural net (CNN), can outperform traditional classifiers by several percentage points (see Figure 18 for the case of explosives detection, top, and cancer detection, bottom). In general, we find that the advantage of ML approaches exists when the material variability or measurement uncertainty is largest, as is the case of real-world XRDT system run for high throughput (and especially when texturing is present). In addition, we have shown that training these classifiers using simulated data generalizes well to experimental data and that our ML algorithms outperform the correlation-based classifier on empirical data [17, 18].

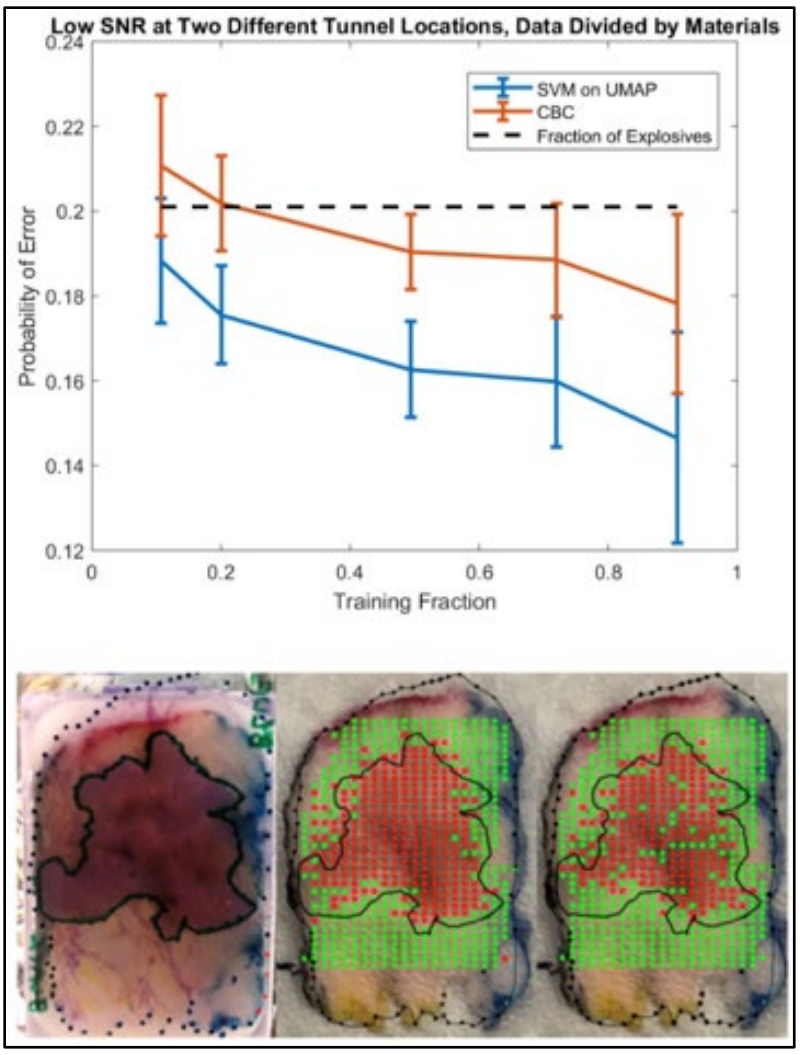

Figure 18: Chart showing the improved error performance of a ML algorithm (blue) versus the traditional algorithm (orange) as a function of the training fraction (top). Images showing cancer classification in tissue (bottom) based on a CNN (middle), traditional classifier (right), and ground truth (left).

In Year 7, we have focused on the problem of spectral unmixing—because the spatial resolution of an XRDT system is typically worse than the sizes of many objects of interest, a single image voxel may end up containing a weighted sum of multiple materials. This mixing is, however, well-described as linear. As such, one must include an additional step between recovering the spectrum at a given voxel and performing classification—namely, one must first recover the abundances and associated spectra of the separate materials present at that location and then perform classification. While we have implemented this successfully with simple cases, we plan to improve spectral unmixing in the constrained case where endmembers are known with providing those and an anomaly class to unmix each pixel. We also plan to look into using synthetic data for pretraining of unsupervised methods of unmixing for case where potential endmembers/materials are too large beyond having a complete database.

D. Milestones

Year 6 Milestone?	Milestone	Description	Status
Yes	XRD database extension	Measure at least 10 instantiations for at least 10 more materials (spanning SoC and prohibited materials) and include transmission information and relevant metadata. Database will enable system-level simulations and algorithm development for XRDT systems.	In process—COVID-19 closed the lab. Duke reopened it, and now we will complete this data acquisition.
Yes	Explosives database fusion	Successful incorporation into URI database. Single-format database available to interested parties from a single access point.	Complete
Yes	MCGPU test report	<10% error between simulation and experiment and time benchmarking versus GEANT4. Validated, rapid, user-friendly X-ray simulation tool available for the community.	Validation work is complete, but timing analysis is pending. Documentation and application to a use case of interest is in progress.
Yes	Classifier test report	Statistically significant performance improvement (in terms of Pe) relative to correlation-based classifier. Algorithm will be incorporated into the Smiths prototype XRDT scanner.	This work is in progress.

E. Final Results at Project Completion (Year 7)

- Year 7
  - XRD database of explosive materials, incorporated in the URI Explosives Database
  - Validated MCGPU simulation tool for simulating X-ray diffraction for real materials
  - New data processing approaches for X-ray diffraction identification and classification
  - Publication of research results
- Over the life of the program
  - First tabletop ED Laue diffractometer system built capable of investigating texture
  - First measurements of XRD texture in a broad range of stream of commerce materials/objects
  - First simulation framework for simulating XRD texture in a meaningful way
  - Demonstration of measurement configurations that mitigate the effect of texture
  - First application of nonlinear dimension reduction and machine learning algorithms for improved XRD-based classification
  - Demonstration of the value of combining coding and collimation for XRD system
  - Demonstration of measurement strategies for mitigating the effects of texture in material identification
  - Demonstration that texture can be a valuable feature for identifying materials

III. RELEVANCE AND TRANSITION

A. Relevance of Research to the DHS Enterprise

This work was directly relevant to the goals of DHS S&T and the TSA, which include seeking new techniques for improving airport security. An integral part of this effort included new methods for identifying threats through a combination of hardware and software, as well as developing tools for understanding and predicting the dependence of the measured signals on the material properties of an object. We proposed to develop these tools and extend the fundamental science behind XRDT systems. Our work benefitted ongoing and future DHS-funded efforts, such as:

- The BAA 13-05 programs at the University of Arizona, Duke University, and SureScan Corp. on information theoretic analysis of X-ray imaging systems
- The Rapiscan Labs, Smiths Detection, and HALO X-ray Technologies Ltd. programs on the development of checkpoint and checked baggage XRDT systems and associated algorithms
- LRBAA 14-02, LRBAA 18-01, and BAA 17-R-03 studies on related technology (e.g., hybrid XRDT and AT/CT scanners, next-generation detectors, and deep-learning classification algorithms)
- Other ALERT task orders (such as the Opioid Detection task order)
- Founding of Quadridox, Inc. to transition technology and expertise to a group capable of working at higher technology readiness levels and make use of sensitive information (e.g., Quadridox is participating in the Air Cargo task order)

The results of this work will continue to aid the TSA, TSL, and NIST in developing standards, calibration phantoms, simulants, and robust classification methods for XRD applications that have not previously been explored.

A.1. Facilitating Next-Generation Scanners

XRDT offers a way to reduce false alarms (Pfa) while maintaining detection (Pd) in baggage screening systems. This ALERT project is playing an important role in furthering the development of these XRDT systems by generating necessary insights and information to be used by OEMs as they develop specific commercial products. Reduced detection errors (Pe) at the checkpoint can save DHS millions of dollars annually while improving throughput, reducing divestment, and ensuring passenger safety.

- Affect XRD imaging system design/determine requirements on coding/sampling approach.
    - Metric: Provided Pd/Pfa improvement resulting from choice of illumination structure and coding/collimation (e.g., CAXI versus XDi system tradeoffs).
- Improve threat detection / provide an understanding of to what degree XRD systems can improve the ability to identify and localize threats. This will also provide a connection between current and next generation technologies (e.g., helping to connect AT/CT with XRDT capabilities and opportunities).
    - Metric: Identified how well materials that are difficult to resolve using transmission (AT/CT) can be identified using XRD.

A.2. Testing and Evaluation

The fast MCGPU simulation tools that we have developed and will refine through Year 7 will allow for the testing and evaluation of deployed and in-development AT, CT, and XRDT scanners. In addition, the XRD

database is essential for performing simulation, as XRD form factors (along with relevant variability) for complex materials can only be obtained empirically and are necessary for accurate simulation of transmission or scatter signals. These tools enable quantitative assessment of the possible performance of any X-ray-based scanner, thus helping determine the future roadmap for checkpoint solutions and component development.

- Creation of tools (the database, simulation, data processing) to enable government and OEMs to evaluate current and future technologies.
    - Metric: Material library contains scans of over 50 explosives and 100 stream of commerce materials (with >5 instantiations per material). MCGPU was shown to be 100 times faster than GEANT4 while providing nearly identical results.

A.3. Standards/Certification

Knowledge about the XRD form factors and inherent material variability can help agencies such as TSL and NIST develop standards, phantoms, and stimulants for evaluating the performance of and certification requirements for next-generation scanners.

- Stakeholders understand luggage from an XRD perspective (e.g., appreciate that confounders, interferents, and simulants are well-established for CT/AT systems, but wholly unknown in XRD) and develop solutions parallel to those in the CT/AT space.
    - Metric: Analyzed and disseminated XRD signature database, texturing taxonomy, and assessment of performance impact of material texturing. This information has been shared with the TSL and is informing some of their XRD testbed design and analysis.

B. Status of Transition at Project End

- The simulation tools and algorithms are currently in use by Smiths, Duke, and Quadridox on other projects (both for DHS and in the medical sector).
- The XRD database is available for use via the URI web interface but has been directly shared with and is being used by Rapiscan, Halo, and Smiths.
- Findings and insights about texturing and its prevalence in stream of commerce materials have been shared with TSL and are playing a role in their investigations of XRD for false alarm reduction.

C. Transition Pathway and Future Opportunities

- **Quadridox, Inc**.: Cofounded by Profs. Greenberg and Kapadia (as well as two other university colleagues), Quadridox is a university spin-out company whose focus is to transition the tools, technologies, and expertise generated at the university into real-world solutions for DHS. Quadridox's main purpose is to work with the government and OEMs to further technology in the security space. Quadridox is currently working with DHS S&T to build a prototype XRDT scanner and, as such, is seriously interested in using (and potentially commercializing) the tools generated in this ALERT program. In addition, Quadridox is developing a suite of commercial tools for virtual testing and evaluation of X-ray systems, and both the simulation tools and XRD databases developed in this ALERT program play a critical role in these activities. Thus, Quadridox represents a key transition vehicle for this ALERT program.

- **Related government contracts**: Drs. Greenberg and Kapadia are involved in other contracts with DHS through Duke University that rely and build directly on the results generated in this program. Examples include SureScan's BAA 13-05 project on fixed gantry CT analysis, Duke's BAA 14-02 project focused on design a hybrid AT-XRDT or CT-XRDT system, and Kromek's BAA 17-03 project focused on developing detector modules for coded aperture XRDT systems. We are also using the tools and methods developed here as part of the ALERT Opioid Detection Task Order to analyze the detectability of opioids for CBP applications. Work on this ALERT effort therefore benefits both DHS S&T and its partners and serves as a natural method for transitioning our results.
- **Direct interaction with major OEMs**: In addition to simply making our results available, we are actively working with several major OEMs to help them answer scientific and engineering questions that most interest them. Rapiscan, Quadridox/Smiths, and HALO are building prototype XRDT systems and have received data from and provided input to us throughout this project that target specific questions of interest.
- **Creation of knowledge products and training**: We documented our findings by publishing papers and books, attending conferences, and more. In addition, we are training students in the problems and techniques relevant to the overall DHS enterprise.

D. Customer Connections

- Kristofer Roe, Souleymane Diallo, Christopher Gregory, Matthew Mertzbacher, Smiths Detection (weekly communication, database shared, collaborating on Duke/Smiths joint BAA 14-02 program for transmission + XRDT study)
- Adam Grosser, Kris Iniewski, Redlen Tech (monthly communication, joint proposals in place to TSA, DHS S&T, OEMs)
- Simon Godber/Keith Rogers, Paul Evans, Halo Tech (monthly communication, database shared)
- Dan Strellis/Ed Franco, Rapiscan (collaboration under development, database shared)
- Robert Klueg, Ron Krauss, TSL (potential collaboration discussed)
- Jack Glover/Larry Hudson, NIST (potential collaboration discussed)
- David Lockley, DSTL (Monte Carlo code shared, annual licensing agreement in progress)
- Brian Harris, Kromek (discussion of detector specifications needed, based on findings herein)
- Alex DeMasi, contractor supporting TSL (shared texture results and ALERT ED Laue testbed design details)

IV. PROJECT ACCOMPLISHMENTS AND DOCUMENTATION

A. Education and Workforce Development Activities

1. Student Internship, Job, and/or Research Opportunities
    a. Summer research opportunities afforded to three high school students
    b. Hosted three REU students for the summer

B. Peer Reviewed Journal Articles

Pending –

1. Carpenter, J., Hazineh, D., & Greenberg, J.A. "Application of Energy-Dispersive Laue Diffractometry to Texture-Based Material Identification." *Journal of Applied Crystallography*, submitted.
2. Hazineh, D., & Greenberg, J.A. "Empirically-Informed Approach to Modeling Texture in an X-Ray Diffraction Tomography System." *Nuclear Instruments and Methods in Physics Research B*, submitted.
3. Hazineh, D., & Greenberg, J.A. "Coding and Collimation for X-ray Diffraction Tomography" *Applied Optics*, in preparation.
4. Japzon, M., & Kapadia, A. "Rapid Monte-Carlo Simulation of X-Ray Diffraction Imaging Systems Using MC-GPU." *Nuclear Instruments and Methods in Physics Research B*, in preparation.
5. Royse, C., Wolter, S., & Greenberg, J.A. "Application of Machine Learning to X-ray Diffraction-Based Explosives Detection." *NIMA*, in preparation.
6. Hazineh, D., & Greenberg, J.A. "Comparison of Direct and Coded Aperture X-Ray Diffraction Tomography in the Absence of Texturing." *Applied Optics*, in preparation.
7. Zhao, B., Yuan, S., Wolter, S., & Greenberg, J.A. "Application of Machine Learning to X-Ray Diffraction-Based Explosives Detection." *Machine Learning and Data Mining in Pattern Recognition*, in preparation.
8. Hazineh, D., Yue, J., & Greenberg, J.A. "Quantifying the Degree of Texture Using an Energy-Dispersive Laue Diffractometer." *NIMB*, in preparation.
9. Greenberg, J.A., Hazineh, D., & Gehm, M. "Energy-Angle Correlations in Energy-Dispersive Laue Diffraction." *Optics Express*, in preparation.
10. Hazineh, D., MacGibbon, C., & Greenberg, J.A. "Comparison of Direction and Coded Aperture X-Ray Diffraction Tomography in the Presence of Texturing." *Applied Optics*, in preparation.
11. Hazineh, D., MacGibbon, C., Kapadia, A.K., & Greenberg, J.A. "Simulation of Anisotropic X-Ray Diffraction Patterns Using Empirically-Measured Texture Masks." *NIMB*, in preparation.

C. Other Publications

Pending –

1. Greenberg, J.A., & Carpenter, J. "Application of X-Ray Diffraction to Explosives Detection." *Counterterrorist Detection Techniques of Explosives*, 2020, in preparation. Edited by Avi Kagan and Jimmie Oxley.

D. Peer Reviewed Conference Proceedings

1. Japzon, M., Nacouzi, N., Sharma, S., & Kapadia, A.J. "Optimization of X-Ray Diffraction Images of Medical Specimens by Monte Carlo Methods." *AAPM Annual Meeting 2019*, San Antonio, Texas, July 2019.
2. Kapadia, A.J., Stryker, S., McCall, S.J., & Greenberg, J.A. "The Role of X-Ray Diffraction Imaging in Digital Pathology." *SPIE Medical Imaging*, virtual, February 2020 [11320-37].

E. Student Theses or Dissertations Produced from This Project

1. Xiao, J. "X-Ray Diffraction Imaging for Breast Tissue Characterization." MS Thesis, Duke University, April 2020.

F. Databases

1. XRD diffractometer database incorporated into the URI Explosives Database (XRD signatures acquired in reflection mode at 8 keV for >400 materials, including explosives and benign materials). Continually updated. Shareable upon request
2. ED Laue database updated (angle- and energy-dependent XRD scatter signal in transmission mode for 510 measurements of >50 materials, including only benign materials commonly found in luggage). Continually updated. Shareable upon request.

G. Models

1. Updated Monte Carlo simulation in GEANT4 for texture-based modeling of X-ray diffraction (available to end users at the end of Year 7). Shareable upon request.

V. REFERENCES

[1] Shanks, N. E. L., & Bradley, A. L. W. Handbook of Checked Baggage Screening: Advanced Airport Security Operation. (John Wiley & Sons, 2005).

[2] G. Harding, M. Newton, & J. Kosanetzky, "Energy-dispersive X-ray diffraction tomography." Phys. Med. Biol, 35(1), 1990, 33.

[3] K. MacCabe, K. Krishnamurthy, A. Chawla, D. Marks, E. Samei, & D. Brady. "Pencil Beam Coded Aperture X-ray Scatter Imaging." Opt. Express 20, 2012, 16310-16320.

[4] S. O. Diallo, K. Tadlock, C. Gregory, S. Wolter, J. A. Greenberg, & K. Roe. "Towards an x-ray-based coded aperture diffraction system for bulk material identification." Proc. SPIE 10632, Anomaly Detection and Imaging with X-Rays (ADIX) III, 1063209 (27 April 2018).

[5] Edward Franco, Dan A. Strellis, Rapiscan Systems Labs. (United States); Kenneth P. MacCabe, Rapiscan Systems Ltd. (United States). "Application of coded aperture x-ray scatter imaging to checkpoint screening." SPIE ADIX 2018 (Orlando, FL).

[6] J.A. Greenberg, K. Krishnamurthy, & D. Brady. "Snapshot molecular imaging using coded energy-sensitive detection." Optics Express 21, 2548, 2013.

[7] Kosciesza, D. et al. in 2013 IEEE Nuclear Science Symposium and Medical Imaging Conference (2013 NSS/MIC), 1-5.

[8] Harding, G. "Compact Multi-focus X-ray Source, X-ray Diffraction Imaging System, and Method for Fabricating Compact Multi-focus X-ray Source." U.S. Patent (2009).

[9] Send et al. "Application of a pnCCD for energy-dispersive Laue diffraction with ultra-hard X-rays." Journal of Applied Crystallography, 49(222) (2016).

[10] Venkatesh Sridhar, Sherman J. Kisner, Sondre Skatter, & Charles A. Bouman. "Model-Based Reconstruction for X-ray Diffraction Imaging." Proc. SPIE, vol. 9847, pp. 98470K-98470K-11, April 17, 2016.

[11] Ke Chen, & David A. Castañón. "Architectures and algorithms for x-ray diffraction imaging." Proc. SPIE 9020, Computational Imaging XII, 902006, March 7, 2014.

[12] Qian Gong, David Coccarelli, Razvan-Ionut Stoian, Joel Greenberg, Esteban Vera, & Michael Gehm. "Rapid GPU-based simulation of x-ray transmission, scatter, and phase measurements for threat detection systems." Proc. SPIE 9847, Anomaly Detection and Imaging with X-Rays (ADIX), 98470Q, May 12, 2016. DOI: 10.1117/12.2223244.

[13] Lakshmanan MN, Kapadia AJ, Sahbaee P, Wolter SD, Harrawood BP, Brady DJ, & Samei E. "An x-ray scatter system for material identification in cluttered objects: a Monte Carlo simulation study." Nuclear Inst. and Methods in Physics Research, B, Volume 335, 2014, pp. 31-38.

[14] https://www.fda.gov/about-fda/cdrh-offices/monte-carlo-simulation-x-ray-transport-gpu-cuda-mc-cpu

[15] Joel A. Greenberg, Chris MacGibbon, Dean Hazineh, Jesse Yue, Brian Keohane, & Scott Wolter. "The role of texturing in x-ray diffraction tomography." Proc. SPIE 1063210, Anomaly Detection and Imaging with X-Rays (ADIX) III (2018)

[16] D. Hazineh, & J. A. Greenberg. "Coding versus collimation in pencil-beam X-ray diffraction tomography." Proc. SPIE 10999-8, Anomaly Detection and Imaging with X-Rays (ADIX) IV (2019).

[17] C. Royse, S. D. Wolter, & J.A. Greenberg. "Emergence and distinction of classes in XRD data via machine learning." Proc. SPIE 10999-12, Anomaly Detection and Imaging with X-Rays (ADIX) IV (2019).

[18] D. Nacouzi. "Smarter Cancer Detection Through Neural Network Classification of High-Resolution X-ray Diffraction Tissue Scans." Master's Thesis, Duke Medical Physics Program, 2019.

This page intentionally left blank.

THRUST R2

TRACE & VAPOR SENSORS

Project Number	Project Title	Lead Investigator(s)	Other Faculty Investigator(s)
R2-A.3	A Novel Method for Evaluating the Adhesion of Explosives Residues	Stephen P. Beaudoin	
R2-B.1	Orthogonal Sensors for Trace Detection	Otto J. Gregory	Michael J. Platek Alan Davis
R2-B.3	Multi-Functional Nano-Electro-Opto-Mechanical Sensing Platform	Matteo Rinaldi	Zhenyun Qian
R2-B.4	Mid-Infrared Photonic Integrated Circuits for Stand-Off Detection of Trace Explosives	Anthony Hoffman Michael Wanke	
R2-C.2	Multiplexed Mid-Infrared Imaging of Trace Explosives	Scott Howard	Vijay Gupta

This page intentionally left blank.

R2-A.3: A Novel Method for Evaluating the Adhesion of Explosives Residues

I. PARTICIPANTS INVOLVED FROM JULY 1, 2019 TO JUNE 30, 2020

Faculty/Staff			
Name	**Title**	**Institution**	**Email**
Stephen P. Beaudoin	PI	Purdue University	sbeaudoi@purdue.edu
Graduate, Undergraduate and REU Students			
Name	**Degree Pursued**	**Institution**	**Month/Year of Graduation**
Cara Stevenson	PhD	Purdue University	8/2021
Jordan Monroe	BS	Purdue University	12/2020
Tyler Roberts	BS	Purdue University	5/2021

II. PROJECT DESCRIPTION

A. Project Overview

The goal of this project is the application of a new interpretation and modeling approach to a traditional experimental method, the centrifuge method, for measuring the adhesion of explosives residues to surfaces. The approach was applied to develop a lookup table containing force constants for the residue-surface systems that are indexed to the particle sizes of a residue. This table is being finalized and will be delivered at the end of the no-cost extension period. The constants are used in a simple, closed-form algebraic model that can be evaluated on a handheld calculator to predict the adhesion force of the residues. The approach was focused on two types of residues: (1) particulate residues such as Royal Demolition eXplosive (RDX), pentaerythritol tetranitrate (PETN), and black powder, and (2) compounded residues such as C4 and Semtex. The work was successful with RDX, but a straightforward, inexpensive, quantitative method for determining the removal of microgram quantities of compounded residues in the centrifuge was not identified.

Figure 1 shows the configuration of the centrifuge, with emphasis on the orientation of the residues on the surface relative to the axis of rotation. The residues adhere to the surface primarily through van der Waals forces. The inertial force from the centrifuge's motion acts to dislodge them. By monitoring the rotational speed required to remove residues of a given size, it is possible to determine the residue adhesion force. From the adhesion force and residue size distribution, the distribution of effective Hamaker constants (the force constants in van der Waals adhesion force descriptions) of model spherical particles against a flat substrate is calculated using the well-established approximate relationship shown in Equation 1 [1]:

$$\textbf{Equation 1:}\quad \boldsymbol{F_{vdW}(D) = \frac{A_{eff}R}{6D^2}}$$

where $F_{vdW}(D)$ is the van der Waals adhesion force, A_{eff} denotes the effective Hamaker constant of the system, R is the radius of the particle, and D represents the separation distance between the two surfaces in contact, which is generally regarded to be 0.4 nm. Figure 2 shows how the modeling and simulation approach developed here can be used to describe the adhesion force distribution of a population of particles against a

surface. In Figure 1, F_{ad} represents F_{vdW} and F_{cent} represents the force to remove particles from the surfaces in the centrifuge. When F_{cent} is just slightly larger than F_{ad}, the particles are removed, so by tracking the particles adhering as a function of the rotational speed, we can measure the particle adhesion force. Figure 2 shows three replicates of the removal of RDX powder from stainless steel as a function of rotational speed in the centrifuge. This is the type of dataset from which the model representations of RDX adhesion are developed.

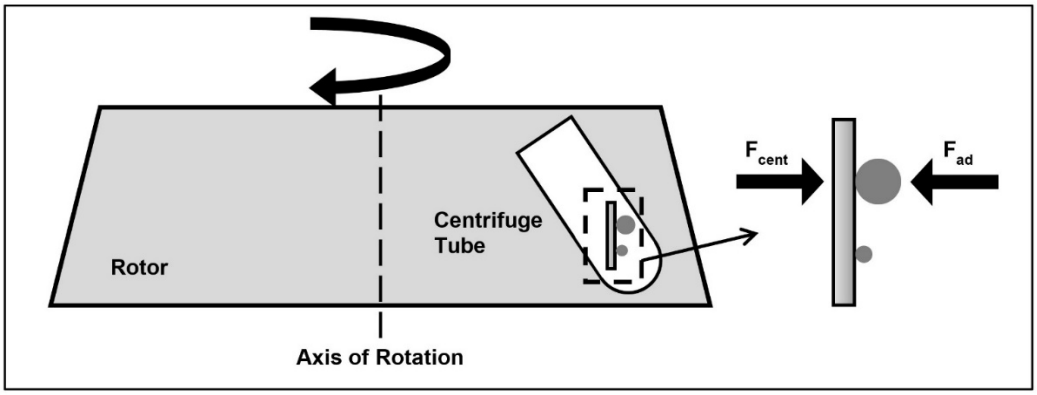

Figure 1: Schematic of the centrifuge apparatus illustrating the adhesion and inertial forces on the particles.

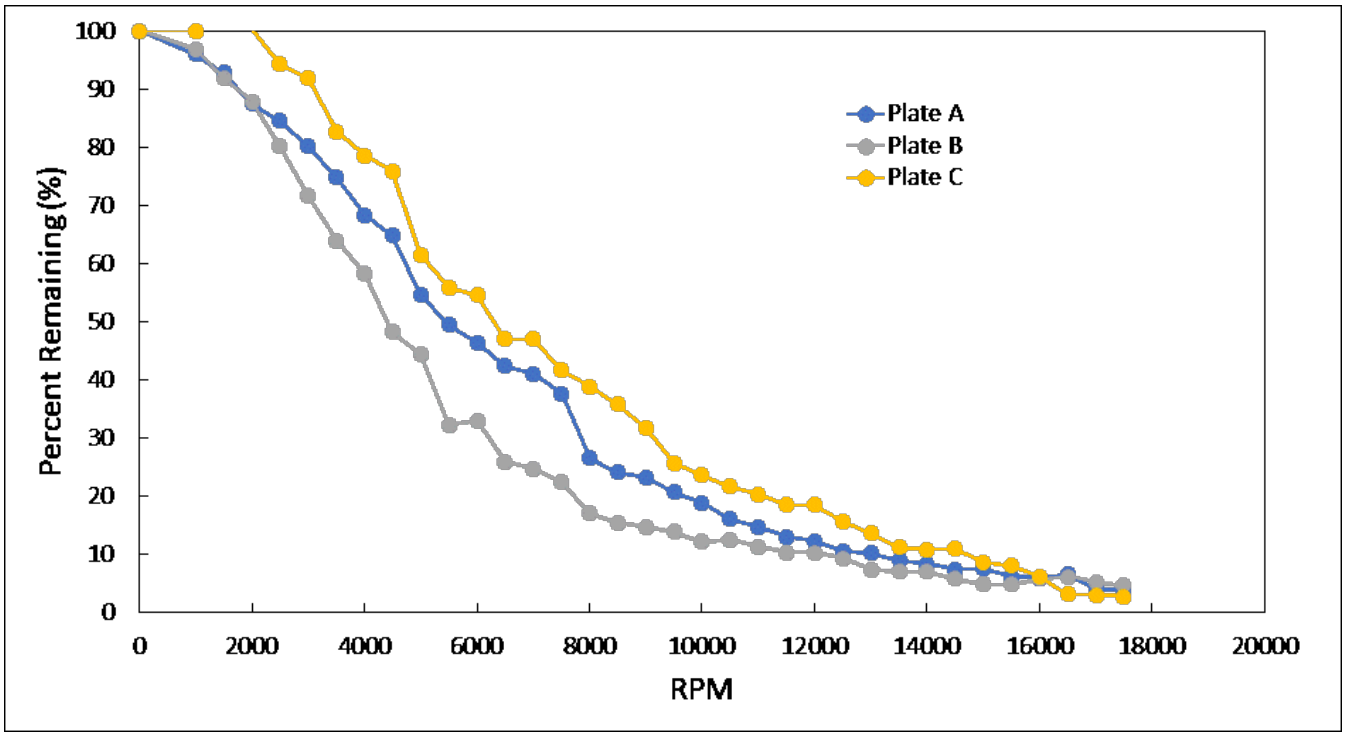

Figure 2: Three replicates of the removal of RDX powder from stainless steel plates during a centrifuge experiment.

The goals of this project were to:

- Fully validate the centrifuge method and implement it in order to study the adhesion of particulate RDX explosive to steel, silicon, aluminum, and acrylonitrile butadiene styrene (ABS) plastic surfaces.

- Create lookup tables of effective Hamaker constants that describe the adhesion of particulate RDX to various surfaces in terms of perfect spheres of residue, for use in defining the limiting adhesion forces that must be overcome during contact sampling.
- Complete and disseminate a MATLAB code (MATLAB executable) that can be used by commercial and government partners to implement the enhanced centrifuge method to prepare lookup tables of explosive adhesion to surfaces.
- Develop a robust model- and simulation-based method to design centrifuge experiments so that the community can quickly and inexpensively determine accurate, effective Hamaker constants. This requires the use of a particle adhesion simulator, which will be disseminated as a MATLAB executable, knowledge of the topography of the surface on which the explosives powder resides, and a modeling framework to relate the size distribution of the particles, the topography of the surface, and the experimental conditions used to develop the effective Hamaker constant distributions.
- Transfer the results of this research to the Transportation Security Lab (TSL), including a series of "how-to" tutorials, so that TSL can apply and disseminate the method as a standard approach in the community.

B. State of the Art and Technical Approach

The state of the art in contact sampling is well developed. Virtually all contact sampling protocols used in conjunction with ion mobility spectrometry (IMS) detection involve swabs made of Teflon-coated fiberglass, Nomex, paper, or muslin. These materials are provided by the manufacturers of the IMS equipment and are designed to be compatible with a specific device. The swabs are optimized to endure repeated exposure to the thermal cycling in the IMS, but not for their effectiveness in removing residues from surfaces. The technical approach pursued here involves fundamental studies of the way that residues deform and yield under the swiping load applied during contact sampling. By developing this understanding, it is possible to elucidate how a swab must contact a residue in order to remove the maximum amount of residue from a surface. With particulate solid residues, this is relatively straightforward to understand: it is necessary to come into contact with the particles. If the adhesion force between the particles and the swab is greater than between the particle and the surface, then it will be collected. In the case of the compounded residues, the behavior is substantially more complex. Specifically, these residues will deform under the sampling load, and it is not clear where they may yield when the trap attempts to lift them from the surface. There have been virtually no studies of this phenomenon, although there has been work on the deformation of compounded, highly filled composites, primarily for work in granular solids [2–11]. Our goal has been to quantify the particulate residue removed from a surface under inertial load and to develop a method to model this phenomenon. In addition, we sought to develop a method to quantify the compounded residue that stretches and breaks off the surfaces of interest in the centrifuge when the inertial removal force is applied. This was the first quantitative study of the residue removal process via applied load. In either case, we attempted to adapt the centrifuge method to evaluate the force required to remove residues of particulate and compounded explosives from surfaces [12–17]. This method allows for the direct measurement of the force required to remove large numbers of particulate explosives, or populations of compounded explosives residues, from surfaces. When these measurements are made, we characterize the adhesion of a sufficiently large number of particles or compounded residues so that the results can be readily generalized to all systems of interest. Moreover, the measurements specifically capture the effects of the topography, shape, and deformation of the explosives particles or residues, as well as the effects of the topography and deformation of the surface to which they adhere. When the two parts of this project are combined, we obtain a comprehensive understanding of the force required to remove residues of explosives, both particulate and compounded, from surfaces, in addition to a first principles understanding of the way that the explosives

deform and fail during removal. This understanding enables the development of improved residue sampling protocols and materials.

C. Major Contributions

The outcomes produced by this project include:

Year 4

We developed and validated a revolutionary interpretation of classical adhesion force measurements using the centrifuge technique. This enhanced centrifuge technique allows us to measure the adhesion force of a large population of explosive particles and to include the effects of their size, shape, and topography on the adhesion, as well as the effects of the topography of the surface to which they adhere.

We validated the enhanced centrifuge technique, created a customer-friendly code to interpret the measured adhesion force distributions, and developed a method to translate the force distributions into lookup tables that can be readily used to describe residue adhesion.

Year 5

We developed a fully transferable MATLAB executable model that runs on a personal computer without requiring resident MATLAB. It allows members of the community to insert centrifuge data and extract effective Hamaker constant distributions for the adhesion between explosive particles and surfaces. These distributions allow the community members to predict the adhesion force distributions between the particles and the surfaces for particles of any size. The code is configured as a black box with a user-friendly GUI to make it straightforward for users to insert and evaluate their data.

Year 6

We demonstrated that the effective Hamaker constant distributions vary as a function of the particle size and the topography of the particles and the topography of the surface to which they adhere. This demonstrates the validity of the enhanced centrifuge method, and shows the interplay between the length scale of features on the surface, the length scale of the particles, and the adhesion forces.

Year 7

We demonstrated that the adhesion between RDX powder and steel and glass surfaces varies systematically with the topography of the steel or glass, with the size of the RDX particles in the powder, and with the relative humidity. In this case, the key concept identified is that the root mean square (RMS) roughness of the surface is not related to the adhesion of the powder in a straightforward manner. Rather, the adhesion between the explosive powder and the surface is much more closely related to the ability of the roughness on the surface to accommodate the geometry of the particles at the particle scale. In Figure 3, the adhesion between RDX and silica is shown. The adhesion force is represented by the effective Hamaker constants determined using the Enhanced Centrifuge Method. These are directly proportional to the adhesion force. While the smoothest surface adheres to the particles of RDX most strongly, the roughest surface adheres next most strongly, closely followed by the second-smoothest surface. During the no-cost extension period, we will complete similar analysis on stainless steel, aluminum, and ABS plastic surfaces.

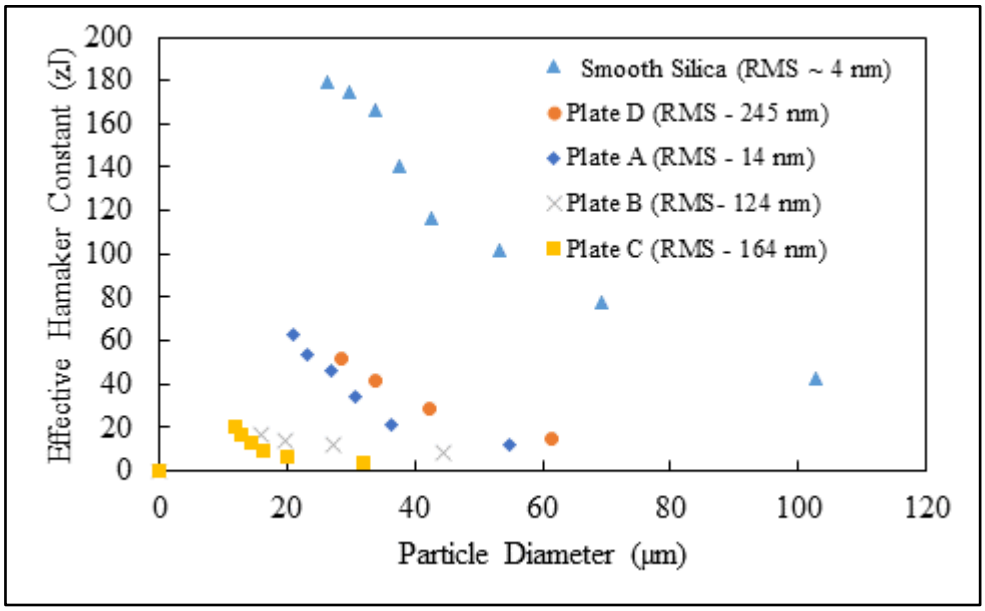

Figure 3: Effective Hamaker constants of RDX against steel and silica surfaces as a function of mean RDX particle diameter.

We developed first generation effective Hamaker constant lookup charts, as shown in Table 1 for RDX adhering to silica and stainless steel. These constants are applied in Equation 1 to determine the adhesion force between the RDX particles and the surfaces listed as a function of particle size and separation distance from the surface.

Silica										Stainless-Steel			
Plate 1 (14 nm)		Plate 2 (245 nm)		Plate 3 (124 nm)		Plate 4 (164 nm)		Pre-polished		Plate 1		Plate 2	
Size (μm)	**Aeff (zJ)**	**Size (μm)**	**Aeff (zJ)**	**Size (μm)**	**Aeff (zJ)**	**Size (μm)**	**Aeff (zJ)**	**Size (μm)**	**Aeff (zJ)**	**Size (μm)**	**Aeff (zJ)**	**Size (μm)**	**Aeff (zJ)**
54.9	12.1	61.5	15.2	44.4	7.9	32.1	4.1	102.8	42.4	59.1	3.5	59.9	8.1
36.4	21.3	42.4	28.9	27.3	12.0	20.1	6.5	69.4	77.3	44.2	4.4	48.3	9.3
30.6	33.8	33.8	41.4	19.8	14.1	16.1	9.4	53.1	101.9	39.7	6.3	44.7	12.5
26.9	46.4	28.4	51.8	15.9	16.3	14.4	13.3	42.6	116.7	32.1	6.5	39.7	14.2
23.1	53.4					13.0	16.8	37.5	140.8	27.7	6.9	35.2	15.2
20.9	63.1					11.8	20.1	33.9	166.4	25.8	8.2	32.1	16.5
								29.8	174.8	24.2	9.4	27.2	15.0
								26.4	179.6	21.2	9.2	24.5	15.0
										18.2	8.3	22.9	15.9
										17.6	9.4	22.0	17.5
										17.3	10.8	19.7	16.5
										16.2	11.1	15.0	11.0
										14.8	10.8	12.7	9.1

Table 1: Lookup table of effective Hamaker constants representing the adhesion of RDX against silica and stainless steel substrates. (Note that "pre-polished silica" had an RMS roughness of ~4 nm.)

We have developed an algorithm to know which rotational speeds to employ in the centrifuge in order to properly implement the Enhanced Centrifuge Method. In particular, during the application of the method, the intervals in rotational speed employed during the powder removal can be tightly coupled to the values of the resulting effective Hamaker constant distribution. When the appropriate rotational speed intervals are employed, this relationship will no longer apply, and the effective Hamaker constant distributions will be only functions of the particle and surface properties. We have developed an algorithm which relates the powder properties (primarily size distribution) and the rotational speed employed in the centrifuge to the

distribution of the particles into bins by size. Because each bin has a unique adhesion force, the binning process produces the effective Hamaker constant distributions. The algorithm is shown in Figure 4.

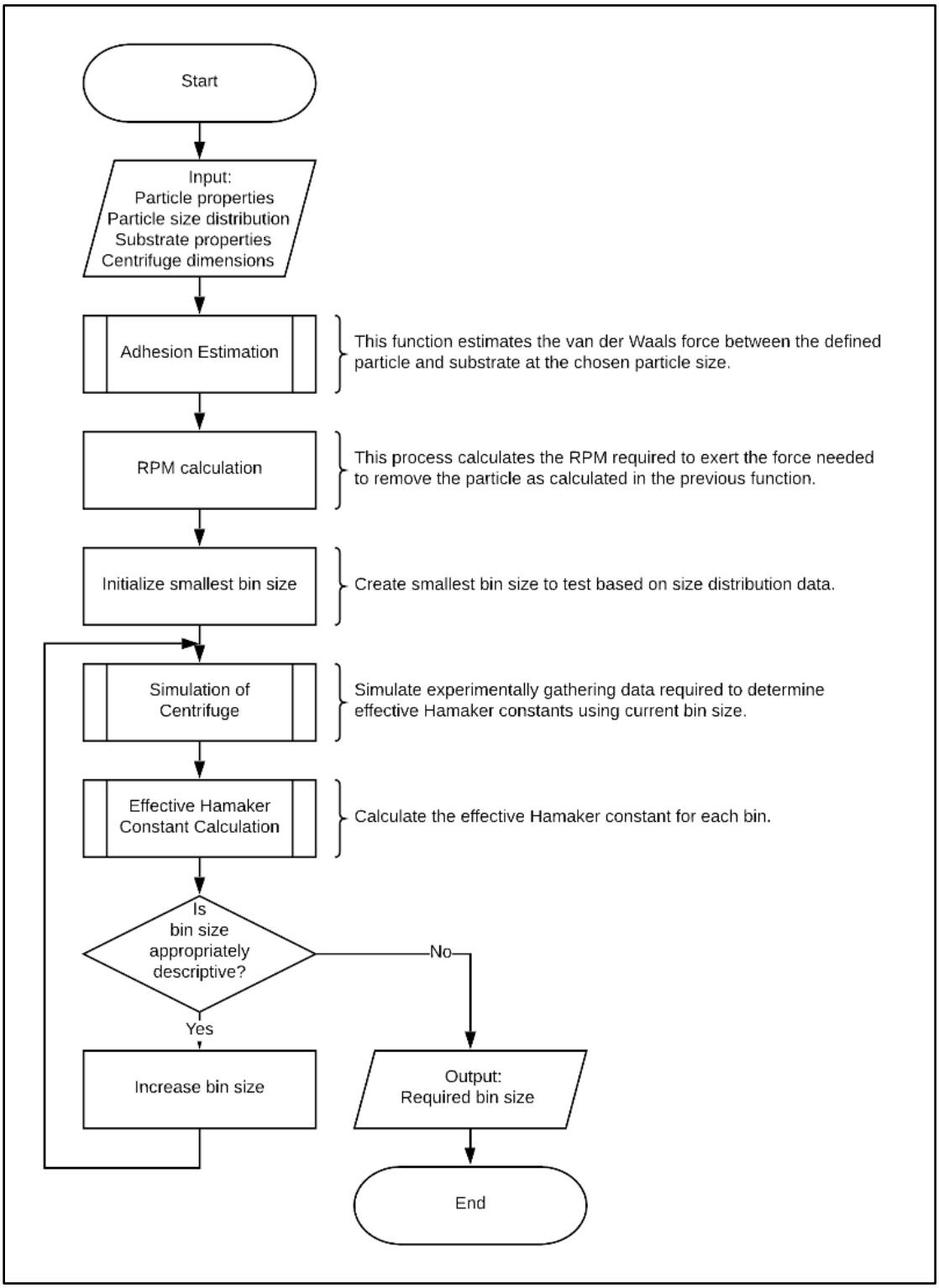

Figure 4: Process flow diagram demonstrating binning algorithm.

D. Milestones

Three milestones were pursued:

1. Determine adhesion force constants for RDX against common surfaces of interest in air transportation security environments;
2. Develop a first order approach for measuring the adhesion forces for compounded explosives against surfaces; and
3. Transfer the enhanced centrifuge method to the community, including a MATLAB-based code to evaluate data, so that the community could design and perform enhanced centrifuge experiments.

The first milestone, determining adhesion force constants for RDX against common surfaces of interest in air transportation environments, was partially achieved, as outlined in Table 1. This was not fully achieved because the lion's share of effort went into the unsuccessful pursuit of milestone 2: develop a first order approach for measuring the adhesion forces for compounded explosives against surfaces.

Milestone 2 was not attained because we could not find a simple, inexpensive, reproducible, and sufficiently sensitive method for quantitatively evaluating trace quantities of a compounded residue on surfaces. We pursued UV spectrophotometry primarily, as an inexpensive and precise approach for measuring residues, but we could not generate the necessary sensitivity.

Milestone 3 was partially achieved. Full completion was prevented because we identified a fundamental challenge in describing surfaces that required solution before the method could be used to design the appropriate operating conditions for experiments.

We anticipate more progress on milestones 1 and 3 during the no-cost extension period.

Programmatic risks and mitigation strategies: In assessing the adhesion forces for powder explosives against surfaces, the topography of the surface to which the explosive powder was adhering was observed to be key to the validity of the determined constants. We explored this phenomenon by systematically varying the surface topography, evaluating quantitatively the resulting force constants, and identifying the topographical features that dominate the adhesion. We also realized that the size of the increments in centrifuge rotational speed had a profound effect on the constants evaluated for particles of any given size. This should not be the case. During the no-cost extension period, we will aim to finalize the relationship between the particle size distribution for the explosive powder and the appropriate rotational speed intervals for the enhanced centrifuge experiments to give ideal experimental results. The goal is shown in Figure 5. As can be seen, for the correct change in rotational speed, the variation in the effective Hamaker constant can be minimized, and thus the intrinsic constant that is influenced only by the topography of the two surfaces and the size and shape of the particles of powder.

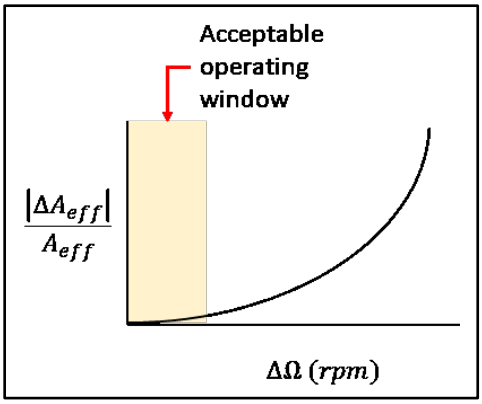

Figure 5: Schematic showing the relationship between the centrifuge rotational speed algorithm and the changes in the effective Hamaker constants.

E. Final Results at Project Completion (Year 7)

We have developed the enhanced centrifuge method to assess the adhesion between explosives powders and surfaces, and to model this adhesion in terms of a simple algebraic model. The model can be readily applied by any member of the community to estimate the range of explosives adhesion to surfaces. We were

scheduled to travel to the TSL for the summer of 2020, to transfer the method to the TSL. This was canceled due to COVID-19. Instead, we are preparing a series of YouTube tutorials that will be disseminated to the TSL and other members of the community to walk them through the method from beginning to end. These will be delivered by the end of the no-cost extension period. We have determined that the success of the method depends on a careful understanding of the topography of the surface to which the energetic material adheres, and we will deliver this understanding in an algorithm for surface evaluation by the end of the no-cost extension period.

III. RELEVANCE AND TRANSITION

A. Relevance of Research to the DHS Enterprise

Relevance #1/Metrics: Develop a method to measure the adhesion between explosives and surfaces of interest in air transportation environments.

Metric 1: Do look up charts exist for selected powdered explosives?

Yes, look up charts created for RDX against glass and steel.

Metric 2: Does the method work for all surfaces (has it been generalized)?

Not fully. The surfaces of interest to DHS will have a range of finishes. We need to investigate these, evaluate the adhesion force constants, and come back with a range of expected values. This will demonstrate the method, and will be completed during the no-cost extension period

Metric 3: Has a method for measuring adhesion of explosives powders to surfaces been developed and transferred to the community?

Not fully. The method has been developed. There are still details of the method to work out, including the effects of the topography of the surface and an algorithm to design the centrifuge experiments. These will be accomplished by the end of the no-cost extension period.

Metric 3: Is there a simple, accurate, inexpensive method to measure the adhesion of compounded explosives to surfaces?

No. We had to abandon this goal as our attempts with UV / visible spectrometry could never be performed in a sufficiently accurate, sensitive manner

B. Status of Transition at Project End

By the end of the no cost extension period, the community will have a series of videos documenting how to perform every aspect of the method, including how to design the experiments and how to interpret the results. Lookup tables will be presented for one-powdered explosive (RDX) on multiple surfaces (glass, stainless steel, aluminum, and ABS plastic) with different finishes. A manuscript will summarize the results in the refereed literature, and the work will be presented at the Trace Explosives Detection Workshop in spring 2021.

C. Transition Pathway and Future Opportunities

We had scheduled for a student to go to TSL and spend the summer of 2020 working there to transition the method to John Brady, but this was canceled due to COVID-19. Instead we will send a manual, a code, and a series of YouTube videos documenting all aspects of the method so that it may be implemented there. These will be sent at the end of the no-cost extension period.

D. Customer Connections

See above.

IV. PROJECT ACCOMPLISHMENTS AND DOCUMENTATION

A. Education and Workforce Development Activities

1. Student Internship, Job, and/or Research Opportunities
    a. Three undergraduate students (one female, one Hispanic) performed research in our lab on this project. All three are expected to go on to graduate study. Two will apply to graduate school this fall, while the other has one more year of study remaining.

B. Peer Reviewed Journal Articles

1. Stevenson, M., Beaudoin, S., & Corti, D. "Toward an Improved Method for Determining the Hamaker Constant of Solid Materials Using Atomic Force Microscopy. I. Quasi-Static Analysis for Arbitrary Surface Roughness." *Journal of Physical Chemistry C*, *124*(5), 10 January 2020, pp. 3014–3027. https://pubs.acs.org/doi/abs/10.1021/acs.jpcc.9b09669.

C. Peer Reviewed Conference Proceedings

1. Coultas-Mckenney, C., Norris, C., Roginski, A., Bradfish, K., Weiglein, E., & Beaudoin, S., "Bringing Particle Scale Properties into Descriptions of Energetic Powder Behavior via the Enhanced Centrifuge Technique." *Annual Meeting of the American Institute of Chemical Engineers*, Orlando, FL. November 2019.
2. Stevenson, M., Beaudoin., S., & Corti, D. "Impact of Surface Roughness on Estimating Hamaker Constants through Non-Contact Atomic Force Microscopy." *Annual Meeting of the American Institute of Chemical Engineers*, Orlando, FL. November 2019.

D. Requests for Assistance/Advice

1. From DHS
    a. Request for Jordan Monroe to spend the summer of 2020 at DHS TSL to transfer the enhanced centrifuge technique to the TSL. Jordan was scheduled to spend the summer teaching the method to TSL staff, but the visit was canceled due to COVID-19. We instead are preparing manuals, videos, and computer code to illustrate and assist with the method.

IV. REFERENCES

[1] M. Brookes, Synthetic Thumb for Residue Creation, in: Trace Explos. Sampl. Secur. Appl. Fundam. Adv. Trace Sampl. Detect. - TESSA02, 2015: pp. 70–82.

[2] A. Salman, G. Reynolds, H. Tan, Breakage in Granulation, in: J. Williams, T. Allen (Eds.), Handb. Powder Technol. Granulation, Vol. 11, Elsevier Science B.V., Netherlands, Amsterdam, 2007: pp. 979–1040.

[3] J. Litster, B. Ennis, The Science and Engineering of Granulation Processes, Kluwer Academic Publishers, Dordrecht, 2003.

[4] L. Liu, R. Smith, J. Litster, Wet Granule Breakage in a Breakage Only High-Shear Mixer: Effect of Formulation Properties on Breakage Behaviour, Powder Technol. 189 (2009) 158–164.

[5] R. Smith, J. Litster, Examining the Failure Modes of Wet Granular Materials Using Dynamic Diametrical Compression, Powder Technol. 224 (2012) 189–195.

[6] S. Iveson, N. Page, Dynamic Strength of Liquid-Bound Granular Materials: The Effect of Particle Size and Shape, Powder Technol. 152 (2005) 79–89.

[7] S. Iveson, J. Beathe, N. Page, The dynamic strength of partially saturated powder compacts: the effect of liquid properties, Powder Technol. 127 (2002) 149–161.

[8] S. Iveson, N. Page, Brittle to Plastic Transition in the Dynamic Mechanical Behavior of Partially Saturated Granular Materials, J. Appl. Mech. 71 (2004) 470–475.

[9] M.L. Sweat, A.S. Parker, S.P. Beaudoin, Compressive behavior of high-viscosity granular systems: Effects of viscosity and strain rate, Powder Technol. 302 (2016). doi:10.1016/j.powtec.2016.06.047.

[10] M.L. Sweat, A.S. Parker, S.P. Beaudoin, Compressive behavior of high viscosity granular systems: Effect of particle size distribution, Powder Technol. 311 (2017). doi:10.1016/j.powtec.2017.01.065.

[11] M.L. Sweat, A.S. Parker, S.P. Beaudoin, Compressive Behavior of Idealized Granules for the Simulation of Composition C-4, Propellants, Explos. Pyrotech. 41 (2016). doi:10.1002/prep.201600036.

[12] M.C. Thomas, S.P. Beaudoin, An enhanced centrifuge-based approach to powder characterization: Particle size and Hamaker constant determination, Powder Technol. 286 (2015) 412–419. doi:10.1016/j.powtec.2015.08.010.

[13] M.C. Thomas, S.P. Beaudoin, An Enhanced Centrifuge-Based Approach to Powder Characterization: Experimental and Theoretical Determination of a Size-Dependent Effective Hamaker Constant Distribution, Powder Technol. 306 (2017) 96–102.

[14] H. Krupp, Particle adhesion theory and experiment, Adv. Colloid Interface Sci. 1 (1967) 111–239. doi:10.1016/0001-8686(67)80004-6.

[15] G. Boehme, H. Krupp, H. Rabenhorst, G. Sandstede, Adhesion measurements involving small particles, Trans. Inst. Chem. Eng. 40 (1962) 252–259.

[16] H. Mizes, Small particle adhesion: measurement and control, Colloids Surfaces A Physicochem. Eng. Asp. 165 (2000) 11–23. doi:10.1016/S0927-7757(99)00442-2.

[17] G.R. Salazar-Banda, M.A. Felicetti, J.A.S. Gonçalves, J.R. Coury, M.L. Aguiar, Determination of the adhesion force between particles and a flat surface, using the centrifuge technique, Powder Technol. 173 (2007) 107–117. doi:10.1016/j.powtec.2006.12.011.

R2-B.1: Orthogonal Sensors for Trace Detection

I. PARTICIPANTS INVOLVED FROM JULY 1, 2019 TO JUNE 30, 2020

Faculty/Staff			
Name	**Title**	**Institution**	**Email**
Otto J. Gregory	PI	University of Rhode Island	gregory@egr.uri.edu
Michael J. Platek	Research Engineer	University of Rhode Island	platek@ele.uri.edu
Alan Davis	Research Professor	NUWC/URI	davis@ele.uri.edu
Graduate, Undergraduate and REU Students			
Name	**Degree Pursued**	**Institution**	**Month/Year of Graduation**
Peter Ricci	BS/PhD	University of Rhode Island	5/2019 (BS), 5/2024 (PhD)
Alyssa Kelly	BS	University of Rhode Island	5/2019 (BS)
Kevin Rivera	MS/PhD	University of Rhode Island	5/2019 (MS), 5/2023 (PhD)

II. PROJECT DESCRIPTION

A. Project Overview

In Year 7, we have dramatically improved the sensitivity and selectivity of our orthogonal sensors for the trace detection of explosives by using ultrathin yttrium-stabilized zirconia (YSZ) as the substrate for our sensor platform (Figure 1a). Due to its highly anisotropic thermal conductivity, the lateral dissipation of heat is minimized, such that it remains in the vicinity of the catalyst (Figure 1b). As a result, the detection of peroxide-based and nitrogen-based explosives at the part-per-billion (ppb) level is now possible at very low temperatures (75°C–175°C). Prior to using these low-mass YSZ substrates, temperatures >500°C were required to get responses in the ppb range. For example, the detection limits for triacetone triperoxide (TATP) and 2,4-dinitrotoluene (DNT) using the latest sensor platform at 175°C are 78 ppb and 2 ppb, respectively. By systematically reducing the thickness of the YSZ platform from 40 μm to 8 μm, the response time was dramatically reduced and the sensitivity to TATP was dramatically increased (Figure 2). All of this was accomplished without sacrificing the catalytic surface area.

a)

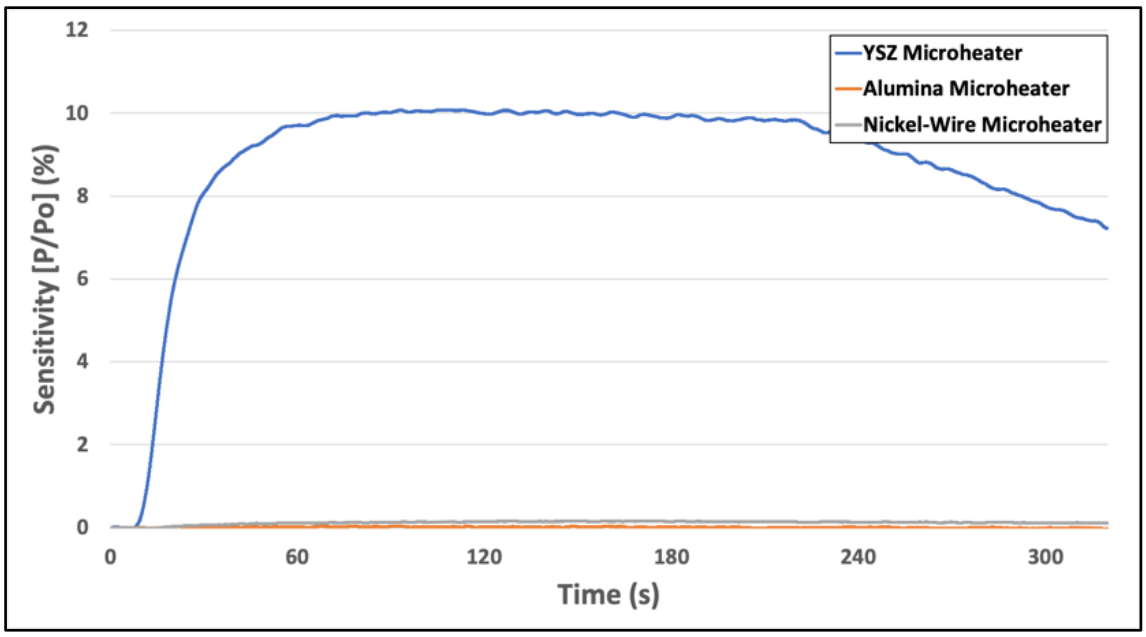

b)

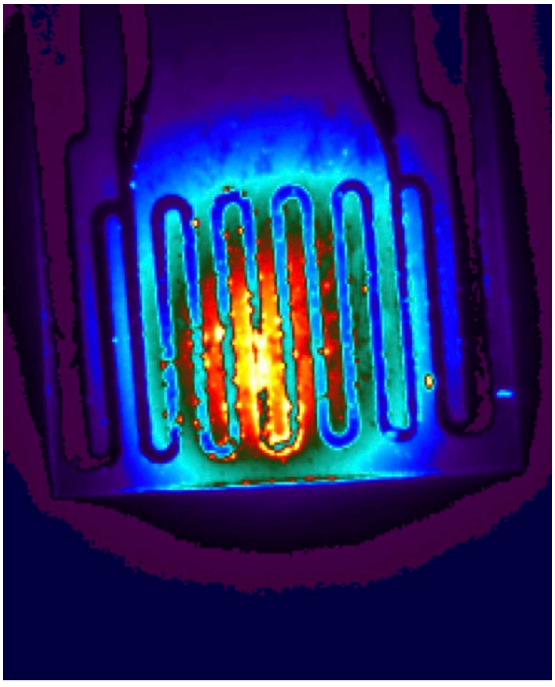

c)

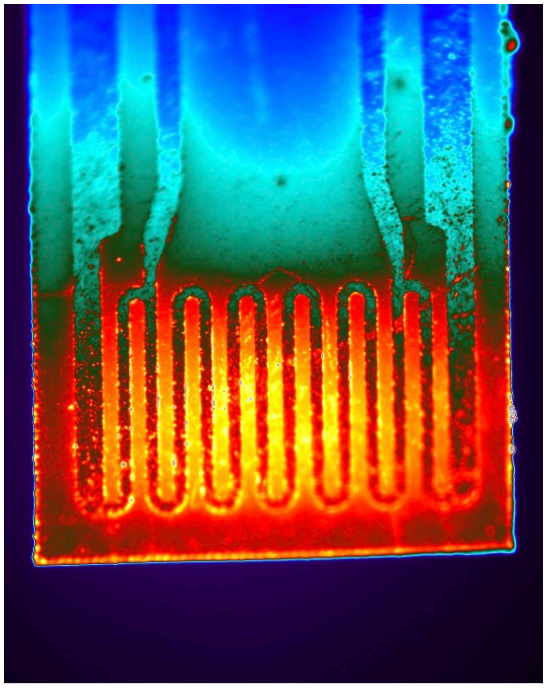

Figure 1: Response of three different microheater platforms to 20 parts per million TATP at 175°C, employing (a) a tin oxide catalyst, (b) high-resolution infrared images of sensors fabricated on YSZ, and (c) alumina substrates. Note the localized heating in (b) relative to the heating of the entire substrate in (c).

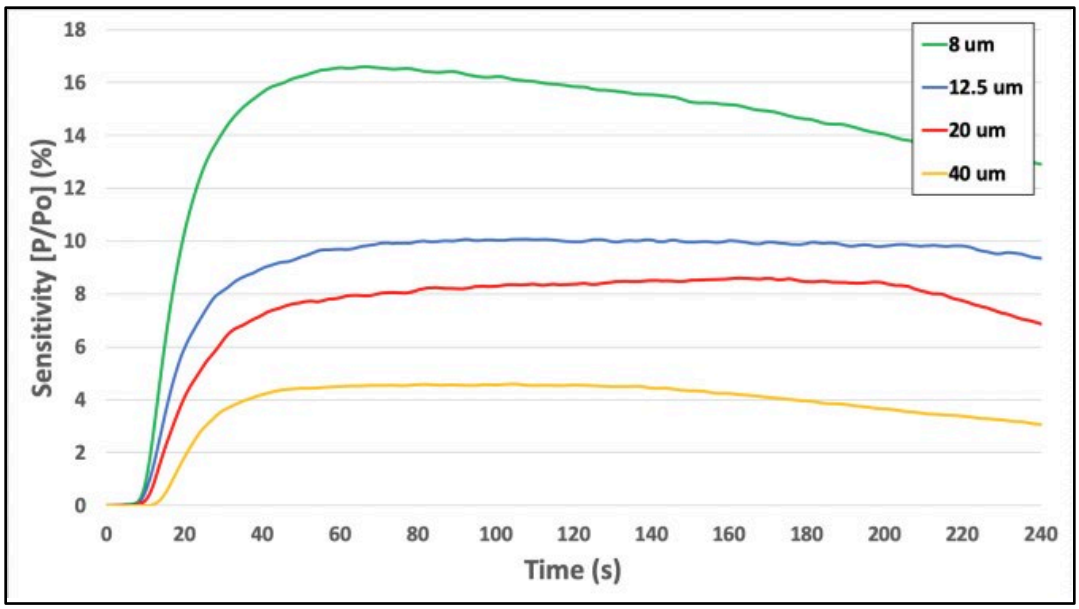

Figure 2: Responses of four palladium-based microheaters of varying thickness of YSZ substrate to 20 parts per million TATP (T = 175°C).

Copper and palladium-based (Pd) microheaters were recently fabricated and tested using our sensor platform. An unexpected outcome in so doing was the general catalytic effect associated with Pd microheaters. In previous studies, we showed that Pd nanoparticles dispersed into a tin oxide (SnO) matrix had a dramatic effect on sensor response [1]—by combining the specific catalytic response associated with SnO and the general catalytic effect associated with Pd, we were able to achieve unprecedented responses to a number of energetic materials relative to those responses using copper and nickel microheaters (Figure 3). With these two modifications, a stand-alone explosives trace detection (ETD) system for highly deployable detection that can be used with drones and wearables is now envisioned.

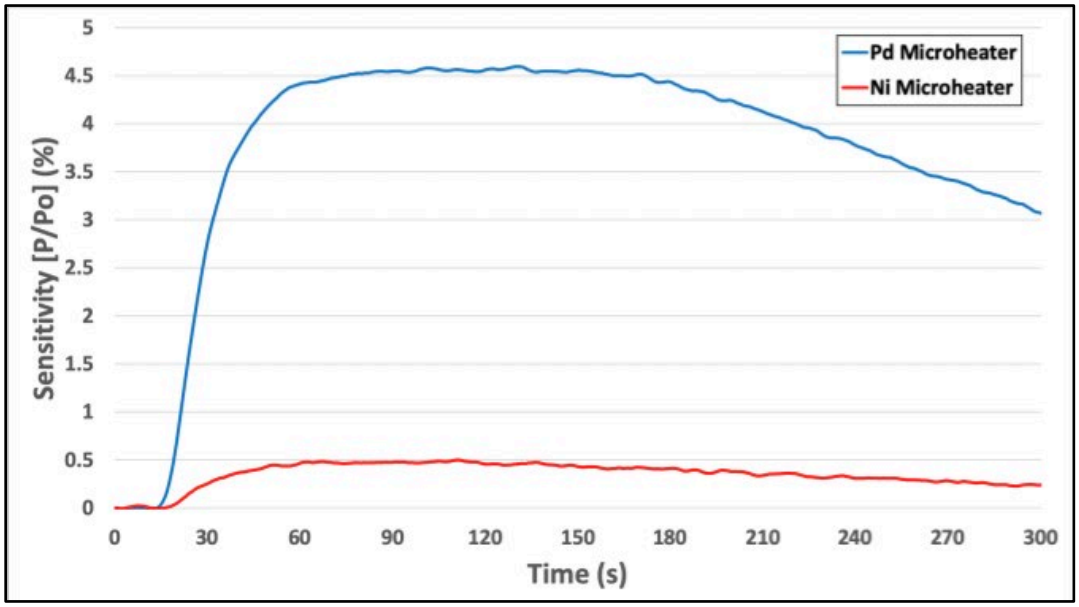

Figure 3: Responses of two YSZ-based sensors to 20 parts per million TATP. The sensors employed two different microheater metallizations (T = 175°C).

Due to these recent developments in sensor performance, we began to focus our efforts on sensor arrays. With an array of sensors of this type, a set of "fingerprints" unique to a specific analyte can be generated to further mitigate false positives and negatives. These "fingerprints" rely on endothermic/exothermic reactions that occur between the catalyst and the analyte. To model the functionality of the sensor arrays, Pd-based microheaters were fabricated employing four different catalysts (SnO, CuO, ZnO, and MnO) and were tested against three different analytes to generate unique "fingerprint" signatures. Overall, the SnO catalyst was found to be the most sensitive, with average sensitivity of 15%, and the MnO and CuO catalysts showed better selectivity for all three analytes. We selected hydrogen peroxide as one of the analytes to explore specificity for TATP: for example, a ZnO catalyst showed a uniquely endothermic response to 4 parts per million (ppm) H_2O_2, whereas the SnO and CuO catalysts showed exothermic responses (Figure 4a). In addition, an MnO catalyst was responsive to H_2O_2 and not TATP, even though acetone and H_2O_2 are well-known decomposition products of TATP (Figures 4a and 4b). Based on these results, an array of microheaters employing different catalysts will greatly improve selectivity.

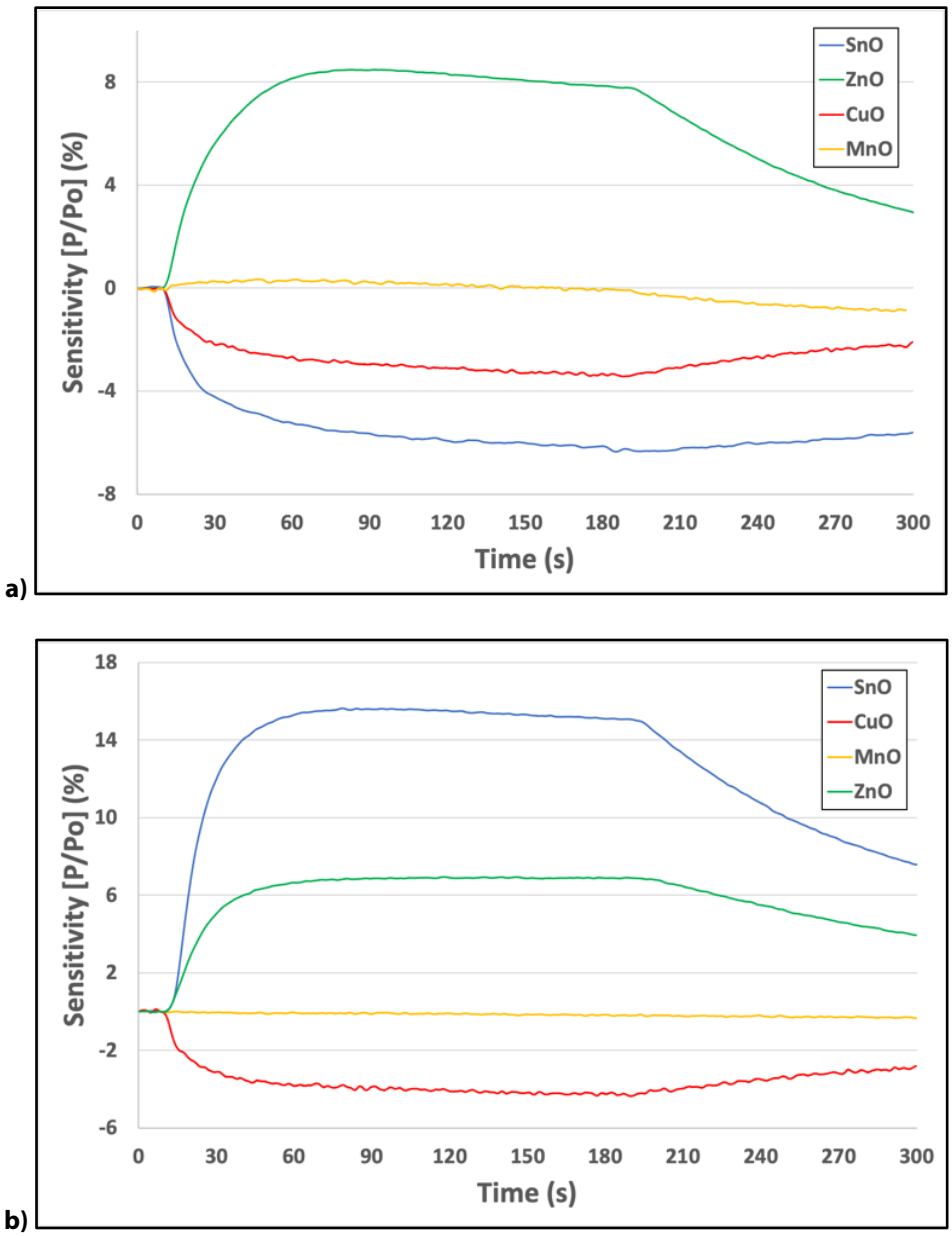

Figure 4: Responses of four YSZ-based sensors employing different metal oxide catalysts to (a) 4 ppm H_2O_2 and (b) 20 ppm TATP (T = 175°C).

In addition to explosives, we have utilized the "digital dog nose" platform for the trace detection of other compounds, most notably fentanyl. Fentanyl is a synthetic opioid pain reliever that has been shown to be 50 to 100 times more potent than morphine. This opioid is considered a highly controlled substance due to its high risk for addiction as well as severe respiratory distress and even death. Currently, fentanyl and related narcotics are being smuggled into the United States via transportation and mail distribution centers. Thus, there is a need for a portable detection system capable of continuously screening fentanyl and related narcotics in real time. Toward that end, we have focused our efforts on the detection of fentanyl and other extremely low vapor pressure compounds, which are very challenging to detect in the vapor phase. For example, fentanyl has a vapor pressure of only 3.17×10^{-11} atm. However, due to the greatly improved sensitivity and response time of our YSZ-based sensors, we believe our digital dog nose platform is well

suited to reliably detect compounds such as fentanyl at these trace levels. Another low vapor pressure threat we have targeted is cyclotrimethylenetrinitramine (RDX), or "plastic explosive", which has a vapor pressure of only 6.16×10^{-12} atm. This makes it a perfect simulant for the detection of very dangerous opioids like fentanyl. Figure 5 shows the response of our YSZ-based sensors to RDX (a) at a variety of temperatures and (b) at a variety of concentrations. Due to the much improved sensitivity of our platform, the detection of 6 parts per trillion (ppt) RDX has been achieved at temperatures ranging from 75°C to 175°C with sensitivities of 1%–8% respectively (Figure 5a). This YSZ platform has also allowed the detection limits to be substantially lowered. Figure 5b shows the sensor response to RDX at concentrations ranging from 0.4–6.0 ppt. Based on our ability to detect RDX at remarkably low vapor pressures, we now believe our sensor platform is capable of detecting fentanyl continuously and in real time.

a)

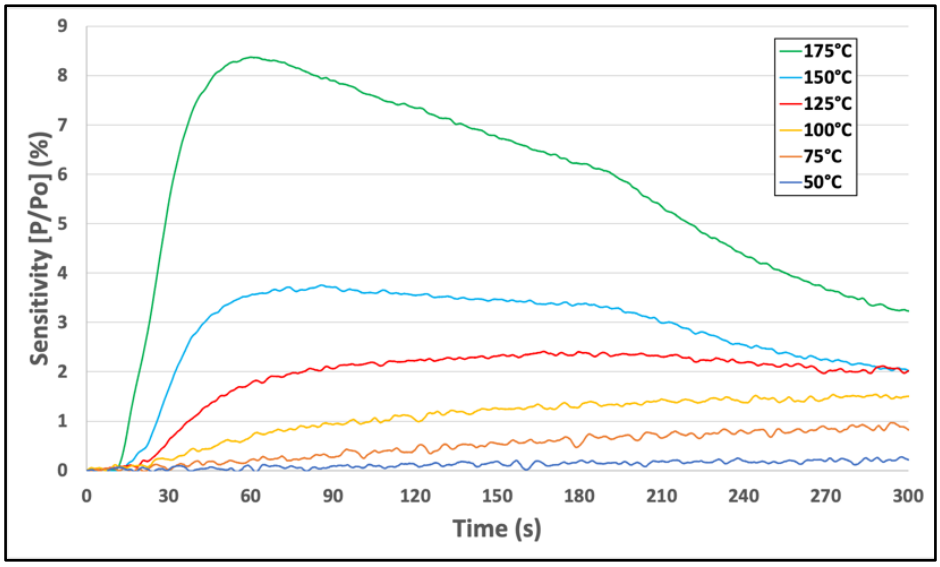

b)

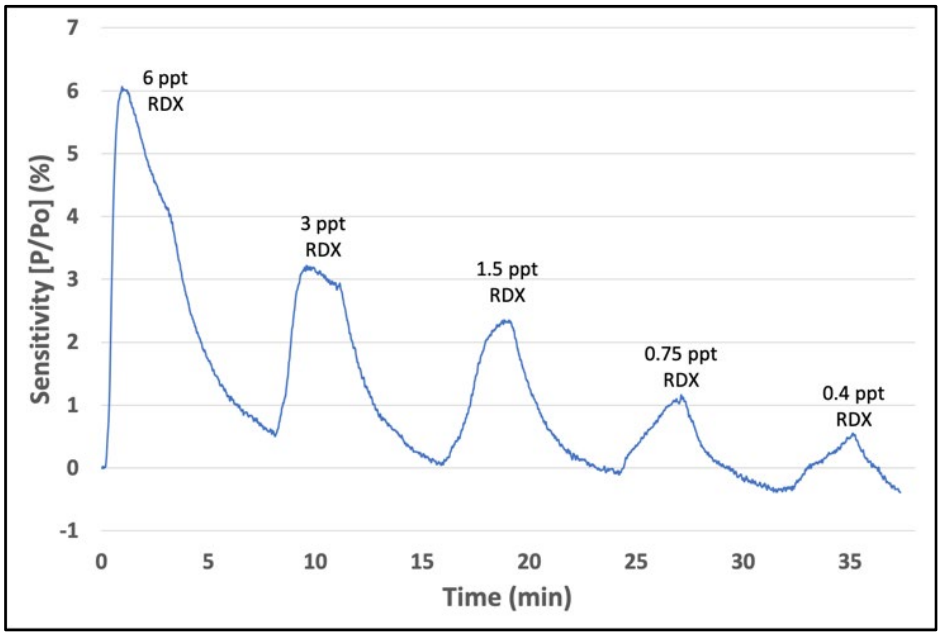

Figure 5: (a) Response of a YSZ-based sensor to 6 ppt RDX at a variety of operating temperatures and (b) a variety of concentrations (T = 175°C).

B. State of the Art and Technical Approach

The main deliverable for this research project was a portable ETD system, capable of continuously monitoring a wide variety of threat molecules in the vapor phase. Our digital dog nose is passive and noninvasive, and it operates in a manner similar to a dog's nose, where vapor is continuously drawn across sensors in a single pass, after which the vapors are expelled from the system. As the vapor is drawn across the active sensor elements, the energetic molecules are detected using a derivative of microcalorimetry where the heat effect associated with the catalytic decomposition of the energetic molecule is measured. By monitoring the electrical power difference between two microheaters (a catalyst-coated microheater and a "bare" microheater) maintained at a constant temperature, the sensor response is the heat effect associated with catalytic decomposition. In this way, the catalyst-coated microheater senses any sensible heat effects plus any heat effects associated with decomposition of the explosive molecule, whereas the "bare" microheater senses any sensible heat effects and thus is the reference. The difference between the two signals (power difference) is attributed to the energy released during catalytic decomposition.

Our sensing approach also relies on the heat effect associated with oxidation/reduction reactions that occur on the surface of the catalyst, after decomposition of the energetic molecules. This response is much more specific, and when "printed" on ultrathin ceramic substrates, it is much more sensitive and selective to different explosive molecules than other techniques [1-3]. Specifically, we monitor the heat effects associated with catalytic decomposition as well as the oxidation/reduction reactions taking place on the catalyst surface when an energetic molecule decomposes. We have shown previously [1-5] that the decomposition of TATP takes place via catalytic decomposition as opposed to ordinary thermal decomposition, as suggested by Chen and Bannister [6] and Dubnikova et al. [7, 8]. Several analytical methods have been successfully used to detect TATP at trace levels [9-12], but each has their own set of limitations. Many of these analytical techniques use large-scale equipment and require complex operational protocols. Colorimetric sensor arrays [9], for example, have been used to detect TATP at the 2 ppb level, but this method requires swabbing and thus is not amenable for continuous monitoring. One advantage of the colorimetric sensing of TATP, however, is that it is insensitive to humidity. Microeletromechanical-systems–based (MEMS-based) sensors, on the other hand, can meet the requirements for portable detection, and thus, a number of MEMS platforms have been used to detect explosives. MEMS-based sensors include metal oxide semiconductor devices [10], bulk acoustic wave resonators [11], and differential thermal analyzers [12].

C. Major Contributions

Year 1

1. Incorporated a reference microheater such that differential measurement could be made: using a reference microheater, hydrodynamic effects and sensible heat effects could be subtracted from the catalyst-coated microheater responses, such that the heat effect due to catalytic decomposition alone could be measured.
2. Implemented preconcentrator into the overall detection system to boost sensor response and thus sensitivity.
3. Detected nitrogen-based explosives (ammonium nitrate, 2,6-DNT, etc.) at the trace levels (<1 ppm).

Year 2

4. Used Combinatorial sputter deposition of Pd nanoparticles into a SnO catalyst matrix to improve sensor selectivity, sensitivity, and response time.

5. Detected peroxide-based explosives (TATP) and potential decomposition products (H_2O_2) at the low ppm level (<5 ppm).

Year 3

6. Developed thermally grown metal oxide nanowires as a catalyst support to increase the overall surface area of the metal oxide catalyst.
    - Increased catalyst surface area by four orders of magnitude (100 μm^2 to 4,000,000 μm^2).

Year 4

7. Implemented 25-μm diameter nickel wires as the microheaters in our sensor platform.
    - Lowered thermal mass of our sensor platform from 190 mg to 48 ug (5,000 times reduction).
    - Decreased overall power requirement (4 W to 1 W).
    - Improved sensor sensitivity.
8. Investigated the effects on sensor performance that humidity has (12%, 50%, 75%, and 100% RH).
9. Developed a nitrogen purge procedure to regenerate metal oxide catalyst after prolonged exposure to humid conditions.
10. Developed a portable digital dog nose sensor system that could be used for field trials.

Year 5

11. Undertook a series of seminal experiments to establish the sensing mechanism of our orthogonal sensors for trace detection.
    - Verified that catalytic decomposition precedes subsequent redox reactions between the decomposition products and the metal oxide, resulting in improved sensitivity and selectivity.
12. Improved detection limits of our sensor platform to peroxide-based (TATP) and nitrogen-based (2,4-DNT) explosives.
    - Demonstrated that detection now possible in the hundred ppb level.

Year 6

13. Implemented 40 μm yttria-stabilized zirconia (YSZ) as the substrate for our sensor platform.
    - Perfected combination of low thermal mass without sacrificing catalyst surface area.
    - Dramatically lowered detection temperatures from 500°C to 175°C.
    - Decreased power requirements from 2 W to 500 mW.
    - Improved sensor sensitivity by 500 times.
14. Developed portable digital dog nose platform for high throughput sensing.

Year 7

15. Implemented yttria-stabilized zirconia (YSZ) substrates 8 μm thick for our sensor platform.
    - Detected at temperatures lower than 175°C.
    - Decreased power requirement from 500 mW to <400 mW.

- Improved sensor sensitivity (ppt detection now a reality).
- Lowered sensor response time to <10 seconds.

16. Developed Pd-based microheaters to improve sensor sensitivity (16% to 30%).
    - Pd provides a catalyst amplifying effect due to its general catalytic properties.
17. Lowered detection limits of our orthogonal sensor platform to <ppb.
18. Developed ultraselective sensor arrays with up to 9 catalyst-coated sensors for "fingerprinting."
19. Detected extremely low vapor pressure compounds such as RDX and fentanyl.

D. Milestones

Milestone 1: Fabrication of Orthogonal Sensors on Ultrathin YSZ Substrates (Q1- 2019)

- **1.1:** We fabricated thin-film microheaters on ultrathin yttrium-stabilized zirconia (YSZ) substrates with thicknesses ranging from 8 μm to 40 μm. Ultrathin yttrium-stabilized zirconia substrates were supplied by our industry partner ENrG Inc.
    - STATUS: Completed (08/2019) 100%.
- **1.2:** We fabricated Cu and Pd thin-film microheaters on our thermodynamic sensors with thicknesses varying from 0.1 μm to 0.8 μm on ultrathin yttrium-stabilized zirconia substrates supplied by our industry partner ENrG Inc.
    - STATUS: Completed (08/2019) 100%.
- **1.3:** We fabricated orthogonal sensors (conductometric and thermodynamic platforms) on ultrathin YSZ substrates.
    - **1.31:** We completed the fabrication of orthogonal sensors utilizing Cu and Pd microheaters, SnO, CuO, ZnO, and FeO metal oxide catalysts as well as other metal oxides with multiple oxidation states.
        - STATUS: Completed (09/2019) 100%.
    - **1.32:** We optimized heat treatment of catalysts (time at temperature) to maximum sensor response.
        - STATUS: Completed (09/2019) 100%.
    - **1.33:** We fabricated thin-film microheaters and metal oxide catalysts on YSZ substrates having thicknesses ranging from 8 μm to 40 μm.
        - STATUS: Completed (09/2019) 100%.
    - **1.34:** We fabricated very thin (<1 μm) Cu microheaters and electrodes for orthogonal sensors.
        - STATUS: Completed (09/2019) 100%.

Milestone 2: Demonstration of Orthogonal Sensors Fabricated on Ultrathin YSZ Substrates (Q1-2019/Q2-2019)

- **2.1:** We tested orthogonal sensors fabricated on ultrathin YSZ substrates against different explosives, including peroxide-based and nitrogen-based explosives (TATP, 2,4 DNT).
- **2.2:** We tested our orthogonal sensors fabricated on YSZ substrates against different opioids/narcotics.

- **2.3:** We achieved faster response times and lower power requirements for orthogonal sensors fabricated on ultrathin YSZ.
- **2.4:** We lowered the detection limits by using sensors fabricated on ultrathin YSZ. Part per trillion detection limits were demonstrated for some explosives.
- STATUS: Completed (2/2020) 100%.

Milestone 3: Fabrication and Testing of Microheater Arrays with Detection Algorithms (Q2-2019/Q3-2020)

- **3.1:** We made new CAD drawings of microheater patterns with line widths and line spaces ranging from 10 μm to 50 μm to minimize lateral heat dissipation and keep the catalyst at a uniform temperature.
  - STATUS: Completed (11/2019) 100%.
- **3.2**: We fabricated thin-film microheater arrays utilizing the new microheater designs.
  - STATUS: Completed (3/2020) 100%.
- **3.3:** We evaluated sensor performance utilizing thin-film microheater arrays.
  - **3.31:** We investigated cross talk (heat transfer) from one thin-film microheater to another using infrared imaging techniques: the effect of line width and line space was studied using designs with 50-μm, 25-μm, and 10-μm line width and line space.
  - **3.32:** We fabricated SnO, CuO, and FeO catalysts on the thin-film microheaters arrays.
  - **3.33:** We established sensor metrics, including response time and power, for different microheater arrays and analytes.
  - STATUS: Completed (3/2020) 100%.
- **3.4**: We patterned arrays of microheaters with different catalysts and tested them against explosives and narcotics. **(Q3-2020/Q4-2020)**
  - **3.41:** We fabricated sensor arrays on ultrathin YSZ and used them to detect explosives and narcotics.
  - **3.42:** We developed new interconnect schemes for thin-film microheater arrays to maximize the number of microheaters in a given array.
  - STATUS: Completed (3/2020) 100%.
- **3.5:** We developed algorithms to uniquely identify analytes of interest, minimizing false positives and negatives, and used them to optimize the energy budget and duty cycle.
  - STATUS: Completed (6/2020) 100%.

Milestone 4: Field Testing Sensor Arrays on Ultrathin YSZ at the Naval Research Lab (Q3-2020)

- **4.1:** We integrated thin-film microheater arrays into our portable trace detection system.
- **4.2:** We used our portable ETD system with integrated microheater arrays to detect a variety of explosives.
- **4.3:** We did not travel to the Naval Research Laboratory's vapor test bed for confirmation of detection limits and demonstration of sensor response in the presence of select interferents using their proprietary vapor generator; trace levels of analytes w/interferents can be delivered in a highly controlled manner traced to National Institute of Standards and Technology standards.

- STATUS: Did not complete (see below).

Milestone 5: Integration of Sensor Arrays for Drone and CT Applications Using High Throughput Design (Q4-2020)

- **5.1**: We finalized the design for high throughput sensing using sensor arrays formed on ultrathin YSZ substrates.
  - STATUS: Completed (12/2019) 100%.
- **5.2:** We fabricated sensors with a modified "pitot tube" design for high throughput sensing.
  - **5.21:** We optimized the size and pattern of vias and microchannels within the ultrathin YSZ substrates for effective sampling of high flow-rate streams.
  - **5.22:** We fabricated micromachined channels and vias within the ultrathin YSZ substrates having thicknesses ranging from 8 μm to 40 μm.
  - STATUS: Completed (1/2020) 100%.
- **5.3:** We demonstrated sensor arrays with modified "pitot tube" design using micromachined channels and vias within the ultrathin YSZ substrates for high throughput sensing.
  - **5.31:** We demonstrated high flow-rate sensing at flow rates up to 100 cubic feet per minute.
  - **5.32:** We evaluated detection limits, response times, false alarm rates, etc. for our high throughput sensor in a CT tunnel environment.
  - STATUS: Completed (5/2020) 100%.
- **5.4**: We packaged sensor arrays using micromachined channels and vias within the ultrathin YSZ substrates used for high throughput sensing.
  - STATUS: Completed (5/2020) 100%.
- **5.5**: We finalized the interconnect schemes for sensor arrays used for high throughput sensing.
  - **5.51:** We demonstrated the ability to detect explosives in the head space of a CT tunnel in real time.
    - STATUS: Completed (4/2020) 100%.
  - Due to the COVID-19 pandemic and the restrictions placed on travel and gathering, testing at the Naval Research Laboratory in Washington, DC planned in Year 7 did not happen. In short, we were not able to field test our ultrathin, low thermal mass sensor arrays at the Naval Research Lab's vapor test bed (Milestone 4). As soon as things are relaxed and we can travel there, we plan to complete the testing of our low thermal mass sensor arrays.

E. Final Results at Project Completion (Year 7)

There were many successful results over the life of the project, but those with the biggest impact on DHS and its stakeholders were realized in Year 7. Perhaps the result with the single greatest impact on transition was lowering thermal mass (i.e., moving to extremely low thermal mass substrates for our sensor platform). At the starts of our project we were using relatively thick (1 mm) aluminum oxide substrates for our thermodynamic sensor platform. Over the course of the project we systematically reduced the thermal mass by a factor of 5,000, eventually using YSZ substrates 10 μm thick. This not only improved the sensitivity and response times (30 s to less than 1 s) of our thermodynamic sensor but also greatly improved the selectivity of our sensor.

Other benefits were realized along the way as well. The power requirements were dramatically lowered as the thermal mass was lowered, resulting in more efficient thermal cycling of our sensor, which made truly portable detection systems possible. The ultrathin YSZ substrates with their highly anisotropic thermal properties minimized the lateral dissipation of heat, which in turn enabled us to dramatically lower the operating temperature of the catalyst. As a result, the operating temperature of our sensor was lowered from 500°C to <175°C. Lastly the resolution of the sensor was improved as the thermal mass was reduced, which enabled us to not only identify the threat but also determine quantitatively how much of the threat was present in the vapor.

Another related successful result was lowering the detection limits for all the explosives of interest. Using the ultrathin, low thermal mass YSZ sensors with Pd microheaters, detection limits in the part per trillion range are now possible. At the start of this project, detection limits in the part per million range were not even possible. This means that the resolution for detection was improved by more than four orders of magnitude over the life of the project.

And finally, the third successful result was that very low vapor pressure analytes, such as RDX and fentanyl, could be detected using our orthogonal trace detection system. Simply put, this means that threats that don't really have a vapor pressure can be detected, including threats that are packaged or concealed, which could provide a complementary tool for those screening at airports and postal distribution centers.

III. RELEVANCE AND TRANSITION

A. Relevance of Research to the DHS Enterprise

- One of the operational homeland security challenges that our orthogonal sensor technology addresses is the detection of explosives in the CT tunnel environment. Our technology can provide inexpensive add-on capability to TSA and others to achieve a redundant or additional screening system to augment some of the shortcomings associated with CT.
- Another operational homeland security challenge that our ETD system addresses is the ability to detect opioids as well as explosives. We have demonstrated that our ETD system can detect fentanyl, which is extremely difficult to detect by other methods. One of the issues mentioned by several DHS stakeholders is that commercial trace detection systems should be able to detect narcotics as well as explosives.

B. Status of Transition at Project End

We have been working with several commercialization partners, funded through the FlexTech Alliance for the past eighteen months, to develop and commercialize a new class of ultrathin, flexible circuits. This will enable high-performance silicon electronics to be directly packaged with a solid-state lithium battery technology on thin-film MEMs-like sensor platform from University of Rhode Island (URI). In short, the team received a $2.8 million award in September 2018 to develop a sensor platform for drone applications whereby monolithic sensors are integrated with thin-film batteries to produce a sensor system with integrated processing. This will enable the integration of a power module, sensor, signal processing, and telemetry electronics into a package with total thickness <250 μm. Such packaging will enable our sensors to be used in small drones, wearables, and other volume/weight-sensitive detection platforms. Furthermore, with only small changes to the catalyst, we will be able to detect a number of analytes, including toxics and narcotics, and provide an enabling technology to the military and first responders.

By using ultrathin YSZ as the substrate for our sensor platform, unparalleled sensitivity and selectivity for the detection of energetic materials was achieved. In addition, a significant reduction in the power required

to operate the sensor was achieved, which makes onboard portable applications such as drones or wearables possible. Table 1 shows a comparison of sensor microheaters utilizing different YSZ substrate thicknesses. Microheaters fabricated on 8 µm YSZ required the least power (215 mW) while Pd microheaters on 8 µm YSZ required the lowest overall energy (0.78 J). Due to the similar power requirements for the Cu (215 mW) and Pd (260 mW) microheaters, the Pd microheaters were chosen for packaging due to the catalyst amplification effect associated with Pd (16.2% versus 5.2%).

	Power Requirement (mW)	Sensitivity‡ (%)	Response Time* (s)	Energy (J)
Cu (40 µm YSZ) †	320	**0.5**	**10**	3.2
Cu (20 µm YSZ) †	300	2.75	9	2.7
Cu (12.5 µm YSZ) †	245	3.2	8.5	2.08
Cu (8 µm YSZ) †	**215**	5.2	6	1.29
Pd (40 µm YSZ) †	**370**	4.5	8.75	**3.24**
Pd (20 µm YSZ) †	330	8.5	5	1.65
Pd (12.5 µm YSZ) †	280	10	4.5	1.26
Pd (8 µm YSZ) †	260	**16.2**	**3**	**0.78**

* Response time was arbitrarily determined to be the t10 time or time required to reach 10% of the overall response
† All microheaters fabricated with 0.5µm metallization thickness
‡ All microheaters employed a 0.9µm thick SnO catalyst

Table 1: Copper- and palladium-based sensors fabricated on YSZ substrates of varying thickness.

Our sensor platform employs a proprietary Anderson Loop circuit to maintain the desired operating temperature as well as measure the resulting heat effects due to catalytic decomposition. Unfortunately, the Anderson Loop circuit requires significantly higher power levels than those required for drones and wearables, and thus an alternative circuit (ALA) was designed. A breadboard design for the ALA was completed and coupled with a microheater that was directly bonded to the surface of a battery made by ITN Energy Systems, as shown in Figure 6. Continued development efforts led to a new ALA circuit, based on a printed circuit board (PCB), with lower noise and power requirements (Figure 7). The new ALA circuit showed ~20 mW of noise compared to the ~80 mW observed from the previous iterations.

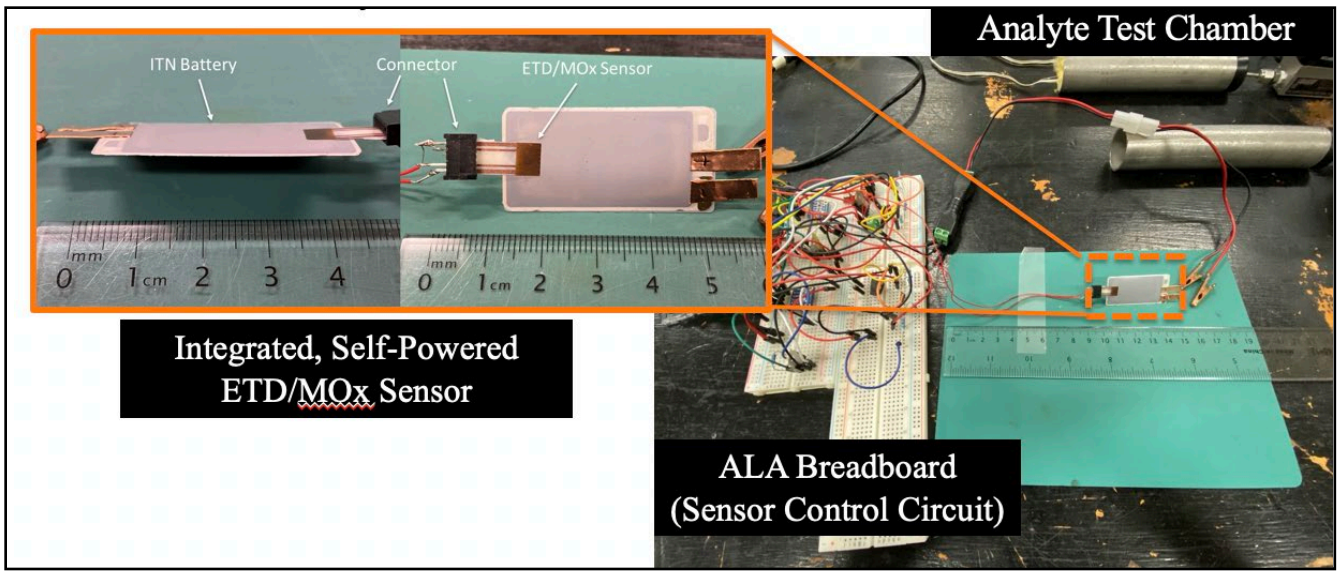

Figure 6: Self-powered sensor, where the URI's ETD was directly bonded to the surface of the ITN battery.

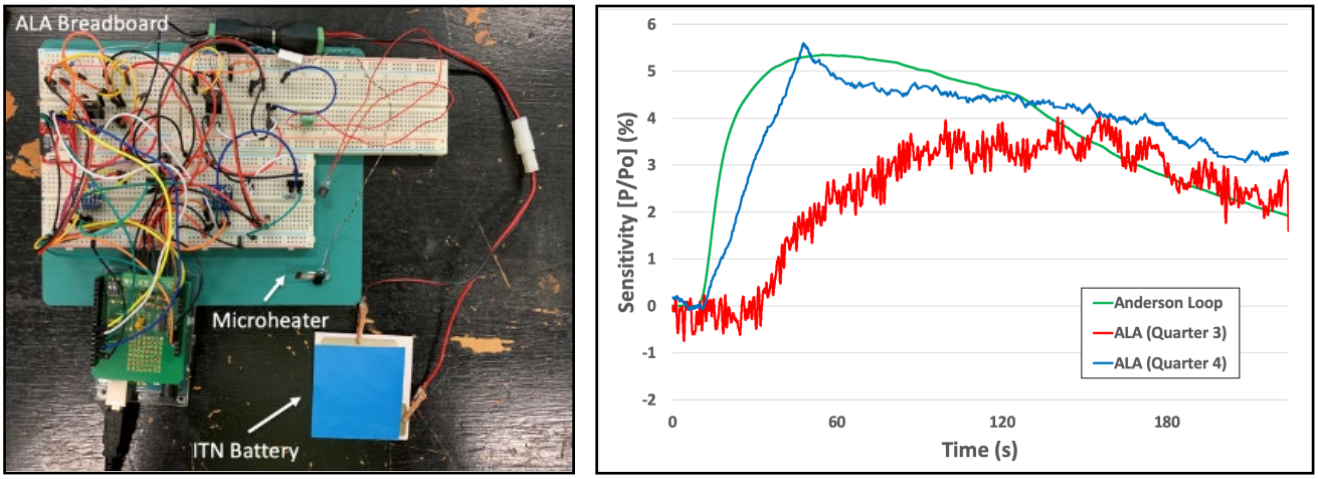

Figure 7: (left) ALA breadboard circuit powered by an ITN battery and (right) comparison of ALA circuit response and noise floor with the power-hungry Anderson Loop (SnO catalyst).

Given the improvements in sensitivity and response time when using Pd microheaters, a comparison between the performance of YSZ-based sensors using the original power-hungry Anderson Loop and the new ALA circuit was assessed. Figure 8 shows the ALA circuit has similar performance and lower power compared to the Anderson Loop.

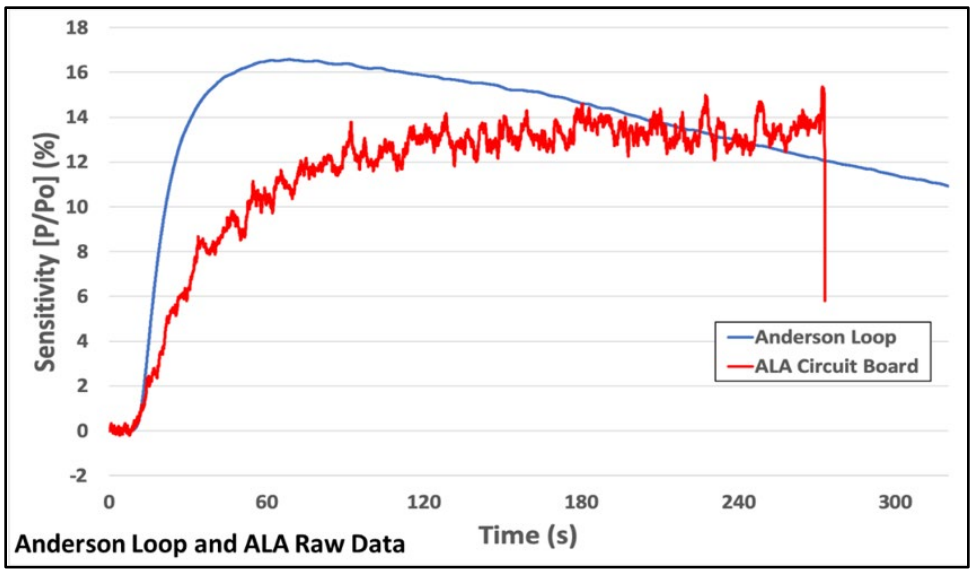

Figure 8: Comparison of the responses of a Pd microheater with a SnO catalyst fabricated on a YSZ substrate to 20 ppm TATP powered by the Anderson Loop (blue) and an ALA circuit (red).

C. Transition Pathway and Future Opportunities

There is considerable potential for transition using our orthogonal sensors for the trace detection of explosives (and narcotics) in future screening systems. This includes mounting our sensors onto the surface of an unmanned aerial vehicle wing with a low vertical profile (low drag) or wearable sensors for firefighters and first responders. The detection of explosives, toxics, and narcotics are the targets for these applications. In other applications, such as the CT tunnel environment, screening the head space around baggage for explosives and narcotics in the time it takes to X-ray baggage is now possible with the high flow-rate version of our sensor. We have been working with several commercialization partners, funded through the FlexTech Alliance, to develop and commercialize a thin-film, MEMs-like version of our orthogonal sensor. Our partners are helping us develop thin-film arrays of chemical sensors that can detect a broad spectrum of compounds in real time as part of an early detection warning system. This "smart skin" sensing platform will employ multiple thin-film microheaters fabricated on ultrathin YSZ substrates. Each microheater will be coated with a different catalyst to form "active" sensor elements, and one will remain uncoated and serve as a reference. In this way, a broad spectrum of threat molecules can be detected in real time.

D. Customer Connections

Name	Title	Institution	Email	Phone
Mark Fischer	Senior Scientist (Explosives)	FLIR	Mark.Fischer@FLIR.com	401-372-9535 x 11615
John Olenick	CEO/President	ENrG Inc.	jolenick@enrg-inc.com	716-390-6740
Kathy Olenick	Business Developer	ENrG Inc.	kolenick@enrg-inc.com	716-873-2939 x 102
Brian Berland	Chief Science Officer	ITN Energy Systems	Bberland@itnes.com	303-285-5107
Alan Davis	Research Professor	NUWC/University of Rhode Island	davis@ele.uri.edu	401-874-5482

IV. PROJECT ACCOMPLISHMENTS AND DOCUMENTATION

A. *Peer Reviewed Journal Articles*

1. Ricci, P.P., Rossi, A.S., & Gregory, O.J. "Orthogonal Sensors for the Trace Detection of Explosives." *IEEE Sensors Letters, 3*(10), October 2019, pp. 1–4. https://doi.org/10.1109/LSENS.2019.2944587.
2. Ricci, P.P., & Gregory, O.J. "Continuous Monitoring of Vapor Phase Threats Using Ultrasensitive, Low-Power Sensors." *IEEE Sensors Journal*, in press.

B. *Peer Reviewed Conference Proceedings*

1. Ricci, P.P., & Gregory, O.J. "Trace Detection of Explosives Using Metal Oxide Nanostructured Catalysts." *TechConnect 2019*, Boston, MA, June 2019.
2. Gregory, O.J., Olenick, J., & Olenick, K. "Ribbon Ceramic: Novel Form Factor Enabling Thermal Product Applications." *NATAS 2019*, Newport, RI, August 2019.
3. Ricci, P.P., & Gregory, O.J. "Ultrasensitive, Thin-Film Sensors for the Trace Detection of Explosives." *NATAS 2019*, Newport, RI, August 2019.
4. Ricci, P.P., & Gregory, O.J. "Low-Power Sensors for the Trace Detection of Threats in the Vapor Phase." *FLEX 2020*, San Jose, CA, February 2020.
5. Ricci, P.P., & Gregory, O.J. "Ultrasensitive, Orthogonal Sensors for the Trace Detection of Explosives." *ISADE 2020*, Charlotte, NC, April 2020.

C. *Other Presentations*

1. Interviews and/or News Articles:
   a. Hampton, M. "Wanted: A Bomb Detector as Sensitive as a Dog's Nose." *IEEE Spectrum*, 11 October 2019. https://spectrum.ieee.org/tech-talk/semiconductors/devices/using-a-twopronged-approach-to-detect-explosive-substances-from-bombs.
   b. CBS News. "'Innovation Checkpoint' and 'Digital Dog Nose': TSA Tests New Security Technology." 25 November 2019. https://www.cbsnews.com/news/tsa-testing-advanced-airport-security-technology-digital-dog-nose-innovation-checkpoint/.
   c. CBS Boston. "URI Researchers Test New TSA Tech 'Digital Dog Nose,' Gel to Flash-Freeze Explosives." 25 November 2019. https://boston.cbslocal.com/2019/11/25/university-of-rhode-island-uri-tsa-tech-digital-dog-nose/.
   d. Larson, B. "High Tech: TSA Testing A 'Digital Dog Nose.'" Fox News, 27 November 2019. https://video.foxnews.com/v/6109645048001#sp=show-clips.
   e. Liberatore, S. "TSA Is Testing New 3D Rotating Scanning Technology to See Through Your Baggage and 'Digital Dog Noses' to Detect Explosives at Airport Security in an Effort to Speed Up Lines." *Daily Mail*, 25 November 2019. https://www.dailymail.co.uk/sciencetech/article-7724599/TSA-testing-new-technology-cut-wait-time-check-in.html.

V. REFERENCES

[1] Ricci, P.P. and Gregory, O. J. "Continuous Monitoring of Vapor Phase Threats Using Ultrasensitive, Low-Power Sensors," *IEEE Sensors Journal*. in press.

[2] Ricci, P.P., Rossi, A.S., and Gregory, O.J. "Orthogonal Sensors for the Trace Detection of Explosives," *IEEE Sensors Letters,* vol. 3, no. 10, pp. 1-4, Oct. 2019.

[3] Rossi, A.S., Ricci, P.P., and Gregory, O.J. "Trace Detection of Explosives Using Metal Oxide Catalysts." *IEEE Sensors Journal*, *19*(14), 2019.

[4] Chu, Y., Mallin, D., Amani, M., Platek M. J., and Gregory, O.J. "Detection of Peroxides Using Pd/SnO2 Nanocomposite Catalysts." *Sensors and Actuators; B Chemical*, *197*, 2014, p. 376–384.

[5] Amani, M., Chu, Y., Waterman, K. L., Hurley, C. M., Platek, M. J., and Gregory, O.J. "Detection of Triacetone Triperoxide (TATP) Using a Thermodynamic Based Gas Sensor." *Sensors and Actuators; B Chemical*, *162*, 2012, pp. 7-13.

[6] Chen, C., and Bannister, W. "Research, Development, and Demonstration of Exothermal Explosive Detection System Based on Microthermal Analysis." *DOT/TSA/AR-ICC5372, Transportation Security Research and Development*; Transportation Security Administration, Washington, D.C., March 2003.

[7] Dubnikova, F., Kosloff, R., Oxley, J.C., Smith, J.L., and Zeiri, Y. "Role of Metal Ions in the Destruction of TATP: Theoretical Considerations." *Journal of Physical Chemistry A*, *115*(38), 2011, pp. 10565–10575.

[8] Dubnikova, F., Kosloff, R., Almog, J., Zeiri, Y., Boese, R., Itzhaky, H., Aaron, X., and Keinan, E. "Decomposition of Triacetone Triperoxide is an Entropic Explosion." *Journal of the American Chemical Society, 127*(4), 2015, pp. 1146-1149.

[9] Lin, H., and Suslick, K.S. "A Colorimetric Sensor Array for Detection of Triacetone Triperoxide Vapor." *Journal of the American Chemical Society, 132*, 2010, pp. 15519–15521.

[10] Warmer, J., P. Wagner, P., Schöning, M.J., and Kaul, P. "Detection of Triacetone Triperoxide Using Temperature Cycled Metal-Oxide Semiconductor Gas Sensors." *Phys. Status Solidi A, 212*(6), 2015, pp. 1289–1298.

[11] Pinnaduwage, L., Gehl, A., Hedden, D., Muralidharan, G., Thundat, T., and R. Lareau. "Explosives: A Microsensor for Trinitrotoluene Vapour." *Nature, 425*, 2003, pp. 474.

[12] Olsen, J. K., Greve, A., Senesac, L., Thundat, T., and Boisen, A. "Differential Thermal Analysis Microsystem for Explosive Detection." *SPIE Defense, Security, and Sensing, International Society for Optics and Photonics*, 2011, pp. 80312.

This page intentionally left blank.

R2-B.3: Multi-Functional Nano-Electro-Opto-Mechanical Sensing Platform

I. PARTICIPANTS INVOLVED FROM JULY 1, 2019 TO JUNE 30, 2020

Faculty/Staff			
Name	**Title**	**Institution**	**Email**
Matteo Rinaldi	PI	NEU	rinaldi@ece.neu.edu
Zhenyun Qian	Research Faculty	NEU	qian@ece.neu.edu
Graduate, Undergraduate and REU Students			
Name	**Degree Pursued**	**Institution**	**Month/Year of Graduation**
Sungho Kang	PhD	NEU	05/2021
Vageeswar Rajaram	PhD	NEU	12/2020
Sila Calisgan	PhD	NEU	5/2022

II. PROJECT DESCRIPTION

A. Project Overview

Infrared-based human detection technologies have been extensively used in motion-triggered automation, indoor/outdoor security, search-and-rescue, and many other applications. The relatively high-power consumption of state-of-the-art motion detectors limits their battery life and increases the maintenance cost of sensor networks deployed in remote or hazardous locations. Passive infrared (PIR) is one of the key sensing technologies being utilized in such short-range persistent surveillance. Current PIR sensors have a limited lifetime when deployed in places like caves, tunnels, mines and underground facilities where energy harvesting (e.g., sunlight) is not available. However, persistent surveillance of such environments in proximity of the border is the most important means for border patrol to prevent smuggling or intrusion in restricted areas.

By exploiting our deep scientific knowledge of uncooled infrared (IR) detectors and zero-power microelectromechanical systems, we have developed wireless miniaturized human detectors with near-zero standby power (<10 nW) for applications in underground caves and tunnels. We developed an ultraminiaturized (coin-size), low-cost, and easily retrofitted wireless IR sensor capable of continuously monitoring the appearance of thermal radiation from the human body without consuming any power in standby (i.e., when human bodies are not present). The wireless IR sensor wakes up (i.e., drains power from the battery) only upon detection of the presence of humans nearby to transmit a radio frequency signal indicating the location of the human activity event. The miniaturized wireless IR sensors can be easily retrofitted to hide in the walls of underground caves and tunnels; and, thanks to the complete elimination of standby power consumption, it can wirelessly reveal thousands of intrusion events without draining the sensor coin battery (lifetime extended to approximately ten years, limited by battery self-discharge).

B. State of the Art and Technical Approach

The state-of-the-art motion detectors heavily rely on their limited power source (i.e., battery), leading to a short sensor lifetime, requiring high maintenance cost associated with the sensor network deployment in remote or hazardous locations. For example, solar-powered integrated fixed towers (IFT) equipped with

radar, day and night cameras, and thermal imaging were deployed along the southwest border to provide long-range persistent surveillance enhance the situational awareness. Furthermore, the border patrol heavily relies on portable systems and unattended ground sensors (UGS) to address areas where rugged terrain and dense ground cover may allow adversaries to penetrate through blind spots or avoid the coverage areas of fixed surveillance systems. Passive infrared (PIR) sensors have been utilized in short-range persistent surveillance; nevertheless, their high dependence on external energy for sensor operation (such as sunlight) inhibits their deployment in places like caves, tunnels, mines, and underground facilities [1].

On the other hand, our technologies utilize the energy of infrared radiation emitted from a human body to operate and determine the presence of the person within a detection range without consuming any electrical power. We leveraged our deep scientific knowledge of uncooled infrared detectors and zero-power microsensing systems to develop wireless, miniaturized human detectors with near-zero standby power for applications in underground caves and tunnels. The proposed approach relies on both the spectrally selective thermal detectors technology developed under the ALERT project R2-B.3 [2, 3] and the zero-power infrared (ZIR) digitizing sensors technology developed under the DARPA N-ZERO program [4]. The core element of the technology is a micromechanical switch that is selectively triggered by IR radiation above a threshold (Figure 1). More specifically, the device selectively harvests energy contained in the specific IR signal of interest (i.e., IR radiation from human bodies) and uses it to mechanically create a conducting channel between two electrical contacts (i.e., a large, sharp off-to-on state transition with an on/off conductance ratio >10^{12} and a practically infinite subthreshold slope) when the strength of the signal is above a predetermined threshold, without the need of any additional power source. Differently from PIR technology, our sensors produce a binary signal directly corresponding to the presence and absence of the triggering IR radiation and do not require any active electronics for signal conditioning.

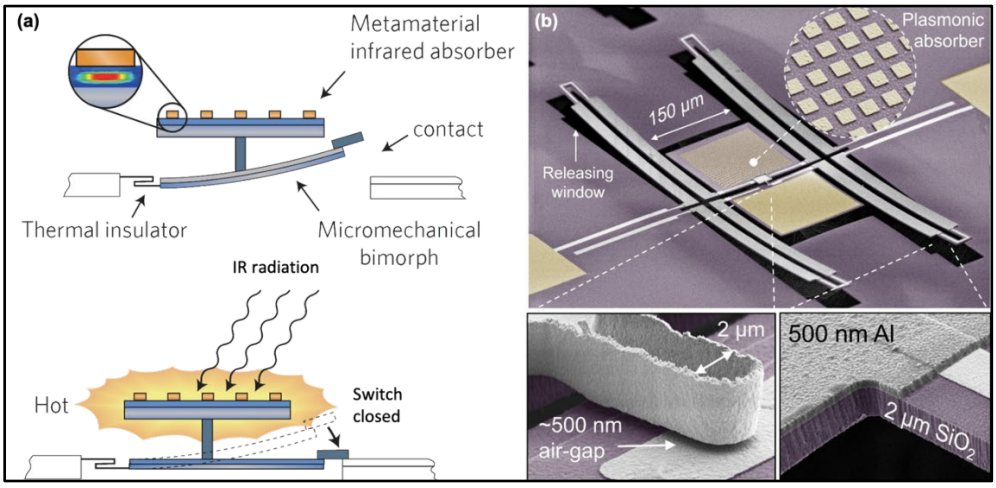

Figure 1: (a) Working principle of zero-power IR sensors [5]; (b) scanning electron microscope image of a fabricated device [4].

Caves and tunnels have much less temperature variability than surface domains that are directly exposed to solar flux, precipitation, and air convection. Moreover, rocks and concretes have 20% to 30% lower emissivity than skin and cloth (Figure 2a) at the IR wavelengths a human body emits. A relatively constant and large contrast between human bodies and the background guarantees a reliable threshold-based detection. The main research challenges preventing the implementation of such micromechanical photoswitch (MP) based zero-power human detectors are (1) the integration of ultrathin IR absorbers that

feature near-unity absorption in a broad mid- to long-IR spectral band (6–12 μm) and (2) the further scaling of the MP detection threshold to tens of nW to enable long range detection of human body radiation.

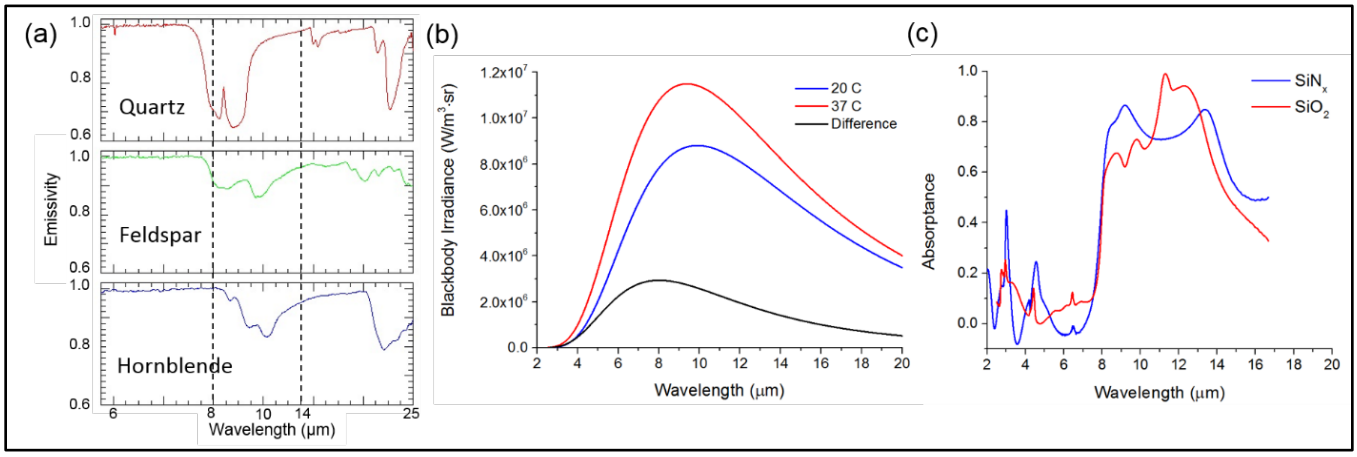

Figure 2: (a) Emissivity spectra of three common constituents of rocks. The emissivity of skin and cloth are between 0.95 and 1. (b) Radiative emission spectra of blackbody sources at 37°C and 20°C, and the difference between the two spectra. (c) Measured absorption spectra of 2-μm SiN_x and SiO_2 [6].

Human bodies emit IR radiation mainly at 8–14 μm. In order to discriminate the background radiation, the sensor should be configured to capture the difference between the two emission spectra (Figure 2b), which peaks at ~8 μm with a wide spread from 6–12 μm. To effectively collect most of the IR energy, we demonstrated broadband long-wavelength IR absorbers composed of a 2-μm SiO_2 slab backed by a metal reflector. A ZIR sensor with an ultralow IR detection threshold of ~140 nW, suitable for human body detection, has been experimentally demonstrated by the PIs' team [7]. When detecting a human body from a distance, the available IR power will inevitably be smaller. Therefore, we further optimized the device design in terms of thermal isolation and IR absorption to scale down the detection threshold to ~40 nW, which corresponds to a detection range as far as 10 m with a focusing lens by adding a highly absorptive dielectric layer such as SiN_x or SiO_2 (Figure 2c). Another important aspect of the ZIR sensor is the reliability. The demonstrated prototypes have already been proven to have relatively high reliability for the envisioned application: over eight thousand consecutive on/off cycles without failure have been demonstrated [4]. Detectors based on single devices with a wide field of view or multiplexed microswitches with a concentrating lens that image different target areas are feasible with our technology. These passive, unpowered human detectors can trigger wireless alarm signals, which can start an action, such as turning on recording media that sits unpowered until the microswitch is closed, enabling unattended operation limited only by the open-circuit life of the accompanying battery.

C. Major Contributions

C.1. Device Design

An analytical model has been developed to improve the thermo-mechanical performance of the previously demonstrated zero-power IR photoswitches and previously verified with the commercially available computer-aided finite element model (FEM) simulation tool, COMSOL. The analytical model eliminates the need of numerical calculation, which can be time inefficient since each data point for each geometry combination involves more than nine parameters. On the other hand, the analytical model can be utilized to study the relationship between each variable geometric parameter and the sensor figure of merits (e.g.,

device threshold power, thermal sensitivity, stiffness, and time constant). The analytical program connects all the design parameters to find an optimized solution for each one and to analyze its trade-offs among different figures of merit. The new analytical approach considers the contribution of strain energy in each section of mechanical beams (i.e., two bimaterial beams and a thermal isolation region) via the fundamental solid mechanical modeling. On the other hand, the bimorph thermal actuator model was utilized to accurately describe IR-thermal properties of the sensor. The total device emissivity has been calculated based on the weighted emissivity of aluminum and silicon dioxide to take into consideration their difference in volume and, as a consequence, their different thermal mass. Most importantly, the thickness of the thermal isolation link is separated from the rest of cantilever (i.e., bimaterial beams and the IR absorbing/reflecting heads) in order to give an extra degree of freedom during the optimization process.

The analytical model was utilized to design a low IR threshold device to meet the required device sensitivity for the target application via the loop-based optimization process (Figure 3). The aim was to maintain the stiffness (k) similar to the one previously demonstrated (k = 0.02 N/m) while increasing the thermal sensitivity (S) as much as possible (it has been doubled from a value of 0.982 m/W to 2.10 m/W). Table 1 shows the figure of merits of the new design. Figure 4 helps understand the nine parameters we have been working on. L3, W3, and t3 refer to the length, width, and thickness of bimaterial legs, respectively; while L1, W1, t, L2, and W2 refer to the lengths, widths, and thickness of the isolation region link that connects the two bimaterial legs.

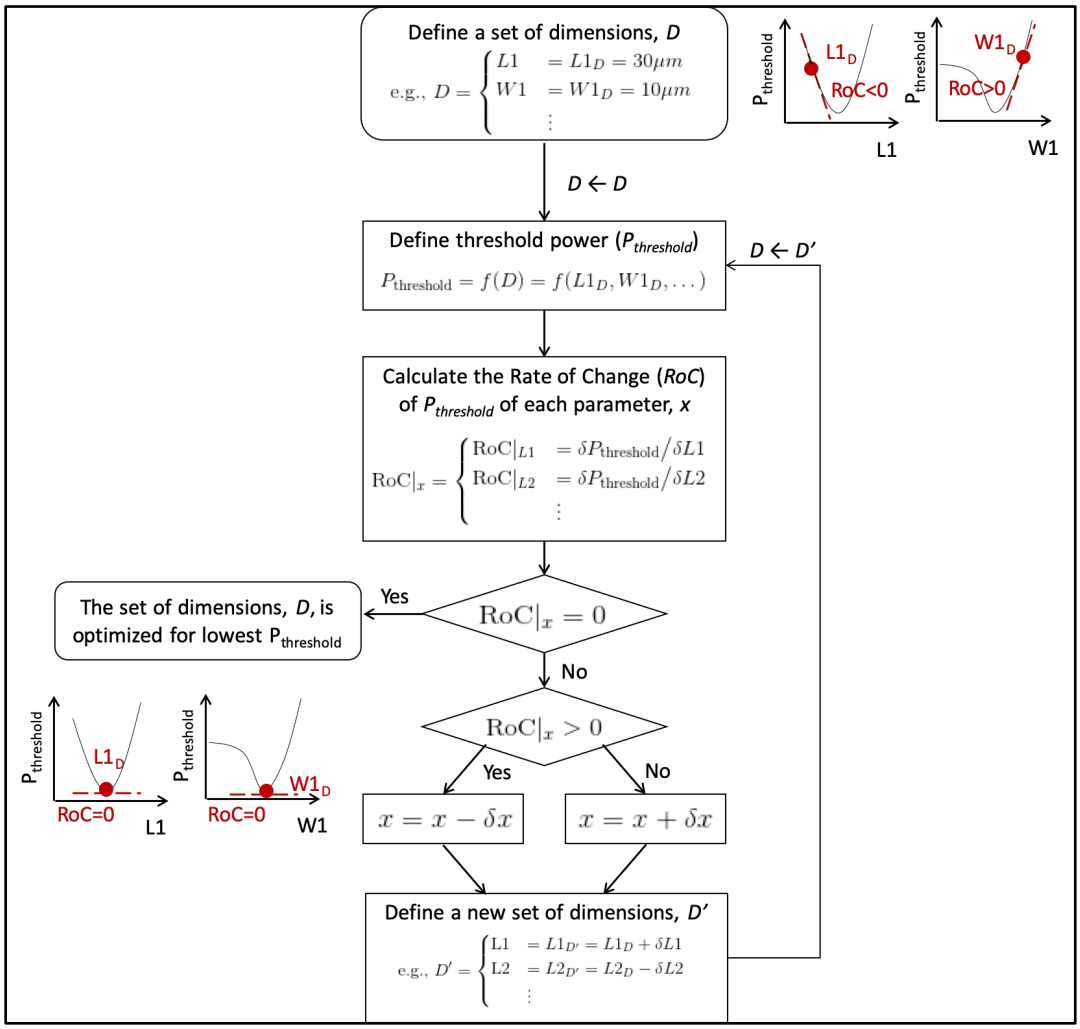

Figure 3: The loop-based optimization process for the low IR threshold device design.

Analytical Model	Previous Demonstration	Primary Design of the New Generation
Stiffness (N/m)	0.022	0.020
Thermal sensitivity (m/W)	0.982	2.100
Time constant (sec)	0.246	0.125
Threshold, 500 nm gap (nW)	509	240

Table 1: Primary design figures of merit.

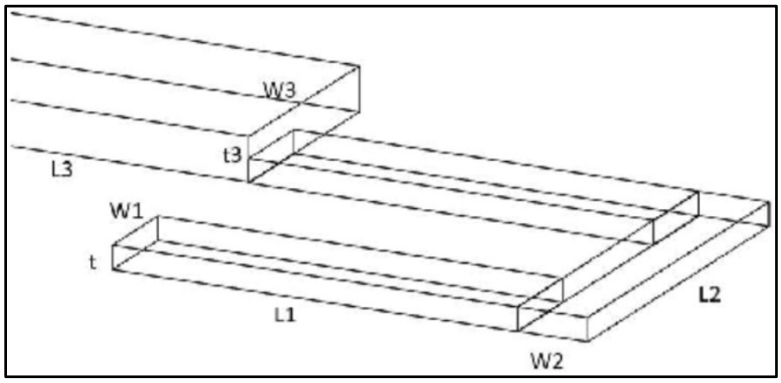

Figure 4: Graphical explanation on the parameters of Table 1 where *t3 = t_ox + t_al*.

The stiffness and thermal sensitivity calculation based on the analytical model have been confirmed by Comsol simulations (Figure 5). The simulated stiffness of the device is 0.02 N/m, which agrees well with the analytical model (0.019 N/m). Furthermore, by applying 500 nW of incident IR power on the whole area of the head, we get a displacement of 1,060 nm, confirming also the analytical value of the thermal sensitivity to be 2.1 m/W.

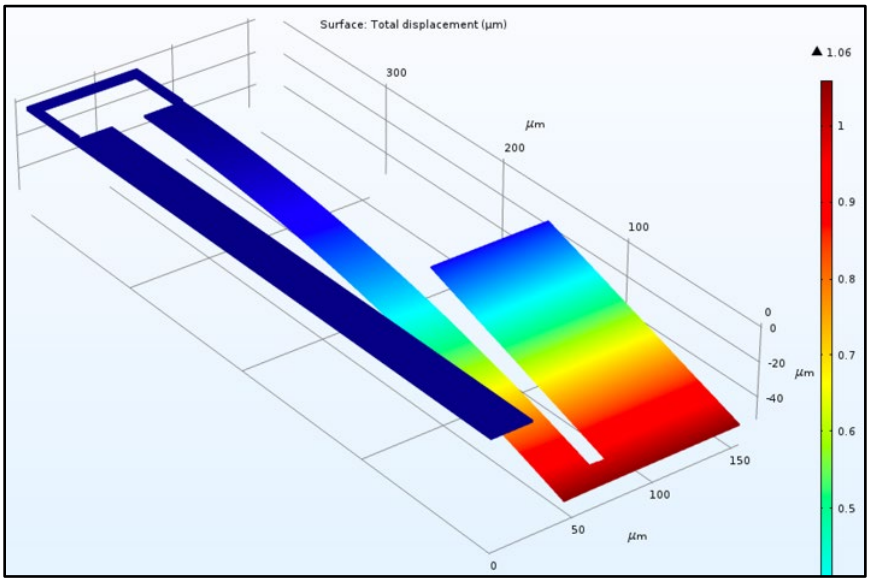

Figure 5: Comsol simulation of the primary design: displacement of 1,050 nm due to 500 nW applied on the head of the device.

The new mask layout includes the optimized device designs as primary devices with two types of contact tips: rectangular and triangular. Nonprimary (secondary) devices include other designs focused on the improvement of the thermal sensitivity with varying stiffnesses, as well as the designs focused on improving the time constant. Last but not least, proven designs from previous demonstrations, as well as some special designs (i.e., not fully supported by theory but with the potential of great advantages in certain aspects), were included in the mask layout. FEM Comsol simulations were employed to verify the effectiveness of most designs. The following shows which designs are included in the mask:

- Primary designs
  - Low threshold power
  - Rectangular and triangular contact tips
  - Different head sizes
- Secondary designs
  - Low time constant
  - High thermal sensitivity
- Other designs
  - Experimental designs
  - Array of primary designs
  - Test structures

C.2. Broadband Absorber Designs

The presence of a human can be detected using the thermal energy emitted in a long-wave infrared (LWIR) regime (e.g., a human body at 37°C has peak IR emissions at around λ = 8–12 μm). In order to harvest the LWIR electromagnetic energy efficiently, we designed different absorber designs that can be integrated in the existing IR sensor. We have demonstrated a LWIR photoswitch using the bulk dielectric (SiO_2) slab backed by an optically thick metal layer as the integrated absorber (Figure 6). The measured absorptance of such a bulk absorber shows consistently high absorptance in the spectral region of interest (η >60% in 8–16 μm). However, the device suffers asymmetry induced by the different material stacks in the absorbing and reflecting heads (a reflecting head has an additional optically thick metal layer as a reflector) (Figure 6). In order to minimize the device asymmetry, we have proposed the two possible absorber designs: (a) plasmonic-dielectric absorber; and (b) metal-germanium-metal absorber.

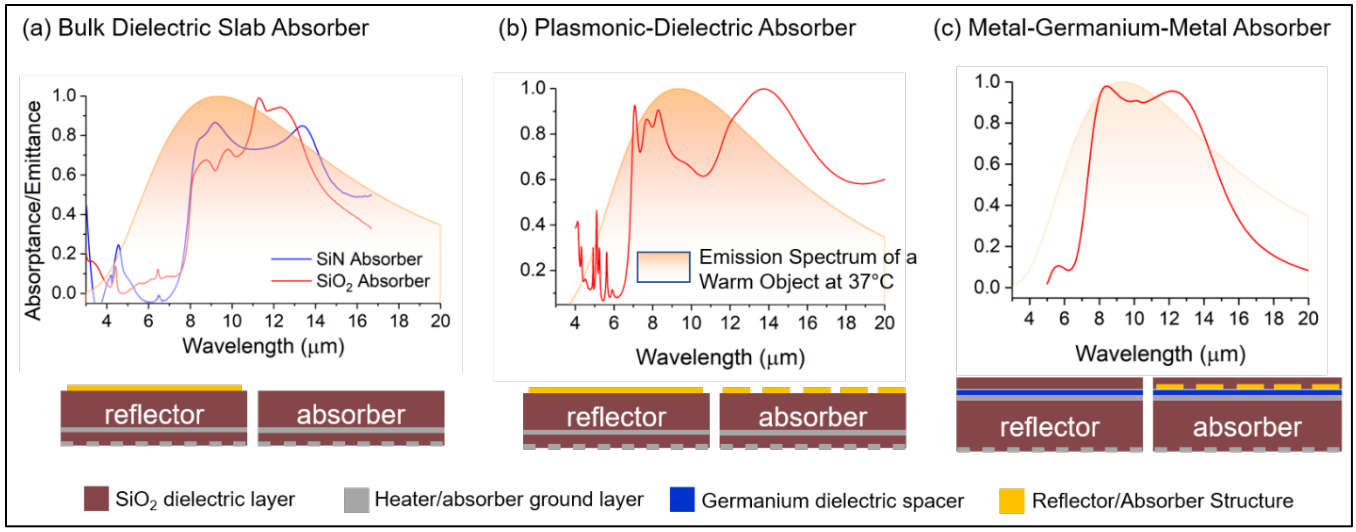

Figure 6: Proposed LWIR broadband absorbers for leaf temperature sensing.

The plasmonic-dielectric absorbers take advantage of both the high loss of SiO_2 slab due to the vibrational modes of longitudinal-optical phonons and the highly capacitive metamaterial sheet patterned on top of the dielectric slab. The numerical calculation (simulated with a commercially available full-wave simulation software, Computer Simulation Technology) shows a high absorptance in the LWIR regime with a broader absorption bandwidth (η >60% in λ = 7–20 μm) than the dielectric slab alone (Figure 6b). The metal-germanium-metal absorber shares the same working principles as the MIM IR absorbers demonstrated for spectrally selective near-IR and mid-wavelength IR absorption. This configuration replaces the SiO_2 subwavelength dielectric layer with an optically dense material, germanium, and the gold plasmonic nanostructures with high-loss metal layer, titanium, to achieve highly absorptive and broadband absorption in LWIR spectral regime. The numerical simulation shows a near-perfect absorption in the LWIR region of interest (η>90% in λ = 8–13 μm) (Figure 6c). Note that it will be necessary to incorporate a protective layer (such as an optically thin SiO_2 layer as shown in the cross-sectional schematic figure) to prevent from etching in an XeF_2 device release fabrication step. It is also worth noting that the proposed absorbers are designed such that they incorporate the microheaters in both absorbing and reflecting heads.

C.3. Fabrication and Characterization of New Devices

The photomasks of the new mask layout for the optimized devices were manufactured. Differently from the previous fabrication process, the new process involves three additional photomasks (eleven in total). The device design optimizations proposed previously were implemented in the new batch of devices. These recently fabricated devices were tested to verify whether the design changes had an effect on improving the device sensitivity. The sensitivity S is defined as the displacement induced at the tip of the switch contact per unit input power. For a given contact gap g, a larger S results in a smaller threshold P_t. One of the major design features of the new batch is the integration of microheaters on all devices to simulate the temperature rise caused by IR absorption. The integration of the heaters also affords an accurate and efficient way to quickly estimate the threshold and sensitivity of each device on the wafer. In the experiments described below, the sensitivity of the optimized device was calculated by measuring the threshold power and the contact gap.

To find the sensitivity, the voltage V_{heater} across the microheater (R = 63.8 kΩ) was increased until the power dissipated as heat was sufficiently high to actuate the contacts and close the switch. The value of this power

is calculated by the equation $P_t = V_{heater}^2/R$. Note: the device was tested in a vacuum probe station to ensure that there was no heat loss through convection in air.

The status of the switch was monitored continuously by applying a separate bias V_{bias} across the switch terminals and monitoring the current using a source meter (Keithley 2450). Figure 7a shows the circuit schematic overlaid on an optical image of the tested device. The heater layer is on the bottom of the device while the electrical routing for the switch is on the top and is electrically insulated from the heater. Figure 7b shows the measured current across the switch as the heater is turned on and off with a V_{heater} that corresponds to a power just above P_{heater}. As shown, when triggered on, the current changes with a conductance ratio of more than 4 orders of magnitude from ~0.1 nA to 0.7 µA for a V_{bias} = 10 mV (the non-zero off current is due to instrument noise). This essentially demonstrates the zero subthreshold leakage of the switches, which is a key factor for zero standby power consumption. P_t for the tested device was measured to be 492 nW.

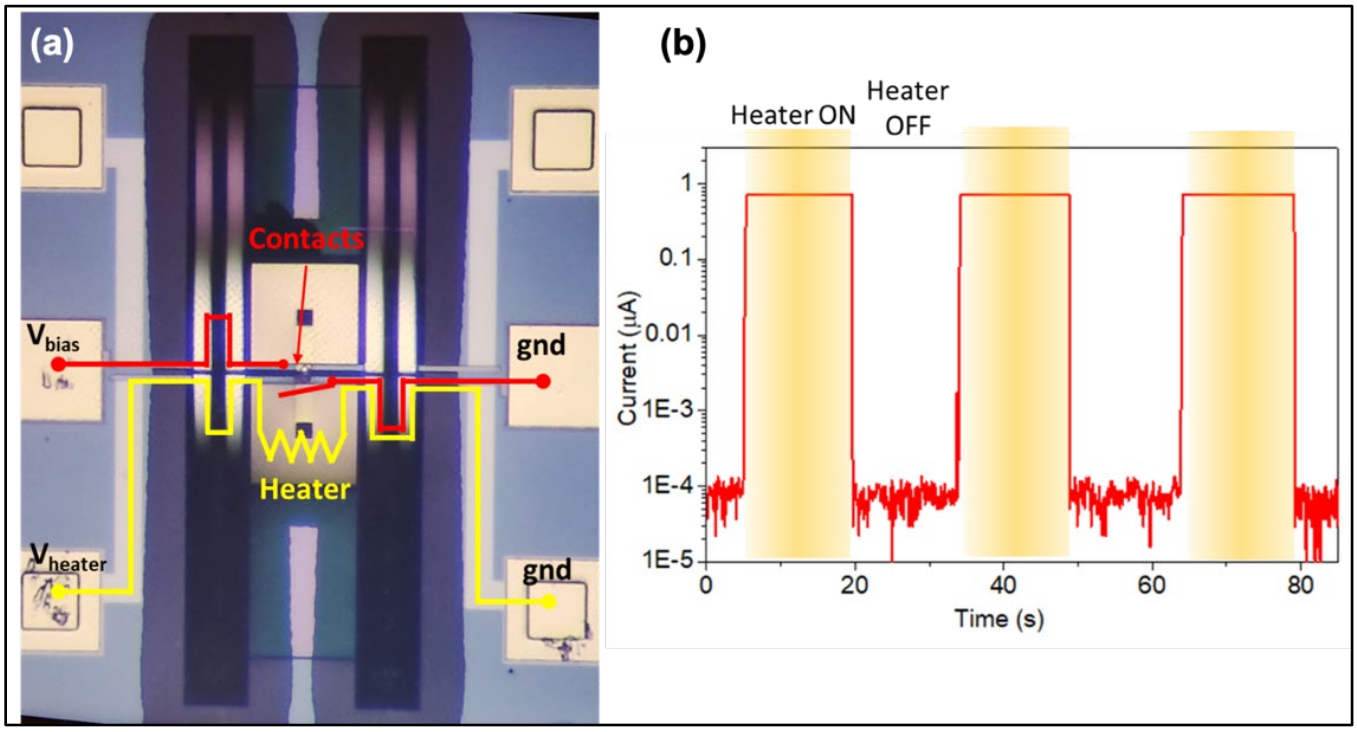

Figure 7: (a) Optical image of tested device with an overlay of the electrical routing schematic. (b) Current across the switch as the heater is turned on and off with a $P_{heater} \geq P_t$.

Next, the contact gap (g) was estimated using the pull-in voltage technique. Since the contacts are effectively a pair of capacitors with an overlap area A and a vacuum as a dielectric, increasing V_{bias} causes charges to accumulate on either contact. Since the contacts are attached to cantilevers (i.e., springs) the electrostatic force developed between the contacts due to these charges causes the contacts to move toward each other. At a certain Voltage $V_{bias} = V_{\text{pull-in}}$, the system becomes unstable and the contacts snap closed (i.e., pull-in). The value of this pull-in voltage is given by:

$$V_{pull\text{-}in} = \sqrt{\frac{8kg^3}{27\varepsilon_o A}}$$

where k is the effective stiffness of the cantilevers (0.0075 N/m from simulations). By sweeping the voltage V_{bias} (without applying any heater power) until the contacts close, $V_{pull\text{-}in}$ can be measured and g can be readily calculated. The overlap area A (67.7 μm²) was measured using an optical microscope at high magnification. For the tested device, $V_{pull\text{-}in}$ = 2.23 V and thus g = 1.095 μm. This results in a sensitivity of the device $S = g/P_t$ = 2.22 *nm/nW.* This is very close to the designed sensitivity of 2.46 nm/nW (determined using analytical modeling). It is worth noting that this is an improvement of ~2.2 times over the previous designs. This experiment thus proves that the new designs indeed have a better sensitivity and thus can be used to achieve unprecedented threshold levels.

C.4. Zero-Power Human Detection

We successfully demonstrated zero-power detection of a hand (at a 16-inch distance) without using a focal lens, owing to the optimized micromechanical structure and thermal expansion material, hence the reduced threshold (Figure 8). We have characterized the infrared radiation from a human body at a varying angle (top, side, and front-facing) and distance (from 0.5 to 2.0 m), using a commercial thermal detector with an active area of 10-mm diameter (Figure 9). Furthermore, we have identified that using a Fresnel focusing lens, the available IR power density can be increased by more than 10 times, which drastically increases the working distance of our sensor. Because of the aforementioned results in terms of device optimization, characterization, and optics-level sensitivity improvement, we have successfully demonstrated a zero-power detection of a human body at ~13 feet distance (Figure 10).

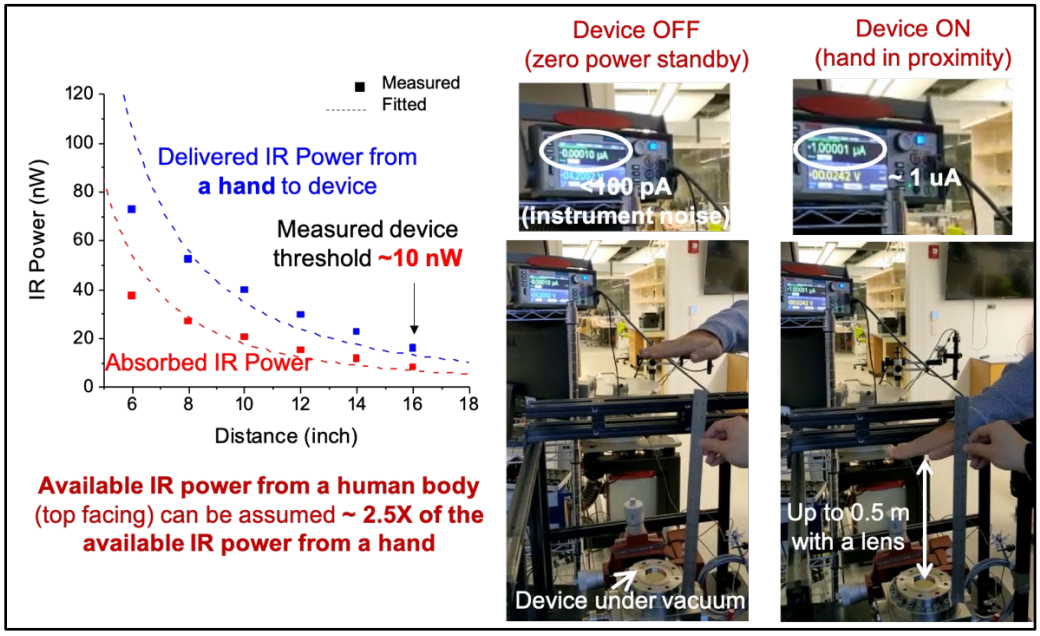

Figure 8: First demonstration of zero-power hand detection.

Tool:
Commercial thermal detector with active area of Φ 10 mm
(3489x larger than our sensor)

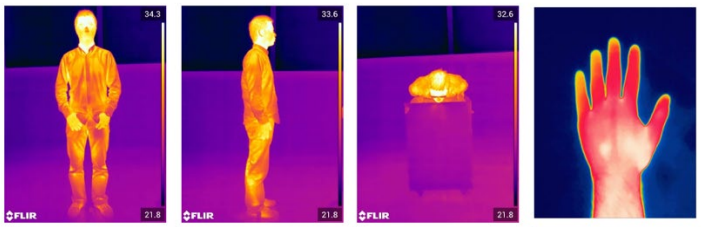

Measurement	Front Facing	Side Facing	Top Facing	Hand
Power @ 0.5m (1.6 ft)	~ 440 µW	~ 330 µW	~ 203 µW	~ 75 µW
Power @ 1m (3.3 ft)	~ 220 µW	~ 158 µW	~ 50 µW	~ 20 µW
Power @ 2m (6.6 ft)	~ 65 µW	~ 45 µW	~ 22 µW	~ 5 µW
Power density @ 1m	2.8 W/m^2	2.0 W/m^2	0.64 W/m^2	0.25 W/m^2
Power delivered to 150x150 µm^2 device @ 1m	63 nW	45 nW	14 nW	5.6 nW
Normalization	100%	~72%	~23%	~ 9%

Figure 9: Characterization of available IR power radiated from a human body at a varying angle and distance.

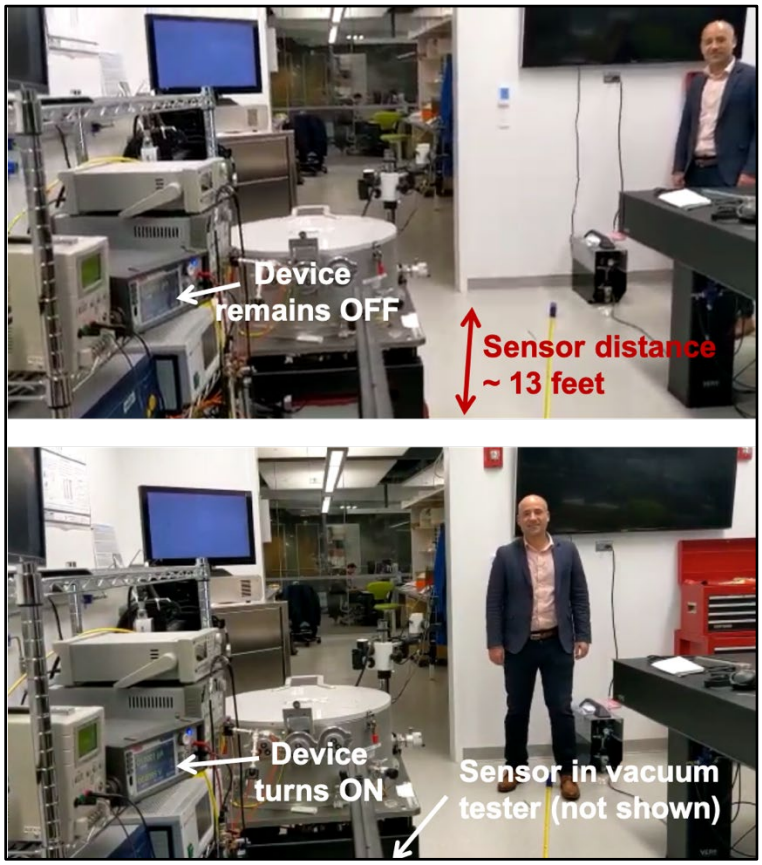

Figure 10: First demonstration of zero-power human detection.

D. Milestones

- **Design of optimized IR sensor with threshold ~40 nW (completed):** When detecting a human body from a larger distance, the delivered IR power to the sensor will inevitably be much smaller due to the inverse-square law. We successfully demonstrated a group of optimized sensor designs with a threshold as low as ~39.4 nW, which was verified through both the analytical model and finite element simulation.
- **Design of experimental setup for human body detection (completed):** The current experimental setup only supports incident infrared light from the top of the testing chamber. Measurement using only a hand instead of a full body as the target was performed for now. Modification of the existing setup with an additional optical path has been designed and implemented to support the test with a human body in horizontal direction (with varying distance) as the target.
- **Device fabrication and characterization (completed):** The first batch of newly designed sensors has been fabricated. The integrated heaters were utilized to measure the IR threshold. The ultra-low IR threshold reaching ~7 nW was demonstrated with a voltage bias. Full characterization was completed, and modified plans are being implemented for the next batch fabrication based upon the characterization. This includes the in situ test functionality for flipped heads, use of a high substrate resistance wafer, and sidewall coating to prevent unwanted pull-in.
- **Reliability test and design optimization (in progress):** The previously demonstrated prototypes have already been proven to have relatively high reliability for the envisioned application: over eight thousand consecutive on/off cycles without failure have been demonstrated. The proposed characterization of the common failure mechanism and demonstration of one million cycles of operation has been postponed after ~60% toward completion due to the ongoing laboratory shutdown due to COVID-19 restrictions.
- **Demonstration of a working prototype in lab environment (completed):** With design iteration, we experimentally demonstrated a working prototype of the zero-power infrared sensor capable of detecting a human body from more than ~4 meters away (expected to have >10-meter detection range, currently limited by the compartmented laboratory space).
- **Finalize a collaboration plan with United Technologies Corporation (completed):** The team has received a $550K grant from the National Science Foundation for a collaboration with United Technologies Corporation.

E. Final Results at Project Completion (Year 7)

We have successfully designed, fabricated, and characterized the first prototype of zero-power human detector suitable for realization of sensor networks deployed in remote or hazardous locations. This sensor network can be deployed with substantially low maintenance cost associated with sensor installation and management. We envision that the demonstrated work can significantly enhance border protection to prevent smuggling or intrusion in restricted areas where the conventional fixed surveillance system is not suitable. The following research works were conceived and successfully executed: (1) We have developed a rigorous thermomechanical analytical model to predict sensor performance to optimize the device geometries. The resulting device has shown much improved sensor performances (thermal sensitivity, stiffness, and device response time) compared to the previous generation, suitable for ultralow threshold IR radiation detection of a human body; (2) the new batch of devices was fabricated and characterized with the proper experimental setup, showing an ultralow IR detection threshold reaching ~7 nW; (3) we have successfully demonstrated the first zero-power human detection capability using the fabricated device with

a working distance reaching ~4 meters; and (4) the team has secured two technology transition funding to develop minimum viable products for border protection and fire prevention applications.

III. RELEVANCE AND TRANSITION

A. Relevance of Research to the DHS Enterprise

- **Relevance #1/metrics:** IR digitizing microsystems that can remain dormant, with near-zero power consumption, until awakened by specific IR spectral signatures associated with a threat (e.g., human intrusion). These completely passive digitizing IR sensor microsystems can harvest the energy contained in a specific IR spectral signature (i.e., IR emission peaks of energetic materials) to produce a digitized output bit capable of waking up short-duty cycle powered electronics for further signal analysis and communications.
- **Relevance #2/metrics:** A wireless sensor network to be deployed in the difficult-to-reach places such as caves, tunnels, mines, and underground facilities. These ultraminiaturized (coin-size), low-cost, and easily retrofitted wireless IR sensor is capable of continuously monitoring the appearance of thermal radiation from human body, without consuming any power in standby.

B. Status of Transition at Project End

- The patent for the base technology was granted in May 2020.
- A provisional patent application was filed to protect the specific device designs developed in this work.
- An internal technology transition funding (GapFund360 Phase 1&2) was secured to develop the minimum viable product for occupancy sensing.
- External funding from the NSF technology translation program, Partnerships for Innovation, was secured to develop the minimum viable product for flame detection based on the same core technology developed in this project.
- A startup company, Zepsor Technologies, has been founded aiming to bring to market zero standby power sensors for various internet-of-things applications including distributed wireless fire monitoring systems, battery-less infrared sensor tags for occupancy sensing, and distributed wireless monitoring systems of plant health parameters for digital agriculture.

C. Transition Pathway and Future Opportunities

- Awarded with internal funding for technology transfer (GapFund360), the project targets the development of battery-less IR sensor tags for reliable occupancy sensing in indoor environment, which is suitable for many DHS-related (DHS: Department of Homeland Security) applications such as airport security.
- Potential commercialization partners (Pendar Technologies, Analog Devices, and Boeing) have already been engaged with performance testing and transition development work.
- The PI holds intellectual property of the technology relevant to the project.
- Prototypes of the technology are being fabricated at Northeastern University for use and testing.

- The proof of concept will be shared with the identified potential customers to explore technology transition: DHS, Defense Advanced Research Projects Agency (DARPA), Analog Devices, Qualcomm, Pendar Technologies, Boeing, and Avago.

D. Customer Connections

- DHS
- United Technologies Corporation: Joseph Mantese
- DARPA Microsystems Technology Office: Ronald Polcawich, Benjamin Griffin, and Whitney Mason
- Air Force Office of Science Research: Kenneth Goretta, Gernot Pomrenke, and Harold Weinstok
- Analog Devices
- Qualcomm
- RF Micro Devices
- Pendar Technologies
- Avago

IV. PROJECT ACCOMPLISHMENTS AND DOCUMENTATION

A. Education and Workforce Development Activities

1. Course, Seminar, and/or Workshop Development
   a. 2019 fall semester course: Introduction to MEMS
2. Student Internship, Job, and/or Research Opportunities
   a. Research assistantship for two graduate students

B. Peer Reviewed Journal Articles

1. Qian, Z., Rajaram, V., Kang, S., & Rinaldi, M. "High Figure-of-Merit NEMS Thermal Detectors Based on 50-nm Thick AlN Nano-Plate Resonators." *Applied Physics Letters, 115*(26), 2019. https://doi.org/10.1063/1.5128643.

C. Poster Sessions

1. "Zero-Power Wireless Sensor Nodes for Unattended Threat Monitoring." Presented by Ryan Kang and Vageeswar Rajaram. 7th ALERT Industrial Advisory Board Meeting Poster Session. Northeastern Innovation Campus, Burlington, MA. 4 November 2019.

D. Other Presentations

1. "Research Highlight: Zero-Power Sensors." Presented by Matteo Rinaldi. 7th ALERT Industrial Advisory Board Meeting. Northeastern Innovation Campus, Burlington, MA. 4 November 2019.

E. Technology Transfer/Patents

1. Patent Awarded
    a. Zero Power Plasmonic Microelectromechanical Devices. Patent Number US 10,643,810 B2. Granted May 2020.

F. Patent Applications Filed (Including Provisional Patents)

1. Zero Power Micromechanical Switch-Based Sensing and Monitoring System, PCT Application No. PCT PCT/US2020/014478.
2. Zero-Power Wireless System for Crop Water Content Monitoring, PCT Application No. PCT/US2020/014427.

V. REFERENCES

[1] Homeland Security, "Integrated Fixed Towers."

[2] S. D. Calisgan et al., "Spectroscopic Chemical Sensing Based on Narrowband MEMS Resonant Infrared Detectors," in *2018 IEEE SENSORS*, 2018, vol. 0, pp. 1–4.

[3] S. Kang, Z. Qian, V. Rajaram, S. D. Calisgan, and M. Rinaldi, "Chip-Scale MEMS-CMOS Multispectral Infrared Chemical Sensor," *2019 IEEE Micro Electro Mech. Syst.*, no. January, pp. 133–136, 2019.

[4] Z. Qian, S. Kang, V. Rajaram, C. Cassella, N. E. McGruer, and M. Rinaldi, "Zero-Power Infrared Digitizers Based on Plasmonically Enhanced Micromechanical Photoswitches," *Nat. Nanotechnol.*, vol. 12, no. 10, pp. 969–973, Sep. 2017.

[5] V. A. Aksyuk, "Internet of Things: Sensing without Power," *Nat. Nanotechnol.*, vol. 12, no. 10, pp. 940–941, Sep. 2017.

[6] J. Kischkat et al., "Mid-Infrared Optical Properties of Thin Films of Aluminum Oxide, Titanium Dioxide, Silicon Dioxide, Aluminum Nitride, and Silicon Nitride," *Appl. Opt.*, vol. 51, no. 28, p. 6789, 2012.

[7] S. Kang, S. Calisgan, Z. Qian, V. Rajaram, N. McGruer, and M. Rinaldi, "Broadband Long-Wavelength Infrared Micromechanical Photoswitch for Zero-Power Human Detection," in *2018 Solid-State, Actuators, and Microsystems Workshop Technical Digest*, 2018, no. d, pp. 187–189.

R2-B.4: Mid-Infrared Photonic Integrated Circuits for Stand-Off Detection of Trace Explosives

I. PARTICIPANTS INVOLVED FROM JULY 1, 2019 TO JUNE 30, 2020

Faculty/Staff			
Name	**Title**	**Institution**	**Email**
Anthony Hoffman	Co-PI	University of Notre Dame	ajhoffman@nd.edu
Michael Wanke	Co-PI	Sandia National Laboratories	mcwanke@sandia.gov
Graduate, Undergraduate and REU Students			
Name	**Degree Pursued**	**Institution**	**Month/Year of Graduation**
Ahmet Cagri Aydinkarahaliloglu	PhD	University of Notre Dame	05/2021
Galen Harden	PhD	University of Notre Dame	07/2020
Owen Dominguez	PhD	University of Notre Dame	4/2020
Junchi Lu	PhD	University of Notre Dame	05/2021
Irfan Khan	PhD	University of Notre Dame	05/2021
Anjan Goswami	PhD	University of Notre Dame	05/2024

II. PROJECT DESCRIPTION

A. Project Overview

This project aims to develop a mid-infrared photonic integrated circuit (MIR-PIC) and use the device for stand-off detection of trace explosives in the solid phase. The proposed MIR-PIC is a mid-infrared (mid-IR) heterodyne receiver where a Schottky barrier diode has been integrated into a high-performance, mid-IR quantum cascade laser (QCL). The final year of this project focuses on leveraging highly scalable semiconductor growth and metal-organic chemical vapor deposition (MOCVD), to demonstrate high-performance devices that can be transitioned to industry. We also explored alternative device designs, to simplify fabrication, including all-optical lithography and a dual-use top contact that provides current injection and a nonlinear diode response.

This research addresses the void of high-performance, compact technologies capable of measuring the phase and amplitude of mid-IR light that has interacted with a sample under test. This semiconductor transceiver operates by mixing light scattered off the sample under test and coupled back into the QCL waveguide with the internal field of the waveguide. Changes in the phase and amplitude of the scattered light are detected by measuring the voltage over the integrated diode.

Compared to existing optical stand-off detection technologies, there is no need for an external detector or optics, as the entire sensor operates at room temperature, and the sensitivity and detection limits are anticipated to improve by orders of magnitude. The proposed MIR-PIC is ultracompact (~5 mm × 300 mm) and low cost, making it appropriate for commercial-scale production, and it can be integrated into large format arrays for imaging. Single devices will enable rapid stand-off detection of explosives, and arrays of these devices will enable imaging with phase, amplitude, and spectral content for improved detection.

The MIR-PIC represents a fundamentally new type of mid-IR semiconductor transceiver that will enable phase- and amplitude-sensitive imaging in the mid-IR via an ultracompact device. This research will have significant impact on the homeland security enterprise due to the complementary sensing and imaging modalities the MIR-PICs enable, as well as the low-cost, small footprint, and improved sensitivity of these devices.

Ultimately, the sensors can be used for detecting explosives residues on skin, clothing, personal items (travel bags, briefcases, etc.), containers, vehicles, and other substrates. Myriad other fields—including medicine, drug enforcement, and environmental monitoring—will also benefit.

B. State of the Art and Technical Approach

B.1. State of the Art Synopsis

Mid-infrared light interacts strongly with the fundamental vibrational and rotational modes of molecules. This strong light-matter interaction results in molecular fingerprints across the mid-IR that can be used for sensitive detection of trace amounts of molecules of interest [1, 2]. The mid-IR is playing an increasing role in the detection of trace gasses and materials across many fields, including the detection of explosives and their precursors. This State of the Art Synopsis focuses on stand-off detection using mid-infrared light and the mid-IR optical sources used in these measurements.

B.2. Mid-Infrared Stand-Off Detection

Passive infrared stand-off detection of explosives measures the spectrally dependent emissivity of a sample under test. Typically, the thermal emission spectrum is measured using a Fourier transform infrared spectrometer (FTIR) and a cooled HgCdTe detector. Hyperspectral imaging using a mid-IR focal plane array and FTIR have been used to detect trace amounts of explosives [3, 4]. However, the use of passive stand-off detection in real-world scenarios is ultimately limited by the low thermal emission of the sample (sub-μW), the cost and size of the FTIR and detector, and the requirement of cryogenically cooled detectors.

Active stand-off detection uses an optical source to illuminate the sample under test. Here, we focus on coherent illumination since the delivered power is much higher and the beam can be collimated. Tunable CO_2 lasers and optical parametric oscillators have been used as sources previously [5, 6], but these systems are prohibitively expensive, large, and cumbersome for wide-scale deployment. Mid-infrared QCLs are rapidly becoming the source of choice for active stand-off detection because they are commercially available over much of the mid-IR spectrum, emit watt-level power, operate at room temperature, are spectrally tunable via temperature and/or voltage, and are compact [7]. Active stand-off detection of trace explosives is typically achieved by measuring the diffuse reflection of light scattered from an illuminated sample, and the measured spectrum is compared to a library of spectra for explosives [8- 10]. Recent progress using QCLs as the optical source has focused on narrow line-width lasers for gas sensing [11], improved sensitivity [12], and increased spectral coverage [13].

For most state-of-the-art sensors, the sensitivity of the system is limited by the relative intensity noise (RIN) of the QCL because a low-noise detector and amplified chain are employed [14]. While the low-noise detector and amplifiers are sufficient for laboratory work, they are not desirable for wide-scale deployment due to the added size, weight, cost, and complexity. The RIN of lasers has been suppressed using many techniques including balanced detectors, active laser intensity stabilization, and heterodyne detection [14]. Mid-IR balanced detectors are difficult to obtain and must be cryogenically cooled, and intensity stabilization adds significant complexity and cost to the spectroscopy setup. Heterodyne detection has been achieved using discrete optical components. Heterodyne-enhanced detection of NO has been demonstrated using a mid-IR

QCL and a room-temperature HgCdTe detector; the overall sensor operates at 3.7 times the fundamental quantum shot limit [14]. Similar heterodyne techniques have been applied to explosives detection in the mid-IR, but the optical configuration of the sensor is not practical for field work—our project integrates the source and mixer into a single device.

Terahertz (THz) QCLs with integrated Schottky barrier diodes for heterodyne detection have been demonstrated by a member of our team (Wanke) [15, 16]. These transceivers operated at cryogenic temperatures due to challenges with the THz QCL active core, and performance was limited in part by the internal field of the THz QCL. A challenge with realizing heterodyne detection in a mid-IR QCL is the need for a high-performance laser with large internal fields.

B.3. High-Performance Mid-Infrared Quantum Cascade Lasers

Mid-IR QCLs were first demonstrated twenty-two years ago [17]. Since then, the performance of QCLs has rapidly and drastically increased to include room-temperature continuous-wave operation, single-mode emission, multi-wavelength and tunable broadband lasing, high wall-plug efficiency (WPE) operation, and more [7]. QCLs are now available from several commercial vendors, and Thorlabs has some lasers available for same-day shipping [18]. Recent progress on QCLs has focused on improving the output power and WPE (electrical to optical conversion efficiency) of the devices [19, 20], broadening the gain spectrum [21], and generating frequency combs [22]. Much of the progress in high-power, high-WPE QCLs has been enabled by carefully considering the effects of interface roughness on the optical and electrical properties of the lasers [20, 23–26]; this work will be key to the MIR-PICs in this project and Hoffman is involved in this area of research.

B.4. Technical Approach

Figure 1 is a schematic of a MIR-PIC deployed as a sensor. The device comprises a mid-IR waveguide (blue, horizontal line) with a mid-IR QCL active core (the active core resides inside of the waveguide), and an integrated Schottky barrier diode (gold dot).

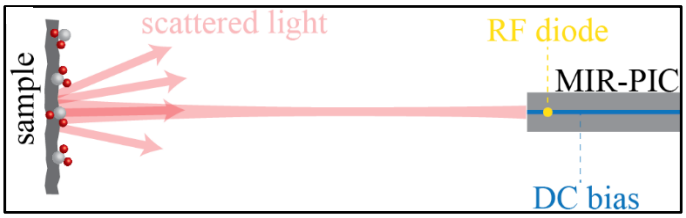

Figure 1: Schematic for stand-off detection of solid phase trace explosives using a MIR-PIC.

A schematic of a MIR-PIC is depicted in Figure 2. The active core of the QCL generates mid-IR photons via electron transitions between the bound sub-bands of hundreds of coupled quantum wells which are then guided in the waveguide. During operation, some of the generated photons are emitted from the facet of the waveguide, scatter off of the sample under test (*c.a.* 3" to 12" away), and re-enter the waveguide. These photons are then mixed by the Schottky diode with the internal field (photons) of the waveguide, Figure 3. This nonlinear mixing results in a voltage over the diode that oscillates at the difference frequency between the internal field and the light that re-entered the cavity, called the intermediate frequency (IF). For a multi-mode Fabry-Perot cavity, a mixing response in the diode is observed at the free spectral range (mode spacing) [15, 16]. For cavities ~3 mm long, the IF is ~14 GHz, a frequency that is easily accessible using common microwave equipment available in our laboratories.

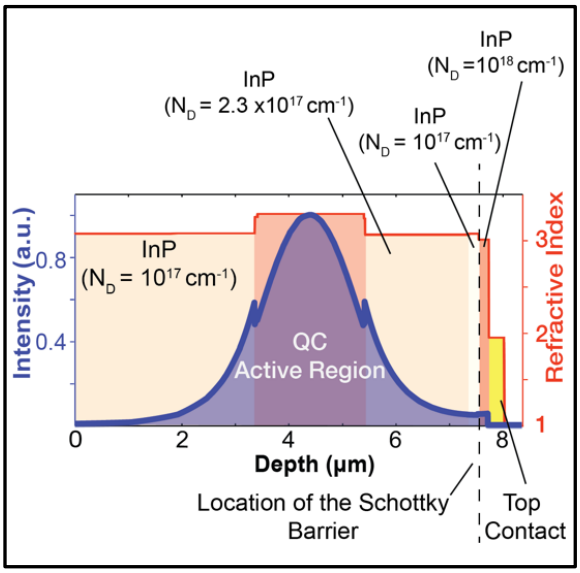

Figure 2: New InP-based design. This design is being grown by Adtech Optics via MOCVD. The mode profile and the refractive index of the device is shown. The mode intensity at the Schottky Diode is designed to be 3% of its maximum intensity.

While mixing has been demonstrated in THz photonic integrated circuits [24, 25], our project aims to develop a platform for the mid-infrared. This is an important advancement for two reasons. First, mid-infrared quantum cascade active regions have been demonstrated to operate at room temperature in continuous-wave mode. Such performance is extremely important for commercial transition of these devices. Second, mid-infrared light interacts strongly with fundamental vibrational and rotational modes of molecules. This strong light-matter interaction ultimately directly influences the detection limits of the sensors.

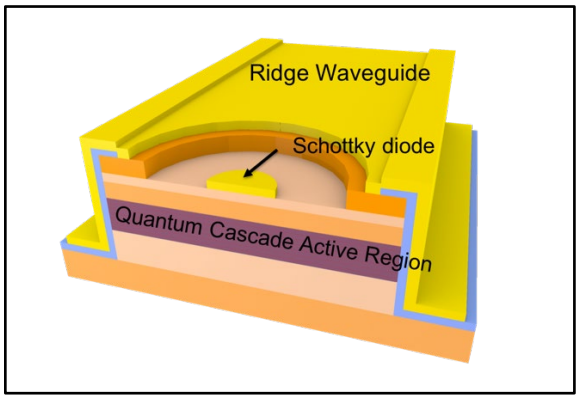

Figure 3: Schematic of a MIR-PIC, highlighting the high-performance quantum cascade active region design, Schottky barrier diode, and ridge waveguide.

The final year of this project focused on advancing the MIR-PIC technology to lower the barrier for commercial transition. We investigated two pathways to achieve this goal. The first approach is to demonstrate room-temperature operation of a MIR-PIC operating in CW mode for devices fabricated from wafers grown via metal organic chemical vapor deposition (MOCVD). Our second approach is to demonstrate nonlinear mixing on the top contact of the waveguide ridge, rather than on a Schottky barrier diode. This will reduce the complexity of the fabrication process, reducing the cost per device and potentially improving device yield and performance.

To realize these Year 7 goals, we developed collaborations with Sandia National Laboratories (SNL) and Adtech Photonics, Inc. (Adtech). Dr. John Klem at

SNL, through a Center for Integrated Nanotechnologies User Proposal, performed strain-balanced growth of two wafers via molecular beam epitaxy (MBE) for MIR-PICs that incorporate and forgo the Schottky diode. Adtech provided heavily subsidized growth of MOCVD-grown wafers.

Figure 4 shows a portion of the conduction band that we have designed for strain-balanced growth on InP substrates via MBE. The calculated figure of merit for the design is comparable to some of the highest performance devices designed to date. Figure 4 depicts the waveguide design that accompanies this active region design. While the calculated optical loss of the waveguide is slightly higher than the highest performing devices, it is well within the range of high-performance waveguide designs.

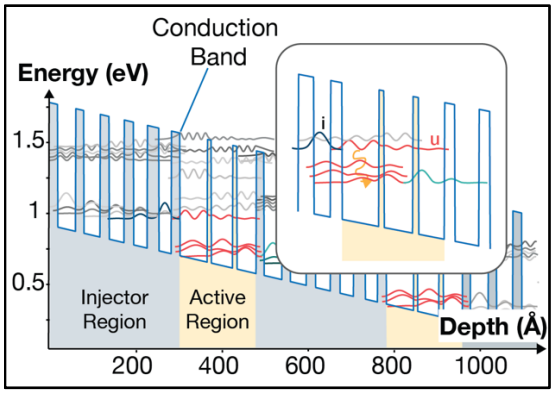

Figure 4: New active region design. Two periods of the conduction band of the active region for strain-balanced In0.66GaAs/ In0.31AlAs on InP. The grey and red curves are the calculated single electron wavefunctions. The curves in red and green are most closely related to the designed optical transition. The applied field is 73.1 kV/cm, and the optical transition is at 6.29 µm.

A distinction between these new devices and our previously tested designs is that the waveguide incorporates a thick layer of InP. For QCLs, an InP waveguide is desirable due to the superior thermal conductivity of the material, which allows efficient extraction of heat from the active region. For a MIR-PIC, the temperature performance is similarly expected to improve, but it is not clear how the overall performance of the MIR-PIC will be influenced. The main reason for this uncertainty is the higher ideality factor for diodes fabricated in InP. Our waveguide design incorporates strategies to mitigate the higher ideality factor. Growth of this heterostructure was completed by Adtech on May 2, 2019.

We fabricated structures for understanding electron transport in these devices and laser ridges to understand the optical properties (e.g., optical gain) of the design structure. An example of the optical gain spectrum measured for a characteristic device is shown in Figure 5. We measured the gain coefficient and the waveguide loss of the devices. In general, the gain coefficient is large (12.09 cm^{-1}/J), but it is still smaller than the highest performing device. We do notice larger waveguide loss in the devices that try to leverage the top metal as the nonlinear diode (16 cm^{-1}); the loss is about 50% greater than conventional QCLs. Gain measurements, along with parameters such as the turn-on voltage, differential resistance, and operating voltage—all of which can be temperature-dependent—can be related to the design and the performance of lasers and MIR-PICs.

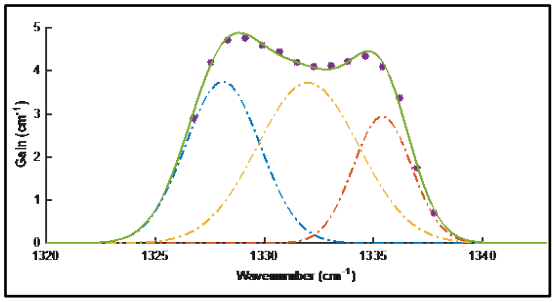

Figure 5: Gain spectrum obtained from Hakki-Paoli calculations. Experimental data (purple stars) was acquired at 80K, and a Gaussian fit was used to estimate the gain shape (green line). Individual transitions that make up the gain shape are depicted in dashed lines

Our next step in the characterization is to measure the microwave response of the MIR-PIC by measuring the voltage over the diode. Figure 6 is a schematic of two circuits we have implemented for testing devices (a) with integrated diodes and (b) without integrated diodes. During this characterization, the devices are operated in continuous wave mode (constant voltage/current). A bias-T is used to couple only the microwave signal into a network analyzer for measuring the spectrum of the generated microwave signal.

The full characterization of the devices was impeded by laboratory closures due to COVID-19. Figure 7 depicts the microwave difference frequency of the amplified spontaneous emission (ASE) spectrum. Our equipment is capable of measuring AC signals below 35 GHz, and there is a strong spectral response around 25 GHz. While the laboratories were shut down, we developed equivalent circuit models and numerical models for MIR-PICs operating at 25 GHz. While we did not originally intend to develop these models as part of this program, they have provided valuable information on improving the overall MIR-PIC performance.

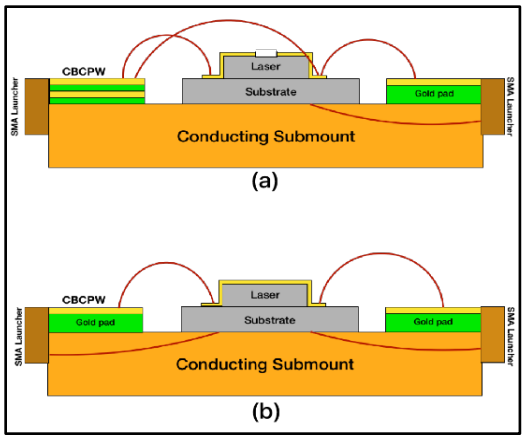

Figure 6: Wiring schematics mixing experiments. (a) Wiring diagram for laser with the diode on. CBCPW is isolated from the ground of the laser. (b) Wiring diagram for laser without a diode. Contacts also used as the nonlinear element. Ground of CBCPW is connected to the laser ground.

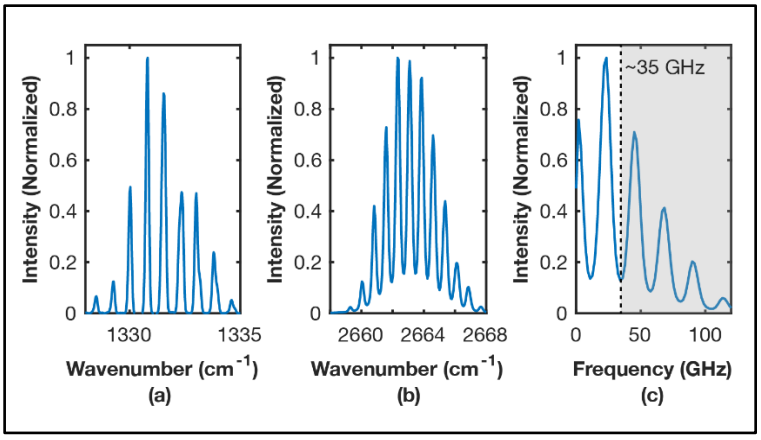

Figure 7: ASE spectrum and calculated sum/difference frequency generation. (a) ASE spectrum acquired at 80K (experimental data). (b) Simulated sum frequency generation. (c) Simulated difference frequency generation. Only signals below ~35 GHz can be detected because of equipment limitations.

An equivalent circuit model for a MIR-PIC and all associated circuitry is given in Figure 8. One immediate insight from these models that we gained is the short stub with designed impedance Z_1 that is now incorporated into our device design, Figure 8.

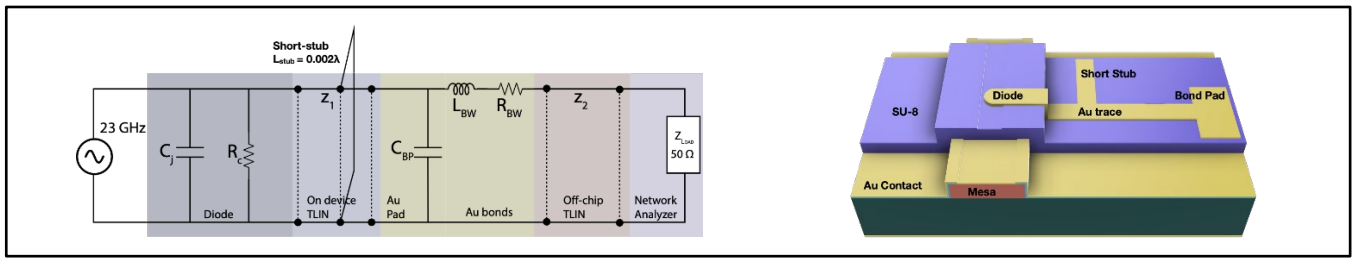

Figure 8: Equivalent circuit model for microwave feed line at 23 GHz and updated device design. (left) 23 GHz corresponds to the difference frequency generated by the Schottky Diode. Impedance matching is done off-chip to increase the flexibility of the design. (right) SU-8 is used as a dielectric layer because of its low price, low loss tangent, and low dielectric coefficient at 24 GHz.

In addition to the equivalent circuit models, we developed models in a standard commercial microwave package to better analyze design devices and circuits. Smith charts depicting the input impedance, Z_{in}, at 48 THz (optical frequencies) and 10 to 30 GHz (microwave frequencies) are given in Figure 9. These models are useful for impedance matching circuits to the MIR-PIC and are available by contacting PI Hoffman.

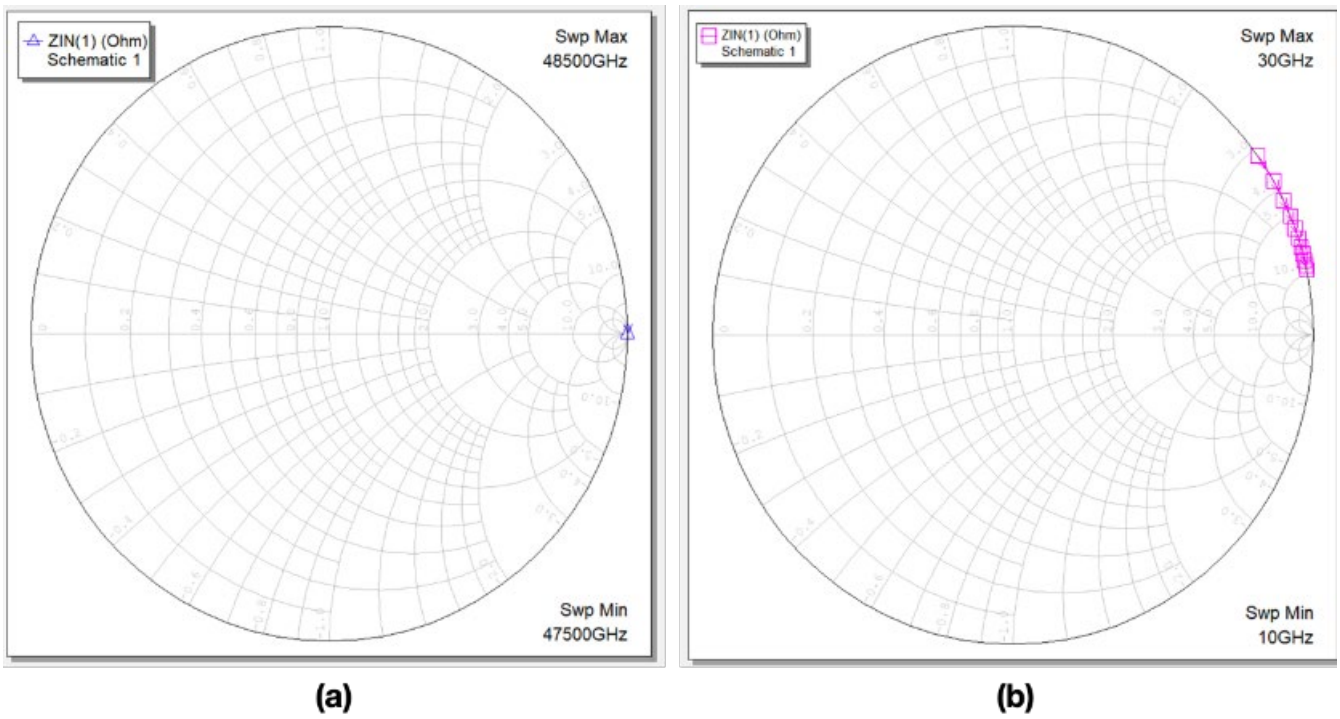

Figure 9: Smith charts showing the input impedance of the MIR-PIC (a) at frequencies from 47.5 THz to 48.5 THz. (b) at frequencies from 10 GHz to 30 GHz.

C. Major Contributions

Year 7:

- Designed a quantum active region to compare MOCVD- and MBE-grown MIR-PICs. The transceivers had differing waveguides, as necessitated by the available materials.
- Fabricated and characterized MIR-PIC devices for semiconductor wafers grown via MBE and MOCVD.
- Developed rigorous microwave models for the entire MIR-PIC device using the industry-standard, commercial software package Microwave Studio. These models are available by contacting Hoffman.
- Developed equivalent circuit models for the MIR-PIC transceiver that are useful for studying trade-offs in device performance and circuit design.
- Developed alternate MIR-PIC fabrication strategies to reduce fabrication costs and improve device yield. These new approaches reduce the complexity of fabrication. We have pursued multiple improvements: replacing air bridges with contacts deposited on benzocyclobutene (BCB); fabricating the diodes using photolithography; and, fabricating devices with the entire top contact serving as the Schottky diode.
- Accessed MIR-PICs that use the top metal as the mixing diode and device contact.
- Developed coplanar waveguide submounts with impedance matching to efficiently extract the microwave signal from the MIR-PIC.

Year 6:

- We made significant updates to our simulation and design software to enable designs in InP-based material systems. This was needed because we shifted our focus to InP-based devices to demonstrate the feasibility of transition for these devices.
- We fabricated devices from a new wafer grown by Adtech (using MOCVD) and devices from wafers grown by Sandia National Laboratories (using MBE).
- We have improved the intermediate frequency amplitude by approximately four times.

Year 5:

- We developed numerical code to model the quantum and optical properties of the MIR-PICs. Using these models, we designed MIR-PIC devices to address problems with the devices used for our preliminary study that prevented the devices from operating in continuous wave mode. Specifically, we developed a quantum cascade gain region capable of providing double the gain of our previous design. These new active region designs employ ultrastrong coupling to improve the injection of electrons into the upper-laser level.
- We used our optical models to design new optical waveguides, focusing on the optical loss, field strength at the metal contact, and confinement factor. We reduced the optical loss by approximately 60% by modifying the field strength at the metal contact and the doping of the cladding layers. The field strength at the metal contact is now 20% of the peak field in the active region; we estimate that this will be sufficient for the MIR-PICs in this project. In order to improve gain, we have also increased the optical confinement factor by ~30% by adding additional active regions. We expect that these changes should enable continuous wave operation of the MIR-PIC.
- We fabricated MIR-PIC devices and performed basic electrical and optical characterization. The devices operated in pulsed and continuous wave mode.

D. Milestones

- Compare the performance of MIR-PICs grown via MBE and MOCVD.
  - Wafers grown via MBE and MOCVD have both been processed, and characterization is complete on the MOCVD devices. Delays due to equipment failure in the Notre Dame Nanofabrication Facility and COVID-19 have slowed testing of the MBE-grown samples.
- Design, fabricate, and characterize a MIR-PIC that allows mixing on the top device contact rather than a separate Schottky diode.
  - Devices have been designed and fabricated. Continuous-wave characterization has been performed, but laboratory closures due to COVID-19 have prevented full microwave characterization.
- Determine the detection sensitivity of devices without an integrated diode for trace solid phase explosives.
  - While this research is still planned for June, the laboratory closure has significantly delayed the experimental characterization. However, during the closure, we have developed rigorous microwave models that could be used for estimating this limit or better optimizing devices for sensitivity.
- Develop rigorous microwave models for MIR-PICs.
  - We designed microwave models for the entire MIR-PIC package that incorporate realistic device parameters. In many cases the device parameters are from actual experiments. These models can be used to analyze trade-offs between the package design and the MIR-PIC performance.

There were three delays that slowed progress in Year 7:

1. MBE semiconductor growth
2. cleanroom down time
3. laboratory closures due to COVID-19

Our mitigation strategies for each are as follows.

1. While we were waiting on the MBE wafers, we focused our fabrication and characterization efforts on the MOCVD samples. (60%)
2. Our fabrication flow required reactive ion etching; however, the cleanroom equipment required for the etch was unavailable from January to March due to a number of cascading failures. We therefore developed wet-etch recipes for the fabrication of the MIR-PICs. (100%)
3. During the laboratory closure, we focused on developing microwave models for the MIR-PICs. (100%)

E. Final Results at Project Completion (Year 7)

- Demonstrated novel, ultracompact MIR-PIC transceivers that operate as both a source and receiver.
- Compared MIR-PICs fabricated using MBE- and MOCVD-grown wafers to investigate commercially scalable technologies
- Developed rigorous microwave and quantum models for MIR-PIC design.
- Engaged leading companies in mid-infrared devices (Thorlabs and Adtech Photonics) for transitioning MIR-PICs to a commercial product.

III. RELEVANCE AND TRANSITION

A. Relevance of Research to the DHS Enterprise

This project addresses the need for ultracompact, sensitive sensors for the stand-off detection of trace explosives in the solid phase (ng/cm^2). Such capabilities could be integrated into handheld devices, unmanned aerial vehicles, remote operated vehicles, and existing security-screening infrastructure as primary or confirming sensors.

- Stand-off detection of explosives is critical for the safety of Homeland Security personnel. We will demonstrate stand-off detection at distances greater than 3 feet but not likely until spring of 2021 at the earliest.
- Compact sensors with high detection sensitivity are needed for the detection of trace explosives. We will demonstrate detection of an explosive in the solid phase. Our sensitivity targets are sub-ng/cm^2; however, since this sensor is entirely new, these detection limits may not be achievable immediately or within the time frame of this project. A goal of this project is to study the relationship between the design and performance of the MIR-PIC and the detection limits when the MIR-PIC is used as a sensor.

Sensitive, stand-off detection could have a transformative impact on the detection of explosives by enabling widespread screening of individuals, vehicles, and objects. The high sensitivity could enable the use of these devices as a primary or confirming sensor, and the ultracompact footprint could enable handheld deployment.

B. Status of Transition at Project End

Our vision for this technology within the homeland security enterprise is to develop a linear array of MIR-PICs for rapidly scanning and imaging letters and packages in sorting facilities or baggage and personal items in screening stations at airports. The array of MIR-PICs would comprise devices that target different spectral regions, enabling preliminary detection of many different solid phase trace explosives or contaminants. We have developed single MIR-PICs and are now working toward scaling those devices into arrays. We are now collaborating with Adtech Photonics, Inc., a leader in QCL technologies. Adtech Photonics employs state-of-the-art growth using MOCVD, a highly scalable semiconductor growth technology. Professor Hoffman has collaborated with several members of the technical staff, and together they have demonstrated world-record QCLs. Mary Fong, the CEO of Adtech Photonics, has directly expressed interest in commercializing the technology in this project.

C. Customer Connections

- Mary Fong, Adtech Photonics LLC. Frequency of contact varied depending on the project status. Adtech Photonics provided semiconductor growth via MOCVD for this project at a heavily-subsidized cost. We have had conversations regarding transitioning to a product.
- Yamac Dikmelik, Thorlabs. Frequency of contact was less than quarterly. We have had discussions with Thorlabs about transitioning the MIR-PICs to a product. Those conversations guided the Year 7 goals.

IV. PROJECT ACCOMPLISHMENTS AND DOCUMENTATION

A. Education and Workforce Development Activities

1. Course, Seminar, and/or Workshop Development
    a. Hoffman incorporates aspects of this research into his graduate-level Nanophotonics and Quantum Optics course. He is also developing an Advanced Condensed Matter course that will include lectures discussing topics relevant to the design of semiconductor devices for optical detection of explosives.
2. Student Internship, Job, and/or Research Opportunities
    a. Undergraduate students working in Hoffman's laboratory participate in group meetings where they are engaged in the research in this project and the needs of DHS.
3. Interactions and Outreach to K–12, Community College, and/or Minority-Serving Institution Students or Faculty
    a. Hoffman has participated in the Indiana STARBASE Program, a DOD-sponsored program for introducing K–12 students to STEM in "hands-on" activities.

B. Peer Reviewed Journal Articles

Pending –

1. Harden, G., Lee, K., Jena, D., Xing, H., & Hoffman, A.J. "Optical Gain and Gain Saturation in Optically-Pumped AlGaN/AlN Quantum Wells." In preparation.

C. Student Theses or Dissertations Produced from This Project

1. Ahmet Cagri Aydinkarahaliloglu will defend his PhD candidacy in fall 2020 with the planned title, "Mid-Infrared Photonic Integrated Transceivers for Intermode Heterodyne Mixing."

D. New and Existing Courses Developed and Student Enrollment

New or Existing	Course/Module/ Degree/Cert.	Title	Description	Student Enrollment
Existing	Course	Nanophotonics and Quantum Optics	This graduate-level course discusses the fundamentals of nanophotonics, including mid-infrared light-matter interactions and quantum well semiconductor devices, which are central to this project	15

E. Software Developed

1. Models
   a. We developed microwave models in industry-standard software packages for the entire MIR-PIC package. Currently, these are available by contacting the PI. We are happy to provide them through an alternative mechanism though.
2. Other
   a. We developed software for controlling mid-infrared detector arrays. Aspects of this software were shared with Prof. Howard, PI of another ALERT project.

V. REFERENCES

*** Indicates publications by senior personnel that are relevant to this project (Total: 6)**

[1] C. Gmachl, F. Capasso, D.L. Sivco, and A.Y. Cho, "Recent progress in quantum cascade lasers and applications," *Rep. Prog. Phys.* **64**, 1533 (2001).

[2] S.S. Kim, C. Young, B. Vidakovic, S.G.A. Gabram-Mendola, C.W. Bayer, and B. Mizaikoff, "Potential and Challenges for Mid-Infrared Sensors in Breath Diagnostics," *IEEE Sensors Journal* **10**, 145 (2010).

[3] K.E. Brown, M.T. Greenfield, S.D. McGrane, and D.S. Moore, "Advances in explosives analysis—part II: photon and neutron methods," *Anal. Bioanal. Chem.* **408,** 49 (2015).

[4] J.M. Therialt et al., "A novel infrared hyperspectral imager for passive standoff detection of explosives and explosive precursors," *Chemical, Biological, Radiological, Nuclear, and Explosives Sensing XII* 8018N, (2015).

[5] A. Mukherjee, S. Von der Porten, and C.K.N. Patel, "Standoff detection of explosive substances at distances of up to 150 m," *Appl. Opt.* **49**, 2072 (2010).

[6] Z. Zhang, R.J. Clewes, C.R. Howle, and D.T. Reid, "Active FTIR-based stand-off spectroscopy using a femtosecond optical parametric oscillator," *Opt. Lett.* **39**, 6005 (2014).

[7]* Y. Yao, A.J. Hoffman, and C.F. Gmachl, "Mid-infrared quantum cascade lasers," *Nature Photonics* **6**, 432 (2012).

[8] F. Fuchs et al., "Infrared Hyperspectral Standoff Detection of Explosives," *Chemical, Biological, Radiological, Nuclear, and Explosives Sensing XII* 8710, (2013).

[9] J.D. Suter, B. Bernacki, and M.C. Phillips, "Spectral and angular dependence of mid-infrared diffuse scattering from explosives residues for standoff detection using external cavity quantum cascade lasers," *Appl. Phys. B* **108**, 965 (2012).

[10] R. Furstenberg et al., "The challenge of changing signatures in infrared stand-off detection of trace explosives," *Chemical, Biological, Radiological, Nuclear, and Explosives Sensing XV* 9073, (2014).

[11] N.A. Macleod, F. Molero, and D. Weidmann, "Broadband standoff detection of large molecules by mid-infrared active coherent laser spectroscopy," *Opt. Express* **23**, 912 (2015).

[12] T.K. Boyson et al. "Pulsed quantum cascade laser hypertemporal real-time headspace measurements," *Opt. Express* **22**, 10519 (2014).

[13] C.K.N. Patel, "Quantum Cascade Lasers: A Game Changer for Defense and Homeland Security IR Photonics," *Micro- and Nanotechnology Sensors, Systems and Applications* III 8031 (2011).

[14] Y. Wang, M. Nikodem, and G. Wysocki, "Cryogen-free heterodyne-enhanced mid-infrared Faraday rotation spectrometer," *Opt. Express* **21**, 740 (2013).

[15**]*** M.C. Wanke et al. "Monolithically Integrated Solid-state Terahertz Transceivers," *Nature Photon.* **4**, 565 (2010).

[16] G.C. Dyer, C.D. Nordquist, M.J. Cich, A.D. Grine, C.T. Fuller, J.L. Reno, and M.C. Wanke, "Rectified diode response of a multimode quantum cascade laser integrated terahertz transceiver," *Optics Express* **21**, 2996 (2013).

[17] J. Faist et al., "Quantum Cascade Laser," *Science* **264**, 553 (1994).

[18] https://www.thorlabs.com/newgrouppage9.cfm?objectgroup_id=6826

[19] A. Bismuto et al., "High power and single mode quantum cascade lasers," *Optics Express* **24**, 260609 (2016).

[20**]*** P.Q. Liu et al., "Highly power-efficient quantum cascade lasers," *Nature Photonics* **4**, 95 (2010).

[21] N. Bndyopadhyay et al., "Ultra-broadband quantum cascade laser, tunable over 760 cm^{-1}, with balanced gain," *Opt. Express* **23**, 21159 (2015).

[22] G. Villares et al., "Dispersion engineering of quantum cascade laser frequency combs," *Optica* **3**, 252 (2016).

[23**]*** J.B. Khurgin et al., "Role of interface roughness in the transport and lasing characteristics of quantum-cascade lasers," *Appl. Phys. Lett.* **94**, 091101 (2009).

[24] Y. Chiu et al., "Importance of interface roughness induced intersubband scattering in mid-infrared quantum cascade lasers," *Appl. Phys. Lett.* **101**, 171117 (2012).

[25**]*** M.P. Harter, Y. Dikmelik, and A.J. Hoffman, "Electron localization in quantum cascade heterostructures due to interface roughness," *Conference on Lasers and Electroopitcs* San Jose, 2014.

[26**]*** Y. Cui, M.P. Harter, Y. Dikmelik, and A.J. Hoffman, "Importance of Coherence and Dephasing in a Density Matrix View of Modeling the Quantum Cascade Laser Gain Spectrum," *under review at IEEE Journal of Quantum Electronics.*

R2-C.2: Multiplexed Mid-Infrared Imaging of Trace Explosives

I. PARTICIPANTS INVOLVED FROM JULY 1, 2019 TO JUNE 30, 2020

Faculty/Staff			
Name	**Title**	**Institution**	**Email**
Scott Howard	PI	University of Notre Dame	showard@nd.edu
Vijay Gupta	Collaborator	University of Notre Dame	vgupta2@nd.edu
Graduate, Undergraduate and REU Students			
Name	**Degree Pursued**	**Institution**	**Month/Year of Graduation**
David Benirschke	PhD	University of Notre Dame	12/2019
Bernardo Cruz	PhD	University of Notre Dame	06/2022
Varun Mannam	PhD	University of Notre Dame	06/2022
Xiaotong Yuan	PhD	University of Notre Dame	06/2022
Cara Ravasio	BS	University of Notre Dame	06/2020

II. PROJECT DESCRIPTION

Explosive residues leave distinct infrared "signatures" that can be detected by illuminating the residues with infrared light. While many scientists have studied these signatures, no technology is readily available that will allow for imaging and detection of the residues in real-world systems.

Project R2-C.2 developed technology platforms for low-cost and sensitive imaging of explosive residue signatures. This was done by developing semiconductor fabrication techniques to enable commercial infrared (IR) laser arrays to be used as compact illumination sources. Intellectual property for this process has been licensed to Department of Defense contractor, Indiana Integrated Circuits. This project also developed new chemical residue imaging platforms leveraged with off-the-shelf and low-cost infrared cameras for detection of explosives. These low size, weight, power, and cost (SWAP-C) systems were integrated into the Army Research Laboratory's (ARL's) electromagnetic environmental sensing and detection platform. In integrating the IR imaging system, a new distributed sensing/coordination/analysis system was implemented to allow for any generic distributed sensor system to collect data which could then be processed either remotely or on board as necessary. The IR imaging platform was then implemented with the on-board computing and communication system for aerial drones for remote, distributed detection. To overcome the increased noise from using low SWAP-C devices, a convolutional neural network was implemented to quickly denoise IR images and a new machine-learning technique was developed to identify chemical signatures by both the spectroscopic absorption and thermal time constants of the chemical film. Both of the new analysis techniques were integrated into the new distributed sensor network communication model.

Applications for these technologies include the incorporation of both the laser module and imaging systems into a variety of screening locations. Portable (deployed with security personnel), fixed (e.g., integrated with document scanners, cargo/luggage processing), and remote (e.g., unnamed aerial vehicle distributed sensor

networks) platforms are being developed to both quickly identify potential threats and to aid in the detailed diagnosis of potential threats.

A. Project Overview

The overall goal of this project is to develop technology to enhance the ongoing work of the ALERT Center of Excellence by developing mid-infrared (MIR) laser-based imaging platforms capable of remote, distributed imaging and sensing of explosive residues.

A.1. Aims

- Development of low SWAP-C (size, weight, power, and cost) optical sources and imaging systems for spectroscopic imaging of explosive films.
- Integration of MIR imaging systems with remote, distributed electromagnetic sensing platforms (e.g., aerial unmanned vehicle platforms).
- Development and evaluation of novel statistical and machine-learning techniques to overcome the limitations of using low SWAP-C (i.e., noisy) detection systems for hyperspectral explosive residue imaging. The techniques will be compatible with the low-computational power integrated MIR imaging systems developed above.

A.2. Realized End-State

- A new wafer-scale laser-array to beam-combining waveguide fabrication technique was developed that demonstrated record array-to-array coupling between two MIR waveguide chips. This can be used to combine arrays of spectroscopic sources (such as those developed by ALERT partner Pendar Technologies) as well as applications in IR scene projection for other homeland security enterprise (HSE) and DoD applications. The IP is patented and licensed to DoD contractor, Indiana Integrator Circuits. This work answers the research question, "how do you combine arrays of MIR lasers, each with a different emission wavelength, into a module with a single emission output location?"
- For the first time, low-cost, commercial, uncooled vanadium oxide bolometer focal plane arrays (FPAs) were characterized for spectroscopic imaging of chemical films. The published results showed that these low SWAP-C imaging systems can achieve the signal-to-noise ratio (SNR) required for hyperspectral imaging with frame rates faster than 1 frame per second. This work answers the research question, "can newly available, off-the-shelf, low SWAP-C MIR imaging systems be capable of quantitative spectroscopic imaging?"
- MIR image acquisition, analysis, and distribution was implemented on board the computing and communications hardware for remote aerial vehicles.
- A client, broker, subscriber networking framework was developed and demonstrated for the low SWAP-C MIR imaging systems as part of the Icarus distributed sensing software platform developed by ARL's Electronic Warfare (EW) group (Sensors and Electron Devices Directorate). To integrate the system, we improved the systems bandwidth and network latency to allow for streaming of real-time data to a centralized broker. The architecture allows for parallel analysis and chains of sequence of analysis across multiple cameras using real-time data. Distributed analysis of the data (spectroscopic imaging, denoising, and machine-learning classification) was carried out on remote servers as well as on-board systems.

- Hyperspectral imaging of high energetic material films and improvised explosive device (IED) precursors was demonstrated using the low SWAP-C imaging platforms. Detailed noise analysis was conducted to develop new denoising models required to improve low SWAP-C imaging performance.
- Noise analysis of the low SWAP-C imaging platforms found non-Gaussian noise characteristics. Previous detection algorithms assumed Gaussian distribution of pixel intensities. The project demonstrated that using generalized extreme value (GEV) distribution in a Bayesian probabilistic detection model allowed for high sensitivity chemical film detection. This work answers the research question, "does using probabilistic models using GEV distributions improve spectroscopic imaging sensitivity and performance?"
- A new machine-learning technique was developed and evaluated to classify chemical residues by their spectroscopic absorption and thermal time constant (i.e., heating and cooling rates). This enables both chemical integration ("absorption fingerprint") and characterization of the local microenvironment (thermal time constant analysis, e.g., detection of presence of plastic explosive binder). This work answers the research question, "can inclusion of thermal time constant data improve MIR spectroscopic imaging specificity?"
- Convolutional neural networks were developed and characterized for real-time denoising of MIR images. Since uncooled, low SWAP-C imaging arrays have higher intrinsic noise than the more expensive, larger, high power-consumption counterparts, we employed a new machine-learning–based technique to "restore" the SNR that was sacrificed to achieve low SWAP-C performance. This work answers the research question, "can the increase in imaging noise found in low SWAP-C cameras be improved computationally using machine-learning approaches?"
- All imaging and analysis were implemented as part of the ARL Icarus distributed sensing software platform and integrated on to the unmanned aerial vehicle computing platforms for the ARL–Notre Dame "RadioHound" electromagnetic sensing platform.

A.3. Significance and Value to ALERT and HSE

This project enhanced ongoing ALERT efforts by enabling lower cost and higher resolution imaging technology to detect signatures characterized by other ALERT projects which will be described later in this report, to provide a technology to enhance the commercial offerings of ALERT industrial partners, and to provide new low-cost spectroscopic explosive imaging platforms useful throughout the HSE. Development of the distributed sensor client/broker/subscriber platform for the ARL Icarus distributed sensor software platform has value broadly throughout the HSE and Defense enterprise by enabling easy integration of generic sensors and data analysis chains for real-time acquisition, image distribution, analysis, and data presentation to the operator and decision makers.

B. State of the Art and Technical Approach

MIR spectroscopic imaging has been demonstrated to be a powerful tool for trace explosives detection by several groups (e.g., [1-4]), including ALERT researcher, Professor Samuel Hernandez-Rivera of the University of Puerto Rico at Mayagüez (Project R3-C). Professor Hernandez-Rivera employs quantum cascade laser (QCL) systems that have been used to deliver high-spectral-energy-density radiation onto highly energetic materials deposited on complex substrates. Through standard preprocessing (second derivative, standard normal variate, and multiplicative scatter correction) and principal component analysis or linear regression analysis, pentaerythritol tetranitrate (PETN) and trinitrotoluene (TNT) can be detected on wood, cardboard, and aluminum substrates. Our groups have also previously characterized such signatures for Semtex, TNT, and explosive precursor hexamine on various substrates. For example, the MIR reflection "fingerprint" of Semtex is shown in Figure 1.

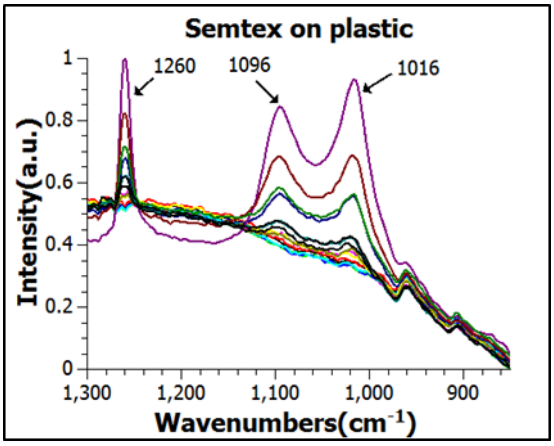

Figure 1: Demonstration of detection of Semtex film on plastic substrate. Data acquired at Notre Dame in collaboration with Professor Beaudoin, Purdue University.

While such laboratory demonstrations are interesting, the practical impact has been demonstrated by collaboration between Fraunhoffer Institutes in Germany, which have developed a trailer-based platform capable of detecting trace explosive residues at a distance of 10 m (Figure 2) [5-6]. These remarkable demonstrations showed that remote detection of explosive residue using MIR spectroscopic imaging at ~10 m is possible. However, to achieve such standoff capabilities, the platforms are large and power hungry and require expensive detector arrays.

Figure 2: Demonstration of standoff explosive residue detection from [6]. Left, image of trailer platform. Right, detection of AIN residue (yellow marks) after an improvised-explosive-device blast.

To address the need for low-cost spectroscopic arrays, we investigated using low-cost (<$250, Seek Thermal and FLIR) imaging arrays to perform spectroscopic MIR imaging of nitride films with thicknesses of 1–2 μm. Thorough noise analysis and spectroscopic imaging of nitride films were presented in [7], and example images are depicted in Figure 3. These results proved that low-cost MIR imaging arrays are capable of sensitive spectroscopic measurements of trace chemical residues.

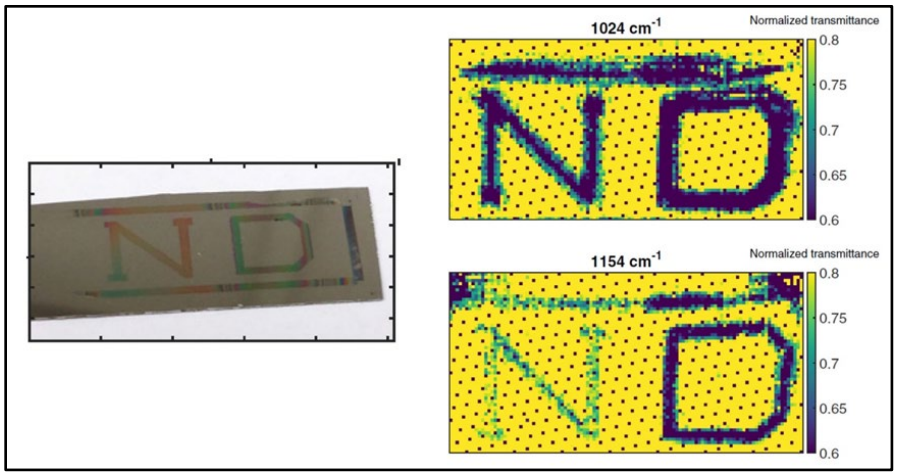

Figure 3: Silicon nitride films in the shape of an "N" (1 µm) and "D" (2 µm) are deposited on a germanium substrate (left). Differential absorption imaging was performed by using the low-cost MIR imaging arrays as detectors in a Fourier-transform infrared (FTIR) spectrometer (right). Results above show subtle difference in relative transmission through the "N" and "D" due to subtle differences in nitride deposition conditions.

B.1. Technical Approach

This project is investigating three complimentary technical advancements: (1) On chip heterogeneous integration of widely disparate wavelength MIR lasers; (2) a low-cost vanadium oxide bolometer for explosive detection (which superseded the original goal of investigating MIR coded aperture imaging technology due to the bolometer array's superior size, weight, power, and cost profile); and (3) development of optical sensor selection algorithms to improve sensitivity and speed of complete sensor systems.

B.2. On Chip Heterogeneous Integration of Widely Disparate Wavelength MIR Lasers

The most commonly used and commercially available semiconductor MIR light source is a QCL [8]. QCLs are made into widely tunable devices that can have large ranges over the entire absorption band of explosives residues using external cavity (EC) feedback. These devices, known as EC-QCLs, select wavelength by rotating the incident angle of light on a diffraction grating. Such a system has been of particular interest recently, to detect trace explosives residues on various targets [1-3]. These systems require moving parts and manual assembly; integration would be preferred for simplicity, lower cost, and to improve mechanical reliability. Arrays of lasers can be fabricated in such a way that the lasing wavelength of adjacent lasers is slightly offset, thus producing a discretely tunable source by selectively turning on and off individual lasers [9]. This is the basis of the technology of Pendar Technologies. These lasers have a lateral offset, and thus can use external free space optics to combine the beams into a single output [10]. External beam combining, while not requiring moving parts, requires free space optics and alignment, which adds complexity and renders the devices susceptible to mechanical instability.

The technical approach we are employing is to combine laser arrays on a single chip and on separate chips into a single module using a novel interchip alignment and optical coupling technique. In this technique, individual laser chips are fabricated with extending copper nodules. The chip with nodules is combined with similar chips to form a quasi-monolithic "quilt," from which the name Optical Quilt Packaging (OQP) is derived (see Figure 4).

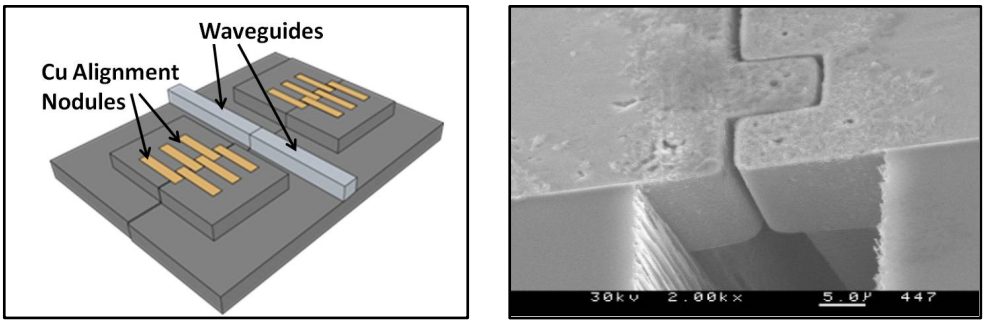

Figure 4: Illustration of OQP (left). SEM micrograph of interlocking quilt packaging nodule structure (right)

The proposed OQP leverages advances in electronic quilt packaging, a novel technique developed at the University of Notre Dame (UND) for high-speed electronic interconnections. Electronic quilt packaging integrates diverse electronic device technologies into a quasi-monolithic module by connecting separate die with solid metallic contacts along the vertical faces for both mechanical and electrical connection. Research at UND has demonstrated the world-record low inter-die insertion loss of less than 0.1 dB from 50 MHz to 100 GHz [11] with submicron alignment.

B.3. MIR Spectroscopic Imaging of Trace Explosives

To increase signal-to-background detection of trace samples of explosives, we will employ MIR spectroscopic imaging. MIR imaging arrays are prohibitively expensive, so we are exploring time and frequency multiplexed imaging with the laser modules developed in this project to improve speed (frame rate) and sensitivity (minimal detectable concentration) of differential reflection spectroscopy by replacing the relatively high-noise infrared detector array with a more sensitive (and less expensive) single element photodetector. MIR trace explosives imaging systems typically employ bolometer (i.e., thermal) or semiconductor detector (i.e., photonic) FPAs. Semiconductor detector arrays exhibit a wavelength dependence on the material; materials useful in the MIR tend to be prohibitively expensive for multipoint distributed sensing. Bolometer-based FPAs can be prohibitively slow for many differential measurement schemes of moving objects; however, recent commercialization of bolometer-based FPAs have drastically reduced system cost by more than 100 fold, opening up new possibilities to investigate using distributed networks of explosive detection systems. To our knowledge, we are the first to explore leveraging these advances and have published the first papers demonstrating hyperspectral chemical imaging using low-cost, microbolometer arrays.

B.4. Improving MIR Spectroscopic Imaging Sensitivity and Specificity

To improve sensitivity and specificity, we are developing a new trace explosive technique based on imaging the thermal relaxation of chemical film residue. MIR explosive residue detection sensitivity and specificity (and therefore accuracy and speed) are limited by the ability to differentiate between the spectral absorption features; however, in real-world environments, substrate and chemical confusants can dramatically reduce performance. Traditionally, this is overcome by imaging samples at many different illumination wavelengths simultaneously; however, such an approach increases system cost and complexity. Our new approach is to not only image the reflected light spectrum but also measure the speed at which thermal energy is dissipated in each point of the image. This added data dimension gives chemical information on the matrix (i.e., binder) of explosive residue and is different for explosives compared to other compounds. We are, to our knowledge, the first to explore this method. It is based on our PI's extensive work on biomedical fluorescence lifetime imaging, which is used to quantitatively measure the chemical microenvironment [12-18].

Low SWAP-C detectors are typically uncooled microbolometer arrays, and as such, have increased noise compared to the more expensive and power-hungry cooled arrays. To overcome this limitation, co-PI Vijay Gupta is investigating using both Bayesian analytical techniques and machine-learning (dynamic time warping) techniques to increase detection confidence as well as provide a method for efficient sensor selection to maximize confidence using the least number of detection wavelengths. Initial work using Bayesian-based detection has found that noisy microbolometer data actually follows a GEV distribution, not a Gaussian distribution. We believe this to be attributed to the characteristics of bolometer array read-out circuitry, and it yields different analytical models that are commonly used for detection. The GEV distribution is evident in Figure 5 , which shows a pixel intensity histogram of a MIR QCL illuminated scene acquired by a Seek Thermal microbolometer array. Hypothesis testing using GEV yields near unity receiver operator characteristic (ROC) when discriminating hydrocarbons on cardboard; this work is currently being prepared for submission to *IEEE Sensors* and has been extended to explosive residues and dynamic time-warp machine learning in Year 7.

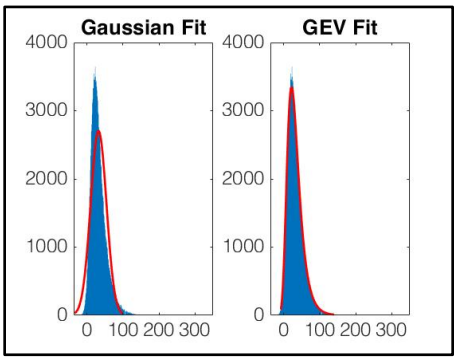

Figure 5: Histograms of pixel values on low SWAP-C MIR imaging platform when field-of-view illuminated by MIR QCL.

B.5. Distributed and Remote Platform Development

The low SWAP-C MIR hyperspectral imaging platform has been enabled by commercially available vanadium oxide microbolometer arrays from several companies (e.g., FLIR and Seek Thermal) that are low-cost (<$250), low-power (<500 mW), small size (2 cm × 2 cm) and low weight (~1 oz). The devices can be controlled over USB and are therefore compatible with a multitude of low-cost single-board computers (SBCs), such as the Raspberry Pi. These traits make them ideal for a low-cost distributed detection platform when combined with a centralized (or ground unmanned vehicle) laser platform or an on-board low-power, pulsed-mode QCL. In Year 7, we integrated our MIR spectroscopic imaging platform inside the radio frequency (RF) EW group in the Sensors and Electron Devices Directorate at the ARL's platform for distributed RF spectrum mapping and sensing. Co-PI Professor Jon Chisum is leading this aspect of the collaboration pursuant to which he has developed the RF sensing component of the platform, and organized field testing with ARL (Figure 6). We have implemented a proof-of-concept demonstration of MIR spectroscopic imaging using these sensor platform nodes by including our custom client-server software written in Python to control and acquire data from MIR microbolometer arrays. We have developed a professional software architecture to enable control and cloud-based data analysis of stand-alone sensing nodes. Additionally, we are leveraging a recent Office of Naval Research (ONR) commitment to fund the translation of the ground-based nodes to unmanned aerial drones. The ONR component is focused on developing on-board RF spectrum mapping and on enhancing communications to support both strong WiFi (i.e., where infrastructure is developed) as well as weak field-based LTE (e.g., in remote areas, forward operating bases, and sea-based platforms). The DHS/ALERT component focuses on (1) the architecture for imaging control and communications, (2) back-end storage and analysis (e.g., real-time on-board "pre-screening" or cloud-based, machine-learning–based analysis), and (3) a graphical user interface for imaging system control and data access.

Figure 6: Current wireless sensor nodes for distributed MIR imaging.

C. Major Contributions

Year 1: The design and predicted performance of chip-to-chip optical coupling between a QCL ridge waveguide and a single-mode Ge-on-Si waveguide arrays was first published. The system was expected to achieve ~2–6 dB coupling loss within the design tolerance of our system. Our approach is therefore feasible as it would exceed previous state-of-the-art results that demonstrated at best 10 dB couple loss [19-20].

Year 2: Fabrication process was developed and demonstrated for coupling Ge-on-Si waveguide structures via OQP with a chip-to-chip distance. The system used new Ge-on-Si waveguide OQP modules, fabricated and aligned via OQP with interchip distance, and interchip spacing was reduced from 10 μm to 4.6±1.1 μm and lateral misalignment of 920±150 nm. In Year 2, we also optimized our system for peak sensitivity by performing MIR spectroscopic imaging using FTIR. Spectral analysis of the complete explosive (energetic material, binder, and plasticizer) yields the required laser spectra, tuning ranges, power spectral density, and imaging speeds for a required sensitivity and specificity. Trace samples (gloved thumbprints) of C4 (91% RDX) and Semtex-1A (76% PETN, 4.6% RDX) were deposited on bare car-body aluminum, car-body aluminum with car paint and clear coat, and low-reflectivity plastic. Samples were provided by ALERT Thrust leader Professor Steve Beaudoin of Purdue University (Projects R2-A.1, R2-A.3, and R2-D.1). While the HEM components of C4 and Semtex (PETN and RDX) are commonly characterized in the MIR [1] on similar substrates [21], and C4 is well characterized in laboratory settings [4], we sought to establish performance parameters of composite explosives on realistic substrates.

Year 3: OQP fabrication optimization continued, reducing interchip gap of fabricated chips to 1.4±0.3 μm. Insertion loss using MIR OQP was experimentally developed for the measured for the first time to be ~9 dB. We began evaluation of the low-cost vanadium oxide bolometer array that will be used extensively going forward. Chemometric analysis software tools were written for hyperspectral imaging analysis using the new VoX bolometer array that could do PCA analysis imaging on QCL illuminated samples in real time.

Year 4: The project demonstrated a microelectromechanical-systems–based MIR chip-to-chip optical coupling technique, OQP, and demonstrated coupling between two waveguide arrays joined by OQP. The coupling loss between Ge-on-Si passive MIR waveguides is found to be ~4.1 dB, which is the lowest butt-coupling loss ever reported between two chips [22].

Characterization of a low SWAP-C vanadium oxide bolometer array was performed and achieved a 4-times reduction in weight (2.0/0.5 lbs.) and a 48-times reduction cost ($12,000/$250) but takes 93 times longer to achieve the same noise equivalent temperature difference (1.551-second acquisition time for low SWAP-C systems at room temperature compared to 16.6 ms for detector system cooled to 45 mK). Additionally, a proof-of-concept spectral imaging experiment of nitride thin films was demonstrated [7].

Year 5: We developed further hardware modifications and signal processing analysis of the microbolometer imaging platform that lead to an increase in acquisition speed from ~7 frames per second to more than 30 frames per second without negatively affecting the signal-to-noise ratio. We also began our collaboration with Prof. Jon Chisum and the Army Research Lab to integrate our MIR imaging platform in wireless, solar-powered, distributable hardware platforms. Real-time spectroscopic data is streamed to custom control software developed by our group for analysis. This platform subsequently became our primary imaging platform.

Year 6: The project demonstrated a plug-and-play, low SWAP-C, MIR imaging system utilizing a commercially available low-cost vanadium oxide microbolometer controlled via a Raspberry Pi and Python. The camera system was enhanced beyond the reported Year 4 result [7] to achieve 32 frames per second without reducing signal-to-noise ratio. Client-server remote operation was also demonstrated [23].

Year 7: A Bayesian statistical approach was demonstrated to segment polymer films on cardboard using the unique statistical nature of the low SWAP-C vanadium oxide bolometer arrays using MIR spectroscopic imaging. Single-frame analysis could properly identify all 199 images of hydrocarbon films on cardboard [24]. Additionally, convolutional neural networks were applied to the imaging data to increase speed by a factor of 4 for the same signal-to-noise ratio.

D. Milestones

- **MIR spectroscopic imaging sensitivity improvements:** To overcome the increased imaging noise that occurs using low SWAP-C–based spectroscopic imaging platforms, we pursued the milestone of using Bayesian statistical techniques to improve detection sensitivity and specificity. We did meet this milestone, however, we did it using machine learning (convolutional neural networks) and not Bayesian statistics. We trained a U-net convolutional neural network, with 12,000 near-infrared images of varying statistical noise properties and demonstrated a 6–9 dB in imaging signal to noise ratio using the low SWAP-C imaging arrays. Image acquisition subsequently increased by a factor of 4 to achieve the same noise level. Denoising is performed in real-time and is compatible with the on-board imaging system in our distributed platform. We originally proposed using cloud computing, but we ended up not needing it to reach this milestone. As part of this milestone, we proposed developing thermal time constant imaging for detection of HEMs as an additional method to increase MIR trace explosive residue imaging sensitivity. Thermal time constants on the order of milliseconds (expected time constant for HEM in binder) are expected to be characterized for the first time and will be a new tool for future HEM detection platform development. While this specific worked was slowed by the University shut down last Spring, we continued developing this approach through extracting 2D thermal diffusivity images of common objects with data collected using our imaging platform in the garage of our technician. Identical materials with different thermal properties were correctly identified using the approach. One-hundred percent of the statistical denoising approach has been achieved in the milestone, and ~50% of the thermal time constant imaging has been achieved.
- **Distributed and remote platform development:** A complete, remote MIR spectroscopic imaging platform has been developed, packaged, and field-tested as a component of the ARL's RF EW group's RF spectrum sensing and mapping platform. During the university shutdown, we in fact used this distributed platform to have different students remotely operating the IR imaging system simultaneously. A signal acquisition and processing pipeline was developed to have multiple "data consumers" (algorithms) analyze data in real time and share the data, remotely, with other "consumers" for further analysis. The system currently consists of ground-based, stand-alone, wireless, mesh network sensor nodes. We have been delayed pursuing aerial drones due to the university shutdown, however, the platform meets the payload specs for aerial drone deployment. Ninety percent of the milestone has been reached (system development, testing, and ground based demonstration). The remaining 10% would be aerial platform demonstration.

E. Final Results at Project Completion (Year 7)

- MIR image acquisition, analysis, and distribution was implemented on board the computing and communications hardware for remote aerial vehicles.
- A client, broker, subscriber networking framework was developed and demonstrated for the low SWAP-C MIR imaging systems as part of the Icarus distributed sensing software platform developed by the ARL's EW group. To integrate the system, we improved the systems bandwidth and network latency to allow for streaming of real-time data to a centralized broker. The architecture allows for parallel analysis

and chains of sequence of analysis across multiple cameras using real time data. Distributed analysis of the data (spectroscopic imaging, denoising, and machine-learning classification) was carried out on remote servers as well as on-board systems.

- Hyperspectral imaging of high energetic material films and IED precursors was demonstrated using the low SWAP-C imaging platforms. Detailed noise analysis was conducted to develop new denoising models required to improve low SWAP-C imaging performance.
- Noise analysis of the low SWAP-C imaging platforms found non-Gaussian noise characteristics. Previous detection algorithms assumed Gaussian distribution of pixel intensities. The project demonstrated that using GEV distribution in a Bayesian probabilistic detection model allowed for high sensitivity chemical film detection. This work answers the research question, "does using probabilistic models using GEV distributions improve spectroscopic imaging sensitivity and performance?"
- A new machine-learning technique was developed and evaluated to classify chemical residues by their spectroscopic absorption and thermal time constant (i.e., heating and cooling rates, Figure 7). This enables both chemical integration ("absorption fingerprint") and characterization of the local microenvironment (thermal time constant analysis, e.g., detection of presence of a plastic explosive binder). This work answers the research question, "can inclusion of thermal time constant data improve MIR spectroscopic imaging specificity?"

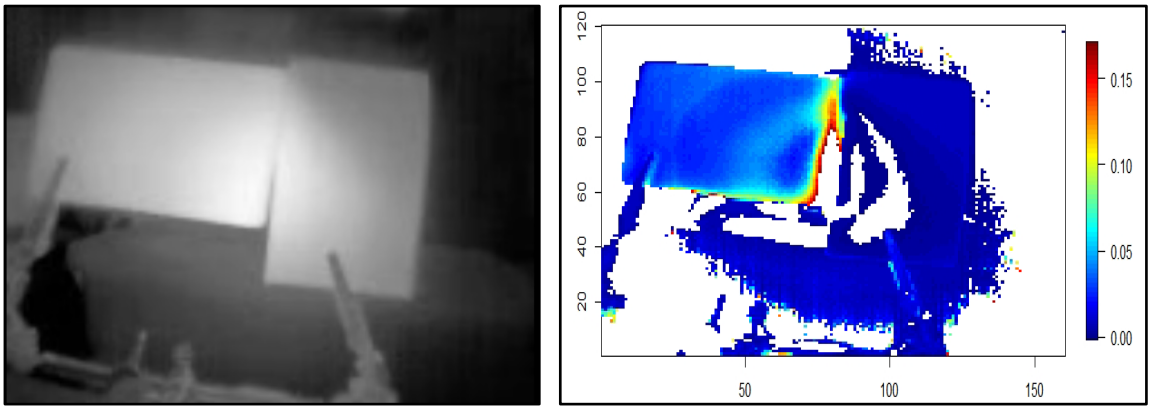

Figure 7: FLIR Lepton image of plastic (left) and glass (right) targets. Demonstration of thermal time constant imaging to segment the materials (right).

- Convolutional neural networks (CNN) were developed and characterized for real-time denoising of MIR images (Figure 8). Since uncooled, low SWAP-C imaging arrays have higher intrinsic noise than the more expensive, larger, high power-consumption counterparts, we employed a new machine-learning–based technique to "restore" the SNR that was sacrificed to achieve low SWAP-C performance. This work answers the research question, "can the increase in imaging noise found in low SWAP-C cameras be improved computationally using machine-learning approaches?"

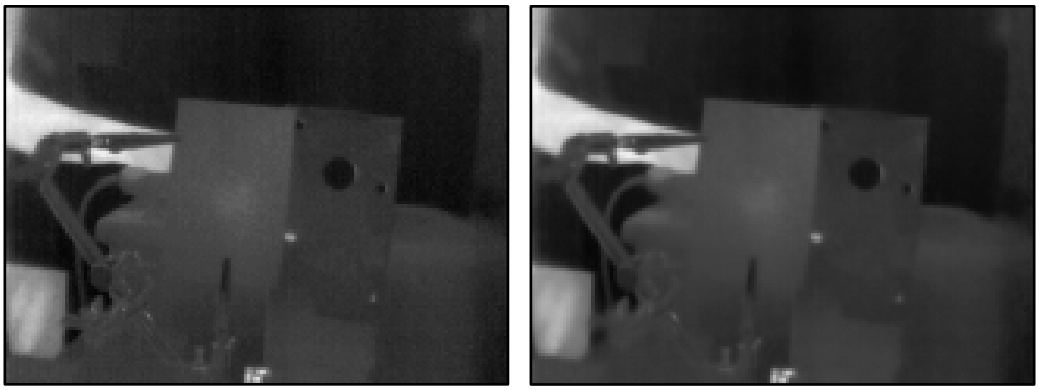

Figure 8: FLIR Lepton raw image (left) and denoised (right) using CNN. Eight-times increase in imaging speed is achieved using machine learning.

- All imaging and analysis were implemented as part of the ARL Icarus distributed sensing software platform and integrated onto the unmanned aerial vehicle computing platforms for the ARL-UND "RadioHound" electromagnetic sensing platform.

III. RELEVANCE AND TRANSITION

A. Relevance of Research to the DHS Enterprise

Remote, standoff detection of explosives residues is a crucial challenge throughout the HSE. While sensitive standoff imaging of residues on the order of 100 μg/cm^2 and less can be achieved with state-of-the-art equipment, such setups are prohibitively expensive and power hungry. Those limitations severely restrict usage. We address this by developing platforms using off-the-shelf commercial components including low SWAP-C arrays and low-power single-board computers, and we developed machine-learning algorithms and distributed sense/compute models to overcome the limitations of low SWAP-C devices. Our final platform cost 50–100 times less than state-of-the-art approaches and reaches image performance comparable to the more expensive systems. The low SWAP-C platform is also compatible with remote, distributed sensors on weight-sensitive platforms such as for aerial drones.

B. Status of Transition at Project End

The primary end-user application of the project is a distributed MIR spectroscopic imaging platform capable of trace explosive residue imaging. To achieve that end goal, we have demonstrated that low SWAP-C vanadium oxide detectors can perform MIR spectroscopic imaging of trace explosives. We have also developed new machine-learning algorithms to overcome the increased noise in low SWAP-C detector arrays and developed and integrated a new sensor and data analysis architecture on top of the ARL's "Icarus" EW sensing platform. We then demonstrated IR imaging and analysis on remote nodes using the Icarus sensor-control platform.

C. Transition Pathway and Future Opportunities

Transition will be facilitated through the existing collaboration between Co-PI Chisum and the RF EW group at ARL. The sensor-node platform (without MIR imaging capabilities) has been tested as part of the NATO Cyber EW working group field-testing in the UK and Norway in addition to ARL testing performed in the US and is of interest more broadly from within that group. Through Year 7 funding, we have developed an interface for generic sensors (including our IR imaging systems) into their platform and created an analysis

"client-subscribe-broker" model to allow for multiple parallel data-analysis workflows on real-time data being acquired by sensors. We have demonstrated MIR imaging capabilities, and machine-learning data analysis, alongside existing RF sensing capabilities on both of the ground-based mesh networks. The results of this work have been committed in real time to the ARL platform.

D. Customer Connections

- Jason Kulic (jason.kulick@indianaic.com), Indiana Integrated Circuits, LLC: monthly meetings through Year 5.
- Charles Dietlein, Sensors and Electron Devices, Army Research Laboratory: direct collaborator of Co-PI Chisum. Has already had successful field-testing campaigns for wireless spectrum-sensing platforms, a multi-year ongoing collaboration. Years 6 and 7.
- Kevin Jim, Oceanit, DoD Contractor: collaborator evaluating MIR imaging systems on aerial drones with Navy contract. Completed contract work during Year 6.

IV. PROJECT ACCOMPLISHMENTS AND DOCUMENTATION

A. Peer Reviewed Journal Articles

1. Aquino, B., Benirschke, D., Gupta, V., & Howard, S. "A Bayesian Approach to Binary Classification of Mid-Infrared Spectral Data with Noisy Sensors." *IEEE Sensors Journal, 20*(13*),* March 2020, pp. 6964-6970. https://doi.org/10.1109/JSEN.2020.2978757.

B. Student Theses or Dissertations Produced from This Project

1. Benirschke, D. "Realization of a Commercially Available, Low-Cost, Spectroscopic, Mid-Infrared Imaging Platform for Enabling Applications and Thermal Time-Harmonic Imaging." PhD, Electrical Engineering, University of Notre Dame, 6 September 2019.

C. New and Existing Courses Developed and Student Enrollment

New or Existing	Course/Module/ Degree/Cert.	Title	Description	Student Enrollment
Existing	Course	EE10115: Introduction to Embedded Systems and Internet of Things (SP 2020)	A project-based first-year undergraduate engineering elective course that teaches students the principles of low-power, wireless sensor technology	90

D. Technology Transfer/Patents

1. Patents Awarded
   a. Hall, D.C., Bernstein, G.H., Hoffman, A., Howard, S., & Kulick, J.M. "Inter-chip alignment." US Patent 10,410,989, 2019.

V. REFERENCES

[1] J. D. Suter, B. Bernacki, and M. C. Phillips, "Spectral and angular dependence of mid-infrared diffuse scattering from explosives residues for standoff detection using external cavity quantum cascade lasers," *Appl. Phys. B*, vol. 108, no. 4, pp. 965–974, Sep. 2012.

[2] C. Bauer, U. Willer, and W. Schade, "Use of quantum cascade lasers for detection of explosives: progress and challenges," *Opt. Eng.*, vol. 49, no. 11, p. 111126, Nov. 2010.

[3] F. Fuchs *et al.*, "Imaging standoff detection of explosives using widely tunable midinfrared quantum cascade lasers," *Opt. Eng.*, vol. 49, no. 11, p. 111127, Nov. 2010.

[4] C. S. C. Yang *et al.*, "Spectral Characterization of RDX, ETN, PETN, TATP, HMTD, HMX, and C-4 in the Mid-Infrared Region," *Tr-1243*, no. April, Apr. 2013.

[5] F. Fuchs *et al.*, "Standoff trace detection of explosives with infrared hyperspectral imagery," in *Proceedings of SPIE Micro- and Nanotechnology Sensors, Systems, and Applications VII*, 2015, p. 94672O.

[6] R. Ostendorf *et al.*, "Recent Advances and Applications of External Cavity-QCLs towards Hyperspectral Imaging for Standoff Detection and Real-Time Spectroscopic Sensing of Chemicals," *Photonics*, vol. 3, no. 2, p. 28, May 2016.

[7] D. Benirschke and S. Howard, "Characterization of a low-cost, commercially available, vanadium oxide microbolometer array for spectroscopic imaging," *Opt. Eng.*, vol. 56, no. 4, p. 040502, Apr. 2017.

[8] Y. Yao, A. J. Hoffman, and C. F. Gmachl, "Mid-infrared quantum cascade lasers," *Nat. Photonics*, vol. 6, no. 7, pp. 432–439, Jun. 2012.

[9] B. G. Lee *et al.*, "DFB quantum cascade laser arrays," *IEEE J. Quantum Electron.*, vol. 45, no. 5, pp. 554–565, May 2009.

[10] B. G. Lee *et al.*, "Beam combining of quantum cascade laser arrays.," *Opt. Express*, vol. 17, no. 18, pp. 16216–24, Aug. 2009.

[11] D. Kopp *et al.*, "Quilt Packaging: A Coplanar Chip-to-Chip Interconnect Offering Ultra-Wide Bandwidth," in *Proc. of 2010 International Conference on Compound Semiconductor Manufacturing Technology*, 2010, p. 309.

[12] Y. Zhang, D. Benirschke, O. Abdalsalam, and S. S. Howard, "Generalized stepwise optical saturation enables super-resolution fluorescence lifetime imaging microscopy," *Biomed. Opt. Express*, vol. 9, no. 9, p. 4077, Sep. 2018.

[13] Y. Zhang *et al.*, "Saturation-compensated measurements for fluorescence lifetime imaging microscopy," *Opt. Lett.*, vol. 42, no. 1, p. 155, Jan. 2017.

[14] A. A. Khan, S. K. Fullerton-Shirey, and S. S. Howard, "Easily prepared ruthenium-complex nanomicelle probes for two-photon quantitative imaging of oxygen in aqueous media," *RSC Adv.*, vol. 5, no. 1, pp. 291–300, Nov. 2015.

[15] S. S. Howard, A. Straub, N. G. Horton, D. Kobat, and C. Xu, "Frequency-multiplexed in vivo multiphoton phosphorescence lifetime microscopy," *Nat. Photonics*, vol. 7, no. 1, pp. 33–37, Jan. 2013.

[16] A. A. Khan, G. D. Vigil, Y. Zhang, S. K. Fullerton-Shirey, and S. S. Howard, "Silica-coated ruthenium-complex nanoprobes for two-photon oxygen microscopy in biological media," *Opt. Mater. Express*, vol. 7, no. 3, p. 1066, Mar. 2017.

[17] Y. Zhang, A. A. Khan, G. D. Vigil, and S. S. Howard, "Investigation of signal-to-noise ratio in frequency-

domain multiphoton fluorescence lifetime imaging microscopy," *J. Opt. Soc. Am. A*, vol. 33, no. 7, p. B1, Jul. 2016.

[18] Y. Zhang, A. A. Khan, G. D. Vigil, and S. S. Howard, "Super-sensitivity multiphoton frequency-domain fluorescence lifetime imaging microscopy," *Opt. Express*, vol. 24, no. 18, p. 20862, Sep. 2016.

[19] T. Ahmed *et al.*, "FDTD modeling of chip-to-chip waveguide coupling via optical quilt packaging," in *SPIE Optical Engineering + Applications*, 2013, vol. 8844, pp. 88440C-88440C–7.

[20] T. Ahmed *et al.*, "Optical Quilt Packaging: A New Chip-to-Chip Optical Coupling and Alignment Process for Modular Sensors," in *Cleo: 2014*, 2014, vol. 2014-Janua, p. JTu4A.56.

[21] M. C. Phillips, J. D. Suter, B. E. Bernacki, and T. J. Johnson, "Challenges of infrared reflective spectroscopy of solid-phase explosives and chemicals on surfaces," in *Proc. SPIE*, 2012, vol. 8358, pp. 83580T-83580T–10.

[22] T. Ahmed *et al.*, "Mid-Infrared Waveguide Array Inter-Chip Coupling Using Optical Quilt Packaging," *IEEE Photonics Technol. Lett.*, vol. 29, no. 9, pp. 755–758, May 2017.

[23] D. Benirschke *et al.*, "Realization of a plug-and-play, low SWAP-C, MIR imaging system utilizing a commercially available low-cost VOx microbolometer array for enabling imaging applications," in *Electro-Optical and Infrared Systems: Technology and Applications XV*, 2018, vol. 10795, p. 12.

[24] B. Aquino, D. Benirschke, V. Gupta, and S. Howard, "A Bayesian Approach to Binary Classification of Mid-Infrared Spectral Data With Noisy Sensors," *IEEE Sens. J.*, pp. 1–1, Mar. 2020.

THRUST R3

BULK SENSORS & SENSOR SYSTEMS

Project Number	Project Title	Lead Investigator(s)	Other Faculty Investigator(s)
R3-A.2	Computational Models & Algorithms for Millimeter-Wave Whole Body Scanning for Advanced Imaging Technology	Carey Rappaport	Mohammad Tajdini Ann Morgenthaler
R3-A.3	Multi-Transmitter/Multi-Receiver Blade Beam Torus Reflector for Efficient Advanced Imaging Technology	Carey Rappaport	Jose Martinez Dan Busuioc
R3-B.1	Hardware Design for "Stand-off" & "On-the-Move" Detection of Security Threats	Jose Martinez	Juan Heredia Juesas
R3-C	Standoff Detection of Explosives: Infrared Spectroscopy Chemical Sensing	Samuel P. Hernández-Rivera	Ricardo Infante-Castillo

This page intentionally left blank.

R3-A.2: Computational Models and Algorithms for Millimeter-Wave Whole Body Scanning for Advanced Imaging Technology

I. PARTICIPANTS INVOLVED FROM JULY 1, 2019 TO JUNE 30, 2020

Faculty/Staff			
Name	**Title**	**Institution**	**Email**
Carey Rappaport	PI	NEU	c.rappaport@northeastern.edu
Mohammad Tajdini	Post-Doc	NEU	mmtajdini@gmail.com
Ann Morgenthaler	Consultant	Ann Morgenthaler Consulting	7bradford@gmail.com
Graduate, Undergraduate, and REU Students			
Name	**Degree Pursued**	**Institution**	**Month/Year of Graduation**
Guanying Sun	PhD	NEU	5/2022
Mahshid Asri	MS, PhD	NEU	5/2020 (MS), 5/2023 (PhD)
Elizabeth Wig	MS	NEU	5/2020
David Femi Lamptey	BS	NEU	5/2025
Allison Care	BS	NEU	5/2025

II. PROJECT DESCRIPTION

A. Project Overview

Active millimeter-wave (mm-wave) radar advanced imaging technology (AIT) is the best available imaging technology for detecting objects concealed on the human body at security checkpoints [1-5]. An important need for AIT person screening is to reduce false alarms due to innocent foreign objects worn under clothing [6]. While currently deployed mm-wave nearfield radar systems, such as the L3 ProVision scanner, can adequately detect and image concealed foreign objects, with current processing they are incapable of ruling out filled beverage containers, medical devices, money belts, or other commonly worn items. The resulting alarms necessitate pat-downs, slow the progress of the traveling public, require significant manpower dedicated to alarm resolution, and detract from the overall passenger experience.

Project R3-A.2 has been investigating new approaches to processing mm-wave nearfield radar data to determine the dielectric constant and thickness of electromagnetically penetrable slabs [7-11]. Using measured data from the high definition (HD) AIT system developed by PNNL, these approaches consider the differential paths taken by rays that pass through dielectric slabs on the way to the conductive human skin backplane. The current AIT systems provide sufficient information about the scattering to generate the overall shape of a foreign dielectric object, but with appropriate processing they can also calculate how thick the dielectric object is and whether its dielectric constant is consistent with a material of interest. The algorithms conceived of and developed in R3-A.2 are being implemented as fully automatic approaches to classify anomalies, some of which were representative low-dielectric materials. Project R3-A.2 algorithms have shown in laboratory testing to discriminate concealed foreign materials, both single frequency raster scanned

focused systems (such as the Smiths Detection eqo[1] system) [12-16] and wideband frequency modulated continuous wave or stepped frequency systems (such as the L3 ProVision[2], PNNL[3]). Armed with this material classification information, security personnel have a much clearer sense of the potential threat, leading to fewer false alarms—and fewer pat-downs at checkpoints. Since even a 10% reduction in false alarms results in tens of millions of dollars in reduced TSA labor costs, as well as faster throughput at security checkpoints and a much happier traveling public, this project has enormous value to the homeland security enterprise.

The goals of the project are to:

- Determine the best means of identifying features of 3D image data that indicate the presence and material characteristics of concealed foreign object on all parts of the body.
- Use the most advanced mm-wave image data available to develop an appropriate algorithm to exploit these features.
- Isolate anomalies and infer their complex dielectric constants.
- Compare this inferred dielectric information with that of potential threats and nuisance objects, and report alarms for potential hazards and pass innocent objects.
- Score the performance of the algorithm relative to know ground truth to establish receiver operating characteristics (ROCs) and show the potential for effectiveness.

B. State of the Art and Technical Approach

The current effort is to establish a new paradigm for foreign object material characterization, so that explosive threats can be more reliably detected. While currently imaged objects such as firearms and knives can be recognized by shape, explosive volumes can take on any shape and thickness. We endeavor to determine the range of foreign object dielectric constant and rule out innocent materials that would have dielectric constants outside this range.

The technical approach used is to determine the front dielectric slab position and the delayed back slab position, both relative to the nominal body surface position, as shown in the cross-sectional image of a body part. Guided by information about the existence and surface location of an anomaly, as provided by the front end automatic target recognition algorithm, our algorithm determines if the object (a) is essentially lossless with a dielectric constant between 2 and 6, corresponding to high explosive, (b) contains bright reflectivity regions 1.5 times that of nominal skin, indicating a metallic object, or (c) is very lossy with a high dielectric constant, associated with a container filled with water-based liquid. If any of these conditions are met, further screening is necessary. To our knowledge, we are the only research group that is using this method—or any method that incorporates images that protrude or are depressed relative to the body surface.

C. Major Contributions

- Conceived and simulated the imaging response for the elliptical torus reflector “blade beam” reflector antenna. This fully multistatic nearfield imaging radar eliminates dihedral artifacts, provides high gain, can be operated quickly, and is less expensive than currently deployed AIT systems (2015).

[1] https://www.smithsdetection.com/products/eqo/

[2] http://www.sds.l-3com.com/advancedimaging/provision-2.htm

[3] Three-dimensional radar imaging techniques and systems for near-field applications, https://doi.org/10.1117/12.2229235

- Established a fast and robust algorithm for elliptical torus reflector imaging of experimentally measured data (2016).
- Developed an optimized feed distribution for efficiently gathering wide-angle radar signals across the entire 120-degree aperture (2017).
- Identified the source and developed an algorithm to correct for grating lobe artifacts from spatial undersampling of elements in receiver array (2018).
- Combined high resolution 2D multi-view angle "projected" images with the richer 3D raw reflectivity data to generate cross sectional slices and contour lines that indicate the shape of the body part as Figure 1 (2018).

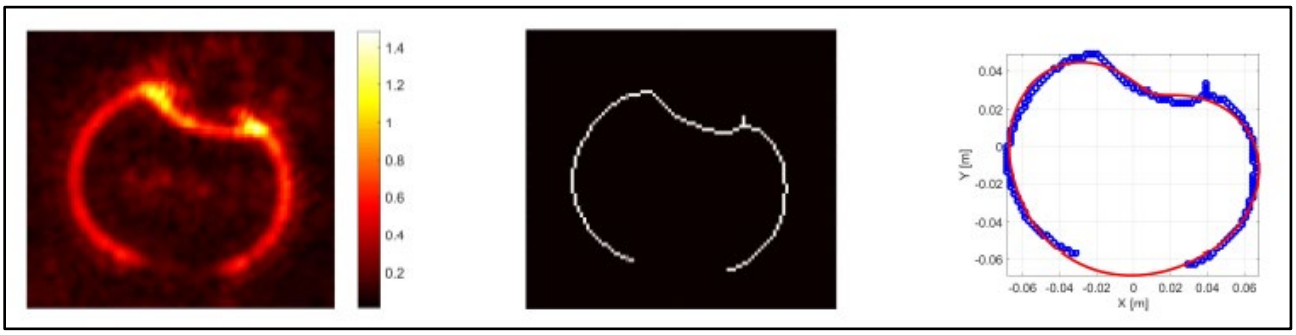

Figure 1: Reflectivity of a cross-section of the lower right thigh contour data of Figure 3 at z = 0.60 m with the depression due to the presence of an affixed slab of petroleum jelly (left), the extracted contour using Canny edge detector filter and morphological processing (middle), and seven-term Fourier series fit to blue contour data (right).

- Exploited the surface curvature and highlighted protruding objects, taking careful consideration of depth dimension (2019).
- Automatically determined the nominal scanned body surface with and without attached foreign objects using high definition advanced imaging technology (HD AIT) measured image data using a Fourier series in circumferential angle. Repeated the series fit after excluding poorly fitting contour points to generate the nominal body contour without the attached anomaly, as shown in Figure 2 (2019).

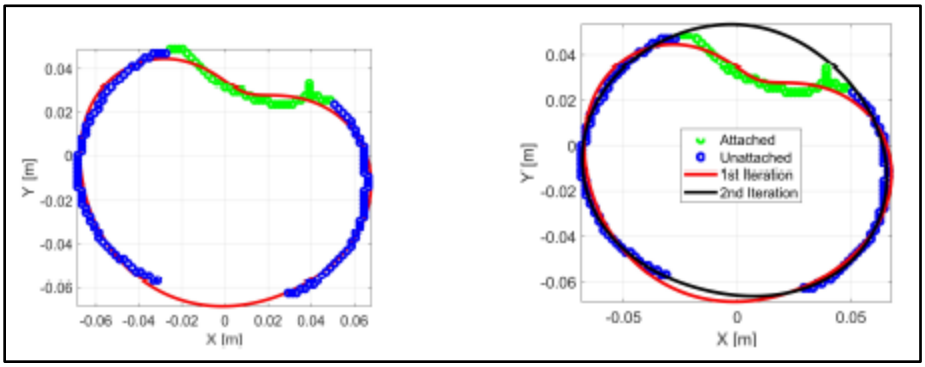

Figure 2: The extracted contour of Figure 1 with points each having a minimum distance from the red fit contour above a threshold value; (left) these thresholded points and all points between them are separated and shown with green color; (right) the second iteration of seven term Fourier series fit shown with black color using only the remaining blue points, and the black contour is used for the estimation of the nominal body surface position to characterize the affixed object.

- Determined the front foreign object reflection and the back (on skin) object reflection, as shown in Figure 3 (2019).

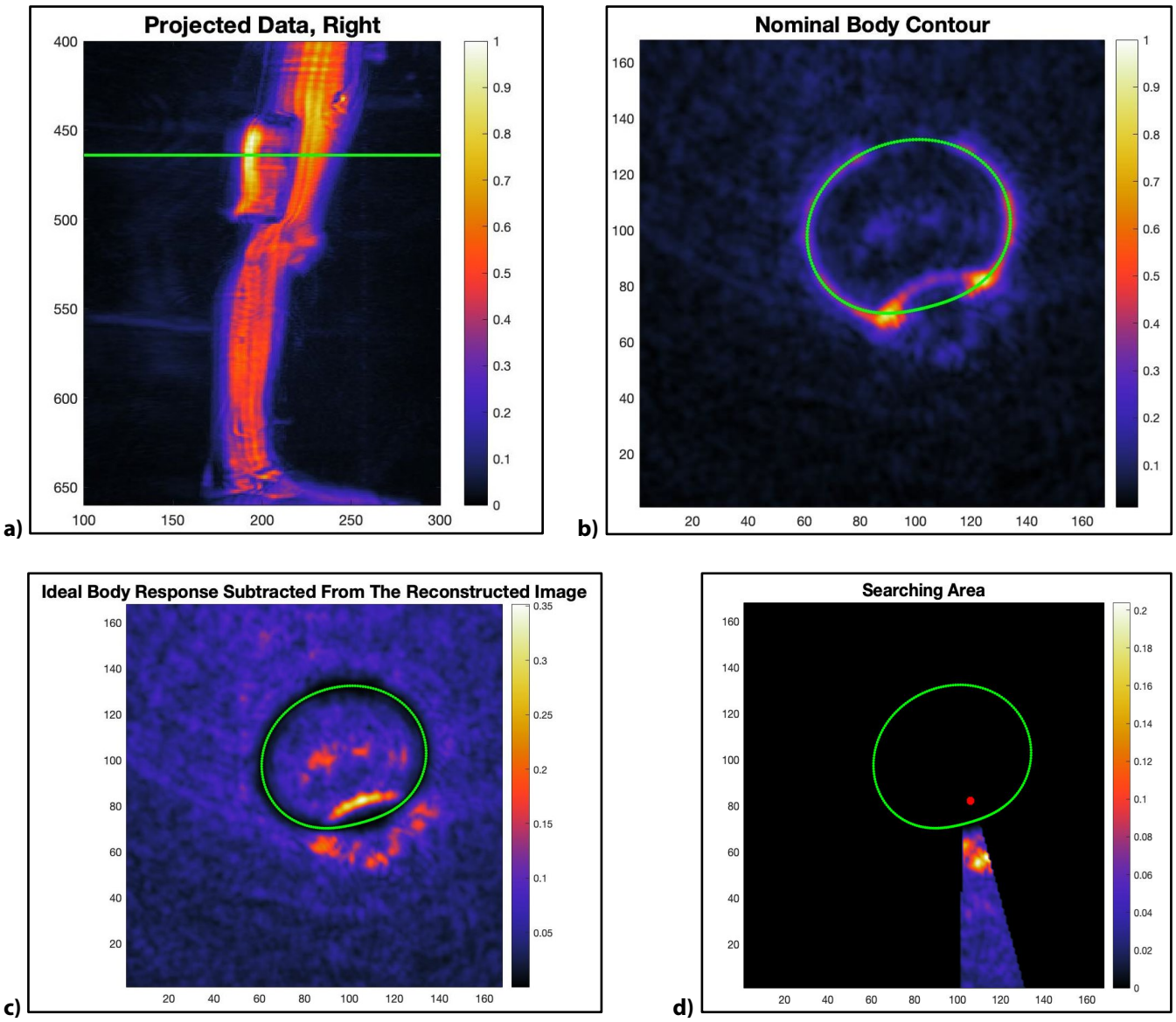

Figure 3: (a) Petroleum jelly attached to the lower right thigh; (b) green curve shows nominal body contour generated with a seven-term Fourier series in φ; (c) back surface of the dielectric displaced *d'* from nominal contour. By subtracting the ideal body response from the data, the displaced body pixels become dominant and can be found by thresholding the image; (d) front surface of dielectric extending *d* from nominal contour with red dot showing depressed body displacement.

- Used the imaged positions of these reflections to determine the dielectric constant and loss factor of the foreign object (2019).
- Configured the material characterization algorithm to automatically choose the appropriate cross-section slices, find the nominal body contour, isolate the anomaly response, determine its complex dielectric constant, and indicate the potential threat level for all parts of the body (2020).

D. Milestones

- All research milestones were met, and new milestones were established. These are (i) automatic application of the material characterization algorithm goes beyond the intended goal of R3-A.2, as it became part of an associated task order; (ii) support of the receiver/transmitter positioning error compensation effort shown in R3-A.3; and (iii) analysis of the effectiveness of the dual frequency combined point spread function concept applied to the elliptical torus reflector AIT system described in R3-A.3.
- The greatest hinderance for the project has been the unavailability of real measured image data for important common anomalies on the body. Requests have been made, and there is indication that new measurements at government laboratories are forthcoming, which, once received, will be used in the ongoing research under the task order "Maturation and Validation of Dielectric Characterization Algorithms" led by Professor Rappaport, which will continue until April 2021.

E. Final Results at Project Completion (Year 7)

The material characterization algorithm yields excellent results in predicting the complex permittivity for lossless materials, such as high explosives. In an example case study, the response from a bag of petroleum jelly is shown in Figure 3. The conventional projected image, shown in Figure 3a, clearly indicates an anomaly on the thigh (at the height of the green line), but it does not provide any guidance in identifying its material composition. The cross section with computed nominal body contour, shown in Figure 3b, shows weak responses due to the anomaly. Removing the strong body contour reflectivity and rescaling in intensity brings out the depressed anomaly back-surface/skin image, and an even weaker front-surface response, Figure 3c. Enhancing just the responses that are outside the body contour and in the vicinity of the back-surface response, shown in Figure 3d, highlights the front-surface response. Using the distances of the average back-surface response from the nominal contour *d*' and the average front-surface response from the body contour *d* (or object thickness), provides dielectric information that is within 3% of its ground truth of 2.15. This is done entirely automatically, with no operator intervention, which proves the automated algorithm works very well. Other tests have yielded similar results for dielectric materials of interest [17-20].

For typically found benign objects such as paper, leather, rubber, and alcohol, the loss tends to be larger than for threats. The back-surface response is either considerably lower than the front-surface response, or indistinguishable from the background entirely. This constitutes the distinguishing feature for these items. Containers filled with water-based liquids have very strong dielectric constants that display as strong deformations to the nominal body contour.

This method can be used to separate threats from benign objects in the security screening of people, thus reducing the number of body pat-downs needed.

III. RELEVANCE AND TRANSITION

A. Relevance of Research to the DHS Enterprise

The algorithms developed in this project are specifically tuned to existing wideband mm-wave portal systems. They have provided greater characterization of concealed threats, thereby reducing the probability of false alarms and thereby increasing efficiency and reducing wait time and labor.

B. Status of Transition at Project End

Algorithmic research is continuing in the form of the task order Maturation and Validation of Dielectric Characterization Algorithms until April 2021.

C. Transition Pathway and Future Opportunities

The characterization algorithm for wideband mm-wave scanners has been developed for Kaggle Prize data, but it is being configured to be platform independent. As such, AIT scanner vendors will be able to add our material characterization algorithm to their processing suite. Since the algorithm is flexible and fast, and well-supported by the Department of Homeland Security (DHS), it is likely that it will be accepted by the vendors.

D. Customer Connections

In the past twelve months and in the coming year, we have been having and will have biweekly telephone meetings with DHS representative Brian Lewis and monthly meetings with DHS's John Fortune as part of our Materials Characterization task order.

IV. PROJECT ACCOMPLISHMENTS AND DOCUMENTATION

A. Education and Workforce Development Activities

1. Student Internship, Job, and/or Research Opportunities
    a. Guanying Sun is pursuing research for her dissertation based on this project.
    b. Mahshid Asri completed her master's thesis based on this project.
    c. Elizabeth Wig completed her master's thesis based on this project.
    d. Femi Lampty has been a paid undergraduate researcher working on this project.
    e. Allison Care has been a volunteer researcher working on this project.

B. Peer Reviewed Journal Articles

Pending –

1. Sadeghi, M., Tajdini, M.M., Wig, E., & Rappaport, C. "Single Frequency Fast Dielectric Characterization of Concealed Body-Worn Explosive Threats." *IEEE Transactions on Antennas and Propagation*, accepted for publication.

C. Peer Reviewed Conference Proceedings

1. Asri, M., & Rappaport, C. "Automatic Permittivity Characterization of a Weak Dielectric Attached to Human Body Based on Using Wideband Radar Image Processing." *2019 IEEE International Symposium on Antennas and Propagation*, Atlanta, GA, July 2019.
2. Morgenthaler, A., & Rappaport, C. "Modeling Focused CW Mm-Wave Scattering of a Penetrable Dielectric Slab Affixed to a Human Body." *2019 IEEE International Symposium on Antennas and Propagation*, Atlanta, GA, July 2019.

3. Tajdini, M., & Rappaport, C. "Focused CW Mm-Wave Characterization of Lossy Penetrable Dielectric Slab Affixed to Human Body." *2019 IEEE International Symposium on Antennas and Propagation*, Atlanta, GA, July 2019.
4. Asri, M., Tajdini, M.M., Wig, E., & Rappaport, C. "Automatic Permittivity and Thickness Characterization of Body-Borne Weak Dielectric Threats Using Wideband Radar." *European Conference on Antennas and Propagation*, Copenhagen, Denmark, March 2020.
5. Sun, G., Nemati, M., & Rappaport, C. "Improving the Reconstruction Image Quality of Multiple Small Discrete Targets Using the Phase Coherence Method." *European Conference on Antennas and Propagation*, Copenhagen, Denmark, March 2020.
6. Tajdini, M.M., Jaisle, K., & Rappaport, C. "Image Radar Determining the Nominal Body Contour for Characterization of Concealed Person-Worn Explosives**."** *European Conference on Antennas and Propagation*, Copenhagen, Denmark, March 2020.

D. Other Presentations

1. Rappaport, C. "Multistatic 3D Whole Body Millimeter-Wave Imaging for Explosives Detection." *IEEE Distinguished Lecture*, University of Lund, Lund, Sweden, 5 March 5 2019.
2. Rappaport, C. "Multistatic 3D Whole Body Millimeter-Wave Imaging for Explosives Detection." *IEEE Distinguished Lecture*, Qualcomm, San Diego, 6 December 2019.

E. Student Theses or Dissertations Produced from This Project

1. Asri, M. "Automatic Characterization of Low-Loss Low-Permittivity Body-Born Threats Using Wideband Millimeter-Wave Radar." MS Thesis, ECE, Northeastern University, April 2020.
2. Wig, E. "Mathematical Models for Dielectrics on the Human Body Using Millimeter-Wave Security Scanners." MS Thesis, ECE, Northeastern University, April 2020.

F. Technology Transfer/Patents

1. Patents Awarded
   a. Martinez Lorenzo, J., & Rappaport, C. "Characterization of Dielectric Slabs Attached to the Body Using Focused Millimeter Waves." #10,416,094, 17 September 2019.

Year 6 Patent Not Previously Reported –

a. Gonzales Valdes, B., Martinez Lorenzo, J., & Rappaport, C. "On the Move Millimeter Wave Interrogation System with a Hallway of Multiple Transmitters and Receivers." #10,295,664, 21 May 2019.

V. REFERENCES

[1] J. Skorupski and P. Uchronski, "Evaluation of the effectiveness of an airport passenger and baggage security screening system," Journal of Air Transport Management, vol. 66, pp. 53–64, 2018.

[2] R. Sakano, K. Obeng, and K. Fuller, "Airport security and screening satisfaction: A case study of us," Journal of Air Transport Management, vol. 55, pp. 129–138, 2016.

[3] A. Knol, A. Sharpanskykh, and S. Janssen, "Analyzing airport security checkpoint performance using cognitive agent models," Journal of Air Transport Management, vol. 75, pp. 39–50, 2019.

[4] A. Pala and J. Zhuang, "Security screening queues with impatient applicants: A new model with a case study," European Journal of Operational Research, vol. 265, no. 3, pp. 919–930, 2018.

[5] D. M. Sheen, D. L. McMakin, and T. E. Hall, "Three-dimensional millimeter-wave imaging for concealed weapon detection," IEEE Transactions on microwave theory and techniques, vol. 49, no. 9, pp. 1581–1592, 2001.

[6] A. Angell and C. Rappaport, "Computational modeling analysis of radar scattering by metallic body-worn explosive devices covered with wrinkled clothing," in 2007 IEEE/MTT-S International Microwave Symposium, pp. 1943–1946.

[7] Y. Alvarez, B. Gonzalez-Valdes, J. A. Martinez-Lorenzo, C. M. Rappaport, and F. Las-Heras, "Sar imaging based techniques for low permittivity lossless dielectric bodies characterization," IEEE Antennas and Propagation Magazine, vol. 57, no. 2, pp. 267–276, 2015.

[8] J. A. Martinez-Lorenzo, F. Quivira, and C. M. Rappaport, "Sar imaging of suicide bombers wearing concealed explosive threats," Progress In Electromagnetics Research, vol. 125, pp. 255–273, 2012.

[9] J. Fernandes, C. M. Rappaport, J. A. Martinez-Lorenzo, and M. Hagelen, "Experimental results for standoff detection of concealed body-worn explosives using millimeter-wave radar and limited view ISAR processing," in 2009 IEEE Conference on Technologies for Homeland Security.

[10] S. Alekseev and M. Ziskin, "Human skin permittivity determined by millimeter wave reflection measurements," Bioelectromagnetics, vol. 28, pp. 331–9, 07 2007.

[11] S. I. Alekseev, A. Radzievsky, M. Logani, and M. C. Ziskin, "Millimeter wave dosimetry of human skin," Bioelectromagnetics, vol. 29, pp. 65–70, 01 2008.

[12] M. Sadeghi, E. Wig, A. Morgenthaler, and C. Rappaport, "Modeling the response of dielectric slabs on ground planes using CW focused millimeter waves," in 2017 11th European Conference on Antennas and Propagation, March 2017, pp. 759–763.

[13] M. Sadeghi and C. Rappaport, "Virtual source model for ray-based analysis of focused wave scattering of a penetrable slab on pec ground plane," in 2018 IEEE International Symposium on Antennas and Propagation & USNC/URSI National Radio Science Meeting. IEEE, 2018, pp. 1177–1178.

[14] M. Sadeghi, E. Wig, and C. Rappaport, "Determining the dielectric permittivity and thickness of a penetrable slab affixed to the human body using focused CW mm-wave sensing," in 2018 IEEE International Symposium on Antennas and Propagation & USNC/URSI National Radio Science Meeting. IEEE, 2018, pp. 621–622.

[15] M. Sadeghi, "Characterization of penetrable dielectric slab affixed to the human body using focused CW mm-waves," Master's thesis, Northeastern University, 2018.

[16] E. Wig and C. Rappaport, "Modeling focused ray scattering by a penetrable dielectric slab over skin surface with a finite air gap for millimeter-wave person scanning," in 2018 IEEE International Symposium on Antennas and Propagation & USNC/URSI National Radio Science Meeting. IEEE, 2018, pp. 1335–1336.

[17] D. J. Griffiths, "Introduction to electrodynamics," 2005.

[18] D. H. Staelin, A. W. Morgenthaler, and J. A. Kong, Electromagnetic Waves. Pearson Education, 1994.

[19] A. L. Higginbotham Duque, W. L. Perry, and C. M. Anderson-Cook, "Complex microwave permittivity of secondary high explosives," Propellants, Explosives, Pyrotechnics, vol. 39, no. 2, pp. 275–283, 2014. [Online].

[20] A. Von Hippel and W. B. Westphal. *Tables of Dielectric Materials. Volume 5*. Massachusetts Inst of Tech Cambridge Lab for Insulation Research, 1957.

This page intentionally left blank.

R3-A.3: Multi-Transmitter/Multi-Receiver Blade Beam Torus Reflector for Efficient Advanced Imaging Technology

I. PARTICIPANTS INVOLVED FROM JULY 1, 2019 TO JUNE 30, 2020

Faculty/Staff			
Name	**Title**	**Institution**	**Email**
Carey Rappaport	PI	NEU	c.rappaport@northeastern.edu
Jose Martinez	Faculty	NEU	j.martinez-lorenzo@northeastern.edu
Dan Busuioc	Consultant	DBC Group, Inc.	db.ipaq@gmail.com
Graduate, Undergraduate and REU Students			
Name	**Degree Pursued**	**Institution**	**Month/Year of Graduation**
Mohammad Nemati	PhD	NEU	TBD
Mahshid Asri	MS, PhD	NEU	5/2020 (MS), 5/2023 (PhD)
Muhammad Ghafoor	BS	NEU	5/2021
Maulik Patel	BS	NEU	5/2025
Emily Belk	BS	NEU	5/2023
Thomas Campion	BS	NEU	5/2022

II. PROJECT DESCRIPTION

A. Project Overview

We have developed a custom-designed advanced imaging technology (AIT) person-scanning system that represents the next generation of airport and other secure-area concealed object detectors. The currently employed systems are omnipresent in the United States and worldwide [1-4]. Our system uses an elliptical toroid reflector that allows multiple overlapping beams for focused wide-angle illumination to speed data acquisition and accurately image strongly inclined body surfaces. Building on the concepts and analysis of ALERT's project R3-A.1 [5-7], we have extended the blade beam reflector from a single illuminating antenna into a multibeam toroidal reflector, with multiple feeds. Each feed generates a different incident beam with different viewing angles, while still maintaining the blade beam configuration of narrow slit illumination in the vertical direction. Having multiple transmitters provides horizontal resolution and imaging of a full 110 degrees of body. Furthermore, the reflector can simultaneously be used for receiving the scattered field, with high-gain, overlapping, high-vertical-resolution beams for each transmitting or receiving array element. The multistatic transmitting and receiving array configuration sensing avoids dihedral artifacts from body crevices and reduces nonspecular dropouts [8, 9].

We have extended the toroidal-reflector–based system from a single fixed transmitter (Tx), swinging arc receiver (Rx) design, to a fixed array of seven transmitters with overlapping coverage (Figure 1). We have computationally simulated, designed, and fabricated radar modules; designed mounts; built a radio frequency (RF) switching network; and assembled and tested a fifty-receiver/seven-transmitter fixed array.

The designs for the fixed array of receivers and transmitters are shown in Figure 1. This configuration was the result of many man-hours of work: (i) we minimized the spacing while maintaining the appropriate distance between elements to mimic the performance of an array with about a third as many elements as previous studies; (ii) we positioned transmitters to block receivers minimally, keeping the antenna elements close enough to the mathematically ideal focal arc while allowing for assembly and fine-tuning for real-world optimal repositioning; (iii) we supported the radar module boards in high temperature conditions to ensure that the multistatic signals are received strongly for all target positions from -55 to 55 degrees, and (iv) we designed to allow for heat-sink attachments. We have simplified the cabling and positioning infrastructure for easy and fast channel assignment.

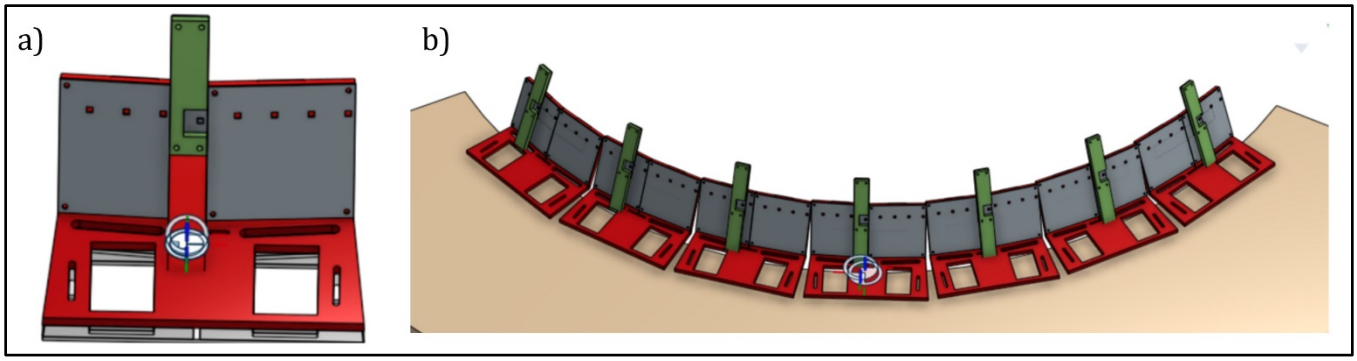

Figure 1: SolidWorks designs of (a) the front view of an individual mount with (green) an attached transmitter board and (gray) two quad receiver boards, showing (small red squares) antenna element positions; and (b) the full seven-mount, fifty-six–receiver array.

B. State of the Art and Technical Approach

The toroidal reflector antenna images in the horizontal plane and translates vertically. As such it acquires signals faster and is prone to fewer mechanical alignment, ruggedness, and wear operation issues than 2D raster scan systems [10]. The toroidal shape can be thought of as a surface of revolution, in which an elliptical profile is swept from -55 to 55 degrees in a 1.06 m circular arc about a vertical axis. The circular horizontal profile is well-approximated by infinitely many parabolas, each with focal length roughly half the circle radius and focal point on a concentric circular arc also having a radius of one half the circle radius. These approximate parabolic contours each act to collimate reflected horizontal rays, while the elliptical vertical contour focuses rays to the secondary focal point in a vertical plane. The resulting reflector reflects rays from any feed point on the focal arc into a "blade beam" that focuses to a line passing through the secondary ellipse focal point. Because of the circular symmetry of the toroidal reflector, there are infinitely many portions that produce blade beams, each inclined in horizontal azimuth. We choose seven equi-angular points on the focal arc for transmitter points, and fifty positions on the arc as receiver positions, as shown in Figure 1. The elliptical contours are chosen as offset to the major ellipse axis to ensure the feeding antenna elements do not block reflected rays. This accounts for the antenna mounts being tilted backwards, which causes each element main beam to be directed upward.

The overall reflector configuration requires precision mounting but can in principle capture the entire front or back horizontal body cross-section practically simultaneously, with 7 × 50 channels (78% more than currently employed systems). In addition, the multistatic configuration avoids dihedral artifacts from body crevices and shadowing drop-outs. The signal processing is also more efficient—and motion artifacts can be reduced, since each horizontal cross-section contour can be computed separately, as soon as it is measured, instead of waiting to have all measurements at all antenna positions taken first.

C. Major Contributions

- Development of an elliptical torus reflector for overlapping multibeam transmission and reception for multistatic operation (2013).
- Fabrication of a reflector and experimental proof of principle (2014).
- Multistatic imaging with elliptical torus using an original Tx/Rx chipset (2015).
- Design of 60-GHz multistatic radar Tx and Rx modules, including separated motherboard/daughterboard configuration, as demanded by the manufacturer's revised specification (2016).
- Design of a separated 60-GHz wideband microstrip antenna (2017).
- Fabrication and testing of RF single Tx/Rx boards (2018).
- Debugging and imaging using individual RF Tx/Rx boards (2019).
- Design and fabrication of quad Rx motherboard and daughterboard to minimize packaging and cabling (2019).
- Correction of a subtle design flaw and second fabrication (2019).
- Debugging of twenty-seven fabrication-delayed quad receiver and transmitter boards (2020).
- Self-calibration protocol, hardware configuration and algorithm to compensate for random receiver and transmitter 180-degree phase errors (2020).
- Thermal compensation of entire test setup (2020).
- Development, testing, and implementation, of position compensation post-processing algorithm to refocus misaligned receiver array elements (2020).

D. Milestones

- Due to the COVID-19–related delays described in the next section, along with the abrupt cancellation of funding by Smiths following their reorganization, almost none of the major milestones originally established were attained. The automatic full 3D reconstruction of a mannequin body surrogate is still to be realized, and the implementation of the dual frequency imaging scheme has not been demonstrated.
- One important goal that was achieved was the demonstration that a fixed array of receivers and transmitters can operate faster than a rotating single receiver. This was a major deliverable at the outset of R3-A.3. Although 3D imaging is still being pursued, the unexpectedly challenging issues of hardware positioning and mounting were solved (Figure 2), as was the thorny issue of calibrating the receivers' starting signal values. This latter difficulty was another flaw in the chip design that resulted in random 180 phase variations. These were overcome by installing a pair of reference transmitters and receivers to correct for the sign flip whenever it occurred.
- New chips by sole source vendor ADI have been pursued to mitigate the random phase effects and significantly increase the operating bandwidth. But this also has been delayed indefinitely by the manufacturer due to performance failures and the COVID-19 shutdown.
- Another midcourse hardware mitigation strategy that was put into place was developing an algorithm to compensate for inaccurate installation of the extremely sensitive positioning. This is discussed in detail in the next section.

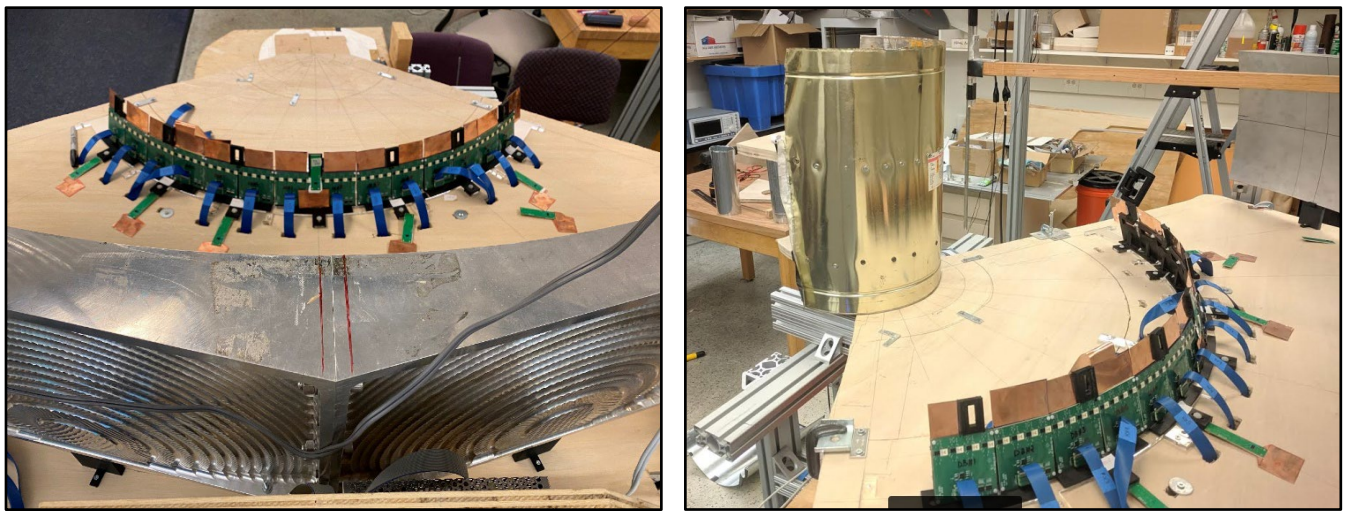

Figure 2: Two views of the fifty-six–element receiver and seven-element transmitter arrays, co-located on a circular arc and tilted to face the center plane of the elliptical torus reflector. The receivers (small grey squares) are mounted four to a board, and the transmitters are singly mounted on narrow green boards. The positions have been extensively analyzed, simulated, and optimized to measure the greatest amount of information in the limited space available.

E. Final Results at Project Completion (Year 7)

The progress on R3-A.3 has been disappointing in Year 7 because of four factors, two of which are due to COVID-19: (i) The custom fabrication of the radar modules was originally contracted to a firm in China in January, just as the country shut down in response to the novel coronavirus outbreak. After two months of uncertain delivery, we shifted the fabrication to a firm in New Hampshire, only to suffer the same stop-work, as COVID-19 and its lockdown reached the United States. The circuit boards were finally delivered, but Northeastern University (NU) shut down soon afterward. All told, the fabrication delay resulted in about three months of lost project time. (ii) Perhaps as a result of the reduced capacity of the fabricator, the quality of the circuit boards was inconsistent. The sole student who was permitted in the NU AIT lab had to painstakingly trace each of fourteen receiver boards and seven transmitter boards, debugging—and occasionally repairing—errors in the delivered hardware. In addition, it became apparent that the chips were generating excessive heat and needed extreme cooling measures. Heat sinks and cooling fans were designed, but high-power fans were required to keep the chip temperature within tolerance (Figure 3). After an additional two and a half months, the RF electronics were finally made operational within the expected performance parameters. (iii) The positions of the installed receivers and transmitters were found to be inexact, and the sensitive imaging results became totally garbled. Since the center wavelength of the radar system is 5 mm, a positioning error of just 2.5 mm would cause a phase error of 180 degrees, or 100% error. Despite great care in fabrication, this installation position error dominated the imaging (Figure 4). We found ways to compensate for it and refocus in postprocessing, but this also took time to develop. (iv) The graduate student, Mohmmad Nemati, who had been running the experimental facility since its inception, accepted full-time employment in May and left for California without completing his dissertation. Replacing him at this last date is problematic.

Figure 3: Elliptical reflector antenna with transmitters and receivers (orange) cooled by large fans. A metallic air duct cylinder body part surrogate target is positioned in the target region.

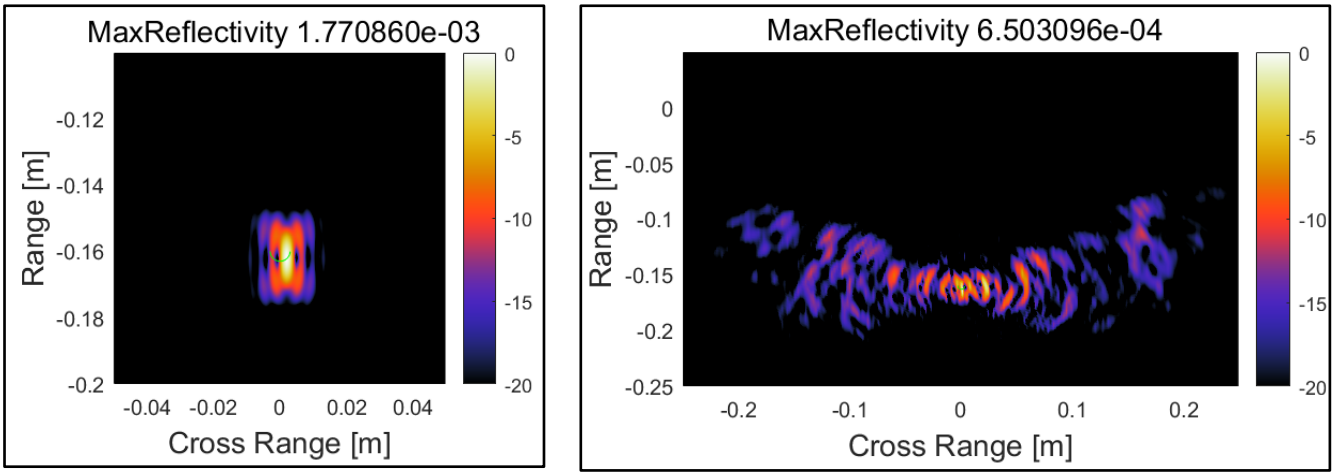

Figure 4: (a) Expected reconstructed image of a simulated thin vertical pole in cross section, producing a tight spot at the correct target position; (b) reconstructed image from experimentally measured radar data from inaccurately aligned receivers.

The most important contribution in R3-A.3 is the position compensation algorithm. This postprocessing algorithm corrects for the slight but extremely sensitive position errors in the hardware installation. Errors too small to measure mechanically cause significant defocusing and destroy the imaging. The example of reconstructing a de facto point scatterer is shown for a modeled case in Figure 4. For reconstruction of large structures, the imaging system must first accurately image the smallest point source objects. The image in Figure 4b clearly indicates the poor, unfocused image of a small localized scatterer. The problem comes from the excess path length between the installed receiver position and the ideal position that is assumed for the imaging algorithm.

The algorithm developed to compensate for the installation position error is simple in principle but challenging to implement. The first step is to determine the phase errors corresponding to the position error for the n^{th} receiver, relative to all the receivers. This can be done by observing the phase at the presumed location of the calibration poles. The difference between the expected phase and the observed phase for the n^{th} receiver, $\Delta\Phi_n$, is a measure of the defocusing. Graphically, this is seen as choosing the shortest distance from each straight receiver signal line in Figure 5b to the pole position (0, -0.15). Since the position error has two components, the phase difference for each receiver must be found for two calibration poles $\Delta\Phi_{n\binom{1}{2}}$.

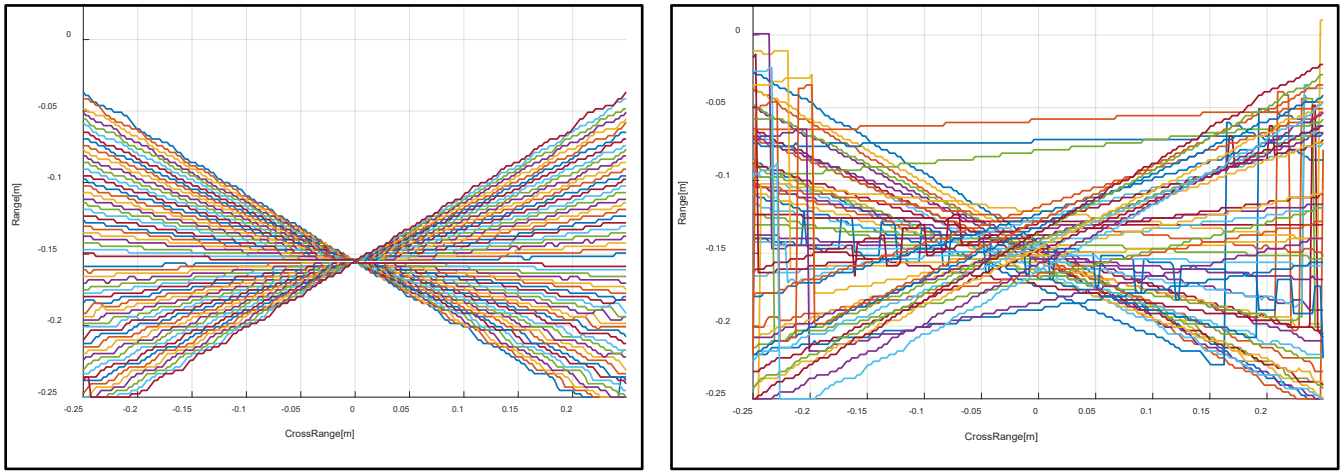

Figure 5: 1D inversions for each of fifty-six receivers separately (different color lines) when the scatterer is a thin metal pole located at (0, -0.15); (a) modeled inversion with no installed position error, indicating that all receivers constructively interfere only at the point target location and destructively interfere at other range and cross-range positions. The 1D images are straight lines for our particular antenna geometry, in which the reflector generates parallel (or plane wave) incident and received rays; (b) 1D inversions based on experimentally measured data using the AIT elliptical torus reflector, indicating five large excursions due to random 180-degree phase errors and many other errors due to inaccurately aligned receivers.

Next, the path length is found for rays traced from the n^{th} installed receiver back through the reflector along the collimated plane-wave rays in the midplane of the reflector to the target calibration pole position. In terms of the ideal receiver position, the installed position of the n^{th} receiver is $(\delta r_i, \theta_i) = \left(r_p - f_r\,, \theta_{n0}\right) + (\delta r_n, \delta\theta_n)$, where f is the offset parabolic reflector midplane section focal length, f_r is the radial component of the focal vector, and r_p is the radius of the torus. The last term is the positioning error, or distance that must be compensated for the n^{th} receiver. Phase is related to distance by $\Phi_n = -k\, r_n$. Assuming the position errors are small relative to the focal length, an effective linearization for each pole results in the phase difference as a simple function of perturbed distances for the n^{th} receiver:

$$\Delta\Phi_{n\binom{1}{2}} = k\left(\frac{f_r}{f}\,\delta r_n + y_{n\binom{1}{2}}\left(\frac{r_p}{f_r} - 1\right)\,\delta\theta_n\right)$$

where

$$y_{n\binom{1}{2}} = r_{\binom{1}{2}}\sin\left(\theta_{\binom{1}{2}} - \theta_{n0}\right)$$

Solving the pair of simultaneous linear equations (one for each pole), the error for the n^{th} receiver is then given by:

$$(\delta r_n, \delta\theta_n) = \left(\frac{f}{kf_r} \frac{y_{n1}\Delta\Phi_{n2} - y_2\Delta\Phi_{n1}}{y_{n1} - y_{n2}}, \qquad \frac{f_r(\Delta\Phi_{n1} - \Delta\Phi_{n2})}{k(f_r - r_p)(y_{n1} - y_{n2})} \right)$$

where r_1 and r_2 are the distances from the center of rotation of the torus to the n^{th} receiver and the first and second thin calibration poles, and θ_{n0}, θ_1, and θ_2 are the angles from the axis of symmetry to the n^{th} receiver and the first pole and the second pole, respectively. Once the position errors have been found, a phase difference correction $\Delta\Phi_{nm}$ for the n^{th} receiver at any image point at (r_m, θ_m) can be found using the first formula with $y_{n\binom{1}{2}}$ replaced with y_{nm}.

Only the receiver positions have been compensated for in the above development. The transmitter positions are also subject to alignment issues, but since they lie on the same focal arc as receivers, the same approach applies to compensate for their position errors.

An example of the effectiveness and precision of the algorithm is demonstrated for a modeled case where the receivers are randomly displaced in radial and angular directions. Thin metal poles at (*x*, *y*) = (-0.02, -0.14) and (0.035, -0.120) (positions are in meters relative to the axis of rotation of the toroidal reflector) are used as the calibration targets. Figure 6 shows the before-and-after compensation pairs of images for nine target position cases (three-by-three grid) in the images space. For each of the nine positions, the left image (before compensation) is smeared and unfocused with little information about where the target should be, while the right image (after compensation) looks almost exactly like the PSF of the point scatterer at the proper position.

Note that this method is much more efficient than reinverting the imaging equations using the derived installed receiver positions because it combines images—each weighted pixel by pixel—instead of recomputing the scattering matrix.

The next step is to apply the postprocessing position error compensation algorithm to collections of point targets, including large body-part surfaces. This will be our approach going forward.

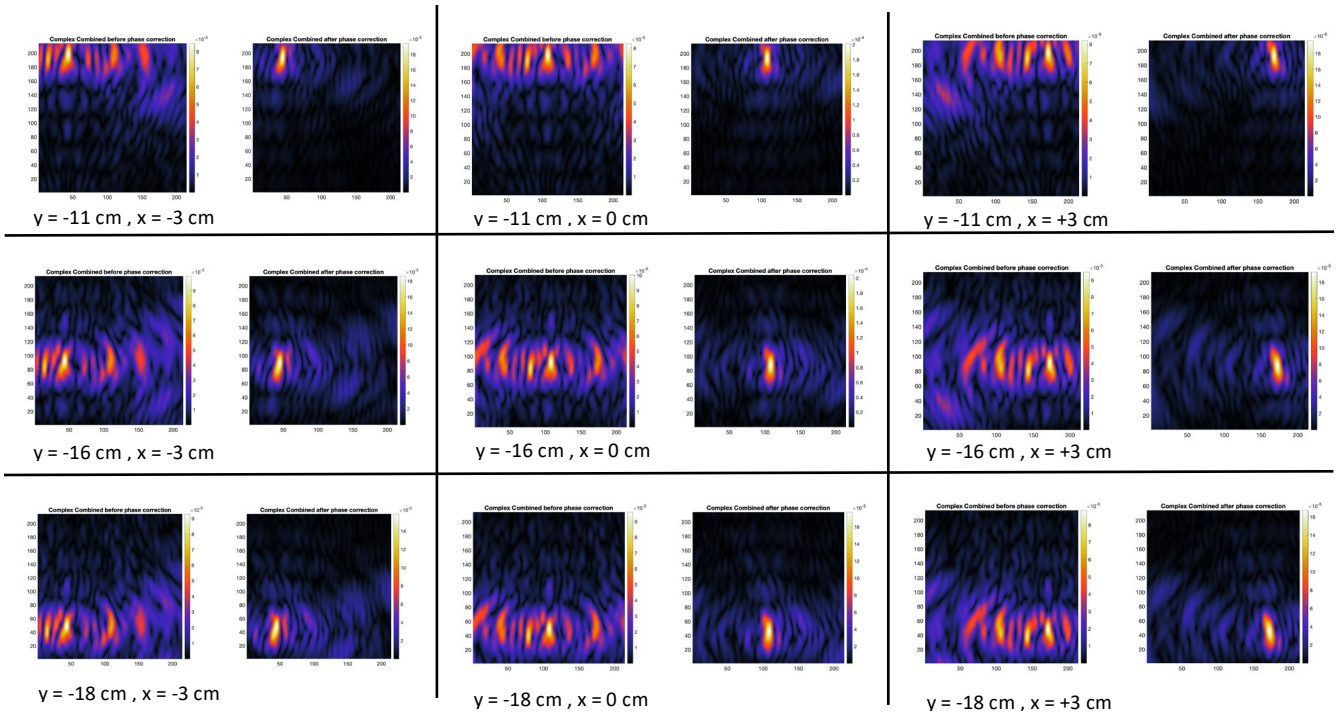

Figure 6: Simulated imaging of a single thin metal pole at nine locations, (left of each pair) without and (right of each pair) with receiver position compensation postprocessing. Receivers have independent random installation errors in both radial and circumferential directions, not exceeding half wavelength (±2.5 mm). These errors defocus the reconstructed image, resulting in smearing and disorganization, while the compensated processed image is crisp, tight, and positioned exactly at each of the various pole positions.

III. RELEVANCE AND TRANSITION

A. Relevance of Research to the DHS Enterprise

- **Relevance #1:** Faster, artifact-free, multistatic (shadow-free) imaging has been important to AIT since TSA's inception. R3-A.3 provides experimental proof that revolutionary improvements are attainable within the constraints of the current concept of operation. By eliminating the shadowing inherent in multimonostatic or bistatic radar, the images of the inside portion of each leg and arm will not suffer from gaps of missing data in the reconstruction. More work is needed to fully demonstrate the reflector-based nearfield imaging radar, but the basic concept is sound.
- **Relevance #2:** The cost for our multistatic design has been shown to be lower than the currently fielded systems. This is due to commercial off-the-shelf 60-GHz radio receiver and transmitter chips that have been repurposed as radar modules. The cost for each module is less than $100, so a seven-transmitter, fifty-receiver multistatic radar would cost about $17 per channel. The processing requires analog-to-digital converters and computer CPU processors, but these costs are low for volume purchasing.
- **Relevance #3:** As R3-A.3 has been developed in conjunction with the algorithm development project R3-A.2, it is automatically well suited for incorporating material characterization. The multistatic reflector-based nearfield radar automatically measures the thickness of foreign objects on the body and can be used to determine the dielectric constant of weak dielectric slabs. This is particularly relevant as a means of ruling out innocent objects, such as cash in a money belt, while alarming on explosive slabs.

B. Transition at Project End

Because of the management realignment and the reprioritization of research and development work at our primary partner, Smiths Detection, our major deliverable in R3-A.3 was cancelled. As such, our plans for transition have not been successful. There is still interest in the experimental AIT project, but commitment of funds is not forthcoming.

C. Transition Pathway and Future Opportunities

We continue to explore improvements in AIT design with both Smiths Detection and Rapiscan, despite scientific staff changes at each organization. Our main proponent at Smiths was laid off due to business activity reduction during the COVID-19 shutdown. We are considering joint proposals to DHS, including the current DHS BAA (HSHQDC-16-R-B0004).

D. Customer Connections

- Christopher Gregory, Smiths Detection, monthly calls
- Dan Strellis, Rapiscan, quarterly calls, occasional email

IV. PROJECT ACCOMPLISHMENTS AND DOCUMENTATION

A. Education and Workforce Development Activities

1. Student Internship, Job, and/or Research Opportunities
    a. Mohammad Nemati is completing his doctorate with a dissertation based on this project.
    b. Guanying Sun is pursuing research for her dissertation using data from this project.
    c. Mahshid Asri completed her master's thesis using data from this project.
    d. Muhammad Ghafoor, Christos Tsevis, Maulik Patel, Thomas Campion, and Emily Belk have been volunteer undergraduate researchers working on this project.

B. Peer Reviewed Conference Proceedings

1. Tajdini, M., & Rappaport, C. "Focused CW Mm-Wave Characterization of Lossy Penetrable Dielectric Slab Affixed to Human Body." *2019 IEEE International Symposium on Antennas and Propagation*, Atlanta, GA, July 2019.
2. Asri, M., & Rappaport, C. "Automatic Permittivity Characterization of a Weak Dielectric Attached to Human Body Based on Using Wideband Radar Image Processing." *2019 IEEE International Symposium on Antennas and Propagation*, Atlanta, GA, July 2019.
3. Morgenthaler, A., & Rappaport, C. "Modeling Focused CW Mm-Wave Scattering of a Penetrable Dielectric Slab Affixed to a Human Body." *2019 IEEE International Symposium on Antennas and Propagation*, Atlanta, GA, July 2019.
4. Sun, G., Nemati, M., & Rappaport, C. "Improving the Reconstruction Image Quality of Multiple Small Discrete Targets Using the Phase Coherence Method." *European Conference on Antennas and Propagation*, Copenhagen, Denmark, March 2020.

C. Other Presentations

1. Rappaport, C. "Multistatic 3D Whole Body Millimeter-Wave Imaging for Explosives Detection." *IEEE Distinguished Lecture*, Qualcomm, San Diego, CA, 6 December 2019.
2. Rappaport, C. "Multistatic 3D Whole Body Millimeter-Wave Imaging for Explosives Detection." *IEEE Distinguished Lecturer* speech, University of Lund, Lund, Sweden, 5 March 2019.

D. Student Theses or Dissertations Produced from This Project

1. Asri, M. "Automatic Characterization of Low-Loss Low-Permittivity Body-Born Threats Using Wideband Millimeter-Wave Radar." MS Thesis, ECE, Northeastern University, April 2020.

E. Technology Transfer/Patents

1. Patents Awarded
   a. Martinez Lorenzo, J., & Rappaport, C. "Characterization of Dielectric Slabs Attached to the Body Using Focused Millimeter Waves." #10,416,094, 17 September 2019.

Year 6 Patent Not Previously Reported –

a. Gonzales Valdes, B., Martinez Lorenzo, J., & Rappaport, C. "On the Move Millimeter Wave Interrogation System with a Hallway of Multiple Transmitters and Receivers." # 10,295,664, 21 May 2019.

V. REFERENCES

[1] J. Skorupski and P. Uchronski, "Evaluation of the effectiveness of an airport passenger and baggage security screening system," *Journal of Air Transport Management*, vol. 66, pp. 53–64, 2018.

[2] R. Sakano, K. Obeng, and K. Fuller, "Airport security and screening satisfaction: A case study of us," *Journal of Air Transport Management*, vol. 55, pp. 129–138, 2016.

[3] A. Knol, A. Sharpanskykh, and S. Janssen, "Analyzing airport security checkpoint performance using cognitive agent models," *Journal of Air Transport Management*, vol. 75, pp. 39–50, 2019.

[4] A. Pala and J. Zhuang, "Security screening queues with impatient applicants: A new model with a case study," *European Journal of Operational Research*, vol. 265, no. 3, pp. 919–930, 2018.

[5] Rappaport, C.M., and Gonzalez-Valdes, B., "The blade beam reflector antenna for stacked nearfield millimeter-wave imaging," *IEEE Antennas and Propagation Society Int'l Symp.*, pp.1-2, 8-14 July 2012.

[6] Gonzalez-Valdes, B., Y. Alvarez, J. A. Martinez-Lorenzo, F. Las-Heras, and C. M. Rappaport, "On the Use of Improved Imaging Techniques for the Development of a Multistatic Three-Dimensional Millimeter-Wave Portal for Personnel Screening," *Progress In Electromagnetics Research, PIER*, vol. 138, pp. 83-98, 2013.

[7] Alvarez, Y., Gonzalez-Valdes, B., Martinez-Lorenzo, J., Las-Heras, F., and Rappaport, C.M., "3D Whole Body Imaging for Detecting Explosive-Related Threats," *IEEE T. Antennas and Propagation*, vol. 60, no. 9, pp. 4453,4458, Sept. 2012.

[8] D. M. Sheen, D. L., McMakin, and T. E. Hall, "Combined illumination cylindrical millimeter-wave imaging technique for concealed weapon detection," *AeroSense, International Society for Optics and Photonics*, pp. 52-60, July 2000.

[9] D. M. Sheen, D. L. McMakin, and T. E. Hall, “Three-dimensional millimeter-wave imaging for concealed weapon detection,” *IEEE Transactions on Microwave Theory and Techniques*, vol. 49, no. 9, pp. 1581–1592, 2001.

[10] Cooper, K.B., Dengler, R.J., Llombart, N., Thomas, B., Chattopadhyay, G., and Siegel, P.H., "THz Imaging Radar for Standoff Personnel Screening," *IEEE T. Terahertz Science and Technology*, , vol. 1, no. 1, pp.169-182, Sept. 2011.

This page intentionally left blank.

R3-B.1: Hardware Design for "Stand-Off" and "On-the-Move" Detection of Security Threats

I. PARTICIPANTS INVOLVED FROM JULY 1, 2019 TO JUNE 30, 2020

Faculty/Staff			
Name	**Title**	**Institution**	**Email**
Jose Martinez	PI	NEU	jmartine@ece.neu.edu
Juan Heredia Juesas	Post-Doc	NEU	j.herediajuesas@neu.edu
Graduate, Undergraduate and REU Students			
Name	**Degree Pursued**	**Institution**	**Month/Year of Graduation**
Matt Skopin	PhD	NEU	12/2024
Weite Zhang	PhD	NEU	12/2022

II. PROJECT DESCRIPTION

A. Project Overview

As the problem of identifying suicide bombers wearing explosives concealed under clothing becomes increasingly important, it becomes essential to detect suspicious individuals at a distance. Systems that employ multiple sensors to determine the presence of explosives on people are being developed. Their functions include observing and following individuals with intelligent video, identifying explosives residues and/or heat signatures on the outer surface of their clothing, and characterizing explosives using penetrating X-rays [1–2], terahertz waves [3–5], neutron analysis [6–7], or nuclear quadrupole resonance (NQR) [8–9]. At present, radar is the only modality that can both penetrate and sense beneath clothing at a distance of 2–50 meters without causing physical harm.

The objective of this project was to develop and evaluate the hardware for an inexpensive, high-resolution radar that can distinguish security threats hidden on individuals at mid-ranges (2–10 meters) using an on-the-move configuration, and at stand-off ranges (10–40 meters) using a van-based configuration (see Figure 1).

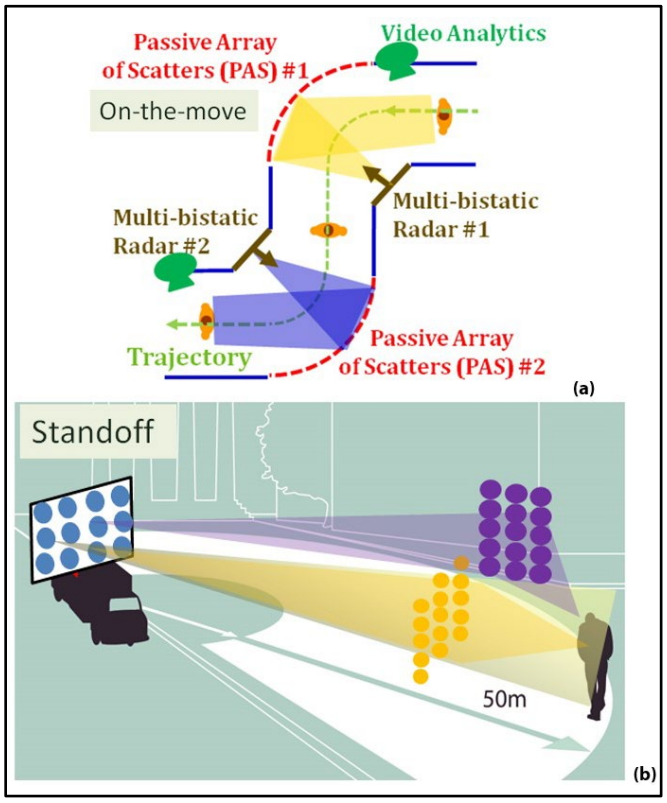

Figure 1: General sketch of the inexpensive, high-resolution radar system used for detecting security threats at (a) mid-ranges using an on-the-move configuration; and (b) stand-off ranges using a van-based configuration.

B. State of the Art and Technical Approach

As pointed out by the International Air Transport Association (IATA), being able to detect security threats without interrupting the motion of the person under scrutiny will be one of the most valuable features of the next-generation personnel screening systems [10]. Current state-of-the-art millimeter-wave (mm-wave) imaging systems for security screening require people to stop and stand in front of the scanning system. Mm-wave generation and acquisition is achieved with a static array of transmitter (Tx) and receiver (Rx) modules [11–12], or movable arrays that create planar [13–14] or cylindrical [15–17] acquisition domains. Most of them are based on monostatic radar and Fourier inversion [11–15]. Monostatic imaging system limitations are mainly related to the appearance of reconstruction dihedral artifacts, as described in [17–19].

The scope of this project was to develop the first inexpensive, high-resolution radar system with a special application to detect and identify potential suicide bombers. Its uniqueness was based on its ability to deploy multistatic configurations [20–23], in which the information from multiple receivers and transmitters are coherently combined by using a common local oscillator. This project had the potential to be the first radar system that is capable of functioning at multiple ranges for both indoor and outdoor scenarios. Unfortunately, limitations on available hardware prevented the realization of the system by the summer of 2020. However, work will continue on the project leveraging non-DHS funding sources with the aim of demonstrating a working system.

Our research program evolved from a 3D imaging mechanical system (Generation 1, Gen-1 [24]) to an intermediate imaging system (Gen-2) capable of imaging small targets in a fully electronic fashion and then to a fully electronic scanning 3D imaging system (Gen-3 [25–26]). The major contributions toward the Gen-3 system are discussed next.

C. Major Contributions

A summary of the Year 7 major contributions follows.

C.1. Hardware Design and Integration of a Multiple-Bistatic Imaging System

- Outcome 1.1: Mechanical assembly of the radar system toward 1,152 multiple-input multiple-output (MIMO) channels
- Outcome 1.2: Design and fabrication of an active phased array and reflect arrays
- Outcome 1.3: Setup of new hardware gantry with four compressive reflector antenna (CRA) arrays

C.2. Calibration Algorithm for Coherent Image Formation in Multiple-Bistatic Imaging System

- Outcome 2: 3D calibration for producing 3D images for the Gen-3 systems

C.3. Imaging Results Using the Multistatic Millimeter Wave Radar System Configuration

- Outcome 3.2: Fully electronic 3D imaging at the 1–2 m range using the modular Gen-3 mm-wave radar system
- Outcome 3.1: Simulation of a system using an array of CRAs

D. Milestones

As we stated in last year's plan, two goals were set for this year:

- Showing preliminary experimental results of real-time imaging using multiple CRAs and HXI's front-end modules.
- Designing a new front end that is more cost-effective and electromagnetically robust than one based on HXI's modules would be.

On one hand, thermal drift and hardware instability of the initial front-end design hindered our ability to achieve the first goal.

On the other hand, important progress was made toward reaching the second goal. Milestones achieved toward reaching the aforementioned goals follow.

D.1. Hardware Design and Integration of a Multiple-Bistatic Imaging System

D.1.a. Mechanical Assembly of the Radar System toward 1,152 MIMO Channels

This year we improved our hardware system, which now possesses the following elements:

- Seven HXI #8302 transmitter (Tx) modules, including one Tx module on the calibration gantry
- Seven HXI #8301 receiver (Rx) modules, including one Rx module for on the calibration gantry
- One HXI #8303 local oscillator module (LOM)
- Fourteen HXI #HSWM41203 single-pole four-throw (SP4T) 4-way antenna switches

The maximum number of available channels in the previous version of the system was 576 (6 transmitter modules × 4 transmitting ports × 6 receiver modules × 4 receiving ports). This configuration enables only the imaging of the front part of the body. To be able to have a fully on-the-move system, the number of coherent channels will need to be doubled. Not only is the electromagnetic stability and thermal drift of HXI's components lacking but also the cost of each transmitting and receiving module is much higher when compared to other alternatives that have reached the market within the last two years. For this reason, this year we not only tried to perform the on-the-move imaging using our current radar components but we also explored more cost-effective and reliable mm-wave radar chips on the market. In pursuit of a system with 1,152 channels, which will afford us ultra-high sensing capacity to image the front and back of a moving person, this year we have tested and validated some off-the-shelf mm-wave mixers (up-converters and down-converters). Those mixers are much more compact and can support much higher output power compared to the current ones. They can provide a better inherent coherence among different Tx/Rx paths, because they are integrated and built in a single printed circuit board (PCB) with one monolithic microwave integrated circuit (MMIC). The latter will reduce the complexity of the calibration procedure when multiple Tx/Rx are used, and it can simplify the use and reliability of the imaging system. Most importantly, those mixers can support user-defined baseband signal input, and as a result of this, we can now perform wave coding by predigital signal processing, including but not limited to the following:

- Binary phase coding of frequency modulated continuous wave (FMCW)
- Orthogonal frequency-division multiplexing of FMCW

These signal processing capabilities resulted in higher signal-to-noise ratio when compared to our previous time-switched MIMO arrays. This year we have also added additional four-way power dividers to the local oscillator (LO), so that additional LO lines are available for the newly introduced mixers. Theoretically, the new augmented LO module has the capability to operate with up to twenty-eight transmitting modules and twenty-eight receiving modules, which is an important increment when compared to the limit of our previous configuration (thirteen transmitting modules and thirteen receiving modules).

D.1.b. Design and Fabrication of an Active Phased Array and Reflect Arrays

Adding active phased arrays in each transmitting and receiving module will also result in a reduction of hardware complexity and imaging speed. This year, we further designed the active phased array. During last year's experiments, we found that our previous phased arrays worked very well for only a limited amount of time. The main reason for this was that the boards were not very stiff, and this made some phase-shift diodes dislodge from the boards. We also observed that our previous substrate combination (RO3003 with RO440F) presented additional manufacturing challenges, since RO4450F showed a reduced peel strength that challenged our foil lamination process.

This year, we have addressed such problems by switching to a RO3003G2 substrate. Specifically, we redesigned our PCB stickup using an RO3003G2 core with FR-4 epoxy underneath, which resulted in enhanced board strength. All the functional units—including the phase shifters, waveguide-to-microstrip transition, antennas, and others—were redesigned under the new stack-up design. Figure 2 shows the S-parameters of two face-to-face waveguide-to-microstrip transitions using new PCB substrates. The return loss was higher than 10 dB after 73.5 GHz. This can be further optimized in the future if this project continues under other DHS funding.

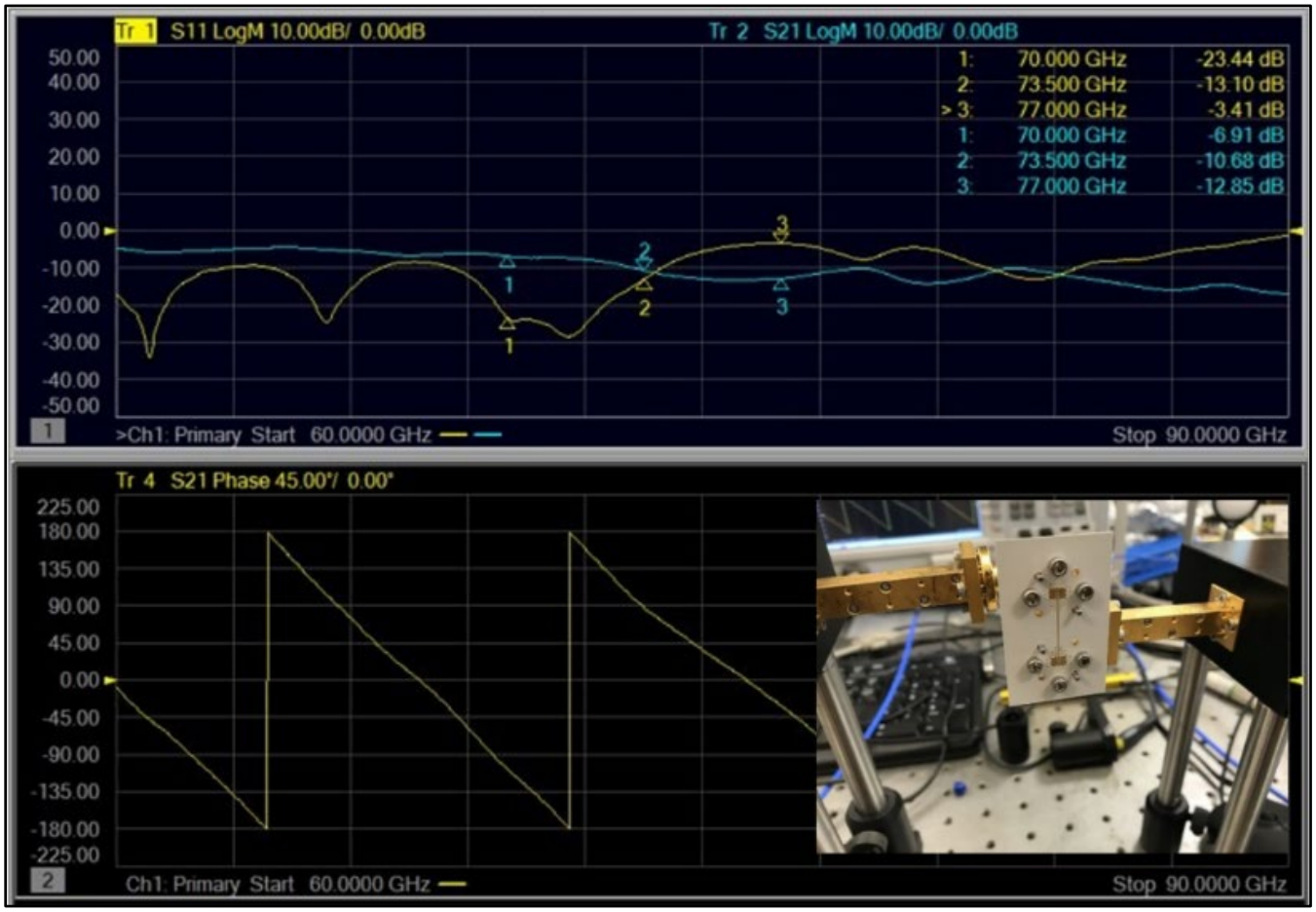

Figure 2: S-parameters of two face-to-face waveguide-to-microstrip transition using new PCB substrates.

This year, we have designed better phase shifters using a 4×4 Butler matrix on microstrip lines. Figure 3 shows the structure of the 4×4 Butler matrix, and Figure 4 shows its ability to steer the beams at 70, 73.5 and 77 GHz, respectively.

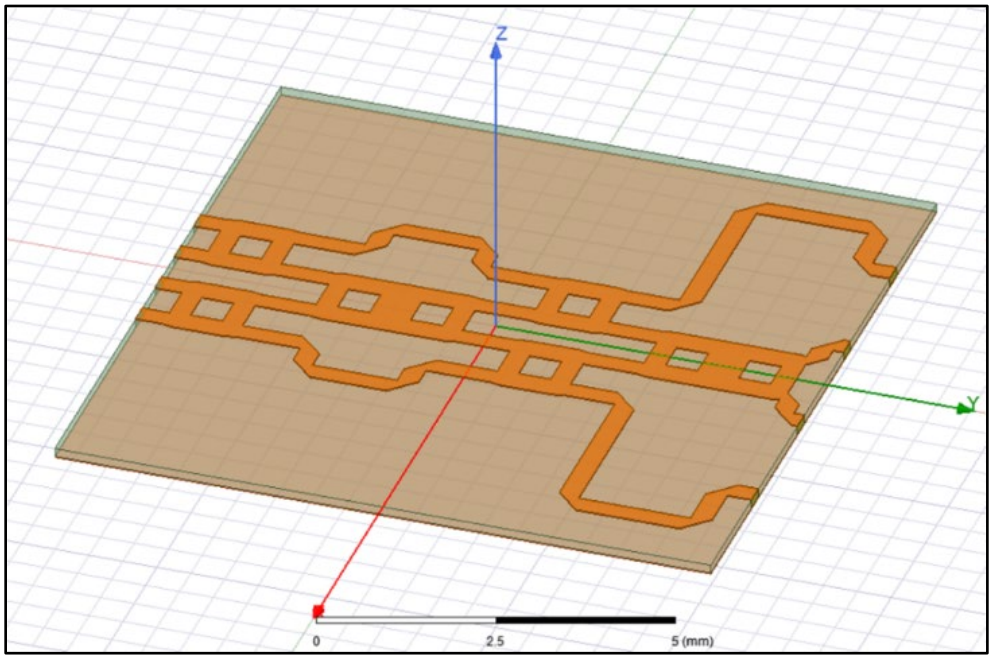

Figure 3: Structure of 4×4 Butler matrix phase shifters.

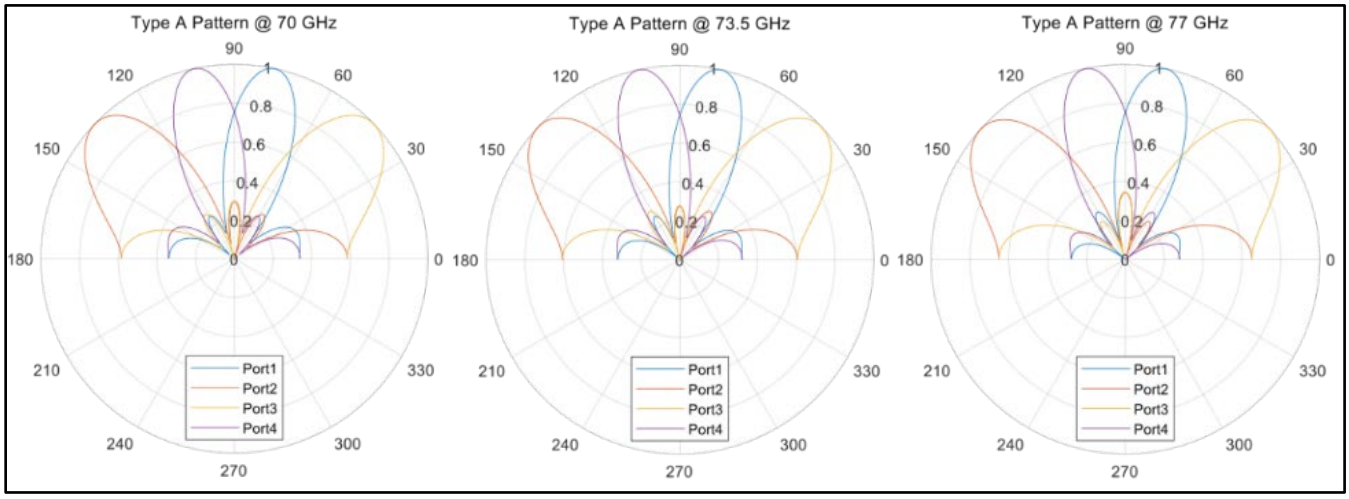

Figure 4: Simulated patterns of 4×4 Butler matrix phase shifters.

This year, we have also used a substrate integrated waveguide (SIW) to provide beam steering. The SIW uses a dielectric substrate with two rows of metallic via-holes, which connect the upper and lower metallic plates. Two SIW designs were carried out this year. The first design is a 2D array that used two 3 dB couplers, as shown in Figure 5. The second design is a 1D array that used a Butler matrix, as shown in Figure 6. The first design can be used with an HXI switch, so that a reduction in grating lobes and better imaging is achieved. The second design can be combined into a cross-shape area array for the new transmitting and receiving modules, so that reduction in granting lobes and better imaging performance is achieved.

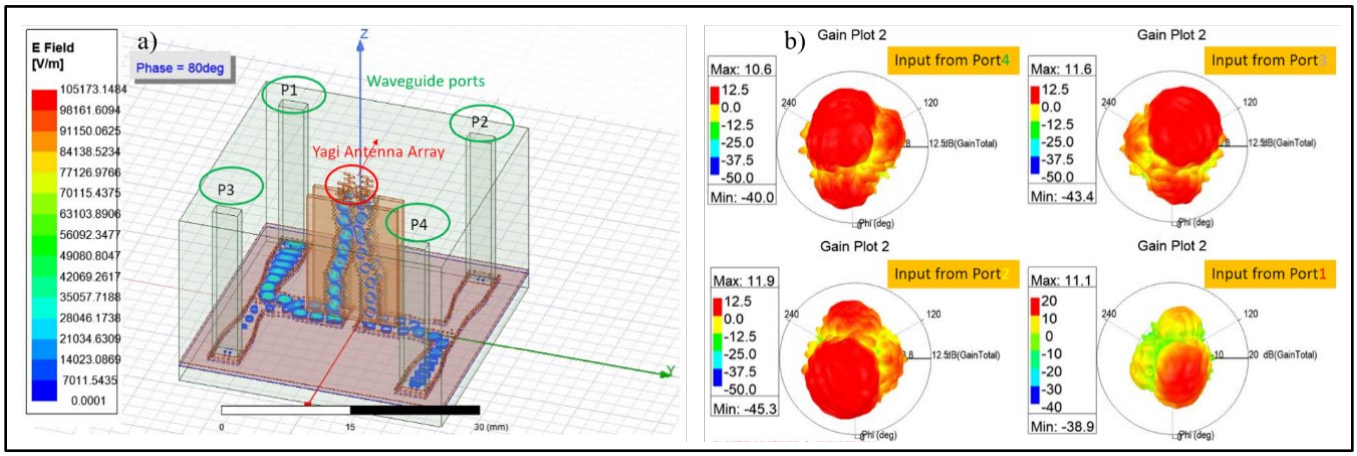

Figure 5: (a) The structure of 2D phased array; (b) simulated pattern.

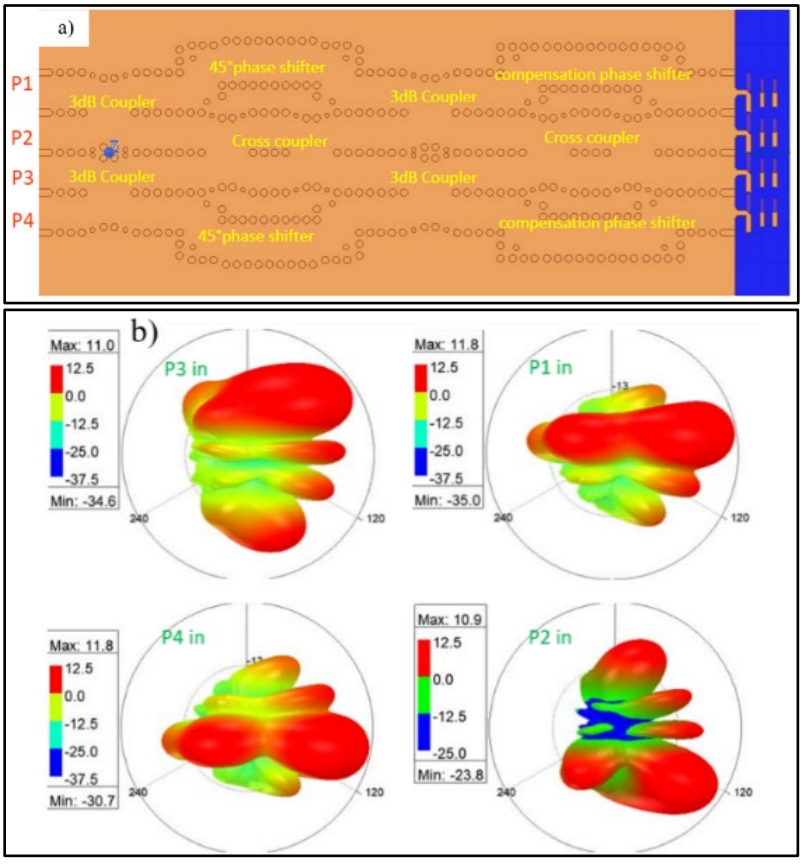

Figure 6: (a) The structure of 1D phased array; (b) simulated pattern.

D.1.c. Setup of New Hardware Gantry with Four CRA Arrays

This year, we have also finalized the new gantry of the CRA imaging system. In Figure 7, the front view of the CRA imaging system is shown in (a), and the back view of the system is shown in (b). The new gantry accommodates four separate arrays of CRAs, which are placed at the four corners of the imaging system. This configuration enables the system to image both front and back of the moving target. Each CRA array supports up to four vertical CRAs, and each one is fed by a MIMO array composed of three transmitting ports and four receiving ports. Each CRA array covers an area of 1.5 meters by 0.5 meters, which enables imaging of human-size targets.

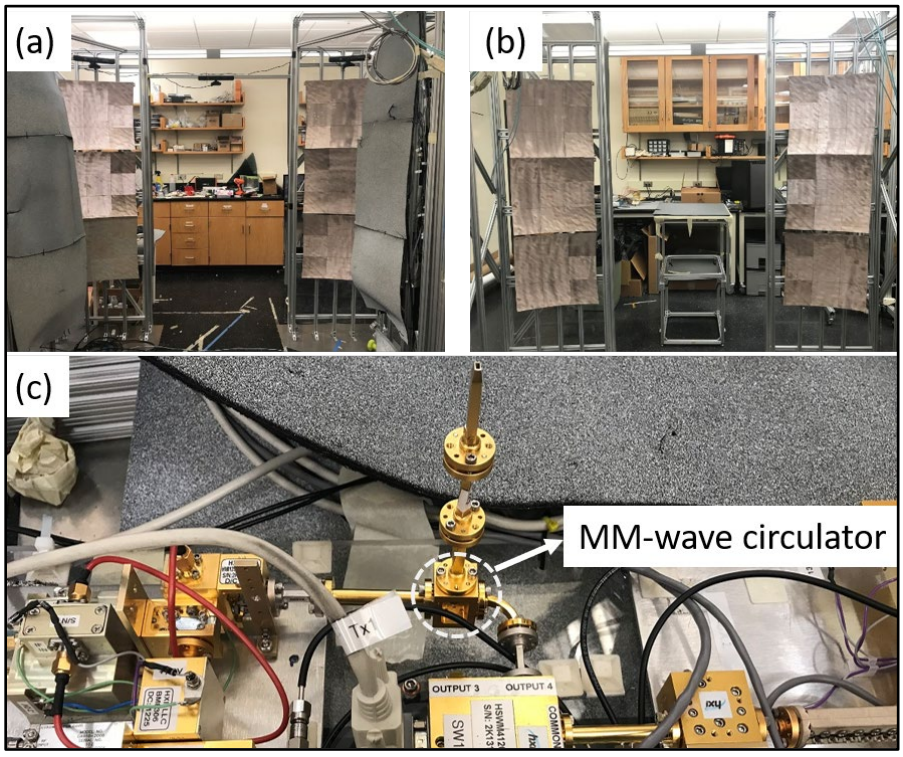

Figure 7: (a) Front view of the CRA imaging system; (b) rear view of the CRA imaging system; and (c) improved calibration configuration of the CRA imaging system.

D.2. Calibration Algorithm for Coherent Image Formation in a Multiple-Bistatic Imaging System

This year, we have advanced the calibration system of the CRA imaging system by using co-located scanning for both the moving transmitter port and the moving receiver port. This is achieved by using a mm-wave circulator, as shown in Figure 7(c). Both the moving transmitter and receiver are connected to the two ports of the circulator and use the common port to transmit and receive the electric fields. In this way, all the calibration fields for any static transmitters and receivers will have the same spatial coordinates, which will improve the accuracy of the calculated sensing matrix. We have also enabled near-field capture of both transmitters and receivers in a single calibration measurement, which can reduce the time for performing a calibration of the imaging system. As shown in Figure 7(c), an SP4T switch is attached to the Tx module to ensure that no power forms when the moving transmitter is coupled into the moving receiver. Although coordinate coherence was achieved, the additional interference between the moving transmitter and receiver modules was observed and had to be removed from the calibration fields to get a reliable sensing matrix. We measured such interferences by using a back-to-back setup, where the moving transmitter and receiver were directly connected, allowing us to enhance the sensing matrix.

D.3. Imaging Results Using the Multistatic Millimeter Wave Radar System Configuration

Preliminary imaging results for a single CRA were presented last year; these results are shown again, for completeness of reported work, in Figure 8 and Figure 9. These results shows that one CRA can image one part of the body relatively well. However, in order to image a human-size target, the coupling between adjacent CRA—each one having a different transmitting and receiving module—must be done.

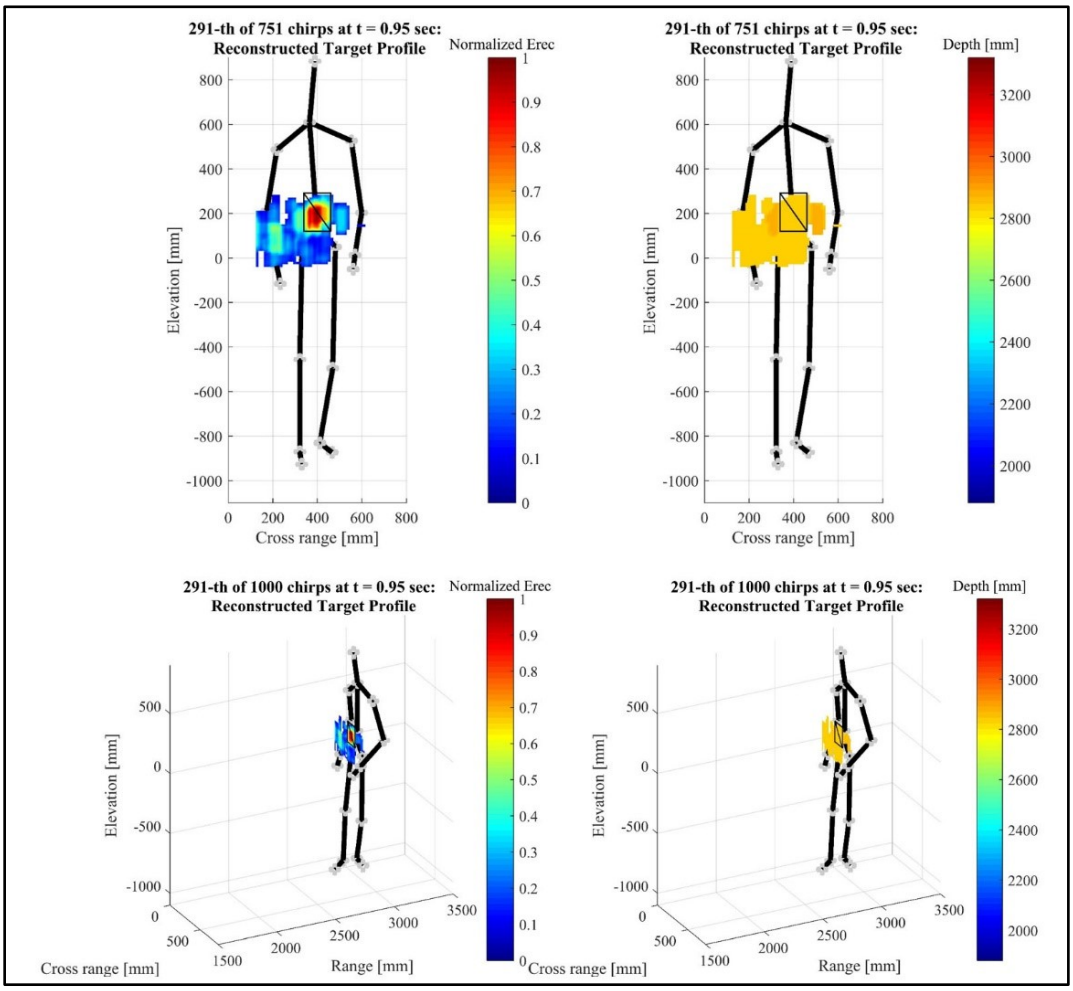

Figure 8: Mm-wave images for the on-the-move human body experiment with a metal box under clothing.

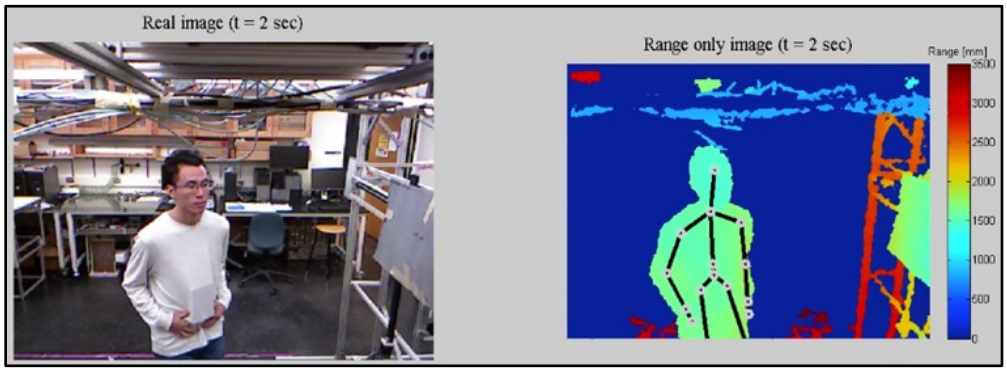

Figure 9: Video and 3D Kinect-based stereo camera images of the on-the move human body experiment.

This year, we aimed at coherently coupling several CRAs to image a human-size target. Our first approach consisted of performing the imaging using the numerically computed sensing matrix and measured electromagnetic fields. This approach was used for three different cases: imaging with the left-middle CRA, imaging with the right-middle CRA, and imaging with the coupling between the left-middle CRA and right-middle CRA. Corresponding imaging results can be seen in Figure 10, where a metallic box is used as a target.

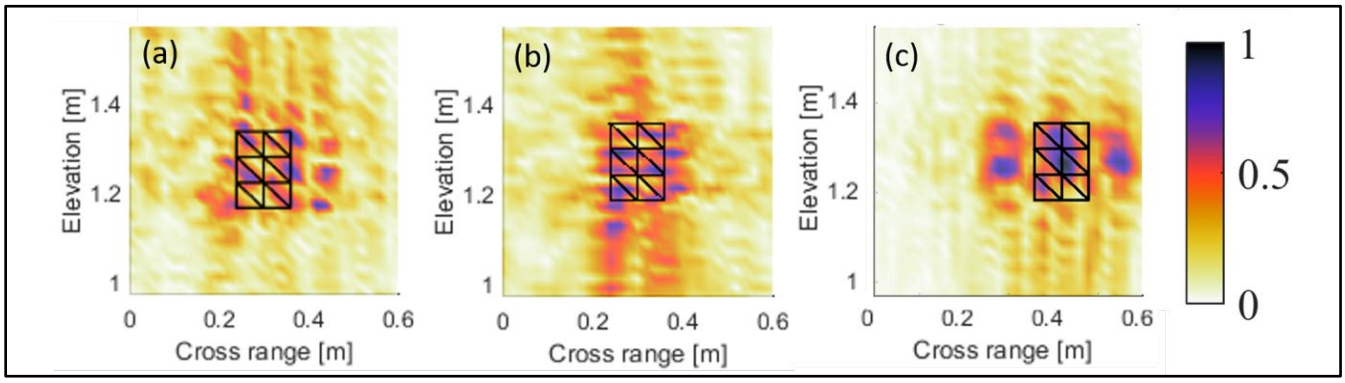

Figure 10: Results from experimental imaging of a metallic box; (a) left-middle CRA, (b) right-middle CRA, and (c) coupling between the left-middle CRA and right-middle CRA.

Our efforts to perform the imaging using multiple reflectors working in a coherent fashion has not been successful when using HXI's front-end modules. We have observed an important thermal drift that causes the measured transfer functions for the transmitting and receiving modules to be unreliable. Using the new low-cost modules has the potential to overcome this limitation. We will continue down this road by using funding from Professor Martinez's current National Science Foundation Faculty CAREER award.

D.4. Study of a New On-the-Move System Hardware and Configuration

D.4.a. Simulation of a System Using an Array of Compressive Reflector Antennas

This year, we also developed simulation models for the Gen-3 mm-wave radar system. In the simulation, we used four CRAs to perform the imaging of different targets. Figure 11 shows the imaging results when the target is a horizontal T-shaped metallic object. HXI's mm-wave switches restrict our ability to place the transmitting and receiving ports in an optimal location, thus making the reconstruction not as accurate as we would like. For this reason, the phased arrays described above—which provide better inter-element spacing—were designed, and their imaging results are presented in the next subsection.

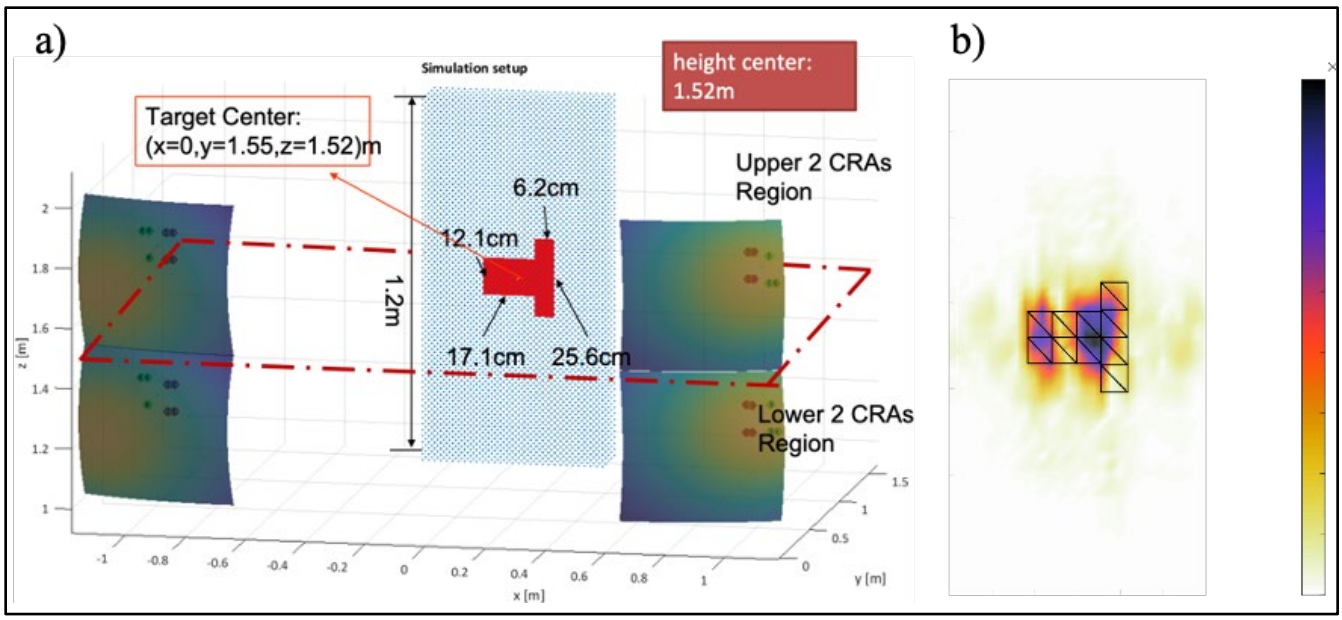

Figure 11: Simulation of four CRAs with a metallic box; (a) simulation setup; (b) corresponding imaging results.

D.4.b. Simulation of a System Using CRA with Active Phased Array

The imaging performance of the CRA system using the active phased arrays was also assessed this year. For the phased array antennas, we designed a plus-shaped antenna configuration with vertically placed Rx antennas and horizontally placed Tx antennas. Figure 12 shows the imaging results of a reversed T-shaped target using the antenna from our phased array. The distance between each antenna element is about two times of the wavelength associated with the center frequency. This result shows that the CRA system with active phased arrays successfully reconstructs the target profile. The active phased array has a good potential to decrease the volume and complexity of our Gen-3 system, where the bulky mm-wave front end of HXI's modules can be replaced with a PCB-based mm-wave front end.

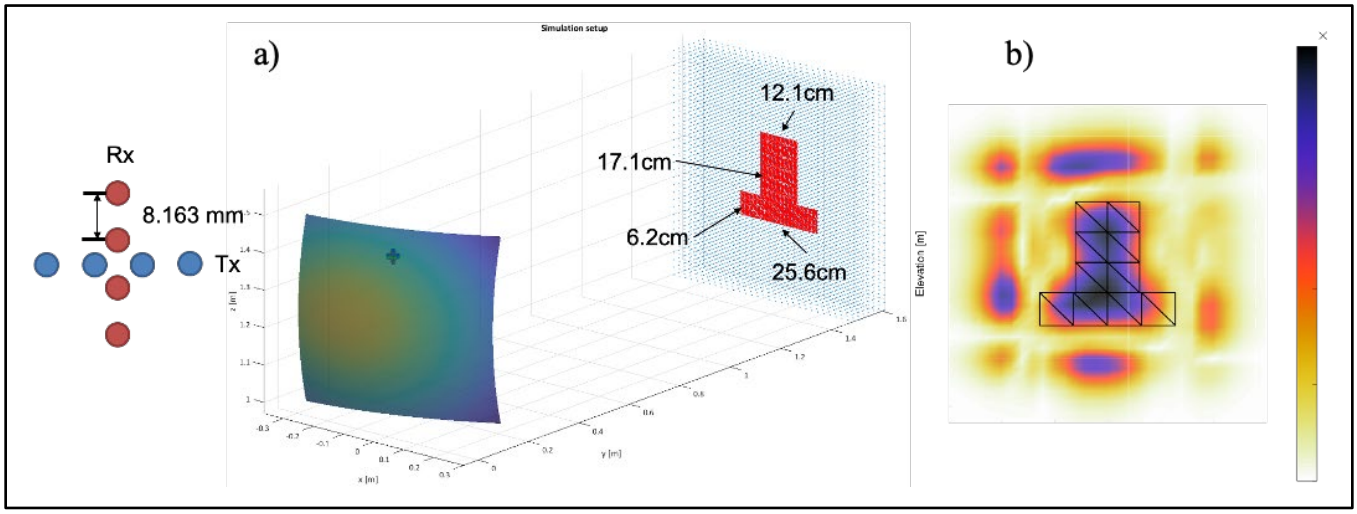

Figure 12: (a) Imaging setup using a plus-shaped array with a reversed T-shaped target; (b) imaging results.

E. Final Results at Project Completion (Year 7)

This project has achieved important milestones during the seven years of funding. These include, but are not limited to, the following:

1. Design from scratch of a mm-wave system to enable on-the-move imaging
2. Development of the mm-wave imaging algorithms
3. Mechanical design of the imaging system
4. Design and fabrication of arrays of CRAs

At the beginning of the project, we settled with HXI's front-end modules, which were probably the only option of functional modules working at 70–77 GHz. This choice, as well as its hardware limitation legacy experienced during the lifetime of the project, has hindered our ability to achieve coherence between multiple transceiver modules. After realizing this over the last year, we have shifted to address this problem by using different front-end modules that are smaller, provide digital signal processing, are more energy efficient, and are thermally stable. Though this project has concluded in the ALERT COE portfolio, we will continue to pursue this goal using the PI's NSF CAREER award. In addition, new funding will be sought from DHS and potentially other sources as well.

III. RELEVANCE AND TRANSITION

A. Relevance of Research to the DHS Enterprise

The following features of this project were of special relevance to the Department of Homeland Security enterprise:

- Noninvasive, minimally disruptive on-the-move scanning with quality imaging and high throughput; fast data collection, in less than 10 ms.
- Full body imaging with interrupted forward movement during mm-wave pedestrian surveillance; in multiview.
- A small number of nonuniform sparse arrays of Tx/Rx radar modules will minimize the cost of on-the-move; seven transmitters, seven receivers, and fourteen switches.

B. Status of Transition at Project End

Several companies (HXI, Smiths Detection, and Rapiscan) have collaborated with our research team on the tasks performed for the R3-B.1 project. This collaboration has played a pivotal role in the design, fabrication, integration, and validation of our radar system. Our Gen-3 prototype has the potential to be the first system capable of imaging moving targets at speed. The following steps will be taken to enable its transition to the market.

1. Professor Martinez hired a new Gordon Engineering Leadership student, Matt Skopin, who worked toward creating a deployable prototype to image security threats at speed. Matt has been in charge of making sure that the prototype is mechanically and electronically robust so it can be tested in the field.
2. Our prototype is modular and adaptable, so that fundamental research contributions developed at Professor Martinez's SICA lab (i.e., low cost mm-wave phased arrays and silicon-based chips) can be incorporated into our prototype without changing the architecture of the system.

C. Transition Pathway and Future Opportunities

Several companies (HXI, Smiths Detection, and Rapiscan) have been collaborating with our research team on the tasks performed for the R3-B.1 project. However, the PI has started a new spin-off, MatrixSpace, with Gregory Waters (CEO, greg.waters@matrixspace.com; former CEO of Integrated Device Technology), who is currently developing much lower cost mm-wave chips that can be used to increase resolution and performance of the system. This should be a viable solution to address the unreliable behavior of the current modules.

Transition goal #1: Exploring the use of MatrixSpace's mm-wave modules, which have lower cost, reduced drift, and enhanced reliability when compared to those of HXI. In pursue of this goal, we have already engaged in a conversation with MatrixSpace's Greg Waters, and we will explore the possibility of doing a joint demonstration by May 2021, the end of the no-cost extension period for ALERT funding.

D. Customer Connections

- HXI: Mr. Earle Stewart
- Smiths Detection: Dr. Kris Roe
- L3 Communications: Dr. Simon Pongratz
- MatrixSpace: Gregory Waters
- New proposals related to the topic of this research will be submitted to other federal funding agencies.

IV. PROJECT ACCOMPLISHMENTS AND DOCUMENTATION

A. Education and Workforce Development Activities

1. Interactions and Outreach to K–12, Community College, and/or Minority Serving Institution Students or Faculty
    a. The PI participated in the Building Bridges Program, which provides opportunities for high school students to visit the laboratories at Northeastern University and gain hands-on research experience, in order to engage them in STEM education.
    b. The PI participated in the Young Scholars Program at Northeastern University, in which two high school students spent six weeks in his lab learning about sensing and imaging.
2. Other Outcomes that Relate to Educational Improvement or Workforce Development
    a. Populating the research group with undergraduates brings homeland security technologies to undergraduate engineering students and establishes a pipeline to train and provide a rich pool of talented new graduate student researchers.

B. Peer Reviewed Journal Articles

Pending –

1. Heredia-Juesas, J., Molaei, A., Tirado, L., & Martinez-Lorenzo, J.A. "Consensus and Sectioning-Based ADMM with Norm-1 Regularization for Imaging with a Compressive Reflector Antenna." *IEEE Transactions on Antennas and Propagation*, under review. arXiv preprint:1811.05571.
2. Molaei, A., Tirado, L., Bisulco, A., Gehrke, C., Zhu, A., & Martinez-Lorenzo, J.A. "3D Printed Conical Horn Antenna Equipped with Orbital Angular Momentum Lenses for High-Capacity Millimeter-Wave

Applications." *IEEE Antennas and Wireless Propagation Letters*, under review.

C. Peer Reviewed Conference Proceedings

1. Heredia-Juesas, J., Tirado, L., Molaei, A., & Martinez-Lorenzo, J.A. "ADMM Based Consensus and Sectioning Norm-1 Regularized Algorithm for Imaging with a CRA." *2019 IEEE International Symposium on Antennas and Propagation and USNC-URSI Radio Science Meeting (AP-S/URSI 2019)*, Atlanta, GA, 7-12 July 2019.

D. Technology Transfer/Patents

1. Patents Awarded
    a. Martinez-Lorenzo, J. "Compressive coded antenna/meta-antenna." United States Patent 10,698,101, 30 June 2020.
    b. Martinez-Lorenzo, J., et al. "Ultrasonic-based system for detection of metallic security threats containers on cargo." United States Patent 10,477,785, 19 November 2019.
    c. Rappaport, C., & Martinez-Lorenzo, J. "Characterization of dielectric slabs attached to the body using focused millimeter waves." United States Patent 10,416,094. 17 September 2019.
2. Licenses Issued
    a. MatrixSpace is licensing the patent on the compressive reflector antenna.
3. Spin-Off Companies Started
    a. MatrixSpace

V. REFERENCES

[1] J. Yinon, "Field detection and monitoring of explosives," Trends in analytical chemistry, vol. 21, no. 4, pp. 415–423, 2002.

[2] J. Yinon, Forensic and Environmental Detection of Explosives. Chichester: John Wiley and Sons, 1999.

[3] M. Leahy-Hoppa, M. Fitch, X. Zheng, L. Hayden, and R. Osiander, "Wideband terahertz spectroscopy of explosives," Chemical Physics Letters, vol. 424, no. 8, pp. 227–230, 2007.

[4] D. J. Cook, B. K. Decker, and M. G. Allen, "Quantitative thz spectroscopy of explosive materials," in Optical Terahertz Science and Technology, Orlando, Florida, 14-16 March 2005.

[5] H. Liu, Y. Chen, G. J. Bastiaans, and X. Zhang, "Detection and identification of explosive rdx by thz diffuse reflection spectroscopy," Optics Express, vol. 14, pp. 415–423, 1 2006.

[6] P. Shea, T. Gozani, and H. Bozorgmanesh, "A tnt explosives-detection system in airline baggage," Nuclear Instruments and Methods in Physics Research Section A: Accelerators, Spectrometers, Detectors and Associated Equipment, vol. 299, no. 20, pp. 444–448, December 1990.

[7] C. L. Fink, B. J. Micklich, T. J. Yule, P. Humm, L. Sagalovsky, and M. M. Martin, "Nuclear instruments and methods in physics research section b: Beam interactions with materials and atoms," Evaluation of neutron techniques for illicit substance detection, vol. 99, no. 1-4, pp. 748–752, May 1995.

[8] H. Itozaki and G. Ota, "International journal on smart sensing and intelligent system," Nuclear quadrupole resonance for explosive detection, vol. 1, no. 3, pp. 705–715, September 2008.

[9] J. B. Miller and G. A. Barral, "Explosives detection with nuclear quadrupole resonance," American Scientist, vol. 93, pp. 50–57, January-February 2005.

[10] IATA, "Checkpoint of the future: Executive summary." Available at: http://www.iata.org/whatwedo/security/Documents/cof-executivesummary.pdf (Latest accessed on 03.16.15.).

[11] S. S. Ahmed, A. Schiessl, F. Gumbmann, M. Tiebout, S. Methfessel, and L. Schmidt, "Advanced microwave imaging," Microwave Magazine, IEEE, vol. 13, no. 6, pp. 26–43, 2012.

[12] S. S. Ahmed, "Personnel screening with advanced multistatic imaging technology," in SPIE Defense, Security, and Sensing. International Society for Optics and Photonics, 2013, pp. 87 150B–87 150B.

[13] D. Sheen, D. McMakin, and T. Hall, "Three-dimensional millimeter-wave imaging for concealed weapon detection," Microwave Theory and Techniques, IEEE Transactions on, vol. 49, no. 9, pp. 1581–1592, 2001.

[14] X. Zhuge and A. Yarovoy, "A sparse aperture mimo-sar-based uwb imaging system for concealed weapon detection," Geoscience and Remote Sensing, IEEE Transactions on, vol. 49, no. 1, pp. 509–518, 2011.

[15] D. M. Sheen, D. L. McMakin, and T. E. Hall, "Combined illumination cylindrical millimeter-wave imaging technique for concealed weapon detection," in AeroSense 2000. International Society for Optics and Photonics, 2000, pp. 52–60.

[16] Y. Rodrıguez-Vaqueiro, Y. Alvarez Lopez, B. Gonzalez-Valdes, J. A. Martinez, F. Las-Heras, and C. M. Rappaport, "On the use of compressed sensing techniques for improving multistatic millimeter-wave portal-based personnel screening," Antennas and Propagation, IEEE Transactions on, vol. 62, no. 1, pp. 494–499, 2014.

[17] B. Gonzalez-Valdes, Y. Alvarez-Lopez, J. A. Martinez-Lorenzo, F. Las Heras Andres, and C. M. Rappaport, "On the use of improved imaging techniques for the development of a multistatic three-dimensional millimeter-wave portal for personnel screening," Progress In Electromagnetics Research, vol. 138, pp. 83–98, 2013.

[18] G. Yates, A. Horne, A. Blake, and R. Middleton, "Bistatic sar image formation," IEEE Proceedings-Radar, Sonar and Navigation, vol. 153, no. 3, pp. 208–213, 2006.

[19] R. Burkholder, I. Gupta, and J. Johnson, "Comparison of Monostatic and bistatic radar images," Antennas and Propagation Magazine, IEEE, vol. 45, no. 3, pp. 41–50, 2003.

[20] B. Gonzalez-Valdes, C. Rappaport, M. Lorenzo, and A. Jose, "On-the-move active millimeter wave interrogation system using a hallway of multiple transmitters and receivers," in Antennas and Propagation Society International Symposium (APSURSI), 2014 IEEE. IEEE, 2014, pp. 1107–1108.

[21] B. Gonzalez-Valdes, C. Rappaport, and M. J.A., "On the move millimeter-wave interrogation system with a hallway of multiple transmitters and receivers," Patent US 14 562 094, 12 05, 2014.

[22] M. Soumekh, "Bistatic synthetic aperture radar inversion with application in dynamic object imaging," Signal Processing, IEEE Transactions on, vol. 39, no. 9, pp. 2044–2055, 1991.

[23] S. S. Ahmed, A. Schiessl, and L.-P. Schmidt, "A novel active realtime digital-beamforming imager for personnel screening," in Synthetic Aperture Radar, 2012. EUSAR. 9th European Conference, April 2012, pp. 178–181.

[24] Y. Alvarez, Y. Rodriguez-Vaqueiro, B. Gonzalez-Valdes, S. Matzavinos, C. M. Rappaport, F. Las-Heras and J. A. Martinez-Lorenzo. "Fourier-based Imaging for Multistatic Radar Systems." IEEE Transactions on Microwave Theory and Techniques, 62(8):1798–1810, Aug 2014. doi: 10.1109/TMTT.2014.2332307.

[25] J. Heredia Juesas, G. Allan, A. Molaei, L. Tirado, W. Blackwell and J. A. Martinez-Lorenzo. “Consensus-based Imaging using ADMM for a Compressive Reflector Antenna.” Accepted for publication. AP-S 2015—IEEE AP-S International Symposium, Vancouver, Canada, July 2015.

[26] J. A. Martinez-Lorenzo, J. Heredia-Juesas and William Blackwell. “Single-Transceiver Compressive Antenna for High-Capacity Sensing and Imaging Applications.” CD Proc., Accepted for publication in EuCAP 2015 —VIII European Conference on Antennas and Propagation, Lisbon, Portugal, April 2015.

This page intentionally left blank.

R3-C: Standoff Detection of Explosives: Infrared Spectroscopy Chemical Sensing

I. PARTICIPANTS INVOLVED FROM JULY 1, 2019 TO JUNE 30, 2020

Faculty/Staff			
Name	**Title**	**Institution**	**Email**
Samuel P. Hernández-Rivera	PI	UPRM	samuel.hernandez3@upr.edu
Ricardo Infante-Castillo	DHS MSI-SRTP-2017; Follow-On Grant-2018	UPR-Arecibo	ricardo.infante1@upr.edu
Graduate, Undergraduate and REU Students			
Name	**Degree Pursued**	**Institution**	**Month/Year of Graduation**
Edgardo L. González Arvelo	PhD	UPRM	6/2022
Nelson Granda-Paz	PhD	UPRM	6/2021
Vladimir Villanueva-López	PhD	UPRM	6/2021
Jorge L. Plata-Enríquez	PhD	UPRM	6/2022
Francheska M. Colón-González	MS	UPRM	6/2020
Annette M. Colón-Mercado	MS	UPRM	6/2020
Wilmaris Muñiz López	MS	UPRM	6/2021
Gabriela I. Padilla-Rivera	MS	UPRM	6/2020
Edwin R. Caballero-Agosto	MS	UPRM	6/2021
Veronica G. Adorno-Pita	BS	UPRM	6/2021
Diego A. Alejandro Rivera	BS	UPRM	6/2020
Sofía Álvarez-Pérez	BS	UPRM	6/2021
Marcos L. Arbelo Velázquez	BS	UPRM	5/2020
Emanuel Irizarry-Monroig	BS/REU Summer 2018	UPRM	6/2020
Elvin S. Lebrón-Ramirez	BS	UPRM	6/2021
Bianca M. López-Pagán	BS	UPRM	12/2019
Gustavo G. Maldonado-Figueroa	BS	UPRM	6/2021
Emy Mina-Barzola	BS	UPRM	6/2022
Tania L. Montanez-Ortiz	BS	UPRM	6/2021
Wilfredo A. Munoz-Gomez	BS	UPRM	6/2020
Marializ Nieves-Maldonado	BS	UPRM	6/2020
Emanuel Ocasio-Reyes	BS	UPRM	6/2021
Dickson D. Ortiz-Zayas	BS	UPRM	6/2021
Frank G. Otero-Alejandro	BS	UPRM	6/2021
Luis S. Ríos-Vega	BS	UPRM	6/2021
Ferdinand O. Rivera-Gonzalez	BS	UPRM	6/2021
Norman Y. Rivero-Bernard	BS	UPRM	6/2022
Destiny L. Rodriguez-Portela	BS	UPRM	6/2021

Graduate, Undergraduate and REU Students			
Name	**Degree Pursued**	**Institution**	**Month/Year of Graduation**
Jubal Rodríguez Reyes	BS	UPRM	6/2021
Tatiana P. Serrano-Zayas	BS	UPRM	6/2021
Giancarlo L. Vargas Alers	BS	UPRM	6/2020
Mariana P. Vazquez-Ortiz	BS	UPRM	6/2022
Karla M. Vazquez-Velez	BS	UPRM	6/2022
Michelle Vecchioly-Casiano	BS	UPRM	6/2021

II. PROJECT DESCRIPTION

A. Project Overview

The goal of the R3-C research component at the University of Puerto Rico at Mayagüez (UPRM) was to use mid-infrared (MIR) laser spectroscopy for the detection of explosives. The end-state of this project was to detect residues of explosives on surfaces that could be present due to an explosion or as a threat to citizens at a distance. Our approach was based on using a tunable quantum cascade laser (QCL) source as a chemical sensor for explosive residues left due to terrorist activities. The infrared spectroscopy (IRS) modalities presented in this work were coupled to chemometrics methods of multivariate analysis (MVA) for the classification, discrimination, and prediction of the threats.

The specific aims of the research included:

- Detection of high explosives (HEs) on metallic/matte substrates at close distances using QCL-GAP (QCL grazing angle probe) systems (~15cm)
- Use of MVA routines and an artificial neural network (NN) for the detection of the HEs
- Detection of HE traces at off-normal incidence geometries using a MIR source

The challenges/obstacles that the research intended to address included:

- Establishing the differences between standards and real-world samples for the detection of HEs
- Detection of HEs with MIR laser spectroscopy on moving targets

Overcoming these challenges required transitioning from commercially available laser spectrometers operating at close distances (~15 cm) to a homebuilt system with the following characteristics:

- Highly collimated laser beams using a telescope for sensing at long distances (10–30 m)
- Higher power laser source systems 50–200 mW
- Wide spectral coverage: 1000 cm^{-1}: 830–2000 cm^{-1} (5–12 um)
- Fast scanning systems: 5 s

The work performed under R3-C addressed the detection of HE residues deposited on real-world substrates. The focus is mainly on real-world samples, including bare and painted metal parts, clothing, travel bags, personal bags, laptop bags/cases, and other relevant substrates. Laser spectroscopy signatures obtained for these surfaces allow for the identification/quantification of explosives by coupling the technique to multivariate analysis.

B. State of the Art and Technical Approach

Chemicals in complex matrices can be identified and quantified based on their unique vibrational spectrum [1-6]. IRS and Raman scattering (RS) are the two main branches of vibrational spectroscopy. IRS is a well-established discipline developing constantly. However, energy sources in the MIR have lacked incremental developments, and until now, thermal sources dominated IRS and FT-IR [1-6]. Therefore, remote detection capabilities for IRS and RS are limited by their photonic mechanisms. Both techniques characterize, detect, identify, and quantify threat chemicals, including HEs and homemade explosives (HMEs) [6-17]. Their ability has allowed countermeasures to deter terrorist threats by focusing on remote detection and other interests for national defense [7-17].

There is a need to detect hazardous threat chemicals at trace or near-trace levels on substrates at longer distances. To successfully realize this goal, more powerful MIR sources need to be developed which led to the consideration of collimated, coherent, and polarized sources. A QCL, which is a unipolar semiconductor injection laser based on sub-interband transitions in a multiple-quantum-well heterostructure, was used as QCLs have the following advantages over other types of lasers [18-22]:

- Ability to produce a laser beam from tens to hundreds of milliwatts of pulsed power under ambient conditions
- Commercial availability
- Ability to enable the development of ruggedized systems for detection of chemical/biological (CHES/BIO) threats

Most of the previous investigations to detect HEs at trace levels have focused on the detection of HE residues deposited on ideal, highly reflective substrates, such as highly polished metallic surfaces [23]. There are very few reports published on the effects of nonideal, low-reflectivity substrates on the spectra of the target HEs [24]. The work by Suter and collaborators (which measures the spectral and angular dependence of MIR diffuse scattering from explosive residue deposited on a painted car door using an external cavity QCL (EC-QCL)) is the foundation for part of our research [25]. However, our approach is significantly different because it focuses on the detection, identification, and discrimination of HEs on highly interfering backgrounds. These substrates include wood, natural and synthetic fibers, such as cotton shirts or pants, nylon, and black polyester from laptop bags or travel cases, and simulated human skin [24]. The work also centers on using robust chemometrics techniques for “on-the-fly” pattern recognition and discriminant analysis, with an expected turnaround response time from milliseconds to a few seconds. The main difference between the contributions of this research and the current state-of-the-art research is in bridging the gap between lab experiments under well-controlled conditions and the real-world detection of explosives residues [26].

QCL spectroscopy was used previously for sensitive detection of nitroamine, nitroaromatics, aliphatic nitrate, and peroxide-based HEs at long-distances (meters from the source) [23-25,27-33]. Also, it has been used for remote detection of a variety of HEs. However, the implementation of MVA with QCL has been limited, especially with variating deposition techniques. In addition to principal component analysis (PCA) we employed soft independent modeling of class analogies (SIMCA), support vector machines (SVM), partial least squares coupled to discriminant analysis (PLS-DA) and *k*-nearest neighbors (KNN). KNN has become a hot topic for discrimination analysis. In this work, HEs were deposited by spray, spin coating, sample smearing, and partial immersion. QCL spectra were acquired and then analyzed using PCA. Also, experiments varying the angle of incidence to determine the optimal source and detector position for acquisition of MIR laser reflectance spectra was implemented. Spectra were then analyzed with KNN to classify each HE.

C. *Major Contributions*

C.1. Detection of HEs on Reflective Substrate Using MIR laser spectroscopy (Year 1)

The first stage of this project involved confirming the performance of a commercial QCL spectrometer (LaserScan™ Block Engineering) for detecting HEs by validation experiments. The MIR spectroscopic system acquired reflectance spectra of films and deposits of chemicals on substrates. Some of the results obtained with the QCL system are included in Figure 1. The reflectance spectra measured with QCL and FT-IR spectroscopy of nitroaromatic 2,4,6-trinitrotoluene (TNT), aliphatic nitrate ester pentaerythritol tetranitrate (PETN), aliphatic nitramine 1,3,5-trinitroperhydro-1,3,5-triazine (RDX), and triacetone triperoxide (TATP) are shown in the figure [34, 35]. The MIR laser spectra were collected on a smooth aluminum (Al) substrate. These spectra serve the purpose of validating the technique for the detection of HEs, explosive mixtures/formulations, and chemical precursors. The MIR laser spectra were collected in open-air conditions. Thus, water vapor lines were observed on some of the spectra. TATP samples had particularly evident water vapor lines because the samples sublimated rapidly, even at room temperatures. In other cases, the inherent strength of the MIR signatures of the HEs made the water vapor lines imperceptible. There are operational parameters worth discussing: the LaserScan™ was designed for short focal length work (~15 cm). Highly reflective polished metallic substrates (e.g., Al, stainless steel, or gold) required a defocused MIR laser beam since the specular radiation collected in back reflection mode saturated the detector. Alternatively, using an incidence angle of 9–10° avoided detector saturation.

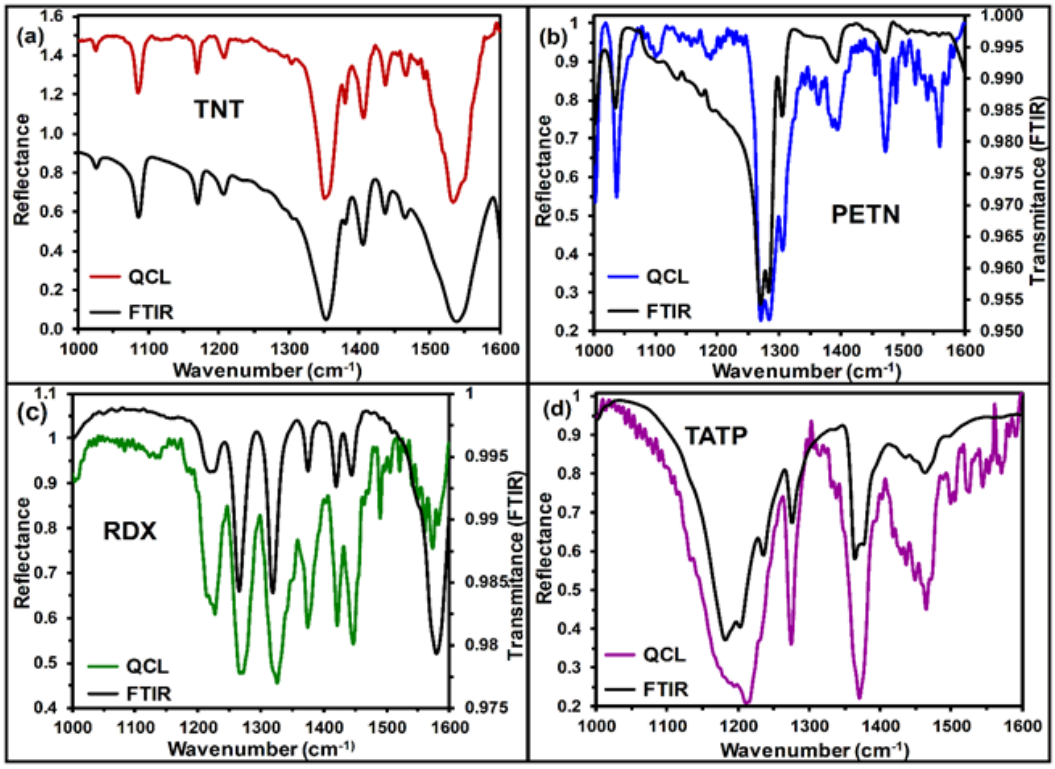

Figure 1: QCL and FTIR (ref.) spectra of HEs deposited on highly reflective polished Al substrates: (a) TNT, (b) PETN, (c) RDX, and (d) TATP. The quality and intensities of the bands are equal or better than those measured by FT-IR.

C.2. Detection of HEs on Nonreflective (Matte) Substrates Using QCL Spectroscopy (Years 1–2)

The spectroscopic system based on QCL was next used to obtain MIR reflectance spectra of HEs deposited on nonideal, low reflectivity matte substrates such as travel bags (TB), cardboard (CB), and wood (W). We tested various deposition methods, including spin coating, sample smearing, partial immersion, and spray deposition for preparing standards and samples used in the study. The HEs used include TNT, PETN, and RDX. Low surface concentrations (1–15 mg/cm^2) of HEs were used in the investigation. Figure 2 shows representative QCL spectra of TNT, PETN, and RDX on Al, CB, W, and TB.

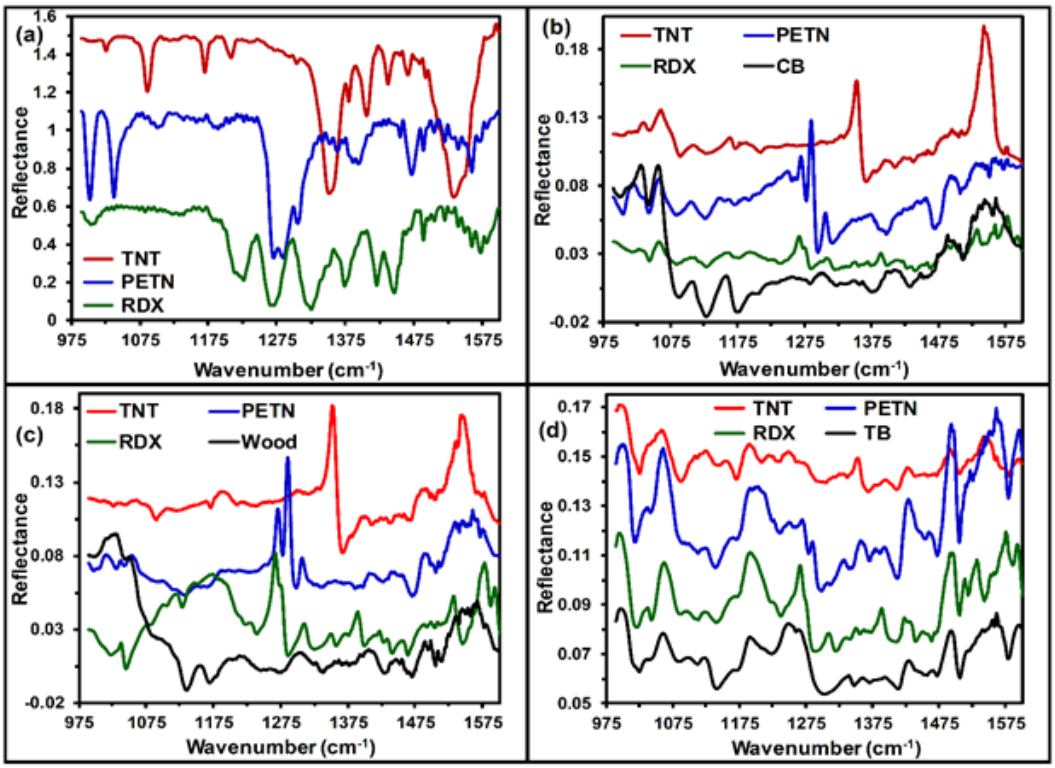

Figure 2: QCL spectra of HEs on substrates: (a) Al, (b) CB, (c) wood, and (d) TB. Surface concentrations were 15 µg/cm2. QCL spectra of substrates are included to establish the degree of spectral interference.

MIR laser reflectance spectra were used for the surface concentration profiles to perform quantitative MVA. A total of nine different surface concentration profiles were assembled: three HEs × three substrates (plus three replicas of each combination). QCL spectra of clean Al substrates were used as backgrounds. Figure 3a shows some of the RDX spectra recorded on wood substrates; Figure 3b shows spectra for TNT on CB at various surface concentrations, and Figure 3c shows measured QCL reflectance spectra for PETN on wood. However, the QCL methodology used for detection of explosives on non-reflective (matte) substrates did not require the use of multivariate analyses (MVA) for identification of HEs, but rather, as illustrated in Figure 3d, a single acquisition (3 s) of CB was subtracted from the corresponding QCL spectrum of PETN on CB to obtain the difference spectrum of PETN. Comparison with the QCL transflectance spectrum of PETN on Al demonstrates that several of the aliphatic nitrate ester signature bands can be readily assigned by comparison with the reference QCL spectrum. The only requirement for this type of remote detection experiment is to be able to acquire a QCL spectrum of a non-contaminated (non-dosed) segment of the substrate. The LaserScan™ spectroscopic system allowed the detection of HEs deposited at low surface concentrations (1–15 mg/cm^2) on three types of nonideal low reflectivity substrates: travel bag fabrics (TB),

cardboard (CB), and wood (w). Spectral identification using spectral correlation algorithms were not efficient enough for identifying HEs when present on nonideal low reflectivity, highly mid-infrared absorbing substrates. However, multivariate analyses were efficient enough to attain the goals of this investigation. Finally, PLS models demonstrated the capability of predicting surface concentrations of HEs on the substrates tested using a maximum of eight latent variables (LV) to obtain values of R^2 higher than 0.9 [24, 26].

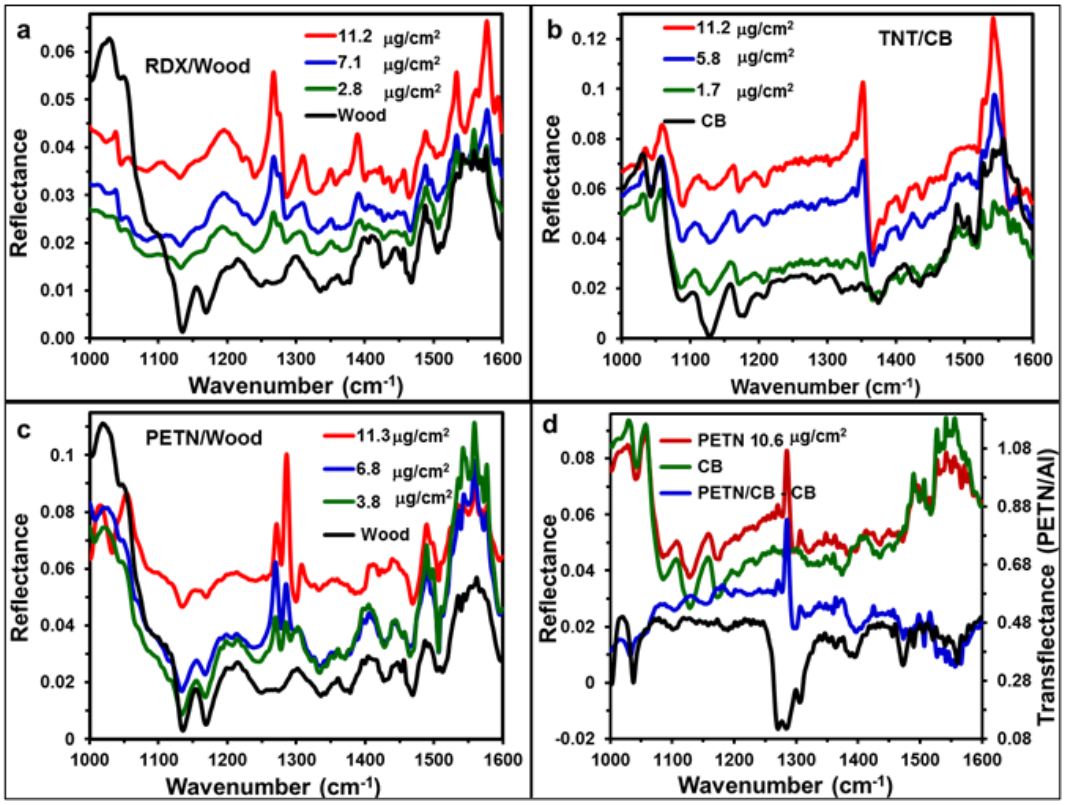

Figure 3: Surface concentration profiles for (a) RDX on wood; (b) TNT on CB; and (c) PETN on wood. Difference spectrum (d): PETN/CB minus CB and comparison with QCL transflectance spectrum PETN/Al (used as reference).

C.3. QCL Spectroscopic Library of Explosives (Year 2)

Spectral signatures of explosives were recorded by MIR spectroscopy using a QCL system. Explosive samples were deposited on aluminum and real-world substrates such as travel baggage, cardboard, and others. Explosives used in this stage of the project were RDX, PETN, and 2,4-dinitrotoluene (2,4-DNT). The deposition method utilized was sample smearing.

C.4. Classical Least Squares–Assisted MIR Laser Spectroscopy Detection of High Explosives on Fabrics (Years 3–5)

MIR laser spectroscopy was used to detect the presence of residues of HEs on fabrics. The discrimination of the vibrational signals of HEs from a highly MIR-absorbing substrate was achieved by a simple and fast spectral evaluation, without preparation of standards, using the classical least squares (CLS) algorithm [36]. CLS focuses on minimizing the differences between the spectral features of the actual spectra acquired by MIR spectroscopy and the spectral features of calculated spectra modeled from linear combinations of the spectra of neat components: HEs, fabrics, and bias. Samples in several combinations of cotton fabrics / HEs were used to validate the methodology. Several experiments were performed focusing on binary, ternary, and quaternary mixtures of TNT, RDX, PETN, and fabrics. The parameters obtained from linear combinations

of the calculated spectra were used to perform discrimination analyses and to determine the sensitivity and selectivity of HEs to the substrates and each other. However, discrimination analysis was not necessary to achieve the successful detection of HEs on cotton fabric substrates [37].

C.5. QCL Spectroscopy at Grazing-Angle Incidence Using Fast Fourier Transform Preprocessing (Years 4–7)

A simple optical layout for a grazing angle probe (GAP) mount for coupling to a MIR QCL spectrometer was designed and developed. This assembly enables reflectance measurements at high incident angles. In the case of optically thin films and deposits on MIR reflective substrates, a double-pass effect occurs, accompanied by the absorption of deposited samples in a reflection-absorption infrared spectroscopy modality. The optical system allows MIR light to pass through the sample twice. Applications to the detection of traces of explosives using the QCL-GAP were also developed. They have been published in various peer-reviewed journals. Principal component analysis and partial least squares multivariate chemometrics methods were employed to analyze MIR spectra to evaluate an analytical methodology for confirming the presence of residues of pharmaceutically active ingredients (irbesartan) and of traces of explosives (RDX) that have been deposited on metallic substrates. The performance of spectral preprocessing via fast Fourier transform (FFT) analysis was evaluated for the ability to extract more robust and accurate information from the obtained reflectance spectra. According to the figures of merit or distinguishing attributes of this new technique, FFT with chemometric routines can obtain sensitivity and specificity values of 1.000. The limit of detection obtained for RDX was 7 ng/cm^2. The experimental results demonstrate that the proposed system, when used together with proper chemometrics routines, constitutes a powerful tool for the development of methodologies that have lower detection limits for a range of applications that involve detecting traces of analytes that reside on substrates as contaminants [38].

C.6. Design and Construction of a Homebuilt MIR Laser Spectrometer System (Years 6–7)

Commercial MIR lasers (QCLs) are already predispersive systems: the grating selected wavelength of the output beam can be scanned very fast, maintaining high accuracy and precision. However, coupling to fast detection systems, in our case, was not a trivial problem to solve. The first approach to obtain data acquisition routines based on National Instruments (NI) LabView™ from researchers affiliated with National Labs or from other researchers in the field was not successful. A commercial solution to the problems was not within reach (>$35k). Thus, several members of our research team had to be involved in the solution of the problem. The first successful experiments are reported here. First, the development of an interface using LabView™ to acquire spectroscopic data from a QCL source and a mercury-cadmium-telluride (MCT) cryocooled detector has not been thoroughly discussed in the literature. A few research papers have focused on parts of the algorithms that can be employed [39-41]. However, none fully describes a procedure that can be programmed as a Virtual Instrument (VI) code in LabView, including acquisition and data processing required to interface a fast laser with an equally fast data acquisition board (analog to digital card) and detector. Software developed in LabView to implement the required interface was created for this purpose.

An ultrafast conversion data acquisition card (DAQ; 200 mega samples/s) was used to capture the signals from the preamplifier, which is connected to the MCT detector, as shown in Figure 4. The system can acquire potential difference (volts) as a function of time and performs the signal processing required to obtain the spectroscopic information related to the samples. The advantage of developing this in-house system was that it facilitated coupling QCL systems with traditional IRS and FT-IR techniques to perform studies with the advantages of a laser source. Among these techniques are transmission, absorbance, diffuse reflectance infrared spectroscopy (DRIRS), attenuated total reflectance (ATR), and grazing angle incidence reflectance (GAIR) which enables the most sensitive IRS technique: reflectance-absorption infrared spectroscopy (RAIRS).

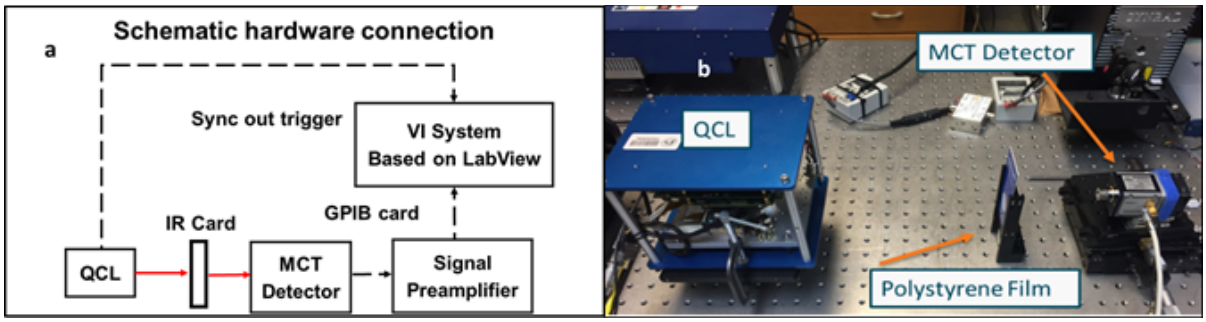

Figure 4: (a) Schematic diagram of the transmission setup using QCL-MCT; (b) calibration of QCL-MCT using a polystyrene film in transmission mode.

C.7. Variable Angle of Incidence MIR Laser Spectroscopy Method for Diffuse Reflectance Measurements (Years 7–8)

The study focused on the development of a MIR laser reflectance method to perform spectroscopic measurements at ten angles of incidence from 12° to 84° for PETN (81.4 μg/cm^2), RDX (47.4 μg/cm^2), and Tetryl 62.7 μg/cm^2. The energetic materials were deposited on substrates with different properties such as the index of refraction, reflectivity (metallic or nonmetallic), and surface roughness. Those differences produce complex infrared spectra, which make it challenging to identify vibrational signatures by sight. Previous results have shown that higher angles of incidence (grazing angle) provide high signal to noise ratios and cover a more extensive sampling area. However, real-life applications could require measurements at an angle of incidence different from grazing angles. QCL has a powerful source of mid-IR that could compensate for the scattering due to the nature of the experiments and still obtain a strong signal. Deep learning emerged as an advanced artificial intelligence method that discovered patterns in the spectra without supervision; therefore, its synergy with QCL spectroscopy leads to the development of more sophisticated detection systems capable of identifying threats in public places by using copius amounts of data collected in airports security checkpoints and laboratories. The algorithm resembles our brain's process of learning. A set of NN layers made of compound nodes "learns" from reliable spectra labeled with its corresponding class. After the learning stage finishes, the algorithm is ready for classification. The goal of the project was to cover a wide range of angles of incidence with respect to the surface normal vector of the substrate using a robust a MIR laser, as shown in Figure 5. The goal was to construct a database that could be coupled with AI algorithms for identification and classification of HEs. The method proposed in this study could be used in airports to inspect surfaces of baggage using diffuse reflectance laser spectroscopy. The acquisition of spectra at several angles of incidence increases the probability of detecting threats independent of the position with respect to the QCL and the detector of the luggage in a conveyor belt.

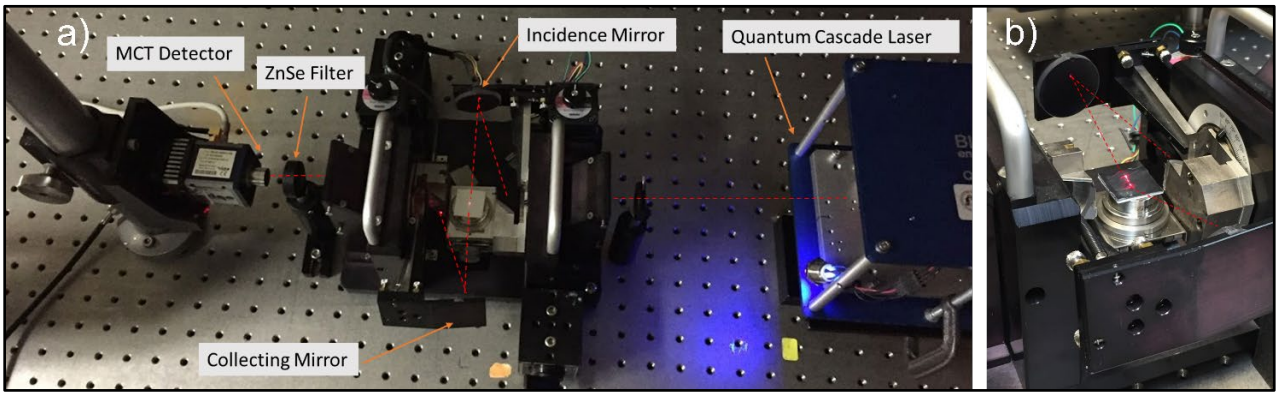

Figure 5: (a) Optical setup for multi-angle incidence diffuse reflectance spectroscopy. (b) Side view.

A total of 450 spectra were collected containing 830 bands from 930 to 1,375 cm^{-1}. A total of 80% of the spectra are separated and labeled with their corresponding class used to train the NN model. A PCA was used as a preprocessing step to select only the most significant bands. Those bands represent the representative features that identify each class. The parameters of the model (the weights) were optimized at each iteration to minimize the percentage of misclassified samples. The training finished when the number of iterations was reached. Afterward, the validation stage began. The remaining 20% of the spectra collected were used to test the model (test set). The results are presented using a confusion matrix. The values in the diagonal of the matrix represent the spectra correctly classified. The overall performance of each stage is shown in the right lower corner of the matrix (shaded in gray), as shown in Figure 6. The green shaded values represent the percentages of the success rate. No additional data was collected for validation. Hence, the values on the validation confusion matrix are zero. Finally, the overall performance of the model is display on the "All Confusion" matrix, which combines the results from the confusion matrix for the training set and the confusion matrix for the test set. Several trials were conducted to find the best parameters of the model, such as the number of classes and if PCA data reduction was applied successfully.

C.7.a. First Trial: Classification Based Only on HEs

A general KNN model, only considering three classes (PETN, RDX, and tetryl), was generated for classification of the samples belonging to these classes. Initially, the NN model was overfitting the data, but it was not generalizing. This conclusion is generated from the training confusion matrix and test confusion matrix. Figure 6 show a 97.2% of overall accuracy. Still, there was only 34.1% of overall accuracy for the testing. These results were computed using three layers arranged as follows: three nodes in the first layer, one node in the second layer, and finally, two nodes in the last layer. The number of iterations was set to 7,000, and only 22% of the data was selected for training.

Figure 6: Preliminary results—confusion matrix of targets (1) PETN, (2) RDX, and (3) tetryl.

C.7.b. Second Trial: Classification Based Only on HEs and Substrates

Improving the prediction capability required the research team to create more classes for the same data, as shown in Table 1. The parameters employed for the second trial were similar to the first trial: three layers arranged as follows: three nodes in the first layer, one node in the second layer, and finally two nodes in the last layer. The number of iterations was set to 4,000, and only 20% of the data was selected for the test set. In this case, an overall accuracy for the training stage was 96.7% as can be seen in Figure 7. For the testing stage, an overall accuracy of 12.2% is shown in Figure 8. This means that the network was training well but the prediction had a low accuracy. The overall true positives of the model were 80% as we can see in Figure 9. However, the model needs to be improved to increase prediction in the testing stage.

1	2	3	4	5	6	7	8	9
PETN Al	PETN Glass	PETN Vinyl	RDX Al	RDX Glass	RDX Vinyl	Tetryl Al	Tetryl Glass	Tetryl Vinyl

Table 1: Classes for training the KNN model.

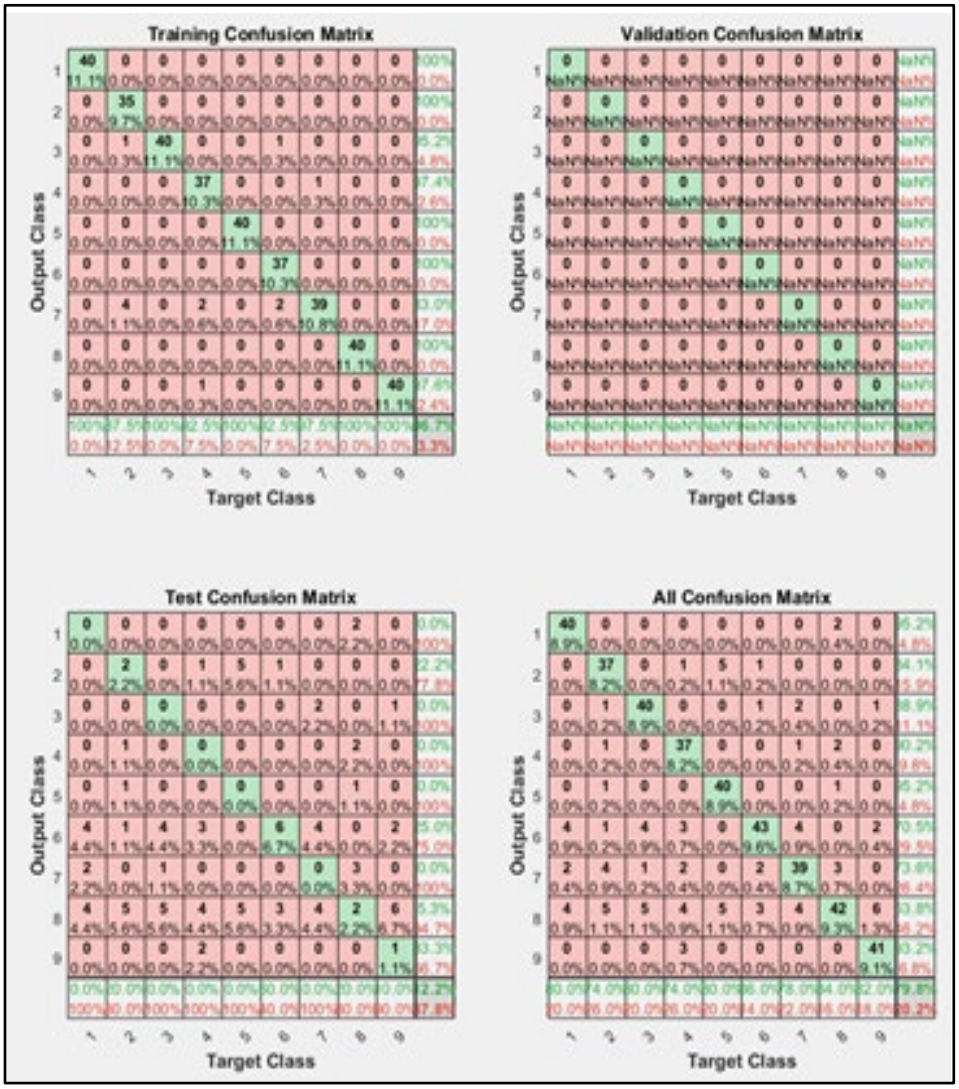

Figure 7: Preliminary results—confusion KNN matrix used to separate nine classes.

C.7.c. Third Trial—Classification Based Only on Energetic Material and Substrate

The same parameters employed in the second trial were used for the third model. The number of contributing bands (vectors) was reduced to twenty using PCA. This reduction retained the twenty most significant bands that contribute more significantly to the spectroscopic data set. The overall accuracy for testing data increased to 27.8% while the overall accuracy for the training data decreased to 56.4%. It is essential to highlight that the comprehensive training time for the 896 bands was around 1 hour. Using 20 bands the model converged in 3 minutes. We are currently working on improving the predictability of the deep learning model by preprocessing the spectra and also by increasing the number of nodes per layer.

C.8. Characterization and Classification of Standards Samples Using QCL-GAP Laser Spectroscopy (Years 7–8)

The use of MIR lasers (QCLs) provides the user with the capability to detect substances that may present interferences even at low concentrations. Our approach entails the signal enhancement of HEs by using the GAP. The results using a Block Engineering, LLC portable system coupled to the GAP mount are presented for the characterization of standards obtained from the Naval Research Laboratory (NRL, Washington, DC) as a part of the SED-V Program: DHS Methods of Optical Detection of Explosives (MODEx). Figure 8 shows the samples first analyzed and used to characterize the HEs, which included: RDX, tetryl, and PETN deposited on acrylonitrile butadiene styrene (ABS) and Al used as matte and reflective substrates as shown respectively. The acquired spectra of the characterization for the HEs are presented in Figure 9a and Figure 9b. The normalized spectra for each HE are shown in comparison to the pure substance synthesized in our laboratory. The IR spectrum of the tetryl was simulated using the OPT + FREQ job setup in Gaussian (Gaussian, Inc. Connecticut, USA) with density functional theory (DFT), 6-311 + G(2d,p) basis set and B3LYP hybrid functional.

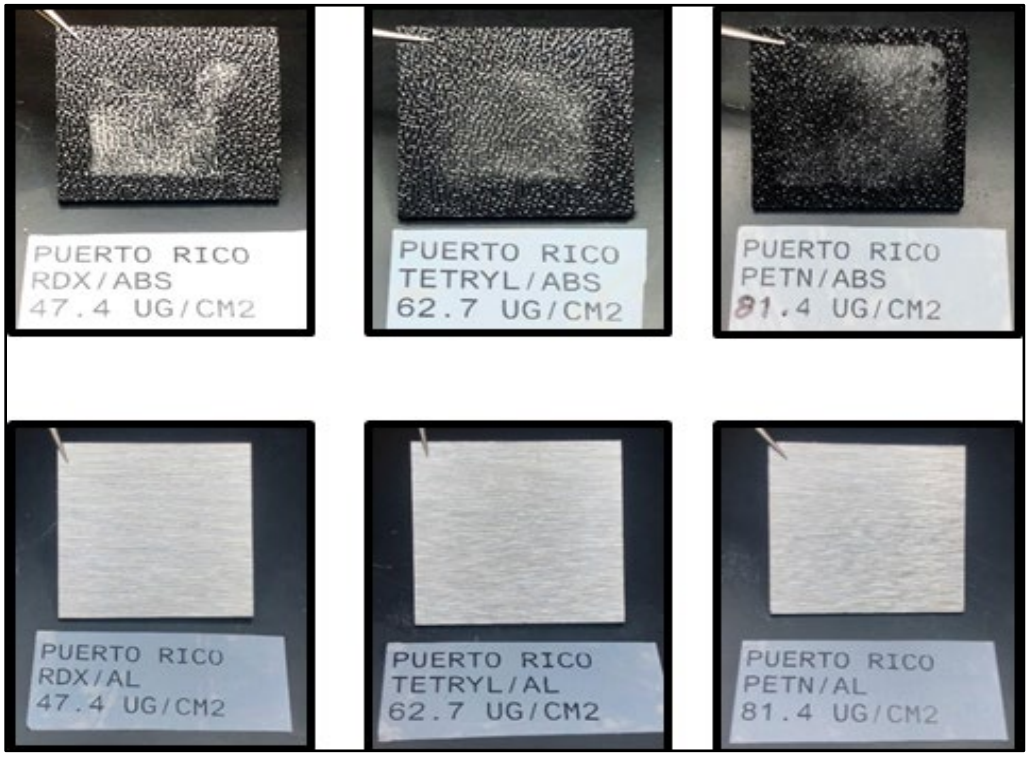

Figure 8: White light micrographs of ABS and Al substrates loaded with HEs used for spectral acquisition.

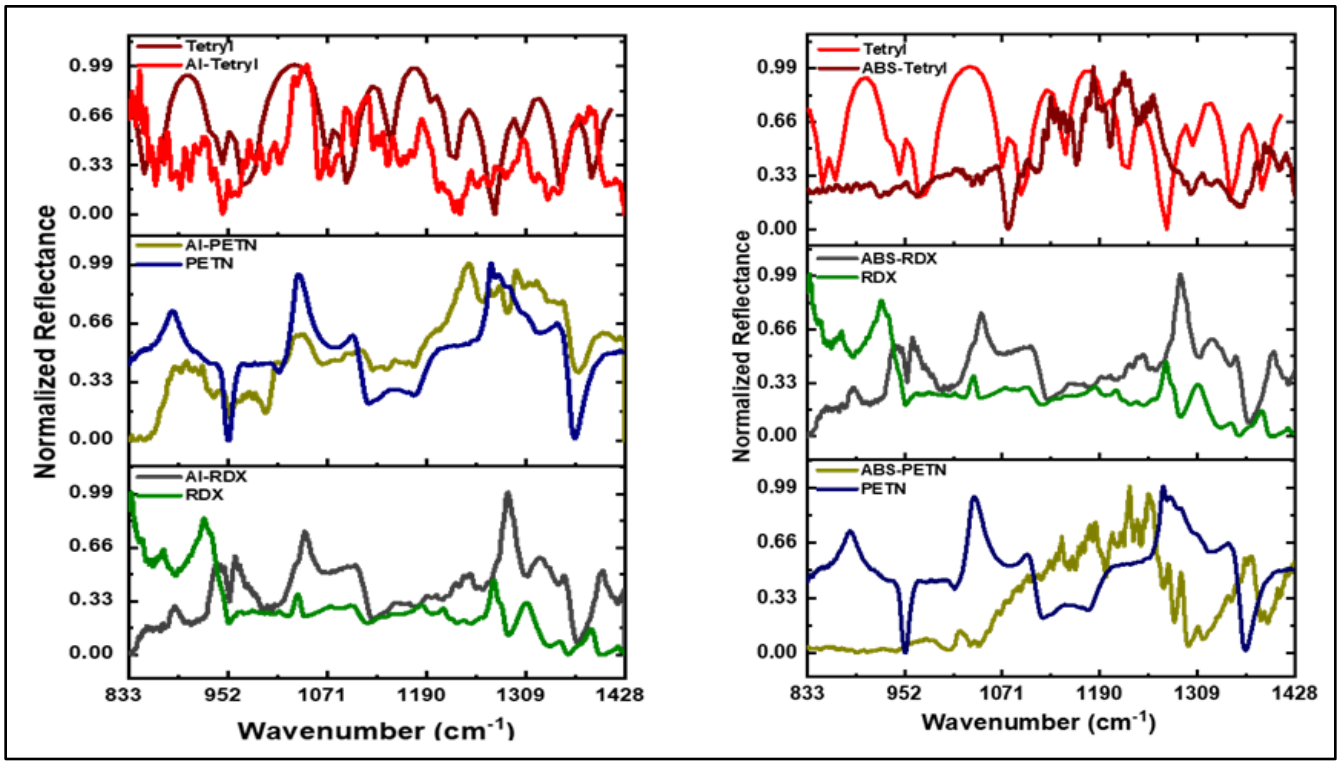

Figure 9: Normalized reflectance spectra of various HEs deposited on the substrates used as standards (a) Al reflective substrate; (b) ABS matte substrate.

PCA models for the standards were generated using MVA routines to differentiate between the explosives deposited and the substrates used for the analysis. The complete MIR spectral region from 833 to 1,428 cm^{-1} was used to investigate these variables. Scores for principal component 1 (PC-1) and PC-2 presented the two most notable variations (percent variance) for the spectra acquired on both substrates. Figure 10 shows the scores plot (PCA plot) for ABS, where PC-1 accounted for 46% of the total spectral variance, and a value of 37% for PC-2. Most of the information contained in PC-1 and PC-2 showed a complete separation between the classes of HEs for both substrates. The classes considered include the substrates with the three types of HEs at different concentrations to identify the variance between the vibrational signatures of the HEs. The percentage of the variance is mainly attributed to the difference in the signals for the HEs. A second score plot, shown in Figure 11, was generated for the samples deposited on Al. The PC-1 score plot shows the main variation in vibrational signatures for the analytes, where the most prominent signals are attributed. In this case, PC-1 explained 46% of the total variance, while PC-2 contributed to 20%. Both PCA scores plots for ABS and Al required the preprocessing steps of the Savitzky-Golay first derivative using a second-order polynomial fit of 15 points followed by minimization of scattering effects by particle-size distribution using standard normal variate (SNV).

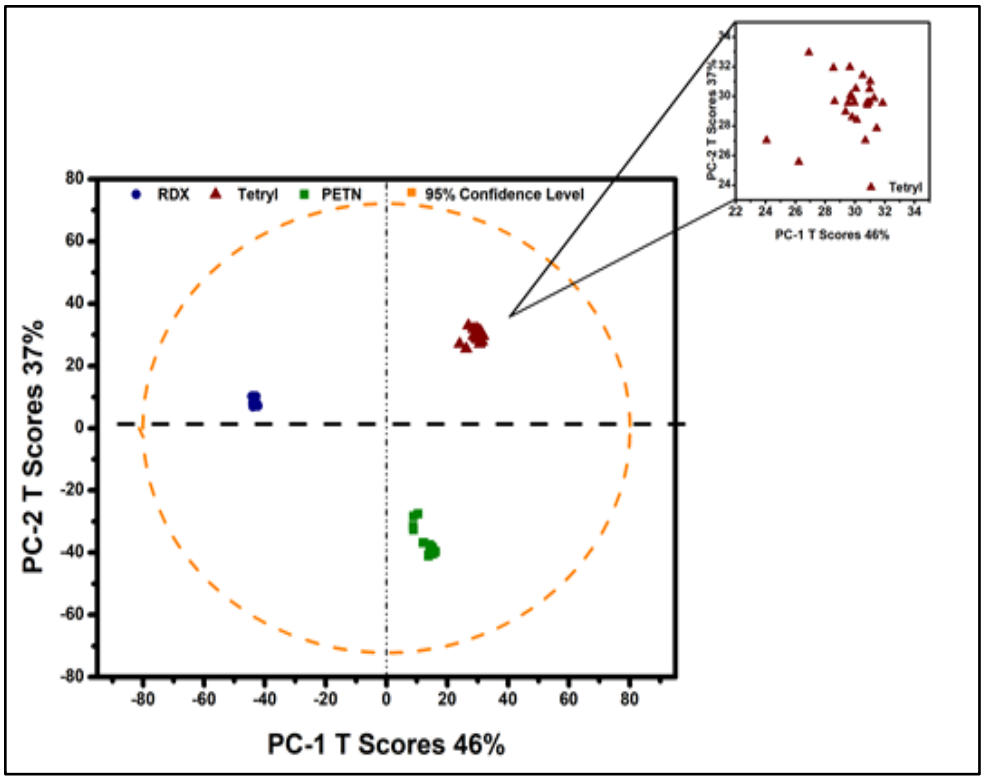

Figure 10: Scores plot for PETN, RDX, and tetryl on ABS substrate in terms of PC-2 versus PC-1. The 95% confidence level used in the analysis is also shown.

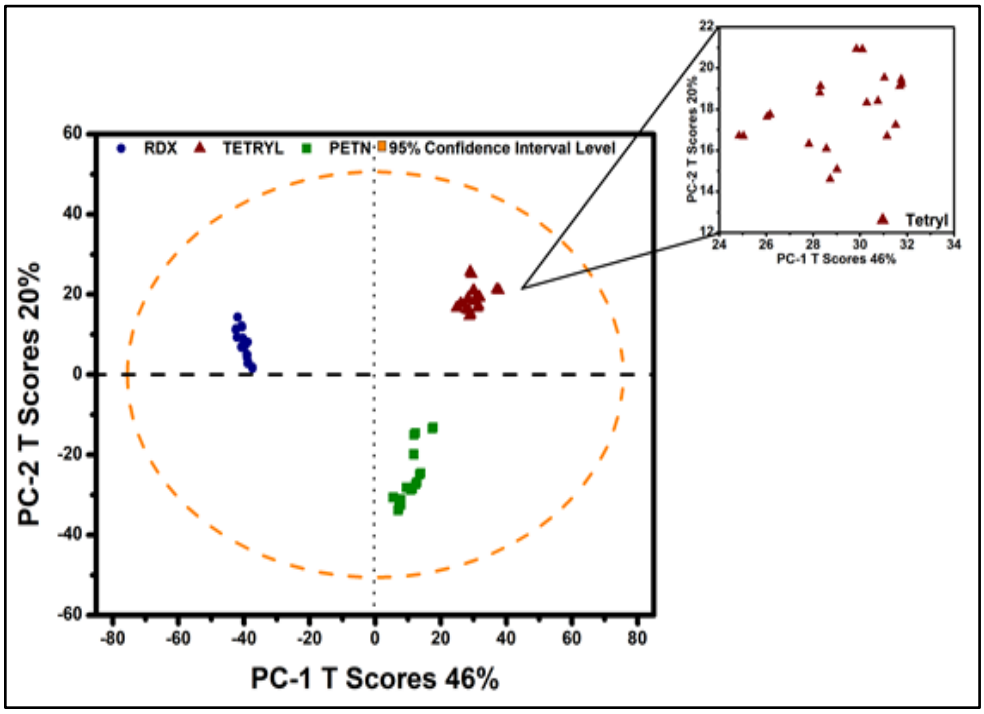

Figure 11: Scores plot for PETN, RDX, and tetryl on Al substrate in terms of PC-2 versus PC-1. The 95% confidence level used in the analysis is also shown.

C.9. PCA Classification of Standards Versus Commercial Aerosol Deposition Samples

Samples representing "real-world" surfaces were prepared by using a Paasche VL series Double Action Internal Mix Airbrush (Harwood Heights, IL, USA), as shown in Figure 12. Samples containing the HE, PETN, were deposited on the surface on reflective substrates stainless steel (SS), aluminum (Al), and Teflon as matte. The MIR spectra obtained from each deposition were characterized and used to classify between the standards and the samples, representing how the HE might be found in a heterogeneous surface.

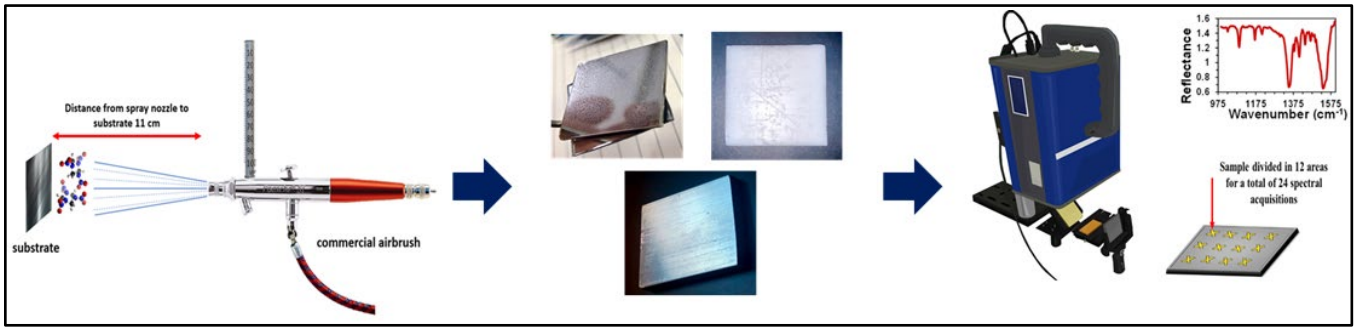

Figure 12: Setup for the MIR QCL-GAP system, including the aerosol deposition on SS, Teflon, and Al substrates.

PCA models were used as a method to validate the HE deposited utilizing the aerosol. The models showed significant variations in the classification of the HE, and it depended on the properties of the substrate. The preprocessing treatment that best classified the HE required Savitzky-Golay first derivative with 2nd order polynomial fit of 15 points followed by SNV. Figure 13 shows the PCA plot generated for the HE in Al, partially reflective standards in comparison to the Al samples with the PETN deposited using the spray. The PC-1 explained 30% of the variance, while PC-2 accounts for 26%. In this case, it was expected that the PETN used for the aerosol deposition samples collided with the PETN standards. The difference in the classification may be attributed to the difference in the Al substrate used in comparison to the standard.

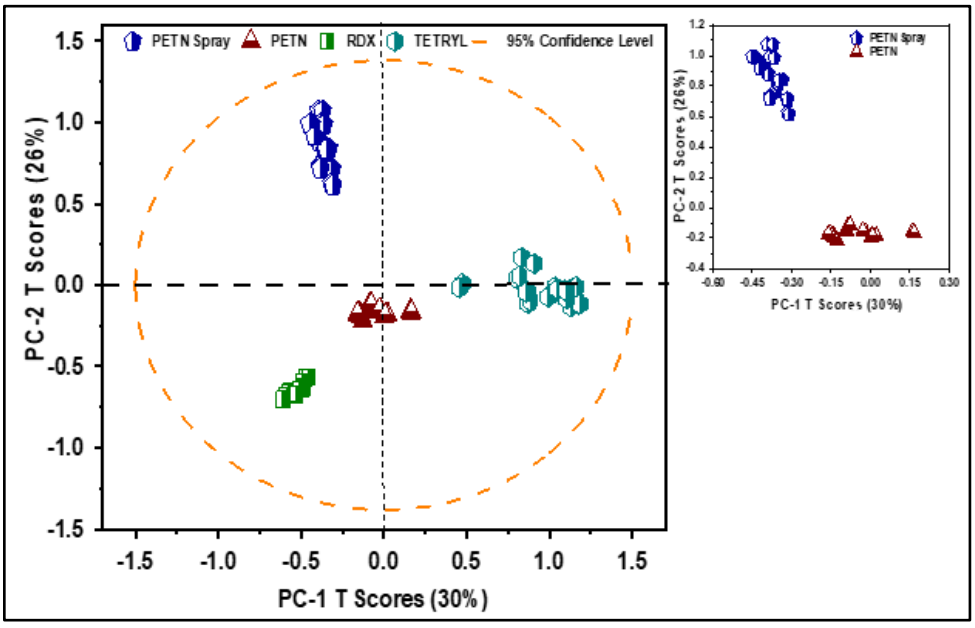

Figure 13: Scores plot PETN, RDX, and tetryl on Al substrates. PETN deposited using aerosol in spray Al is shown for validation of the HE.

A second score plot was generated for the nonreflective (matte) substrates. Teflon with PETN deposited using aerosol was compared to the HE deposited on ABS. These samples were used as the lowest reflective substrates, an essential aspect of the RAIRS experiments. The classification score plot for the HE in ABS standards and PETN in Teflon is shown in Figure 14. The PETN for both samples, standards, and nonstandards were classified with similar scores. PC-1 explained a percentage of 31%, while the PC-2 score explained the variance of 22%. The nitroaromatic compounds, RDX, and tetryl were also classified in this model. This model of the nonreflective substrate was able to fully classify PETN samples deposited on both ABS and Teflon, merging the PETN under one classification. The results for this model prove that the MVA routine used can differentiate between other HEs. The third model for the classification of the data included the highly reflective substrate, stainless steel with the PETN deposited utilizing the spray, and was compared to the partial reflective substrate Al as a standard. The model grouped the different compounds in the score plot but was not able to fully classify the PETN using the spray with the PETN standard. The plot for this model is shown in Figure 15.

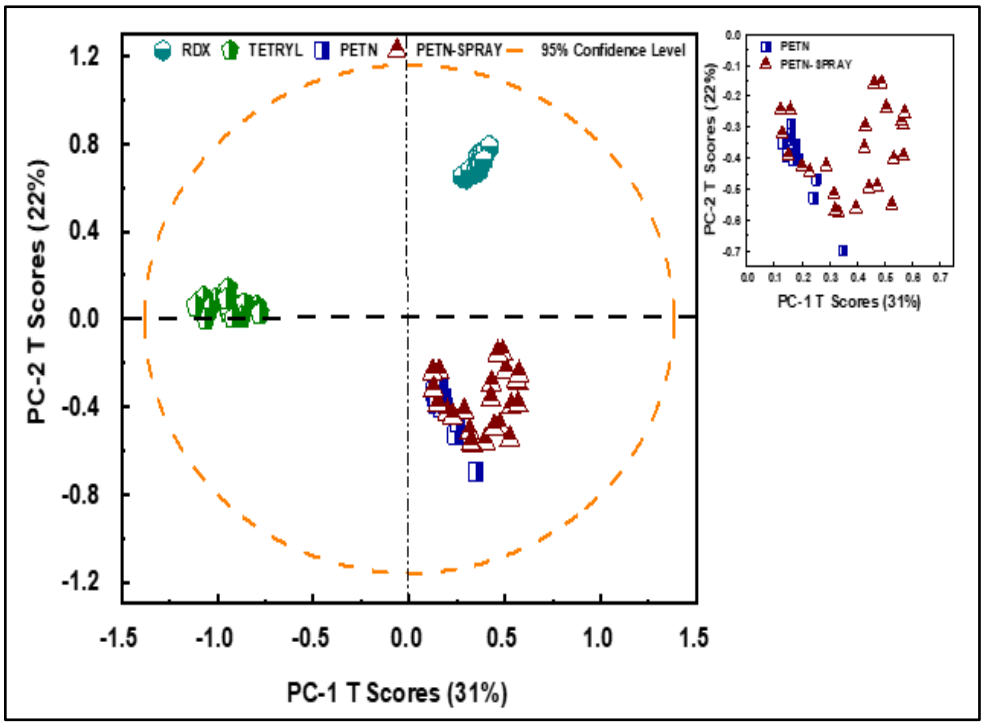

Figure 14: Scores plot for PETN, RDX, and tetryl on the ABS matte substrate. PETN deposited using air spray-on technique on Teflon substrates is shown for the validation of the HE.

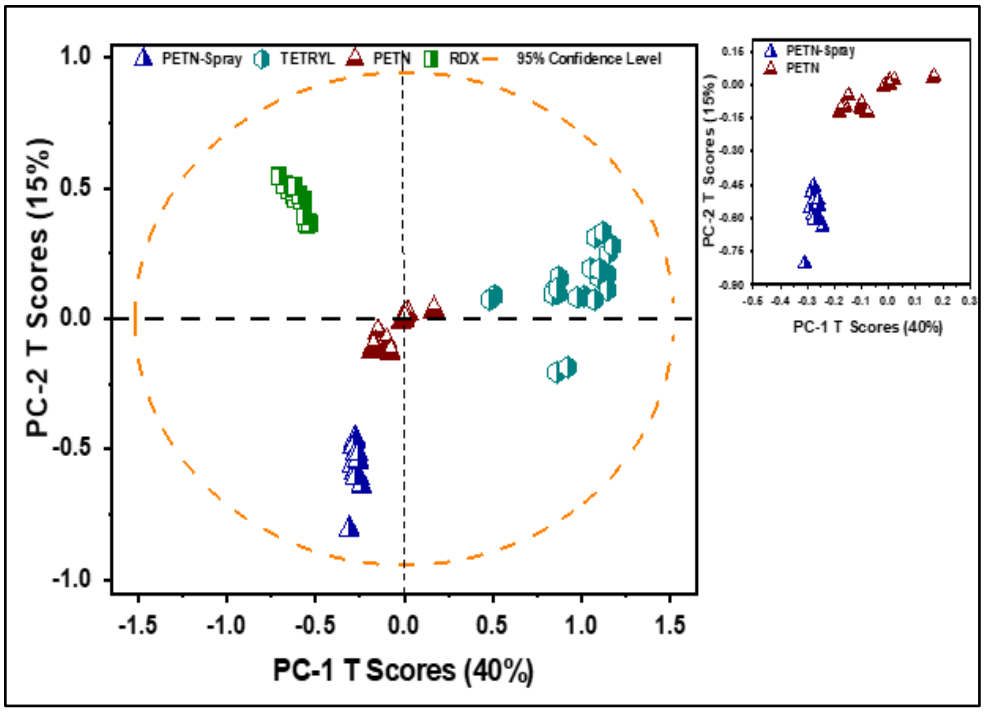

Figure 15: Scores plot for PETN, RDX, and tetryl on Al substrate. PETN deposited using air spray on SS reflective substrate.

The variations in the signals that classified the HEs and created the presented models were evaluated in terms of the loadings for the three models. The difference in the reflectiveness of the substrate may have caused interferences in this model, as well as the deposition method used. The deposition for this analysis plays a significant aspect since it is expected that a homogeneous deposition using a printer or direct deposition is more reliable than spray due to the loss of sample during the sample preparation. The use of other PC scores could aid in the classification of the PETN while varying the preprocessing treatments.

D. Expected Milestones at Project End

The key milestones from this year's project are related to the application of MVA routines for accurate detection using MIR QCL spectroscopy. In line with the no-cost extension provided on the ALERT Year 7 award, we will continue to work towards the completion of the following milestones up to or before May 2021:

- Finish the design of the multipass system (August 2020)
- Couple the setup to MVA routines to evaluate the effectiveness of the system (December 2020)
- Enhance factors: Ag/Au nanoparticles embedded on substrates for creation of materials for detection at lower concentrations: surface enhanced infrared reflectance (SEIRR); project recently started.
- Finish the computational chemistry of target chemicals (December 2020)

E. Final Results at Project Completion (Year 7)

One of the most important outcomes and contributions from this research component is the characterization of trace and near-trace to semi-bulk amounts of HEs. Deposition methods of HEs on substrates of interest to the homeland security enterprise, in general, must be characterized both morphologically and

spectroscopically. The project has achieved significant advances related to trace-level HE detection with the coupling of the QCL spectrometer to the GAP (QCL-GAP). The deposition methods were varied by introducing samples that represent real-world heterogeneous surfaces with the HE. Classification models were created using the acquired spectroscopic data containing the vibrational signatures. The validation aspect was achieved by using the NRL standards. The models were able to classify the HEs according to the substrate, and HE deposited.

Another contribution of this project was realized by the variation of the incident angle from 12° to 84° for the HEs under study. The investigation was carried out using the QCL with a neural network analysis algorithm for the sorting of the classes by creating confusion and test matrices. A total of nine classes were analyzed to predict the HEs when using spectra with the variation of the angles. KNN is still under the MVA tool in our lab and is expected to continue providing results based on the training of data to improve the prediction of samples.

III. RELEVANCE AND TRANSITION

A. Relevance of the Research to the DHS Enterprise

Over the years, incidents involving attacks have fortunately decreased due to technological advancements and rigorous security measures; however, threats still exist. The detection, identification, and quantification of HEs, homemade explosives (HMEs), precursors, and new green explosives continue to be a high priority for security agencies.

- Development of a methodology for detection, identification, discrimination, and quantification of explosives in the presence of highly interfering backgrounds
- Mass range from bulk (0.1 g) to trace (10 ng) at close distances (~15 cm) for potential operation at checkpoints and mid to long remote distances
- The methodology under development will provide a positive/negative result or a confidence level indication to the operator for the presence of explosives within (<3 s), with a goal of (1 s)
- The methodology will operate effectively in field environments at multiple distances with varying amounts of humidity, air particulates, temperature, light, and wind
- The methodology will be useful in providing evidence of post-terrorist events by detecting explosives residues on dirt, concrete, wood, cardboard, bricks, and other surfaces
- Two invention disclosures for patent applications on coupling technology under development for robust separation and quantification methodologies
- Neural network analysis, multivariate routines, and partial least squares discriminant analysis for data analysis and generation of prediction models

The impact of developing QCL-GAP technology through this effort is particularly essential to the HE trace detection community in security and defense applications. It is particularly important for development of methods that can determine if individuals have been in contact with HE illicitly. QCL-GAP system operated in standoff mode with chemometrics-based MVA should become a new technological approach for rapid detection of HE traces.

B. Status of Transition at Project End

- Will continue to seek partnerships for the ongoing development of methods of detection of explosives and hazardous chemicals with companies that fabricate laser sources for MIR or are involved in explosives detection instruments/methodologies
- Have already shared papers and described the invention disclosures that have resulted from this project to most of the potential partners
- Plan to submit a proposal to DHS Small Business Innovation Research (SBIR) Topic solicitation in the subject area of Research and Development of Countering Biological Weapons of Mass Destruction threats. The first phase of the topic solicitation pitch paper was recommended for competition in two of the topics selected. The proposal was submitted on June 19, 2020.

C. Transition Pathway and Future Opportunities

C.1. Sub-Project 1

The sub-project described in Task 1 will be either a "spinoff" small startup with alumni from the UPRM chemistry doctoral program in Applied Chemical Sciences and former ALERT-II R3-C students in the form of a Small Business Innovation Research (SBIR) proposal channeled through the Puerto Rico Science Trust. Another possible mechanism is to apply to DHS, Department of Defense, or the National Science Foundation for an SBIR together with Michele Hinnrichs and VERLUZ, LLC (PAT, Inc.). We have already submitted an invention disclosure for a patent ("Grazing Angle Probe Mount for Quantum Cascade Lasers"; Ser.#: 62/587,557; filing date 11/17/2017). The planned prototype would be a portable explosives detection system (EDS), physically coupled to MIR fiber optics, user friendly, and completely contained in a small frame rugged box.

The goal of Sub-Project 1 is to fully develop QCL-GAP setups coupled to MVA for the detection of HEs on reflective and non-reflective substrates and to transition the technology through an SBIR to build a portable system prototype.

The expected outcomes include:

- Developing portable QCL systems setups for the detection of HEs on non-reflective substrates
- Building a lab-based fiber optics coupled QCL-GAP
- Completing the design and development of the multipass system
- Strengthening our research, education, and training STEM facilities, focusing on explosives sensing concepts and data analysis at the University of Puerto Rico.

This ongoing process is visualized to allow for continuous, sustainable participation of undergraduate students and development of faculty from the BS program focused on Technology in Industrial Chemical Processes at UPR at Arecibo. Students and faculty members will be pipelined into UPRM MS and PhD programs and further into DHS, US government, and private sector internships and work opportunities.

C.2. Sub-Project 2

Planning of a joint venture with Michele Hinnrichs (VERLUZ, LLC; Humacao, PR), a division of Pacific Advanced Technology, Corp. (Solvang, CA), Targeted SBIR: DHS (Jim Jensen, DHS program manager,

Edgewood Chemical Biological Center, Aberdeen Proving Grounds, Aberdeen, MD). Other possible sources of funding are DoD-DTRA, other DoD divisions, and NSF.

The goal of Sub-Project 2 is to transition Laser-Induced Thermal Imaging Spectroscopy (LITIS) together with VERLUZ, LLC.

The expected outcomes include:

- Establishing the feasibility of LITIS on reflective and dielectric (i.e., non-reflective) substrates using various HEs/substrates combinations
- Establishing the limits of detection and quantification of the technique
- Establishing a joint venture with an industrial partner (VERLUZ, LLC) for developing an instrument capable of detecting explosive residues at a distance using an active sensing modality.

C.3. Sub-Project 3

Intellectual property stemming from this task will be made available, cost-free, possibly through a mechanism similar to the one used by the University of Rhode Island, with its database of explosives properties.

The goal of Sub-Project 3 is to predict the performance and thermochemical properties of new energetic materials using computational chemistry, from a given molecular structure without using experimental measurements.

The expected outcomes include:

- Predicting the detonation parameters without experimental data for a systematic set of novel green energetic materials with high nitrogen and low carbon content as triazoles, tetrazoles, azidotetrazoles, triazene, nitro-substituted cage compounds, and oxygen-rich organic peroxides
- Training students in computational chemistry to integrate the information provided by different programs of molecular modeling and chemometrics routines for the prediction of explosive properties

IV. PROJECT ACCOMPLISHMENTS AND DOCUMENTATION

A. Education and Workforce Development Activities

1. Student Internship, Job, and/or Research Opportunities
    a. Annette M. Colón-Mercado, MS student, summer 2020, research internship, Naval Research Lab, Indian Head division, Washington, DC (canceled due to COVID-19)
    b. Francheska M. Colón González, MS student, summer 2020, research internship, Sandia National Laboratories, Albuquerque, New Mexico (canceled due to COVID-19)
2. Training to Professionals or Others
    a. Raman Spectroscopy Workshop I, October 2019, Society for Applied Spectroscopy (SAS-UPRM)
    b. Raman Spectroscopy Workshop II, November 2019, SAS-UPRM
    c. Raman Spectroscopy Workshop III, March 2020, SAS-UPRM

B. Peer Reviewed Journal Articles

1. Pacheco-Londoño, L.C., Galán-Freyle, N.J., Figueroa-Navedo, A.M., Infante-Castillo, R., Ruiz-Caballero, J.L., & Hernández-Rivera, S.P. "Quantum Cascade Laser Back-Reflection Spectroscopy at Grazing-Angle Incidence Using the Fast Fourier Transform as a Data Preprocessing Algorithm." *Journal of Chemometrics*, *33*, 29 July 2019, p. e3167. https://doi.org/10.1002/cem.3167.
2. Pacheco-Londoño, L.C., Ruiz-Caballero, J.L., Ramírez-Cedeño, M.L., Infante-Castillo, R., Gálan-Freyle, N.J., & Hernández-Rivera, S.P. "Surface Persistence of Trace Level Deposits of Highly Energetic Materials." *Molecules*, *24*(19), 26 September 2019, p. 3494. https://doi.org/10.3390/molecules24193494.
3. Galán-Freyle, N.J., Ospina-Castro, M.L., Medina-González, A.R., Villarreal-González, R., Hernández-Rivera, S.P., & Pacheco-Londoño, L.C. "Artificial Intelligence Assisted Mid-Infrared Laser Spectroscopy in situ Detection of Petroleum in Soils." *Applied Sciences*, *10*(4), 15 February 2020, p. 1319. https://doi.org/10.3390/app10041319.
4. Pacheco-Londoño, L.C., Warren, E., Galán-Freyle, N.J., Villarreal-González, R., Aparicio-Bolaño, J.A., Ospina-Castro, M.L., Shih, W.C., & Hernández-Rivera, S.P. "Mid-Infrared Laser Spectroscopy Detection and Quantification of Explosives in Soils Using Multivariate Analysis and Artificial Intelligence." *Applied Sciences*, *10*(6), 31 May 2020, p. 1319. https://doi.org/10.3390/app10041319; https://doi.org/10.3390/app10124178.

Pending –

1. Colón-González, F.M., Perez-Almodovar, L.A., Barreto-Pérez, M., Vargas-Alers, G.L., Santos-Rolón, J.M., & Hernández-Rivera, S.P. "Raman Scattering Detection of High Explosives on Human Hair." *Optical Engineering*, submitted February 2020.
2. Colón-Mercado, A.M., Vázquez-Vélez, K.M., Caballero-Agosto, E., Villanueva-López, V., Infante-Castillo, R., & Hernández-Rivera, S.P. "Detection and Classification of High Explosives Samples Deposited on Various Substrates Types Using a Mid-infrared Laser Grazing Angle Probe Assisted by Multivariate Analysis." *Optical Engineering*, submitted February 2020.
3. Galán-Freyle, N.J., Pacheco-Londoño L.C., Figueroa-Navedo, A.M., Ortiz-Rivera, W., Castro-Suarez, J.R., & Hernández-Rivera, S.P. "Modulated-Laser Source Induction System for Remote Detection of Infrared Emissions of High Explosives Using Laser-Induced Thermal Emission (LITE)." *Optical Engineering*, submitted February 2020.

C. Other Presentations

1. Poster Sessions
   a. Caballero-Agosto, E.R., Infante-Castillo, R., & Hernández-Rivera, S.P. "1H, and 13C NMR Chemical Shifts Prediction Models for Peroxi-Based Compounds with Computational Chemistry" [poster]. Industrial Advisory Board Meeting, Awareness and Localization of Explosive-Related Threats, Northeastern University Innovation Campus at Burlington, MA. 4 November 2019.
   b. Colón-Gonzalez, F.M., & Hernández-Rivera, S.P. "Detection of HE's on Human Hair by Raman Spectroscopy" [poster], Industrial Advisory Board Meeting, Awareness and Localization of Explosive-Related Threats, Northeastern University Innovation Campus at Burlington, MA. 4 November 2019.

c. Colón-Mercado, A.M., López-Pagán, B.M., Ruíz-Caballero, J.L., & Hernández-Rivera, S.P. "Enhanced Detection of High Energetics Materials in Substrates Using Tunable Quantum Cascade Laser-Grazing Angle Probe" [poster], Industrial Advisory Board Meeting, Awareness and Localization of Explosive-Related Threats, Northeastern University Innovation Campus at Burlington, MA. 4 November 2019.

2. Interviews and/or News Articles

a. Colón-Mercado, A.M. "Meet the ALERT Students." Industrial Advisory Board Meeting, Awareness and Localization of Explosive-Related Threats, Northeastern University Innovation Campus at Burlington, MA. 4 November 2019.

b. Colón-Mercado, A.M. "Student from RUM Stands Out in DHS Security Challenge." *Primera Hora*, local PR newspaper, 23 November 2019. https://www.primerahora.com/noticias/puerto-rico/notas/estudiante-del-rum-se-destaca-en-competencia-del-departamento-de-seguridad-nacional/.

D. Student Theses or Dissertations Produced from This Project

1. Colón-González, F.M. "Detection and Discrimination of High Explosives on Human Hair by Raman Scattering." MS Thesis, University of Puerto Rico at Mayagüez, May 2020.

2. Colón-Mercado, A.M. "Quantum Cascade Laser-Grazing Angle Spectroscopy Detection of High Explosives Deposited on Various Substrates Using Air Spray." MS Thesis, University of Puerto Rico at Mayagüez, May 2020.

3. Padilla-Rivera, G.I. "TNT and MO Photodegradation in Deionized and Salt Waters with Visible Light Assisted by Photoactivation of Modified TiO_2." MS Thesis, University of Puerto Rico at Mayagüez, May 2020.

E. New and Existing Courses Developed and Student Enrollment

New or Existing	Course/Module/Degree/Cert.	Title	Description	Student Enrollment
Existing	Certificate program course in forensic chemistry	Chemistry of Explosives	For students of chemistry and chemical engineering	15

F. Technology Transfer/Patents

1. Patent Applications Filed (Including Provisional Patents)

a. Hernández-Rivera, S.P., & Castro-Suarez, J.R. "Coupling of Thin-Layer Chromatography (TLC) to Quantum Cascade Laser Spectroscopy (QCLS) for Qualitative and Quantitative Field Analyses of Explosives and Other Pollutants." U.S. Patent 10,379,033 B1, 13 August 2019.

G. Software Developed

1. Databases

a. Ongoing: Library of vibrational spectra of HEs, HMEs, and precursors.

2. Algorithms

   a. Fast Fourier Transform preprocessing programmed in MATLAB 8.6.0.267246 (R2015b; MathWorks Inc., Natick, USA). This algorithm is being used to remove interference fringes from thin HE films generated by GAP-QCL RAIRS measurements. Used in Pacheco-Londoño, L.C., Galán-Freyle, N.J., Figueroa-Navedo, A.M., Infante-Castillo, R., Ruiz-Caballero, J.L., & Hernández-Rivera, S.P. "Quantum Cascade Laser Back-Reflection Spectroscopy at Grazing-Angle Incidence Using the Fast Fourier Transform as a Data Preprocessing Algorithm." *Journal of Chemometrics*, *33*, 29 July 2019, p. e3167. https://doi.org/10.1002/cem.3167.

V. REFERENCES

[1] Schraeder, B. (1995) "Early history of vibrational spectroscopy," in "Infrared and Raman Spectroscopy: Methods and Applications," Edited by Schrader, B., VCH, Weinheim, Germany.

[2] Sheppard, N. (2002) "The Historical Development of Experimental Techniques in Vibrational Spectroscopy," in "Handbook of Vibrational Spectroscopy," Chalmers, J. M. and Griffiths, P. R. Eds., Wiley, Chichester, West Sussex, England, Vol. 1, pp. 1-32.

[3] Griffiths, P. R., (2002) "Introduction to Vibrational Spectroscopy," in "Handbook of Vibrational Spectroscopy," Chalmers, J. M. and Griffiths, P. R. Eds., Wiley, Chichester, West Sussex, England, Vol. 1, pp. 1-11.

[4] Griffiths, P. R. and de Haseth J. A. (2007) "Fourier Transform Infrared Spectrometry," 2nd Ed., John Wiley & Sons, Inc., Hoboken, NJ.

[5] Larkin, P., (2011) "Infrared and Raman Spectroscopy: Principles and Spectral Interpretation" Elsevier Waltham, MA.

[6] Yinon J. and Zitrin S., (1996) "Modern Methods and applications in the analysis of explosives," John Wiley & Sons Ltd., Chichester, UK.

[7] Castro-Suarez, J. R., Ortiz-Rivera, W., Galán-Freyle, N., Figueroa-Navedo, A., Pacheco-Londoño, L. C. and Hernández-Rivera, S. P., "Multivariate Analysis in Vibrational Spectroscopy of Highly Energetic Materials and Chemical Warfare Agents Simulants" in "Multivariate Analysis in Management, Engineering, and the Sciences," Valim de Freitas, L., and Barbosa Rodrigues de Freitas, A.P., eds., ISBN 978-953-51-0921-1, Hardcover, 254 pages, Publisher: InTech, Rijeka, Croatia, 2013, DOI: 10.5772/3301.

[8] Steinfeld, J. I. and Wormhoudt, J., (1998) Anu. Rev. Phys. Chem. 49, 203.

[9] Committee on the Review of Existing and Potential Standoff Explosives Detection Techniques, (2004) "Existing and Potential Standoff Explosives Detection Techniques," National Research Council, National Academy of Sciences Committee, Washington, DC.

[10] Parmenter, J. E., (2004) "The challenge of standoff explosives detection," Proceedings of the 38th Annual International Carnahan Conference on Security Technology, 355-358, IEEE: New York, NY.

[11] Schubert, H. and Rimski-Korsakov, A., (2005) "Standoff Detection of Suicide-Bombers and Mobile Subjects," Proceedings of the NATO Advanced Research Workshop on Standoff Detection of Suicide Bombers and Mobile Subjects, NATO Security through Science Series B: Physics and Biophysics, Pfinztal, Germany, Springer, Germany.

[12] Moore, D. S., (2004) Rev. Sci. Instrum. 75: 2499.

[13] Moore, D. S., (2007) Sens. Imaging, 8(1): 9.

[14] Marshall, M., and Oxley, J. C., (2009) "Aspects of Explosives Detection," Elsevier, Amsterdam, The Netherlands.

[15] Caygill, J. S., Davis, F., Higson, S. P. J., (2012) ''Current Trends in Explosive Talanta. 2012. 88: 14-29.

[16] Tourné, M., (2013) J. Forensic Res. S12: 002.

[17] Fountain III, A. W. Christesen, S. D. Moon, R. P. and Guicheteau, J. A., (2014) Appl. Spectrosc. 68(8): 795.

[18] Faist, J., Capasso, F. Sirtori, C., Sivco, D. L., Baillargeon, J. N., Hutchinson, A. L., Chu, S. G., and Cho. A. Y. (1996) Appl. Phys. Lett. 68(26): 3680-3682.

[19] Capasso, F., Gmachl, C., Paiella, R., Tredicucci, A., Hutchinson, A. L., Sivco, D. L., Baillargeon, J., N. Cho, A. Y. and Liu, H. C., (2000) IEEE J. Sel. Top. Quantum Electron. 6, 931.

[20] Gmachl, C., Capasso, F., Sivco, D. L. and Cho, A. Y., (2001) Rep. Prog. Phys. 64, 1533.

[21] Beck, M., et al., (2002) Science 295, 301.

[22] Mizaikoff, B. and Lendl, B., (2002) "Sensor Systems Based on Mid-Infrared Transparent Fibers," in "Handbook of Vibrational Spectroscopy," Chalmers, J. M. and Griffiths, P. R. Eds., Wiley, Chichester, West Sussex, England, Vol. 2.

[23] Deutsch, E. R., Kotidis, P., Zhu, N., Goyal, A. K., Ye, J., Mazurenko, A., Norman, M., Zafiriou, K., Baier, M., Connors, R., (2014) Proc. SPIE. 2014. 9106 91060A-9.

[24] Castro-Suarez, J. R., Pollock, Y. S. and Hernández-Rivera, S. P. (2013) Proc. SPIE. 8710: 871010-871010.

[25] Suter, J. D., Bernacki, B., and Phillips. M. C., (2012) Appl. Phys. B: Lasers Opt. 108(4): 965–974.

[26] Castro-Suarez, J.R., Hidalgo-Santiago, M., Hernández-Rivera, S.P., (2015) Appl. Spectrosc. 69(9): 1023-1035.

[27] Pushkarsky, M. B., Dunayevskiy, I. G., Prasanna, M., Tsekoun, A. G., Go, R. and Patel, C. K. N., (2006) Proc. Natl. Acad. Sci. U.S.A. 2006. 103(52): 19630–19634.

[28] Patel. C. K. N. (2009) Proc. SPIE. 7484: 748402.

[29] Bauer, C., Willer, U. and Schade. W., (2010) Opt. Eng. 49(11): 111126-111126-7.

[30] Pacheco-Londoño, L. C., Castro-Suarez, J. R. and Hernández-Rivera. S. P., (2013) Adv. Opt. Tech. 2013. Article ID: 532670.

[31] Van Neste, C. W. Senesac, L. R. and Thundat, T., (2009) Anal. Chem. 81, 1952-1956.

[32] Hildebrand, J., Herbst, J., Wöllenstein, J. and Lambrecht. A., (2009) Proc. SPIE. 7222: 72220B.

[33] Fuchs, F., Hugger, S., Kinzer, M., Aidam, R., Bronner, W., Losch, R. and Yang. Q., (2010) Opt. Eng. 49(11): 111127-111127-8.

[34] Pacheco-Londoño, L.C., Castro-Suarez, J.R., Galán-Freyle, N.J., Figueroa-Navedo, A.M., Ruiz-Caballero, J.L., Infante-Castillo, R., Hernández-Rivera, S.P.; "Mid-Infrared Laser Spectroscopy Applications I: Detection of Traces of High Explosives on Reflective and Matte Substrates", Chapter 2, pp. 11-34, DOI: 10.5772/intechopen.81923, in "Infrared Spectroscopy: Principles, Advances, and Applications" Ed. M. El-Azary, IntechOpen, London, UK, 2019. ISBN: 978-1-78984-968-4; OnLine: 978-1-78984-969-1.

[35] Pacheco-Londoño, L.C., Galán-Freyle, N.J., Padilla-Jiménez, A.C., Castro-Suarez, J.R., Figueroa-Navedo, A.M., Ruiz-Caballero, J.L., Infante-Castillo, Rios-Velazquez, C. Hernández-Rivera, S.P. "Mid-Infrared Laser Spectroscopy Applications in Process Analytical Technology: Cleaning Validation, Microorganisms, and Active Pharmaceutical Ingredients in Formulations", Chapter 3, pp. 35-57, DOI:

10.5772/intechopen.82402, in “Infrared Spectroscopy: Principles, Advances, and Applications” Ed. M. El-Azary, IntechOpen, London, UK, 2019. ISBN: 978-1-78984-968-4; OnLine: 978-1-78984-969-1.

[36] Gallagher, N. B., Blake, T. A., Gassman, P. L., Shaver, J. M., Windig, W., Appl. Spectrosc., (2006) 60(7): 713-722.

[37] Pacheco-Londoño, L.C., Aparicio-Bolaño, J.A., Galán-Freyle, N.J., Román-Ospino, A.D. and Hernandez-Rivera, S.P., App. Spectrosc., (2019) 73(1) 17-29 DOI 10.1177-0003702818780414.

[38] Pacheco-Londoño, L. C.; Galán-Freyle, N. J.; Figueroa-Navedo, A. M.; Infante-Castillo, R.; Ruiz-Caballero, J. L.; Hernández-Rivera, S. P. Quantum Cascade Laser Back-reflection Spectroscopy at Grazing-angle Incidence Using the Fast Fourier Transform as a Data Preprocessing Algorithm. J. Chemom. 2019, 33 (9). https://doi.org/10.1002/cem.3167.

[39] Yeh, K. Bhargava, R., Mahadevan-Jansen, A., Petrich, W., Eds.; 2016; p 970406. https://doi.org/10.1117/12.2230003.

[40] Morales-Rodríguez, M. E. McFarlane, J. Kidder, M. K. Int. J. Anal. Chem. 2018, 2018, 1–9. https://doi.org/10.1155/2018/7896903.

[41] Schwaighofer, A., Montemurro, M., Freitag, S., Kristament, C., Culzoni, M. J., Lendl, B. Anal. CHEs. 2018, acs.analcHEs.8b01632. https://doi.org/10.1021/acs.analcHEs.8b01632.

THRUST R4

VIDEO ANALYTICS & SIGNATURE ANALYSIS

Project Number	Project Title	Lead Investigator(s)	Other Faculty Investigator(s)
R4-A.1	Dynamics-Based Video Analytics	Octavia Camps Mario Sznaier	
R4-A.3	Human Detection & Re-Identification for Mass Transit Environments	Rich Radke	
R4-B.1	Toward Advanced Baggage Screening: Reconstruction & Automatic Target Recognition	Charles Bouman	
R4-B.2	Multi-Energy, Limited-View Computed Tomography	Eric Miller	James Webber Kenny Yau
R4-C.1	Advanced Multispectral Computed Tomography Algorithms	Clem Karl	David Castañón

This page intentionally left blank.

R4-A.1: Dynamics-Based Video Analytics

I. PARTICIPANTS INVOLVED FROM JULY 1, 2019 TO JUNE 30, 2020

Faculty/Staff			
Name	**Title**	**Institution**	**Email**
Octavia Camps	Co-PI	Northeastern University	o.camps@northeastern.edu
Mario Sznaier	Co-PI	Northeastern University	m.sznaier@northeastern.edu
Graduate, Undergraduate and REU Students			
Name	**Degree Pursued**	**Institution**	**Month/Year of Graduation**
Sadjad Esfeden Asghari	PhD	Northeastern University	12/2021
Wenqian Liu	PhD	Northeastern University	5/2021
Dan Luo	PhD	Northeastern University	12/2023
Bengizu Ozbay	PhD	Northeastern University	12/2021
Dong Yin	PhD	Northeastern University	12/2022
Yuexi Zhang	PhD	Northeastern University	12/2021
Armand Comas	MS, PhD	Northeastern University	6/2019 (MS), 6/2024 (PhD)
Timothy Rupprecht	MS	Northeastern University	8/2020
Can Uner	MS	Northeastern University	12/2019

II. PROJECT DESCRIPTION

A. Project Overview

Video-based methods can provide advanced warning of terrorist activities and threats. In addition, they can assist and substantially enhance localized, complementary sensors that are more restricted in range, such as radar, infrared, and chemical detectors. Moreover, since the supporting hardware is relatively inexpensive and largely already deployed (stationary and mobile networked cameras, including camera cell phones, capable of broadcasting and sharing live video feeds), the additional investment required is minimal.

Arguably, a critical impediment to fully realizing this potential was the absence of reliable technology for robust, real-time interpretation of the abundant, multi-camera video data. The dynamic and stochastic nature of this data, compounded with its high dimensionality, and the difficulty to characterize distinguishing features of benign versus dangerous behaviors, makes automatic threat detection extremely challenging. Indeed, state-of-the-art turnkey software relies heavily on human operators, which in turn severely limits the scope of its use.

This research effort was motivated by an emerging opportunity to address these challenges, exploiting advances at the confluence of robust dynamical systems, computer vision, and machine learning. A fundamental feature and key advantage of the envisioned methods is the encapsulation of metadata on targeted behavior using dynamics-based and statistical-based invariants. Drawing on solid theoretical

foundations, robust system identification and adaptation methods, along with model (in)validation and artificial intelligence tools, we designed algorithms for quantifiable characterization of threats and benign behaviors, provable uncertainty bounds, and alternatives for viable explanations of observed activities.

Specifically, this research sought to predict and isolate threats in crowded public spaces—such as sports arenas, airports, bus terminals—and vulnerable urban spaces, as illustrated in Figure 1.

Figure 1: This research sought to predict and isolate threats in crowded public spaces, such as sport arenas and transport terminals, and vulnerable urban spaces.

Toward this goal, we developed algorithms to:

- answer the "who, what, where, and why" questions from video data;
- identify security breaches at portals;
- track movements across distributed camera networks;
- detect suspicious, potentially threatening activities; and
- flag objects left behind.

The resulting systems integrate real-time data from multiple sources over dynamic networks, covering large areas, extracting meaningful behavioral information on a large number of individuals and objects, and striking a difficult compromise between the inherent conservatism demanded from threat detection and the need to avoid a high false-alarm ratio, which heightens vulnerability by straining resources.

The impact of successful video analytics such as the ones developed in this project are very relevant to the Department of Homeland Security (DHS). Our goal was to provide tools to automatically process vast amounts of visual data, most of which is not relevant, and to localize, both in space and time, critical actionable information that is needed to ensure safety in large public spaces.

B. State of the Art and Technical Approach

Recent advances in the accuracy and efficiency of object detectors [1, 2], particularly pedestrian detectors, have inspired and fueled multi-target tracking approaches for detection. These techniques proceed by detecting the targets frame by frame, using a high quality object detector, and then associating these detections by using online or offline trackers [3-5]. Often, these associations are based on appearance and location similarity; however, these approaches fail when the appearance of the targets is discriminative and the targets display simple motion patterns. While there are trackers that rely less on appearance [6-10], they often require the tuning of a large number of parameters and the expertise to adapt the algorithms to these more challenging scenarios. Alternatively, Ding et al. [11] showed that it is possible to use dynamics

to compare tracks and disambiguate between targets without assuming a motion model a priori; however, the computational and memory complexity of this approach has limited its application to short trajectories of a few targets.

Multiple cameras are used to cover wide areas and provide different viewpoints of targets. Maintaining consistent identity labels across cameras is a difficult problem since the appearance of the targets can be quite different when seen from different angles. Previous approaches to this problem include matching features such as color and apparent height [12-14, 15], using 3D information from camera calibration [13, 16-20], using the epipolar constraint [21-23], modeling the relationship between the appearance of a target in different views through a linear time invariant system [24], or computing homographies between views [25-29]. When the cameras do not have overlapping fields of view, targets must be re-identified (re-IDed) across cameras. A good overview of existing re-ID methods can be found in [30-34] and the references therein.

The three most important aspects in re-ID are the features used, the matching procedure, and the performance evaluation. Most re-ID approaches use appearance-based features that are viewpoint quasi-invariant [35-40], such as color and texture descriptors; however, the number of features used varies greatly across approaches, making it difficult to compare their impact on performance. Using standard metrics such as Euclidean distance to match images based on these types of features results in poor performance due to the large variations in pose, illumination, and limited training data. Thus, recent approaches [34, 41-44] design classifiers to learn specialized metrics that enforce features from the same individual to be closer than features from different individuals. Yet, state-of-the-art performance remains low, slightly above 30% for the best match. Performance is often reported on standard datasets, and while they are challenging, they bring in different biases. Moreover, the number of datasets and the experimental evaluation protocols used also vary greatly across approaches, making it difficult to compare them.

Video frame prediction is an active research topic [45-54]. Most approaches use convolutional networks, such as 3D convolutional networks [55] or generative adversarial networks (GANs) [56] to synthetize future frames. Many techniques work directly on pixel values [52, 57-60] while others [61, 62] use/predict optical flow as well. However, the performance of convolutional schemes is limited by short-range dependencies, and they often experience blurriness in the predicted frames.

Human pose estimation [63-67], which seeks to estimate the locations of human body joints, has many practical applications such as smart video surveillance[68, 69], human computer interaction [70], and virtual reality (VR) / augmented reality (AR) [71]. The most general pose estimation pipeline extracts features from the input and then uses a classification/regression model to predict the location of the joints. Recently, Bertasius et al. [72] introduced a Pose Warper capable of using a few manually annotated frames to propagate pose information across the complete video. However, it relies on annotations of every k^{th} frame, and thus it fails to fully exploit the dynamic correlation between them.

Dynamics, and more precisely dynamic invariants, can be used to extract critical information from data streams. Robust identification of piecewise affine dynamic systems has been the subject of recent intensive research, leading to a number of techniques meant to identify subsystem dynamics and switching surfaces [73]. A common feature is the computational complexity entailed in dealing with noisy measurements. In this case, algebraic procedures [74] lead to nonconvex optimization problems, while optimization methods lead to mixed integer/linear programming [75]. Similarly, methods relying on probabilistic priors [76] also lead to computationally complex combinatorial problems. An alternative approach is provided by clustering-based methods [77, 78]. Since these methods rely on local identification, they require “fair sampling” of each cluster, which places constraints on the data that can be used. More recently, the PIs of

this project have developed new sparsification-based techniques for identification of switched affine models that allow for several types of noise [79-81].

Finding dynamic invariants from corrupted data often requires the ability to solve optimization problems. Semidefinite programs seek to minimize a linear function subject to affine matrix equality and positive semidefinite constraints. These problems are convex (albeit nonsmooth) and thus tractable. Indeed, recent research efforts have led to numerous algorithms (for instance interior point algorithms) with polynomial complexity; excellent surveys are given in [82] and [83]. Of particular interest to this project are semidefinite programs resulting from the relaxation of constrained rank minimization problems [84, 85]. It has been recently shown [86] that in these cases, gradient-based methods outperform interior point ones. Polynomial optimization problems are highly nonconvex; however, one can find convex liftings leading to standard semidefinite programs. Two (related) approaches are usually used: the "sums of squares" approach [87], which provides convex certificates for positivity of a polynomial over a semi-algebraic set, and its dual approach, referred to as the "moments" approach [88]. Here, sufficient and asymptotically necessary conditions for a sequence to be a moment sequence of some Borel measure are used to convexify the problem [89].

C. Major Contributions

C.1. Year 7

C.1.a. Dynamics-Based Video Prediction

Humans and animals rely on making accurate predictions in order to survive in a dynamic world, as illustrated in Figure 2. Accurate predictions of the location of objects in the environment and their motion is of vital importance for autonomous navigation, estimating human intention, and controlling robots. Motivated by this need, there has been significant interest in the task of video prediction, where the goal is to synthesize future frames from previous ones.

Figure 2: Good timing is everything. In order to survive as they move in a dynamic world, humans and animals rely on having accurate predictions of where things are going to be.

During Year 6, we introduced a novel architecture, DYAN, to predict future frames from a given short video clip of a scene [90]. DYAN uses a dictionary made of a set of dynamics-based atoms to identify a dynamic model for the scene optical flow, which is used to generate future frames. This approach produces high-quality, realistic frames, but when looked at carefully, one can observe that the predictions exhibit significant lagging when compared against the ground-truth frames. We observed that one cause for this lag is that DYAN uses a Eulerian point of view: it makes predictions at a pixel location based on the previous values at this same location. This can lead to incorrect predictions when objects move in the scene

and partially occlude each other or the background. To address this shortcoming, in Year 6 we preprocessed the input flows using a recursive warping. The modified architecture, W-DYAN, tries to approximate a Lagrangian point of view, where predictions are made by following points in the 3D scene, using the optical flow as a surrogate for tracking.

In Year 7, we further improved the DYAN and W-DYAN architectures by introducing a new module to reduce prediction lag caused by abrupt changes of input dynamics and to allow the networks to process arbitrary long sequences.

Abrupt changes in dynamics happen at occlusion boundaries (Eulerian point of view) and when objects change their motion patterns (Eulerian and Lagrangian points of view). To detect these changes, the proposed module uses a recursive Kalman filter on the latent dynamic encoding of the input data. Since the filter is recursive, it allows the network to process the data as it becomes available in an online fashion. Given a new frame, the filter updates its generative model and the error covariance of its predictions. The filter compares the new measurement with its prediction from previous data and determines if it is within the current estimated error covariance. If it does, the new measurement is used to refine the current model and covariance. If it doesn't, a dynamic change is detected, and a new model is initialized. A diagram of the new architecture, K-DYAN (KW-DYAN), combining this module with DYAN (W-DYAN) is shown in Figure 3.

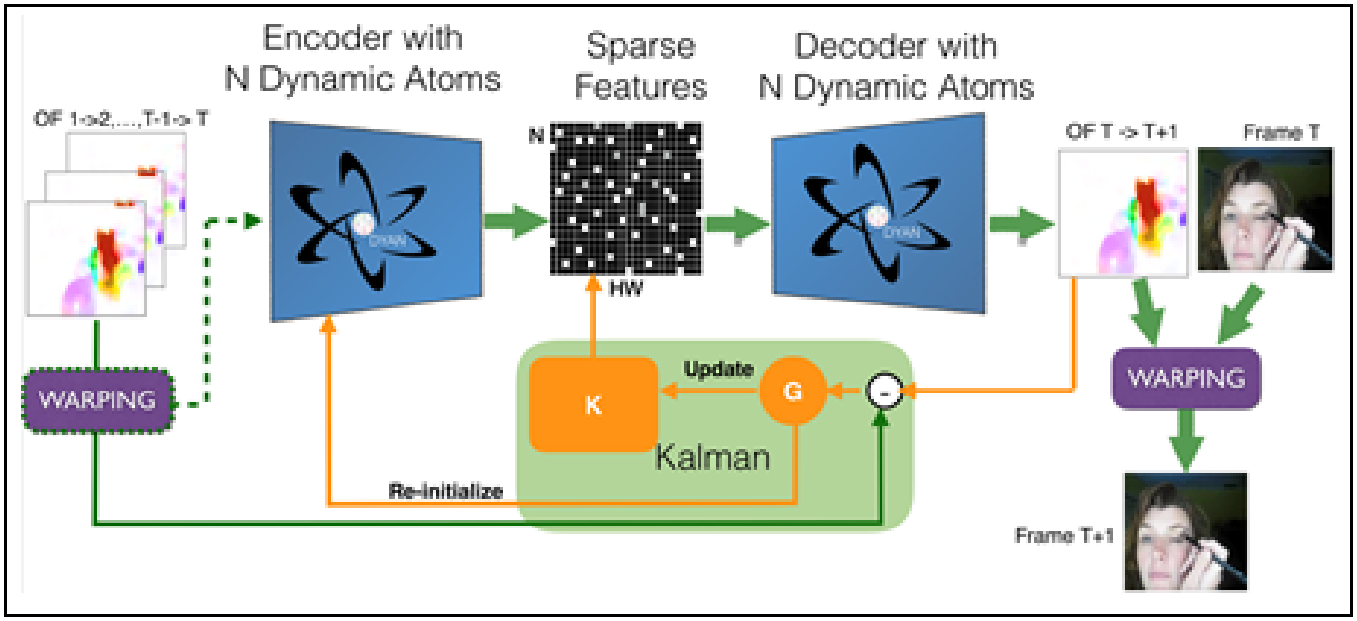

Figure 3: KW-DYAN's architecture. The latent space is filtered to estimate the error covariance, which is used by gate G to detect changes in the input dynamics, decide when to forget old inputs, and reset the system identification. The optional (dashed boundary) warping module at the input aligns the input optical flows to reduce the number of changes in dynamics in the input. All recurrent connections are shown in orange.

Figure 4 shows a qualitative example illustrating the benefits of using Kalman filtering with DYAN (K-DYAN) and warped WDYAN (KW-DYAN). As the figure shows, the module is able to significantly reduce the lag while still producing sharp images.

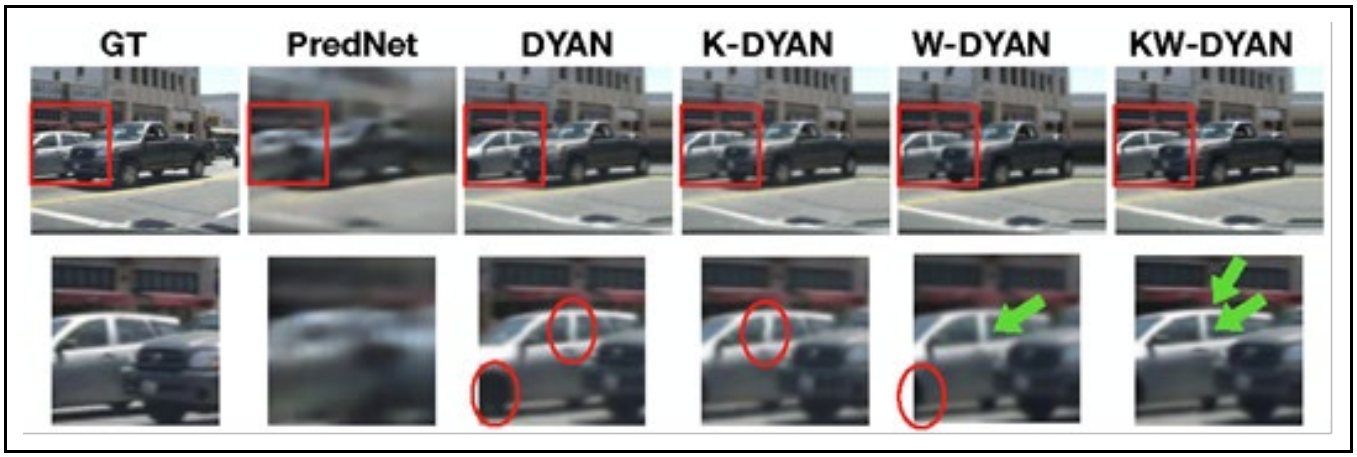

Figure 4: Qualitative example predicting the fifth future frame for the sequence set10V011 from the Caltech dataset. Top row shows the ground truth and predicted frames. Bottom row shows details inside the red box. Circled in red: incorrect position of the front tire and orientation of the window frame of the car. Green arrows: sharper roof line, correct orientation of the window frame.

We evaluated KW-DYAN and its variants and compared them against the state-of-the-art in Table 1 and Table 2, using the Caltech and UCF101 datasets, respectively. For next frame prediction, the networks predict the next optical flow and warp the last given frame. Comparisons were done with commonly used numerical measurements—mean peak-signal–to–noise ratio (PSNR) [58], mean square error (MSE), and structural similarity index measure (SSIM) [91]—to evaluate performance at the pixel level. Additionally, we report learned perceptual image patch similarity (LPIPS) distance [92], since it has been shown to be a good perceptual metric, and mean of the maximum optical flow (MMF) metric, proposed by us, to measure prediction lag. For the Human 3.6 M dataset, we evaluated long-term prediction performance using the mean of Euler angle error. Quantitatively, the higher PSNR/SSIM and the lower the MSE/LPIPS/MMF, the better the performance. As seen in the tables, the new architectures decreased lagging while still performing as good or better in the other metrics.

Method	Parameters	MSE x 10^3	SSIM	LPIPS x 10^{-2}	MMF
CopyLast	-	2.2	0.91	1.98	2.82
BeyondMSE [58]	8.9 million	3.26	0.88	-	-
PredNet [93]	6.9 million	-	0.91	7.47	-
ContextVP [49]	8.6 million	1.94	0.92	6.03	-
DualMoGan [94]	11.3 million	2.41	0.89	-	-
SDCNet [62]	-	1.62	0.92	-	-
CtrlGen [95]	-	-	0.90	6.38	-
FGVP [96]	-	-	0.92	5.04	-
DYAN	80	0.87	0.95	2.2	1.93
K-DYAN	82	0.69	0.96	2.1	1.75
W-DYAN	80	0.70	0.96	2.3	1.62
KW-DYAN	82	0.74	0.95	1.8	1.55

Table 1: Quantitative results for predictions on Caltech dataset, compared to best available open source methods.

Method	Parameters	PSNR	SSIM	LPIPS x 10^{-2}	MMF
CopyLast	-	28.6	0.89	3.8	6.25
BeyondMSE[58]	8.9 million	30.11	0.88	-	-
ContextVP[49]	8.6 million	34.9	0.92	-	-
DVF[61]	8.9 million	32.86	0.93	-	-
DYAN	80	34.26	0.95	**3.8**	5.59
K-DYAN	82	**34.90**	0.96	4.1	**4.95**
W-DYAN	80	32.07	**0.97**	4.4	5.75
KW-DYAN	82	33.59	0.95	4.1	5.87

Table 2: Quantitative results for predictions on UCF101 dataset, compared to best available open source methods. Red indicates the best scores.

C.1.b. Efficient Human Pose Estimation

In [97] we proposed an efficient pose estimation pipeline based on two observations: all frames are not equally informative, and the dynamics of the body joints can be modeled using simple dynamics. The new pipeline, shown in Figure 5, uses a light-weighted key frame proposal network (K-FPN) to select a small number of frames to apply a pose estimation model. One of the main contributions of our approach is a new loss function based on the recovery error in the latent feature space for unsupervised training of this network. The second module of the pipeline is an efficient human pose interpolation module (HPIM), which uses a dynamics-based dictionary to obtain the pose in the remaining frames.

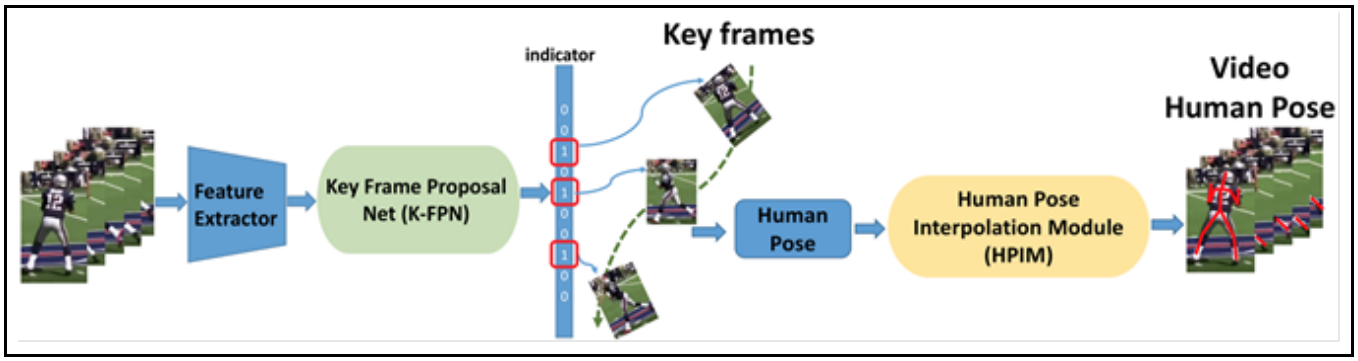

Figure 5: Proposed pipeline for video human pose detection. The K-FPN net, which is trained unsupervised, selects a set of key frames. The HPIM, trained to learn human pose dynamics, generates human poses for the entire sequence from the poses in the selected key frames.

Figure 6 shows two sample outputs of our pipeline, where the poses shown in purple were interpolated from the automatically selected red key frames. The advantages of the proposed approach are as follows:

- It uses a very light, unsupervised model to select "important" frames.
- It is highly efficient, since pose is estimated only at key frames.
- It is robust with respect to challenging conditions present in the non-key frames, such as occlusion, poor lighting conditions, and motion blur.
- It can be used to reduce annotation efforts for supervised approaches by selecting which frames should be manually annotated.

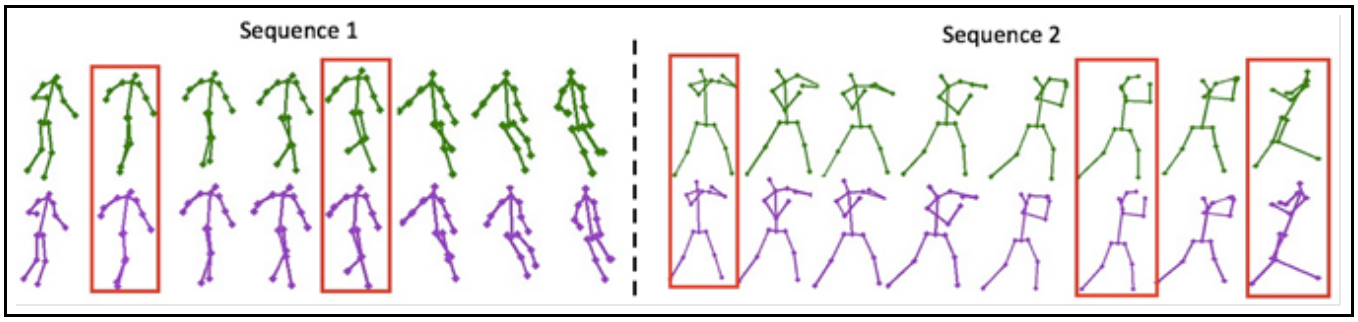

Figure 6: Two examples of the output of our pipeline, (top) ground truth and (bottom) poses recovered from the automatically selected key frames (red boxes).

The architecture of the frame selection network K-FPN is shown in Figure 7. It is trained completely unsupervised by minimizing the loss:

$$|[I - \rho^{-1}DD^{T}S]^{-1}Y|_F^2 + \lambda \sum_i s_i$$

where D is a dynamics-based DYAN dictionary, S is a diagonal matrix with diagonal elements s_i, which are the selection variables (1 for key frames, 0 otherwise), and Y is a tensor of image features of the input video. The first term of the loss penalizes reconstruction error of the input features from the features of the key frames while the second term penalizes the number of key frames.

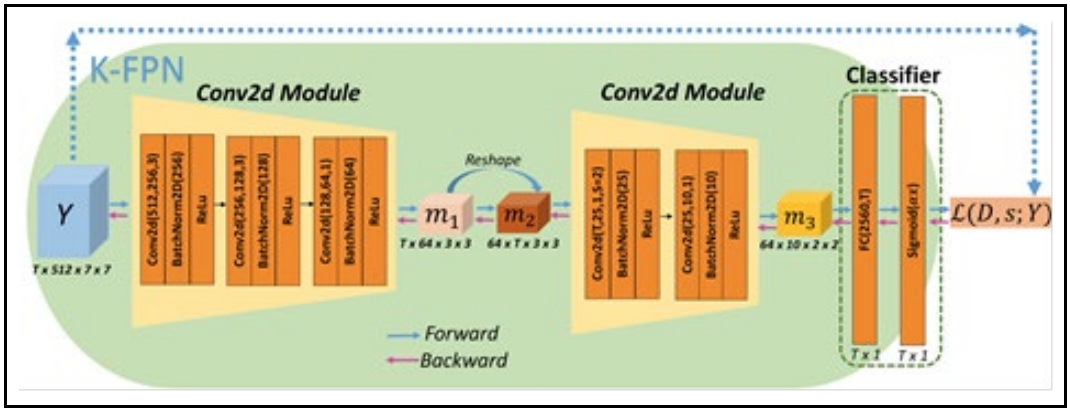

Figure 7: K-FPN architecture.

The network has two Conv2D modules followed by a fully connected and an adaptive Sigmoid layer, where the Sigmoid layer forces the output logits to be close to binary.

The HPIM efficiently interpolates the pose for the entire sequence, H, from the poses in the selected keyframes, H_r:

$$\boldsymbol{H} = \left(\boldsymbol{D}^{(h)}\boldsymbol{D}^{(h)^T}\right)\boldsymbol{P}_r^T\left[\boldsymbol{P}_r\left(\boldsymbol{D}^{(h)}\boldsymbol{D}^{(h)^T}\right)\boldsymbol{P}_r^T\right]^{-1}\boldsymbol{H}_r$$

where P_r is the selection matrix, $D^{(h)}$ is a dynamics-based DYAN dictionary for the poses, and $\left(D^{(h)}D^{(h)^T}\right)$ can be precomputed.

We evaluated the proposed approach on two widely used datasets: Penn Action (Table 3) and sub-JHMDB (Table 4). The input features *Y* were obtained using the ResNet family [98]. Our approach achieves the best performance and is 1.6 times faster (6.8 ms versus 11 ms) than the previous state-of-art [99] for the Penn Action dataset, using an average of 17.5 key frames. Moreover, if we use our lightest model (Resnet34), our approach is 2 times faster than [99] with a minor PCK degradation. For the sub-JHMDB dataset, we run more than 2 times faster than [100] without any degradation in accuracy.

Method	Time (ms)	Avg PCK	#Key Frames (avg,stdev)
Nie et al. [101]	-	48.0	N/A
Iqal et al. [102]	-	81.1	N/A
Gkioxari et al. [103]	-	91.9	N/A
Song et al. [104]	-	96.8	N/A
Luo et al. [105]	25.0	97.7	N/A
DKD (small CPM) [99]	12.0	96.8	N/A
Baseline [100]	11.3	97.4	N/A
DKD (ResNet50) [99]	11.0	97.8	N/A
Ours (ResNet50)	**6.8**	**98.0**	(17.5,4.9)
Ours (ResNet34)	**5.3**	**97.40**	(15.2,3.3)

Table 3: Performance evaluation on Penn Action dataset. Red indicates the best results.

Method	Time(ms)	Avg PCK	#Key Frames (avg,stdev)
Park et al.		52.5	N/A
Nie et al. [101]	-	55.7	N/A
Iqal et al. [102]	-	73.8	N/A
Song et al. [104]	-	92.1	N/A
Luo et al. [105]	24.0	93.6	N/A
DKD (ResNet50) [99]	-	94.0	N/A
Baseline [100]	10.0	94.4	N/A
Ours (ResNet50)	**7.0**	**94.7**	(17.8,1.4)
Ours (ResNet34)	**4.7**	**94.5**	(16.3,1.8)

Table 4: Performance evaluation on sub-JHDMB dataset. Red indicates the best results.

C.1.c. Explainable Variational Autoencoders and Anomaly Detection

Applications in safety-critical and consumer-focusing areas demand a clear understanding of the reasoning behind an algorithm's predictions, in addition certainly to robustness and performance guarantees. Consequently, there has been substantial recent interest in devising ways to understand and explain the underlying "why" driving the output of "what."

While progress in algorithmic generative modeling has been swift, explaining such generative algorithms is still a relatively unexplored field of study. There are certainly some ongoing efforts in using the concept of visual attention in generative models, but the focus of these methods is to use attention as an auxiliary information source for the particular task of interest, and not visually explain the generative model itself.

In [106], we take a step toward bridging this gap, proposing the first technique to visually explain variational autoencoders (VAE), by means of gradient-based attention. The intuition behind the proposed approach is that the latent space of a trained VAE captures key properties of the encoder, and thus explanations conditioned on the latent space will be informative about the downstream predictions.

More concretely, as illustrated in Figure 8, given a learned Gaussian distribution in the latent space, we use the re-parameterization trick to sample a latent code. Then, by backpropagating the activations in each dimension of the latent code to a convolutional layer in the model and aggregating all the resulting gradients, we generate the attention map.

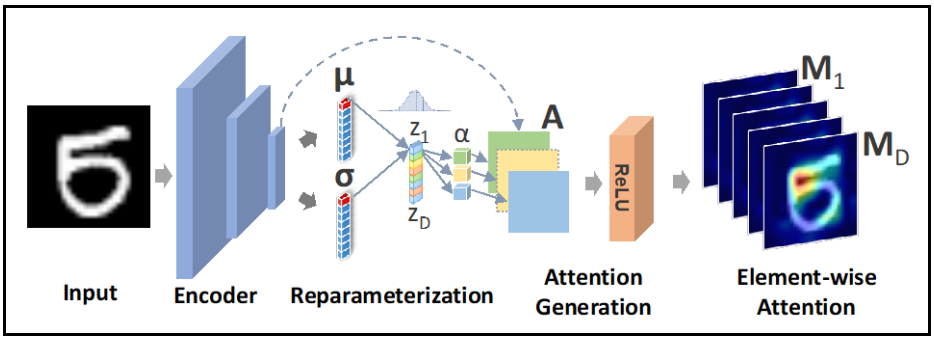

Figure 8: Element-wise attention generation with a VAE.

Let $q(z|x)$ be the posterior distribution inferred by the trained VAE for a sample x. For each element of latent vector z, we backpropagate gradients to the last convolutional feature map A, to obtain the attention map M^i corresponding to the element z_i:

$$M^i = ReLU\left(\sum_{k=1}^{n} \alpha_k A_k\right)$$

where the scalar α_k is given by:

$$\alpha_k = GAP\left(\frac{\partial z_i}{\partial A_k}\right) = \frac{1}{T}\sum_{p=1}^{h}\sum_{q=1}^{w}\frac{\partial z_i}{\partial A_k^{pq}}$$

and GAP is the global average pooling operator and A_k is the k^{th} feature channel of the feature map A.

Figure 9 shows an example of an attention map M. There, we can see that each component of the latent space has consistently high localization responses. All responses can be aggregated for an overall attention map using, for example, the mean of all the attention maps.

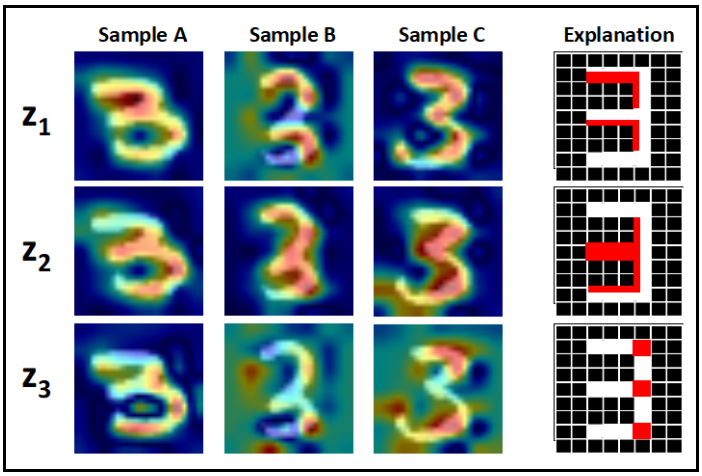

Figure 9: Each element in the latent space vector can be explained separately with the proposed attention map.

The attention maps obtained this way can also be used to localize anomaly regions, as illustrated in Figure 10 and Figure 11, given a one-class VAE trained on "normal" data (digit '1', for instance). When the VAE is given as input for an anomaly (i.e., digit "4"), the latent space for the given sample will be very different from the learned normal distribution. By simply computing the sum of all elements in the mean vector, we can obtain a score and backpropagate it to compute an anomaly attention map.

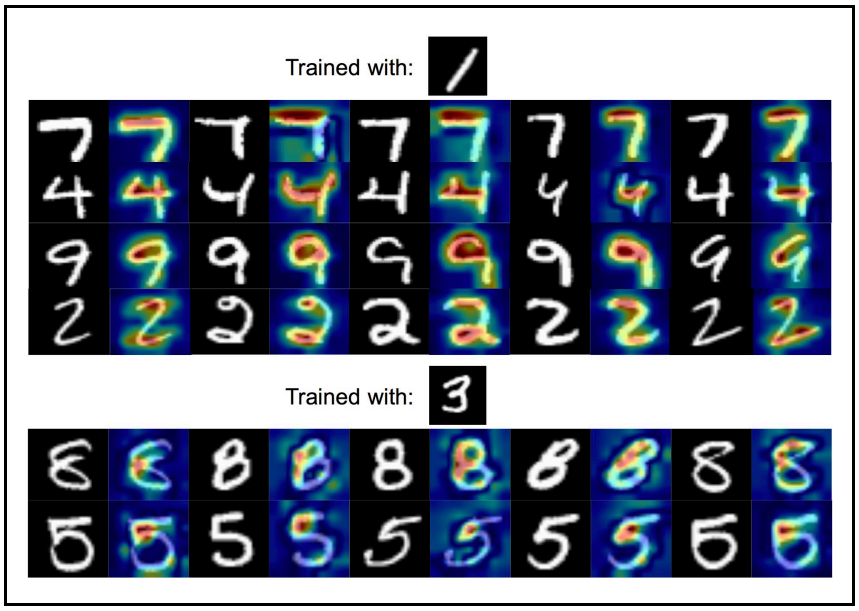

Figure 10: Anomaly localization for Modified National Institute of Standards and Technology database images.

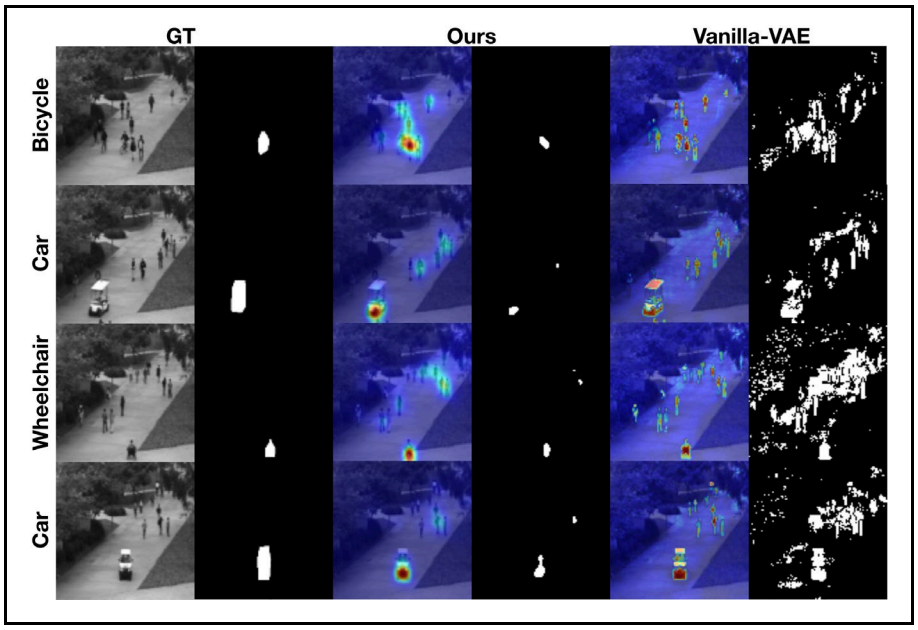

Figure 11: Anomaly detection using VAE attention maps; (left to right) original test image, ground truth masks, our attention maps, anomaly detection, and difference between input and VAE reconstruction. The anomalies in these examples are moving cars, bicycles, and wheelchair.

C.1.d. CLASP: Correlating Luggage and Specific Passengers

In addition to our core research work, we are working on a project with Rensselaer Polytechnic Institute (RPI) and Marquette University using ALERT's mock airport security checkpoint at the Kostas Research Institute. This supplement to ALERT's core cooperative agreement, Correlating Luggage and Specific Passengers (CLASP), allows us to generate large amounts of realistic data while facilitating ground truth annotation. We expect that this dataset will be the starting point for addressing many problems relevant to TSA.

During Year 7, we continued working on the CLASP task order project. In particular, we focused on the problem of activity recognition and passenger interactions. Toward this goal, we implemented several prototype learning neural networks that take combinations of RGB frames and detect actions such as putting down or picking up objects in or from bins on the conveyor belt and giving an object to another passenger.

Figure 12 shows a sample frame where the networks detect the action of putting objects in the conveyor belt bins. In our experiments, we tested using RGB alone, optical flow alone, and RGB and optical flow on a video with 67 bin transfers and 1 person-to-person transfer. RGB-alone had a precision of 0.88 and a recall of 0.90, while optical flow alone had 0.86 precision and 0.84 recall. Combining both inputs, precision improved to 0.91 and recall to 0.94.

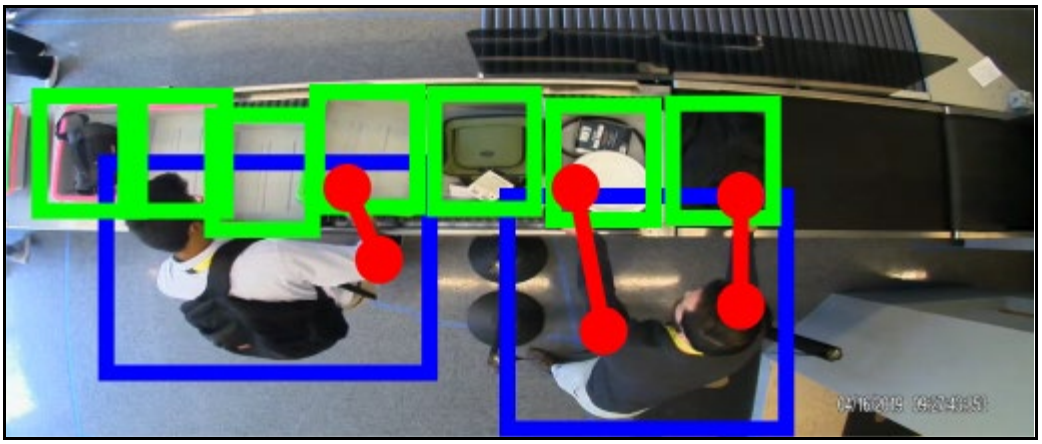

Figure 12: CLASP action detection (person to bin).

C.2. Years 1–6

The outcomes achieved in previous years (Years 1–6) are briefly summarized below.

- Tracking [107-109]:
  - We developed an algorithm that uses dynamics-based invariants to robustly track multiple targets with similar appearances. Our algorithm is faster and has better performance than the previous state-of-the-art algorithms. We have also developed a set of robust tools for tracking, including filtering and covariance propagation.
- Activity recognition [108, 110-119]:
  - We proposed an efficient algorithm to detect casual interactions by sparsifying a dynamics-based graph, where each node represents a time sequence associated with the location of an agent. This was applied to flag activity of people trying to breach security by moving into the secure area of the airport via the exit lane.
  - We developed a set of tools to compare and classify temporal sequences and applied them to the problem of activity recognition.
  - We developed a learning neural that takes an input human pose from an actor (e.g., joints or heat map of joints) and uses our DYAN encoder to capture dynamic information and classify activities.
  - We proposed a computationally efficient algorithm for the identification of error-in variables switched systems that can be used to segment activities from time traces of the position of a person's centroid in a video sequence.
- Human re-identification [120-123]:
  - In collaboration with Transportation Security Administration (TSA) and the Cleveland Hopkins International Airport (CLE), we collected and annotated a dataset for human re-identification at CLE. In collaboration with Great Cleveland Rapid Transit Authority (GCRTA) and the DHS Center of Excellence VACCINE (Visual Analytics for Command, Control, and Interoperability Environments), we collected and annotated a second dataset (where targets changed appearance) at bus terminals in Cleveland, OH.

- We benchmarked re-id algorithms and proposed a better kernel-based metric learning approach. We also addressed the problem of re-identifying targets in appearance-impaired scenarios, when targets have similar appearance or change appearance between views.

- Video prediction [90]:
  - We introduced a novel dynamics-based neural network, DYAN, that captures the dynamics of an input video sequence to predict future frames. The network is very compact, with only 80 parameters and achieved state-of-art performance.
  - We introduced a new metric to quantify prediction lagging.
  - We modified DYAN, using a recursive warping module to reduce temporal lagging in the predictions.
- Mathematical tools [108, 109, 111, 112, 114, 116, 117, 124-132]:
  - We developed theory-connecting machine learning and systems identification. For example, we developed the following tools:
    - A method for robustly estimating the fundamental matrix in stereo camera systems
    - A method for linear robust regression in the presence of gross outliers
    - A method for subspace clustering capable of incorporating prior information, which is suitable for motion and planar surfaces segmentation
    - An algorithm to chronologically sort crowd-sourced images in order to recover temporal information of an event
    - A robust algorithm for linear subspace clustering using a sum-of-squares approach
- Deep-model–based approaches [90, 133]:
  - We started incorporating our dynamics-based and statistical-based approaches into deep models. For example, we developed a deep architecture using moments embedding for fine-grain classification of objects that can only be distinguished by fine details. We also developed a deep architecture that incorporates dynamics-based layers for video encoding.
- Multi-camera motion segmentation [134]:
  - We developed an approach for motion segmentation of data collected with unsynchronized multiple cameras that combines shape and dynamical information but does not require spatiotemporal registration or shared features across video streams.
- CLASP [135]:
  - We implemented a set of algorithms for tasks related to CLASP, including passenger and bin detection, and upper body human pose estimation. The performance of the algorithms has been evaluated using data captured at ALERT's mock airport security checkpoint located at the NU Kostas Research Institute (KRI) in Burlington, MA.

D. Milestones

During Year 7, we continued working on the problems of activity segmentation, video prediction, and passenger-luggage association. We achieved the following milestones:

- Improved and tested dynamic-invariants–based deep architectures for video prediction to reduce prediction lag and process arbitrary length inputs.
- Designed and implemented an efficient deep pipeline to estimate human pose. The proposed approach is two times faster than the previous state of art.
- Designed and implemented a visual attention mechanism to explain variational autoencoders, which can be used for anomaly detection.
- Designed, implemented, and tested three preliminary architectures for action recognition for the CLASP project that can process RGB, optical flow, and a combination of the two to detect actions in real time.

E. Final Results as Project Completion (Year 7) / No-Cost Extension

Due to the current situation with COVID-19, we have not been able to collect (and label) additional data at the KRI for our CLASP research. This delay has impacted our ability to train and test our algorithms for activity detection and activity prediction. As a consequence, we have not been able to complete several of the anticipated milestones. Thus, we are planning to resume and continue this work through the no-cost extension period, ending in May 2021, to accomplish the following expected milestones:

- **MILESTONE 1**—Collect and annotate more data at the CLASP facility at KRI that captures a passenger's actions, from a side view.
  - NEXT STEPS: The collected data will be used to augment public available datasets and train a deep network for person and person-to-person activities for CLASP data. In particular, we will focus on interactions between passengers and transportation security officers during secondary screening and integrate human pose inputs.
- **MILESTONE 2**—Update the K-DYAN encoder to detect occlusions and fill gaps.
  - NEXT STEPS: We plan to extend the Kalman module to also run "backward in time" to provide further noise smoothing and to detect spatial occlusions and train a GAN to fill gaps.
- **MILESTONE 3**—We have implemented a prototype network to perform activity classification, which has been trained and tested using standard activity recognition datasets. However, the current network is not robust to partial detections and occlusions. We are making improvements to the current architecture by incorporating optical flow as part of the inputs.
  - NEXT STEPS: In addition to optical flow, we will incorporate human pose estimates as part of the input. Furthermore, we will use network distillation to eliminate the need to compute optical flow and pose during testing time in order to reduce computational complexity.
- **MILESTONE 4**—Fine-tune and test the new network performance using CLASP data.
  - NEXT STEPS: Once milestones 1 and 3 are completed, we will perform fine-tuning with CLASP data and will reevaluate the performance.
- **MILESTONE 5**—Extend the network to also perform action prediction. Train and test its performance using standard activity recognition datasets.
  - NEXT STEPS: This will start after milestone 4 is completed.
- **MILESTONE 6**—Fine-tune and test its performance using CLASP data.
  - NEXT STEPS: This will start after milestones 1 and 4 are completed.

III. RELEVANCE AND TRANSITION

A. Relevance of Research to the DHS Enterprise

This research addressed the challenge of processing vast amounts of video data in real-time to enhance security by: detecting dangerous situations as they evolve; providing supporting actionable information to mitigate damage; and aiding during forensic analysis of events.

Examples of benefits that a successful "who is doing what, where, and why" system could provide, include:

- Faster throughput in airport security lines without compromising security;
- Avoidance of airport terminal closure due to breach of security incidents (such as a person reaching the secure gates area through an exit, thus bypassing security);
- Quick identification of recurrent thieves in public transportation terminals; and
- Faster forensic analysis of security incidents.

All of these applications not only have a tangible effect in ensuring public safety, but also have clear economic benefits, such as reducing human resources needed at airport security checkpoints and reducing crime in bus terminals.

B. Status of Transition at Project End

The products of this research effort have direct application to the security and surveillance of large public spaces, such as airports, mass transport system terminals, sport venues, etc. In addition to directly supporting the homeland security enterprise's mission, systems endowed with activity analysis capabilities can assist law enforcement, allow elderly people to continue living independently, and help first responders and emergency workers prevent hazards from developing into full blown catastrophic situations. Finally, as part of this work, we continue collecting and labeling data, which will be distributed to the video analytics community to be used as benchmarks to aid the advancement of the state-of-the-art.

We engaged with potential customers by reaching out to DHS-related agencies such as TSA, and by presenting our work at professional and industrial meetings. Portions of this work have already been deployed and tested at CLE, where it was used by TSA officers to detect security threats caused by persons bypassing airport security at terminal exits. We believe that the system could be transferred to other airports in the near future. In addition, we are working on a project with RPI and Marquette University using ALERT's mock airport security checkpoint at KRI. This supplement to ALERT's core cooperative agreement, named Correlating Luggage and Specific Passengers (CLASP), allows us to generate large amounts of realistic data while facilitating ground truth annotation. We expect that this dataset will be the starting point for addressing many problems relevant to TSA. Finally, through the transition team at ALERT, we will also reach out to other DHS entities, such as the US Customs and Border Protection or the US Coast Guard, to explore transitioning our video-analytics-based threat detection and assessment tools to agency specific needs.

C. Transition Pathway and Future Opportunities

Our goal is to address the user needs for surveillance of large public spaces, such as airport terminals and bus stations. As part of this research, we are developing video analytics algorithms and implementing prototype systems, which are being tested using real-world data to show their feasibility.

D. Customer Connections

These are our customers from previous years:

- CLE airport commissioner, Mr. Fred Szabo
- CLE TSA, Mr. Michael Young (retired)
- GCRTA security chief, Mr. John Joyce
- DHS Science and Technology, Apex Screening at Speed Program manager, Mr. John Fortune

IV. PROJECT ACCOMPLISHMENTS AND DOCUMENTATION

A. Education and Workforce Development Activities

1. Course, Seminar, and/or Workshop Development
   a. Professor Octavia Camps taught regular and advanced courses in computer vision, where students worked on projects for object detection, tracking, and activity classification.
   b. Professor Mario Sznaier taught a course in control theory, where students applied concepts of system identification to design vision-based systems that can be used for surveillance.
2. Student Internship, Job, and/or Research Opportunities
   a. Wenqian Liu worked as a summer intern at Amazon.
   b. Armand Comas worked as an intern at MERL.

B. Peer Reviewed Journal Articles

1. Dai, T., & Sznaier, M. "A Semi-Algebraic Optimization Approach to Data-Driven Control of Continuous-Time Nonlinear Systems." *IEEE Control Systems Letters*, *5*(2), 18 June 2020, pp. 487–492. https://doi.org/10.1109/LCSYS.2020.3003505.

C. Peer Reviewed Conference Proceedings

1. Berberich, J., Sznaier, M., & Allgower, F. "Signal Estimation and System Identification with Nonlinear Dynamic Sensors." *IEEE Conference on Control Technology and Applications*, Hong Kong, China, 19–21 August 2019.
2. Taskazan, B., Miller, J., Inyang-Udoh, U., Camps, O., & Sznaier, M. "Domain Adaptation Based Fault Detection in Label Imbalanced Cyberphysical Systems." *IEEE Conference on Control Technology and Applications*, Hong Kong, China, 19–21 August 2019.
3. Dai, T., & Sznaier, M. "Worst-Case Optimal Data-Driven Estimators for Switched Discrete-Time Linear Systems." *IEEE Conference on Decision and Control,* Nice, France, 11–13 December 2019.
4. Miller, J., Zheng, Y., Roig-Solvas, B., Sznaier, M., & Papachristodoulou, A. "Chordal Decomposition in Rank Minimized Semidefinite Programs with Applications to Subspace Clustering." *IEEE Conference on Decision and Control*, Nice, France, 11–13 December 2019.
5. Ozbay, B., Camps, O., & Sznaier, M. "Efficient Identification of Error-in-Variables Switched Systems via a Sum-of-Squares Polynomial Based Subspace Clustering Method." *IEEE Conference on Decision and Control*, Nice, France, 11–13 December 2019.

6. Singh, R., & Sznaier, M. "A Convex Optimization Approach to Finding Low Rank Mixed Time/Frequency Domain Interpolants with Applications to Control Oriented Identification." *IEEE Conference on Decision and Control*, Nice, France, 11–13 December 2019.
7. Asghari-Esfeden, S., Sznaier, M., & Camps, O. "Dynamic Motion Representation for Human Action Recognition." *IEEE 2020 Winter Conference on Applications of Computer Vision*, Aspen, CO, 1–5 March 2020, pp. 557–566.
8. Liu, W., Li, R., Zheng, M., Karanam, S., Wu, Z., Bhanu, B., Radke, R., & Camps, O. "Towards Visually Explaining Variational Autoencoders." *IEEE/CVF Conference on Computer Vision and Pattern Recognition*, Seattle, WA, 16–18 June 2020, pp. 8642–8651.
9. Singh, R., & Sznaier, M. "A Loewner Matrix Based Convex Optimization Approach to Finding Low Rank Mixed Time/Frequency Domain Interpolants." *2020 American Control Conference*, Denver, CO, 1–3 July 2020.
10. Dai, T., Sznaier, M., & Roig-Solvas, B. "Data-Driven Quadratic Stabilization of Continuous LTI Systems." *2020 IFAC World Congress*, Berlin, Germany, 12–17 July 2020.
11. Miller, J., Zhang, Y., Sznaier, M., & Papachristodoulou, A. "Decomposed Structured Subsets for Semidefinite Optimization." *2020 IFAC World Congress*, Berlin, Germany, 12–17 July 2020.
12. Ozbay, B., Sznaier, M., & Camps, O. "An Algebraic Approach to Efficient Identification of a Class of Wiener Systems." *2020 IFAC World Congress*, Berlin, Germany, 12–17 July 2020.
13. Zhang, Y., Wang, Y., Camps, O., & Sznaier, M. "Key Frame Proposal Network for Efficient Pose Estimation in Videos." *European Conference on Computer Vision*, 23–28 August 2020.

Pending –

1. Comas Massague, A., Zhang, C., Feric, Z., Camps, O., & Yu, R. "Learning Disentangled Representations of Video with Missing Data." *Neural Information Processing Systems,* 5–12 December 2020, under review.
2. Liu, W., Comas Massague, A., Zhang, Y., Luo, D., Camps, O., & Szanier, M. "KW-DYAN: A Recurrent and Warping DYAN for Better Video Prediction." *Neural Information Processing Systems,* 5–12 December 2020, under review.
3. Miller, J., Wang, J., Sznaier, M., & Camps, O. "Model Fitting by Semialgebraic Clustering." *Neural Information Processing Systems,* 5–12 December 2020, under review.
4. Ozbay, B., Sznaier, M., & Camps, O. "SOS-Spaces: A Sum-of-Squares Polynomial Based Subspace Clustering Method." *Neural Information Processing Systems,* 5–12 December 2020, under review.
5. Sznaier, M. "A Convex Optimization Approach to Learning Koopman Operators." *Neural Information Processing Systems,* 5–12 December 2020, under review.
6. Chamanbaz, M., Sznaier, M., Lagoa, C.M., & Dabbene, F. "Probabilistic Discrete Time Robust H2 Controller Design." *59th IEEE Conference on Decision and Control*, Jeju Island, Korea, 14–18 December 2020, accepted.
7. Dai, T., & Sznaier, M. "A Semi-Algebraic Optimization Approach to Data-Driven Control of Continuous-Time Nonlinear Systems." *59th IEEE Conference on Decision and Control*, Jeju Island, Korea, 14–18 December 2020, accepted.

8. Miller, J., Singh, R., & Sznaier, M. "MIMO System Identification by Randomized Active-Set Methods." *59th IEEE Conference on Decision and Control*, Jeju Island, Korea, 14–18 December 2020, accepted.

D. Other Presentations

1. Seminars

   a. Camps, O. "Compact and Interpretable Dynamics-Based Video Representations." *2020 IEEE/CVF Area Chair Meeting, Conference on Computer Vision and Pattern Recognition*, San Diego, CA, February 2020.

E. Software Developed

1. We developed a suite of algorithms for fine grain classification, video prediction, motion segmentation, and outlier rejection. The code can be downloaded from http://robustsystems.coe.neu.edu.

V. REFERENCES

[1] N. Dalal and B. Triggs, "Histograms of oriented gradients for human detection," in *Computer Vision and Pattern Recognition, 2005. CVPR 2005. IEEE Computer Society Conference on*, 2005, vol. 1: IEEE, pp. 886-893.

[2] P. Felzenszwalb, D. McAllester, and D. Ramanan, "A discriminatively trained, multiscale, deformable part model," in *Computer Vision and Pattern Recognition, 2008. CVPR 2008. IEEE Conference on*, 2008: IEEE, pp. 1-8.

[3] B. Benfold and I. Reid, "Stable multi-target tracking in real-time surveillance video," in *Computer Vision and Pattern Recognition (CVPR), 2011 IEEE Conference on*, 2011: IEEE, pp. 3457-3464.

[4] J. Xing, H. Ai, and S. Lao, "Multi-object tracking through occlusions by local tracklets filtering and global tracklets association with detection responses," in *Computer Vision and Pattern Recognition, 2009. CVPR 2009. IEEE Conference on*, 2009: IEEE, pp. 1200-1207.

[5] L. Zhang, Y. Li, and R. Nevatia, "Global data association for multi-object tracking using network flows," in *Computer Vision and Pattern Recognition, 2008. CVPR 2008. IEEE Conference on*, 2008: IEEE, pp. 1-8.

[6] A. Andriyenko, K. Schindler, and S. Roth, "Discrete-continuous optimization for multi-target tracking," in *Computer Vision and Pattern Recognition (CVPR), 2012 IEEE Conference on*, 2012: IEEE, pp. 1926-1933.

[7] M. Betke, D. E. Hirsh, A. Bagchi, N. I. Hristov, N. C. Makris, and T. H. Kunz, "Tracking large variable numbers of objects in clutter," in *Computer Vision and Pattern Recognition, 2007. CVPR'07. IEEE Conference on*, 2007: IEEE, pp. 1-8.

[8] E. Brau, D. Dunatunga, K. Barnard, T. Tsukamoto, R. Palanivelu, and P. Lee, "A generative statistical model for tracking multiple smooth trajectories," in *Computer Vision and Pattern Recognition (CVPR), 2011 IEEE Conference on*, 2011: IEEE, pp. 1137-1144.

[9] R. T. Collins, "Multitarget data association with higher-order motion models," in *Computer Vision and Pattern Recognition (CVPR), 2012 IEEE Conference on*, 2012: IEEE, pp. 1744-1751.

[10] Z. Wu, T. H. Kunz, and M. Betke, "Efficient track linking methods for track graphs using network-flow and set-cover techniques," in *Computer Vision and Pattern Recognition (CVPR), 2011 IEEE Conference on*, 2011: IEEE, pp. 1185-1192.

[11] T. Ding, Mario Sznaier, and Octavia I. Camps, "Fast track matching and event detection," presented at the IEEE Conference on Computer Vision and Pattern Recognition, Anchorage, Alaska, 2008.

[12] Q. Cai and J. K. Aggarwal, "Tracking human motion in structured environments using a distributed-camera system," *IEEE Transactions on Pattern Analysis and Machine Intelligence,* vol. 21, no. 11, pp. 1241-1247, 1999.

[13] T.-H. Chang and S. Gong, "Tracking multiple people with a multi-camera system," in *Multi-Object Tracking, 2001. Proceedings. 2001 IEEE Workshop on*, 2001: IEEE, pp. 19-26.

[14] D. Comaniciu, V. Ramesh, and F. Berton, "Adaptive resolution system and method for providing efficient low bit rate transmission of image data for distributed applications," ed: Google Patents, 2004.

[15] K. Nummiaro, E. Koller-Meier, T. Svoboda, D. Roth, and L. Van Gool, "Color-based object tracking in multi-camera environments," *Pattern Recognition,* pp. 591-599, 2003.

[16] J. Black and T. Ellis, "Multi camera image tracking," in *In International Workshop on Performance Evaluation of Tracking and Surveillance*, 2001: Citeseer.

[17] R. T. Collins, O. Amidi, and T. Kanade, "An active camera system for acquiring multi-view video," in *Image Processing. 2002. Proceedings. 2002 International Conference on*, 2002, vol. 1: IEEE, pp. I-I.

[18] S. L. Dockstader and A. M. Tekalp, "Multiple camera tracking of interacting and occluded human motion," *Proceedings of the IEEE,* vol. 89, no. 10, pp. 1441-1455, 2001.

[19] A. Mittal and L. S. Davis, "M2tracker: A multi-view approach to segmenting and tracking people in a cluttered scene," *International Journal of Computer Vision,* vol. 51, no. 3, pp. 189-203, 2003.

[20] Z. Wu, N. I. Hristov, T. L. Hedrick, T. H. Kunz, and M. Betke, "Tracking a large number of objects from multiple views," in *Computer Vision, 2009 IEEE 12th International Conference on*, 2009: IEEE, pp. 1546-1553.

[21] A. Gaschler, D. Burschka, and G. Hager, "Epipolar-based stereo tracking without explicit 3d reconstruction," in *Pattern Recognition (ICPR), 2010 20th International Conference on*, 2010: IEEE, pp. 1755-1758.

[22] K. Ni and F. Dellaert, "Stereo tracking and three-point/one-point algorithms-a robust approach in visual odometry," in *Image Processing, 2006 IEEE International Conference on*, 2006: IEEE, pp. 2777-2780.

[23] D. Stoyanov, G. P. Mylonas, F. Deligianni, A. Darzi, and G. Z. Yang, "Soft-tissue motion tracking and structure estimation for robotic assisted MIS procedures," in *International Conference on Medical Image Computing and Computer-Assisted Intervention*, 2005: Springer, pp. 139-146.

[24] V. I. Morariu and O. I. Camps, "Modeling correspondences for multi-camera tracking using nonlinear manifold learning and target dynamics," in *Computer Vision and Pattern Recognition, 2006 IEEE Computer Society Conference on*, 2006, vol. 1: IEEE, pp. 545-552.

[25] S. Calderara, R. Cucchiara, and A. Prati, "Bayesian-competitive consistent labeling for people surveillance," *IEEE Transactions on Pattern Analysis and Machine Intelligence,* vol. 30, no. 2, 2008.

[26] Y. Caspi and M. Irani, "A step towards sequence-to-sequence alignment," in *Computer Vision and Pattern Recognition, 2000. Proceedings. IEEE Conference on*, 2000, vol. 2: IEEE, pp. 682-689.

[27] S. M. Khan and M. Shah, "Tracking multiple occluding people by localizing on multiple scene planes," *IEEE transactions on pattern analysis and machine intelligence,* vol. 31, no. 3, pp. 505-519, 2009.

[28] L. Lee, R. Romano, and G. Stein, "Monitoring activities from multiple video streams: Establishing a common coordinate frame," *IEEE Transactions on pattern analysis and machine intelligence,* vol. 22, no. 8, pp. 758-767, 2000.

[29] S.-N. Lim and L. Davis, "An ease-of-use stereo-based particle filter for tracking under occlusion," *Human Motion–Understanding, Modeling, Capture and Animation,* pp. 225-239, 2007.

[30] A. Bedagkar-Gala and S. K. Shah, "A survey of approaches and trends in person re-identification," *Image and Vision Computing,* vol. 32, no. 4, pp. 270-286, 2014.

[31] G. Doretto, T. Sebastian, P. Tu, and J. Rittscher, "Appearance-based person reidentification in camera networks: problem overview and current approaches," *Journal of Ambient Intelligence and Humanized Computing,* vol. 2, no. 2, pp. 127-151, 2011.

[32] S. Gong, M. Cristani, S. Yan, C. C. Loy, and P. Re-Identification, "Springer Publishing Company," ed: Incorporated, 2014.

[33] R. Vezzani, D. Baltieri, and R. Cucchiara, "People reidentification in surveillance and forensics: A survey," *ACM Computing Surveys (CSUR),* vol. 46, no. 2, p. 29, 2013.

[34] W.-S. Zheng, S. Gong, and T. Xiang, "Reidentification by relative distance comparison," *IEEE transactions on pattern analysis and machine intelligence,* vol. 35, no. 3, pp. 653-668, 2013.

[35] S. Bak, E. Corvee, F. Bremond, and M. Thonnat, "Multiple-shot human re-identification by mean riemannian covariance grid," in *Advanced Video and Signal-Based Surveillance (AVSS), 2011 8th IEEE International Conference on*, 2011: IEEE, pp. 179-184.

[36] M. Bauml and R. Stiefelhagen, "Evaluation of local features for person re-identification in image sequences," in *Advanced Video and Signal-Based Surveillance (AVSS), 2011 8th IEEE International Conference on*, 2011: IEEE, pp. 291-296.

[37] M. Farenzena, L. Bazzani, A. Perina, V. Murino, and M. Cristani, "Person re-identification by symmetry-driven accumulation of local features," in *Computer Vision and Pattern Recognition (CVPR), 2010 IEEE Conference on*, 2010: IEEE, pp. 2360-2367.

[38] N. Gheissari, T. B. Sebastian, and R. Hartley, "Person reidentification using spatiotemporal appearance," in *Computer Vision and Pattern Recognition, 2006 IEEE Computer Society Conference on*, 2006, vol. 2: IEEE, pp. 1528-1535.

[39] D. Gray and H. Tao, "Viewpoint invariant pedestrian recognition with an ensemble of localized features," *Computer Vision–ECCV 2008,* pp. 262-275, 2008.

[40] X. Wang, G. Doretto, T. Sebastian, J. Rittscher, and P. Tu, "Shape and appearance context modeling," in *Computer Vision, 2007. ICCV 2007. IEEE 11th International Conference on*, 2007: IEEE, pp. 1-8.

[41] Z. Li, S. Chang, F. Liang, T. S. Huang, L. Cao, and J. R. Smith, "Learning locally-adaptive decision functions for person verification," in *Proceedings of the IEEE Conference on Computer Vision and Pattern Recognition*, 2013, pp. 3610-3617.

[42] A. Mignon and F. Jurie, "Pcca: A new approach for distance learning from sparse pairwise constraints," in *Computer Vision and Pattern Recognition (CVPR), 2012 IEEE Conference on*, 2012: IEEE, pp. 2666-2672.

[43] S. Pedagadi, J. Orwell, S. Velastin, and B. Boghossian, "Local fisher discriminant analysis for pedestrian re-identification," in *Proceedings of the IEEE Conference on Computer Vision and Pattern Recognition*, 2013, pp. 3318-3325.

[44] W.-S. Zheng, S. Gong, and T. Xiang, "Person re-identification by probabilistic relative distance comparison," in *Computer vision and pattern recognition (CVPR), 2011 IEEE conference on*, 2011: IEEE, pp. 649-656.

[45] P. Luc, N. Neverova, C. Couprie, J. Verbeek, and Y. LeCun, "Predicting deeper into the future of semantic segmentation," in *of: ICCV 2017-International Conference on Computer Vision*, 2017, p. 10.

[46] V. Vukotić, S.-L. Pintea, C. Raymond, G. Gravier, and J. C. Van Gemert, "One-step time-dependent future video frame prediction with a convolutional encoder-decoder neural network," in *International Conference on Image Analysis and Processing*, 2017: Springer, pp. 140-151.

[47] J. Van Amersfoort, A. Kannan, M. A. Ranzato, A. Szlam, D. Tran, and S. Chintala, "Transformation-based models of video sequences," *arXiv preprint arXiv:1701.08435,* 2017.

[48] M. Babaeizadeh, C. Finn, D. Erhan, R. H. Campbell, and S. Levine, "Stochastic variational video prediction," *arXiv preprint arXiv:1710.11252,* 2017.

[49] W. Byeon, Q. Wang, R. Kumar Srivastava, and P. Koumoutsakos, "Contextvp: Fully context-aware video prediction," in *Proceedings of the European Conference on Computer Vision (ECCV)*, 2018, pp. 753-769.

[50] F. Leibfried, N. Kushman, and K. Hofmann, "A deep learning approach for joint video frame and reward prediction in atari games," *arXiv preprint arXiv:1611.07078,* 2016.

[51] R. Mahjourian, M. Wicke, and A. Angelova, "Geometry-based next frame prediction from monocular video," in *2017 IEEE Intelligent Vehicles Symposium (IV)*, 2017: IEEE, pp. 1700-1707.

[52] C. Vondrick, H. Pirsiavash, and A. Torralba, "Generating videos with scene dynamics," in *Advances in neural information processing systems*, 2016, pp. 613-621.

[53] E. Denton and R. Fergus, "Stochastic video generation with a learned prior," *arXiv preprint arXiv:1802.07687,* 2018.

[54] M. Oliu, J. Selva, and S. Escalera, "Folded recurrent neural networks for future video prediction," in *Proceedings of the European Conference on Computer Vision (ECCV)*, 2018, pp. 716-731.

[55] L. B. D. Tran, R. Fergus, L. Torresani, and M. Palur, "Learning spatiotemporal features with 3d convolutional networks.," presented at the Int. Conf. on Computer Vision (ICCV), 2015.

[56] I. Goodfellow *et al.*, "Generative adversarial nets," in *Advances in neural information processing systems*, 2014, pp. 2672-2680.

[57] N. Kalchbrenner *et al.*, "Video pixel networks," in *International Conference on Machine Learning*, 2017, pp. 1771-1779.

[58] M. Mathieu, C. Couprie, and Y. LeCun, "Deep multi-scale video prediction beyond mean square error," *arXiv preprint arXiv:1511.05440,* 2015.

[59] J. Oh, X. Guo, H. Lee, R. L. Lewis, and S. Singh, "Action-conditional video prediction using deep networks in atari games," in *Advances in neural information processing systems*, 2015, pp. 2863-2871.

[60] M. Ranzato, A. Szlam, J. Bruna, M. Mathieu, R. Collobert, and S. Chopra, "Video (language) modeling: a baseline for generative models of natural videos," *arXiv preprint arXiv:1412.6604,* 2014.

[61] Z. Liu, R. A. Yeh, X. Tang, Y. Liu, and A. Agarwala, "Video frame synthesis using deep voxel flow," in *Proceedings of the IEEE International Conference on Computer Vision*, 2017, pp. 4463-4471.

[62] F. A. Reda *et al.*, "Sdc-net: Video prediction using spatially-displaced convolution," in *Proceedings of the European Conference on Computer Vision (ECCV)*, 2018, pp. 718-733.

[63] V. Belagiannis and A. Zisserman, "Recurrent human pose estimation," in *2017 12th IEEE International Conference on Automatic Face & Gesture Recognition (FG 2017)*, 2017: IEEE, pp. 468-475.

[64] A. Newell, K. Yang, and J. Deng, "Stacked hourglass networks for human pose estimation," in *European conference on computer vision*, 2016: Springer, pp. 483-499.

[65] L. Pishchulin, M. Andriluka, P. Gehler, and B. Schiele, "Strong appearance and expressive spatial models for human pose estimation," in *Proceedings of the IEEE international conference on Computer Vision*, 2013, pp. 3487-3494.

[66] A. Toshev and C. Szegedy, "Deeppose: Human pose estimation via deep neural networks," in *Proceedings of the IEEE conference on computer vision and pattern recognition*, 2014, pp. 1653-1660.

[67] S.-E. Wei, V. Ramakrishna, T. Kanade, and Y. Sheikh, "Convolutional pose machines," in *Proceedings of the IEEE conference on Computer Vision and Pattern Recognition*, 2016, pp. 4724-4732.

[68] M. Cristani, R. Raghavendra, A. Del Bue, and V. Murino, "Human behavior analysis in video surveillance: A social signal processing perspective," *Neurocomputing,* vol. 100, pp. 86-97, 2013.

[69] S. Park and M. M. Trivedi, "Understanding human interactions with track and body synergies (TBS) captured from multiple views," *Computer Vision and Image Understanding,* vol. 111, no. 1, pp. 2-20, 2008.

[70] J. Shotton *et al.*, "Real-time human pose recognition in parts from single depth images," in *CVPR 2011*, 2011: Ieee, pp. 1297-1304.

[71] H.-Y. Lin and T.-W. Chen, "Augmented reality with human body interaction based on monocular 3D pose estimation," in *International Conference on Advanced Concepts for Intelligent Vision Systems*, 2010: Springer, pp. 321-331.

[72] G. Bertasius, C. Feichtenhofer, D. Tran, J. Shi, and L. Torresani, "Learning temporal pose estimation from sparsely-labeled videos," in *Advances in Neural Information Processing Systems*, 2019, pp. 3027-3038.

[73] S. Paoletti, A. L. Juloski, G. Ferrari-Trecate, and R. Vidal, "Identification of hybrid systems a tutorial," *European journal of control,* vol. 13, no. 2-3, pp. 242-260, 2007.

[74] Y. Ma and R. Vidal, "Identification of deterministic switched ARX systems via identification of algebraic varieties," in *International Workshop on Hybrid Systems: Computation and Control*, 2005: Springer, pp. 449-465.

[75] J. Roll, A. Bemporad, and L. Ljung, "Identification of piecewise affine systems via mixed-integer programming," *Automatica,* vol. 40, no. 1, pp. 37-50, 2004.

[76] A. L. Juloski, S. Weiland, and W. Heemels, "A Bayesian approach to identification of hybrid systems," *IEEE Transactions on Automatic Control,* vol. 50, no. 10, pp. 1520-1533, 2005.

[77] G. Ferrari-Trecate, M. Muselli, D. Liberati, and M. Morari, "A clustering technique for the identification of piecewise affine systems," in *International Workshop on Hybrid Systems: Computation and Control*, 2001: Springer, pp. 218-231.

[78] H. Nakada, K. Takaba, and T. Katayama, "Identification of piecewise affine systems based on statistical clustering technique," *Automatica,* vol. 41, no. 5, pp. 905-913, 2005.

[79] C. Feng, C. M. Lagoa, and M. Sznaier, "Hybrid system identification via sparse polynomial optimization," in *American Control Conference (ACC), 2010*, 2010: IEEE, pp. 160-165.

[80] N. Ozay, C. Lagoa, and M. Sznaier, "Robust identification of switched affine systems via moments-based convex optimization," in *Decision and Control, 2009 held jointly with the 2009 28th Chinese Control Conference. CDC/CCC 2009. Proceedings of the 48th IEEE Conference on*, 2009: IEEE, pp. 4686-4691.

[81] N. Ozay, M. Sznaier, C. Lagoa, and O. Camps, "A sparsification approach to set membership identification of a class of affine hybrid systems," in *Decision and Control, 2008. CDC 2008. 47th IEEE Conference on*, 2008: IEEE, pp. 123-130.

[82] L. Vandenberghe and S. Boyd, "Semidefinite programming," *SIAM review,* vol. 38, no. 1, pp. 49-95, 1996.

[83] S. Boyd and L. Vandenberghe, *Convex optimization*. Cambridge university press, 2004.

[84] M. Fazel, H. Hindi, and S. P. Boyd, "A rank minimization heuristic with application to minimum order system approximation," in *American Control Conference, 2001. Proceedings of the 2001*, 2001, vol. 6: IEEE, pp. 4734-4739.

[85] M. S. Lobo, M. Fazel, and S. Boyd, "Portfolio optimization with linear and fixed transaction costs," *Annals of Operations Research,* vol. 152, no. 1, pp. 341-365, 2007.

[86] J. Wright, A. Ganesh, S. Rao, Y. Peng, and Y. Ma, "Robust principal component analysis: Exact recovery of corrupted low-rank matrices via convex optimization," in *Advances in neural information processing systems*, 2009, pp. 2080-2088.

[87] D. Henrion and A. Garulli, *Positive polynomials in control*. Springer Science & Business Media, 2005.

[88] J. B. Lasserre, *Moments, positive polynomials and their applications*. World Scientific, 2009.

[89] J. B. Lasserre and M. Putinar, "Positivity and optimization for semi-algebraic functions," *SIAM Journal on Optimization,* vol. 20, no. 6, pp. 3364-3383, 2010.

[90] W. Liu, Abhishek Sharma, Octavia Camps, and Mario Sznaier, "DYAN: A Dynamical Atoms-Based Network for Video Prediction," presented at the European Conference on Computer Vision (ECCV), Munich, Germany, 2018.

[91] Z. Wang, A. C. Bovik, H. R. Sheikh, and E. P. Simoncelli, "Image quality assessment: from error visibility to structural similarity," *IEEE transactions on image processing,* vol. 13, no. 4, pp. 600-612, 2004.

[92] R. Zhang, P. Isola, A. A. Efros, E. Shechtman, and O. Wang, "The unreasonable effectiveness of deep features as a perceptual metric," in *Proceedings of the IEEE conference on computer vision and pattern recognition*, 2018, pp. 586-595.

[93] W. Lotter, G. Kreiman, and D. Cox, "Deep predictive coding networks for video prediction and unsupervised learning," *arXiv preprint arXiv:1605.08104,* 2016.

[94] X. Liang, L. Lee, W. Dai, and E. P. Xing, "Dual motion GAN for future-flow embedded video prediction," in *Proceedings of the IEEE International Conference on Computer Vision*, 2017, pp. 1744-1752.

[95] Z. Hao, X. Huang, and S. Belongie, "Controllable video generation with sparse trajectories," in *Proceedings of the IEEE Conference on Computer Vision and Pattern Recognition*, 2018, pp. 7854-7863.

[96] H. Gao, H. Xu, Q.-Z. Cai, R. Wang, F. Yu, and T. Darrell, "Disentangling propagation and generation for video prediction," in *Proceedings of the IEEE International Conference on Computer Vision*, 2019, pp. 9006-9015.

[97] Y. Zhang, Yin Wang, Octavia Camps, and Mario Sznaier, "Key Frame Proposal Network for Efficient Pose Estimation in Videos," in *European Conference on Computer Vision (ECCV)*, 2020.

[98] K. He, X. Zhang, S. Ren, and J. Sun, "Deep residual learning for image recognition," in *Proceedings of the IEEE conference on computer vision and pattern recognition*, 2016, pp. 770-778.

[99] X. Nie, Y. Li, L. Luo, N. Zhang, and J. Feng, "Dynamic kernel distillation for efficient pose estimation in videos," in *Proceedings of the IEEE International Conference on Computer Vision*, 2019, pp. 6942-6950.

[100] B. Xiao, H. Wu, and Y. Wei, "Simple baselines for human pose estimation and tracking," in *Proceedings of the European conference on computer vision (ECCV)*, 2018, pp. 466-481.

[101] B. Xiaohan Nie, C. Xiong, and S.-C. Zhu, "Joint action recognition and pose estimation from video," in *Proceedings of the IEEE Conference on Computer Vision and Pattern Recognition*, 2015, pp. 1293-1301.

[102] U. Iqbal, M. Garbade, and J. Gall, "Pose for action-action for pose," in *2017 12th IEEE International Conference on Automatic Face & Gesture Recognition (FG 2017)*, 2017: IEEE, pp. 438-445.

[103] G. Gkioxari, A. Toshev, and N. Jaitly, "Chained predictions using convolutional neural networks," in *European Conference on Computer Vision*, 2016: Springer, pp. 728-743.

[104] J. Song, L. Wang, L. Van Gool, and O. Hilliges, "Thin-slicing network: A deep structured model for pose estimation in videos," in *Proceedings of the IEEE conference on computer vision and pattern recognition*, 2017, pp. 4220-4229.

[105] Y. Luo *et al.*, "Lstm pose machines," in *Proceedings of the IEEE conference on computer vision and pattern recognition*, 2018, pp. 5207-5215.

[106] W. Liu *et al.*, "Towards visually explaining variational autoencoders," in *Proceedings of the IEEE/CVF Conference on Computer Vision and Pattern Recognition*, 2020, pp. 8642-8651.

[107] C. Dicle, O. I. Camps, and M. Sznaier, "The way they move: Tracking multiple targets with similar appearance," in *Proceedings of the IEEE International Conference on Computer Vision*, 2013, pp. 2304-2311.

[108] Y. Cheng, Y. Wang, M. Sznaier, and O. Camps, "Subspace clustering with priors via sparse quadratically constrained quadratic programming," in *Proceedings of the IEEE Conference on Computer Vision and Pattern Recognition*, 2016, pp. 5204-5212.

[109] Y. Wang, M. Sznaier, O. Camps, and F. Pait, "Identification of a class of generalized autoregressive conditional heteroskedasticity (GARCH) models with applications to covariance propagation," in *Decision and Control (CDC), 2015 IEEE 54th Annual Conference on*, 2015: IEEE, pp. 795-800.

[110] M. Ayazoglu, B. Yilmaz, M. Sznaier, and O. Camps, "Finding causal interactions in video sequences," in *Proceedings of the IEEE International Conference on Computer Vision*, 2013, pp. 3575-3582.

[111] F. Xiong, Y. Cheng, O. Camps, M. Sznaier, and C. Lagoa, "Hankel based maximum margin classifiers: A connection between machine learning and wiener systems identification," in *Decision and Control (CDC), 2013 IEEE 52nd Annual Conference on*, 2013: IEEE, pp. 6005-6010.

[112] L. Lo Presti, M. La Cascia, S. Sclaroff, and O. Camps, "Hankelet-based dynamical systems modeling for 3D action recognition," *Image and Vision Computing,* vol. 44, pp. 29-43, 2015.

[113] Y. Cheng, Y. Wang, and M. Sznaier, "A convex optimization approach to semi-supervised identification of switched ARX systems," in *Decision and Control (CDC), 2014 IEEE 53rd Annual Conference on*, 2014: IEEE, pp. 2573-2578.

[114] N. Ozay, M. Sznaier, and C. Lagoa, "Convex certificates for model (in) validation of switched affine systems with unknown switches," *IEEE Transactions on Automatic Control,* vol. 59, no. 11, pp. 2921-2932, 2014.

[115] L. Lo Presti, M. La Cascia, S. Sclaroff, and O. Camps, "Gesture modeling by hanklet-based hidden markov model," in *Asian Conference on Computer Vision*, 2014: Springer, pp. 529-546.

[116] X. Zhang, Y. Wang, M. Gou, M. Sznaier, and O. Camps, "Efficient temporal sequence comparison and classification using gram matrix embeddings on a riemannian manifold," in *Proceedings of the IEEE Conference on Computer Vision and Pattern Recognition*, 2016, pp. 4498-4507.

[117] O. Camps, M. Sznaier, and X. Zhang, "Convex behavioral model (in) validation via Jensen-Bregman divergence minimization," in *American Control Conference (ACC), 2016*, 2016: IEEE, pp. 4575-4579.

[118] S. Asghari-Esfeden, M. Sznaier, and O. Camps, "Dynamic Motion Representation for Human Action Recognition," in *The IEEE Winter Conference on Applications of Computer Vision*, 2020, pp. 557-566.

[119] X. Zhang, M. Sznaier, and O. Camps, "Efficient Identification of Error-in Variables Switched Systems Based on Riemannian Distance-Like Functions," presented at the IEEE Conference on Decision and Control (CDC), 2018.

[120] F. Xiong, M. Gou, O. Camps, and M. Sznaier, "Person re-identification using kernel-based metric learning methods," in *European conference on computer vision*, 2014: Springer, pp. 1-16.

[121] M. Gou, X. Zhang, A. Rates-Borras, S. Asghari-Esfeden, M. Sznaier, and O. Camps, "Person re-identification in appearance impaired scenarios," *arXiv preprint arXiv:1604.00367,* 2016.

[122] O. Camps *et al.*, "From the lab to the real world: Re-identification in an airport camera network," *IEEE Transactions on Circuits and Systems for Video Technology,* vol. 27, no. 3, pp. 540-553, 2017.

[123] S. Karanam, M. Gou, Z. Wu, A. Rates-Borras, O. Camps, and R. J. Radke, "A comprehensive evaluation and benchmark for person re-identification: Features, metrics, and datasets," *arXiv preprint arXiv:1605.09653,* 2016.

[124] Y. Cheng, J. A. Lopez, O. Camps, and M. Sznaier, "A convex optimization approach to robust fundamental matrix estimation," in *Proceedings of the IEEE Conference on Computer Vision and Pattern Recognition*, 2015, pp. 2170-2178.

[125] M. Sznaier, M. Ayazoglu, and T. Inanc, "Fast structured nuclear norm minimization with applications to set membership systems identification," *IEEE Transactions on Automatic Control,* vol. 59, no. 10, pp. 2837-2842, 2014.

[126] M. Sznaier and O. Camps, "Uncertainty and Robustness in Dynamic Vision," *Encyclopedia of Systems and Control,* pp. 1493-1499, 2015.

[127] Y. Wang, C. Dicle, M. Sznaier, and O. Camps, "Self scaled regularized robust regression," in *Proceedings of the IEEE Conference on Computer Vision and Pattern Recognition*, 2015, pp. 3261-3269.

[128] B. Yılmaz and M. Sznaier, "Efficient identification of Wiener systems using a combination of atomic norm minimization and interval matrix properties," in *Decision and Control (CDC), 2015 IEEE 54th Annual Conference on*, 2015: IEEE, pp. 109-114.

[129] C. Dicle, B. Yilmaz, O. Camps, and M. Sznaier, "Solving Temporal Puzzles," in *Proceedings of the IEEE Conference on Computer Vision and Pattern Recognition*, 2016, pp. 5896-5905.

[130] Y. Wang, O. Camps, M. Sznaier, and B. R. Solvas, "Jensen Bregman LogDet Divergence Optimal Filtering in the Manifold of Positive Definite Matrices," in *European Conference on Computer Vision*, 2016: Springer, pp. 221-235.

[131] Y. Wang, M. Sznaier, and O. Camps, "A super-atomic norm minimization approach to identifying sparse dynamical graphical models," in *American Control Conference (ACC), 2016*, 2016: IEEE, pp. 1962-1967.

[132] M. Sznaier and O. Camps, "Sos-rsc: A sum-of-squares polynomial approach to robustifying subspace clustering algorithms," in *Proceedings of the IEEE Conference on Computer Vision and Pattern Recognition*, 2018, pp. 8033-8041.

[133] M. Gou, F. Xiong, O. Camps, and M. Sznaier, "MoNet: Moments Embedding Network," in *Proceedings of the IEEE Conference on Computer Vision and Pattern Recognition*, 2018, pp. 3175-3183.

[134] X. Zhang, B. Ozbay, M. Sznaier, and O. Camps, "Dynamics Enhanced Multi-Camera Motion Segmentation from Unsynchronized Videos," in *Proceedings of the IEEE Conference on Computer Vision and Pattern Recognition*, 2017, pp. 4668-4676.

[135] Y. Z. A. Islam, D. Yin, O. Camps, and R. J. Radke, "Correlating belongings with passengers in a simulated airport security checkpoint," presented at the 12th International Conference on Distributed Smart Cameras, 2018.

This page intentionally left blank.

R4-A.3: Human Detection & Re-Identification for Mass Transit Environments

I. PARTICIPANTS INVOLVED FROM JULY 1, 2019 TO JUNE 30, 2020

Faculty/Staff			
Name	**Title**	**Institution**	**Email**
Rich Radke	PI	RPI	rjradke@ecse.rpi.edu
Graduate, Undergraduate and REU Students			
Name	**Degree Pursued**	**Institution**	**Month/Year of Graduation**
Meng Zheng	PhD	RPI	5/2020

II. PROJECT DESCRIPTION

A. Project Overview

Large networks of cameras are ubiquitous in urban life, especially in densely populated environments such as airports, train stations, and sports arenas. For cost and practicality, most cameras in such networks are spaced widely so that their fields of view are nonoverlapping. Automatically matching humans that reappear across different cameras in such networks is a critical problem in homeland security-related surveillance applications.

This issue is highly related to the computer vision research problem of human re-identification or "re-id." Given a cropped rectangle of pixels representing a human in one view, a re-id algorithm produces a similarity score for each candidate in a gallery of similarly cropped human rectangles from a second view. Early re-id system designs focused on two major problems: (1) feature extraction, in which the goal is to determine effective ways to extract representative information from each cropped rectangle to produce feature representations, and (2) metric learning, in which the goal is to produce high similarity scores for feature representations from the same person, and low similarity scores for feature representations for different persons. With the recent explosion of Convolutional Neural Networks (CNNs) and deep learning, deep networks have been gradually adopted in re-id system design and have achieved great success. The most recent research in re-id has been focused on developing various deep CNN-based networks that combine feature extraction and metric learning as an integrated module to facilitate end-to-end training. In practice, a re-id system must be fully autonomous from the point that a user draws a rectangle around a person of interest to the point that candidates are presented to them; thus, the system must also automatically detect and track humans in all cameras with speed and accuracy.

This project addresses the design and deployment of real-world re-id algorithms specifically designed for large-scale surveillance systems in mass transit environments. This involves:

- The design and analysis of new state-of-the-art computer vision algorithms for human detection and tracking, feature representation learning, and deep CNN model design for cross-view matching;
- The evaluation of the suitability of such algorithms for real-world homeland security applications, taking into account tracking/detection errors, latency/congestion, and human-computer interfaces to software systems;

- The design and dissemination of new experimental protocols and datasets that more closely resemble the types of re-id problems practitioners will encounter in real-world deployments; and
- The design of novel algorithms that can be directly integrated into real-world surveillance systems for practical Department of Homeland Security (DHS) use for person re-id and trajectory reconstruction.

The latter three aspects differentiate our approach from most related re-id research. That is, in academic research the re-id problem is often reduced to comparing one candidate rectangle of pixels to another, which is only a small part of a fully automated re-id system. In addition, we take into account that the candidate rectangles are likely to be generated by an automatic (and possibly inaccurate) human detection and tracking subsystem; that many cameras may be involved; that new subjects are constantly appearing in the target camera(s); that the overall system needs to operate in real time; and that the system may be in operation for very long periods of time. We provided practical solutions that can be directly integrated into real-world surveillance systems to automatically calculate motion trajectories of persons of interest, given the cropped rectangles of the person's first appearance. Our solution differs from conventional re-id algorithms, which typically require a substantial amount of manual intervention to achieve the same goal.

The end-state of the research is a suite of re-id/trajectory recovery algorithms that are directly applicable to the homeland security enterprise (HSE) and ready for large-scale system integration, as well as several re-id benchmark databases of interest to the homeland security community. The project also produced an up-to-date assessment of the re-id state of the art that can help DHS stakeholders understand what is technologically feasible in this area, informing policies and technology solicitations.

B. State of the Art and Technical Approach

To date, the majority of deep CNN-based person re-id research has been focused on image-based re-id, which considers the cross-view similarity between single person images as discussed above. However, recent progress in big data and deep learning has facilitated the storage and processing of large-scale data, which recently influenced the re-id research community. Person tracklets (or image sequences), which consist of consecutive frames of cropped person images, typically contain richer temporal information than single frames and are more helpful for re-identification tasks. Thus, we proposed a deep CNN-based network architecture, with spatiotemporal consistent attention for cross-view person tracklet matching, to deal with the video-based re-id problem.

As with image-based re-id, illumination and viewpoint changes, occlusions, and misalignment issues are critical challenges for cross-view person tracklet matching. However, the availability of multiple image frames for each identity under the same or different camera views raises additional problems for video-based re-id. Specifically, how to extract cross-view invariant spatiotemporal feature representations and effectively aggregate temporal information along the image sequence are critical questions in video scenarios. In our work in Year 6 [1], we showed the effectiveness of introducing attention as a principled part of the training process of the deep re-id network, which is able to automatically spatially localize regions of interest while ignoring irrelevant noisy backgrounds of person images. In Year 7, we extended the involvement of attention and attention-consistency supervision from the spatial dimension to the temporal dimension, to automatically discover 3D attentive regions and learn inter-view and intra-view consistent feature representations for same-person image sequences.

Recently, the success of 2D CNN designs have attracted broad attention in the computer vision community [2, 3]. These designs are critical to various computer vision tasks such as image classification, detection, and semantic segmentation. 3D CNNs, on the other hand, due to the lack of large-scale 3D pretraining data comparable to ImageNet [4], are more limited in application for computer vision tasks. However, recent progress [5-7] in 3D CNNs has shown superior performance in various video-based tasks, such as action

recognition compared to 2D CNNs, due to their advantage in involving temporal cues in the convolution procedure, enabling spatiotemporally correlated feature representations. Despite the superiority of vanilla 3D CNN architectures in dealing with video-based data, real-world difficulties in re-id systems, such as occlusions and background noise as mentioned above, will deteriorate the effectiveness of the learned features. Thus we incorporate the gradient-based attention technique [8] with a vanilla 3D CNN architecture, which generates spatiotemporal attention maps to automatically discover attentive image regions along the temporal dimension. Both spatial and temporal consistency constraints are applied to lead the network to find consistent attentive regions along same-person image sequences under different camera views.

For temporal aggregation of feature vectors, we suspected that the conventional approach of average or max pooling [9] could deteriorate re-identification performance if person images along the sequence are misaligned. Instead, we applied an additional temporal convolution layer [10] to automatically find consistent information along the feature sequence, at the same time including useful temporal variations to obtain aggregated feature representations for person image sequences. To this end, we proposed a 3D CNN network called the Spatiotemporal Consistent Attentive Network (SCAN) as a video extension to our work [1] for image data. The pipeline of the proposed SCAN method is shown in Figure 1. The proposed SCAN method is learned in an end-to-end way, with 3D attention maps explicitly regularized for spatiotemporal invariant feature learning, producing robust cross-view matching for same-person tracklets. Experimental results show that our SCAN method achieved 82.7%, 93.4%, and 93.3% rank-1 performance on the Motion Analysis and Re-identification Set (MARS) [11], DukeMTMC-VideoReID (Multi-Target, Multi-Camera) [12], and Person Re-ID (PRID) [13] benchmark datasets, which are comparable to the state-of-the-art video-based re-id algorithms [12, 14-15].

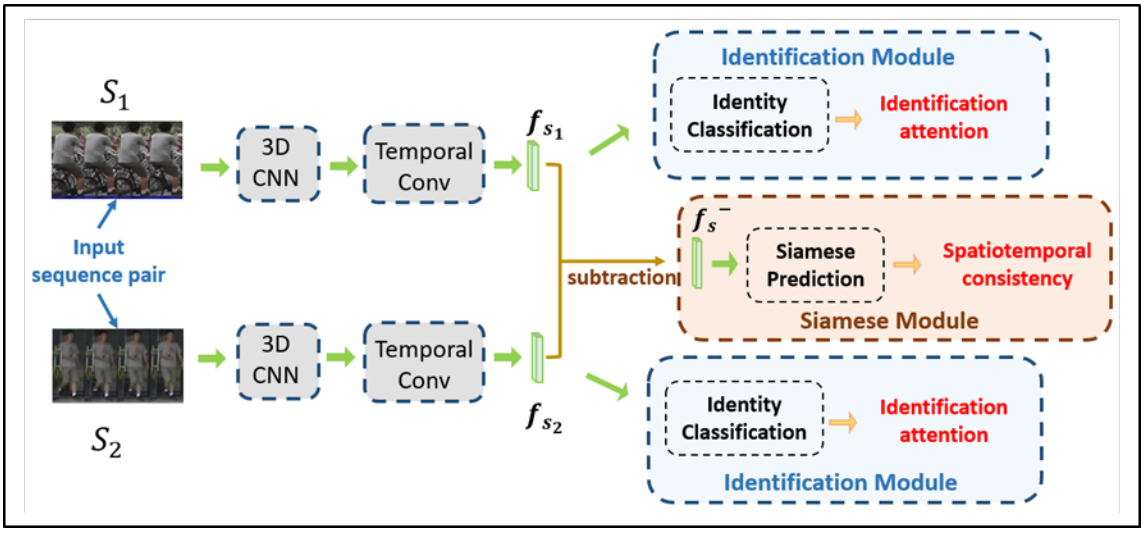

Figure 1: Pipeline of the proposed SCAN method for video-based re-id.

In our Year 6 ALERT-funded paper [1], we introduced the Consistent Attentive Siamese Network (CASN), which is able to generate attention from classification-based re-id models to spatially localize informative regions and provide visual explanations given person identity label information, showing superior performance compared to state-of-the-art re-id algorithms. In particular, depending on the dataset, we reported 5%–7% improvements in rank-1 accuracy compared to general competing algorithms, and substantial 10%–30% improvements in rank-1 accuracy compared specifically to attention-based methods. In Year 7, we took a step further to develop a similarity attention generation technique that produces attention from similarity distances between feature points in the deep embedding space. The generated

attention is able to explain why the input data points (pairs/triplets of person images) are similar/dissimilar by localizing meaningful spatial regions in the input person image set. Compared to CASN, the proposed similarity attention generation model has a much cleaner and more simplified architecture that is able to achieve comparable/superior performance in person re-identification tasks. More importantly, it is the first method proposed to interpret the reasoning behind CNN-based metric learning models by means of gradient-based attention.

Existing deep similarity predictors for person re-id [16-18] are trained in a distance-learning fashion where the big-picture goal is to embed features of same-person data points close to each other in the learned embedding, while also pushing features of data from other person classes further away. Consequently, most techniques distill this problem into optimizing a ranking objective that respects the relative ordinality of pairs [19], triplets [20], or even quadruplets [18] of training examples. However, a key limitation of these approaches is their lack of decision reasoning (i.e., explanations for why the model predicts the input set of person images is similar or dissimilar). An illustrative example of our proposed Similarity Attention Network is shown in Figure 2. A more detailed presentation of the approach is described in our paper [21], which is currently under review for the European Conference on Computer Vision 2020 (ECCV). As we demonstrate in our paper, our method offers not only model explainability but also decision reasoning that can further be infused into the model training process, in turn helping bootstrap and improve the generality of the trained re-id model.

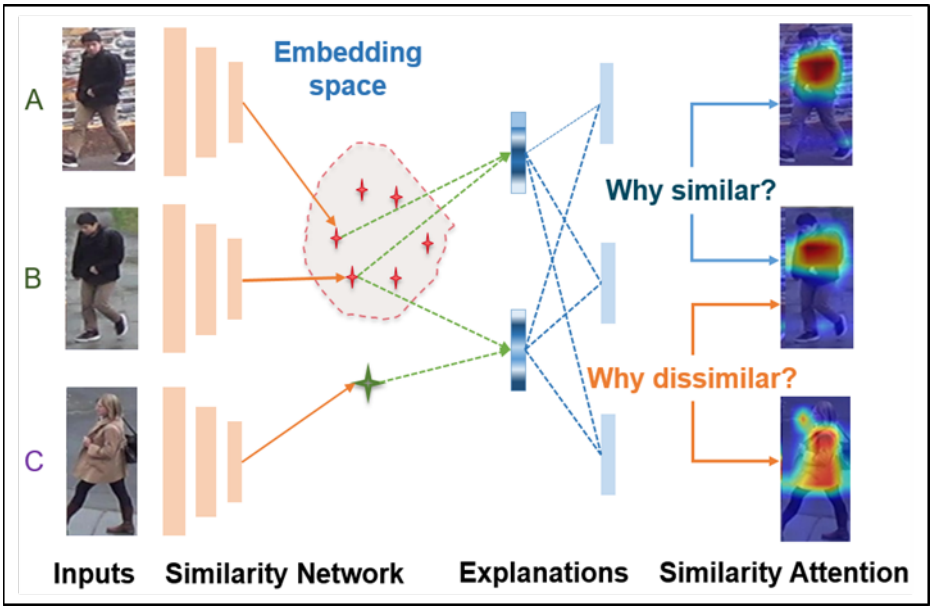

Figure 2: We present the first gradient-based similarity attention and similarity mining framework, giving a new attention-driven learning paradigm for similarity predictors that results in similarity model explainability and improved downstream performance.

The output of existing re-id algorithms is typically a list of candidate images ranked by the corresponding similarity scores computed by the algorithm. However, for real-world applications of re-id, this is not enough. For example, a suspect typically will need to be consistently tracked throughout a wide-area camera network, not just a single camera, so that the user of the system (e.g., a security officer) can monitor and recover the spatial and temporal information about his/her travel path. To achieve this with conventional re-id algorithms, system users would have to manually, incrementally select correct matches from the camera-to-camera ranked lists produced by the algorithm and then reconstruct the person of interest's path based on the selected appearances. With the list of candidate images likely to be large in dense mass-transit

environments (e.g., airports) where such systems are typically installed, the burden on the system operator to manually go through even a part of the list and recover the travel path can be immense. To address this key practical necessity, in Year 7 we introduced spatiotemporal trajectory recovery, the problem of automatically reconstructing the timestamped spatial trajectory of a person of interest in a camera network. We illustrate the problem and its difference to standard re-id in Figure 3. Given a person of interest, a traditional re-id algorithm will produce ranked candidate lists for each camera in the network. On the other hand, our proposed trajectory recovery involves a complete spatial and temporal path reconstruction of the person of interest as the individual moves through the camera network. Specifically, as shown in Figure 3, the output is a timestamped sequential list, including camera identity and image sequence, that shows where the person of interest was in the camera network and at what time. End users of a surveillance system can then use this data to easily retrieve the desired forensic information for the person of interest. To the best of our knowledge, this is the first work in the re-id community proposed to solve the trajectory recovery problem.

With standard re-id evaluation measures not directly relevant for the problem, we introduced three new evaluation metrics that consider various spatiotemporal aspects in the context of practical, real-world use of our algorithm. Specifically, we consider (1) the percentage of recovered reappearance duration comparing to ground-truth reappearance duration; (2) similarity between recovered trajectory and ground-truth trajectory; and (3) the percentage of recovered tracking lifetime (time difference between the first and last identified appearance) with respect to ground-truth tracking lifetime to evaluate our algorithm. The experimental results on our RPIfield dataset [22] show that our trajectory recovery algorithm is able to automatically reconstruct trajectories of the persons of interest with 80.1%, 82.5% and 97.0% accuracy evaluated with the above three metrics respectively. The detailed description of this algorithm and experimental results are under review at the journal *IEEE Transactions on Biometrics, Behavior, and Identity Science*.

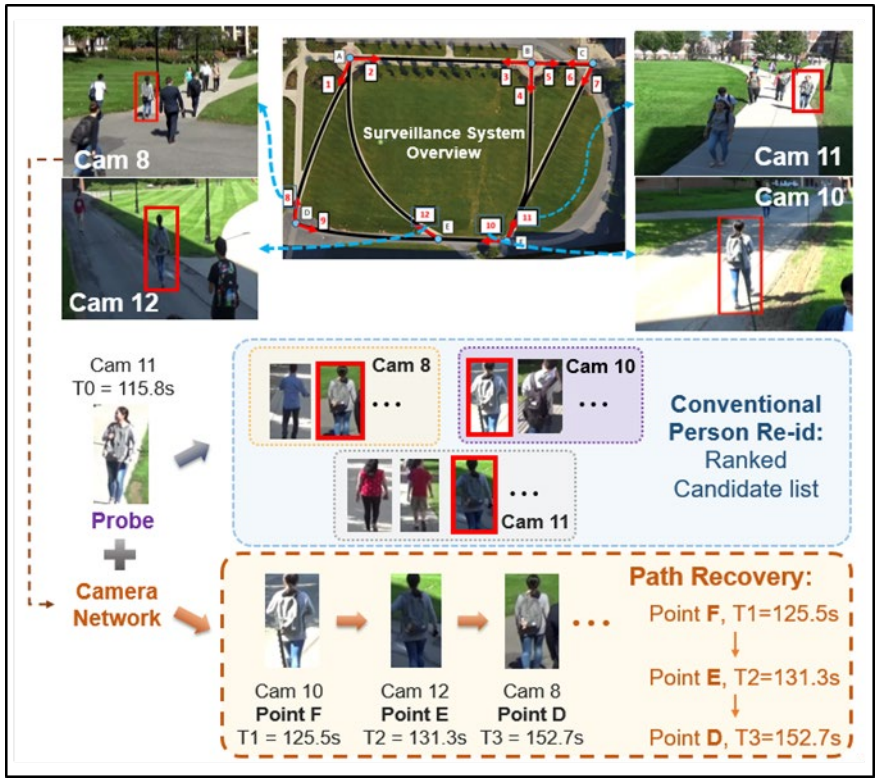

Figure 3: An illustration of the trajectory recovery problem in a wide-area multi-camera system, compared to conventional person re-identification.

C. Major Contributions

As described in more detail in the previous sections, the major contributions from Year 7 include:

- (Year 7) We proposed a novel network based on 3D convolution called the Spatiotemporal Consistent Attentive Network (SCAN) for video-based person re-id. The proposed SCAN is able to localize complete spatial regions along the temporal dimension for person tracklets by means of gradient-based 3D CNN attention, while learning intra- and inter-view consistent attentive sequence features by utilizing 3D attention as the guidance for network training. We performed extensive experiments on three benchmark video re-id datasets along with a functionality study of the individual attention modules in our new method, demonstrating the superiority of our proposed 3D attention and attention-consistency mechanism in performing video-based re-id tasks.
- (Year 7) We presented new techniques to explain and visualize, with gradient-based attention, predictions of similarity models. We showed our resulting similarity attention is generic and applicable to many commonly used similarity architectures. We presented a new paradigm for learning similarity functions with our similarity-mining learning objective, resulting in improved downstream model performance. We also demonstrated the versatility of our framework in learning similarity-attention-driven models for related surveillance applications (e.g., anomaly detection) in addition to person re-id tasks. This work is currently under review for the ECCV 2020. An application of the proposed algorithm in anomaly detection and disentangled latent representation, with which we collaborated with Northeastern University, was selected for oral presentation at the IEEE Conference on Computer Vision and Pattern Recognition, 2020.
- (Year 7) We proposed the first method to automatically reconstruct the trajectory of persons of interest by re-identifying them through a network of cameras. To efficiently compute the motion path of the persons of interest, we developed an incremental pruning strategy with a novel confidence score calculation strategy based on appearance similarity and transition-time modeling. Experimental results on the RPIfield dataset [22] show that the proposed trajectory recovery algorithm is able to consistently retrieve the crucial appearances of the persons of interest starting from their first appearance until their last reappearance, presenting the user with easy-to-read spatial and temporal reconstruction information. This work is under second review for a Minor Revision at *IEEE Transactions on Biometrics, Behavior, and Identity Science*, 2020.

Milestones achieved in the project since its inception include:

- (Year 6) We presented a novel deep architecture, called the Consistent Attentive Siamese Network (CASN), for image-based person re-id, which achieves state-of-the-art performance on popular benchmark datasets. The proposed technique makes spatial localization of the person of interest a principle part of the learning process, providing supervision only by means of person identity labels. This makes spatial localization end-to-end trainable and automatically discovers complete attentive regions. The proposed CASN defines a new framework that enforces attention consistency as part of the learning process, providing supervision that facilitates end-to-end learning of consistent attentive regions of images of the same person. This is the first proposed Siamese attention mechanism that jointly models consistent attention across similar images through a Siamese learning framework, resulting in a powerful method that can help explain the reasoning behind the network's prediction. This work was presented at the IEEE Conference on Computer Vision and Pattern Recognition, 2019.
- (Year 6) We developed a preliminary “chained re-id” algorithm that can recover the spatial path of a tagged person by following them through a network of cameras. Previously, all of our re-id research and development had focused on re-identifying a target person in a second camera (and then stopping).

In contrast, we investigated the operationally important problem of reconstructing the timestamped reappearances of people across many cameras (e.g., Person X appeared in Camera 1 at 12:30, Camera 4 at 12:33, Camera 2 at 12:35, etc.). We developed a human-in-the-loop Graphical User Interface program to completely recover the trajectory of the persons of interest. This approach was refined and automated in Year 7, as discussed above, to remove the human from the loop.

- (Year 5) We created a new large-scale real-world re-id dataset, RPIfield [22], using 12 disjoint surveillance cameras placed around an outdoor field at RPI. RPIfield contains the largest number of camera views in the context of benchmarking datasets in the re-id research community. It includes 112 known "actors" walking along predefined paths among ~4000 distractors, which simulates the mass-transit environments of interest to DHS. With timestamp information preserved for every person image, the dataset allows extensive temporal analysis of re-id algorithms that was not previously addressable by existing benchmarking datasets.
- (Year 5) Temporal attribute analysis of re-id algorithms is mostly ignored in academic re-id research; however, these considerations are essential to real-world deployment. Specifically, for a real-world re-id system that automatically detects and tracks people for a long time (e.g., several days), the gallery sets will be continuously populated with incoming candidate images. Consequently, existing measures adopted to evaluate re-id algorithms, such as CMC curves, fall short because they ignore such time-varying behavior of the gallery. In Year 5, we extended the idea of Rank Persistence Curve (RPC) proposed in Year 4, extensively evaluating and analyzing the temporal performance of benchmarking re-id algorithms on our new RPIfield [22] dataset. This kind of analysis is critical for bridging the gap between real-world system application and academic research in this area.
- (Year 4) In Year 4, we initially proposed the Rank Persistence Curve (RPC) methodology. We designed both qualitative and quantitative evaluation metrics that are generic and can be used to evaluate the "temporal robustness" of any re-id algorithm. We assessed preliminary results using a custom re-id dataset we built specifically to model such temporal aspects of real-world re-id, constructed from the camera views collected by the ALERT team at the Greater Cleveland Rapid Transit Authority (GCRTA) in Years 2 and 3. However, this dataset was quite limited and necessitated the collection of a larger dataset in Year 5 as described above.
- (Years 4–5) The ALERT Airport Re-Identification Dataset was curated and released on ALERT's website, generating substantial interest from the research community. The dataset has been requested and downloaded 280 times since it was made available, and 13 industrial organizations have made use of the data, including Bosch, Intel and Mitsubishi. See more information below.
- (Year 4) We began to investigate the transition of the best-performing re-id algorithms identified by our extensive benchmarking analysis (see below) to a large environment equipped with multiple pan-tilt-zoom (PTZ) cameras. The goal is to actively orient the cameras in conjunction with real-time re-id, for example, to keep promising candidates in sight by panning and acquire higher resolution images by zooming. The problem is complicated by the issue that there may be more candidates than cameras, requiring time-sharing schemes to be developed to entertain multiple hypotheses.
- (Years 3–5) The public release of several datasets and code for vision algorithms has facilitated rapid progress in re-id research over the past decade. However, directly comparing re-id algorithms reported in the literature has become difficult since a wide variety of features, experimental protocols, and evaluation metrics are employed. In order to address this need, we undertook an extensive review and performance evaluation of single- and multi-shot re-id algorithms. The experimental protocol incorporates the most recent advances in both feature extraction and metric learning. All approaches

were evaluated using a new large-scale dataset created using videos from Cleveland Hopkins International Airport (CLE) as well as existing publicly available datasets. This study is the largest and most comprehensive re-id benchmark to date, and has been accepted and published online at *IEEE Transactions on Pattern Analysis and Machine Intelligence* in February 2018.

- (Years 3–4) We refined and improved the end-to-end system solution for the re-id problem installed in CLE in Year 2. We constructed a new large-scale dataset that accurately mimics the real-world re-id problem using videos from CLE and conducted several new experiments in the concourse testbed. The overall system architecture and the challenges of bringing academic re-id research to a real-world deployment were described in an overarching journal paper that should be quite valuable to both the academic and industrial research communities. This work appeared online in *IEEE Transactions on Circuits and Systems for Video Technology* in April 2016 and was published in March 2017.
- (Years 3–4) We introduced an algorithm to describe image sequence data using affine hulls and to learn feature representations directly from these affine hulls using discriminatively trained dictionaries. While existing metric learning methods typically employ the average feature vector as a data exemplar, this discards the rich information present in the sequence of images available for a person. We show that using affine hull representations computed with respect to the learned dictionary results in superior re-id performance when compared to using the average feature vector, as done in existing methods. This work was accepted by *IEEE Transactions on Circuits and Systems for Video Technology* and appeared online in July 2017.
- (Year 3) We proposed a new approach to address the person re-id problem in cameras with nonoverlapping fields of view. Unlike previous approaches that learn Mahalanobis-like distance metrics in some embedding space, we propose to learn a dictionary that is capable of discriminatively and sparsely encoding features representing different people. To tackle viewpoint and associated appearance changes, we learn a single dictionary in a projected embedding space to represent both gallery and probe images in the training phase. We then discriminatively train the dictionary by enforcing explicit constraints on the associated sparse representations of the feature vectors. In the testing phase, we re-identify a probe image by simply determining the gallery image that has the closest sparse representation to that of the probe image in the Euclidean sense. Extensive performance evaluations on two publicly available multi-shot re-id datasets demonstrate the advantages of our algorithm over several state-of-the-art dictionary learning, temporal sequence matching, spatial appearance, and metric-learning-based techniques. This work was presented at the IEEE International Conference on Computer Vision (ICCV) in December 2015.
- (Years 2–3) We introduced an algorithm to hierarchically cluster image sequences and use the representative data samples to learn a feature subspace maximizing the Fisher criterion. The clustering and subspace learning processes are applied iteratively to obtain diversity-preserving discriminative features. A metric learning step is then applied to bridge the appearance difference between two cameras. The proposed method was evaluated on three multi-shot re-id datasets, and the results outperformed state-of-the-art methods. This work was presented at the British Machine Vision Conference in September 2015.
- (Year 2) We proposed a novel approach to solve the problem of person re-id in nonoverlapping camera views. We hypothesized that the feature vector of a probe image approximately lies in the linear span of the corresponding gallery feature vectors in a learned embedding space. We then formulated the re-id problem as a block sparse recovery problem and solved the associated optimization problem using the alternating directions framework. We evaluated our approach on the publicly available PRID (person re-id) 2011 and iLIDS-VID multi-shot re-id datasets and demonstrated superior performance in

comparison with the current state of the art. This work was presented at the IEEE/ISPRS 2nd Joint Workshop on Multi-Sensor Fusion for Dynamic Scene Understanding in June 2015.

- (Year 2) We proposed a novel metric learning approach to the human re-id problem with an emphasis on the multi-shot scenario. First, we perform dimensionality reduction on image feature vectors through random projection. Next, a random forest is trained based on pairwise constraints in the projected subspace. This procedure repeats with a number of random projection bases so that a series of random forests are trained in various feature subspaces. Finally, we select personalized random forests for each subject using their multi-shot appearances. We evaluated the performance of our algorithm on three benchmark datasets. This work was presented at the IEEE Winter Conference on Applications of Computer Vision (WACV) in January 2015.
- (Year 2) An end-to-end system solution of the re-id problem was installed in an airport environment, with a focus on the challenges brought by the real-world scenario. We addressed the high-level system design of the video surveillance application and enumerated the issues we encountered during our development and testing. We described the algorithm framework for our human re-id software and discussed considerations of speed and matching performance. Finally, we reported the results of an experiment conducted to illustrate the output of the developed software, as well as its feasibility for the airport surveillance task. This work was presented at the eighth ACM/IEEE International Conference on Distributed Smart Cameras (ICDSC) in November 2014.
- (Years 1–2) In collaboration with the R4-A.1 project, the design and deployment of an on-site re-id algorithm for the new branching testbed at CLE occurred, leveraging a software architecture using Data Distribution Service (DDS), including an experimental graphical user interface for tagging subjects of interest and viewing top-ranked matching candidates.
- (Years 1–2) ALERT-guided design and deployment of a new six-camera branching testbed leading from the exit of the central security checkpoint in CLE to each of the three concourses.
- (Year 1) Development of a novel re-id algorithm that mitigates perspective changes in surveillance cameras. We built a model for human appearance as a function of pose using training data gathered from a calibrated camera. We then applied this "pose prior" in online re-id to make matching and identification more robust to viewpoint. We further integrated person-specific features learned over the course of tracking to improve the algorithm's performance. We evaluated the performance of the proposed algorithm and compared it to several state-of-the-art algorithms, demonstrating superior performance on standard benchmarking datasets as well as a challenging new airport surveillance scenario. This work was published in *IEEE Transactions on Pattern Analysis and Machine Intelligence* in May 2015.
- (Year 1) Developed an algorithm for keeping a pan-tilt-zoom (PTZ) camera calibrated. We proposed a complete model for a PTZ camera that explicitly reflects how focal length and lens distortion vary as a function of zoom scale. We show how the parameters of this model can be quickly and accurately estimated using a series of simple initialization steps and followed by a nonlinear optimization. Our method requires only ten images to achieve accurate calibration results. Next, we show how the calibration parameters can be maintained using a one-shot dynamic correction process; this ensures that the camera returns the same field of view every time the user requests a given (pan, tilt, zoom), even after hundreds of hours of operation. The dynamic calibration algorithm is based on matching the current image against a stored feature library created at the time the PTZ camera is mounted. We evaluated the calibration and dynamic correction algorithms on both experimental and real-world

datasets, demonstrating the effectiveness of the techniques. This work was published in *IEEE Transactions on Pattern Analysis and Machine Intelligence* in August 2013.

- (Year 1) Establishment of an initial tag and track testbed in CLE that included a selection of cameras leading from the parking garage to the terminal.

D. Milestones

As described in our Year 6 Report, the major milestones planned for Year 7, which were achieved, included:

- The development of an effective, end-to-end training deep network for the video-based re-id problem, to learn spatiotemporal attentive and cross-view invariant feature representations for person tracklets. To demonstrate our effectiveness and improvement over the state of the art, we used the standard measure of rank-k performance with an emphasis on rank-1 performance (i.e., the percentage in which the algorithm's top match is the correct candidate). We achieved this milestone with 82.7%–93.4% rank-1 performance on several benchmark video-based re-id datasets, which is described in more detail in our section "State of the Art and Technical Approach." The outcome is a pre-trained end-to-end package that could easily be adopted by DHS practitioners.
- To continue the study of a robust "chained-re-id" algorithm to automatically recover the trajectory of a person of interest in a network of cameras, which has immediate applications to real-world multicamera surveillance environments. This milestone was achieved with the new trajectory recovery algorithm and additional novel evaluation metrics described in the previous section. We performed extensive experiments and individual algorithm module studies on the RPIfield dataset [22] with the proposed evaluation metrics. The outcome is an algorithm module able to process timestamped person image sequences from a large camera network, along with side information about the topology of the network, to produce maps and corresponding camera-by-camera thumbnails of the recovered person trajectory.

We also achieved an additional milestone in Year 7 not on the original list:

- We presented a new paradigm for learning similarity functions for person re-id using our similarity-mining learning objective, resulting in improved downstream model performance. We achieved state-of-the-art rank-1 performance compared to the most recent re-id algorithms, which is better than as published in our Year 6 ALERT-funded paper [1]. We also demonstrated the versatility of our framework in learning attention-driven models for anomaly detection, which is also a crucial problem in modern surveillance system development. We collaborated with Northeastern on developing this work, which will be presented orally at the *IEEE Conference on Computer Vision and Pattern Recognition*, 2020.

E. Final Results at Project Completion (Year 7)

The achieved final results in Year 7 include:

- The development of an effective, end-to-end training deep network for the video-based re-id problem, achieving 82.7%–93.4% rank-1 performance on various benchmark video-based re-id datasets, which matches the most recent state of the art. This end-to-end deeply learned re-id model can be directly integrated into large-scale real-world surveillance systems for cross-view person tracklet matching.
- The development of a state-of-the-art similarity-attention-driven deep re-id model, which is able to provide explicit reasoning behind the similarity predictions (i.e., why the person image pair was found to be similar or dissimilar), by means of gradient-based spatial localization, while additionally

producing state-of-the-art re-id performance in terms of rank-1 matching accuracy. This algorithm can be combined with any existing temporal aggregation method and easily plugged into existing real-world systems for direct use of person re-id, while presenting explicit visualizations of why the algorithm produces right/wrong predictions in the form of heatmaps.

- The development of an algorithm module to process timestamped person image sequences from a large camera network, along with side information about the topology of the network, producing maps and corresponding camera-by-camera thumbnails of the recovered person trajectory. This is the first work proposed in the re-id community that solves the problem of trajectory recovery of persons of interest moving in a wide-area camera network. Our proposed solution automatically outputs possible moving trajectories of the person of interest, which avoids intractable manual labeling effort from real-world end users required by conventional re-id. The developed algorithm module is easy to integrate into real-world systems for direct use, which does not require any extra transition effort.

  The contributions with the highest impact over the life of the project (described more fully in the previous section) include:

  - Our benchmarking, categorization, and code dissemination efforts that culminated in our highly cited survey in *IEEE Transactions on Pattern Analysis and Machine Intelligence* in 2018. This extensive review and performance evaluation of single- and multi-shot re-id algorithms defined an experimental protocol that incorporated the most recent advances in both feature extraction and metric learning.
  - Our fundamental theoretical work on viewpoint-invariant human re-identification that laid the groundwork for many further advancements in the field. In particular, two of our papers [24, 25] published in 2015 have 123 and 162 citations as of July 2020.
  - Our real-world implementation of a real-time, multicamera system at Cleveland Hopkins International Airport that demonstrated the feasibility and challenges of bringing a previously academic problem into DHS practice. This early effort formed the basis of our group's emphasis on the real-world operational aspects of re-id algorithms.

III. RELEVANCE AND TRANSITION

A. Relevance of Research to the DHS Enterprise

- Video surveillance is an integral aspect of homeland security monitoring, forensic analysis, and intelligence collection. The research projects in this area were directly motivated (and in fact, requested) by DHS officials as critical needs for their surveillance infrastructure, in particular for agencies such as the Transportation Security Administration (TSA). As ALERT evolved, video surveillance, in particular for mass transit environments, took on an increasingly prominent role, as a result of associated task orders and follow-on funding (e.g., Counterflow and Tag and Track efforts at CLE and the Correlating Luggage and Specific Passengers program at Kostas Research Institute at Northeastern University).
- For evaluating typical re-id systems, the metric we seek to maximize is the rank-k performance; that is, the percentage of tagged subjects who appear in the short list of k best matches automatically predicted by the algorithm. In Year 7, on the one hand, we developed novel, effective re-id algorithms that achieved state-of-the-art/competitive rank-1 performance on the most popular benchmark re-id datasets. These end-to-end learning algorithms can be plugged in as a submodule to real-world

surveillance systems, which will produce more accurate candidate lists in a graphical user interface than existing competitive methods. On the other hand, we developed a novel trajectory recovery algorithm which provides the first proposed solution for reconstructing a person of interest's trajectory in a network of cameras. The output of our algorithm is one or multiple possible timestamped reappearances along with spatial locations, which directly addresses the concern of real-world users who usually want to retrieve this information from conventional re-id algorithms but currently would need substantial manual selection effort to achieve this.

B. Status of Transition at Project End

In Years 1–4, the video analytics group built a strong relationship with Cleveland TSA, CLE, and the Greater Cleveland Regional Transit Authority (GCRTA). In our first project, we transferred a set of counterflow algorithms to detect people entering the airport exit lanes, and worked with the TSA and airport officials to display the counterflow events in their coordination center for further analysis and action. We then worked with the same group to develop re-id and tracking algorithms to satisfy their needs and match their CONOPS, so that the presented results fit their operation. The developed re-id algorithms were implemented on a custom-built PC at CLE, with a working user interface, as detailed in the joint publication [26]. Our research in Years 5–7 of developing effective deep person re-id networks could naturally be integrated and tested on simulated or real-world surveillance systems, due to its end-to-end learning architecture. Specifically in Year 7, we worked on realizing higher-level functions of re-id (i.e., systems that can automatically recover trajectories of persons of interest walking through a network of cameras). These two aspects could be easily transited to real-world applications, in the form of algorithm module development. Possible avenues for transition/industrial collaboration were discussed with the ALERT team in December 2018 (e.g., nonairport scenarios like ports/shipping, customs, campus security / public safety). It would be particularly interesting to partner with the re-id effort apparently underway at Lincoln Labs.

Another aspect of transition in which our project is strong is the creation, packaging, and dissemination of algorithms and datasets that can immediately be adopted by DHS stakeholders. These include several benchmark datasets/codebases published in the past three years (e.g., the ALERT Airport Re-Id Dataset, the RPIField Dataset, the DukeMTMC4ReID dataset, the easy-to-use GitHub codebase that accompanies our survey paper [23]).

C. Transition Pathway and Future Opportunities

With the research of four graduate students concluded over the lifetime of ALERT, the project leaves behind a large codebase with state-of-the-art re-id performance directly applicable to DHS surveillance systems. Our early experience at CLE demonstrated that interfacing our algorithms to a legacy surveillance system requires a substantial effort, as well as months of negotiations that generally have to occur above the individual project level. As a center, ALERT continues to push strongly into this space (e.g., the current effort to integrate the CLASP algorithms at KRI into a domestic airport). If these CLASP agreements are successful, the target airport would be a natural venue to transition the re-id algorithms developed in this project.

Three of the four ALERT PhD students still work closely together, first at Siemens Corporate Research in Princeton, New Jersey and now at United Imaging Intelligence in Cambridge, Massachusetts. They would be willing to advise future students or staff on concrete transitions to field sites once agreements are in place.

D. Customer Connections

This project historically involved regular contact with DHS, CLE, GCRTA, and law enforcement collaborators, including:

- Michael Young, former Federal Security Director, TSA at CLE
- Jim Spriggs, former Federal Security Director, TSA at CLE
- John Joyce, Chief of Police/Director of Security, GCRTA
- Don Kemer, Transportation Security Manager, Coordination Center, TSA at CLE
- Fred Szabo, Commissioner, CLE
- Michael Gettings, Lieutenant, Cleveland Transit Police

Of these, Michael Young was in weekly contact with the PI and students over the course of the transition project at CLE and had substantial input over the direction of the project.

Little contact was made with these individuals in Years 4–7 due to retirements and reorganizations. The proposed research in this thrust would be quite relevant to airports and rail stations, if the contacts were to be reestablished and sufficient resources made available. There is currently considerable interest and ongoing negotiations from airport officials with respect to the related CLASP project, and some of these contacts may also be interested in the re-id problem. George Naccara, retired CIO, MassPort is playing a key role in the current CLASP transition effort.

IV. PROJECT ACCOMPLISHMENTS AND DOCUMENTATION

A. Education and Workforce Development Activities

1. Student Internship, Job, and/or Research Opportunities
    a. PhD student Meng Zheng defended her thesis in March 2020 and graduated from RPI in May 2020. She joined United Imaging Intelligence in Cambridge, Massachusetts in June 2020.

B. Peer Reviewed Journal Articles

Pending –

1. Zheng, M., Karanam, S., & Radke, R.J. "Towards Automated Forensic Reconstruction in Wide-Area Multi-Camera Networks." *IEEE Transactions on Biometrics, Behavior, and Identity Science*, submitted May 2020.

C. Peer-Reviewed Conference Proceedings

1. Liu, W., Li, R., Zheng, M., Karanam, S., Wu, Z., Bhanu, B., Radke, R.J., & Camps, O. "Towards Automated Forensic Reconstruction in Wide-Area Multi-Camera Networks." *IEEE Conference on Computer Vision and Pattern Recognition,* 2020.

Pending –

1. Zheng, M., Karanam, S., Wu, Z., Chen, T., & Radke, R.J. "Learning Similarity Attention." *European Conference on Computer Vision*, in review, 2020.

D. Student Theses or Dissertations Produced from This Project

1. Zheng, M. "Design of Real-World Person Re-Identification Systems." PhD Thesis, Department of Electrical, Computer, and Systems Engineering, Rensselaer Polytechnic Institute, May 2020.

V. REFERENCES

[1] M. Zheng, S. Karanam, Z. Wu, and R. J. Radke, "Re-Identification with Consistent Attentive Siamese Networks," in *CVPR*, 2019.

[2] K. He, X. Zhang, S. Ren, and J. Sun, "Deep Residual Learning for Image Recognition," in *CVPR*, 2016.

[3] A. Krizhevsky, I. Sutskever, and G. E. Hinton, "ImageNet Classification with Deep Convolutional Neural Networks," in *NIPS*, 2012.

[4] J. Deng, W. Dong, R. Socher, L. Li, K. Li, and F. Li, "ImageNet: A Large-Scale Hierarchical Image Database," in *CVPR*, 2009.

[5] D. Tran, L. Bourdev, R. Fergus, L. Torresani, and M. Paluri, "Learning Spatiotemporal Features with 3D Convolutional Networks," in *ICCV*, 2015.

[6] C. Szegedy, W. Liu, Y. Jia, P. Sermanet, S. Reed, D. Anguelov, D. Erhan, V. Vanhoucke, and A. Rabinovich, "Going Deeper with Convolutions," in *CVPR*, 2015.

[7] K. Hara, H. Kataoka, and Y. Satoh, "Can Spatiotemporal 3D CNNs Retrace the History of 2D CNNs and ImageNet?" in *CVPR*, 2018.

[8] R. R. Selvaraju, M. Cogswell, A. Das, R. Vedantam, D. Parikh, and D. Batra, "Grad-CAM: Visual Explanations from Deep Networks via Gradient-Based Localization," in *ICCV*, 2017.

[9] L. Zheng, Y. Yang, and A. G. Hauptmann, "Person Re-identification: Past, Present and Future," in *arXiv:1610.02984*, 2016.

[10] N. McLaughlin, J. M. D. Rincon, and P. Miller, "Recurrent Convolutional Network for Video-Based Person Re-identification," in *CVPR*, 2016.

[11] L. Zheng, Z. Bie, Y. Sun, J. Wang, C. Su, S. Wang, and Q. Tian, "MARS: A Video Benchmark for Large-Scale Person Re-Identification," in *ECCV*, 2016.

[12] Y. Wu, Y. Lin, X. Dong, Y. Yan, W. Ouyang, and Y. Yang, "Exploit the Unknown Gradually: One-Shot Video-Based Person Re-Identification by Stepwise Learning," in *CVPR*, 2018.

[13] M. Hirzer, C. Beleznai, P. M. Roth, and H. Bischof, "Person Re-identification by Descriptive and Discriminative Classification," in *SICA*, 2011.

[14] S. Li, S. Bak, P. Carr, and X. Wang, "Diversity Regularized Spatiotemporal Attention for Video-based Person Re-identification," in *CVPR*, 2018.

[15] Y. Liu, Y. Junjie, and W. Ouyang, "Quality Aware Network for Set to Set Recognition," in *CVPR*, 2017.

[16] M. Opitz, G. Waltner, H. Possegger, and H. Bischof, "BIER - Boosting Independent Embeddings Robustly," in *ICCV*, 2017.

[17] W. Kim, B. Goyal, K. Chawla, J. Lee, and K. Kwon, "Attention-Based Ensemble for Deep Metric Learning," in *ECCV*, 2018.

[18] W. Chen, X. Chen, J. Zhang, and K. Huang, "Beyond Triplet Loss: A Deep Quadruplet Network for Person Re-identification," in *CVPR*, 2016.

[19] W. Li, R. Zhao, T. Xiao, and X. Wang, "DeepReID: Deep Filter Pairing Neural Network for Person Re-identification," in *CVPR*, 2014.

[20] D. Cheng, Y. Gong, S. Zhou, J. Wang, and N. Zheng, "Person Re-identification by Multi-Channel Parts-Based CNN with Improved Triplet Loss Function," in *CVPR*, 2016.

[21] M. Zheng, S. Karanam, T. Chen, R. J. Radke, and Z. Wu, "Learning Similarity Attention," in *arXiv: 1911.07381*, 2019.

[22] M. Zheng, S. Karanam, and R. J. Radke, "RPIfield: A New Dataset for Temporally Evaluating Person Re-Identification," in *CVPR Workshops*, 2018.

[23] S. Karanam, M. Gou, Z. Wu, A. Rates-Borras, O. Camps, and R.J. Radke, "A Systematic Evaluation and Benchmark for Person Re-Identification: Features, Metrics, and Datasets," *IEEE Transactions on Pattern Analysis and Machine Intelligence*, 2018.

[24] Z. Wu, Y. Li, and R. J. Radke, Viewpoint Invariant Human Re-Identification in Camera Networks Using Pose Priors and Subject-Discriminative Features. *IEEE Transactions on Pattern Analysis and Machine Intelligence*, Vol. 37, No. 5, pp. 1095-1108, May 2015.

[25] S. Karanam, Y. Li, and R. J. Radke, Person Re-Identification with Discriminatively Trained Viewpoint Invariant Dictionaries, International Conference on Computer Vision (ICCV), December 2015.

[26] O. Camps, M. Gou, T. Hebble, S. Karanam, O. Lehmann, Y. Li, R.J. Radke, Z. Wu, and F. Xiong, "From the Lab to the Real World: Re-Identification in an Airport Camera Network," *IEEE Transactions on Circuits and Systems for Video Technology,* special issue "Group and Crowd Behavior Analysis for Intelligent Multi-camera Video Surveillance," Vol. 27, No. 3, pp. 540-553, March 2017.

This page intentionally left blank.

R4-B.1: Toward Advanced Baggage Screening: Reconstruction & Automatic Target Recognition

I. PARTICIPANTS INVOLVED FROM JULY 1, 2019 TO JUNE 30, 2020

Faculty/Staff			
Name	**Title**	**Institution**	**Email**
Charles Bouman	Co-PI	Purdue University	bouman@purdue.edu
Graduate, Undergraduate and REU Students			
Name	**Degree Pursued**	**Institution**	**Month/Year of Graduation**
Wenrui Li	PhD	Purdue University	9/2022
Venkatesh Sridhar	PhD	Purdue University	9/2020

II. PROJECT DESCRIPTION

A. Project Overview

3D computed tomography (CT) has been widely deployed in air transportation security applications such as check-baggage screening because of its ability to better detect threats. Based on this success, there is great interest in deploying CT in other areas of transportation security, such as checkpoint security for carry-on baggage and cargo inspection. However, for applications such as checkpoint screening and cargo, it is likely not practical to support the traditional rotating gantry structure or even rotating tables that can collect a full set of projection views assumed by traditional Fourier-based reconstruction methods. This means that this new generation of scanners will need to depend on a new generation of image reconstruction algorithms that go beyond the limitations of Fourier-based reconstruction methods, such as filtered back-projection (FBP).

The following are major challenges faced by next-generation CT systems for Transportation Security Administration (TSA) applications.

- **Large volumes:** Cargo scanning at the resolution required to detect threats will drive systems to reconstruct enormous numbers of voxels. Using existing methods, this has two undesirable consequences. First, it requires more views, which slows down physical scanning; and second, the increase in the amount of data and voxels dramatically slows reconstruction.
- **Dense materials:** In cargo applications, large volumes of dense material will make scanning difficult since photon penetration will be limited.
- **Sparse views:** Physical and practical constraints will likely limit the number of views that can be acquired by fieldable scanning systems for both baggage and checkpoint scanning. This means that reconstruction algorithms will need to be able to reconstruct accurate 3D volumes from sparse views.
- **Beam hardening and scatter due to metal:** Heterogeneous materials such as metals create a combination of beam hardening and scatter effects that break traditional models of reconstruction. While beam hardening for a single material without scatter can be compensated for, it is nearly impossible to accurately compensate for the beam hardening in a single-energy system when it is combined with

scatter effects and multiple materials. This creates large-scale artifacts that can cause erroneous segmentation and missed detection of threats.

B. State of the Art and Technical Approach

Over the last decade, model-based iterative reconstruction (MBIR) and other regularized iterative reconstruction methods have changed how people think about 3D reconstruction from CT data [1–4]. By using MBIR, we have demonstrated that 3D reconstruction from sparse views is possible [5, 6]. However, major challenges still remain. While MBIR reconstruction methods offer some solutions to these problems [7, 8], these algorithms suffer from very high computational requirements, continued (but reduced) susceptibility to beam-hardening/scatter artifacts due to metal, and continued (but reduced) degradation in quality from sparse view data.

A new generation of reconstruction algorithms that blend physical models with artificial intelligence (AI) or machine learning (ML) methods hold great promise in addressing these challenges. The breakthroughs of ML and in particular deep learning (DL) methods have opened new directions for both dramatically reducing computation and dramatically improving quality of reconstructions. The challenge of ML-based methods is to integrate the well-understood models of physics with the information that can be extracted from large corpuses of data. In some cases, this blending of data and physics models can be subtle, such as in the modeling of metal artifacts that requires the integration of well-understood physics models with empirical models of scatter distribution in the presence of unknown physical scattering parameters.

Following is a list of advanced technologies that will likely be critical to future CT imaging technologies needed by the Department of Homeland Security (DHS).

- **Integrated data, physics, and sensor models:** Next generation CT algorithms will need to integrate multiple sources of information from the physical sensor measurements, the known physics of the materials, and the empirical data distributions in order to create accurate 3D reconstructions with the limitations of sparse view data, measurement distortion due to scattering and beam hardening, heterogeneous materials, large and dense objects, and detector and photon counting noise sources. To meet this challenge, a new generation of algorithms should be developed for the integration of heterogeneous information that we call multi-agent consensus equilibrium (MACE) [9]. MACE methods are based on the plug-and-play (PnP) methods [10, 11], but they generalize to multiple sources of information that may not be formulated in an optimization framework. This framework can be used to integrate traditional physics-based models with ML models based on DL [12, 13].
- **Integrated beam-hardening and scatter models:** The complex interactions of beam-hardening and scatter are extremely difficult to accurately model for heterogeneous materials scanned with single energy CT. To address this, one can use a blend of physics and ML modeling to integrate the known physics of CT sensors with the higher order data-driven sensor models. By integrating this type of model with prior image models, our goals was to reduce metal artifacts and improve segmentation accuracy.
- **Integrated segmentation models:** The ultimate goal of reconstruction is to accurately detect targets, and this is critically dependent upon accurate segmentation. ML methods provide a formal basis for incorporating segmentation into the reconstruction process either through training or ML-based prior models. Our goal was to use the methods such as PnP to integrate in segmentation models, or to directly train ML methods to incorporate segmentation into the reconstruction process.
- **Fast reconstruction:** ML methods can be used in a variety of ways to speed up reconstruction [14, 15, 16]. One approach is to train DL methods to remove noise, but this is not effective for artifact reduction. An alternative approach that we have pioneered is to use DL methods to accurately approximate MBIR

reconstructions in a method we call DL-MBIR [14, 15]. One particular extension of this is 2.5D DL-MBIR, which uses convolutional neural networks to accurately approximate MBIR reconstructions. A goal was to use the 2.5D processing structure to achieve quality near full 3D processing, with computation that is very close to 2D.

- **Incorporation of side information:** In many applications, such as cargo scanning, there is side information available, such as manifests, that describe cargo contents that can be potentially used to improve reconstruction quality or improve segmentation or detection accuracy. This will require the formulation of general methods for incorporating side information in the reconstruction, segmentation, and threat detection process.
- **Dynamic sparse-view selection:** Large dense objects present special challenges in 3D imaging due to the difficulty of achieving sufficient penetration. While some of these can be addressed using high Kv X-ray sources and photon counting detectors, these hardware upgrades add cost and also may not be sufficient. There is a need to develop methods for dynamic acquisition of sparse views [17] that can achieve higher signal-to-noise ratio (SNR) given a fixed time budget by selecting views that are more informative based on dynamic measures of object content and structure. We have based this approach on our previous research in statistical learning approach to dynamic sampling (SLADS) [18], which has proven to be useful in dynamic 2D scanning of materials using scanning electron microscopy and other point-probe measurement methods.

We worked with ALERT to obtain data from previous task orders, and we also used simulated data to perform experiments.

B.1. Research on Direct Sparse-View Reconstruction Using Long Short-Term Memory Processing of Stacked Back-Projections

Over the past few years, sparse-view CT has captured the attention of the CT community since sparse-view data acquisition can drastically reduce scan time and dosage. However, in sparse-view applications, conventional CT reconstruction algorithms will suffer from severe streak artifacts and image distortion since projection data is undersampled. MBIR can solve sparse-view CT reconstruction problems. However, the high computational cost of MBIR makes it unsuitable for calculating reconstruction in real time.

Also over the past five years, DL has emerged as a fundamentally new approach to image reconstruction. The two major advantages of deep neural networks (DNNs) are that they can be trained to produce high-quality reconstructions from sparse and noisy data and that they are much more computationally efficient than iterative reconstruction methods.

We proposed stacked back-projection (SBP) as a general structure for direct tomographic reconstruction that preserves all the sinogram information, avoids the need for computationally intractable dense networks, and allows for the natural introduction of convolutional neural network (CNN) structures in reconstruction. We also proposed a DNN based on long short-term memory (LSTM), with SBP as an efficient computational structure that yields high quality reconstructions. In this approach, our model has a convolutional LSTM followed by a U-Net. Further, to avoid a high dependency of the output on the last view projection of SBP, we developed a rotational LSTM that can train two parallel LSTMs using different projections as the last view. Compared to CNN-based methods, our approach incorporates a convolutional LSTM that improves algorithmic convergence and leads to better reconstruction quality.

We train our networks on simulated data and validate our approach on both simulated and real data. We demonstrate that the SBP-LSTM architecture produces higher quality images as compared to post-processing of FBP images and SBP-CNN architecture.

B.1.a. Stacked Back-Projection

Figures 1 and 2 illustrate the procedure of the SBP generation. As shown in Figure 1, all the sinogram views acquired from a single 2D slice are first filtered by a ramp filter. Then, for each single-view projection, we back-project it as listed in the outer ring in Figure 1.

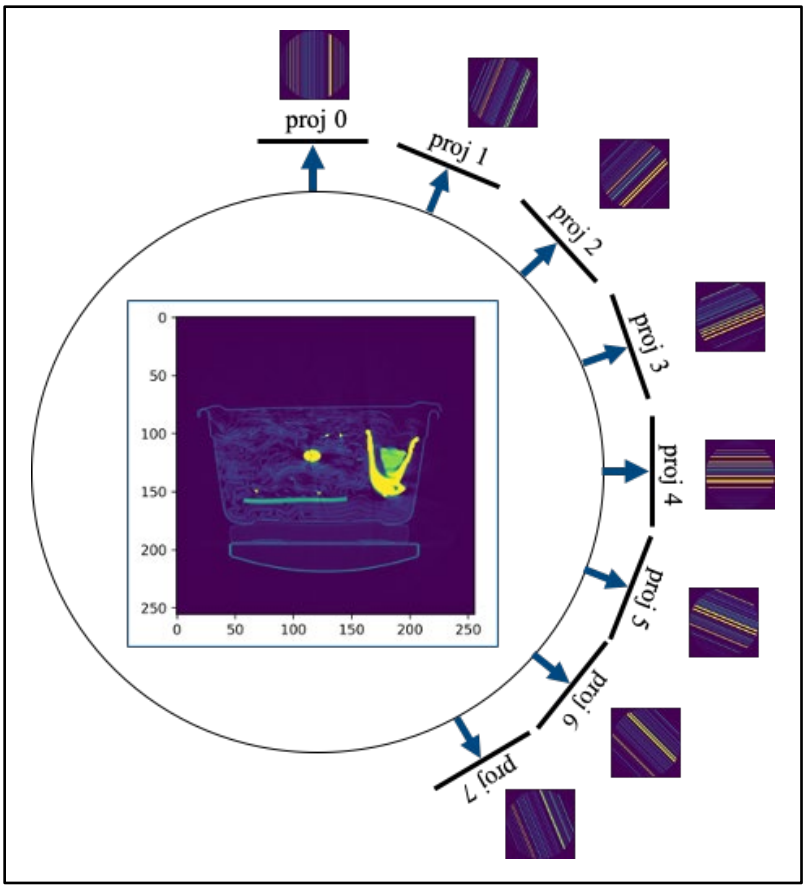

Figure 1: Single-view back-projection generation. In this example, sinogram is projected from sixteen equispaced views $[0, \pi]$.

Figure 2 depicts a pipeline from sinogram to SBP. Sixteen single-view back-projections are stacked together following the order of the equispaced views $[0, \pi]$.

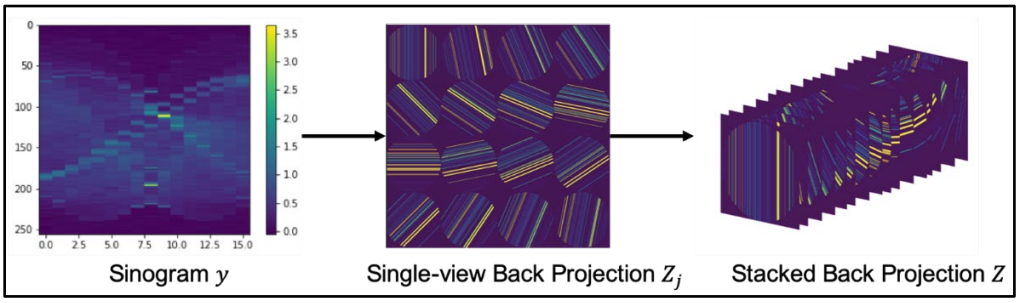

Figure 2: SBP generation. In this example, sinogram is projected from sixteen equispaced views $[0, \pi]$.

B.1.b. Deep Neural Network Models

Since we want to demonstrate the effect of using SBP as input to the deep neural network, we first implement a baseline model using FBP as input. According to [1], many deep neural networks have been proposed to learn the artifacts of the image generated from the measurement by some analytic methods. For example, Wang et al. propose several different neural networks [2-6] to recover a normal dose CT image from a noisy low dose CT image.

The architecture of our learning model is shown in Figures 3 and 4. We use both the FBP image (256 × 256 × 1) and SBP image (256 × 256 × 16) as input to our CNN model to demonstrate the effect of using SBP. We base our CNN model on the U-Net [7] by adding three convolutional blocks before the original U-Net.

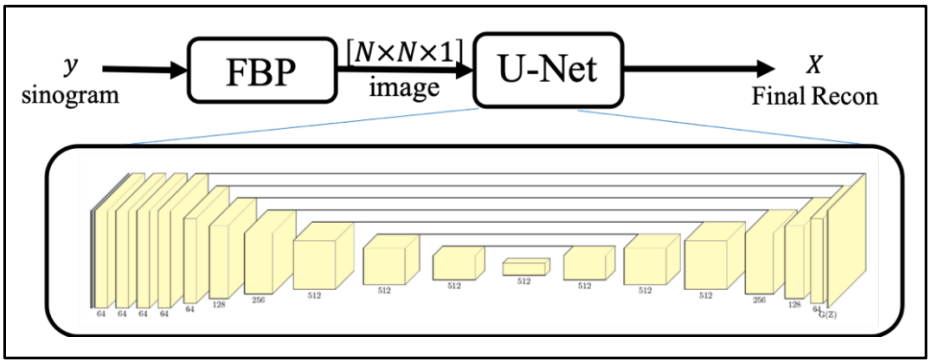

Figure 3: FBP + U-Net. The first block consists of a 3 × 3 convolution layer (with 64 filter, stride = 1) and a rectified linear unit (ReLU) activation function. We do not use activation functions in the final block. The remaining blocks consist of a 3 × 3 convolution layer (with 64 filter, stride = 1), ReLU activation function, and batch normalization.

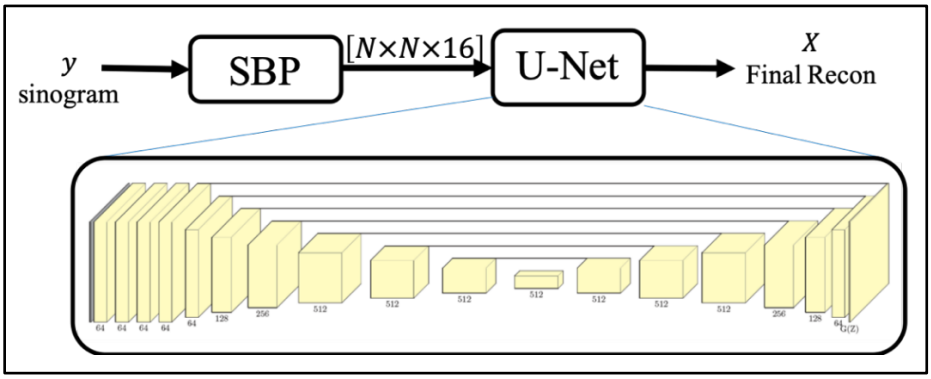

Figure 4: SBP + U-Net. Other layers remain the same as in Figure 3.

LSTM model for SBP: When using a CNN as above, we treat each single-view back projection as a channel, like the RGB channels in a color image, and stack them together in a manner by which the order of the channel does not affect the reconstruction. However, projections of a sinogram generated under a sorted angle sequence have order. Therefore, we introduce a sequential processing network to better handle the SBP data. This is reminiscent of Le et al. [8], who use LSTM to correlate adjacent views in 3D mesh segmentation.

The architecture of our proposed model is shown in Figure 5. We treat multiple views as a temporal sequence. In practical training, we need to expand and rearrange the original SBP into a 4D tensor consisting of time, rows, columns, and channels. After rearrangement, the number of views of the corresponding sinogram is consistent with the dimensionality of time, while the dimensionality of channels is one.

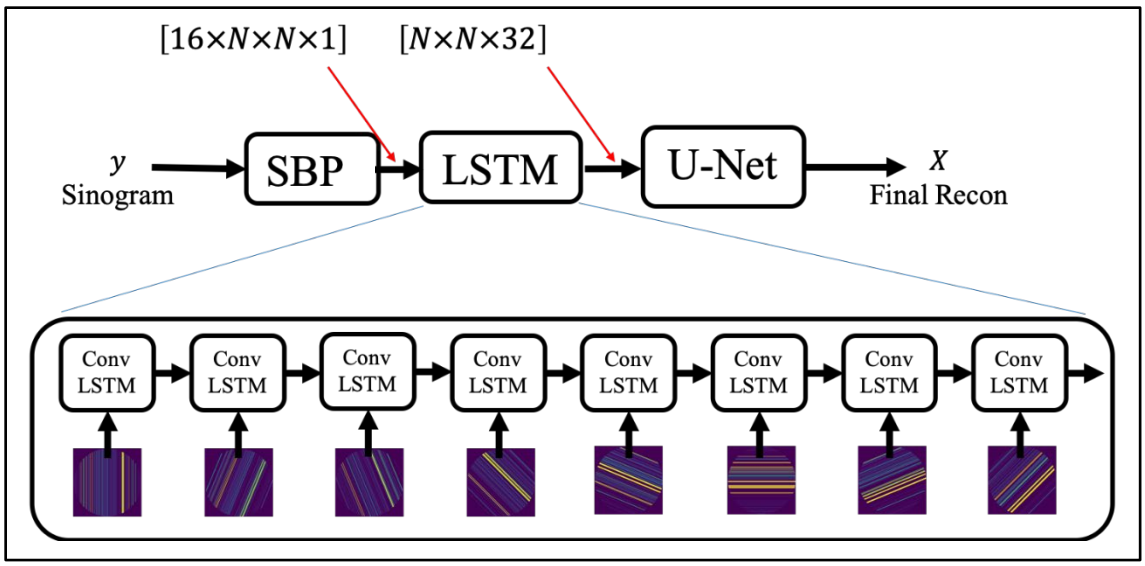

Figure 5: SBP + LSTM + U-Net. The first three blocks are replaced by the convolutional LSTM layer (kernel size = 3, strides = 1, padding = "same," and number of output filters in convolution = 32). Other layers remain the same as in Figure 3.

We base our recurrent layer on convolutional LSTM. Convolutional LSTM replaces a fully connected operation with a convolutional operation, which leads to a novel combination of LSTM and CNN. A traditional CNN-LSTM model uses CNN to extract features, followed by an LSTM and a dense layer, as in [8]. Our proposed model first uses the rearranged SBP tensor as input to the convolutional LSTM; the output is the hidden state output of the last sequence step, which is a 3D tensor shown in Figure 5. The output of the convolutional LSTM will plug into the U-Net. The convolutional LSTM can correlate adjacent views and can better separate low-noise projections from noisy projections. Also, the U-Net can further remove streak artifacts.

Rotational stride: Since we output only the last sequence step of the convolutional LSTM, we need to introduce a half rotational stride to avoid a high dependency of the output on the last view projection. As shown in Figure 6, by using a rotational stride of $\pi/2$, we actually train two parallel convolutional LSTMs. Then we concatenate the last hidden states ($N \times N \times 32$) of two LSTMs as the final output ($N \times N \times 64$) of our LSTM.

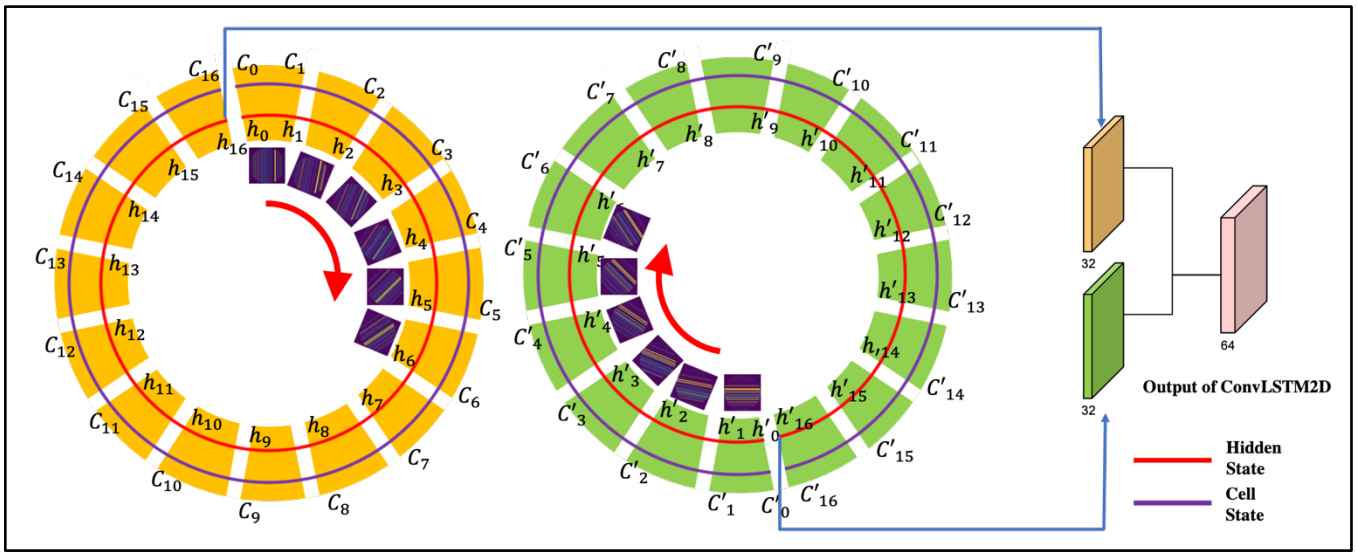

Figure 6: Half rotational stride convolutional LSTM.

Loss function: For reconstructing an X-ray CT image for security applications, the range from 0 to 2,000 Hounsfield units (HU) (scaled so that air = 0 HU and water = 1,000 HU) is critical. Therefore, we used a modified MSE loss to train our models:

$$L_{MSE} = \|f(x) - f(\hat{x})\|^2$$

$$\text{where, } f(x) = \frac{x}{|x|+2000}$$

B.1.c. Experimental Results

To test our approach, we used 980 synthetic sinograms generated from the ALERT Task Order 4 (Advances in Automatic Target Recognition for CT-Based Object Detection Systems) CT dataset by Python as well as 200 sinograms from the ALERT Task Order 3 (Research and Development of Reconstruction Advances in CT-Based Object Detection Systems) CT dataset, using an Imatron Model C300 scanner X-ray CT system.

Figure 7 together with Table 1 compare both qualitative and quantitative results of the image reconstruction algorithms using 16 view simulated data. Both root mean squared error (RMSE) and structural image similarity metric (SSIM) are used as quantitative measures of image quality. For Figure 7, a display range of 0 to 2,000 HU is used. Notice that that proposed SBP+LSTM+U-Net algorithm produces the best overall results and reduces striking artifacts such as those highlighted in the red box. Perhaps surprisingly, SBP+LSTM+U-Net even performs better than the much more computationally expensive MBIR algorithm with a simple Q-GGMRF prior model. Also notice that for our example the introduction of CGAN training does not significantly improve the result relative to more a more standard MSE loss function.

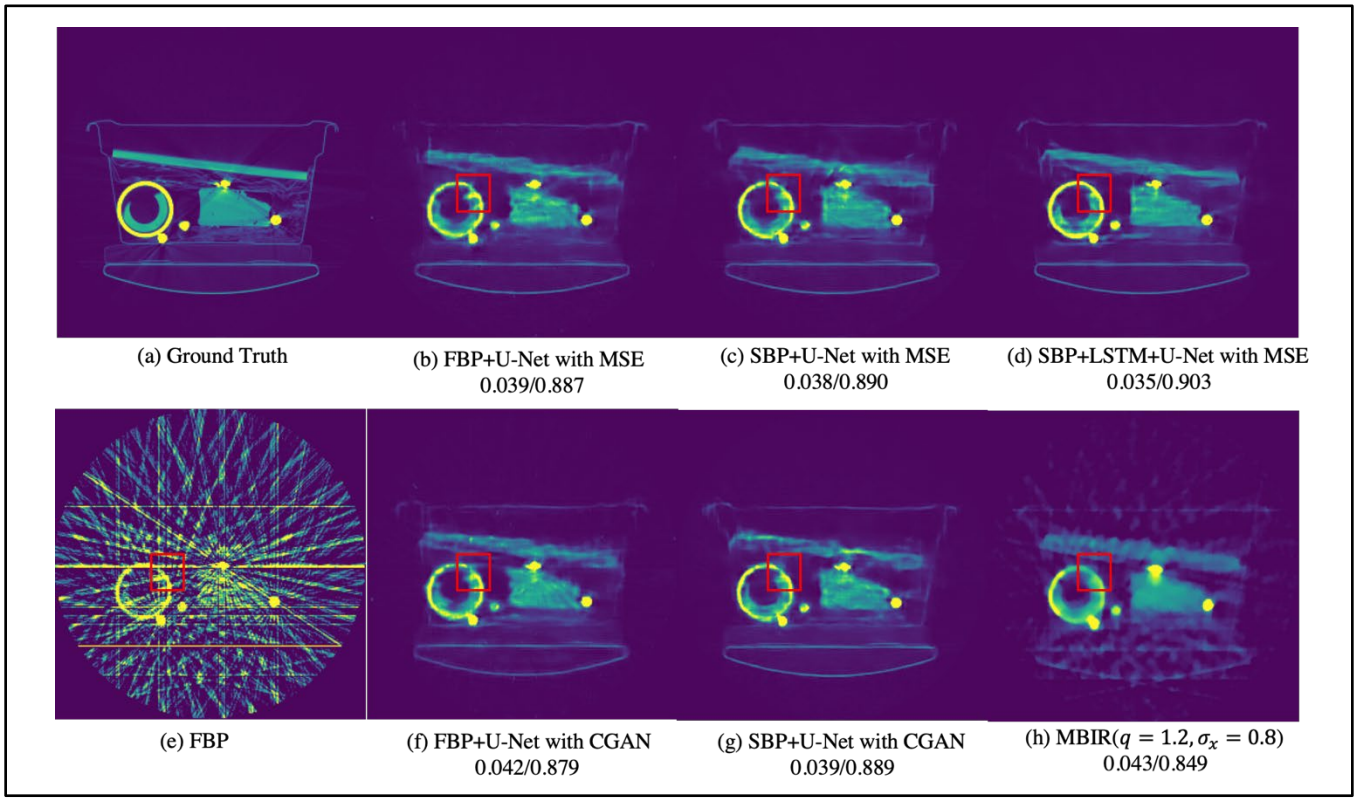

Figure 7: Results on a simulated image. Modified RMSE/SSIM. Display range is 0 to 2,000 HU. Both DL-based methods can successfully suppress most of the streak artifacts. However, FBP + U-Net fails to suppress the remaining streak artifacts shown in the red frame. SBP + LSTM + U-Net can sharpen the reconstruction image and recover important information from low-noise projections.

Model	Training Loss	RMSE	SSIM
FBP + U-Net	MSE	0.0331	0.9028
SBP + U-Net	MSE	0.0321	0.9074
FBP + U-Net	CGAN	0.0339	0.8957
SBP + U-Net	CGAN	0.0320	0.9068
SBP + LSTM + U-Net (unidirectional with rotational stride)	MSE	0.0303	0.9153
MBIR	N/A	0.0374	0.8686

Table 1: Quantitative evaluation on simulated data. SBP + LSTM + U-NET has the best modified RMSE and SSIM metric among all the methods.

Figure 8 together with Table 2 compare both qualitative and quantitative results of the image reconstruction algorithms using 16 view real data subsampled from a full set of views. Again, the RMSE and SSIM are used as metrics of image quality, but since this is real data ground truth is not available to use as a reference image. Therefore, we use the reconstruction form the full set of views as our reference, and this is done using and MBIR and FBP reference for fairness. Perhaps not surprisingly, the MBIR algorithm results in the best image quality when an MBIR reference image is used. However, when an FBP reference image is used, then SBP+LSTM+U-Net algorithm results in the best image quality. Also, visually, the SBP+LSTM+U-Net algorithm results in comparable image quality to MBIR, with less streaking and better overall sharpness, but perhaps more artifacts in some locations. So on the real data, the SBP+LSTM+U-Net algorithm results in comparible image quality to MBIR but with much lower computation.

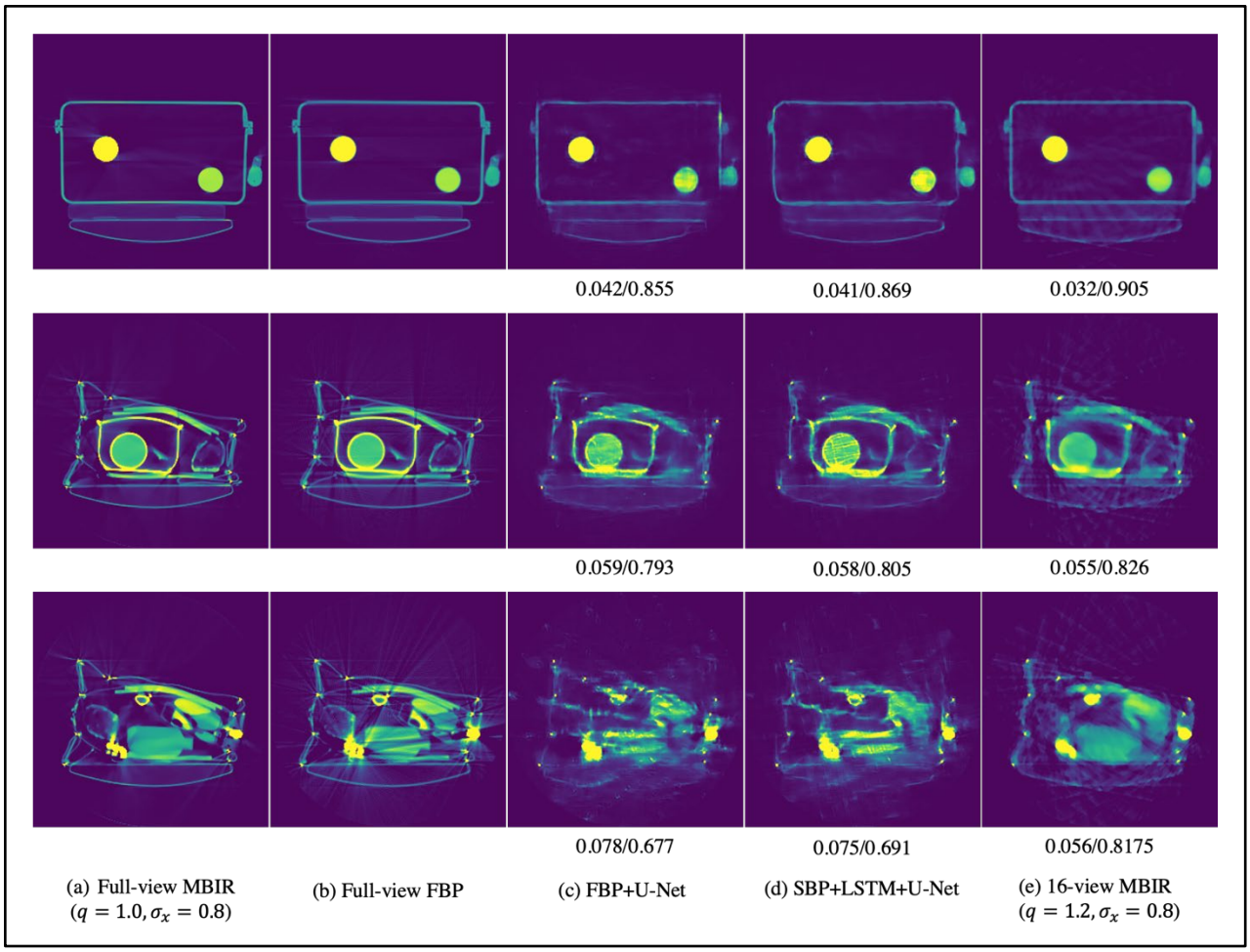

Figure 8: Sparse-view reconstruction on real sinogram. Modified RMSE/SSIM compared with full-view MBIR. Display range is from 0 to 2,000 HU. The MBIR reconstruction on sparse-view sinogram has a more accurate result than our proposed method on real data. However, our proposed method still outperforms other deep models on real data.

Model	Training Loss	RMSE (Relative to Full-View MBIR)	SSIM (Relative to Full-View MBIR)	RMSE (Relative to Full-View FBP)	SSIM (Relative to Full-View FBP)
FBP + U-Net	MSE	0.0606	0.7695	0.0493	0.8110
SBP + U-Net	MSE	0.0613	0.7740	0.0501	0.8112
FBP + U-Net	CGAN	0.0609	0.7781	0.0493	0.8124
SBP + U-Net	CGAN	0.0605	0.7758	0.0502	0.8123
SBP + LSTM + U-Net (unidirectional with rotational stride)	MSE	0.0589	0.7870	0.0470	0.8242
MBIR	N/A	0.0505	0.8404	0.0514	0.7983

Table 2: Quantitative evaluation on real data. Calculating the RMSE and SSIM between the sparse view reconstruction and a reference image computed using the full set of views and either MBIR or FBP. Notice that SBP+LSTM+U-Net and MBIR have the best overall image quality.

B.2. Source Code and Licensing for High-Performance Iterative CT Reconstruction

The parallel super-voxel iterative coordinate optimization (PSV-ICD) method [12] is a high-performance implementation of MBIR for multicore CPU systems. This approach has fast algorithmic convergence since it is based on the ICD method [9] and is roughly 187 times faster on a 20-core CPU system as standard serial ICD reconstruction on a single CPU core [12].

Figure 9 illustrates how the PSV-ICD accelerates the computation MBIR by reorganizing the projection data and system-matrix entries for each super-voxel (SV, a group of spatially close voxels) into a compact contiguous memory layout called the SV-buffer. This approach has two major benefits. First, the data access for the voxel-wise ICD update in a given SV is faster due to sequential memory access and superior cache-locality. Second, the computation of each voxel-wise ICD update can be accelerated using SIMD vector processing units. To efficiently utilize each CPU core, the update of multiple SVs that are spatially far apart is parallelized across CPU cores.

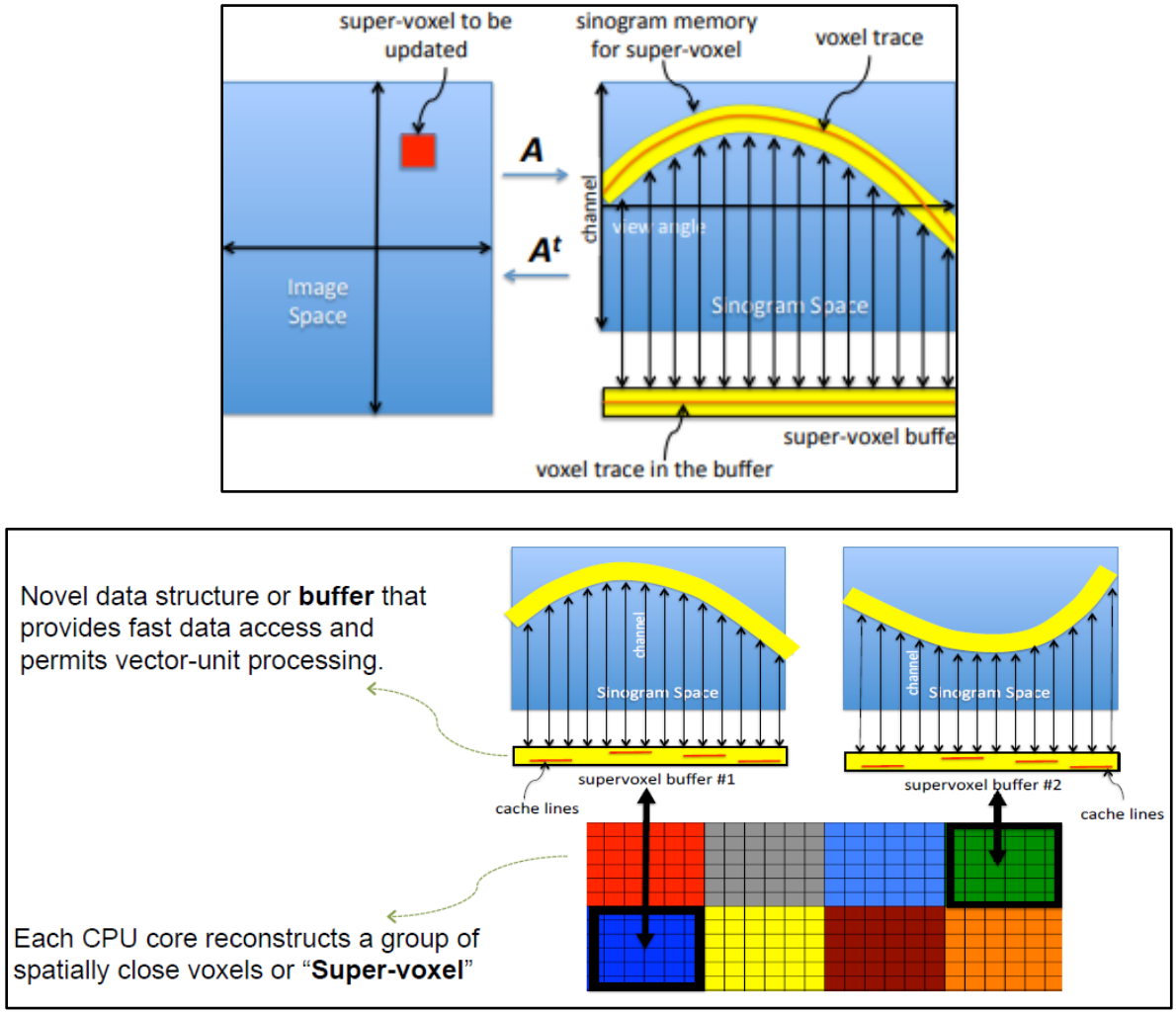

Figure 9: Illustration of high-performance CT reconstruction using the parallel SV-ICD approach; (top) SV buffer formation and (bottom) parallelization of SV-ICD algorithm across CPU cores for reconstructing single slice. The projection data for each SV is reorganized into a more compact data structure called the SV-buffer that permits fast sequential memory access and high data-caching efficiency. Further, the ICD update of different SVs that are spatially far apart is parallelized across multiple CPU cores.

In collaboration with High Performance Imaging LLC (HPI), we publicly released an open-source version of the PSV-ICD algorithm suitable for use on a high-performance multicore compute node. The software, which is available on GitHub (https://github.com/HPImaging), is licensed under the BSD-3-Clause License.

We also built an open-source Python package, svmbir, on GitHub (https://github.com/cabouman/svmbir) that makes the SV MBIR code easy to use and integrate into user software. Enhanced versions of the software suitable for CPU and GPU clusters are available from HPI for commercial licensing.

B.3. Research on Distributed Iterative High-Resolution CT Reconstruction

Tomographic reconstruction algorithms can be roughly divided into two categories: analytical reconstruction methods and regularized iterative reconstruction methods, such as MBIR. MBIR methods have the advantage that they can improve reconstructed image quality particularly when projection data are sparse and/or the X-ray dosage is low. This is because MBIR integrates a model of both the sensor and object being imaged into the reconstruction process. However, the high computational cost of MBIR often makes it less suitable for solving large reconstruction problems in real time.

We proposed a MACE algorithm for distributing both the computation and memory of MBIR reconstruction across a large number of parallel nodes [11, 16, 17]. In MACE, each node stores only a sparse subset of views and a small portion of the system matrix, and each parallel node performs a local sparse-view reconstruction, which—on repeated feedback from other nodes—converges to the global optimum.

Our distributed approach can also incorporate advanced denoisers as priors to enhance reconstruction quality. In this case, we obtain a parallel solution to the serial framework of PnP priors [15, 18], which we call MACE-PnP. Further, a direct implementation of MACE is not practical since it involves repeated application of proximal operators that are themselves iterative. To make MACE practical, we introduced a partial-update method [11, 16] that eliminates nested iterations and proves that it converges to the same global solution.

Finally, we validated our approach on a distributed memory system with real CT datasets taken from security and synchrotron imaging applications, respectively. We also demonstrate an implementation of our approach on a massive supercomputer that can perform large-scale 3D reconstruction in real time.

B.3.a. MACE and MACE-PnP Algorithms

Figure 10 illustrates our two approaches to this distributed CT reconstruction problem. While both the approaches integrate multiple sparse-view reconstructions across a compute cluster into a high-quality reconstruction, they differ based on how the prior model is implemented.

Figure 10 (top) depicts our basic MACE approach that utilizes conventional edge-preserving regularization as a prior model and converges to the maximum a posteriori (MAP) estimate. Figure 10 (bottom) shows our second approach called MACE-PnP which allows for distributed CT reconstruction using PnP priors. These PnP priors [15] substantially improve reconstructed image quality by implementing the prior model using a denoising algorithm based on methods such as BM3D [19] or deep residual CNNs [20]. We prove that MACE-PnP provides a parallel algorithm for computing the standard serial PnP reconstruction of [15].

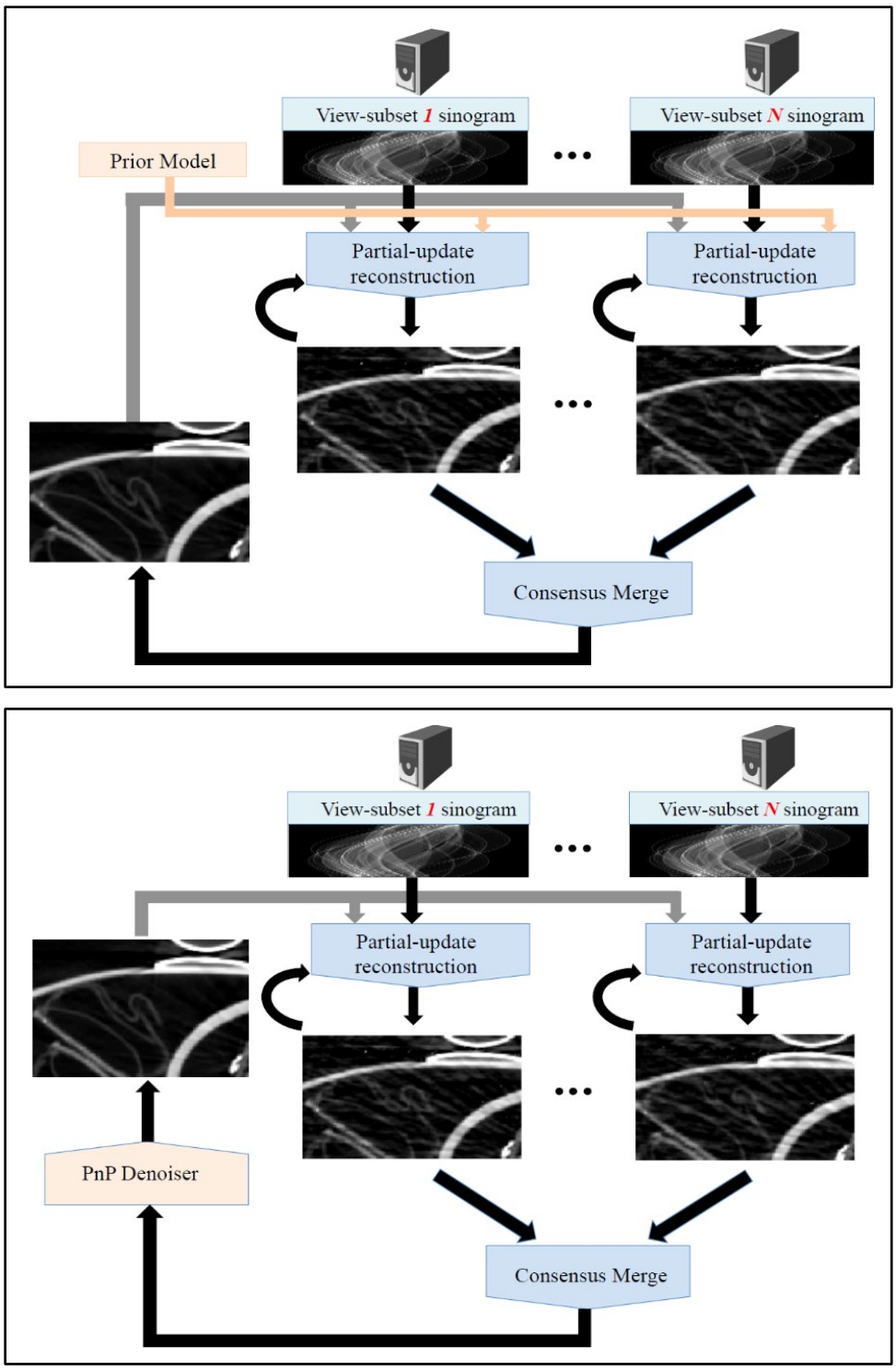

Figure 10: Illustration of the MACE algorithm for distributing CT reconstruction across a parallel cluster of compute nodes. The MACE algorithm works by splitting data into view subsets and reconstructing them in parallel. The individual reconstructions are then merged in an iterative loop that results in (top) the MAP reconstruction in the case of conventional prior models or (bottom) standard PnP reconstruction in the case of advanced prior models.

B.3.b. Mathematical Framework for MACE and MACE-PnP Algorithms

B.3.b.i. CT Reconstruction as a MAP Estimation Problem

To parallelize CT reconstruction, we first split the global MAP estimation problem into a sum of N auxiliary functions given by the following:

$$\text{Minimize } (x;\beta) = \sum_{i=1}^{N} f_i(x;\beta)\,,$$

where for each i, $f_i(x)$ represents a sparse-view reconstruction problem associated with the i^{th} view subset. More specifically, we define

$$f_i(x;\beta) = \frac{1}{2}\|y_i - A_i x\|_{\Lambda}^2 + \frac{1}{N}h(x)\,,$$

where y_i is the projection data from the i^{th} view subset, A_i is the projection operator for the i^{th} view subset, $\beta \geq 0$ is the regularization level, and $h(x)$ is the regularizing prior model. So, the MAP estimate x^* is given by the minimization of the objective function $f(x;\beta)$.

B.3.b.ii. MACE Framework

We apply the MACE framework [10] to solve the above reconstruction problem. The key idea of the MACE framework is to integrate N different data models or *agents*, represented by $F_i\,, i = 1, \cdots, N$ and generate a single coherent fit x^*. The MACE framework [10] specifies x^* through the equilibrium conditions

$$F_i(x^* + u_i^*) = x^*, i = 1, \ldots, N$$

$$\sum_{i=1}^{N} u_i^* = 0.$$

To solve the above CT MAP estimation problem using the MACE framework, we define each agent $F_i\,, i = 1, \cdots, N$ as a proximal map associated with the sparse-view reconstruction problem f_i given by

$$F_i(v_i) = \arg\min_x \left\{ f_i(x) + \frac{1}{2\sigma_\lambda}\|x - v_i\|^2 \right\},$$

where $\sigma_\lambda > 0$ is a parameter that can be selected arbitrarily, but that effects convergence speed of our algorithm. In this case, it can be shown that the MACE solution x^* is exactly the MAP estimate.

To represent the MACE conditions more compactly, we define the parallel-agent operator F and consensus operator G as

$$F(v) = \begin{bmatrix} F_1(v_1) \\ \vdots \\ F_N(v_N) \end{bmatrix}, \text{where } v = \begin{bmatrix} v_1 \\ \vdots \\ v_N \end{bmatrix} \text{and}$$

$$G(v) = \begin{bmatrix} \bar{v} \\ \vdots \\ \bar{v} \end{bmatrix}, \text{where } \bar{v} = \frac{1}{N}\sum_{i=1}^{N} v_i\,.$$

Then, the MACE equilibrium conditions are compactly represented as

$$F(v^*) = G(v^*),$$

where v^* is then the equilibrium solution to the MACE equations. Once v^* is known, then the desired solution to our CT MAP estimation problem is given by the component-wise average of v^*,

$$x^* = \frac{1}{N}\sum_{i=1}^{N} v_i^*$$

It can be shown that the solution to the MACE equations is also the solution to the following fixed-point problem [10]:

$$(2F - I)(2G - I)w^* = w^*,$$

where w^* is defined through a change of coordinates given by $v^* = (2G - I)w^*$. Consequently, the fixed-point solution can be computed using the Mann iteration given by

$$w^{k+1} = (1 - \rho)w^k + \rho(2F - I)(2G - I)w^k$$

where again ρ is a user-selectable parameter between 0 and 1 that affects convergence speed of the algorithm. Importantly, note that the above approach parallelizes CT reconstruction across N view subsets, since the proximal operators $F_1,\ldots,F_N$ in F that compute the individual sparse-view reconstructions can be applied independently.

B.3.b.iii. MACE-PnP Framework

In this section, we generalize our approach to incorporate PnP priors implemented with advanced denoisers. Since we will be incorporating the prior as a denoiser, for this section we drop the prior terms in the equations of section B.3.b.i by setting $\beta = 0$. So let $f(x) = f(x;\beta)$ denote the CT log likelihood function with $\beta = 0$ and no prior term, and let $F(x)$ denote its corresponding proximal map.

Then Buzzard et al. in [10] show that the PnP framework of Sreehari et al. in [15] can be specified by the following equilibrium conditions:

$$F(x^* - \alpha^*; \sigma) = x^*$$

$$H(x^* + \alpha^*) = x^*$$

where H is the PnP denoiser used in place of a prior model. This framework supports a wide variety of denoisers including BM3D [19] and residual CNNs [20] that can be used to improve reconstruction quality as compared to conventional prior models [15, 18].

Let $f_i(x) = f_i(x;\beta)$ denote the CT log likelihood function with $\beta = 0$ and no prior term, and let $F(x)$ denote its corresponding proximal map. Then we can show that the below equilibrium conditions are exactly equivalent to that of the PnP framework [16].

$$F_i(x^* + u_i^*; \sigma) = x^*, i = 1, \ldots, N$$

$$H(x^* + \alpha^*) = x^*$$

$$\alpha^* + \textstyle\sum_{i=1}^{N} u_i^* = 0.$$

Once again, we formulate a fixed-point method to solve the above problem. One specific way is to use an approach similar to the one in section B.3.b.i, where all agents are applied in parallel. However, we take a slightly different approach in which the denoising is applied in series rather than in parallel. To do so, we define the parallel-operator F and consensus operator G_{H} as

$$F(v) = \begin{bmatrix} F_1\left(v_1\,;\,\sqrt{N}\sigma\right) \\ \vdots \\ F_N\left(v_N;\,\sqrt{N}\sigma\right) \end{bmatrix}, \text{where } v = \begin{bmatrix} v_1 \\ \vdots \\ v_N \end{bmatrix} \text{and}$$

$$G_H(v) = \begin{bmatrix} H\bar{v} \\ \vdots \\ H\bar{v} \end{bmatrix}, \text{where } \bar{v} = \frac{1}{N}\sum_{i=1}^{N} v_i\,.$$

Then we show that x^* in the above equilibrium conditions can be computed by finding the fixed-point of map T_H defined by $T_H = (2F - I)(2G_H - 1)$ [16]. More specifically, to compute x^* we first find w*, the fixed-point of T_H by using the Mann iteration

$$w^{k+1} = (1-\rho)w^k + \rho T_H w^k,$$

where $0<\rho<1$, and then applying the denoiser H to the component-wise average of w^*. Note that this method is parallelizable across N view subsets, since the parallel operator F typically dominates the computation in comparison with consensus operator G_H.

B.3.b.iv. Partial-Update Method for Speeding Up MACE and MACE-PnP

A direct application of the MACE and MACE-PnP algorithms is not practical, since the proximal operators F_{i} = 1,…,N that are evaluated in each Mann iteration require iterative optimization on their own. This results in nested loops of optimization that slow down the convergence speed.

To overcome this issue, we proposed a partial-update method that replaces the proximal operator with fast noniterative updates. In [16] we show that this method significantly speeds up the MACE and MACE-PnP algorithms without sacrificing convergence. We refer to this modified version of MACE with partial updates as partial-update MACE.

B.3.c. Experimental Results

We compare the image quality and convergence of our distributed MACE approach against a standard single-node reconstruction method. The single-node method is conventional ICD reconstruction from all views on a single node [9]. In the MACE approach, the views are distributed across multiple nodes, and we compute each partial update using one pass of ICD optimization.

To measure algorithmic convergence, we specify computation in units called equits. For the case of the conventional serial algorithm, we define one equit to be the computation associated with the update of all the pixels within the region of interest using the entire set of sinogram views. Since this definition accounts for the number of views being processed by the node, note that on a distributed implementation, one equit is equivalent to having each node perform one full ICD iteration using its subset of views.

Figure 11 (left) shows the distributed MACE reconstruction using N = 16 nodes for a single slice of the ceramic-composite dataset acquired by the Advanced Light Source (ALS) synchrotron at Lawrence Berkeley National Labs (LBNL). For this dataset, the CT measurements per slice consist of 2,560 sinogram views × 1,024 detector channels, and our reconstruction size is 512 × 512 voxels. From Figure 11 (middle) and

(right), we notice that MACE reconstruction with N = 16 nodes has quality equivalent to the single-node reconstruction, even though each node utilizes <7% of the sinogram views for its local reconstruction.

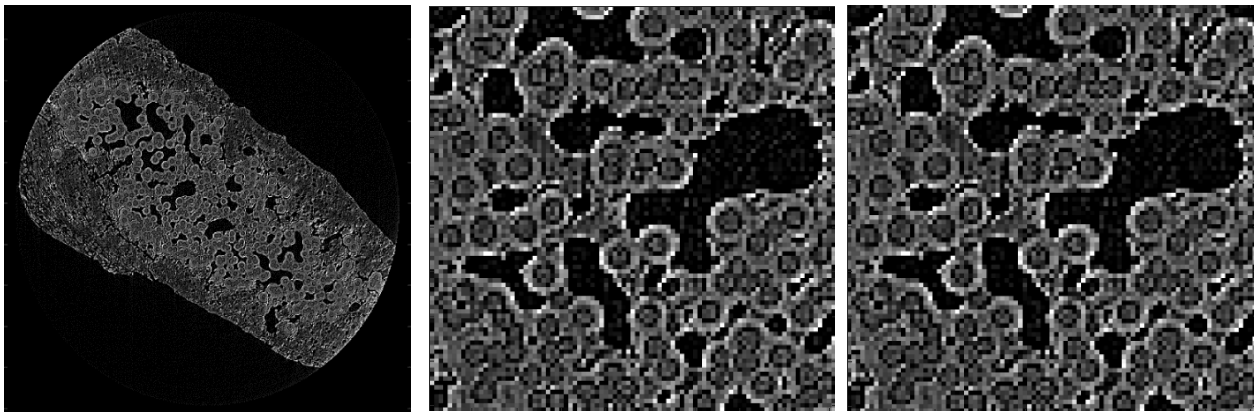

Figure 11: Image quality comparison using the LBNL ceramic composite dataset: (left) MACE reconstruction method with N = 16 nodes; (middle) close-up of the MACE reconstruction method with N = 16 nodes; (right) close-up of single-node reconstruction method. Notice that MACE produces image quality equivalent to the single-node method.

Figure 12(a) shows the distributed MACE-PnP reconstruction using N = 16 nodes and CNN as a prior model for a single slice of the ALERT Task Order 3 baggage scan. For this dataset, the CT measurements per slice consist of 720 sinogram views × 1,024 detector-channels, and our reconstruction size is 512 × 512 pixels. For this experiment, our CNN prior is based on the deep res-net architecture of [20] and was trained using natural images. From Figure 12 (right) we notice that in comparison with conventional Q-GGMRF prior [13, 14], the CNN prior improves quality by reducing streaking artifacts, which can potentially enable better segmentation.

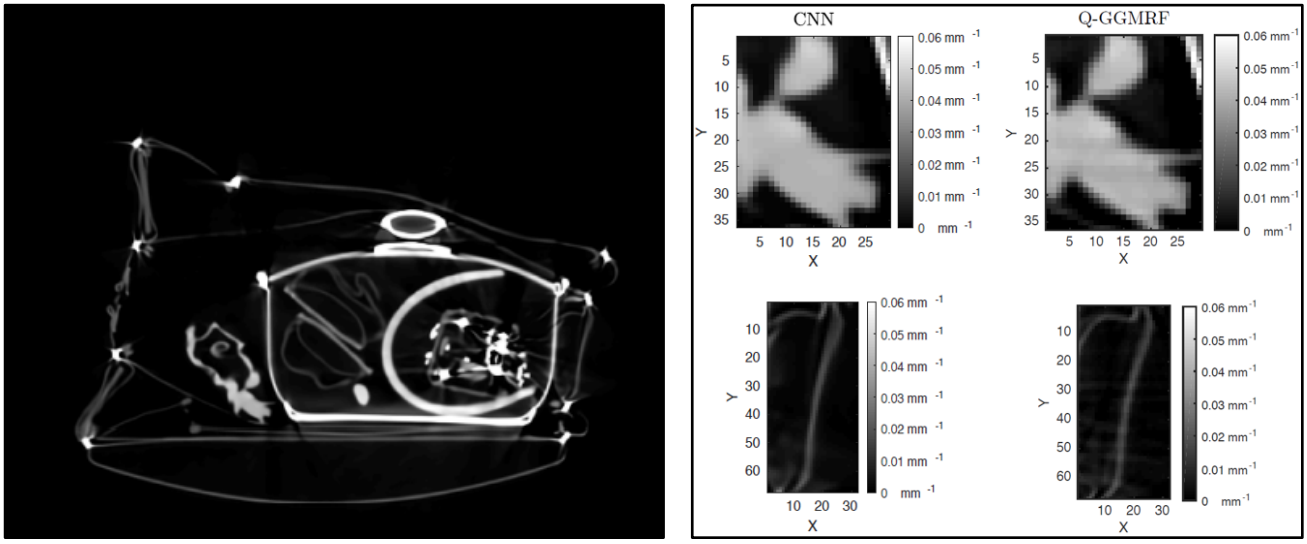

Figure 12: (left) MACE-PnP reconstruction with CNN prior and N = 16 nodes for the ALERT Task Order 3 baggage scan; (right) comparison of CNN prior versus Q-GGMRF prior. Notice that CNN prior reduces streaking artifacts in comparison to conventional edge-preserving regularization.

Figure 13 (left) shows that in the case of MACE with conventional Q-GGMRF prior, the number of equits required for convergence increases with the number of nodes, *N*, and consequently, the speedup is less than linear. However, from Figure 13 (right) we notice that in the case of MACE with CNN prior (MACE-PnP), the number of equits required for convergence does not change significantly from $N = 2$ to 8, and it is in fact less than that required by the serial approach when $N \leq 8$. Consequently, MACE with CNN prior provides a roughly linear speedup and has better parallel efficiency. Table 3 summarizes the relative speedup results for these experiments.

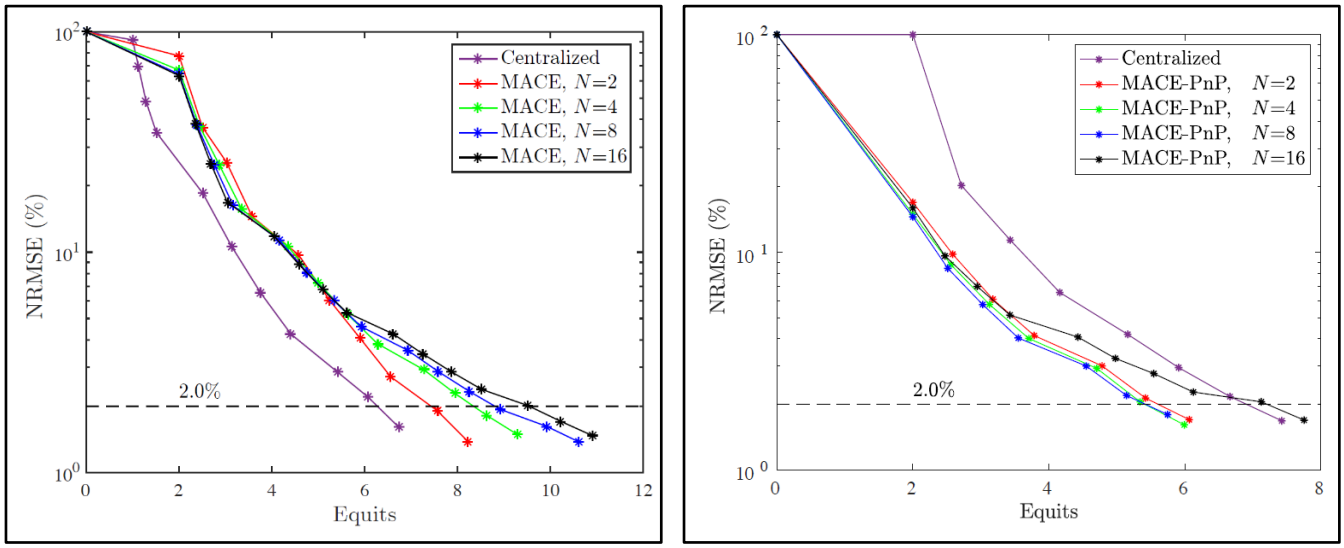

Figure 13: MACE algorithmic convergence using (left) Q-GGMRF prior and (right) res-net CNN prior (MACE-PnP) as a function of the number of nodes *N* for ALERT Task Order 3 baggage scan. In comparison with the Q-GGMRF prior, the CNN prior provides faster convergence and significantly better speedup over the serial reconstruction method.

Prior Model	*N* = 1	*N* = 2	*N* = 4	*N* = 8	*N* = 16
Q-GGMRF	1.00	1.80	3.27	6.00	10.29
BM3D	1.00	2.14	4.29	8.57	16.00

Table 3: MACE algorithmic speedup as a function of number of nodes *N*, for the LBNL ceramic composite dataset. Note that while MACE speedup is less than linear in the case of the Q-GGMRF prior, it is roughly linear in the case of the BM3D prior.

Table 4 illustrates the use of our distributed MACE approach for large-scale reconstruction on the massive National Energy Research Scientific Computing Center (NERSC) supercomputer in real time and analyzes its computational performance. For this experiment, we performed high-resolution reconstruction for a 3D ceramic-composite dataset acquired by the ALS synchrotron at LBNL. The CT measurements consist of 2,560 sinogram views × 1,024 detector channels × 1,200 detector rows, and our reconstruction size is 1280 × 1280 × 1,200 voxels. Each node in the cluster reconstructs 8 slices and utilizes the high-performance SV-ICD method [12] for efficient parallelization across multiple CPU cores. For this dataset, the conventional reconstruction method that does not distribute memory is not practical, since the overall CT system model is very large. From Table 4, we notice that our distributed MACE approach can achieve high-quality reconstructions in real time by reducing both the memory and computation (per iteration) on each node by a factor of *N*, where *N* denotes the number of view subsets. While the speedup of MACE increases with *N*, we notice that after $N = 4$, the parallel efficiency drops and the speedup based on real machine-time is less than the algorithmic speedup based on equits.

#View Subsets (*N*)	#Nodes	#Equits	#Time (seconds)	Algorithmic Speedup	Machine-Time Speedup
1	150	–	–	–	–
2	300	23.91	275	2.00	2.00
4	600	26.67	154	3.58	3.57
8	1200	34.03	121	5.62	4.55

Table 4: High-resolution reconstruction of a large 3D synchrotron dataset using the MACE approach on the NERSC supercomputer. MACE enables reconstruction of large datasets in real time by reducing both the computation and memory footprint per compute node by a factor of *N*, the number of view subsets. Note that while the speedup increases with *N*, the parallel efficiency drops after *N* = 4.

B.4. Major Contributions

Year 1 (2013–2014) outcomes:

- Developed MBIR algorithm for application in sparse view CT.
- Developed multislice helical scan geometry CT code for MBIR reconstruction.
- Developed an "implicit prior" method for image reconstruction. This method was the conceptual precursor to the PnP methods that were later developed and have come to be widely used in the computational imaging community.
- Published the first paper on PnP, which has 284 citations in Google Scholar as of August 25, 2020.
- Implemented 2D MBIR on reformatted Imatron data.

Year 2 (2014–2015) outcomes:

- Developed and implemented metal artifact reduction methods for MBIR reconstruction algorithm for application in sparse view CT.
- Implemented MBIR on Morpho and ALERT Task Order 3 data to demonstrate IQ improvements and improved Pd/Pfa (probability of detection/probability of false alarm) performance for baggage scanning data.
- Completed Secure Sensitive Information (SSI) report on improved performance of MBIR for baggage scanning applications.
- Developed novel segmentation-based beam hardening correction algorithm for MBIR. Resulted in P. Jin, C. A Bouman, and K. D Sauer, Trans. Computation Imaging, 2015, with 146 citations in Google Scholar as of August 25, 2020.

Year 3 (2015–2016) outcomes:

- Developed novel algorithm for joint segmentation and reconstruction using MBIR that won a best paper award from the *IEEE International Conference on Acoustics, Speech and Signal Processing*.
- Developed novel CT automatic target recognition (ATR) algorithm based on segmentation and classification method that was demonstrated in ALERT Task Order 4 competition.
- Invented SV MBIR reconstruction algorithm that has proven to be ~100–2,000 times faster than conventional MBIR and scalable to large-scale supercomputers. The SV-MBIR algorithm resulted in being a finalist for the Gorden Bell prize in 2017. It also was the basis for the formation of a small business,

High Performance Imaging, which currently has three ongoing projects with the Air Force and Air Force contractors as of July 1, 2020.

Year 4 (2016–2017) outcomes:

- Did initial research on MACE that is a follow-up to the PnP methods. This was used by others, including Professor Karl, for application in sparse-view CT reconstruction using DL.
- Implemented 3D SV algorithm on a large-scale supercomputer.

Year 5 (2017–2018) outcomes:

- Used the MACE algorithm to implement a highly parallel reconstruction algorithm for very large CT reconstruction on large-scale supercomputers.
- Demonstrated large-scale CT reconstruction on the NERSC supercomputer using MACE and SV-MBIR technologies.
- Created SBP architecture for direct reconstruction of sparse CT data using DNNs.

Year 6 (2018–2019) outcomes:

- Created SBP-LSTM algorithm for improved 2D image reconstruction quality.
- Developed partial-update PnP methods for large-scale parallel 3D image reconstruction.

Year 7 (2019–2020) outcomes:

- Extended the SBP-LSTM algorithm to 3D cone-beam geometry for fast and accurate CT image reconstruction.
- Published a TCI journal paper on large-scale parallel implementations of SV, MACE algorithms, with PnP priors.

B.5. Milestones

Our Year 7 activities focused on studying the potential of the methods described above to solve problems faced by TSA in baggage, checkpoint, and cargo scanning. In particular, we developed a novel algorithm for direct reconstruction from sinogram data using DNNs that is based on the SBP together with an LSTM architecture. These specific milestones were achieved:

- September 30, 2019—Performed preliminary study of methods and evaluated the potential of these methods for addressing TSA problems in cargo scanning. Identified mechanisms for obtaining simulated and real cargo-scanning data.
- December 31, 2019—Implemented ML-based reconstruction algorithms for real and simulated cargo-scanning data sets.
- March 31, 2019—Tested and optimized ML-based reconstruction algorithms using real and simulated cargo-scanning data sets. Assessed weaknesses and strengths. Formulated plan for optimizing performance in terms of computation speed and image quality.
- June 30, 2019—Evaluated image quality and computation speed of ML-based reconstruction algorithms using standard methods of image quality, such as normalized root mean squared error for simulated data, and artifact measures such as contrast ratio for real data sets.

In addition, we achieved the following milestone in parallel with high-speed MBIR reconstruction.

- June 30, 2019—Developed and implemented a novel algorithm based on the MACE framework for parallel reconstruction of large CT images using both traditional MBIR and PnP priors.

B.6 Final Results at Project Completion (Year 7)

Major project outcomes:

- Demonstrated the first practical methods for sparse view reconstruction. In [21] and [22], we had the first demonstrations that sparse view reconstruction was possible for practical transportation security problems such as cargo scanners. Practical sparse view reconstruction is of critical values since for many problems, including carry-on baggage and cargo, it may not be possible or practical to obtain a full set of views.
- Demonstrated the value of MBIR in reducing reconstruction artifacts that contribute to increased false alarm and missed detection rates [23].
- Introduced novel methods for metal artifact reduction in MBIR reconstruction [24,25]. These publications, done in collaboration with researchers at what was then Morpho Detection, demonstrate that MBIR can be used to reduce metal artifacts that cause false alarms and miss detections in baggage scanning.
- Developed the advanced prior methods for reconstruction that are generally known as plug-and-play (PnP) methods. These methods can dramatically improve reconstructed image quality by allowing the integration of physics models with AI and deep-learning–based prior models [18,15].
- Created a novel high-performance MBIR algorithm, known as super-voxel MBIR (SV-MBIR), that was demonstrated to speed reconstruction by well over a factor of 400 on CPU, GPU, and large-scale cluster computers [12,26,17,11,16]. The multicore CPU version of this algorithm is now available as open-source Python code and makes fast MBIR reconstruction practically accessible to a wide range of users.
- Created novel computationally efficient architecture known as stacked-back projection (SBP) for direct reconstruction of parallel and cone-beam data using deep neural networks [27, 28]. These emerging methods have the potential to achieve reconstruction quality that is near MBIR with a fraction of the computation time.
- Formed a startup company, High-Performance Imaging LLC (HPI), to translate state-of-the-art innovations in CT scanning technology to the problems of transportation security. It currently has a number of active research programs with the Air Force and is also working with US Department of Energy (DOE) researchers to translate the innovations of the ALERT research to important applications in manufacturing, material science, and sensing.

III. RELEVANCE AND TRANSITION

A. Relevance of Research to the DHS Enterprise

Metrics:

- Speed of computation—In the publications [12, 26, 17, 11, 16] we demonstrated reconstruction speedups of the svmbir algorithm relative to conventional parallel state-of-the-art implementations of MBIR of approximately 400 times. This relative speedup was achieved on multicore CPU implementations, multi-GPU implementations, and large-scale clusters such as the DOE's NERSC supercomputer.

- Image quality—Using MBIR with advanced priors and also using direct SBP reconstruction using deep neural networks we were able to demonstrate dramatic reconduction image artifacts for sparse view reconstruction, substantial image quality improvement using metal artifact reduction, and improved segmentation and object detection using integrated reconstruction/segmentation/classification methods.

B. Status of Transition at Project End

In collaboration with HPI, we publicly released an open-source version of the PSV-ICD algorithm suitable for use on a high-performance multicore compute node. The software, which is available on GitHub (https://github.com/HPImaging), is licensed under the BSD-3-Clause License. We are also building an open-source Python package, svmbir, on GitHub (https://github.com/cabouman/svmbir) that makes the SV MBIR code easy to use and integrate into user software. Enhanced versions of the software suitable for CPU and GPU clusters are available from HPI for commercial licensing.

In addition, we are planning on making open-source Python packages available for the SBP-LSTM reconstruction algorithm discussed. Our goal is to develop a version of the SBP-LSTM algorithm that can work for both parallel and cone beam geometry with arbitrary uniform view angle sampling and on-the-fly LSTM processing. With these innovations the package can be used on a wide variety of practical parallel and cone-beam tomography data sets without retraining.

C. Transition Pathway and Future Opportunities

The software and algorithms described in this report and developed over the past seven years are being used to engage with a wide variety of government and commercial organizations including:

- Eli Lilly Corporation: We are using the cone-beam and parallel 3D and 4D MBIR algorithms to image medical devices, such as injectors, in collaboration with Eli Lilly. This collaboration also involves Canadian Light Source and Kinetic Vision.
- Los Alamos National Laboratory (LANL): We are using the software and algorithms developed in this effort as the core of our collaborations with LANL in the areas of hyperspectral neutron imaging, imaging of hydrodynamic events, and ptychographic imaging.
- Argonne National Laboratory's Advanced Photon Source (APS): We are using the parallel-beam geometry SV MBIR code as the basis of our collaborations with APS on topics such as 4D reconstruction form sparse view sampling of dynamic events.

D. Customer Connections

1. Morpho Detection: 2011–2016
    - Collaborated with Samit K Basu, Todd Gable, Walter Garms, Matthew Merzbacher, and Sondre Skatter on:
        - Astrophysics project for cargo scanner
        - Study of iterative reconstruction for checked baggage scanner
        - X-ray diffraction scanner for checked baggage scanner
2. Astrophysics: 2011–2013
    - Simon Bedford and Francois Zayek
        - Astrophysics project for cargo scanner

3. AS&E: 2017-2018
    - Aaron Couture and Jonathan Everett
        - Advanced X-ray diffraction scanner reconstruction done jointly with Tufts University.

IV. PROJECT ACCOMPLISHMENTS AND DOCUMENTATION

A. Peer Reviewed Journal Articles

Pending –

1. Sridhar, V., Wang, X., Buzzard, G.T., & Bouman, C.A., "Distributed Iterative CT Reconstruction Using Multi-Agent Consensus Equilibrium." *IEEE Transactions on Computational Imaging*, accepted 2020.

B. Peer Reviewed Conference Proceedings

1. Wang, X., Sridhar, V., Ronaghi, Z., Thomas, R., Deslippe, J., Parkinson, D., Buzzard, G.T., Midkiff, S.P., Bouman, C.A., & Warfield, S.K. "Consensus Equilibrium Method for Super-Resolution and Extreme-Scale CT Iterative Reconstruction." *SC 19: The International Conference for High Performance Computing, Networking, Storage, and Analysis*, Denver, CO. 17–22 November 2019, pp. 86-1 to 86-13.

C. Other Presentations

1. Webinars
    a. "Plug and Play: A General Approach to AI and Sensor Model Fusion." Best Paper Prize, keynote lecture, *2020 SIAM Imaging Sciences Conference*. https://www.youtube.com/watch?v=GjCmxTqAJDo&feature=youtu.be.

D. Student Theses or Dissertations Produced from This Project

1. Sridhar, V., "Parallel Computational Methods for Model-Based Tomographic Reconstruction and Coherent Imaging." PhD, School of Electrical and Computer Engineering, Purdue University, May 2020.

E. Algorithms

See Section III.

V. REFERENCES

[1] S. Ravishankar, J. C. Ye, and J. A. Fessler, "Image Reconstruction: From Sparsity to Data-Adaptive Methods and Machine Learning,"arXiv:1904.02816 [cs, eess, stat], Apr. 2019, arXiv: 1904.02816.

[2] Q. Yang, P. Yan, Y. Zhang, H. Yu, Y. Shi, X. Mou, M. K. Kalra,Y. Zhang, L. Sun, and G. Wang, "Low-Dose CT Image Denoising Using a Generative Adversarial Network With Wasserstein Distance and Perceptual Loss," IEEE Transactions on Medical Imaging, vol. 37, no. 6,pp. 1348–1357, June 2018.

[3] C. You, L. Yang, Y. Zhang, and G. Wang, "Low-Dose CT via Deep CNN with Skip Connection and Network in Network," arXiv:1811.10564.

[4] C. You, Q. Yang, H. shan, L. Gjesteby, G. Li, S. Ju, Z. Zhang, Z. Zhao, Y. Zhang, W. Cong, and G. Wang,

"Structurally-Sensitive Multi-Scale Deep Neural Network for Low-Dose CT Denoising," IEEE Access, vol. 6, pp. 41 839–41 855, 2018. [Online]. Available: https://ieeexplore.ieee.org/document/8416740/.

[5] H. Chen, Y. Zhang, M. K. Kalra, F. Lin, Y. Chen, P. Liao, J. Zhou, and G. Wang, "Low-Dose CT with a Residual Encoder-Decoder Convolutional Neural Network (RED-CNN)," IEEE Transactions on Medical Imaging, vol. 36, no. 12, pp. 2524–2535, Dec. 2017, arXiv:1702.00288. [Online]. Available: http://arxiv.org/abs/1702.00288.

[6] H. Chen, Y. Zhang, W. Zhang, P. Liao, K. Li, J. Zhou, and G. Wang, "Low-dose CT denoising with convolutional neura network," arXiv:1610.00321 [physics], Oct. 2016, arXiv: 1610.00321. [Online]. Available: http://arxiv.org/abs/1610.00321.

[7] O. Ronneberger, P. Fischer, and T. Brox, "U-Net: Convolutional Net-works for Biomedical Image Segmentation," in Medical Image Computing and Computer-Assisted Intervention – MICCAI 2015, ser. Lecture Notes in Computer Science, N. Navab, J. Hornegger, W. M. Wells, and A. F. Frangi, Eds. Springer International Publishing, 2015, pp. 234–241.

[8] T. Le, G. Bui, and Y. Duan, "A Multi-View Recurrent Neural Network for 3D Mesh Segmentation," Computers & Graphics, vol. 66, pp. 103–112, Aug. 2017.

[9] C. A. Bouman and K. D. Sauer, "A Unified Approach to Statistical Tomography using Coordinate Descent Optimization," IEEE Trans. on Image Processing, vol. 5, no. 3, pp. 480-492, March 1996.

[10] G. T. Buzzard, S. H. Chan, S. Sreehari and C. A. Bouman, "Plug-and-Play Unplugged: Optimization Free Reconstruction Using Consensus Equilibrium," vol. 11, no. 3, SIAM Journal on Imaging Science, 2018.

[11] V. Sridhar, G.T. Buzzard and C. A. Bouman, "Distributed Framework for Fast Iterative CT Reconstruction from View-subsets", Proc. of IS&T Electronic Imaging Conference, 2018.

[12] X. Wang, A. Sabne, S. J. Kisner, A. Raghunathan, C. A. Bouman and S. P. Midkiff, "High Performance Model Based Image Reconstruction", 21st ACM SIGPLAN Symposium on Principles and Practice of Parallel Programming (PPoPP), pp. 2:1-2:12, 2016.

[13] Bouman C.A. and Sauer K., "A Generalized Gaussian Image Model for Edge-Preserving MAP Estimation," IEEE Transacions on Image Processing, vol. 2, no. 3, pp. 296-310, July 1993.

[14] J. B. Thibault, K. D. Sauer, C. A. Bouman and J. Hsieh, "A Three-Dimensional Statistical Approach to Improved Image Quality for Multi-Slice Helical CT," Med. Phys., vol. 34, no. 11, pp. 4526-4544, 2007.

[15] S. Sreehari, S.V. Venkatakrishnan, B. Wohlberg, L. Drummy, J. P. Simmons, and C. A. Bouman, "Plug and Play Priors for Bright Field Electron Tomography and Sparse Interpolation", IEEE Transactions on Computational Imaging, vol. 2, no. 4, Dec. 2016.

[16] Sridhar V., Wang X., Buzzard G.T., and Bouman C.A., "Distributed Iterative CT Reconstruction using Multi-Agent Consensus Equilibrium", accepted to IEEE Transactions on Computational Imaging, 2020. (arXiv preprint:1911.09278).

[17] Wang, X., Sridhar, V., Ronaghi, Z., Thomas, R., Deslippe, J., Parkinson, D., Buzzard, G.T., Midkiff, S.P., Bouman, C.A., & Warfield, S.K. "Consensus Equilibrium Method for Super-Resolution and Extreme-Scale CT Iterative Reconstruction.", SC 19 the International Conference for High Performance Computing, Networking, Storage, and Analysis, pp. 86-1 to 86-13, 2019.

[18] Venkatakrishnan, S.V., Bouman, Charles A. and Wohlberg, Brendt, "Plug-n-play priors for model based reconstruction", IEEE Global Conference on Signal and Information Processing, 2013.

[19] Buades A., Coll, B. and Morel J.M., "A non-local algorithm for image denoising", IEEE Computer Society Conference on Computer Vision and Pattern Recognition (CVPR), 2005.

[20] Zhang K., Zuo W., Chen Y., Meng D. and Zhang L., "Beyond a Gaussian Denoiser: Residual Learning of Deep CNN for Image Denoising", IEEE Transactions on Image Processing.

[21] S. J. Kisner, E. Haneda, C. A. Bouman, S. Skatter, M. Kourinny, and S. Bedford, "Limited View Angle CT Reconstruction," Proceedings of SPIE-IS\&T Electronic Imaging -Computational Imaging X,} vol. 8296, January 23-24, 2012.

[22] Sherman J. Kisner, Eri Haneda, Charles A. Bouman, Sondre Skatter, Mikhail Kourinny, Simon Bedford, "Model-Based CT Reconstruction from Sparse Views," the proceedings of the Second International Conference on Image Formation in X-Ray Computed Tomography, pp. 444-447, Salt Lake City, Utah, June 24-27, 2012.

[23] Sherman J. Kisner, Pengchnog Jin, Charles A. Bouman, Ken Sauer, Walter Garms, Todd Gable, Seungseok Oh, Matthew Merzbacher, and Sondre Skatter, "Innovative Data Weighting for Iterative Reconstruction in Helical CT Security Baggage Scanner," 47th IEEE International Carnahan Conference on Security Technology, Medellin-Colombia, October 8-11, 2013.

[24] Pengchong Jin, Charles A. Bouman, and Ken D. Sauer, "A Model-Based Image Reconstruction Algorithm with Simultaneous Beam Hardening Correction for X-Ray CT," {\em IEEE Transactions on Computational Imaging}, vol. 1, no. 3, pp. 200-216, January 2016.

[25] Pengchong Jin, Dong Hye Ye, and Charles A. Bouman "Joint Metal Artifact Reduction and Segmentation of CT Images Using Dictionary-Based Image Prior and Continuous-Relaxed Potts Model," in the proceedings of the {\em IEEE International Conference on Image Processing}, September 2015.

[26] Amit Sabne, Xiao Wang, Sherman Kisner, Charles Bouman, Anand Raghunathan, and Samuel Midkiff, "Model-based Iterative CT Image Reconstruction on GPUs," 21st ACM SIGPLAN Symposium on Principles and Practice of Parallel Programming (PPoPP '17), February 4-8, 2017.

[27] Dong Hye Ye, Gregery T. Buzzard, Max Ruby, and Charles A. Bouman, "Deep Back Projection for Sparse-View CT Reconstruction," IEEE Global Conference on Signal and Information Processing (GlobalSIP), pp. 1-5, Nov. 20, 2018.

[28] Wenrui Li, Gregery T. Buzzard, and Charles A. Bouman, "Direct Sparse-View CT Reconstruction using LSTM Processing of Stacked Back Projections," International Conference on Computational Photography (ICCP), Aprill 24-26, 2020.

R4-B.2: Multi-Energy, Limited-View Computed Tomography

I. PARTICIPANTS INVOLVED FROM JULY 1, 2019 TO JUNE 30, 2020

Faculty/Staff			
Name	**Title**	**Institution**	**Email**
Eric Miller	PI	Tufts University	eric.miller@tufts.edu
James Webber	Postdoctoral Researcher	Tufts University	James.webber@tufts.edu
Kenny Yau	Research Engineer	Tufts University	Kenny.Yau@tufts.edu

II. PROJECT DESCRIPTION

A. Project Overview

A.1. X-Ray Modeling and Processing

The development of new scanning technologies by Rapiscan Systems has led to the analysis of novel integral transforms and inversion methods in Bragg Scattering Tomography (BST) and Compton Scattering Tomography (CST). The advances made by the teams at Tufts and Rapiscan Systems this year lay the groundwork for better material characterizations and for modification of the currently employed threat detection algorithms, with the ultimate goal to improve the false alarm rates.

Our specific focus was on a Real Time Tomography (RTT) X-ray portal scanner, with the ability to measure simultaneously Bragg scatter, Compton scatter, and transmission (X-ray CT) data. Our aim was to successfully fuse the multiple data streams to enhance the image quality and threat classification accuracy. The square tunnel geometry, collimation technology, and energy sensitive capabilities of the scanner were shown to be crucial to the mathematical analysis and inversion. In particular, we derived explicit inversion formulae for the BST and CST transforms in the RTT geometry. The inversion techniques presented give a fast, analytic means to process the Bragg and Compton signal in order to recover the material properties (e.g., the crystalline structure and electron density of the items present in the image). Knowledge of such material characteristics helps us to better distinguish threat and nonthreat materials, and hence we anticipate that our methods will offer a reduction in the false alarm rates moving forward.

We considered the joint reconstruction of the electron density and attenuation coefficient using Compton and transmission data, with the aim to enhance the edge recovery of both images simultaneously, and to more precisely localize the image space for suspected threats. Our results showed great promise on simulated phantoms.

Following our work in Year 6, we completed the development of a Monte Carlo (MC) MATLAB package for the simulation of the Bragg, Compton, and Rayleigh processes. In Year 7, we set out to verify our BST and CST inversion methods using MC data. The MC code was also applied to simulate data acquisition scenarios of interest to Rapiscan (e.g., to simulate energy histograms and photon counts).

A.2. Optical Image Processing

Trace chemical identification on a surface has important applications, for example in security and forensics in identifying illicit drugs and explosives [1, 2]. The traditional process of bringing a sample to a lab for identification is costly in terms of time and money, not only adding a financial burden but also delaying decisions that require the desired information. While not as powerful as their laboratory counterparts, portable spectrometers capable of trace detection such as those discussed in [3-5] have exhibited adequate performance to enable them to fill a gap in on-site spectroscopy technology. To the best of our knowledge, existing products and technologies still require constant user interaction to scan a surface region for potential threat particles and initiate analyses of said particles.

Tufts University collaborated with Pendar Technologies. The company has expertise in the portable Raman spectrometer domain to address this autonomous technology gap. The project was called the Portable Chemical Fingerprint Identification System (PCFIS).

The goal of the PCFIS project was to create a device that adds autonomous functionality to existing portable microscopy capabilities. Specifically, we wanted to *automatically* scan a $1'' \times 1''$ region of a surface, in general not flat, for potential threat particles; *automatically* analyze the composition of a subset of the potential threats, the number of which is user-specified; and *automatically* provide an image that sharply resolves the entirety of the $1'' \times 1''$ region, called a "flattened image."

The Tufts team focused on the optical image processing necessary for automatically finding potential threat particles and for facilitating Raman spectroscopy. These included a topography estimation algorithm of the $1'' \times 1''$ region using a focal stack of a particular scene; a fast method of producing a large depth-of-field image from the focal stack; a particle detection algorithm that is robust against slowly varying background illumination; and an aim assist algorithm for the device to properly focus the Raman laser beam onto the particle being analyzed. The prototype was able to automatically scan a $1'' \times 1''$ region for particles and analyze the composition of 10–20 particles in 3–5 minutes.

B. State of the Art and Technical Approach

B.1. X-Ray Modeling and Processing

The RTT portal scanner geometry, under principle consideration by the Tufts team this year, is displayed in Figure 1. The scanner sources (with coordinate $\mathbf{s}$) are fixed and switched along the linear array $\{x_2 = -1, x_3 = 0\}$. The sources are assumed to be polychromatic and approximately 2-D fan-beam (in the (x_1, x_2) plane), with opening angle β. The forward scatter (Bragg) detectors (with coordinate $\mathbf{d}_B$) are assumed to be energy-resolved and lie on the $\{x_2 = 1\}$ plane, with small (relative to the scanning tunnel size) offset ϵ in the x_3 direction. The detectors are collimated to record photons that scatter on planes in $\mathbb{R}^3$ (see Figure 1b), where the planes of collimation are orientated to intersect the source (x_1, x_2) plane along horizontal lines (parallel to x_1). Hence the Bragg photon arrivals measured by the portal scanner detectors are scattered from horizontal lines embedded in the (x_1, x_2) plane. An example line of intersection is illustrated by L in Figure 1. The backscatter (Compton) detectors (with coordinate $\mathbf{d}_C$) are located on $\{x_2 = -0.8\}$. They are energy-resolved and uncollimated, allowing for photon arrivals in all directions. The forward (transmission) detectors (with coordinate $\mathbf{d}_A$) lie on the line $\{x_2 = 1, x_3 = 0\}$, and measure the intensity of unattenuated photons.

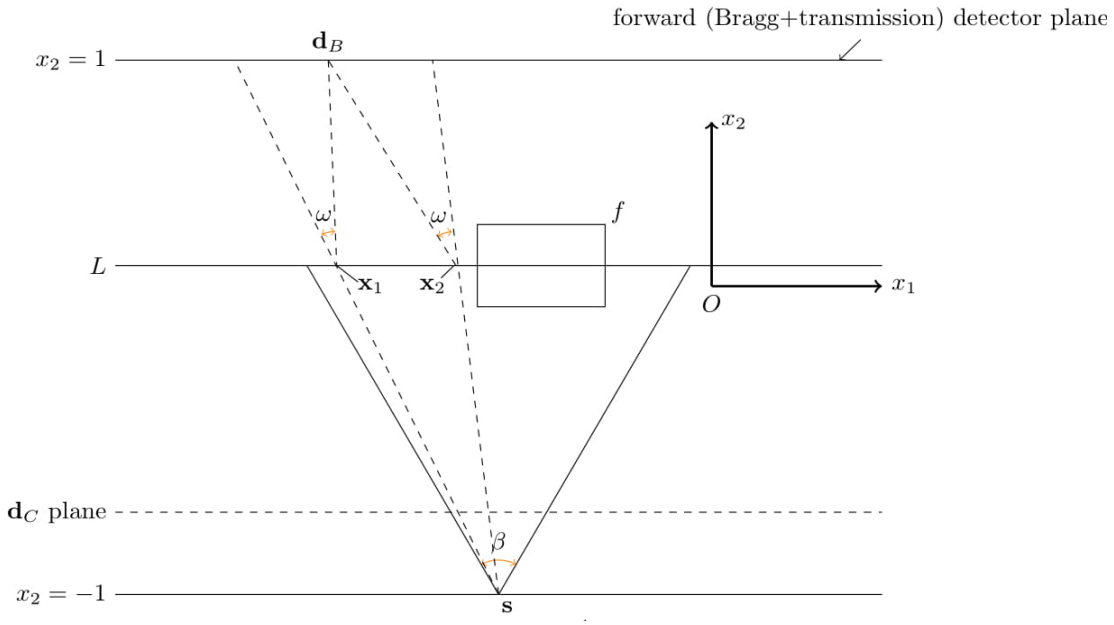

Figure 1a: (x_1, x_2) (source fan-beam) plane cross-section. The source(s) opening angle is β and we have shown two scattering locations at $x_1, x_2 \in L$ with scattering angle ω.

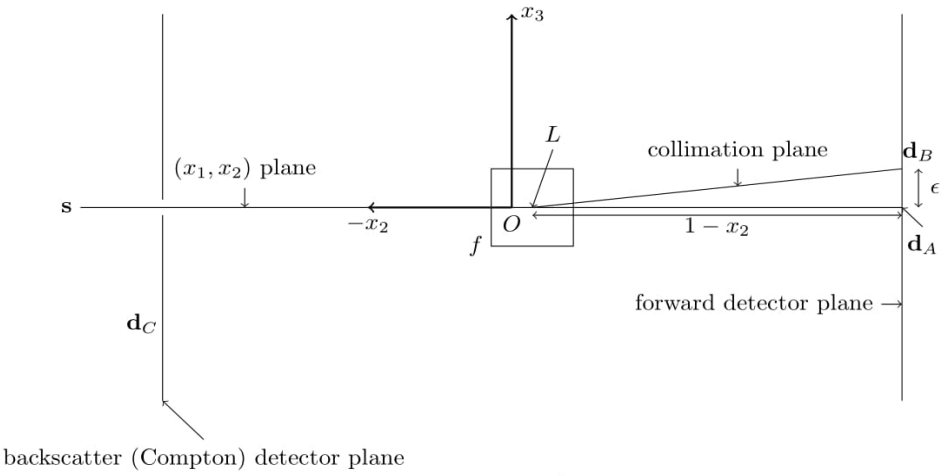

Figure 1b: (x_2, x_3) plane cross-section. Note that L is now orthogonal to the page (parallel to x_1).

Figure 1: The RTT portal scanner geometry. The scanned object is labelled by f. The detectors are collimated to planes, and the scattering events occur along lines $L = \{x_2 = a, x_3 = 0\}$, for some $-1 < a < 1$. The Bragg scatter from L is measured by detectors $\mathbf{d}_B \in \{x_2 = 1, x_3 = \epsilon\}$, for some $\epsilon > 0$. The Compton backscatter is measured by $\mathbf{d}_C \in \{x_2 = -0.8\}$, and the transmission data is measured by $d_A \in \{x_2 = 1, x_3 = 0\}$.

Let $\boldsymbol{x} = (x_1, x_2)$. Then the data streams collected by the RTT are modelled as follows:

1. Transmission—the intensity of unattenuated photons $I_A(E, \mathbf{s}, \mathbf{d}_A)$ is described by the Beer-Lambert law [6]

$$\log \frac{I_0(E)}{I_A(E, \mathbf{s}, \mathbf{d}_A)} = R\mu_E(E, \mathbf{s}, \mathbf{d}_A) = \int_{l_{\mathbf{s},\mathbf{d}_A}} \mu_E(\boldsymbol{x})\, \mathbf{d}\boldsymbol{x},$$

   where $\mathrm{I}_0(\mathrm{E})$ is the initial source intensity and μ_E is the attenuation coefficient at energy E. The integrals are taken over lines $\mathrm{l}_{\mathrm{s,d_A}}$ connecting $\mathrm{s} \in \{\mathrm{x}_2 = -1, \mathrm{x}_3 = 0\}$ and $\mathrm{d_A} \in \{\mathrm{x}_2 = 1, \mathrm{x}_3 = 0\}$, and the transmission data determines the line Radon transform $\mathrm{R}\mu_\mathrm{E}$ of μ_E [7].

2. Bragg forward scatter—the Bragg intensity $I_B(E, \mathbf{s}, \mathbf{d}_B)$ scattered from powder samples is modelled as integrals of the differential cross section function $F(q, \mathbf{x})$ over C^2 curves [8]

$$I_B(E, \mathbf{s}, \mathbf{d}_\mathrm{B}) = \mathcal{B}F(E, \mathbf{s}, \mathbf{d}_\mathrm{B}) = \int_L F\left(E \sin\frac{\omega(\boldsymbol{x}, \mathbf{s}, \mathbf{d}_\mathrm{B})}{2}, \mathbf{x}\right) \mathbf{dx},$$

   where L is a line parallel to x_1 (as in Figure 1a), $q = E \sin\frac{\omega(\mathbf{x},\mathbf{s},\mathbf{d}_\mathrm{B})}{2} \in \mathbb{R}^+$ is the momentum transfer and $\omega(\mathbf{x}, \mathbf{s}, \mathbf{d}_\mathrm{B}) \in [0, \pi]$ is the scattering angle of the interaction, as pictured in Figure 1a. The Bragg transform $\mathcal{B}$ describes the integrals of a function over the 3-D set of 1-D curves in the plane,

$$\mathcal{Q} = \left\{(q, x_1) \in \mathbb{R}^2 : q = E \sin\frac{\omega(\mathbf{x}, \mathbf{s}, \mathbf{d}_\mathrm{B})}{2}\right\}$$

   for each fixed $x_2 \in (-1,1)$, where $E \in \mathbb{R}^+$, $\mathbf{s} \in \{x_2 = -1, x_3 = 0\}$ and $\mathbf{d}_B \in \{x_2 = 1, x_3 = \epsilon\}$, for some $\epsilon > 0$.

3. Compton backscatter – the intensity of Compton backscattered photons $I_C(E, \mathbf{s}, \mathbf{d}_\mathrm{C})$ is modelled as integrals of the electron density n_e over toric sections [9]

$$I_C(E, \mathbf{s}, \mathbf{d}_\mathrm{C}) = \boldsymbol{\mathcal{T}} n_e(E, \mathbf{s}, \mathbf{d}_\mathrm{C}) = \int_{\boldsymbol{T}(E,\mathbf{s},\mathbf{d}_C)} n_e(\mathbf{x})\, \mathbf{d}x.$$

   A toric section is the union of two intersecting circles with the same radius. Here $\boldsymbol{T}(E, \mathbf{s}, \mathbf{d}_\mathrm{C})$ is the toric section with points of self-intersection at $\mathbf{s}$ and $\mathbf{d}_C$, with radius determined by E, and the Compton data is described by the toric section transform $\boldsymbol{\mathcal{T}} n_e$ of n_e. Geometrically, the CST problem is 2-D and the Compton interactions occur in the (x_1, x_2) plane (in Figure 1a). Note that the dimensions used here are not exactly the same as in [9], but the geometry is analogous.

The modelling of transmission data is well established in the literature [7], and the inversion properties of the Radon transform R are well understood [10]. The novel advances made by the team at Tufts this year are towards the physical modelling of the BST and CST problem, and the inversion and stability properties of the transforms $\boldsymbol{\mathcal{T}}$ and $\mathcal{B}$. We also consider the simultaneous reconstruction of n_e and μ_E from the joint data, $\boldsymbol{\mathcal{T}} n_e$ and $R\mu_E$, to improve the image edge resolution.

Using the theory of [11, 12], in [8] we propose new physical models for the RTT geometry that estimate the Bragg scattered signal from line samples of randomly orientated crystallites (powder scattering). When the effects due to attenuation are ignored, the physical models lead us to a new, linear Radon transform, namely $\mathcal{B}$ (as in 2 above). The removal of attenuation from the modelling is a common assumption made in the scattering tomography literature, for example in Compton Scattering Tomography (CST) [13-15]. While neglecting attenuation introduces a systematic error in the modelling, the linearization of the model allows us to apply the theory of linear integral equations and Radon transforms to obtain an explicit solution. Further the linear analysis will likely shed light on the inversion and stability properties in the nonlinear case (with attenuation included) and provides the theoretical groundwork required to move forward with such problems.

The Bragg transform maps F (the reconstruction target) associated with the crystalline material to its integrals over the set of curves Q, as in 2 above. By exploiting the translational invariance of $\mathcal{B}$, and using the established theory of linear Volterra integral equations [16] and analytic continuation ideas, we prove the injectivity and explicit invertibility of $\mathcal{B}$ in Theorem 4.1 of [8]. We also show that $\mathcal{B}$ is a bounded operator in Corollary 4.4 of [8], in a least squares sense. In more detail, Corollary 4.4 gives bounds for the data magnitude in L^2 (i.e., $\|\mathcal{B}F\|_{L^2}$) in terms of the target magnitude $\|F\|_{L^2}$.

This work lays the foundation for new imaging techniques in Bragg spectroscopy, a decades old idea, dating back to the experiments of Debye-Scherrer [17] and the works of [18], which image the crystal structure of point samples using monochromatic, pencil-beam sources. Our analysis considers the BST problem with polychromatic, fan-beam sources, where the (3-D) crystal sample is observed along lines L. The energy-resolving capabilities of the RTT detectors (a technology not available to [17, 18]) allow us also to distinguish the energies of the spectrum, which adds new dimensionality to the data, and plays a crucial role in the derivation of our main theorems (e.g., in Theorem 4.1 of [8]).

We give an extension of the results of Theorem 4.1 of [8] to three dimensions (and further to n dimensions) in Theorem 5.1 of [8]. In 3-D the Bragg transform models the Bragg signal in the scanning geometry displayed in Figure 2. Here the scattering is restricted to planes of crystallites in $\mathbb{R}^3$. This is analogous to the 2-D case in Figure 1, where the scatter is constrained to lines $L \subseteq \mathbb{R}^2$. We anticipate that the scanning modality of Figure 2 will have practical application in the materials characterization of thin films as on page 150 of [19].

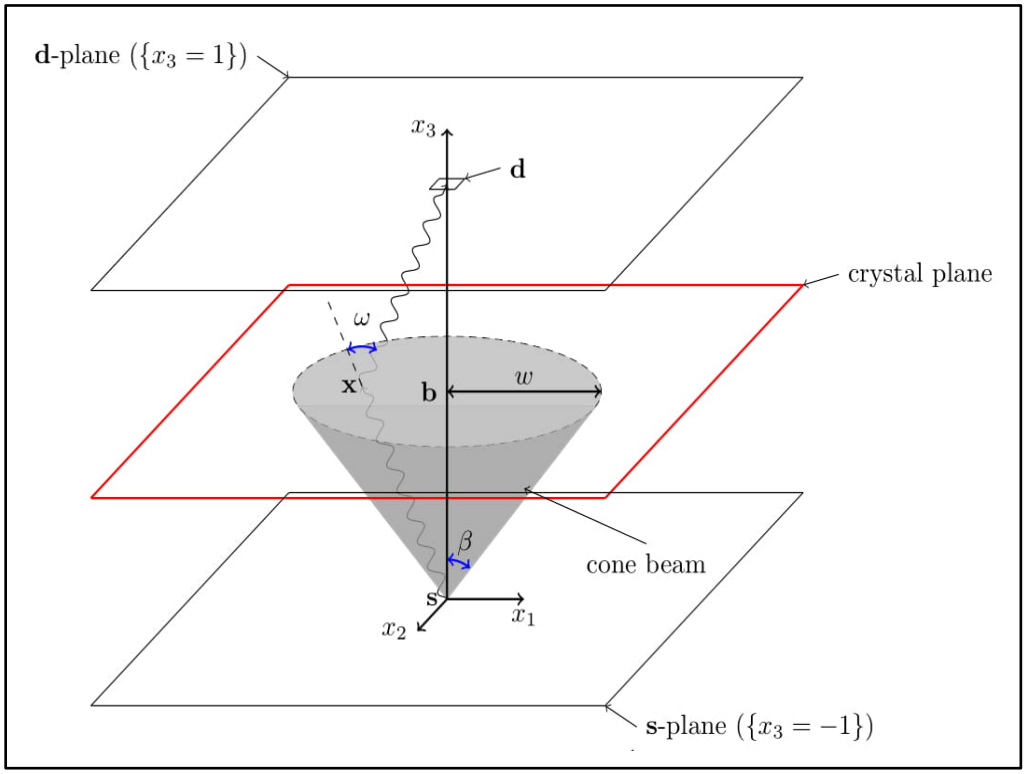

Figure 2: Bragg scanning modality in 3-D. A square detector d is shown opposite a source s, and collects photons (shown as wavy lines) scattered from points x on the crystal plane. The crystal sample (the red plane) is placed between, and is parallel to, the s-plane and d-plane. The center of the base of the cone is b, the source opening angle is β (as in Figure 1), and the source width is $w = |\mathbf{b} - \mathbf{s}|\, tan\, \beta$.

Additionally, in Section 6.2, we use the conditions of our theorems to assist in machine design of the RTT. Roughly speaking, the design condition we derive specifies that the detector offset ϵ not be too large relative to the source fan width $w = (1 - x_2)\tan\beta$ (see Figure 1). Specifically, we provide example detector configurations for varying β, so that the resulting condition is satisfied, thus allowing us to apply the proposed inversion formulae.

In [9] we present new physical models for the CST problem in the RTT geometry, following the theory of [13-15, 20, 21]. We show how the Compton intensity can be approximated by toric section integrals $\mathcal{T}n_e$ of n_e, as in 3 above. As in the Bragg case, the effects due to attenuation are ignored in the CST modelling, which linearizes the forward problem. This allows us to apply linear Radon transforms theory to obtain a closed-form solution for n_e in terms of $\mathcal{T}n_e$. Specifically, by exploiting the translational invariance of the RTT geometry, and using Paley-Wiener-Schwartz theorem ideas, we prove the invertibility of $\mathcal{T}$ in Theorem 3.3 of [9]. This is important, since it shows that the recovery of n_e is unique upon inversion of $\mathcal{T}$, and hence there are no artifacts in the reconstruction due to null space.

In [21], we present new joint reconstruction and regularization techniques inspired by ideas in microlocal analysis and lambda tomography, for the simultaneous reconstruction of μ_E and n_e from $R\mu_E$ and $\mathcal{T}n_e$ data. Using microlocal analysis, we show how the $R\mu_E$ and $\mathcal{T}n_e$ data sets are complimentary in terms of the image edge recovery. Following our theory, we devise a new linear least squares reconstruction scheme using lambda penalties, which we call the "JLAM" method. The lambda penalties work by enforcing a similarity in the locations and directions of the image edges of μ_E and n_e, and hence stabilize the edge recovery in the least squares solution. For example, let us consider the reconstruction of the n_e and μ_E phantoms shown in Figure 3. The phantoms consists of a water ellipsoid, a sulfur ellipsoid, a calcium sulfate ($CaSO_4$) right-angled triangle and a thin film of titanium dioxide (TiO_2) in the shape of a cross. The density ratio of the materials that compose the n_e phantom is approximately $1:2:3:4$ (H_2O : S : $CaSO_4$: TiO_2), and the density values used are taken from the NIST database [22], with the background density (≈ 0) set to the density of dry air (near sea level). The μ_E phantom was simulated similarly, for $E = 100$ keV. The materials considered are widely used in practice. For example $CaSO_4$ is used in the production of plaster of Paris and stucco (a common construction material) [23], and TiO_2 is used in the making of decorative thin films (e.g., topaz) and in pigmentation [24].

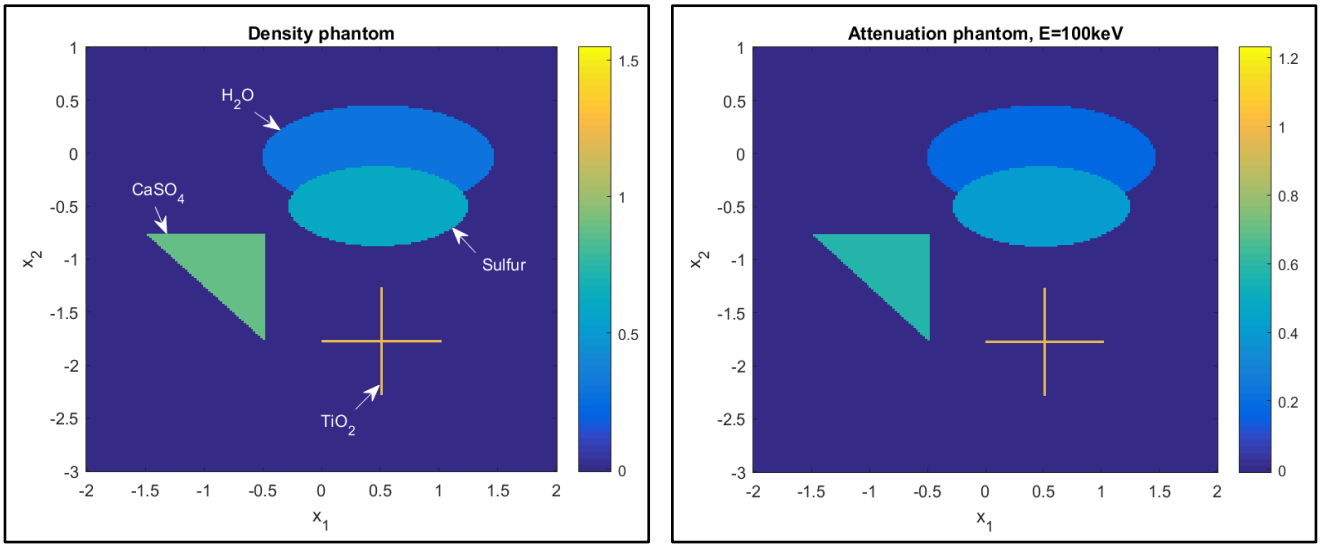

Figure 3: Density (left) and attenuation coefficient (right) phantoms. The associated materials are labelled in each case.

In Figures 4, 5 and 6, we present reconstructions of the n_e and μ_E phantoms from simulated noisy data (using additive Gaussian noise) using separate data with total variation (TV) (a well-studied state-of-the-art edge-preserving regularizer) [25], JLAM and the methods of [25] from the literature, specifically the linear poarallel level sets (LPLS) method. In Figure 4 we see severe artifacts in the reconstruction due to limited data, and the TV regularizers fail to combat the artifacts effectively. In Figure 5, we see an almost complete removal of the artifacts, and the lambda regularizers successfully preserve the edge map of the density. We see a further improvement using LPLS. See Figure 6. While the edge recovery using LPLS and JLAM is comparable, the smoothing properties of LPLS are most optimal, yielding a higher signal-to-noise ratio. In both cases (Figures 5 and 6), the joint reconstruction methods performed well, and significantly improved upon the image quality of Figure 4, using TV with separate data. Given the linearity of JLAM, the ideas of LPLS can be easily integrated with lambda regularization to modify the objectives of the literature and improve further the edge resolution of the reconstruction. To preserve the linearity of JLAM, we could also combine JLAM with a Tikhonov type regularizer. This may help smooth out the distortion observed in the JLAM reconstruction. We intend to pursue such ideas in future work.

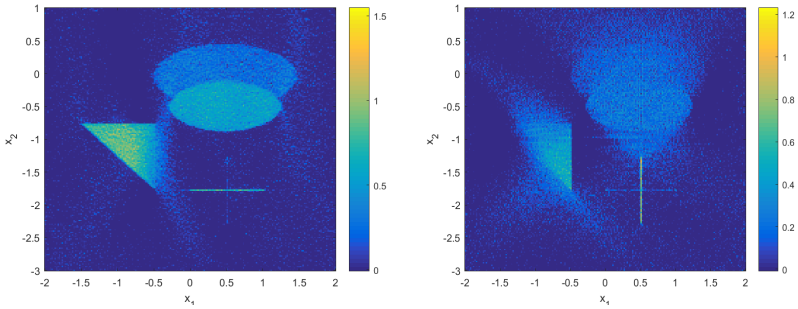

Figure 4: Density (left) and attenuation (right) phantom reconstructions using separate data and TV, with 10% Gaussian noise.

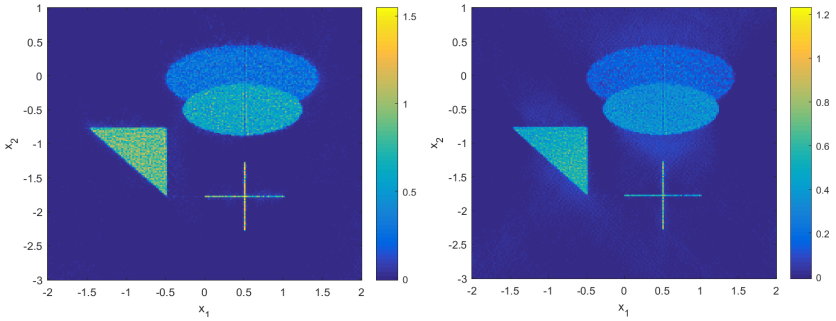

Figure 5: Density (left) and attenuation (right) phantom reconstructions using JLAM, with 10% Gaussian noise.

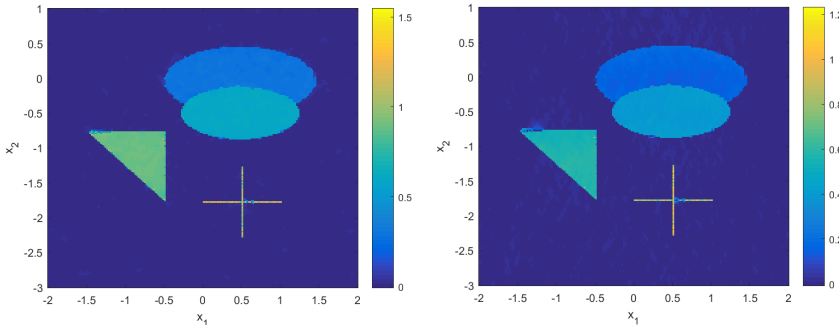

Figure 6: Density (left) and attenuation (right) phantom reconstructions using LPLS, with 10% Gaussian noise.

In addition to our peer reviewed efforts this year, following on from our work in Year 6, we completed the development of a Monte Carlo (MC) MATLAB code to simulate the Bragg, Compton and Rayleigh processes. So far we have applied our MC code to simulate data acquisition scenarios of interest to Rapiscan, and we are beginning to test the theory and inversion formulae of [8, 9, 21] using MC data. For example, let us consider the rectangular object f pictured in Figure 1. Using our MC code, we can simulate energy histograms of the Bragg scattered signal from f, measured by the detector array at $\{x_2 = 1, x_3 = \epsilon\}$, for $\epsilon \approx 0.1$ (see Figure 1). The photon counts are simulated using an X-ray tube [26], with voltage $V = 150$ keV and 10^8 photons per

projection across all energies. The source is Tungsten target, which has characteristic Bremsstrahlung peaks (jumps in intensity) at 60 keV, 66 keV and 68 keV, the largest of which occurs at 60 keV. The energy bins are 3 keV width, and the detector bins are 25 mm wide. So the data is smoothed with respect to the detector coordinate. The effects due to attenuation and self-absorption were also included in the MC simulation. See Figure 7 for energy histograms corresponding to the materials $f = \text{NaCl}$ and $f = \text{Al}$. For each material, we see the intensity peaking around the largest Bremsstrahlung peak (at 60 keV), but overall the count rate is low and the data appears noisy. To reduce the noise, we could increase the count rate per projection. However this would require a longer scanning time, which is undesirable, as we wish to scan in real-time. Hence, based on these experiments, we can anticipate a high noise level in the Bragg data. With this in mind, in future work, we aim to develop practical reconstruction algorithms in BST (based on the inversion formulae of [8]) with sufficient regularization to combat the noise.

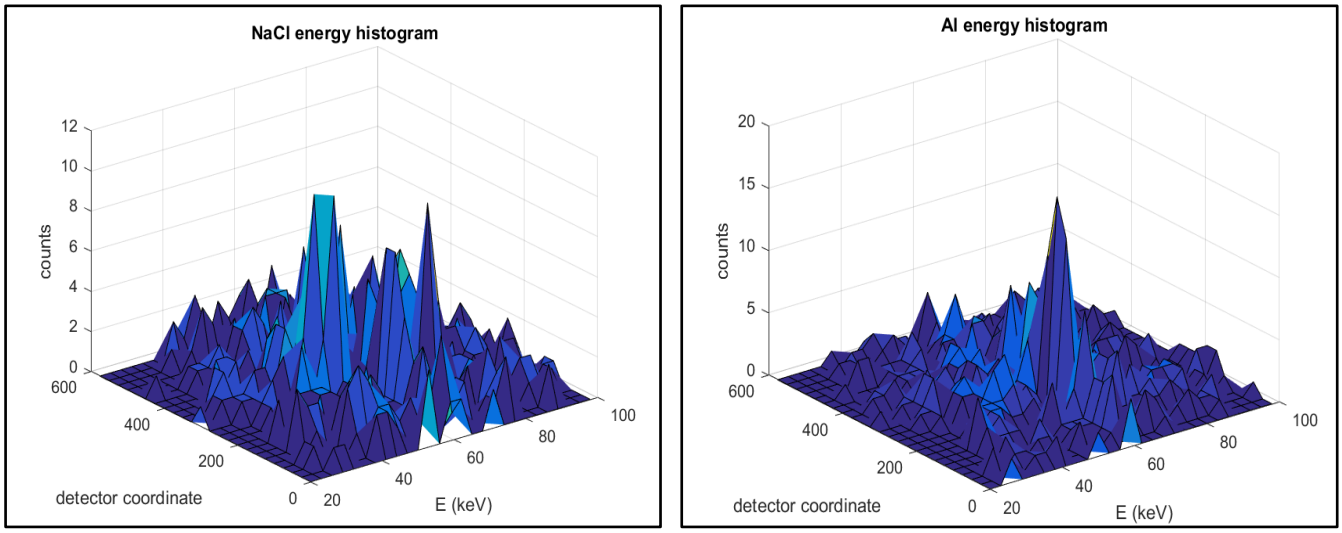

Figure 7: NaCl (left) and Al (right) energy histograms of the Bragg signal.

B.2. Optical Image Processing

The camera and optics used in the prototype required nine focal stacks arranged in a 3×3 grid to cover a $1'' \times 1''$ area. The camera and optics were mounted on a motorized XYZ stage capable of micrometer movement. Control of the prototype is done via a connected laptop PC through a LabVIEW interface.

As shown in Figure 8, the PCFIS prototype is a reflected-light dark-field microscope, where the light collected by the objective has been reflected from the specimen and not transmitted through it [27], and where the specimen is illuminated at an oblique angle such that direct, nondiffracted rays are not collective by the objective [28]. An assumption we make is that the surface diffracts less light that the particles, and so particles will appear bright in a dark field. This was the case in the four types of

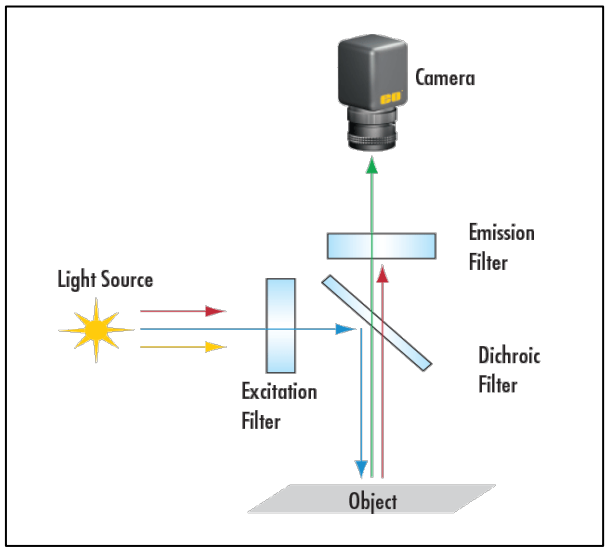

Figure 8: Schematic of dark-field microscopy.

surfaces we tested with (aluminum-coated glass, CD-ROM, curved aluminum, curved glossy black car panel).

Figure 9 shows the state diagram for the autonomous operation of the PCFIS, which uses the algorithms written by Tufts. The upper half of the diagram comprise the data collection, topography estimation, and location of potential threat particles. The lower half, circled in red, is the loop where the system analyzes a subset of the potential threat particles. In the rest of this section, we describe the data collected and the algorithms circled in blue.

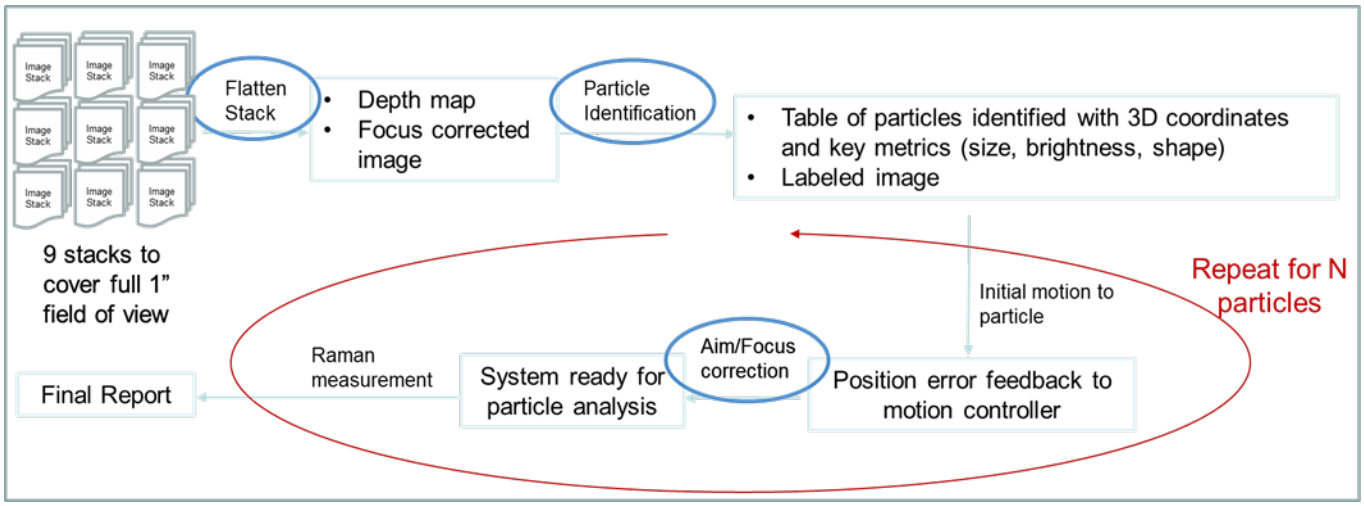

Figure 9: State diagram for the autonomous feature of the PCFIS prototype. Operations circled in blue are the optical image processing components on which members of Tufts worked.

B.3. Data Collection

As illustrated in Figure 10, a focal stack is a sequence of images of the same scene but varying the focal plane. For a typical scene in which various objects are located at different distances from the camera, different objects will appear sharp or blurry in different layers of the focal stack. In our use case, we obtain focal stacks of the surface being interrogated, with the goal of having a sharp version of every part of the surface in at least one layer of the focal stack. Importantly, every layer in a focal stack is associated with a certain depth, as we poll the z-motion motor every time a layer is captured. We obtain nine such stacks, one for every region needed to cover the 1″ × 1″ scan area.

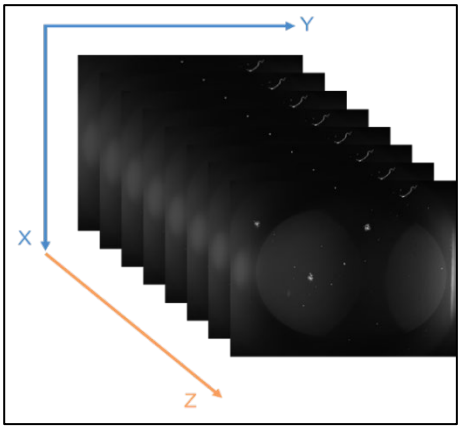

Figure 10: Example of an image stack.

B.4. Focus Stacking

We employed a technique called "focus stacking," commonly used in microscopy and macro photography to synthetically increase the depth-of-field of a camera, in order to obtain a flattened image of an arbitrary curved surface. As a byproduct of creating the flattening image, we can associate every pixel in the image (and thus every point in space) with a certain depth based on which layer in the focal stack was used to create those pixels. This is how we obtained a topography map. Whereas focus stacking algorithms have been studied before [29], to the best of our knowledge, the flattened image has always been the primary goal, and the depth information discarded. For this project, we use both.

Focus metrics evaluate how sharp an image is or how sharp different parts of an image are. Common ones used in the microscopy world can be found in this report [30]. As that paper shows, literature on the comparison between different focus metrics tend to be application-specific. For our application, we looked at a number of focus metrics listed in that paper, with our selection motivated by the need to balance algorithm time complexity and accuracy. Additionally, we explored the FISH metric found in this paper, which was interesting because of its foundation in the Discrete Wavelet Transform (DWT). The focus metric we decided on was FISH because of its vastly superior performance and acceptable computation time.

FISH was applied to images in the focus stack in a block-based fashion. For example, an image that is 1024 × 1024 is divided into blocks of 64 × 64 pixels, and each of these blocks receive a FISH score. Thus, any image to which FISH is applied is associated with a map of FISH scores as illustrated in Figure 11. To lower the computation time for the depth map, we only apply FISH to every third image in our stack with the other images are used later in the pipeline. Once we have finished applying FISH, we look at each block region and note the layer that has the maximum FISH score in that block region. The depth for this layer is assigned to every pixel in that block region.

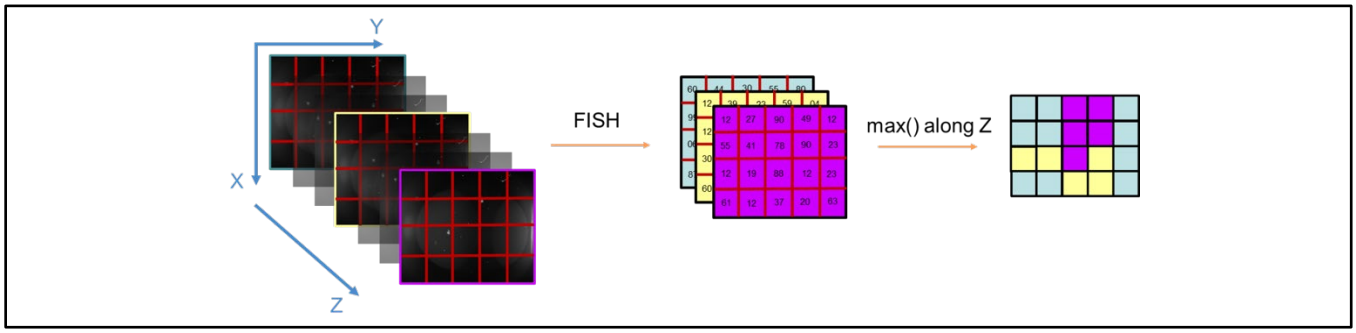

Figure 11: Block diagram of the topography estimation pipeline, using an example of a focal stack that has seven layers; a focal stack (left) where FISH is applied to the highlighted layers; maps of FISH (middle) associated with the highlighted layers; depth map (right).

To create the flattened image, we simply place the pixel in each all of the sharpest blocks next to each other. While one can identify visual artifacts with this method, the final image was fine for use in detecting particles.

B.5. Particle Detection

At its core, particle detection consists of applying a global threshold to the flattened image to obtain a binary image of the brighter portions of the image, and then performing connected component analysis on the binary image. As shown in Figure 12, a preprocessing step, called illumination normalization, seeks to remove slowly varying patterns in background illumination so that particle pixels and background pixels are well-separated in their intensities and uses a global threshold to separate particle pixels and background pixels well.

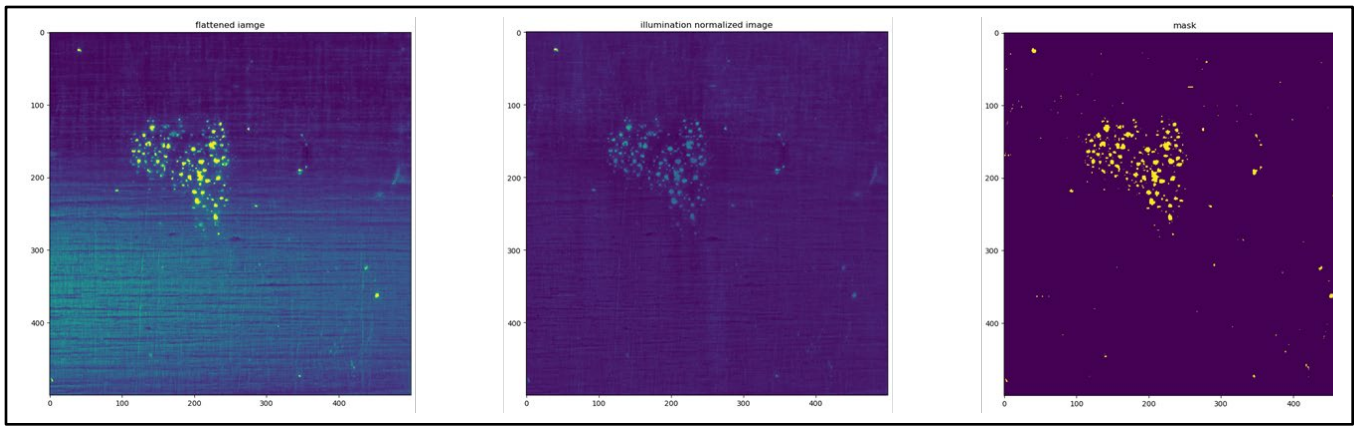

Figure 12: Intermediate images in the particle detection pipeline. Left: Flattened image, obtained from topography estimation. Middle: Illumination-normalized version of flattened image. Right: Binary mask of the previous image, which marks particle pixels.

The illumination normalization preprocessing procedure was taken from [31], which assumes the gray level is proportional to the product of the reflectance of the surface and the illumination on the scene:

$$f(x,y) = r(x,y)\, e(x,y)$$

If a logarithm transform is applied to the image, then the product becomes a sum:

$$\log f(x,y) = \log r(x,y) + \log e(x,y)$$

The method in [27] assumes first that the information on particles is contained in the reflectance, second that the illumination is slowly varying, and third that the reflectance contains high-frequency information. If so, the $\log r(x,y)$ and $\log e(x,y)$ terms are separated in the frequency domain, and we can simply apply a high-pass filter to remove the $\log e(x,y)$, leaving just the $\log r(x,y)$ term. Using the discrete cosine transform (DCT) as a frequency domain representation, the processing is illustrated in Figure 12. This is why the logarithm transform is used. Reversing the logarithm transform completes the normalization.

After illumination normalization, we can be relatively certain that brighter pixels belong to particles and darker pixels belong to the background. A shown in the rightmost part of Figure 12, we now apply a global threshold set equal to the mean pixel value plus three times the standard deviation. Finally, we apply connected component analysis to identify particle sizes, locations, and contrasts.

B.6. Aim Assist

After the motor subsystem has made its initial movement to the particle-of-interest, it is necessary to refine the position of the microscope to ensure that the Raman optics are aligned with the particle of intertest, in this case, the object in the green box in Figure 13. This aim assist step is split into two steps: a *Z*-correction and an *XY*-correction. As seen in Figure 14, for the *Z*-correction, the procedure is the same as that for stack flattening, except this time we use a tighter focal stack around the particle-of-interest: we use all image layers, and we restrict the *XY* dimensions to a smaller region around the particle-of-interest. The block size used is also smaller. The sharpest layer for the block in which the particle lies is the updated depth of the particle.

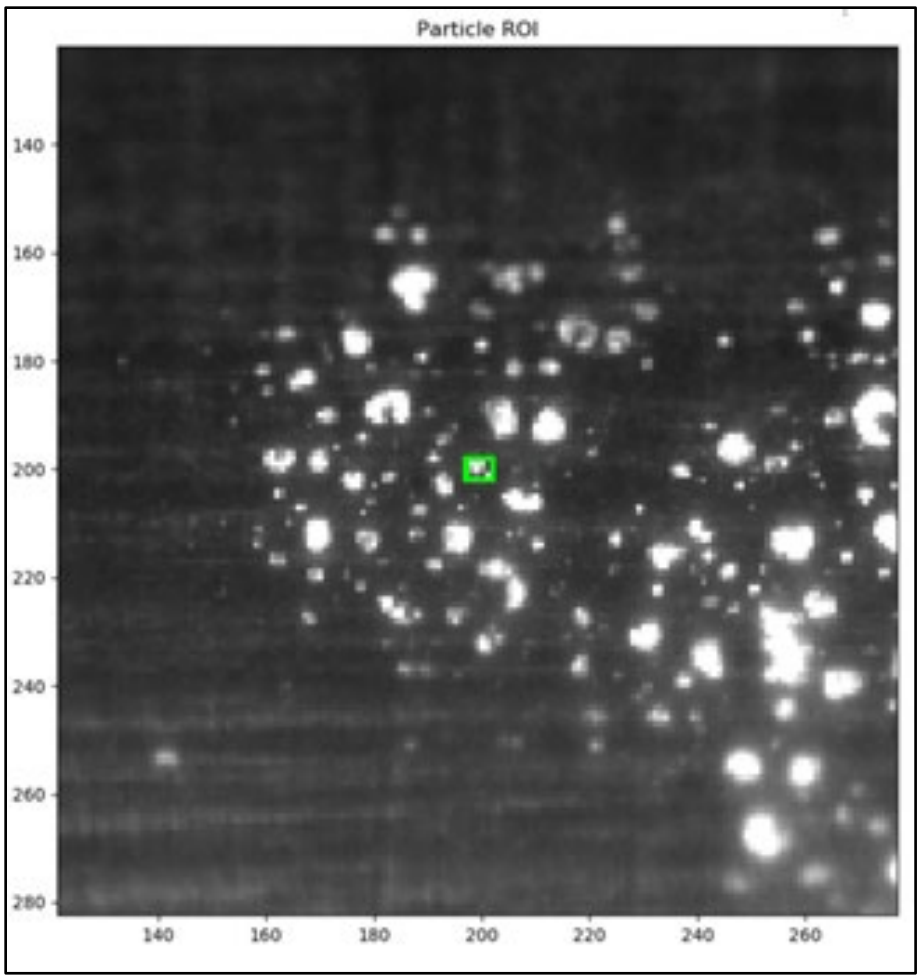

Figure 13: Template of particle and neighborhood from previous data collection.

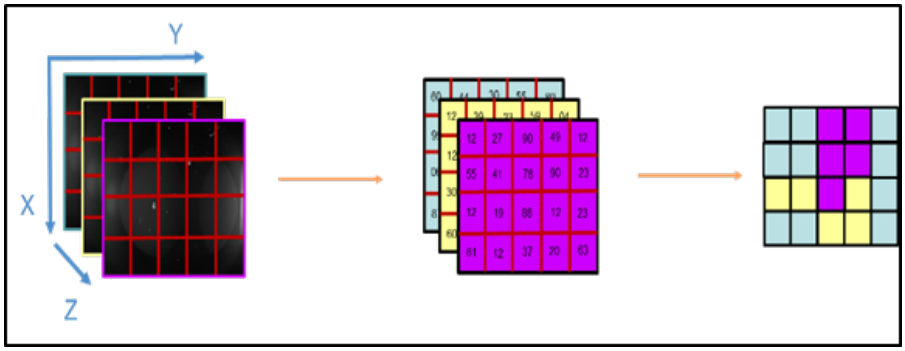

Figure 14: *Z*-correction. The focal stack is tighter in all dimensions and sampled more frequently in *Z*.

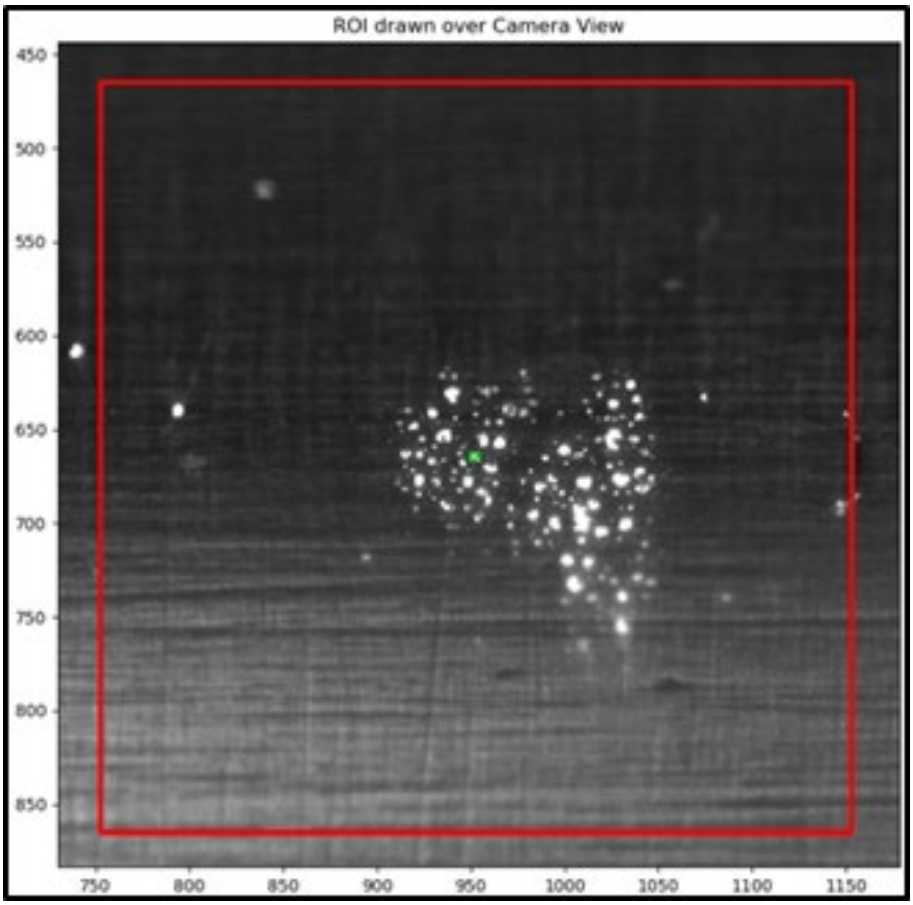

Figure 15: Optical image of the surface collected before beginning XY-refinement, zoomed-up to the particle of interest.

Subsequent to *Z* alignment, an optical image of the surface is collected for *XY* refinement; see Figure 15 for a close up of the region of interest. A 400×400 template region-of-interest around the particle to be interrogated, is then retrieved from the associated sharpest layer from the initial stack of images, see Figure 16 in this case. We create binary masks of the new and old data using the particle-finding procedure from before, then perform a template matching [32] between the new and old data to retrieve an offset by which to move the camera. The correlation surface between the template (Figure 13) and the image (Figure 15) is shown in Figure 16 where the peak at row 465 and column 753 is used to provide the shift in the optics such that the Raman spectrometer will be centered over the particle of interest.

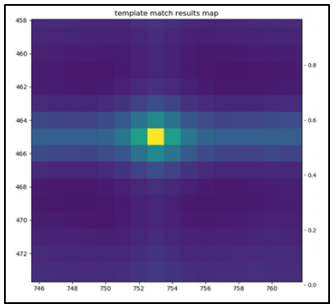

Figure 16: Template match results. Bright spot indicates location returned by algorithm.

C. Major Contributions

C.1. *X-Ray Modeling and Processing*

C.1.a. Year 7

The research advances made over the last year by the ECE group at Tufts are summarized as follows:

- Derived new injectivity theorems and explicit inversion formulae for a spindle torus Radon transform, which describes the CST problem for the RTT portal system of Figure 1. Our results were formulated as a research article [9], which is now published in the Journal of *Inverse Problems*.
- The derivation of new microlocal theorems for the CST problem in the RTT geometry. We developed a novel joint reconstruction and lambda regularization scheme to combat the image artifacts predicted by our microlocal theory. Our results have been formulated as a research article [21], which has been accepted to the journal *Inverse Problems special issue on Modern Challenges in Imaging*. The feedback from the reviewers has been highly positive and we expect publication.
- In recent work, we proposed new physical models for the Bragg scattered signal in the RTT geometry, which has led to the analysis of a new class of Radon transforms in BST. So far we have proven the invertibility of the BST transform and shown how to choose the machine parameters so as to optimize the problem stability. Our results have been formulated as a research article [8], which is under review *at The Journal of Inverse Problems and Imaging*.
- Completed the development of a novel single-scatter MATLAB code for the simulation of the Bragg, Rayleigh and Compton scattered signal. This is currently being used to test our inversion algorithms in BST and CST, and further to simulate data acquisition scenarios of interest to Rapiscan (e.g., to simulate photon counts).
- During Year 6, we worked with Prof. Eric Todd Quinto from the Department of Mathematics at Tufts. Our research focused on a novel microlocal analysis of a toric section transform, arising from a two dimensional CST problem, based on an old RTT design (with rings of sources and detectors, as opposed to the square array of Figure 1). Our results [33] have been published in the *SIAM Journal on Imaging Sciences* (*SIIMS*).
- Communicated our research at academic conferences. For example, at the Cormack Conference on Modern Challenges in Imaging, mini-symposium on security applications (August 5–9, 2019, Tufts University, Medford, MA USA), and the IS&T International Symposium on Electronic Imaging, mini-symposium on computational imaging (January 26–30, Burlingame, CA USA).
- We are now studying the microlocal and stability properties of the BST problem. So far we have derived sufficient conditions for the Bolker assumption, and shown that the RTT geometry satisfies such conditions. Satisfaction of the Bolker assumption implies that the BST inversion is stable and there are no nonlocal artifacts in the reconstruction due to the machine geometry.

C.1.b. Year 6

The Tufts PhD student supported for four years by ALERT, Ms. Hamideh Rezaee, successfully defended her doctoral dissertation and published a paper in the IEEE Transactions on Computational Imaging, on the model-based fusion of attenuation and scatter X-ray data for the joint recovery of electron density and photoelectric absorption. In support of our growing collaboration with Rapiscan Systems (Drs. Ed Morton and Dan Strellis), we began the development of new Monte Carlo (MC) software for the simulation of the

transmitted and scattered signal from randomly orientated crystalline lattices (powders) and amorphous materials. This provided valuable insight to our collaborators at Rapiscan on the expected photon counts and imaging capabilities of a new RTT portal scanner developed by the company. We developed new inversion formulae in Compton Scattering Tomography (CST), based on the RTT geometry.

C.1.c. Year 5

In the process of writing a manuscript detailing the processing method developed by our group under support from ALERT, we were asked by the reviewers of the paper to test the approach on data sets more realistic than those employed to date. To meet this need, we considered (a) the generation of data with Poisson statistics based on the single scatter model used in the processing (i.e., model matched data), as well as (b) the creation of data using sophisticated Monte Carlo codes (specifically, GEANT4) that in essence contain "all" of the physics that would be seen in experimentally obtained data. We developed a collaboration with Dr. Peter Rothschild of Heuresis Corporation to generate the Monte Carlo simulation data for a number of test scenarios. The effort of generating the data and reducing it to a form that can be input to our algorithms took most of Fall 2017 and Winter 2018. We focused on the processing of the Poisson and Monte Carlo data. Initial results demonstrated that even within the context of severely limited view geometries, our formulating of the imaging problems clearly demonstrates that the addition of scatter data to the processing provides significant benefits in terms of recovering the density relative to attenuation-only data sets. It is likely that accurate recovery of the photoelectric signature will not be possible in this data acquisition scenario. We hypothesize that sparse angle data (i.e., data acquired from a small number of angles but fully encircling the object) should yield much improved performance.

C.1.d. Year 4

The initial image formation method developed in Year 3 has been refined, as we have tested the approach on test cases far more complex than those considered during Year 3. Specifically, we have achieved the objectives in Year 4 that were outlined in the Year 3 project report. First, we have developed an objective method based on the discrepancy principle for choosing the regularization parameters defining the cost functions used as the basis for estimating both the mass density and photoelectric (PE) images from X-ray observations. Second, we have augmented the Compton data with energy resolved attenuation data and demonstrated the gain achieved from the fusion of these two data types. Finally, building on our prior efforts in multi-energy CT, we have developed a method for stabilizing the recovery of the PE image, which is based on the use of an NLM regularization scheme.

C.1.e. Year 3

We have demonstrated a method for joint recovery of both density as well as the photoelectric coefficient from severely limited view, multi-energy Compton scatter data. The overall approach is based on a variational formulation of the imaging problem. Physical intuition has guided the specific method used to solve this problem. Initial results on simulated data were quite promising.

C.1.f. Year 2

We have developed a tractable, analytical model capable for X-ray scattering and attenuation. The model has been instantiated in the form of a MATLAB-based code that will be made accessible to the broader DHS community. We believe that the model can be used effectively and efficiently in the context of image reconstruction methods seeking to recover spatial maps of electron density and photoelectric absorption information from limited view, multi-energy X-ray data.

C.1.g. Year 1

Our initial efforts under Phase 2 of ALERT support was the development of a computational forward model for multi-energy, limited view X-ray scanner modeled on the AS&E CANSCAN system, the limited view system that formed the basis for the 13-05 project. At the start of Year 2, we decided to move away from this absorption-only model as we began to explore the potential for scattered photon data to address the many challenges associated with the processing of limited view information.

C.2. Optical Image Processing

Year 7: We have designed, implemented. and transitioned to the Pendar PCFIS system the following:

- A topography estimation algorithm based on measuring the sharpness in different areas of a focal stack
- A particle detection method that returns particle coordinates within a confined search space and provides particles statistics, and that is robust against surfaces with uneven background illumination
- An aim assist method to facilitate the autonomous execution of particle identification using a Raman spectroscopy subsystem

D. Milestones

D.1.X-Ray Modeling and Processing

- **Milestone 1—Month 2:** Complete preliminary analytical model of the RTT XRD geometry with sources, detectors, collimators, and tunnel defined.
  - **Status:** Complete 08/2019
  - **Next steps:** Model is being used in development of advanced image formation methods
- **Milestone 2—Month 3:** Complete first Monte Carlo simulations of both idealized Bragg and Compton scattering spectra projected on a 2-D energy resolving detector.
  - **Status:** Complete 09/2019
  - **Next steps:** Model is being used to generate simulated data for use in exploration of the performance of image formation methods
- **Milestone 3—Month 4**: Complete more realistic Monte Carlo simulations of Bragg and Compton scattering spectra (including Poisson noise, detector energy resolution).
  - **Status:** Completed 09/2019
  - **Next steps:** The work here was basically folded into the previous milestone. Because of the Monte Carlo nature of the model, there was no need to simulate Poisson statistics. Detector energy resolution was included in the model.
- **Milestone 4—Month 5:** Complete realistic Monte Carlo simulations of Bragg and Compton scattering spectra (including scatter from system features like tunnel, belt, and detector structure).
  - **Status:** Never started
  - **Next steps:** As described previously in this report, the Tufts and Rapiscan team felt that the Monte Carlo model developed under Milestones 2 and 3 would be enough for the work to be done by Tufts for Milestones 6 and 7.

- **Milestone 5—Month 6:** Report with results from the Monte Carlo simulations supporting the detector, source, and collimator geometry for the Preliminary Design Review with DHS S&T.
  - **Status:** Never started
  - **Next steps:** As described previously in this report, the Tufts and Rapiscan team felt that the Monte Carlo model developed under Milestones 2 and 3 would be enough for the work to be done by Tufts for Milestones 6 and 7.
- **Milestone 6—Month 8:** Development and validation using both Monte Carlo and RTT data of Bragg tomography and threat classification techniques, combining Bragg scattering models with machine learning classification (e.g., neural network architectures or support vector machines).
  - **Status:** 90% complete. The Tufts team has developed the analytical foundations for a fundamentally new class of methods for the processing of Bragg scatter data collected in the "Venetian blind" sensor configuration of the Rapiscan RTT system. Also, within the context of the Rapiscan RTT geometry, the group at Tufts has developed a unique method for fused image formation from absorption and incoherent scatter data. The formal, microlocal analysis of this approach clearly explains the performance gains associated with this physics-based fusion scheme. The practical algorithm for producing images from data employs a new edge-preserving regularization method scheme for multiparameter inverse problems that produces state of the art results at substantially reduced computational load. This method promises wide applicability for problems and in fields well beyond those of interest in this project.
  - **Next steps:** We have chosen to delay the consideration of machine learning methods until such a time as we have developed a single algorithm for fusing diffraction, attenuation, and scatter X-ray data. Only when we are able to fuse all three of these data types can we best quantify the ultimate performance of X-ray methods for materials characterization.
- **Milestone 7—Month 12:** Development, validation using both Monte Carlo and RTT data and transition of materials characterization methods attenuation data, coherent scatter, and incoherent scatter. The effort will bring together microlocal analysis ideas for handling the incoherent scatter as well as iterative methods for processing the attenuation and Bragg data.
  - **Status:** In progress
  - **Next steps:** This work started in May 2020 and continued throughout the summer of 2020.

D.2. Optical Image Processing

- Enhanced machine vision processing for VICTOR Systems.
  - **Milestone 1—Month 2:** Development and use of an extended set of training data for identification of regions of interest across a broader array of luggage items.
    - **Status:** Never started
    - **Next steps:** The failure of the MODEx program to move beyond Phase I obviated this effort.
  - **Milestone 2—Month 5:** Multi-camera, video-based identification and tracking of luggage items moving along a conveyor belt.
    - **Status:** Never started
    - **Next steps:** The failure of the MODEx program to move beyond Phase I obviated this effort.

- Depth from defocus processing for Pendar PCFIS system.
  - **Milestone 1—Month 6:** Determination of technical specifications of Pendar problem and Selection of candidate depth from defocus processing methods to address Pendar problem.
    - **Status:** 07/2019
    - **Next steps:** Results of this effort formed the basis for Milestones 2–5
  - **Milestone 2—Month 7:** Implementation of candidate methods.
    - **Status:** Completed 09/2019
    - **Next steps:** Results of this effort formed the basis for Milestones 3–5
  - **Milestone 3—Month 9:** Collection of data and evaluation of processing methods.
    - **Status:** Completed 1/2020
    - **Next steps:** None
  - **Milestone 4—Month 10:** Implementation of particle detection and location algorithm. Python code tested on depth-corrected PCFIS images.
    - **Status:** Completed 10/2019
    - **Next steps:** None
  - **Milestone 5—Month 12:** Implementation of image tracking algorithm to follow particle locations as the instrument is aimed successively to the different particles. Python code uses depth corrected PCFIS images and produces updated particle coordinates as an output. The updated are used by the Pendar's motion controller to fine adjust the system aim and focus. Algorithm integrated and tested into PCFIS system.
    - **Status:** Completed 11/2019
    - **Next steps:** None

E. Final Results at Project Completion (Year 7)

E.1. Activities Toward Transition

E.1.a. X-Ray Modeling and Processing

As a result of the work discussed previously in this report, Tufts and Rapiscan submitted a white paper for consideration in response to the DHS LRBAA Securing Borders Research Area, Topic SEC BORD 04-02, Actionable Intelligence Gathering and Sharing. We proposed a three-year effort to develop, validate, and transition to fielded systems algorithms for processing X-ray attenuation and scatter data with the goal of detecting opioids and other illicit narcotics. Fusing attenuation, Compton scatter, and Bragg diffraction data, our proposed algorithms would significantly enhance CBP's abilities in terms of automated opioid and narcotics detection and confirmation. Unfortunately, DHS chose to not support this effort.

Prior to this proposal, ALERT funding at Tufts was dedicated to the development and validation of advanced computational models and associated processing methods for materials identification from X-ray data in support of the growing interests of DHS in fielding scanners at the checkpoint with few, fixed sources and detectors. Of specific interest has been the use of energy resolved observations of both attenuation and incoherently scattered photons for mapping the two physical properties to which X-rays are most sensitive

over the range of energies associated with the scanners currently under development: electron density and photoelectric attenuation coefficient. As a result of the investment by ALERT in the initial computational models and iterative reconstruction methods was a funded BAA 13-05 proposal (HSHQDC-15-C-B0012 Advanced Material Discrimination: Multi-View/Multi-Energy, Limited View, Compton Scatter Tomography) between Tufts and AS&E. That project resulted in the construction of a testbed for collection of experimental data that in turn provided for the validation of our computational models as well as initial image formation results. This effort clearly demonstrated the potential practical utility of scatter data for improving the quantitative accuracy of formed images in the context of the fixed source / detector scanners to be deployed at the checkpoint for which alternate, state of the art processing methods would be insufficient. A direct outcome of the 13-05 effort was the transition of the codes and documentation for the models and algorithms developed at Tufts to the engineers and scientists at AS&E.

E.1.b. Optical Image Processing

The optical image processing pipeline has been transitioned into the Pendar PCFIS. The collaboration between the Tufts team and Pendar greatly accelerated the identification and testing of candidate algorithms to be tested for PCFIS. The broad experience and knowledge base of the Tufts team was used to identify best options to address PCFIS challenges and issues as they emerged, making our team very reactive and greatly reducing both technical and scheduling risk for this effort.

E.2. Final Outputs Realized

E.2.a. X-Ray Modeling and Processing

- Derived new injectivity theorems, microlocal theorems, and explicit inversion formulae for a spindle torus Radon transform, which describes the Compton Scatter Tomography (CST) problem for the Rapiscan RTT portal system. Based on this work, developed a novel joint reconstruction and lambda regularization scheme to combat the image artifacts predicted by our microlocal theory. Extending and enhancing this algorithm for use in CBP-relevant problems is one component of the Rapiscan-Tufts LRBAA proposal.
- Studied the microlocal and stability properties of the Bragg scatter tomography (BST) problem. Derived sufficient conditions for the Bolker assumption, and shown that the RTT geometry satisfies such conditions meaning that that the BST inversion is stable and there are no nonlocal artifacts in the reconstruction due to the machine geometry.
- Demonstrated a method for joint recovery of both density as well as the photoelectric coefficient from severely limited view, multi-energy Compton scatter data. The overall approach is based on a variational formulation of the imaging problem. Physical intuition has guided the specific method used to solve this problem.
- Developed a tractable, analytical model capable for X-ray scattering and attenuation. The model has been instantiated in the form of a MATLAB-based code that can be made accessible to the broader DHS community.
- Transition of the codes and documentation for the models and algorithms developed at Tufts under 13-05 to the engineers and scientists at AS&E.

E.2.b. Optical Image Processing

- Development and validation of image processing pipeline for (a) identification of particles on curved surfaces from image stacks and (b) improved targeting of Rama spectral sensor.
- Implementation and transition of pipeline to Pendar PCFIS.

E.3. Results Documenting Impact

- Journal articles
  - Webber, J.W., & Miller, E.L. "Compton Scattering Tomography in Translational Geometries." *Inverse Problems*, *36*(2), 23 January 2020. https://doi.org/10.1088/1361-6420/ab4a32.
  - Webber, J.W., & Quinto, E.T. "Microlocal Analysis of a Compton Tomography Problem." *SIAM Journal on Imaging Sciences*, *13*(2), 2020, pp. 746-774. https://doi.org/10.1137/19M1251035.
  - Webber, J.W., Quinto, E.T., & Miller, E.L. "A Joint Reconstruction and Lambda Tomography Regularization Technique for Energy-Resolved X-Ray Imaging." *Inverse Problems*, special issue on modern challenges in imaging, *36*(7), 19 June 2020. https://doi.org/10.1088/1361-6420/ab8f82.
  - Webber, J.W., & Miller, E.L. "Bragg Scattering Tomography." *Inverse Problems and Imaging*, under review. Arxiv preprint available at https://arxiv.org/abs/2004.10961.
  - Rezaee, H., Rothschild, P., Tracey, B., & Miller, E.L. "On the Fusion of Energy Resolved Scatter and Attenuation Data for Limited-View X-Ray Materials Characterization with Application to Security Screening." *IEEE Transactions on Computational Imaging*, *5*(4), December 2019, pp. 620-634. DOI: 10.1109/TCI.2019.2909858.
  - Desmal, A., Schubert, J.R., Denker, J., Kisner, S.J., Rezaee, H., Couture, A., Miller, E.L., & Tracey, B.H. "Limited-View X-Ray Tomography Combining Attenuation and Compton Scatter Data: Approach and Experimental Results." *IEEE Access* 7, 2019, pp. 165734-165747. https://doi.org/10.1109/ACCESS.2019.2953217.
- Successful 13-05 project with AS&E including transition of code from Tufts to AS&E
- Successful development and transition into Pendar product of an image processing pipeline for particle identification and Raman spectral microscope target localization
- Current LRBAA proposal effort between Tufts and Rapiscan

III. RELEVANCE AND TRANSITION

A. Relevance of Research to the DHS Enterprise

Both the X-ray and optical components of this project share a common relevance to the homeland security enterprise: namely the development and fielding of sophisticated sensor systems and embedded processing methods for the detection of explosive materials at the checkpoint. Current methods for luggage scanning at the checkpoint are insufficient to meet the future needs and expectations of the traveling public as well as the rapidly emerging and changing threats facing the United States. All viable solutions to this problem are based on the deployment of advanced sensing systems. The success of such systems in turn is driven both by the physical processes being exploited to detect and characterize explosive materials embedded in cluttered environments as well as the processing methods designed to turn sensor data into actionable information.

Meeting the performance specifications set by the Department of Homeland Security requires the exploitation of increasingly subtle physical effects that in turn leads to data whose reliable interpretation is made all the more challenging not only due to noise, but also systematic effects associated with the physics of the sensor coupled with uncertainty in the environment. In the context of the Pendar system for example (a similar case could be made for the Rapiscan project), the spectral signature of a compound of interest changes dramatically as a function of its concentration as well as the surface on which it has been deposited. Both of these complications are essentially uncontrolled in this application thereby rendering useless any sort of "off-the-shelf" processing method. The success of the overall system then requires a carefully designed and very deliberative approach to integrating the engineers and scientists responsible for the processing with those constructing the sensor itself. Over the past seven years, the group at Tufts has pursued just this type of collaboration both with Pendar and AS&E/Rapiscan Systems and, as discussed below have successfully transitioned technologies from academia to our HSE-serving industrial partners.

We are seeking to address challenges associated with automated scanning and threat detection in both checked luggage and baggage that is inspected at checkpoints. The overall goal is to determine spatial maps of material properties in an automated manner from multi-energy X-ray data collected in limited-view types of geometries or optical methods. Any metric that quantifies the accuracy of the material maps can be used to evaluate the performance of our work including:

- Confusion matrices capturing the percentage of correctly and incorrectly labeled pixels for scenarios where ground truth is known.
- If one is concerned with purely binary problems (threat object versus all other types of materials), then the receiver operating characteristic, plotting detection probabilities versus false alarm rates, could be developed.
- Finally, we could visualize accuracy using uncertainty cloud analysis developed as part of ALERT Task Order 3 and employed in "Stabilizing Dual-Energy X-Ray Computed Tomography Reconstructions Using Patch-Based Regularization" by Brian H. Tracey and Eric L. Miller [*Inverse Problems*, *3*(10), 2015, 105004]. These clouds would plot the average value and first standard deviation ellipse of the distribution of photoelectric and electron density over known target regions in our reconstructions. In comparing multiple candidate processing methods, smaller ellipses and means closer to ground truth are indicators of higher accuracy.

B. Status of Transition at Project End

B.1. X-Ray Modeling and Processing

As a result of the work discussed previously in this report, Tufts and Rapiscan have submitted a white paper for consideration in response to the DHS LRBAA Securing Borders Research Area, Topic SEC BORD 04-02, Actionable Intelligence Gathering and Sharing. We have proposed a three-year effort to develop, validate, and transition to fielded systems algorithms for processing X-ray attenuation and scatter data with the goal of detecting opioids and other illicit narcotics. Fusing attenuation, Compton scatter, and Bragg diffraction data, our proposed algorithms will significant enhance Customs and Border Protection's abilities in terms of automated opioid and narcotics detection and confirmation.

B.2. Optical Image Processing

The optical image processing pipeline has been transitioned into the Pendar PCFIS. The collaboration between the Tufts team and Pendar greatly accelerated the identification and testing of candidate algorithms

to be tested for PCFIS. The broad experience and knowledge base of the Tufts team was used to identify best options to address PCFIS challenges and issues as they emerged, making our team very reactive and greatly reducing both technical and scheduling risk for this effort.

C. Transition Pathway and Future Opportunities

C.1. X-Ray Modeling and Processing

This project was a close collaboration between the Tufts team of Dr. Miller and Dr. Webber and the Rapiscan team of Dr. Strellis and Dr. Morton. The group had a teleconference about twice a month to review progress on the project, ensure relevance of the Tufts effort to Rapiscan, and set goals for the next time period. The work being performed at Tufts benefitted Rapiscan by providing a collaboration whereby academia was able concentrate on the exploration of new methods and data extraction processes while allowing Rapiscan participants to concentrate on the application of the technology. Throughout this collaboration, Rapiscan has provided laboratory X-ray diffraction data for Tufts to use in benchmarking their methods. Tufts has provided valuable feedback on the data Rapiscan has provided and has suggested new measurements or materials where new data would be valuable.

The LRBAA proposal represents one future opportunity being pursued. Additionally, the Tufts group will seek to collaborate with Rapiscan in response to any new RFPs released by DHS looking for advanced methods for collecting and processing X-ray data.

C.2. Optical Image Processing

This project is a close collaboration between the Tufts team of Dr. Miller and Mr. Yau and the Pendar team led by Dr. Blanchard. Mr. Yau, hired by Tufts to work on this project, was physically located at Pendar interacting on a continual basis with the PCFIS team. Dr. Miller and Mr. Yau met weekly to discuss progress on the project, address technical issues in need of solution, and set goals for the upcoming week. Prior to programmatic deadlines associated with the PCFIS system, Dr. Miller visited Pendar to provide additional technical support.

The Tufts group will seek to collaborate with Pendar in response to any new RFPs released by DHS looking for advanced methods for collected and processing optical data.

D. Customer Connections

- At Rapiscan: Dr. Dan Strellis and Dr. Ed Morton. We meet with both Dr. Strellis and Dr. Morton once every two weeks to review progress on our project and plan for future efforts.
- At Pendar: Dr. Romain Blanchard. We speak with Dr. Blanchard approximately monthly concerning progress on this project.

IV. PROJECT ACCOMPLISHMENTS AND DOCUMENTATION

A. Peer Reviewed Journal Articles

1. Rezaee, H., Rothschild, P., Tracey, B., & Miller, E.L. “On the Fusion of Energy Resolved Scatter and Attenuation Data for Limited-View X-Ray Materials Characterization with Application to Security Screening.” *IEEE Transactions on Computational Imaging*, *5*(4), December 2019, pp. 620–634. https://doi.org/10.1109/TCI.2019.2909858.

2. Webber, J.W., & Miller, E.L. "Compton Scattering Tomography in Translational Geometries." *Inverse Problems*, *36*(2), 23 January 2020. https://doi.org/10.1088/1361-6420/ab4a32.
3. Webber, J.W., & Quinto, E.T. "Microlocal Analysis of a Compton Tomography Problem." *SIAM Journal on Imaging Sciences*, *13*(2), 2020, pp. 746–774. https://doi.org/10.1137/19M1251035.
4. Webber, J.W., Quinto, E.T., & Miller, E.L. "A Joint Reconstruction and Lambda Tomography Regularization Technique for Energy-Resolved X-Ray Imaging." *Inverse Problems*, special issue on modern challenges in imaging, *36*(7), 19 June 2020. https://doi.org/10.1088/1361-6420/ab8f82.

Pending –

1. Webber, J.W., & Miller, E.L. "Bragg Scattering Tomography." Under review at *Inverse Problems and Imaging*. Arxiv preprint available at https://arxiv.org/abs/2004.10961.

B. Other Conference Proceedings

1. Webber, J.W., Quinto, E.T., & Miller, E.L. "A Joint Reconstruction and Lambda Tomography Regularization Technique for Energy-Resolved X-Ray Imaging." *Computational Imaging XVIII Conference* at the *IS&T Electronic Imaging 2020 Symposium*, Burlingame, CA. 26–30 January 2020.

C. Other Presentations

1. Webber, J.W. Speaker at *The Cormack Conference on Modern Challenges in Imaging*, mini-symposium on security applications. Tufts University, Medford, MA. 5–9 August 2019.
2. Webber, J.W. Speaker at *The IS&T International Symposium on Electronic Imaging*, mini-symposium on computational imaging, Burlingame, CA, 26–30 January 2020.
3. Webber, J.W. "Generalized Radon Transforms and Applications." Mini-symposium. *The 10th International Conference on Inverse Problems: Modelling and Simulation*, Malta. 24–30 May 2020.
4. Webber, J.W., & Miller, E.L. Co-organizers of "Scattering Tomography and Generalized Radon Transforms," mini-symposium at *SIAM Conference on Imaging Sciences*, Toronto, Canada, 6–9 July 2020.

V. REFERENCES

[1] G. J. Edelman, E. Gaston, T. G. van Leeuwen, P. J. Cullen, and M. C. G. Aalders, "Hyperspectral imaging for non-contact analysis of forensic traces," (in English), *Forensic Sci Int,* vol. 223, no. 1-3, pp. 28-39, Nov 30 2012, doi: 10.1016/j.forsciint.2012.09.012.

[2] D. S. Moore, "Instrumentation for trace detection of high explosives," *Review of Scientific Instruments,* vol. 75, no. 8, pp. 2499-2512, 2004, doi: 10.1063/1.1771493.

[3] P. I. Hendricks et al., "Autonomous in Situ Analysis and Real-Time Chemical Detection Using a Backpack Miniature Mass Spectrometer: Concept, Instrumentation Development, and Performance," (in English), *Anal Chem,* vol. 86, no. 6, pp. 2900-2908, Mar 18 2014, doi: 10.1021/ac403765x.

[4] W. R. de Araujo et al., "Portable analytical platforms for forensic chemistry: A review," (in English), *Analytica Chimica Acta,* vol. 1034, pp. 1-21, Nov 30 2018, doi: 10.1016/j.aca.2018.06.014.

[5] "Virsa™ Raman Analyser." https://www.renishaw.com/en/virsa-raman-analyser--44980.

[6] D. F. Swinehart, "The beer-lambert law," *Journal of chemical education,* vol. 39, no. 7, p. 333, 1962.

[7] A. C. Kak, M. Slaney, and G. Wang, "Principles of computerized tomographic imaging," *Medical Physics,* vol. 29, no. 1, pp. 107-107, 2002.

[8] J. Webber and E. Miller, "Braggh Scatter Tomography," *Inverse Problems and Imaging,* 2020.

[9] J. Webber and E. L. Miller, "Compton scattering tomography in translational geometries," (in English), *Inverse Probl,* vol. 36, no. 2, Feb 2020, doi: ARTN 025007, 10.1088/1361-6420/ab4a32.

[10] F. Natterer, *The mathematics of computerized tomography*. SIAM, 2001.

[11] J. J. DeMarco and P. Suortti, "Effect of Scattering on the Attenuation of X Rays," *Physical Review B,* vol. 4, no. 4, p. 1028, 1971.

[12] A. J. C. Wilson and V. Geist, "International Tables for Crystallography. Volume C: Mathematical, Physical and Chemical Tables. Kluwer Academic Publishers, Dordrecht/Boston/London 1992 (published for the International Union of Crystallography), 883 Seiten, ISBN 0-792-3-16-38X.

[13] M. K. Nguyen and T. T. Truong, "Inversion of a new circular-arc Radon transform for Compton scattering tomography (vol 26, 065005, 2010)," (in English), *Inverse Probl,* vol. 26, no. 9, Sep 2010, doi: Artn 099802,10.1088/0266-5611/26/9/099802.

[14] V. P. Palamodov, "An analytic reconstruction for the Compton scattering tomography in a plane," (in English), *Inverse Probl,* vol. 27, no. 12, Dec 2011, doi: Artn 125004, 10.1088/0266-5611/27/12/125004.

[15] T. T. Truong, M. K. Nguyen, and H. Zaidi, "The mathematical foundations of 3D Compton scatter emission imaging," *International journal of biomedical imaging,* vol. 2007, 2007.

[16] F. G. Tricomi, *Integral equations*. Courier Corporation, 1985.

[17] A. Taylor and H. Sinclair, "On the Determination of Lattice Parameters by the Debye-Scherrer Method," (in English), *P Phys Soc Lond,* vol. 57, no. 320, pp. 126-135, 1945, doi: Doi 10.1088/0959-5309/57/2/306.

[18] B. E. Warren, *X-ray Diffraction*. Courier Corporation, 1990.

[19] D. Ballantine Jr *et al.*, *Acoustic wave sensors: theory, design and physico-chemical applications*. Elsevier, 1996.

[20] O. Klein and Y. Nishina, "Über die Streuung von Strahlung durch freie Elektronen nach der neuen relativistischen Quantendynamik von Dirac," *Zeitschrift für Physik,* vol. 52, no. 11-12, pp. 853-868, 1929.

[21] J. Webber, E. T. Quinto, and E. Miller, "A joint reconstruction and lambda tomography regularization technique for energy-resolved X-ray imaging," *Inverse Problems special issue on Modern Challenges in Imaging,* 2020, doi: 10.1088/1361-6420/ab8f82

[22] J. Hubbell, "Photon cross sections, attenuation coefficients and energy absorption coefficients," *National Bureau of Standards Report NSRDS-NBS29, Washington DC,* 1969.

[23] F. Wirsching, "Calcium sulfate," *Ullmann's encyclopedia of industrial chemistry,* 2000.

[24] J. Winkler, *Titanium Dioxide: Production, Properties and Effective Usage 2nd Revised Edition*. Vincentz Network, 2014.

[25] M. J. Ehrhardt *et al.*, "Joint reconstruction of PET-MRI by exploiting structural similarity," (in English), *Inverse Probl,* vol. 31, no. 1, Jan 2015, doi: Artn 015001, 10.1088/0266-5611/31/1/015001.

[26] R. Behling, *Modern Diagnostic X-Ray Sources: Technology, Manufacturing, Reliability*. CRC Press, 2015.

[27] Y. Leng, "Materials Characterization: Introduction to Microscopic and Spectroscopic Methods, 2nd Edition," (in English), *Materials Characterization: Introduction to Microscopic and Spectroscopic Methods, 2nd Edition,* pp. 1-376, 2013, doi: 10.1002/9783527670772.

[28] D. B. Murphy, *Fundamentals of light microscopy and electronic imaging*. John Wiley & Sons, 2002.

[29] M. S. Sigdel, M. Sigdel, S. Dinc, I. Dinc, M. L. Pusey, and R. S. Aygun, "FocusALL: Focal Stacking of Microscopic Images Using Modified Harris Corner Response Measure," (in English), *Ieee Acm T Comput Bi,* vol. 13, no. 2, pp. 326-340, Mar-Apr 2016, doi: 10.1109/Tcbb.2015.2459685.

[30] J. M. Mateos-Pérez *et al.*, "Comparative evaluation of autofocus algorithms for a real-time system for automatic detection of Mycobacterium tuberculosis," *Cytom Part A,* vol. 81, no. 3, pp. 213-221, 2012.

[31] W. L. Chen, M. J. Er, and S. Q. Wu, "Illumination compensation and normalization for robust face recognition using discrete cosine transform in logarithm domain," (in English), *Ieee T Syst Man Cy B,* vol. 36, no. 2, pp. 458-466, Apr 2006, doi: 10.1109/Tsmcb.2005.857353.

[32] R. Brunelli, *Template matching techniques in computer vision: theory and practice*. John Wiley & Sons, 2009.

[33] J. W. Webber and E. T. Quinto, "Microlocal Analysis of a Compton Tomography Problem," *SIAM Journal on Imaging Sciences,* vol. 13, no. 2, pp. 746-774, 2020, doi: 10.1137/19m1251035.

This page intentionally left blank.

R4-C.1: Advanced Multispectral Computed Tomography Algorithms

I. PARTICIPANTS INVOLVED FROM JULY 1, 2019 TO JUNE 30, 2020

Faculty/Staff			
Name	**Title**	**Institution**	**Email**
Clem Karl	PI	BU	wckarl@bu.edu
David Castañón	Professor	BU	dac@bu.edu
Graduate, Undergraduate and REU Students			
Name	**Degree Pursued**	**Institution**	**Month/Year of Graduation**
Sandamali Devadithya	PhD, ECE	BU	6/2021
Usman Ghani	PhD, ECE	BU	6/2021

II. PROJECT DESCRIPTION

A. Project Overview

Explosives represent a continual threat to aviation security. New threats, resilient and adaptable adversaries, and demands for increased throughput continue to stress existing and planned security systems. New limited data geometries, novel sensing paradigms, and increased performance requirements have challenged traditional methods for Computerized Tomography (CT)-based explosives detection in security systems. Furthermore, CT-based systems are being developed and deployed for new missions, such as checkpoint carry-on screening and air cargo screening. Such systems use new sensing geometries with multi-spectral excitation.

In order to extract features that can identify explosives, CT systems are using dual-energy computed tomography (DECT) to estimate a small number of material-specific parameters at each image location and use them for material identification. Multispectral X-ray CT attempts to use the additional energy-dependent material information obtained by making multiple energy-selective measurements of attenuation. Metal and clutter in scenes cause artifacts that confound traditional methods. In addition, new sensing geometries are being explored. All these developments have meant that the application of conventional tomographic imaging approaches, largely coming from the medical domain, are highly suboptimal, and new approaches are required.

In this project, new methods for the formation of enhanced material parameter images from multi-energy CT data have been developed. The methods focus on increasing robustness to noise and artifacts that exist in images obtained by conventional means. The resulting algorithms include approaches for enhanced image quality and material identification. The improved algorithms lead to more accurate material and object identification, resulting in fewer false alarms, greater security, and reduced passenger inconvenience. These algorithms have been tested on simulated and real data.

B. *State of the Art and Technical Approach*

The majority of the work on multispectral X-ray CT focuses on DECT. Several DECT techniques have been suggested since the 1970s [1-3]. They are mostly targeted at medical applications and do not deal with the image artifact mitigation necessary for security applications [4-8]. Extensions of dual-energy techniques for security applications can be found in [8-9]. We overview the basic approach for DECT briefly below.

In DECT, X-ray transmission measurements of an image are collected using two excitations with different spectra. The observed normalized log-sinogram data in DECT sensing follows the nonlinear Beer-Lambert law [1,2,9]:

$$I_s(\ell) = -\ln\left(\frac{\int w_s(E) e^{-\int_\ell \mu(x,E)dx} dE}{\int w_s(E) dE}\right)$$

where $w_S(E)$ is the spectral weighting used in the measurement with spectrum s; $\mu(x,E)$ is the linear attenuation coefficient (LAC) of the material at spatial location x and energy E, and $I_S(\ell)$ is the measurement along ray-path ℓ for spectral weighting $w_S(E)$. Examples of LAC curves and spectral weighting functions are shown in Figure 1.

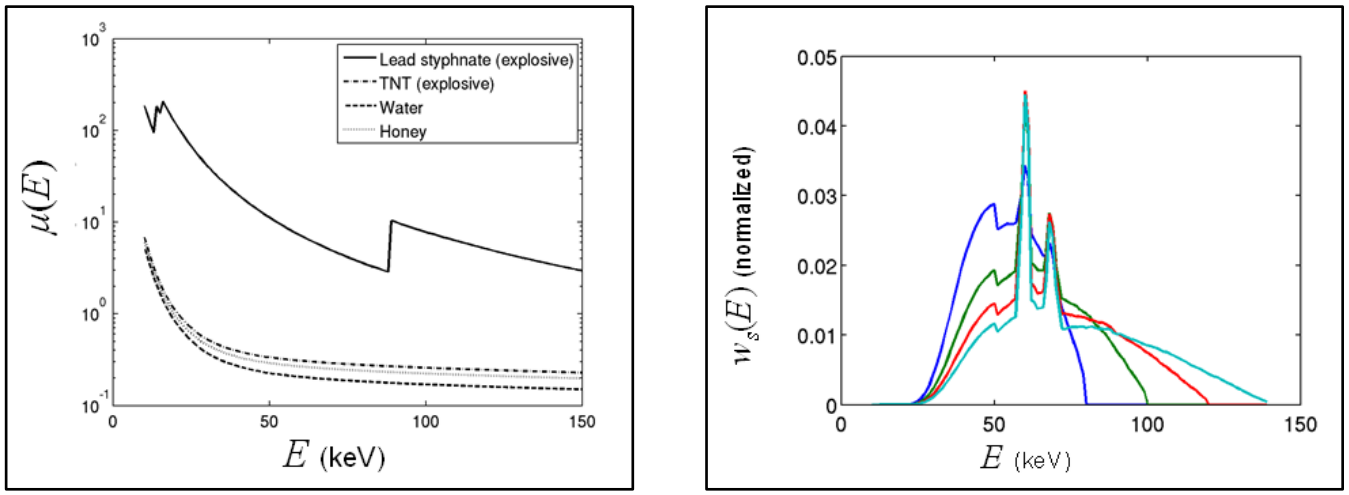

Figure 1: (left) The LAC curves of a few example materials and (right) examples of spectral weighting functions (normalized to unit sum).

The characteristics of the material at spatial location x are captured through the energy dependent function. Typically, this function is approximated as a linear combination of a few basis functions [1, 8]. A common choice of basis functions in DECT are the photoelectric absorption and Compton scatter cross-section functions. The LAC representation in the photo-Compton model is given by:

$$\mu(x,E) = a_p(x) f_p(E) + a_c(x) f_c(E)$$

where $f_p(E), f_c(E)$ are the photoelectric and Compton energy-dependent basis functions; and $a_p(x)$, $a_c(x)$, are the corresponding material-dependent coefficients at each spatial location x. The goal is to separate materials on the basis of their coefficient values.

In many DECT methods, the goal is to reconstruct the coefficient images $a_p(x)$ and $a_c(x)$, given the dual-energy tomographic projection measurements $I_1(\ell)$, $I_2(\ell)$. Since the problem is nonlinear and high dimensional, a

well-known solution approach is to separate it into two decoupled subproblems [1]. In the first subproblem, a nonlinear set of equations is solved at each detector, to obtain the basis coefficient sinograms $A_p(\ell)$, $A_c(\ell)$, defined as:

$$A_p(l) = \int_{\ell} a_p(x)\,dx \text{ and } A_c(l) = \int_{\ell} a_c(x)\,dx.$$

The second subproblem is tomographic reconstruction of the basis coefficient images $a_p(x)$ and $a_c(x)$ from these sinograms. This reconstruction step is usually accomplished by applying filtered back projection (FBP) or iterative reconstruction methods to each sinogram individually; therefore, mutual structure information is not used.

An early focus of this work was on developing reconstruction algorithms that simultaneously formed basis coefficient images and exploited mutual structure information in each sinogram. We called this method structure-preserving dual-energy (SPDE), which was documented in our past publications [10-12].

The general formulation of our SPDE method in vector form is given by the following:

$$\min_{(a_p \geq 0, a_c \geq 0, s)} \| A_p - Ta_p \|_{W_z}^2 + \| A_c - Ta_c \|_{W_z}^2 + \lambda_1 \| Da_p \|_{W_{ps}}^2 + \lambda_2 \| Da_c \|_{W_{cs}}^2 + \lambda_3 \| a_p \|_2^2 + \lambda_4 \| a_c \|_2^2 + \lambda_5 \| Ds \|_2^2 + \lambda_6 \| s \|_2^2$$

where s is a common mutual boundary field; T is the tomographic projection operator; D is a derivative operator; W_z is a data weighting matrix; W_{ps} and W_{cs} are weighting matrices derived from s; and λ_k are nonnegative regularization parameters.

Another major result in our previous work was the development of a joint segmentation/recognition approach for direct estimation of material labels from dual-energy labels. In typical explosive detection systems [10-12], segmentation of reconstructed images is used to identify volumes of interest, from which features are extracted to classify the volume. In our approach, we formulate a combined segmentation/classification optimization problem for dual-energy systems. We extended the previous multi-energy formulation to direct estimation of material labels but combined a dual-energy learned appearance model with a Markov random field material model. In the dual-energy case this formulation becomes:

$$\min_{l_1, l_2, \ldots, l_N} \left\{ \sum_x v_x [-\ln\left(p(\mu_x^L, \mu_x^H | l_x)\right)] + \lambda g_{MRF}(l_1, l_2, \ldots, l_N, s) \right\}$$
$$\text{subject to } l_x \in \{1, 2, \ldots, M\}$$

where μ_j^L, μ_j^H are the formed effective attenuation images obtained from measurements with two different (high and low) spectral weightings at voxel x; l_x is the material label at voxel x; $p(\mu_j^L, \mu_j^H \mid l_x)$ is the learned appearance model for material label l_x at voxel x; v_x are data weights, which down-weight data points in the vicinity of metal; λ is a nonnegative regularization parameter; and $g_{MRF}(l_1, l_2, \ldots, l_N, s)$ is a Markov random field smoothing term, which is based on an estimate of the image boundary field s. This MRF model captures local coherence of material labels and takes into account an estimate of object boundaries to further ensure label homogeneity within an object.

The resulting optimization problem is a nonconvex, discrete label problem, which is generally challenging to solve. To accomplish this optimization, we developed an efficient graph-cut method. Such graph-cut methods [13] have been popular in computer vision and discrete optimization literature but have not been used in this domain. These methods map the original optimization problem to an equivalent graph flow problem, and a minimal cut of this graph provides the optimal solution when there are only two labels. In our experiments, there are multiple labels, so we use a rotation method to obtain a solution. We call this voxel-

based method "learning-based object identification and segmentation," or LOIS. Our algorithm development and initial results were documented in [10-,11].

In our recent work, we extended this approach to learn spatially correlated models of the dual-energy reconstructions for different materials. Using sample reconstructions that include regions with known materials, we learn the conditional probability density of the low and high attenuation images over a neighborhood patch that includes *k* pixels, as:

$$p(\mu_{1,n}^{L}, \ldots, \mu_{k,n}^{L}, \mu_{1,n}^{H}, \ldots, \mu_{k,n}^{H} | \ell_n)$$

where $\mu_{j,n}^{L}$, $\mu_{j,n}^{H}$ refers to the reconstructed low and high attenuation for pixel number *k* in patch at location *n*.

In our work, we use patches consisting of 2×2 pixels to better capture the special energy dependence. We then optimize the following energy function over the labels and patches:

$$\min_{\{\ell_n, n=1,\ldots,NN\}} \sum_{n=1}^{NN} p(\mu_{1,n}^{L}, \ldots, \mu_{k,n}^{L}, \mu_{1,n}^{H}, \ldots, \mu_{k,n}^{H} | \ell_n) + \lambda \sum_{n=1}^{NN} \sum_{n \in \mathcal{N}(n)} \phi(\ell_n, \ell_j)$$

where *NN* is the number of patches; ℓ_n is the label of patch *n*; and $\phi(\ell_n, \ell_j)$ is 0 if $\ell_n = \ell_j$, 1 otherwise. The resulting discrete optimization problem is solved by a multi-label graph-cut algorithm [22], leading to fast assignment of material labels to patches. The development of the patch-based version of the LOIS algorithm was presented in our paper [14] and the thesis [15].

The LOIS approach described above for the joint segmentation/classification of materials requires the formation of CT images. As part of our research under this task, we have also developed approaches that can directly estimate discrete labels associated with spatial regions from single-energy or dual-energy sinograms. This bypasses conventional CT image formation and results in discrete tomography formulations. In our work, we examined the difficult general problem of inverting tomographic data where the scene is constrained to be discrete valued using a variational approach. Our original problem is defined as:

$$\underset{x \in \{\text{Disc Amp}\}}{\operatorname{argmin}} J_{data}(x) + \lambda J_{prior}(x) = \underset{x \in \{\text{Disc Amp}\}}{\operatorname{argmin}} J_{data}(x) + \lambda \|\mathrm{D}x\|_1^1$$

where *x* is the desired, unknown, discrete-valued quantity of interest; $J_{data}(x)$ is a data penalty (e.g., negative log-likelihood) that projects how the label field would generate sinograms that match the observed data; and $\|\mathrm{D}x\|_1^1$ is a total-variation edge-preserving dissimilarity penalty on the reconstructed label field.

The above formulation is a combinatorial formulation: each voxel must be labeled with one of a finite number of material labels (which includes background). As such, this is no longer a convex optimization problem of the type solved by iterative CT algorithms. Furthermore, the data fidelity term now involves matching the sinogram data, rather than matching the learned appearance model in the image space. The tomographic relationship between sinograms and the underlying properties of the label images does not permit the direct application of fast combinatorial algorithms, such as graph cuts, to solve the discrete problem.

Our early work on discrete tomography is documented in [16-17]. Our approach in that work was focused on extensions of graph-cut algorithms that would be applicable to discrete tomography, either through sequential linearization or through the use of decomposition techniques. We ended up pursuing a different algorithmic approach, developing a new variable splitting approach based on the alternating direction method of multipliers (ADMM) from convex optimization theory. ADMM is designed to solve convex optimization problems involving two blocks of variables by splitting the overall hard optimization into a sequence of simpler optimizations [18]. The ADMM algorithm is used for convex optimization with continuous variables, and our discrete optimization framework is notably nonconvex.

The ADMM-based algorithm that we developed, which we term TOMO-SPL, provides an efficient, inherently discrete solution; however, using a particular variable splitting:

$$x^{k+1} = \arg\min_{x \in \Re^n} J_{data}(x) + \frac{\rho}{2}\left\| x - z^k - u^k / \rho \right\|_2^2$$
$$z^{k+1} = \arg\min_{z \in \{\text{Disc Amp}\}} \lambda J_{prior}(z) + \frac{\rho}{2}\left\| x^{k+1} - z - u^k / \rho \right\|_2^2$$
$$u^{k+1} = u^k - \tau\rho\left(x^{k+1} - z^{k+1}\right)$$

Specifically, we reconstruct a continuous approximation to the discrete label field in the form of *x*, and we then solve for the best label *z* to assign to that discrete field that is close to *x*. Our particular splitting thus breaks down (in a joint iterative optimization) a field reconstruction step similar to CT iterative reconstruction, together with a joint segmentation/label step; the former step is done using standard iterative CT techniques, whereas the latter step can be performed efficiently using graph-cut techniques. This work was documented in our papers [19-21].

Another result from Year 4 that integrates learning into reconstruction is the development of a new algorithm to reduce metal artifacts in CT images when data is acquired using a single source spectrum. This is a major problem in both medical and security CT [4-5, 7]. Such metal artifacts arise from many effects, including beam hardening. With a single energy spectrum, one cannot use basis decomposition techniques to correct these artifacts.

Our algorithm is a hybrid approach that corrects the sinogram vector followed by an iterative reconstruction. Many prior sinogram correction algorithms [22–24] identify projection measurements that travel through areas with significant metal content and remove those projections, interpolating their values for use in subsequent reconstruction. In contrast, our algorithm retains the information of random subsets of these metal-affected projection measurements, and uses an average procedure to construct a modified sinogram. To reduce the secondary artifacts created by this interpolation, we apply an iterative reconstruction in which the solution is regularized using a sparsifying transform [25]. The basis functions used in the sparsifying transform are learned from reconstructed imagery, enforcing the natural structure that appears in CT reconstructions. Our experiments indicate that our algorithm reduces the extent of metal artifacts significantly, and it enables accurate recovery of structures in proximity to metal. These results are documented in our publication [26].

In the above discussion, we primarily focused on dual-energy CT systems. The emergence of new threat materials and variations in manufacturing processes have introduced new challenges for separating materials of interest using dual-energy spectra. There has also been an increase in new measurement technologies for extracting additional signatures that would enhance the capability for identifying materials, including commercial photon-counting detectors to facilitate multi-spectral CT and new measurement technologies (e.g., X-ray diffraction imaging and phase contrast imaging). Furthermore, new features are being proposed for dual-energy systems, either in terms of basis materials or in terms of electron density or effective atomic number [1,8,27].

Given these developments, it is important to understand the limits in performance of potential designs for new systems that include changes in architecture, processing, measurement technology, and extracted features. To that end, we developed an approach based on information theory metrics that provides bounds on the explosives detection performance of alternative system architectures with different feature extraction approaches.

A drawback of using information theory is that computing the measures requires knowledge of the underlying probability distributions of the features for different materials. Furthermore, exact computation

can only be conducted for small classes of distributions such as Gaussian, Poisson, or exponential models. An alternative approach uses machine learning and nonparametric techniques, such as kernel density estimation, to estimate the underlying probability distributions of the different material classes from sample values. Unfortunately, most of these nonparametric techniques result in densities for which the relevant information theory divergence measures cannot be computed in closed form. This requires Monte Carlo techniques, a process that can be slow and require many samples when the feature values are multidimensional.

In our work in Year 4, we adapted novel techniques in nonparametric statistics for estimating information-theoretic measures of explosives detection performance directly using graph techniques, avoiding the need to learn distributions. Our algorithms are graph-based estimators based on minimal spanning trees that compute an approximation to a particular *f*-divergence measure. This *f*-divergence can estimate bounds on the Fisher information as well as the Bayes error in binary classification [28]. Unlike many other divergence measures, this *f*-divergence can be estimated directly from data samples without generating estimates of the underlying distributions. In our paper [29], we describe a framework for performance estimation for novel threat detection systems using these performance bounds. We illustrate the framework by computing bounds on the Bayes error for a class of multi-spectral X-ray CT systems using photon-counting detectors with different energy quantization bins.

The use of photon-counting detectors, or with additional illumination spectra beyond two, raises the possibility of extracting more than two features for summarizing material properties. Previous work [1, 8, 27] has established that two features (such as photoelectric and Compton coefficients) are usually sufficient to represent the linear attenuation properties of materials with an effective atomic number below 14. However, this representation is inaccurate for many explosive materials, such as Baratol or lead styphnate, which have component elements with K-edges in the relevant energy range of the CT instruments (usually 30–120 keV). In Year 5, we explored the utility of additional basis representations when photon-counting detectors are used. We developed CT algorithms that can reconstruct the coefficients of the different materials in an image from multi-energy projection sinograms. These algorithms are extensions of the dual-energy approach in [1, 8, 17], using enhanced sparse optimization techniques and statistical methods. The idea is to select basis representations that capture the variability of the LACs in Figure 1 accurately.

Some of the potential basis representations that we explored are based on machine learning features. Given a database of materials with LACs, one can find basis functions using principal component analysis, and select the basis corresponding to the three to five largest principal directions, which typically capture most of the variability among the LACs of the different materials. If we separate the materials into explosives and non-explosives, we can choose basis functions with techniques from discriminant analysis, which can capture the primary differences between the explosive class and the non-explosive class. In particular, we explored the use of the sequential linear discriminant analysis basis suggested in [12]. As a final set of basis functions, we explored extensions of physical bases such as photoelectric and Compton, adding the linear attenuation functions of materials with K-edges in the 30–120 keV region. While this last set of bases may have more functions than spectra used for sinogram measurements, we used a sparse decomposition where the measured photon counts for each spectrum *k,* denoted by b^k and converted to log scale, are decomposed at each detector into sparse coefficients α for the basis using the following optimization:

$$\min_{\alpha} \sum_{k} || \ln(\int_{e \in S_k} w_k(e) e^{-B^T(e)\alpha} de) + \frac{\ln(b^k)}{\ln(I^k)} ||_2^2 + \lambda ||\alpha||_1$$

The resulting decomposition at each detector can be used to construct coefficient images, which provide the needed signals for explosives detection. Our results [15,30] established that this last set of basis functions

could be used to obtain accurate reconstructions of materials with high effective atomic numbers, provided their attenuation was small enough to allow for X-ray penetration.

The main focus of our Year 6 work was on transitioning selected multispectral algorithms developed in earlier years for use in commercial CT systems for Department of Homeland Security (DHS) missions. In particular, we focused on developing algorithms for a dual-energy air cargo CT inspection system developed by our industrial partner, Astrophysics Inc. The challenge was to develop reconstruction and feature extraction approaches that achieve enhanced resolution, reduce artifacts, and increase the accuracy of object recognition, as well as achieving real-time computation objectives so that the resulting algorithms become part of a fielded prototype system.

To enhance the resolution of the resulting dual-energy system, we developed a major improvement for the joint inversion approach, SPDE, that we had developed earlier in our program. In our paper [31], we improved on this approach by developing an edge-preserving total variation (EPTV) regularization algorithm that provides sharp boundary definition, even in regions where the materials are hard to observe. The main idea in this technique is to identify edges from an initial reconstruction, typically from the high energy image. We then define voxel-dependent regularization weights based on the magnitude of the gradient of the image. In two dimensions, these weights are defined as:

$$\mathbf{w}_v = \exp(-(|\mathbf{D}_v\mathbf{x}_{high}|)/\sigma) \quad \mathbf{w}_h = \exp(-(|\mathbf{D}_h\mathbf{x}_{high}|)/\sigma)$$

where D_v and D_h are the vertical and horizontal directional gradients, and σ is a scale parameter. Using these edge-dependent weights, the reconstructed photoelectric and Compton images are generated using a weighted total variation iterative reconstruction technique, as the solution of:

$$\hat{\mathbf{x}}_c = \underset{\mathbf{x}_c \geq 0}{\operatorname{argmin}} \frac{1}{2}||\mathbf{y}_c - \mathbf{A}\mathbf{x}_c||_2^2 + \tau_c||\mathbf{W}_h\mathbf{D}_h\mathbf{x}_c||_1 + \tau_c||\mathbf{W}_v\mathbf{D}_v\mathbf{x}_c||_1$$

$$\hat{\mathbf{x}}_p = \underset{\mathbf{x}_p \geq 0}{\operatorname{argmin}} \frac{1}{2}||\mathbf{y}_p - \mathbf{A}\mathbf{x}_p||_{\mathbf{W}_{yp}}^2 + \tau_p||\mathbf{W}_h\mathbf{D}_h\mathbf{x}_p||_1 + \tau_p||\mathbf{W}_v\mathbf{D}_v\mathbf{x}_p||_1$$

where the matrices W_v and W_h are defined by the weight coefficients derived from the initial reconstruction.

In Year 6 and 7, we continued our metal artifact reduction (MAR) work using deep neural networks, which we started in Year 5. One of the limitations of the MAR approach we developed in [14,15] was the large computation requirements. We have developed deep learning methods for artifact reduction in X-ray tomographic images. Many groups are applying conventional methods from computer vision to post-process images and are attempting to improve them. In contrast, we have focused on removing artifacts directly from tomographic projection data prior to image formation. The advantage of our approach is that it fits well into conventional data processing flows. In particular, once trained, applying a convolutional network to sinogram data can be very fast if it's followed by conventional FBP reconstruction. Thus, our method can plug into existing vendor processing workflows with little alteration. Further, it is much faster during evaluation than computationally intensive iterative methods.

C. Major Contributions

One of the major results of our work in Years 1 and 2 was the development of the SPDE reconstruction framework that generates a unified, joint estimate of the coefficient images for dual-energy CT. We implemented a 2D version of this frame and demonstrated results in reducing the artifacts in dual-energy photoelectric and Compton imagery on two representative slices using data generated for ALERT under Task Order 3 (TO3) [32].

In previous annual reports, we have detailed results of our experiments with this algorithm, documented in [11, 32]. Figure 2 shows results obtained from 95 kVp and 130 kVp data obtained from the Imatron C300 CT scanner under TO3. The top row shows the results of conventional reconstructions of the photoelectric and Compton coefficients. The presence of metal causes severe streaking in the photoelectric image and causes shading and intensity variation in homogeneous regions of the Compton image. Such light and dark streaking can lead to object splitting in subsequent segmentation and label tasks of an automatic target recognition, thus compromising threat identification. In contrast, the bottom row shows our SPDE method. The reduction of streaking artifacts is readily apparent, as is the improved uniformity of homogeneous object regions.

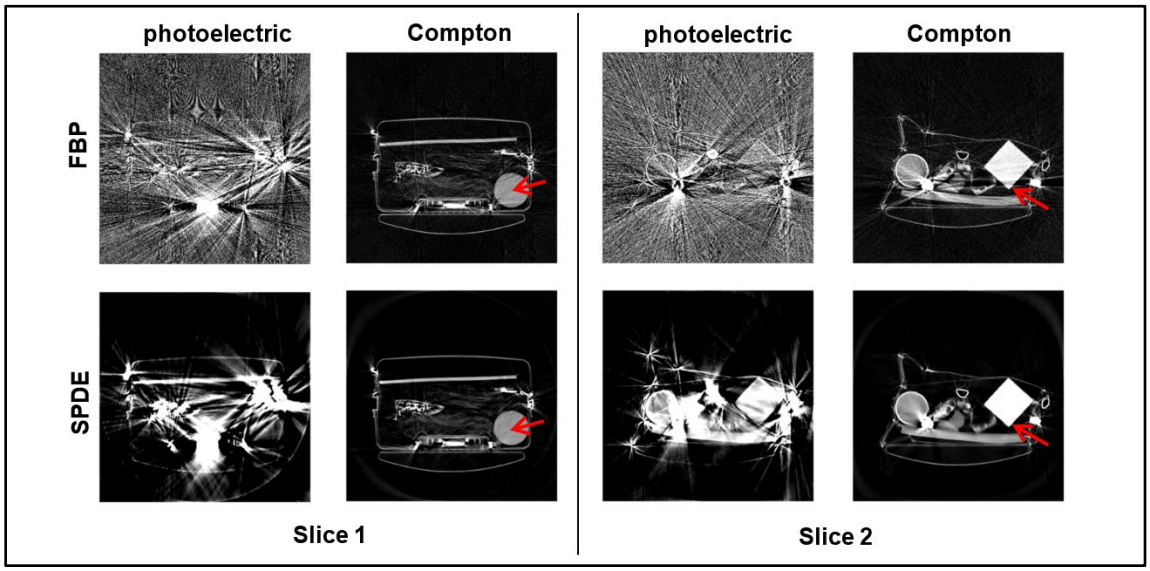

Figure 2: Two example slices from the Imatron data set for TO3; (top) conventional FBP-based photoelectric and Compton reconstructions based on decoupled processing. Severe streaking and shading due to metal are evident; (bottom) new SPDE reconstructions. Reduction of streaking and improved uniformity of object regions are demonstrated.

Another major result of our efforts from Years 2 and 3 was the learning-based joint segmentation and classification algorithm, LOIS, documented in [10-12]. In Year 4, these results were extended to a patch-based formulation to account for spatial correlations in voxel values [14]. To illustrate the improvements of the patch-based LOIS over the voxel-based LOIS algorithm, we tested both algorithms on some of the dual-energy reconstructions obtained from the TO3 dataset [32]. This data was collected on the Imatron scanner with two different peak voltages, 135 kV and 95 kV. Based on multiple images, we trained both a single-pixel appearance model and a 2×2 patch-based appearance model. The improvements are documented in [14].

Another result in Year 4 was the development and implementation of the ADMM-based framework for discrete tomography that we term TOMO-SPL [19-21]. The variable splitting used in this framework breaks the original problem into subproblems that allow for the use of very efficient graph-cut methods, but more importantly, the overall solution method is very robust to data imperfections, as we illustrate next. Figure 3 demonstrates the results of using our discrete tomography algorithm on an extremely sparse angle tomography problem with only eight projections, a very limited-angle problem. The phantom is binary valued. The results show that TOMO-SPL has enhanced accuracy over the alternatives based on gray-scale reconstruction followed by discretization.

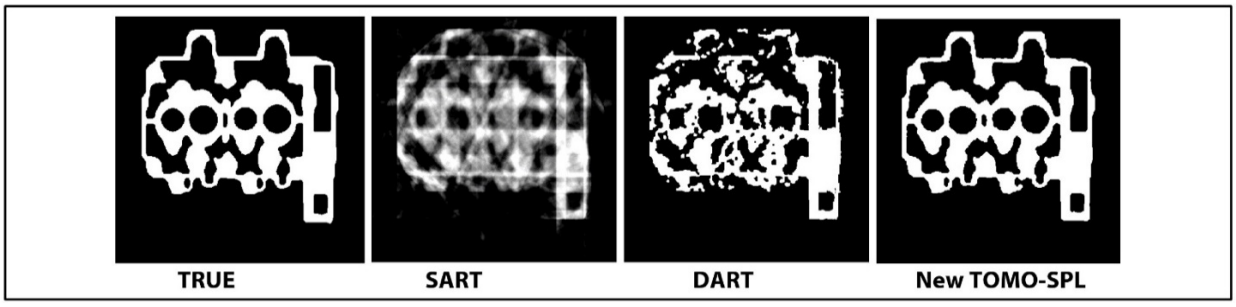

Figure 3: Comparison of results with only eight projections: True is the true field; SART is a conventional thresholded reconstruction based on the SART method; DART is the popular "discrete algebraic reconstruction tomography" method; and TOMO-SPL is our new method. Our new method produces nearly perfect reconstructions even from extremely limited data.

Note that TOMO-SPL preserves the connectivity between regions, prevents splits, suppresses noise, and maintains boundaries. These characteristics would prove valuable for use in new scanner geometries that use limited-angle sensing for speed, size, or power reasons.

Other results in Year 4 included the new approach for MAR documented in [15,26]. The approach combines aspects from dictionary learning together with random sampling to provide enhanced reconstructions in regions with significant metal presence. We tested the algorithms both on simulated data, as well as data obtained from the Imatron scanner with significant metal presence. A key aspect of our algorithm is that it tries to preserve the information in projections that pass through metal regions. In simulated experiments, the average reconstructed attenuation coefficient in regions enclosed by metal was far more accurate than in competing algorithms in the literature.

Another result in Year 4 was our work on performance bounds for detection performance of CT systems using nonparametric statistics. The key concept in our results, as explained in [28,29], is to simulate representative measurements from different materials and reconstruct features as points in n-dimensional space. By computing a minimum spanning tree using Euclidean distances for those points, one computes a statistic—namely the fraction of arcs in the minimum spanning tree that connect a point in one class (explosives) to a point in the other class (non-explosives). This statistic converges to an f-divergence that can be related to upper and lower bounds on the probability of error in detection.

To evaluate our techniques, we constructed a database of 320 materials, with 124 explosives and 196 non-explosives. For each of these materials, we obtained LAC information from National Institute of Standards and Technology models and used this to generate representative LACs as a function of X-ray energy. We then simulated measurements generated by photon-counting detectors with counts aggregated to varying numbers. As features, we reconstructed the average LACs in each detector energy bin. We also simulated measurements for a dual-energy system using photoelectric and Compton basis reconstructions. Our results are reported in the paper [29].

In Year 5 and continuing into Year 6 and 7, we developed deep learning methods for artifact reduction in X-ray tomographic images. Our techniques are focused on removing artifacts directly from tomographic projection data prior to image formation. Once trained, applying a convolutional network to sinogram data can be very fast, making our method suitable for transition, as it is much faster than alternative MAR techniques.

An overview of the approach is shown in Figure 4. We train a fully convolutional network to effectively remove metal artifacts in stream of commerce sinograms, conventionally reconstruct the output, and then

add the metal back in. By using modern conventional networks together with generalized adversarial learning [33], we can apply the network to the entire sinogram and not be limited to small patch-based processing, as some existing methods are. Since obtaining matched pairs of real sinograms for training is challenging, instead, we generate synthetic pairs by coupling a physically accurate X-ray simulator with a bag generator and then augment this synthetic data with modest real measurements via transfer learning.

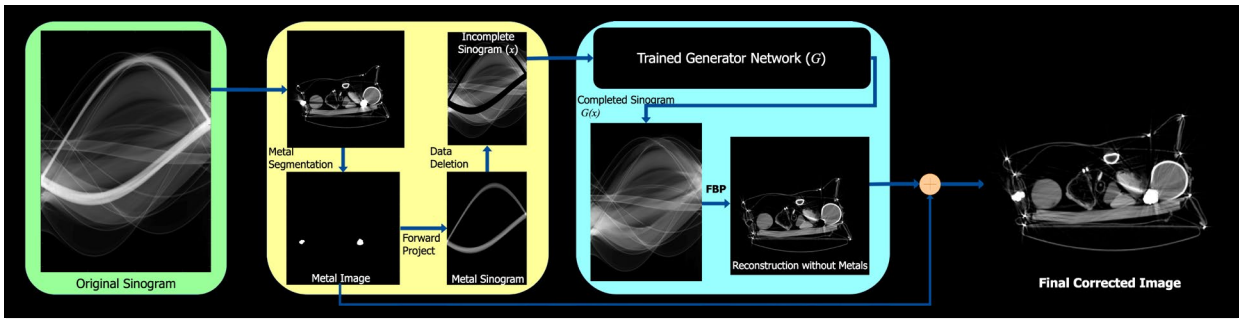

Figure 4: Overview of deep network MAR process.

We show some results in Figures 5 and 6. We compare our novel conditional generative adversarial network (CGAN) method with traditional linear interpolation and weighted nearest neighbor MAR methods. These preliminary results focus only on suppression of artifacts from large metal objects; they have not been optimized. Further results can be found in our papers [34-38]. In Year 6, we further developed these initial results scaling up the training as well as testing of the method. The method was also extended to sparse angle and low-dose tomography problems, where sinogram angular coverage is limited.

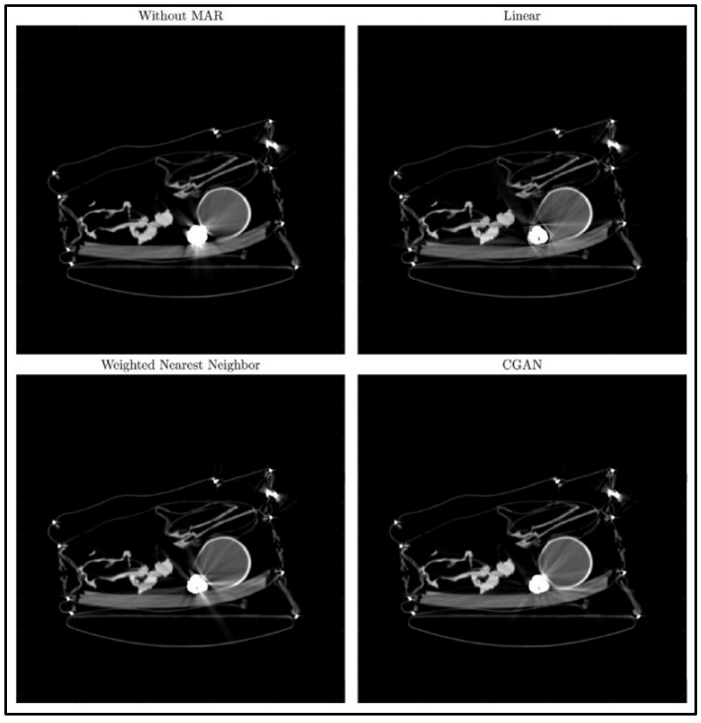

Figure 5: Comparison of MAR techniques for two slices of different suitcases with metal: (top left) original reconstruction; (top right) linear interpolation; (bottom left) weighted nearest neighbor algorithm; and (bottom right) reconstruction using our convolutional network MAR.

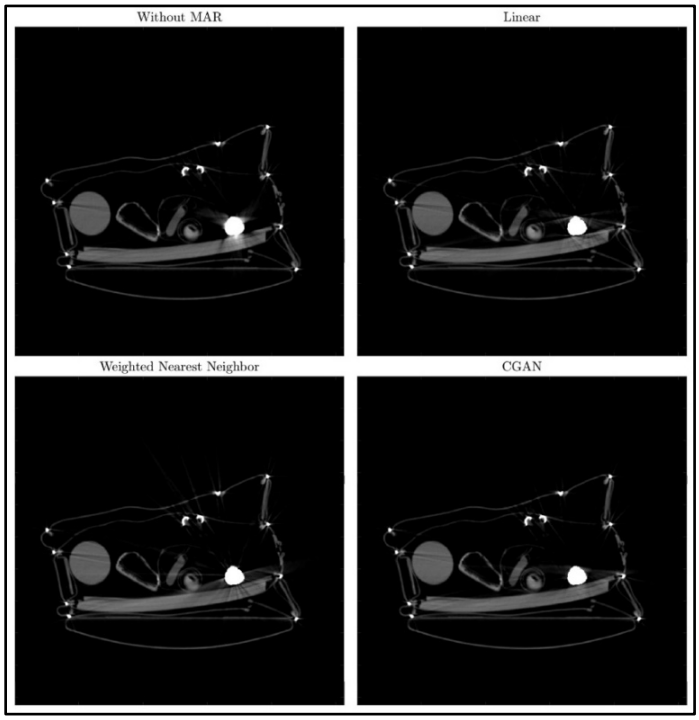

Figure 6: Comparison of MAR techniques for two slices of different suitcases with metal: (top left) original weighted nearest neighbor algorithm; (top right) linear interpolation; (bottom left) weighted nearest neighbor algorithm; and (bottom right) reconstruction using our convolutional network MAR.

In Year 5, we developed new multispectral CT algorithms that use more than two spectra and use a new class of basis functions that can accurately represent energy-dependent X-ray transmission characteristics in few dimensions. Current approaches for dual-energy decomposition use basis functions such as photoelectric and Compton cross-sections that have a continuous dependence on energy. However, many materials of interest—including explosives such as Baratol, where the LAC has discontinuities in energy due to the presence of atoms that include K-edges in the relevant energy region of the excitation—are used as contrast agents in medical imaging [39–41] precisely because their X-ray attenuation increases at specific energies that can be identified using multispectral CT imaging. However, medical imaging approaches for multispectral CT have been limited to direct imaging of each spectral signature separately, avoiding basis decompositions.

One of our main contributions is the development of a new class of basis functions that can represent the LACs of complex materials that include atoms with K-edges in the region of interest. Figure 7 illustrates the LAC of Baratol versus energy, with a discontinuity in energy arising because of the K-edge of barium around 38 keV. As the figure indicates, the LAC of Baratol is poorly approximated using a photoelectric-Compton basis, and imaging with dual-energy systems in this basis leads to Baratol being classified as iron.

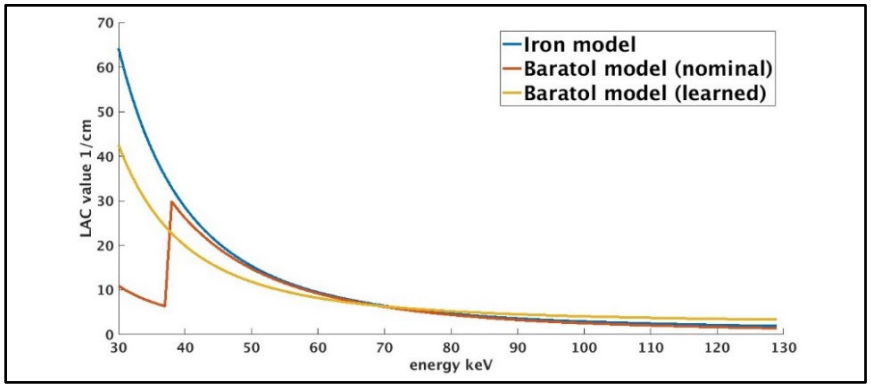

Figure 7: LAC of Baratol versus energy (red); best approximation using photoelectric and Compton basis (orange); and material that is confused with Baratol when using dual-energy CT (blue).

To address this problem, we investigated several approaches at modifying the set of basis functions used for multispectral imaging systems. Specifically, we introduced a new basis transform, termed SPECK, which is a short form for "sparse photoelectric, Compton, and K-edge basis." The first two basis functions in the transform are the photoelectric and Compton basis functions. To these two functions, we added the LAC functions of the atoms that have K-edges in the energy range 30–130 keV. Note that these other basis functions are linearly independent from the first two bases and each other because they have discontinuities at different energy values. However, the number of basis functions K can be larger than the number of spectral measurements in each detector, so we developed a different approach to estimate the decomposed measurements. Specifically, we proposed sparse regression techniques, where the decomposed measurements $A_L^1,\ldots, A_L^K$ are obtained for each detector by solving:

$$[A_L^1,\ldots,A_L^K] = \arg\min_{\underline{A}\geq 0} \sum_{i=1}^{I} (c_L^i - g^i(\underline{A}))^2 + \lambda \sum_{i=1}^{K} |A^i|$$

for a parameter λ that controls the desired level of sparsity in the coefficient vector. The details of this algorithm can be found in [15, 30].

We also developed a multispectral CT reconstruction algorithm that takes the estimated coefficient sinograms from the previous equation and constructs coefficient images in the volume of interest. We implemented a joint reconstruction and recognition algorithm and tested it on simulated data from a multispectral system photon-counting detectors with ten energy bins in the energy range of 30–130 keV. The reconstructed coefficient images were used to recognize the type of material in each region. We compared the performance of the multispectral algorithms using the SPECK basis decomposition, the photoelectric-Compton basis decomposition, reconstruction of the average LAC in each energy bin, and a data-driven basis derived from principal component analysis of a large set of materials. The results in Table 1 show that the multispectral CT with the SPECK basis significantly outperformed the alternatives in material recognition.

Algorithm	Region Classification Accuracy
SPECK coefficients	86.7%
PEC coefficients	75.0%
Direct LAC reconstruction	65.6%
PCA (6 coefficients)	61.6%

Table 1: Material recognition performance for multispectral CT experiments using different basis decompositions.

We also performed a set of experiments to recognize whether a material was an explosive or not using the same basis functions. In these experiments, we trained a random forest classifier on a set of 80 training images containing multiple materials, and then we tested the classification performance on a set of 20 test images. We ran the experiments with different regions of responsibility around each material, where larger regions (10%) indicated a range of 10% variability from the nominal LAC of each material in the test data. The resulting performance is shown in Table 2. The use of the SPECK basis improved explosives detection performance. Furthermore, the performance of the detection algorithms using the SPECK transform exhibited little degradation with increased region of responsibility, unlike the results for other algorithms.

Algorithm	Accuracy (0% variability)	Accuracy (5% variability)	Accuracy (10% variability)
Pho/Compton	94.1%	90.055	89.5%
PCA-6	04.8%	86.0%	83.0%
SPECK	99.4%	96.0%	96.0%
Direct Recon	94.1%	88.8%	85.0%

Table 2: Explosives detection performance for multispectral CT experiments using different basis decompositions.

The final set of results in Year 5 was the development of a novel approach toward joint CT reconstruction, segmentation, and identification. This can be viewed as a significant generalization of our work on discrete CT discussed earlier. In discrete CT, the underlying volume being imaged is composed of regions with constant LACs, and the imaging model is assumed to be linear. In our model, the underlying volume is composed of regions with constant material types, where the LACs of material types can vary within each region and will be energy dependent, as is the case when using Bremsstrahlung X-ray sources. As such, the corresponding imaging model is nonlinear, as discussed earlier.

The resulting algorithm, termed JRIDE (for "joint reconstruction and identification"), is illustrated in Figure 8. The basis decomposition sinograms are inputs to the algorithm. JRIDE reconstructs basis coefficient images as well as the material labels for the different regions in the image.

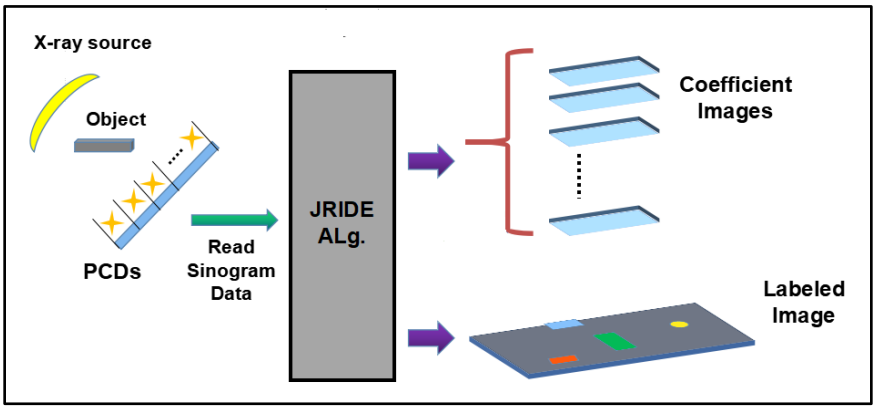

Figure 8: Structure of JRIDE algorithm.

The details of the JRIDE algorithm can be found in [15,42]. JRIDE performs a maximum a posteriori estimate of both the coefficient images as well as the underlying region labels. As such, the problem is posed as a joint optimization over region labels Z and coefficient images W:

$$(W^*, Z^*)(V) \in \arg\min_{W,Z} \frac{1}{2} \sum_{j=1}^{N_v d_c} (\hat{\mathbf{v}}_j - (M_j W)^T)^T \Sigma_j^{-1} (\hat{\mathbf{v}}_j - (M_j W)^T) + \beta \sum_{i=1}^{N_p} \sum_{i' \in \mathcal{N}(i)} ||\mathbf{w}(i) - \mathbf{w}(i')||^2$$

$$+ \sum_{i=1}^{N_p} \frac{1}{2} [(\mathbf{w}(i) - \mathbf{g}_{\ell(i)})^T \Gamma_{\ell(i)}^{-1} (\mathbf{w}(i) - \mathbf{g}_{\ell(i)}) + \log(\det(\Gamma_{\ell(i)})] + \gamma \sum_{i=1}^{N_p} \sum_{i' \in \mathcal{N}(i)} 1_{\ell(i) \neq \ell(i')}$$

The minimization is broken into overlapping minimizations, where given the coefficient image reconstructions W, one finds the best segmentation and material labels for regions Z (a discrete optimization) using an efficient multilabel graph cut algorithm [13]. Subsequently, given the region segmentation and

material labels, the coefficient images can be reconstructed as a continuous optimization problem where the coefficient reconstructions in each segmented region should be consistent with the region's material label.

Our JRIDE algorithm is similar in intent to a recent algorithm proposed for medical imaging in [43], named JE-MAP. The major differences between JRIDE and JE-MAP are twofold: first, JRIDE is based on a rigorous probabilistic maximum a posteriori framework; and second, JRIDE uses an efficient discrete optimization algorithm that is orders of magnitude faster than the corresponding algorithm used in JE-MAP. We evaluated our algorithm, JE-MAP, and an algorithm based on the conventional reconstruction, then we segmented and sequence classified the algorithms using a set of phantoms with 54 different materials present. The results are shown in Table 3. The JRIDE algorithm outperforms JE-MAP significantly, indicating the advantages of using a correct and rigorous probabilistic framework for the joint reconstruction and material identification problem. The results also indicate that there is significant improvement in material identification performance when material properties are used in an integrated manner with reconstruction, as indicated by the difference in performance between the sequential and JRIDE algorithms.

Algorithm	Region Classification Accuracy, No K-Edge Materials	Region Classification Accuracy, All Materials
JRIDE	100.00%	91.66%
Sequential	85.41%	83.33%
JE-MAP	56.25%	47.25%

Table 3: Material identification performance for JRIDE versus alternative algorithms.

The main focus of our Year 6 work was transitioning some of the multispectral algorithms developed in earlier years for use in commercial CT systems for DHS missions. We focused on developing algorithms for a dual-energy air cargo CT inspection system developed by our industrial partner, Astrophysics Inc. The specific prototype system we focused on is known as the Multi-View CT (MVCT) Cargo System. The system is designed as a noninvasive inspection method for the screening and detection of contraband and explosives in cargo skids at ports of entry. In 2017, the system was demonstrated in government trials using some of the single-energy reconstruction algorithms developed in our earlier work. The system has been deployed at J.F.K. International Airport in New York [44]. However, the current algorithms need improved processing to reduce imaging artifacts due to effects of beam hardening, photon starvation, and noise. In addition, the system reconstructs each spectrum independently, leading to a fundamental loss in resolution.

To enhance the resolution of the resulting dual-energy system, we developed a major improvement for the joint inversion approach SPDE that we had developed earlier in our program, described earlier. This approach, EPTV regularization, is described in our paper [31]. Figure 9 shows the differences between the standard FBP reconstruction, the SPDE reconstruction, and our new EPTV reconstruction on two slices of a bag containing metal objects. As the figure indicates, the EPTV reconstructions do a better job of localizing the difficult reconstruction of photoelectric absorption when compared with the SPDE reconstruction. Both reconstructions are far superior to that obtained from filtered back-projection. Our EPTV algorithm can also be applied to single-spectrum reconstructions. We have done a prototype implementation for the Astrophysics MVCT instrument for single-spectrum reconstructions, and we are evaluating the enhancement in resolution in that limited-angle reconstruction scenario.

As the results in Figure 9 indicate, reconstructing photoelectric absorption is a challenging problem in the presence of metal because the majority of the low energy photons that carry the most information about photoelectric absorption fail to reach the detectors. In collaboration with Lawrence Livermore National Laboratory (LLNL), we have explored alternative approaches for basis decomposition that are more suitable

for higher energy systems and provide more stable features in the presence of metal. In particular, we have been using a synthetic monoenergetic basis decomposition which is derived from the photoelectric absorption and Compton scatter basis functions. Figure 10 shows the reconstruction obtained using the EPTV algorithm with the photoelectric and Compton basis functions, versus the synthetic monoenergetic basis (SMB) functions. As the figure indicates, the reconstructions with SMB basis functions at low energies are much more stable than the photoelectric reconstructions, as each of the basis functions can be estimated using the high-energy photons that are more likely to reach detectors in the presence of metal. A significant advantage of SMB features is that there are analytical methods for estimating the effective atomic number Z_{eff} and the electron density ρ_{eff}, which are features that allow for system-independent material characterization [27].

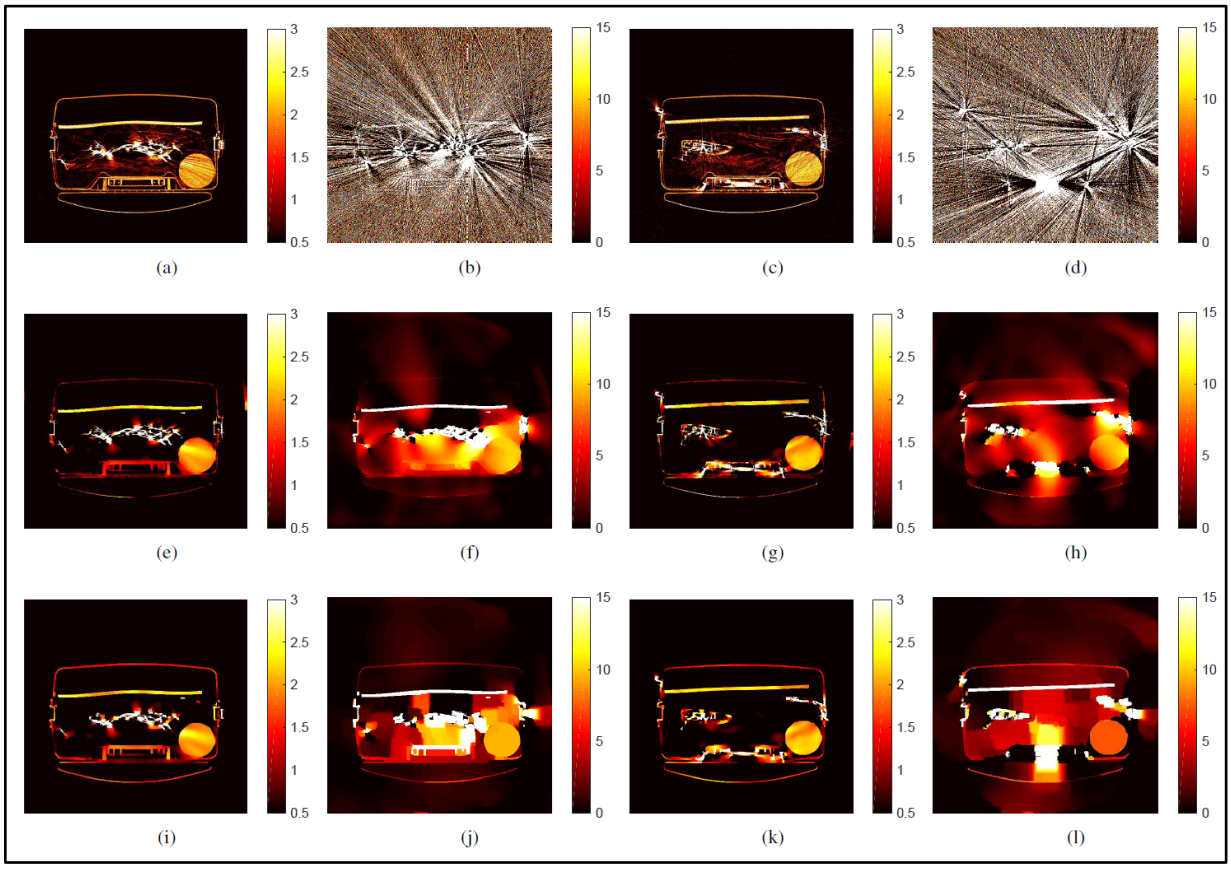

Figure 9: Reconstruction of two slices for container with metal. FBP reconstructions are shown with (a, c) Compton coefficients and (b, d) photoelectric coefficients. SPDE reconstructions are shown with (e, g) Compton coefficients and (f, h) photoelectric coefficients. EPTV reconstructions are shown with (i, k) Compton coefficients and (j, l) photoelectric coefficients.

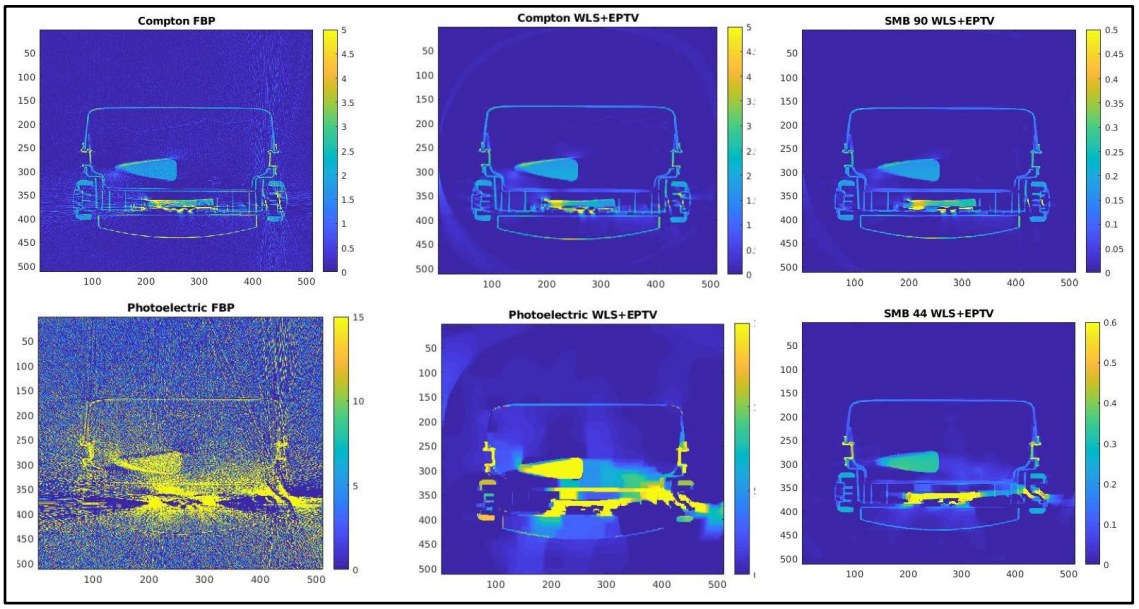

Figure 10: (left) FBP of Compton and photoelectric, (center) EPTV of Compton and photoelectric, and (right) SMB of high and low reconstructions.

In our final Year 7 work, the data-domain deep learning methods were extended to seamlessly include learned image models in a modular framework allowing for improved reconstruction even for very challenging problems. This new framework, called DIP-MIR, combines learned prior models for data and image using consensus equilibrium, as shown in Figure 11.

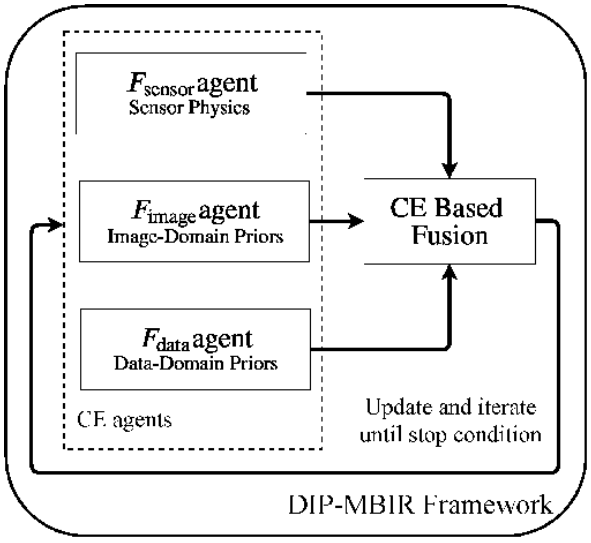

Figure 11: Consensus equilibrium-based framework for inclusion of deep learning of both data and image behavior.

Results from an extremely limited data reconstruction example using 90 degrees worth of data are shown in Figure 12, comparing a state-of-the-art deep network post-processing method to the new integrated approach.

Quantitative metrics in Table 4 confirm the visually apparent improvements provided by the new deep learning framework.

Method	RMSE	PSNR	SSIM
FBP + deep post-processing	103	23.32	0.48
PnP – MBIR existing model based	78	25.65	0.79
New DIP – MBIR deep learning based	51	29.50	0.87

Table 4: Reconstruction performance comparison of different methods in Figure 12.

In Year 7, we continued our transition work for dual-energy imaging with applications to cargo screening. A fundamental issue that arose in the transition effort is that material identification was that the presence of metal in cargo introduced significant artifacts that limited material recognition. We explored approaches for enhancing material recognition in the presence of metal artifacts. In our earlier work, we had developed techniques for compensating for metal artifacts that improved image quality. However, the improved quality often translated into erroneous material recognition, as the sonogram interpolation techniques modified the reconstruction parameters used for recognition.

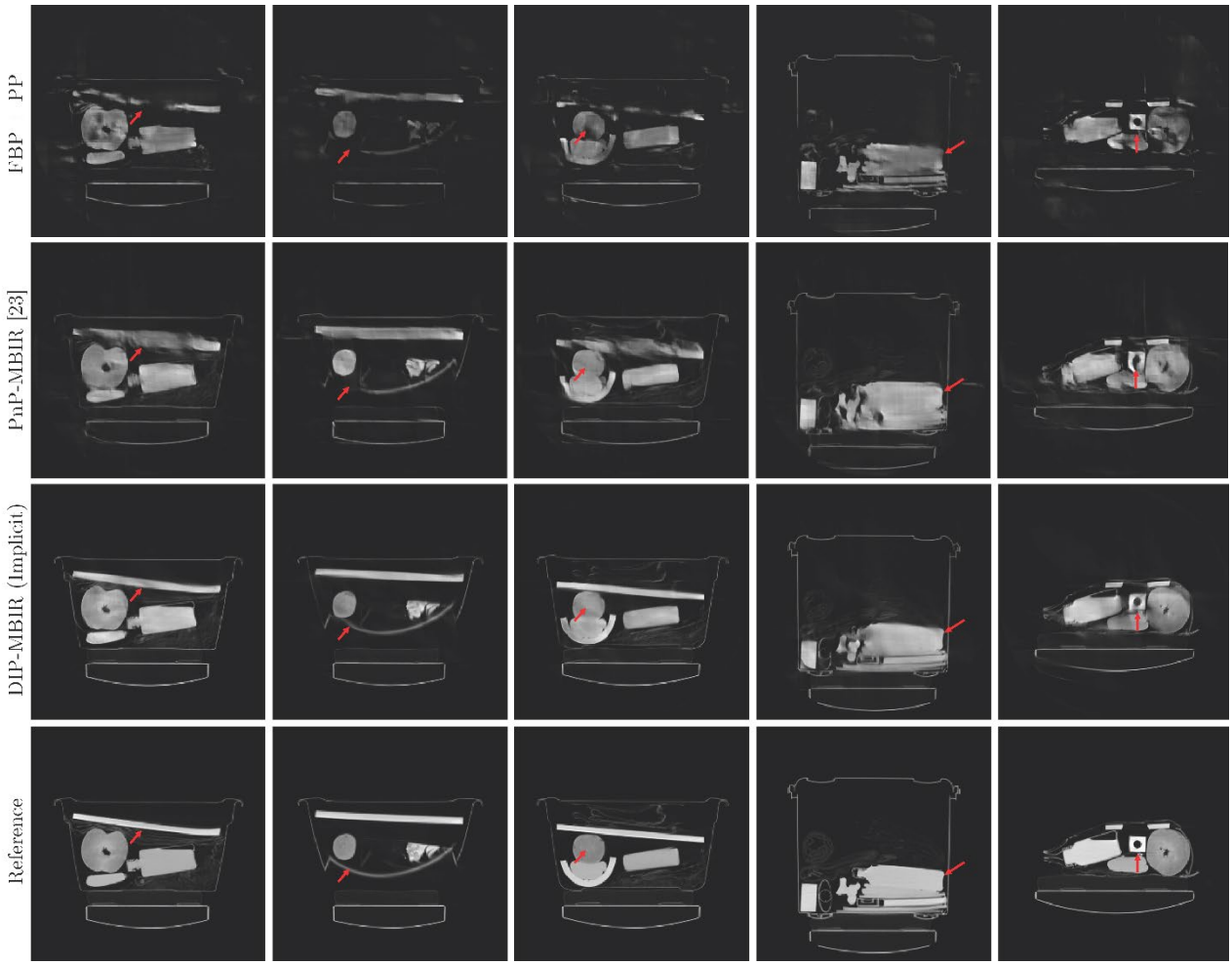

Figure 12: (top row) State-of-the-art deep-learning post-processing and (second row) model-based reconstruction compared to (third row) the new integrated consensus equilibrium-based deep-learning framework and (bottom row) ground truth for a challenging limited-angle tomographic reconstruction problem.

We conducted an in-depth study to determine whether the choice of basis functions in dual-energy reconstructions can mitigate the distortion in material recognition when metal is present. We explored the use of photoelectric and Compton basis (PCB) functions, synthesized monochromatic basis (SMB) functions, and material basis (MB) functions composed of polystyrene and aluminum for reconstruction. Using the reconstructed coefficient images, we generated estimates of effective atomic number and density. We simulated phantoms with regions of homogeneous materials between two copper sheets. The materials used in the simulations included a range of effective atomic number and electron density materials: polypropylene, citric acid, water, sapphire, magnesium, aluminum, black powder, hydrochloric acid, and, calcium chloride. For all cases, we conducted reconstructions using two different algorithms: total-variation (TV) and EPTV, with phantoms with and without metal present.

The results are shown in Table 5. The table depicts the averages of relative mean absolute errors for effective atomic number Z_e and electron density ρ_e across all materials. The results indicate two preliminary conclusions. First, reconstruction with EPTV results in enhanced accuracy for estimation of material properties for all three basis decompositions. The improvements were critical in the presence of metal, where the standard TV reconstruction techniques resulted in sizeable parameter errors, whereas the EPTV reconstructions led to much more accurate parameter estimates for all basis functions. The second conclusion is that material basis reconstructions may generate more robust material property estimates in the presence of metal. These preliminary conclusions require further experimentation with more complex phantoms for validation.

Mean error (%)	Directly from PCB		Sampled LAC from PCB		Sampled LAC from MB		Directly from SMB	
	Z_e	ρ_e	Z_e	ρ_e	Z_e	ρ_e	Z_e	ρ_e
TV (without metal)	0.71	0.75	0.72	0.55	0.99	0.86	0.72	0.65
EPTV (without metal)	0.43	0.56	0.42	0.18	0.98	0.74	0.41	0.24
TV (without metal)	49	2.7	49	33	52	66	40	29
EPTV (without metal)	11.8	1	11.7	0.8	2.4	3.9	5.4	4.8

Table 5: Average error in estimates of effective atomic number Z_e and electron density ρ_e across all materials, when imaged in the presence of metal and without metal.

The above results did not include any explicit sinogram correction to remove metal artifacts. Instead, they relied on the joint reconstruction algorithms to generate accurate coefficient images in the regions of interest. Most sinogram correction techniques have been developed for single energy spectrum systems and reduce artifacts such as metal blooming and streaking, as evidenced in our results in Figures 5 and 6. However, for material recognition, it is important to correct metal artifacts in multispectral images consistently and to estimate accurately the properties of the materials in the region. In Year 7, we conducted an investigation into developing dual-energy algorithms for material property estimation in the presence of metal. We explored approaches that apply dual-energy sinogram correction techniques for MAR prior to basis decompositions, as well as approaches that apply sinogram correction techniques after basis decomposition to the coefficient sinograms. We also explored algorithm variations to down-weight the accuracy of projections that include significant metal content. This is ongoing work that will be completed in the summer of 2020.

Our initial results [45] are shown in Table 6, for two phantoms with significant metal content and four materials of interest: water, nylon, citric acid, and aluminum. In these algorithms, we used both a PCB basis decomposition and a material basis decomposition using aluminum and polystyrene. The results are encouraging; we are able to estimate the effective atomic number and the electron density of materials within 1.5% of their true values using either of the two basis decompositions. Our goal this summer is to transition

these algorithms to work with cargo skids that contain boxes with some metal content, showing that we can generate accurate material property estimates.

Scatter v3	Effective Atomic Number		Effective Electron Density	
	Pho-Comp	Material	Pho-Comp	Material
Aluminum	0.07%	0.68%	0.19%	0.47%
Water	1.52%	2.10%	0.59%	0.80%
Citric Acid	0.53%	0.39%	0.23%	0.20%
Nylon	0.37%	0.46%	0.22%	0.15%
Average	0.62%	0.90%	0.31%	0.40%

Scatter v5	Effective Atomic Number		Effective Electron Density	
	Pho-Comp	Material	Pho-Comp	Material
Aluminum	0.00%	0.66%	0.05%	0.42%
Water	0.79%	0.35%	1.18%	1.74%
Citric Acid	1.88%	1.24%	3.63%	3.61%
Nylon	0.25%	0.32%	0.29%	0.29%
Average	0.73%	0.64%	1.29%	1.51%

Table 6: Average percent error in estimates of effective atomic number Z_e and electron density ρ_e across four materials, with two phantoms, when imaged in the presence of metal. The reconstruction algorithms use the EPTV algorithms with basis decompositions using either PCB or MB bases.

D. Milestones

Major milestones achieved to date include:

- Extended integrated segmentation and labeling framework from 2D to 3D.
- Developed and implemented performance prediction framework.
- Developed ADMM-based discrete tomography methods.
- Fused the artifact mitigation reconstruction and the integrated labeling frameworks into a discrete tomography framework, resulting in the JRIDE algorithm.
- Incorporated dictionary-based representations for multi-energy tomographic inversion and material characterization, resulting in the SPECK feature basis and associated reconstruction algorithms.
- Extended the SPDE framework to multi-energy sensing and from 2D to 3D using the SPECK basis.
- Developed and evaluated extensions of deep learning techniques for MAR in CT systems.
- Developed fast GPU versions of multi-energy CT algorithms for transition to cargo and checkpoint CT systems.
- Developed EPTV joint reconstruction for enhanced resolution.
- Developed multi-spectral CT reconstruction techniques using synthetic measurement bases.
- Transitioned reconstruction algorithms into a prototype MVCT cargo skid scanner, developed by Astrophysics Inc.
- Evaluated performance of multispectral CT algorithms with experimental data in collaboration with LLNL using multispectral micro-CT systems.
- Transitioned multispectral CT algorithms to LLNL through reports for potential integration into Livermore Tomography Tools.
- Developed and evaluated extensions of deep learning techniques for limited-angle CT reconstruction.
- Developed and evaluated new framework for inclusion of deep learning models of data and images for challenging data CT reconstruction problems.

- Developed fast, enhanced resolution versions of multispectral CT algorithms and transitioned to cargo CT systems.
- Evaluated performance of multispectral CT algorithms in prototype cargo system for material recognition.
- Developed approaches for multispectral CT material property recognition in the presence of significant metal content and transitioned them to cargo CT systems.

E. Final Results at Project Completion (Year 7)

This project developed methods to improve imagery for explosives detection and restricted object detection in X-ray-based sensing for checked luggage, checkpoints, and air cargo skids. Furthermore, it developed algorithm technology that takes advantage of new developments in sensor technology, which will enable future systems to address emerging threats, and integrated emerging concepts in machine learning. In Years 6 and 7, some of these reconstruction technologies were transitioned to a commercial cargo screening system. Over the life of the project, new algorithms and methods were developed that provided improvement over conventional methods of reconstruction for mono- and multi-energy X-ray CT scans. These algorithms provide the foundation for future CT systems that use multi-spectral excitation to obtain robust signatures for material identification.

III. RELEVANCE AND TRANSITION

A. Relevance of Research to the DHS Enterprise

The improved artifact suppression methods enhance image quality, object boundary and volume estimates, and object localization. The direct discrete inversion approaches make better use of existing measurements, allowing for better detection. The multispectral CT algorithms can provide enhanced information for discriminating complex, higher effective atomic number explosives better than conventional dual-energy systems, increasing the probability of detection and resulting in fewer false alarms for both checkpoint and checked-luggage systems. The deep learning-based inversion frameworks allow for greatly improved imagery for challenging imaging problems. The multispectral material property reconstruction algorithms that work robustly in the presence of metal provide the foundation for automated threat recognition algorithms that can work in difficult luggage and cargo screening scenarios.

Overall, these methods can increase the probability of detection as well as reduce the number of false alarms, which can, in turn, reduce the need for on-screen anomaly resolution protocol (OSARP) and manual inspection. These concerns will grow as the use of multi-spectral X-ray scanning increases at the checkpoint.

B. Status of Transition at Project End

The most significant transition of this work has been in collaboration with Astrophysics Inc., where we have transitioned subsets of the developed algorithms to a fielded air cargo skid scanner. Algorithms transitioned include several dual-energy reconstruction algorithms for limited angle CT, including edge preserving regularization as well as enhanced material property reconstruction algorithms in the presence of metal for improved automated threat recognition. While several algorithms have been transitioned, additional modifications are in progress as our partner Astrophysics Inc. adds operational requirements for their instrument.

C. Transition Pathway and Future Opportunities

In developing next-generation reconstruction algorithms, we have engaged in extensive discussions with potential transition partners. However, upgrading software in certified instruments is seldom desirable unless there are new requirements that the instrument must satisfy. Hence, we focused our attention on vendors developing new instruments. Our industrial partner, Astrophysics Inc., was developing a novel limited-field-of-view, dual-energy CT scanner for cargo skids and needed algorithms that significantly extended the state of the art for this design. We focused much of our transition work on this direction, and our algorithms have been at the heart of the CT reconstruction used in Astrophysics's Multi-View CT Cargo Scanner. We have continued our discussions with other vendors, looking for new opportunities for transitioning our algorithms.

D. Customer Connections

- Francois Zayek, Astrophysics Inc., ALERT industrial partner, met weekly.
- Harry Martz and Kyle Champley, LLNL, met twice per month.
- Ronald Krauss and Robert Kleug, DHS, met occasionally.

IV. PROJECT ACCOMPLISHMENTS AND DOCUMENTATION

A. Education and Workforce Development Activities

1. Student Internship, Job, and/or Research Opportunities
    a. Ms. Devadithya will be an intern at Lawrence Livermore National Laboratory in the Materials Research Institute working under Dr. Harry Martz. Her internship was delayed until Sept. 2020 because of Livermore workplace restrictions due to the COVID-19 virus.

B. Peer Reviewed Journal Articles

1. Ghani, M.U., & Karl, W.C. "Fast Enhanced CT Metal Artifact Reduction Using Data Domain Deep Learning." *IEEE Transactions on Computational Imaging*, *6*, 27 August 2019, pp. 181–193. https://doi.org/10.1109/TCI.2019.2937221.

Pending –

1. Ghani, M.U., & Karl, W.C. "Integration of Data and Image Priors for Image Reconstruction Using Consensus Equilibrium." Submitted to *IEEE Transactions on Computational Imaging.*

C. Peer Reviewed Conference Proceedings

1. Ghani, M.U., & Karl, W.C. "Integrating Data and Image Domain Deep Learning for Limited Angle Tomography Using Consensus Equilibrium." *IEEE Conference on Computer Vision*, Seoul, Korea. 22 October–2 November 2019.
2. Ghani, M.U., & Karl, W.C. "Integrating Learned Data and Image Models through Consensus Equilibrium," in *Computational Imaging*, Bouman, C.A., & Sauer, K., editors, *Process of Electronic Imaging*, Burlingame, CA. 26–30 January 2020.
3. Ghani, M.U., & Karl, W.C. "Integrating Learned Data and Image Models through Consensus Equilibrium for Model-Based Image Reconstruction." *International Symposium on Biomedical Imaging*, Iowa, IA. April 2020.

4. Devadithya, S., & Castañón, D. "Material Identification in Presence of Metal for Baggage Screening," in *Computational Imaging*, Bouman, C.A., & Sauer, K., editors, *Process of Electronic Imaging*, Burlingame, CA. 26–30 January 2020.

D. Other Presentations

1. Karl, W.C. "Data and Image Domain Deep Learning for Tomographic Computational Imaging." Invited talk in *Institute for Mathematics and its Applications Workshop on Computational Imaging*, 14–18 October 2019.

E. Student Theses or Dissertations Produced from This Project prior to Year 7

1. Chen, K. "Reconstruction Algorithms for Multispectral Diffraction Imaging." PhD Thesis, electrical engineering, Boston University, May 2014.
2. Eger, L. "Enhanced Information Extraction in Multi-Energy X-Ray Tomography for Security." PhD Thesis, electrical engineering, Boston University, May 2014.
3. Tuysuzoglu, A. "Robust Inversion and Detection Techniques for Improved Imaging Performance." PhD Thesis, electrical engineering, Boston University, May 2014.
4. Babaheidarian, P. "Algorithms for Enhanced Artifact Reduction and Material Recognition in Computed Tomography." PhD Thesis, electrical engineering, Boston University, May 2018.
5. Sun, Z. "Reduced and Coded Sensing Methods for X-Ray Based Security." PhD Thesis, electrical engineering, Boston University, September 2016.

Pending –

1. Ghani, M.U. "Data and Image Domain Deep Learning for Tomographic Computational Imaging." PhD Thesis, electrical engineering, Boston University, in progress—expected completion December 2020.
2. Devadithya, S. "Enhanced Reconstruction and Material Recognition in X-Ray CT for Security Applications." PhD Thesis, electrical engineering, Boston University, in progress—expected completion May 2021.

V. REFERENCES

[1] R. E. Alvarez and A. Macovski, "Energy-selective reconstruction in X-ray computerized tomography," *Physics in Medicine & Biology, vol. 21, no. 5,* 11976, pp. 733–744.

[2] A. C. Kak and M. Slaney, "Principles of Computerized Tomographic Imaging," Society of Industrial and Applied Mathematics, 2001.

[3] J. A. Fessler, I. A. Elbakri, P. Sukovic, and N. H. Clinthorne, "Maximum-likelihood dual-energy tomographic image reconstruction," Proc. of SPIE, *vol. 4684*, 2002, pp. 38–49.

[4] K. W. Dolan, R. W. Ryon, D. J. Schneberk, H. E. Martz, and R. D. Rikard, "Explosives detection limitations using dual-energy radiography and computed tomography," Proceedings of the First International Symposium on Explosives Detection Technology, 1991, pp. 252–260.

[5] S. Singh and M. Singh, "Explosives detection systems (EDS) for aviation security," *Signal Processing 83*, 2003, pp. 31–55.

[6] J. Heismann, J. Leppert, and K. Stierstorfer, "Density and atomic number measurements with spectral X-ray attenuation method," *Journal of Applied Physics* 94, 2073-9, 2003.

[7] B. De Man, J. Nuyts, P. Dupont, G. Marchal, and P. Suetens, "Metal streak artifacts in X-ray computed tomography: a simulation study," *IEEE Transactions on Nuclear Science, V. 46*, June 1999, pp. 691–696.

[8] Z. Ying, R. Naidu, and C. R. Crawford, "Dual energy computed tomography for explosive detection," *Journal of X-ray Science and Technology, vol. 14, no. 4*, 2006, pp. 235–256

[9] A. Macovski, *Medical Imaging Systems*, Prentice-Hall, 1983.

[10] L. Martin, A. Tuysuzoglu, W. C. Karl, and P. Ishwar, "Learning-based object identification and segmentation using dual-energy CT images for security," *IEEE Transactions on Image Processing, vol. 24*, *no. 11*, 2015.

[11] L. Martin, W. C. Karl, and P. Ishwar, "Structure-preserving Dual-energy CT for Luggage Screening," Proc. of IEEE International Conference on Acoustics, Speech, and Signal Processing, Florence, Italy, 4–9 May 2014.

[12] L. Martin, "Enhanced Information Extraction in Multi-Energy X-ray Tomography for Security," Ph. D. Thesis, Electrical Engineering, Boston University, May 2014.

[13] Y. Boykov, O. Veksler, and R. Zabih, "Fast approximate energy minimization via graph cuts," *IEEE Transactions Pattern Analysis Machine Intelligence*, *vol. 23, no. 11*, 2001, pp. 1222–1239.

[14] P. Babaheidarian and D. A. Castañón, "Joint Segmentation and Material Recognition in Dual-Energy CT Images," Proc. 2017 IS&T International Symposium on Electronic Imaging, San Francisco, CA, 29 January–2 February 2017.

[15] P. Babaheidarian, "Algorithms for Enhanced Artifact Reduction and Material Recognition in Computed Tomography," Department of Electrical and Computer Engineering, Boston University, January 2018.

[16] A. Tuysuzoglu, W. C. Karl, I. Stojanovic, D. A. Castañón, and S. Unlu, "Graph-Cut Based Discrete-Valued Image Reconstruction," *IEEE Transactions on Image Processing, vol. 24, no. 5*, pp. 1614-1627, 2015.

[17] A. Tuysuzoglu, "Robust Inversion and Detection Techniques for Improved Imaging Performance," Doctoral Thesis, BU, ECE Department, June 2014.

[18] S. Boyd, N. Parikh, E. Chu, B. Peleato, and J. Eckstein, "Distributed optimization and statistical learning via the alternating direction method of multipliers," *Foundation and Trends Machine Learning*, *vol. 3, no. 1*, January 2011, pp. 1–122.

[19] A. Tuysuzoglu, Y. Khoo, and W. C. Karl. "Variable Splitting Techniques for Discrete Tomography," Proceedings of IEEE International Conference on Image Processing, Phoenix, Arizona, 25–28 September 2016.

[20] A. Tuysuzoglu, Y. Khoo, and W. Clem Karl, "Fast and robust discrete computational imaging," in *Computational Imaging*, C. A. Bouman, K. Sauer, editors, Proc. of Electronic Imaging, San Francisco, CA, 29 January – 2 February 2017.

[21] A. Tuysuzoglu, Y. Khoo, W. Clem Karl, and U. Ghani, "Fast and Robust Discrete Computational Imaging," in International Conference on Computational Photography, Stanford University, Stanford, CA, 12–14 May 2017.

[22] Y. Zhang, H. Yan, X. Jia, J. Yang, S. Jiang, and X. Mou, "A hybrid metal artifact reduction algorithm for X-ray CT," *Medical Physics, V. 40*, 2013.

[23] W. A. Kalender, R. Hebel, and J. Ebersberger, "Reduction of CT artifacts caused by metallic implants," *Radiology, vol. 164, no. 2*, 1987.

[24] F. E. Boas and D. Fleischmann, "Evaluation of two iterative techniques for reducing metal artifacts in computed tomography," *Radiology, vol. 259, no. 3*, 2011.

[25] S. Ravishankar and Y. Bresler, "Learning sparsifying transforms," *IEEE Transactions on Signal Processing, V. 61, No. 5*, 2013.

[26] P. Babaheidarian and D. A. Castañón, "A Randomized Approach to Reduce Metal Artifacts in X-Ray Computed Tomography," Proceedings of IS&T International Symposium on Electronic Imaging, San Francisco, CA, 29 January – 2 February 2017.

[27] S. G. Azevedo, H. E. Martz, Jr., M. B. Aufderheide, III, W. D. Brown, K. M. Champley, J. S. Kallman, G. P. Roberson, D. Schneberk, I. M. Seetho, and J. A. Smith, "System-independent characterization of materials using dual-energy computed tomography," *IEEE Transactions on Nuclear Science, V. 63*, February 2016

[28] V. Berisha, A. Wisler, A. O. Hero, III, and A. Spanias, "Empirically estimable classification bounds based on a nonparametric divergence measure," *IEEE Transactions on Signal Processing, V. 64*, February 2016.

[29] T. Montgomery, W. C. Karl, and D. A. Castañón, "Performance Estimation for Threat Detection in CT Systems," *Proc. of SPIE, vol. 10187*, SPIE, Los Angeles, CA, 9–13 April 2017.

[30] P. Babaheidarian and D. A. Castañón, "Feature Selection for Material Identification in Spectral CT,"in Computational Imaging, C. A. Bouman, K. Sauer, editors, Proc. of Electronic Imaging, San Francisco, CA, 28 January – 2 February 2018.

[31] S. Devadithya and D. Castañón, "Edge-preserving Total Variation Regularization for Dual-Energy CT Images," IS&T Symposium on Electronic Imaging, San Francisco, CA, January 2019.

[32] C. R. Crawford, "Research and Development of Reconstruction Advances in CT-Based Object Detection Systems," ALERT TO3 final report, May 2014.

[33] P. Luc, Pauline. C. Couprie, S. Chintala, and J. Verbeek, "Semantic Segmentation using Adversarial Networks." NIPS Workshop on Adversarial Training, Barcelona, Spain, December 2016.

[34] M. U. Ghani and W. C. Karl, "Deep learning based sinogram correction for metal artifacts reduction," in Computational Imaging, C. A. Bouman, K. Sauer, editors, *Proc. of Electronic Imaging*, San Francisco, CA, 28 January – 2 February 2018.

[35] M. U. Ghani and W. C. Karl, "CNN based Sinogram Denoising for Low-Dose CT," in Imaging and Applied Optics 2017 (3D, AIO, COSI, IS, MATH, pcAOP), OSA Technical Digest, Optical Society of America, Orlando, FL, 25–28 June 2018.

[36] M. U. Ghani and W. C. Karl, "Learning based methods for CT correction," in International Conference on Computational Photography 2018, Carnegie Mellon University, Pittsburgh, PA, 4 – 6 May 2018

[37] M. U. Ghani and W. C. Karl, "Sinogram Inpainting using Deep Learning," 2018 IEEE Image, Video, and Multidimensional Signal Processing (IVMSP) Workshop, Zagori, Aristi Village Greece, 10–12 June 2018.

[38] M. U. Ghani and W. C. Karl, "Deep learning in artifact reduction for medical imaging," Gordon Research Conference: Creating Knowledge from Imaging Data, Easton, MA, 17–22 June 2018.

[39] N. G. Anderson, A. P. Butler, et al., "Spectroscopic (multi-energy) VT distinguishes iodine and barium contrast material in mice," *European Radiology, vol. 20, no. 9*, 2010.

[40] Q. Yang, W. Cong, Y. Xi, and G. Wang, "Spectral X-ray CT image reconstruction with a combination of energy-integrating and photon-counting detectors," *PLoS One, vol. 11, no. 5,* 2016.

[41] S. Feuerlein, E. Roessl, R. Proksa, G. Martens, O. Klass, M. Jeltsch, V. Rasche, H. Brambs, M. Hoffmann, and J. Schlomka, "Multienergy photon-counting K-edge imaging: potential for improved luminal depiction in vascular imaging," *Radiology, vol. 249, no. 3*, 2008, pp. 1010–1016.

[42] P. Babaheidarian and D. A. Castañón, "Joint reconstruction and material classification in spectral CT," Proc. of SPIE: Anomaly Detection and Imaging with X-Rays (ADIX) III, SPIE Defense + Security, Orlando, FL, April 2018.

[43] K. Nakada, K. Taguchi, G. S. Fung, and K. Amaya, "Joint estimation of tissue types and linear attenuation coefficients for photon-counting CT," Medical physics 42(9), pp. 5329–5341, 2015.

[44] F. Zayek, "The Multi-View CT Air Cargo Pallet Scanner," ADSA 21 presentation, Northeastern University, November 2019. 2018.

[45] S. Devadithya and D. Castañón, "Material Identification in Presence of Metal for Baggage Screening," IS&T Symposium on Electronic Imaging, San Francisco, CA, January 2020.

This page intentionally left blank.

APPENDIX B: Bibliography of Publications

This page intentionally left blank.

Peer Reviewed Journal Articles

THRUST R1

Bezemer, K., McLennan, L., van Duin, L., Kuijpers, C.J., Koeberg, M., van den Elshout, J., van der Heijden, A., Busby, T., Yevdokimov, A.V., Schoenmakers, P., Smith, J., Oxley, J., & van Asten, A. "Chemical Attribution of the Home-Made Explosive ETN—Part I: Liquid Chromatography–Mass Spectrometry Analysis of Partially Nitrated Erythritol Impurities." *Forensic Science International*, *307*(110102), December 2019. https://doi.org/10.1016/j.forsciint.2019.110102.

Rettinger, R.C, Porter, M., Canaria, J., Smith, J.L., & Oxley, J.C. "Fuel-Oxidizer Mixtures: A Lab and Field Study." *Journal of Energetic Materials*, *38*(2), 23 October 2019, pp. 170–190. https://doi.org/10.1080/07370652.2019.1679282.

THRUST R2

Aquino, B., Benirschke, D., Gupta, V., & Howard, S. "A Bayesian Approach to Binary Classification of Mid-Infrared Spectral Data with Noisy Sensors." *IEEE Sensors Journal, 20*(*13),* March 2020, pp. 6964–6970. https://doi.org/10.1109/JSEN.2020.2978757.

Qian, Z., Rajaram, V., Kang, S., & Rinaldi, M. "High Figure-of-Merit NEMS Thermal Detectors Based on 50-nm Thick AlN Nano-Plate Resonators." *Applied Physics Letters, 115*(26), 2019. https://doi.org/10.1063/1.5128643.

Ricci, P.P., & Gregory, O.J. "Continuous Monitoring of Vapor Phase Threats Using Ultrasensitive, Low-Power Sensors." *IEEE Sensors Journal*, in press.

Ricci, P.P., Rossi A.S., & Gregory O.J. "Orthogonal Sensors for the Trace Detection of Explosives." *IEEE Sensors Letters, 3*(10), October 2019, pp. 1–4. https://doi.org/10.1109/LSENS.2019.2944587.

Stevenson, M., Beaudoin, S., & Corti, D. "Toward an Improved Method for Determining the Hamaker Constant of Solid Materials Using Atomic Force Microscopy. I. Quasi-Static Analysis for Arbitrary Surface Roughness." *Journal of Physical Chemistry C*, *124*(5), 10 January 2020, pp. 3014–3027. https://pubs.acs.org/doi/abs/10.1021/acs.jpcc.9b09669.

Year 6 Publication Not Previously Reported

Jaiswal, R., & Beaudoin, S. "London-van der Waals Force Field of a Chemically Patterned Surface to Enable Selective Adhesion." *Langmuir*, *35*(1), 8 January 2019, pp. 86–94. https://doi.org/10.1021/acs.langmuir.8b03502.

THRUST R3

Galán-Freyle, N.J., Ospina-Castro, M.L., Medina-González, A.R., Villarreal-González, R., Hernández-Rivera, S.P., & Pacheco-Londoño, L.C. "Artificial Intelligence Assisted Mid-Infrared Laser Spectroscopy in situ Detection of Petroleum in Soils." *Applied Sciences*, *10*(4), 15 February 2020, pp. 1319. https://doi.org/10.3390/app10041319.

Pacheco-Londoño, L.C., Galán-Freyle, N.J., Figueroa-Navedo, A.M., Infante-Castillo, R., Ruiz-Caballero, J.L., & Hernández-Rivera, S.P. "Quantum Cascade Laser Back-Reflection Spectroscopy at Grazing- Angle Incidence Using the Fast Fourier Transform as a Data Preprocessing Algorithm." *Journal of Chemometrics*, *33*, 29 July 2019, pp. e3167. https://doi.org/10.1002/cem.3167.

Pacheco-Londoño, L.C., Ruiz-Caballero, J.L., Ramírez-Cedeño, M.L., Infante-Castillo, R., Gálan-Freyle, N.J., & Hernández-Rivera, S.P. "Surface Persistence of Trace Level Deposits of Highly Energetic Materials." *Molecules 2019*, *24*(19), 26 September 2019, pp. 3494. https://doi.org/10.3390/molecules24193494.

Pacheco-Londoño, L.C., Warren, E., Galán-Freyle, N.J., Villarreal-González, R., Aparicio-Bolaño, J.A., Ospina-Castro, M.L., Shih, W.C., & Hernández-Rivera, S.P. "Mid-Infrared Laser Spectroscopy Detection and Quantification of Explosives in Soils Using Multivariate Analysis and Artificial Intelligence." *Applied Sciences, 10*(6), 31 May 2020, pp. 1319. https://doi.org/10.3390/app10041319; https://doi.org/10.3390/app10124178.

THRUST R4

Dai, T., & Sznaier, M. "A Semi-Algebraic Optimization Approach to Data-Driven Control of Continuous-Time Nonlinear Systems." *IEEE Control Systems Letters*, *5*(2), 18 June 2020, pp. 487–492. https://doi.org/10.1109/LCSYS.2020.3003505.

Ghani, M.U., & Karl, W.C. "Fast Enhanced CT Metal Artifact Reduction using Data Domain Deep Learning." *IEEE Transactions on Computational Imaging*, *6*, 27 August 2019, pp. 181–193. https://doi.org/10.1109/TCI.2019.2937221.

Rezaee, H., Rothschild, P., Tracey, B., & Miller, E.L. "On the Fusion of Energy Resolved Scatter and Attenuation Data for Limited-View X-Ray Materials Characterization with Application to Security Screening." *IEEE Transactions on Computational Imaging*, *5*(4), December 2019, pp. 620–634. https://doi.org/10.1109/TCI.2019.2909858.

Webber, J.W., & Miller, E.L. "Compton Scattering Tomography in Translational Geometries." *Inverse Problems, 36*(2), 23 January 2020. https://doi.org/10.1088/1361-6420/ab4a32.

Webber, J.W., & Quinto, E.T. "Microlocal Analysis of a Compton Tomography Problem." *SIAM Journal on Imaging Sciences, 13*(2), 2020, pp. 746–774. https://doi.org/10.1137/19M1251035.

Webber, J.W., Quinto, E.T., & Miller, E.L. "A Joint Reconstruction and Lambda Tomography Regularization Technique for Energy-Resolved X-Ray Imaging." *Inverse Problems*, special issue on modern challenges in imaging, *36*(7), 19 June 2020. https://doi.org/10.1088/1361-6420/ab8f82.

Peer Reviewed Conference Proceedings

THRUST R1

Japzon, M., Nacouzi, N., Sharma, S., & Kapadia, A.J. "Optimization of X-Ray Diffraction Images of Medical Specimens by Monte Carlo Methods." *AAPM Annual Meeting 2019*, San Antonio, Texas, July 2019.

Kapadia, A.J., Stryker, S., McCall, S.J., & Greenberg, J.A. "The Role of X-Ray Diffraction Imaging in Digital Pathology." *SPIE Medical Imaging*, virtual, February 2020 [11320–37].

Oxley, J.C., Smith, J.L., Colizza, K., & Gonsalves, M. "In Vitro Metabolism of TATP." *NTREM*, April 2020, meeting proceedings, meeting canceled.

THRUST R2

Coultas-Mckenney, C., Norris, C., Roginski, A., Bradfish, K., Weiglein, E., & Beaudoin, S. "Bringing Particle Scale Properties into Descriptions of Energetic Powder Behavior via the Enhanced Centrifuge Technique." *Annual Meeting of the American Institute of Chemical Engineers*, Orlando, FL, November 2019.

Gregory, O.J., Olenick, J., & Olenick, K. "Ribbon Ceramic: Novel Form Factor Enabling Thermal Product Applications." *NATAS 2019*, Newport, RI, August 2019.

Ricci, P.P., & Gregory, O.J. "Low-Power Sensors for the Trace Detection of Threats in the Vapor Phase." *FLEX 2020*, San Jose, CA, February 2020.

Ricci, P.P., & Gregory, O.J. "Trace Detection of Explosives Using Metal Oxide Nanostructured Catalysts." *TechConnect 2019*, Boston, MA, June 2019.

Ricci, P.P., & Gregory, O.J. "Ultrasensitive, Orthogonal Sensors for the Trace Detection of Explosives." *ISADE 2020*, Charlotte, NC, April 2020.

Ricci, P.P., & Gregory, O.J. "Ultrasensitive, Thin-Film Sensors for the Trace Detection of Explosives." *NATAS 2019*, Newport, RI, August 2019.

Stevenson, M., Beaudoin., S., & Corti, D. "Impact of Surface Roughness on Estimating Hamaker Constants through Non-Contact Atomic Force Microscopy." *Annual Meeting of the American Institute of Chemical Engineers*, Orlando, FL, November 2019.

Year 6 Publication Not Previously Reported

Calisgan, S., Kang, S., Rajaram, V., Qian, Z., & Rinaldi, M. "Threshold-Triggered Mems-Cmos Infrared Resonant Detector with Near-Zero Standby Power Consumption." *2019 20th International Conference on Solid-State Sensors, Actuators and Microsystems–Transducers 2019 Eurosensors XXIII*, Berlin, Germany, 23–27 June 2019, pp. 637–640.

THRUST R3

Asri, M., & Rappaport, C. "Automatic Permittivity Characterization of a Weak Dielectric Attached to Human Body Based on Using Wideband Radar Image Processing." *2019 IEEE International Symposium on Antennas and Propagation*, Atlanta, GA, July 2019.

Asri, M., Tajdini, M.M., Wig, E., & Rappaport, C. "Automatic Permittivity and Thickness Characterization of Body-Borne Weak Dielectric Threats Using Wideband Radar." *European Conference on Antennas and Propagation*, Copenhagen, Denmark, March 2020.

Heredia-Juesas, J., Tirado, L., Molaei, A., & Martinez-Lorenzo, J.A. "ADMM Based Consensus and Sectioning Norm-1 Regularized Algorithm for Imaging with a CRA." *2019 IEEE International Symposium on Antennas and Propagation and USNC-URSI Radio Science Meeting (AP-S/URSI 2019)*, Atlanta, GA, 7–12 July 2019.

Morgenthaler, A., & Rappaport, C. "Modeling Focused CW Mm-Wave Scattering of a Penetrable Dielectric Slab Affixed to a Human Body." *2019 IEEE International Symposium on Antennas and Propagation*, Atlanta, GA, July 2019.

Sun, G., Nemati, M., & Rappaport, C. "Improving the Reconstruction Image Quality of Multiple Small Discrete Targets Using the Phase Coherence Method." *European Conference on Antennas and Propagation*, Copenhagen, Denmark, March 2020.

Tajdini, M.M., Jaisle, K., & Rappaport, C. "Image Radar Determining the Nominal Body Contour for Characterization of Concealed Person-Worn Explosives." *European Conference on Antennas and Propagation*, Copenhagen, Denmark, March 2020.

Tajdini, M., & Rappaport, C. "Focused CW Mm-Wave Characterization of Lossy Penetrable Dielectric Slab Affixed to Human Body." *2019 IEEE International Symposium on Antennas and Propagation*, Atlanta, GA, July 2019.

THRUST R4

Asghari-Esfeden, S., Sznaier, M., & Camps, O. "Dynamic Motion Representation for Human Action Recognition." *IEEE 2020 Winter Conference on Applications of Computer Vision*, Aspen, CO, 1–5 March 2020, pp. 557–566.

Berberich, J., Sznaier, M., & Allgower, F. "Signal Estimation and System Identification with Nonlinear Dynamic Sensors." *IEEE Conference on Control Technology and Applications*, Hong Kong, China, 19–21 August 2019.

Dai, T., & Sznaier, M. "Worst-Case Optimal Data-Driven Estimators for Switched Discrete-Time Linear Systems." *IEEE Conference on Decision and Control,* Nice, France, 11–13 December 2019.

Dai, T., Sznaier, M., & Roig-Solvas, B. "Data-Driven Quadratic Stabilization of Continuous LTI Systems." *2020 IFAC World Congress*, Berlin, Germany, 12–17 July 2020.

Devadithya, S., & Castañón, D. "Material Identification in Presence of Metal for Baggage Screening," in *Computational Imaging*, Bouman, C.A., & Sauer, K., editors, *Process of Electronic Imaging*, Burlingame, CA, 26–30 January 2020.

Ghani, M.U., & Karl, W.C. "Integrating Data and Image Domain Deep Learning for Limited Angle Tomography Using Consensus Equilibrium." *IEEE Conference on Computer Vision*, Seoul, Korea, 22 October–2 November 2019.

Ghani, M.U., & Karl, W.C. "Integrating Learned Data and Image Models through Consensus Equilibrium." in *Computational Imaging*, Bouman, C.A., & Sauer, K., editors, *Process of Electronic Imaging*, Burlingame, CA, 26–30 January 2020.

Ghani, M.U., & Karl, W.C. "Integrating Learned Data and Image Models through Consensus Equilibrium for Model-Based Image Reconstruction." *International Symposium on Biomedical Imaging*, Iowa, IA, April 2020.

Liu, W., Li, R., Zheng, M., Karanam, S., Wu, Z., Bhanu, B., Radke, R.J., & Camps, O. "Towards Automated Forensic Reconstruction in Wide-Area Multi-Camera Networks." *IEEE Conference on Computer Vision and Pattern Recognition,* 2020.

Liu, W., Li, R., Zheng, M., Karanam, S., Wu, Z., Bhanu, B., Radke, R., & Camps, O. "Towards Visually Explaining Variational Autoencoders." *IEEE/CVF Conference on Computer Vision and Pattern Recognition*, Seattle, WA, 16–18 June 2020, pp. 8642–8651.

Miller, J., Zheng, Y., Roig-Solvas, B., Sznaier, M., & Papachristodoulou, A. "Chordal Decomposition in Rank Minimized Semidefinite Programs with Applications to Subspace Clustering." *IEEE Conference on Decision and Control*, Nice, France, 11–13 December 2019.

Miller, J., Zheng, Y., Sznaier, M., & Papachristodoulou, A. "Decomposed Structured Subsets for Semidefinite Optimization." *2020 IFAC World Congress*, Berlin, Germany, 12–17 July 2020.

Ozbay, B., Camps, O., & Sznaier, M. "Efficient Identification of Error-in-Variables Switched Systems via a Sum-of-Squares Polynomial Based Subspace Clustering Method." *IEEE Conference on Decision and Control*, Nice, France, 11–13 December 2019.

Ozbay, B., Sznaier, M., & Camps, O. "An Algebraic Approach to Efficient Identification of a Class of Wiener Systems." *2020 IFAC World Congress*, Berlin, Germany, 12–17 July 2020.

Singh, R., & Sznaier, M. "A Convex Optimization Approach to Finding Low Rank Mixed Time/Frequency Domain Interpolants with Applications to Control Oriented Identification." *IEEE Conference on Decision and Control*, Nice, France, 11–13 December 2019.

Singh, R., & Sznaier, M. "A Loewner Matrix Based Convex Optimization Approach to Finding Low Rank Mixed Time/Frequency Domain Interpolants." *2020 American Control Conference*, Denver, CO, 1–3 July 2020.

Taskazan, B., Miller, J., Inyang-Udoh, U., Camps, O., & Sznaier, M. "Domain Adaptation Based Fault Detection in Label Imbalanced Cyberphysical Systems." *IEEE Conference on Control Technology and Applications*, Hong Kong, China, 19–21 August 2019.

Wang, X., Sridhar, V., Ronaghi, Z., Thomas, R., Deslippe, J., Parkinson, D., Buzzard, G.T., Midkiff, S.P., Bouman, C.A., & Warfield, S.K. "Consensus Equilibrium Method for Super-Resolution and Extreme-Scale CT Iterative Reconstruction." *SC 19: The International Conference for High Performance Computing, Networking, Storage, and Analysis*, Denver, CO, 17–22 November 2019, pp. 86-1 to 86-13.

Zhang, Y., Wang, Y., Camps, O., & Sznaier, M. "Key Frame Proposal Network for Efficient Pose Estimation in Videos." *European Conference on Computer Vision*, 23–28 August 2020.

This page intentionally left blank.

APPENDIX C: Tables

This page intentionally left blank.

Table 1: Center Accomplishments

Outputs	July 01, 2019 - June 30, 2020
Personnel	
TOTAL	147
Faculty	23
Administrative Staff	12
Technical Staff	12
Graduate Students	61
Undergraduate Students	39
K-12 Teachers	0
K-12 Students	0
Publications That Result from Center Support	
All Publications	53
Co-authored with Students	29
In Peer-Reviewed Technical Journals	17
In Peer-Reviewed Conference Proceedings	36
Strategic Reports	1
Theses	9
Posters	5
News Articles	9
Industrial and Practitioner Participation, Collaboration, and Associated Funding	
Members	9
Technology Transfer	
Inventions Disclosed (Submitted to Agencies by Researchers or Technology Transfer	0
Patent Applications Filed	4
Patents Awarded	5
Licenses Issued	1
Spin-off Companies Started	2
Software Products Developed	8
Knowledge Transfer	
Website Page Views	44,808
Publications Downloaded from Website	2,866
Requests for Assistance or Advice from DHS	3
Requests for Assistance or Advice from Federal, State, Local Government	1
Student Internships in Industry or Government	3
ALERT Graduates Working In	
Industry	2
Government	5
Academic Institutions	8
Undecided/Still Looking/Unknown	5
Degrees to ALERT Students	
Doctoral Degrees Granted	4
Master's Degrees Granted	7
Bachelor's Degrees Granted	9
ALERT-Sponsored Active Information Dissemination/Educational Outreach	
Workshops	
# of Events	3
Total # of Attendees	320
Short Courses	
# of Events	10
Total # of Attendees	225
Educational Outreach Events for Community College or Undergraduate Students	
# of Events	0
Total # of Attendees	0

TABLE 2: ALERT PERSONNEL

Personnel Type	Total	Gender			Citizenship Status								Ethnicity: Hispanic			Disability
		Male	Female	Gender not reported	Race: US citizens and permanent residents only							Other non-US	US/Perm	Non-US	Not reported	
					AI/AN	NH/PI	B/AA	W	A	More than one race reported, minority	More than one race reported, non-minority	Not provided				
All Institutions																
Total	153	77	43	33	1	1	3	49	8	0	3	31	26	37	3	0	2
Leadership/Administration																	
Director	1	1	0	0	0	0	0	0	0	0	0	1	0	0	0	0	0
Associate Director	1	1	0	0	0	0	0	1	0	0	0	0	0	0	0	0	0
Administrative Staff	12	3	8	1	0	0	0	9	1	0	0	0	1	1	0	0	0
Senior Faculty	1	1	0	0	0	0	0	1	0	0	0	0	0	0	0	0	1
Master's Student	3	1	2	0	0	0	0	0	0	0	0	0	3	0	0	0	0
Undergraduate (non-REU) Student	3	0	2	1	0	0	0	1	1	0	0	0	0	0	0	0	0
Consultant	2	0	2	0	0	0	0	2	0	0	0	0	0	0	0	0	0
Subtotal	23	7	14	2	0	0	0	14	2	0	0	1	4	1	0	0	1
Research under Strategic Research Plan																	
Senior Faculty	16	13	2	1	0	0	0	11	1	0	0	4	0	5	0	0	0
Junior Faculty	4	4	0	0	0	0	0	2	0	0	0	2	0	1	0	0	0
Research Staff	6	6	0	0	0	0	1	2	2	0	1	0	0	1	0	0	0
Industry/Government Researcher	1	0	0	1	0	0	0	0	0	0	0	0	0	0	0	0	0
Post Doctoral Associate	5	5	0	0	0	0	0	3	0	0	0	0	2	1	0	0	0
Doctoral Student	44	22	9	13	0	1	0	8	1	0	1	5	17	4	2	0	1
Master's Student	14	4	6	4	0	0	1	2	1	0	0	5	1	4	0	0	0
Undergraduate (non-REU) Student	36	13	11	12	1	0	1	4	1	0	1	14	1	20	0	0	0
Consultant	4	3	1	0	0	0	0	3	0	0	0	0	1	0	1	0	0
Subtotal	130	70	29	31	1	1	3	35	6	0	3	30	22	36	3	0	1
Curriculum Development and Outreach																	
Subtotal	0	0	0	0	0	0	0	0	0	0	0	0	0	0	0	0	0
Core Partners																	
Total	147	73	42	32	1	1	2	45	8	0	3	31	26	36	3	0	2

TABLE 2: ALERT PERSONNEL (CONT.)

Personnel Type	Total	Gender			Citizenship Status								Ethnicity: Hispanic			Disability
		Male	Female	Gender not reported	Race: US citizens and permanent residents only							Other non-US	US/Perm	Non-US	Not reported	
					AI/AN	NH/PI	B/AA	W	A	More than one race reported, minority	More than one race reported, non-minority	Not provided				
Northeastern University																
Total	55	22	22	11	0	0	0	22	3	0	1	3	17	5	1	0	1
Leadership/Administration																	
Director	1	1	0	0	0	0	0	0	0	0	0	1	0	0	0	0	0
Associate Director	1	1	0	0	0	0	0	1	0	0	0	0	0	0	0	0	0
Administrative Staff	12	3	8	1	0	0	0	9	1	0	0	0	1	1	0	0	0
Senior Faculty	1	1	0	0	0	0	0	1	0	0	0	0	0	0	0	0	1
Master's Student	3	1	2	0	0	0	0	0	0	0	0	0	3	0	0	0	0
Undergraduate (non-REU) Student	3	0	2	1	0	0	0	1	1	0	0	0	0	0	0	0	0
Consultant	2	0	2	0	0	0	0	2	0	0	0	0	0	0	0	0	0
Subtotal	23	7	14	2	0	0	0	14	2	0	0	1	4	1	0	0	1
Research under Strategic Research Plan																	
Senior Faculty	2	1	1	0	0	0	0	2	0	0	0	0	0	2	0	0	0
Junior Faculty	2	2	0	0	0	0	0	1	0	0	0	1	0	1	0	0	0
Post Doctoral Associate	3	3	0	0	0	0	0	2	0	0	0	0	1	1	0	0	0
Doctoral Student	14	5	3	6	0	0	0	0	0	0	0	1	9	0	0	0	0
Master's Student	4	1	2	1	0	0	0	2	0	0	0	0	1	0	0	0	0
Undergraduate (non-REU) Student	6	2	2	2	0	0	0	1	1	0	1	0	1	0	0	0	0
Consultant	1	1	0	0	0	0	0	0	0	0	0	0	1	0	1	0	0
Subtotal	32	15	8	9	0	0	0	8	1	0	1	2	13	4	1	0	0
Curriculum Development and Outreach																	
Subtotal	0	0	0	0	0	0	0	0	0	0	0	0	0	0	0	0	0
Boston University																	
Total	4	3	1	0	0	0	0	1	0	0	0	1	2	1	0	0	0
Leadership/Administration																	
Subtotal	0	0	0	0	0	0	0	0	0	0	0	0	0	0	0	0	0

TABLE 2: ALERT PERSONNEL (CONT.)

Personnel Type	Total	Gender			Citizenship Status								Ethnicity: Hispanic			Disability
		Male	Female	Gender not reported	Race: US citizens and permanent residents only							Other non-US	US/Perm	Non-US	Not reported	
					AI/AN	NH/PI	B/AA	W	A	More than one race reported, minority	More than one race reported, non-minority	Not provided				
Research under Strategic Research Plan																
Senior Faculty	2	2	0	0	0	0	0	1	0	0	0	1	0	1	0	0
Doctoral Student	2	1	1	0	0	0	0	0	0	0	0	0	2	0	0	0
Subtotal	4	3	1	0	0	0	0	1	0	0	0	1	2	1	0	0
Curriculum Development and Outreach																
Subtotal	0	0	0	0	0	0	0	0	0	0	0	0	0	0	0	0
Purdue University																
Total	10	5	1	4	0	0	0	4	2	0	0	1	0	1	0	0
Leadership/Administration																
Subtotal	0	0	0	0	0	0	0	0	0	0	0	0	0	0	0	0
Research under Strategic Research Plan																
Senior Faculty	3	3	0	0	0	0	0	3	0	0	0	0	0	1	0	0
Research Staff	1	1	0	0	0	0	0	0	1	0	0	0	0	0	0	0
Doctoral Student	3	1	1	1	0	0	0	1	1	0	0	0	0	0	0	0
Master's Student	1	0	0	1	0	0	0	0	0	0	0	1	0	0	0	0
Undergraduate (non-REU) Student	2	0	0	2	0	0	0	0	0	0	0	0	0	0	0	0
Subtotal	10	5	1	4	0	0	0	4	2	0	0	1	0	1	0	0
Curriculum Development and Outreach																
Subtotal	0	0	0	0	0	0	0	0	0	0	0	0	0	0	0	0
Rensselaer Polytechnic Institute																
Total	2	1	1	0	0	0	0	1	0	0	0	0	1	0	0	0
Leadership/Administration																
Subtotal	0	0	0	0	0	0	0	0	0	0	0	0	0	0	0	0

TABLE 2: ALERT PERSONNEL (CONT.)

Personnel Type	Total	Gender			Citizenship Status								Ethnicity: Hispanic			Disability
		Male	Female	Gender not reported	Race: US citizens and permanent residents only							Other non-US	US/Perm	Non-US	Not reported	
					AI/AN	NH/PI	B/AA	W	A	More than one race reported, minority	More than one race reported, non-minority	Not provided				
Research under Strategic Research Plan																
Senior Faculty	1	1	0	0	0	0	0	1	0	0	0	0	0	0	0	0
Doctoral Student	1	0	1	0	0	0	0	0	0	0	0	0	1	0	0	0
Subtotal	2	1	1	0	0	0	0	1	0	0	0	0	1	0	0	0
Curriculum Development and Outreach																
Subtotal	0	0	0	0	0	0	0	0	0	0	0	0	0	0	0	0
Tufts University																
Total	3	3	0	0	0	0	0	0	1	0	0	1	1	0	0	0
Leadership/Administration																
Subtotal	0	0	0	0	0	0	0	0	0	0	0	0	0	0	0	0
Research under Strategic Research Plan																
Senior Faculty	1	1	0	0	0	0	0	0	0	0	0	1	0	0	0	0
Research Staff	1	1	0	0	0	0	0	0	1	0	0	0	0	0	0	0
Post Doctoral Associate	1	1	0	0	0	0	0	0	0	0	0	0	1	0	0	0
Subtotal	3	3	0	0	0	0	0	0	1	0	0	1	1	0	0	0
Curriculum Development and Outreach																
Subtotal	0	0	0	0	0	0	0	0	0	0	0	0	0	0	0	0
Duke University																
Total	7	7	0	0	0	0	1	1	2	0	1	1	0	0	0	0
Leadership/Administration																
Subtotal	0	0	0	0	0	0	0	0	0	0	0	0	0	0	0	0

TABLE 2: ALERT PERSONNEL (CONT.)

Personnel Type	Total	Gender			Citizenship Status								Ethnicity: Hispanic			Disability
		Male	Female	Gender not reported	Race: US citizens and permanent residents only							Other non-US	US/Perm	Non-US	Not reported	
					AI/AN	NH/PI	B/AA	W	A	More than one race reported, minority	More than one race reported, non-minority	Not provided				
Research under Strategic Research Plan																
Senior Faculty	1	1	0	0	0	0	0	0	1	0	0	0	0	0	0	0
Junior Faculty	1	1	0	0	0	0	0	0	0	0	0	1	0	0	0	0
Research Staff	1	1	0	0	0	0	0	0	0	0	1	0	0	0	0	0
Doctoral Student	1	1	0	0	0	0	0	1	0	0	0	0	0	0	0	0
Master's Student	3	3	0	0	0	0	1	0	1	0	0	0	0	0	0	0
Subtotal	7	7	0	0	0	0	1	1	2	0	1	1	0	0	0	0
Curriculum Development and Outreach																
Subtotal	0	0	0	0	0	0	0	0	0	0	0	0	0	0	0	0
University of Notre Dame																
Total	14	8	1	5	0	0	0	4	0	0	0	2	4	1	0	0
Leadership/Administration																
Subtotal	0	0	0	0	0	0	0	0	0	0	0	0	0	0	0	0
Research under Strategic Research Plan																
Senior Faculty	2	1	0	1	0	0	0	1	0	0	0	1	0	0	0	0
Junior Faculty	1	1	0	0	0	0	0	1	0	0	0	0	0	0	0	0
Doctoral Student	10	6	1	3	0	0	0	2	0	0	0	1	4	1	0	0
Undergraduate (non-REU) Student	1	0	0	1	0	0	0	0	0	0	0	0	0	0	0	0
Subtotal	14	8	1	5	0	0	0	4	0	0	0	2	4	1	0	0
Curriculum Development and Outreach																
Subtotal	0	0	0	0	0	0	0	0	0	0	0	0	0	0	0	0
University of Puerto Rico Mayagüez																
Total	35	15	13	7	1	0	1	3	0	0	0	21	1	27	1	1
Leadership/Administration																

TABLE 2: ALERT PERSONNEL (CONT.)

Personnel Type	Total	Gender			Citizenship Status								Ethnicity: Hispanic			Disability
		Male	Female	Gender not reported	Race: US citizens and permanent residents only							Other non-US	US/Perm	Non-US	Not reported	
					AI/AN	NH/PI	B/AA	W	A	More than one race reported, minority	More than one race reported, non-minority	Not provided				
Subtotal	0	0	0	0	0	0	0	0	0	0	0	0	0	0	0	0
Research under Strategic Research Plan																
Senior Faculty	1	1	0	0	0	0	0	0	0	0	0	1	0	1	0	0
Doctoral Student	4	3	0	1	0	0	0	0	0	0	0	2	1	2	1	0	1
Master's Student	5	0	4	1	0	0	0	0	0	0	0	4	0	4	0	0	0
Undergraduate (non-REU) Student	25	11	9	5	1	0	1	3	0	0	0	14	0	20	0	0	0
Subtotal	35	15	13	7	1	0	1	3	0	0	0	21	1	27	1	0	1
Curriculum Development and Outreach																	
Subtotal	0	0	0	0	0	0	0	0	0	0	0	0	0	0	0	0	0
University of Rhode Island																	
Total	17	9	3	5	0	1	0	9	0	0	1	1	0	1	0	0	0
Leadership/Administration																	
Subtotal	0	0	0	0	0	0	0	0	0	0	0	0	0	0	0	0	0
Research under Strategic Research Plan																	
Senior Faculty	3	2	1	0	0	0	0	3	0	0	0	0	0	0	0	0	0
Research Staff	1	1	0	0	0	0	0	1	0	0	0	0	0	0	0	0	0
Post Doctoral Associate	1	1	0	0	0	0	0	1	0	0	0	0	0	0	0	0	0
Doctoral Student	9	5	2	2	0	1	0	4	0	0	1	1	0	1	0	0	0
Master's Student	1	0	0	1	0	0	0	0	0	0	0	0	0	0	0	0	0
Undergraduate (non-REU) Student	2	0	0	2	0	0	0	0	0	0	0	0	0	0	0	0	0
Subtotal	17	9	3	5	0	1	0	9	0	0	1	1	0	1	0	0	0
Curriculum Development and Outreach																	
Subtotal	0	0	0	0	0	0	0	0	0	0	0	0	0	0	0	0	0

TABLE 2: ALERT PERSONNEL (CONT.)

Personnel Type	Total	Gender			Citizenship Status								Ethnicity: Hispanic			Disability
		Male	Female	Gender not reported	Race: US citizens and permanent residents only							Other non-US	US/Perm	Non-US	Not reported	
					AI/AN	NH/PI	B/AA	W	A	More than one race reported, minority	More than one race reported, non-minority	Not provided				
Associate Institutions and Others																
Total	6	4	1	1	0	0	1	4	0	0	0	0	1	0	0	0
Leadership/Administration																
Subtotal	0	0	0	0	0	0	0	0	0	0	0	0	0	0	0	0
Research under Strategic Research Plan																
Research Staff	2	2	0	0	0	0	1	1	0	0	0	0	1	0	0	0
Industry/Government Researcher	1	0	0	1	0	0	0	0	0	0	0	0	0	0	0	0
Consultant	3	2	1	0	0	0	0	3	0	0	0	0	0	0	0	0
Subtotal	6	4	1	1	0	0	1	4	0	0	0	0	1	0	0	0
Curriculum Development and Outreach																
Subtotal	0	0	0	0	0	0	0	0	0	0	0	0	0	0	0	0

This page intentionally left blank.

Awareness and Localization of Explosives-Related Threats

A Department of Homeland Security Center of Excellence

Lead Partner: Northeastern University

Core Academic Partners:
Boston University • Purdue University • University of Rhode Island

Academic Partners:
Duke University • Marquette University • Rensselaer Polytechnic Institute • Tufts University
University of Notre Dame • University of Puerto Rico at Mayagüez

This material is based upon work supported by the US Department of Homeland Security, Science and Technology Directorate, Office of University Programs, under Grant Award 2013-ST-061-ED0001. The views and conclusions contained in this document are those of the authors and should not be interpreted as necessarily representing the official policies, either expressed or implied, of the US Department of Homeland Security.

Photo Caption: ALERT leadership, researchers, and industry representatives participated in an all-day Technology Demonstration in November 2019 at the Los Angeles/Long Beach Seaport. Chief Victor Todorov of the US Customs and Border Protection (CBP) Office of Field Operations and Ms. Emel Bulat, industrial liaison officer of the ALERT Center, organized and led the event which also included CBP officers and senior personnel from the Department of Homeland Security (DHS) Science and Technology (S&T) Directorate. Attendees included Dr. Michael Silevitch, director of ALERT; Major General Robert Newman (retired), executive director for the Office of Mission and Capability Support at DHS S&T; Dr. Laura Parker, program manager at DHS S&T; Mr. David Taylor, portfolio manager at DHS S&T; and Mr. Edward Morones, assistant port director at CBP.